Appendix H

Quality Assurance/Quality Control and Data Issues

Jeffery D. Long

CONTENTS

TABLES

Appendix H

Quality Assurance/Quality Control and Data Issues

H-1. INTRODUCTION

In August and September 2004, INTEC tank farm soil characterization activities were performed to collect environmental data to support the remedial investigation/baseline risk assessment and feasibility study phases of OU 3-14. Characterization was performed to determine the extent, distribution, and composition of contamination in soils located at identified tank farm release sites. Characterization activities were conducted according to the *Operable Unit 3-14 Tank Farm Soil and Groundwater Remedial Investigation/Feasibility Study Work Plan* (DOE-ID 2004a). The *Tank Farm Soil and Groundwater Field Sampling Plan for the Operable Unit 3-14 Remedial Investigation/Feasibility Study* (DOE-ID 2004b) governed all sampling and analysis activities at the task site.

Characterization of the tank farm soil took place in two phases. The first phase of the field investigation was performed to define the extent and distribution of contamination in the subsurface for known release sites. Cased probeholes were installed and surveyed for gamma radiation. The subsurface gamma radiation surveys produced log plots to show variations in gamma-ray flux at depth. This information was used as a basis to estimate the combined horizontal and vertical extent of the soil contamination zones. It also served as an indicator of zones where other contaminants of potential concern were most likely to exist.

In the second phase of the characterization effort, soil samples were collected to define the composition of contamination from release locations defined during the phase one probing effort. Samples were then sent to an analytical laboratory for organic, inorganic, and radiochemical analyses. Probing and sampling activities were conducted at the CPP-15, CPP-27, CPP-28, CPP-31, and CPP-79 soil contamination sites.

The purpose of this appendix document is to discuss the sampling and analytical effort for the second phase of the characterization project. Sample collection and analysis issues are detailed along with a quality assurance and quality control (QA/QC) evaluation of the data.

H-2. SAMPLING METHODOLOGY

Sampling was conducted in August and September of 2004 according to the *Tank Farm Soil and Groundwater Field Sampling Plan for the Operable Unit 3-14 Remedial Investigation/Feasibility Study* (DOE-ID 2004b). The objective of the phase 2 field effort was to define the composition of contamination from identified release locations from the ground surface down through the alluvium to the top of basalt. Table H-1 contains a list of the samples collected, location and depth, and analyses performed. Samples were collected according to standard collection, handling, and packaging procedures.

H-2.1 Sample Collection

As noted in the field sampling plan, soil samples were collected from CPP-15, -27, -28, -31, and -79. Corehole locations were installed immediately adjacent to applicable probehole locations. Appendix F, *End of Well Reports for the OU 3-14 2004 Tank Farm Soil Investigation at the Idaho Nuclear Technology and Engineering Center*, documents the probing activities using the direct push with dual-tube sampling system. Soil samples were collected at the specified locations and intervals from the ground surface to basalt.

Table H-1. 2004 OU 3-14 field sampling.

Sample Number	Depth (ft)	Date Collected	Analyses Performed[a]
CPP-15			
E05104000	2-4	8/9/04	3A, 9A, RH, RN, TV, AV
E05104001	6-8	8/10/04	3A, 9A, RH, RN, TV, AV
E05104002	10-12	8/10/04	3A, 9A, RH, RN, TV, AV
E05104003	14-16	8/10/04	1G[d], 9A, RH, RN, TV, AV
E05104004	16-18	8/10/04	3A, 9A, RH, RN, TV, AV
CPP-27			
E05104012	2-4	8/12/04	3A, 9A, RH, RN, TV, AV
E05104013	6-8	8/12/04	3A, 9A, RH, RN, TV, AV
E05104014	10-12	8/12/04	3A, 9A, RH, RN, TV, AV
E05104015	14-16	8/12/04	3A, 9A, RH, RN, TV, AV
E05104016	18-20	8/12/04	3A, 9A, RH, RN, TV, AV
E05104017	20-24	8/16/04	3A, 9A, RH, RN, TV, AV
E05104018	24-28	8/16/04	1G[d], 9A, RH, RN, TV, AV
E05104019	28-32	8/16/04	3A, 9A, RH, RN, TV, AV
E05104020	32-36	8/19/04	3A, 9A, RH, RN, TV, AV
CPP-28			
E05104024	2-3	8/18/04	3A, 9A, RH, RN, TV, AV
E05104025	6-7	8/18/04	3A, 9A, RH, RN, TV, AV
E05104026	10-12	9/20/04	3A, 9A, RH, RN, TV, AV, *, **
E05104027	12-14	9/20/04	3A, 9A, RH, RN, TV, AV
E05104028	16-18	9/20/04	3A, 9A, RH, RN, TV, AV
E05104029[b]	22-24	9/21/04	3A, 9A, RH, RN, TV, AV
E05104030	24-28	9/21/04	3A, 9A, RH, RN, TV, AV
E05104031	28-32	9/21/04	1G[d], 9A, RH, RN, TV, AV, *, **
E05104032	32-34	9/21/04	3A, 9A, RH, RN, TV, AV
E05104033	38-40	9/21/04	3A, 9A, RH, RN, TV, AV
E05104034	42-44	9/22/04	3A, 9A, RH, RN, TV, AV
E05104035	44-48	9/22/04	3A, 9A, RH, RN, TV, AV
E05104064	50-52	9/22/04	3A, 9A, RH, RN, TV, AV
E05104065	54-56	9/22/04	3A, 9A, RH, RN, TV, AV, *, **
CPP-31			
E05104036	0-4	8/24/04	3A, 9A, RH, RN, TV, AV
E05104037	6-8	8/24/04	3A, 9A, RH, RN, TV, AV
E05104038	10-12	8/24/04	3A, 9A, RH, RN, TV, AV
E05104039	14-16	8/24/04	3A, 9A, RH, RN, TV, AV
E00905000[c]	16-18	3/21/05	***
E05104040	18-20	8/25/04	1G[d], 9A, RH, RN, TV, AV
E05104041	22-24	8/25/04	3A, 9A, RH, RN, TV, AV

Table H-1. (continued).

Sample Number	Depth (ft)	Date Collected	Analyses Performed[a]
E05104042	26-28	8/25/04	3A, 9A, RH, RN, TV, AV
E05104043	30-32	8/26/04	3A, 9A, RH, RN, TV, AV
E05104044	34-36	8/26/04	3A, 9A, RH, RN, TV, AV
E05104045[b]	36-40	8/26/04	3A, 9A, RH, RN, TV, AV
CPP-79			
E05104048	2-4	9/7/04	3A, 9A, RH, RN, TV, AV
E05104049	6-8	9/7/04	3A, 9A, RH, RN, TV, AV
E05104050	10-12	9/8/04	3A, 9A, RH, RN, TV, AV
E05104051	14-16	9/8/04	3A, 9A, RH, RN, TV, AV
E05104052	16-18	9/8/04	3A, 9A, RH, RN, TV, AV, *, **
E05104053	20-22	9/8/04	3A, 9A, RH, RN, TV, AV
E05104054	24-26	9/8/04	3A, 9A, RH, RN, TV, AV
E05104055	30-32	9/9/04	3A, 9A, RH, RN, TV, AV
E05104056	34-36	9/9/04	3A, 9A, RH, RN, TV, AV, *, **
E05104057	36-38	9/9/04	3A, 9A, RH, RN, TV, AV
E05104058	42-44	9/9/04	3A, 9A, RH, RN, TV, AV
E05104059[b]	44-46	9/13/04	3A, 9A, RH, RN, TV, AV
E05104061	48-52	9/15/04	3A, 9A, RH, RN, TV
E05104062	52-56	9/15/04	3A, 9A, RH, RN, TV
E05104063	56-59	9/15/04	3A, 9A, RH, RN, TV, *, **
Equipment Blank			
E05104060	N/A	9/16/04	9A, RH, RN, 1X, LA, AZ

a. Sample analysis codes:
3A: Semivolatile Organic Compounds (SVOCs) (Appendix IX Target Analyte List [TAL])
Total Metals (TAL)
Toxicity Characteristic Leaching Procedure (TCLP) SVOCs
TCLP Metals
9A: Nitrate/Nitrite - Speciated
Hydrogen Ion (pH)
1G: SVOCs (Appendix IX TAL) including Matrix Spike/Matrix Spike Duplicate
Total Metals (TAL)
TCLP SVOCs
TCLP Metals
RH: Am-241, Tc-99, Np-237, Gamma Spec., Pu-Isotopic, U-Isotopic, Sr-90
RN: C-14, Tritium, I-129
1X: SVOCs (Appendix IX TAL)
TV: TCLP Volatile Organic Compounds (VOCs)
LA: Total Metals
AV: VOCs (Appendix IX TAL)
AZ: VOCs (Appendix IX TAL) - Matrix Spike/Matrix Spike Duplicate
* Pu-241
** Zirconium
*** Gamma Spec, Total Sr, Total Hg
b. Field duplicate sample also collected
c. Soil core collected in August 2004, but radiation levels precluded subsampling. Core was retrieved from archive on 3/21/2005 and placed in shielded hot cell for remote sampling. Limited analysis was performed on the sample at the on-site lab. Results on Table 5-6 in the RI/BRA report main document.
d. Analysis code 1G is the same as 3A but also includes additional volume to analyze quality assurance/quality control samples such as matrix spikes and matrix spike duplicates per ER-SOW-394 requirements.

Two 2-ft sample liners were collected from each 4-ft soil interval and gamma surveyed by the radiological control technician (RCT) using field instrumentation. The higher activity core was subsampled for the various analyses and the second core was placed in the sample archive. If insufficient volume was unavailable in the 2-ft liner, the second liner was also opened to obtain additional sample material. If insufficient volume was available in both liners, as was the case with E05104061, E05104062, and E05104063, a priority was established and specific analyses were cancelled due to insufficient volume. In one case, soil interval radiological levels exceeded contact-handling limits which initially prevented the collection of samples. This interval was placed in the sample archive and later sent to the laboratory for limited analyses.

A technical procedure (TPR-7463) was developed to provide step-by-step instructions for core sampling. Once the sample cores were pulled from the ground, they were transferred inside a sample handling tent. Dependent on core radiological readings, sample cores were placed inside a sample handling box or glovebag. Samplers opened the core and plastic liner. The sample container identified for volatile organic compound (VOC) analysis was filled first. Then the remaining sample material was placed in a bag where it could be mixed and homogenized. Afterwards, the remaining sample bottles were filled from the stirred material. However, sample E0510406201 was not mixed prior to subsampling. If any sample volume remained after the sample bottles were filled, the remaining volume was placed in a labeled bottle for the archive.

Radiological readings of the soil core collected from CPP-31 (16-18 ft) precluded core sampling in the field according to TPR-7463. The core was placed in the archive storage immediately upon collection. Project management later determined that some critical analyses needed to be performed on soil from this core. In March 2005, the soil core was placed into the shielded hot cell at the INTEC Remote Analytical Facility (CPP-684) for sampling according to facility standard operating procedures. The core and plastic liner were opened remotely, and the contents were placed in a number of smaller bottles. Each bottle was transferred outside the hot cell to obtain radiological readings. The bottle with the highest reading was then sampled to obtain a small volume for analysis. Radiological readings from the smaller volume were low enough to allow handling outside the shielded cell according to regular laboratory analytical procedures. Due to limited available volume, the sample (E0090500001) was only analyzed for gamma spectroscopy, total strontium, and total mercury.

Sampling activities were documented in the field sampling logbook (ER-143-2004). The logbook was completed and managed according to Management Control Procedure (MCP)-1194, “Logbook Practices for ER and D&D&D Projects.” The logbook contains a chronological description of the sampling activity. Sample information such as the sample location, sample matrix, analysis requested, gamma survey results, and other observations were recorded in the logbook. Physical information, weather observations, shipping information, and preparation of QC samples were also documented in the sampling logbook.

Samples were collected in precleaned, laboratory-certified containers according to Environmental Protection Agency (EPA)-recommended procedures. Samples were preserved upon sample collection in accordance with the field sampling plan requirements. Samples requiring cooling to 4°C were placed in refrigerators or coolers containing reusable ice.

Samplers adhered to chain of custody (COC) procedures to maintain and document sample possession. The COC procedure was implemented when the sample was collected. A COC form was completed documenting the date and time each sample was collected. Custody of the samples was maintained and documented on the form by the person relinquishing the samples and the person receiving the samples. The original completed COC forms are maintained as part of the project record.

H-2.2 Sample Packaging and Shipment

Samples were packaged for shipment to the contracted laboratory for analysis. Samples were shipped in accordance with the regulations issued by the Department of Transportation (DOT) (49 Code of Federal Regulations [CFR] Parts 171 through 178) and EPA sample handling, packaging, and shipping methods (40 CFR 262.30). Prior to shipment, selected samples were sent to the on-Site laboratory for gamma screening. Table H-2 contains results from the on-site sample screening. Results of the screening and process knowledge were used to scale alpha and beta isotopes in relation to the gamma activity in order to calculate the total shipment activity.

Table H-2. Gamma screening results for sample shipment.

Field Sample Name	Analyte	Result String
E0510400101R5	CS137	1.469E+02 +- 9.9E+00 pCi/g
E0510400301R5	AM241	4.11E+02 +- 6.2E+01 pCi/g
	CS137	1.441E+05 +- 8.1E+03 pCi/g
E0510401801R5	GAMMA SCAN	No Nuclides Identified
E0510402501R5	CS137	2.33E+02 +- 2.0E+01 pCi/g
	TOTAL SR	-9.86E+02 +- 1.2E+01 pCi/g
	BETA	9.60E+02 +- 1.8E+01 pCi/g
E0510402601R5	CS137	3.38E+00 +- 4.1E-01 pCi/g
	ALPHA	-2.0E+00 +- 1.4E+00 pCi/g
	BETA	7.79E+03 +- 1.3E+02 pCi/g
E0510403101R5	CO60	3.58E+02 +- 3.4E+01 pCi/g
	CS137	5.76E+06 +- 6.7E+05 pCi/g
	EU154	1.12E+04 +- 1.0E+03 pCi/g
	ALPHA	2.05E+03 +- 1.2E+02 pCi/g
	BETA	2.1231E+05 +- 9.6E+02 pCi/g
E0510403901R5	CS137	1.66E+05 +- 1.1E+04 pCi/g
E0510404001R5	CS137	6.42E+06 +- 3.6E+05 pCi/g
	EU154	4.62E+03 +- 5.5E+02 pCi/g
E0510404301R5	GAMMA SCAN	No Nuclides Identified
	TOTAL SR	805,240 +- 1888 pCi/g
E0510404901R5	CS137	4.88E+01 +- 4.2E+00 pCi/g
E0510405301R5	CS137	1.32E+00 +- 1.3E-01 pCi/g
	BETA	5.462E+05 +- 2.8E+03 pCi/g
E0510405601R5	CS137	3.61E+06 +- 2.4E+05 pCi/g
	BETA	4.4977E+06 +- 7.9E+03 pCi/g
E0510405901R5	CS137	2.81E+02 +- 3.4E+01 pCi/g
	ALPHA	1.90E+01 +- 3.6E+00 pCi/g
	BETA	5.34E+02 +- 1.3E+01 pCi/g
E0510406301R5	AM241	1.48E+03 +- 1.4E+02 pCi/g
	CS137	8.25E+05 +- 5.1E+04 pCi/g
	ALPHA	3.47E+04 +- 1.1E+03 pCi/g
	BETA	1.0594E+06 +- 4.9E+03 pCi/g

Samples were packaged in appropriate containers as determined by project packaging and transportation personnel. Ice was placed inside the containers to keep the samples preserved at the correct temperature. Tamper-resistant custody seals were placed on the shipping containers to ensure that the sample integrity was not compromised by the unauthorized opening of the container. Samples were shipped via overnight delivery to the contract laboratory for analysis, and all shipments conformed with applicable DOT requirements. In addition, transfers of accountable nuclear material to, from, and within the Idaho National Laboratory (INL) must be controlled and monitored. Where required, shipments were coordinated with the appropriate nuclear materials custodians in accordance with MCP-2752, "Shipments and Receipts of Nuclear Material."

H-3. SAMPLE ANALYSIS

The INL Sampling and Analysis Management (SAM) office was responsible to establish a laboratory contract for the analysis of samples collected during Phase 2 of the characterization effort. Based on the requirements established in the SAP (DOE-ID 2004b), the SAM office identified and selected a qualified laboratory to perform sample analysis. The SAM is responsible to evaluate the project's needs, determine the laboratory's approval status, evaluate the laboratory's acceptance criteria, and consider the laboratory's status under the established make or buy policy. Further the laboratory must be assessed and approved by SAM and QA personnel before use to evaluate its analytical procedures, calibration, and QA/QC program.

The SAM establishes long-term blanket master contracts with qualified laboratories to perform standard methods for radiological, organic, inorganic, and miscellaneous classical analyses. The Analytical Services Statement of Work (SOW) (ER-SOW-394) describes routine requirements for sample handling, custody, storage, data reporting, and delivery schedules. Upon identification of a qualified laboratory, the SAM establishes a project specific Task Order Statement (TOS) that describes any additional analysis requirements or deviations from the Analytical Services SOW.

Upon receipt and review of the SAP (DOE-ID 2004b), SAM personnel identified a subcontracted laboratory, BWXT Services, Inc., to perform the requested analyses. A project-specific TOS (ER-TOS-A2359) was prepared to identify the required analyses to be performed in accordance with ER-SOW-394. Throughout the project, several revisions to the TOS were required to request additional analyses based on the projects needs. Specific samples were selected for Pu-241 and zirconium analyses to help the project identify the source and age of contamination.

A contract was also established with the on-site Analytical Laboratories Department to sample and analyze the archived soil core from CPP-31, 16-18 feet. A task-specific TOS (ER-TOS-S2528) was prepared to identify the required analyses to be performed in accordance with ER-SOW-394. Due to high radiation levels that limited sample handling, the soil core was placed in the laboratory's shielded hot cell for sampling remotely. Limited analyses including gamma spectroscopy, total strontium, and total mercury were requested for this sample.

H-4. DATA REPORTING

When laboratory analysis is complete, the laboratory is required to generate a data report. Laboratory analysis generates raw (as-collected) data including instrument and computer printouts. These raw data are typically subject to mathematical review to reduce the data to a meaningful expression such as a compound concentration identified in specific units. ER-SOW-394 identifies data reporting, data reduction, and transformation requirements the laboratory must follow when reporting data results. The SAM office is responsible to verify and validate the laboratory's compliance with data reporting requirements.

The project SAP (DOE-ID 2004b) identified that the laboratory report the data in a standard plus raw data deliverable (ER-SOW-394). This deliverable includes both standard reporting forms to report the results, as well as raw data reports from the instrumentation, laboratory logbook copies, instrumentation and standards certifications, etc. The laboratory reports are delivered to the SAM office upon completion.

Sample results are reported in sample delivery groups (SDGs). An SDG is defined as up to 20 field samples collected at one site, under one task order, or geographical area received by the laboratory over no more than a 14-day calendar period (ER-SOW-394). Each SDG must encompass only one analysis discipline such as organic, radiological, or inorganic. For each discipline, when more than one analytical fraction is requested as identified by line-item type in the applicable TOS, a separate SDG is established for each fraction. Samples are assigned to an SDG by matrix and batched together in a manner that prevents missed hold times. The SDG number is assigned by the laboratory and is one of the sample numbers included in the SDG. Table H-3 contains a listing of the individual SDGs reported for this project.

The SAM office is responsible to perform data validation upon receipt of the laboratory SDG. Per the project SAP (DOE-ID 2004b), all data packages received by the SAM underwent Level A analytical method data validation. This validation is a thorough evaluation that consists of data confirmation, data clarification, and data appraisal. Data confirmation consists of correlating the reported data with its corresponding raw data. Data clarification is the process of qualifying or flagging the reported analytical results based on adherence to the applicable validation procedure and/or professional judgment of the data validator. Data appraisal consists of the formulation of a comprehensive limitations and validation (L&V) report documenting the validation process. Table H-3 contains references for the validation report for each SDG generated by the laboratory.

Laboratory SDGs were received by the SAM in electronic image .PDF format. The electronic image is initially placed on the SAM internal internet homepage for review by the project. These image files are eventually uploaded to the INL Electronic Data Management System for permanent storage per project requirements. Electronic results are also uploaded into the SAM Integrated Environmental Data Management System. The data are subsequently uploaded to the Environmental Data Warehouse. The SAM ensures that all security requirements for electronic data are implemented and complied with.

H-5. QUALITY ASSURANCE/QUALITY CONTROL

The *Quality Assurance Project Plan for WAGs 1, 2, 3, 4, 5, 6, 7, 10 and Deactivation, Decontamination, and Decommissioning* (DOE-ID 2004c), referred to as the QAPjP, applies QA/QC requirements for all environmental testing, analysis, and data review. The SAP further identifies specific QA/QC requirements that apply to the field sampling investigation.

The SAP (DOE-ID 2004b) establishes QA objectives for the project that specify which measurements must be obtained to produce acceptable data. The technical and statistical qualities of these measurements must be properly documented. Quantitative parameters including precision, accuracy, and completeness, as well as qualitative parameters including representativeness and comparability, were specified objectives identified for evaluation.

The QA objectives for the sampling project were met through a combination of field and laboratory checks. Field checks consisted of the collection of field duplicates and equipment blanks. Laboratory checks consist of initial and continuing calibration samples, laboratory control samples, matrix spikes (MSs), and matrix spike duplicates (MSDs).

Table H-3. Table identifying SDG numbers and validation report numbers.

Sample Location	SDG Number	Type	Validation Report
CPP-15, 27, 28 Shallow	E05104000013A-01	SVOCs	DMG-267-04
CPP-15, 27, 28 Shallow	E05104000013A-02	TCLP SVOCs	DMG-265-04
CPP-15, 27, 28 Shallow	E05104000013A-03	Total Metals (TAL)	DNT-441-04
CPP-15, 27, 28 Shallow	E05104000013A-04	TCLP Metals	DNT-432-04
CPP-15, 27, 28 Shallow	E05104000019A-01	Nitrate/Nitrite pH	DNT-429-04
CPP-15, 27, 28 Shallow	E0510400001AV-01	VOCs	DMG-266-04
CPP-15, 27, 28 Shallow	E0510400001RH-01	Radiochem (all)	SOS-TL330-04R3
CPP-15, 27, 28 Shallow	E0510400001RH-02	Supplemental gamma	BAM-009-05
CPP-15, 27, 28 Shallow	E0510400001TV-01	TCLP VOCs	SOS-TL320-04
CPP-28 (8-56'), 79 (44-60')	E05104026013A-01	TCLP SVOCs	DMG-323-04
CPP-28 (8-56'), 79 (44-60')	E05104026013A-02	SVOCs	DMG-321-04
CPP-28 (8-56'), 79 (44-60')	E05104026013A-03	TCLP Metals	DNT-455-04
CPP-28 (8-56'), 79 (44-60')	E05104026013A-04	Total Metals (TAL)	DNT-462-04
CPP-28 (8-56'), 79 (44-60')	E05104026019A-01	Nitrate/Nitrite pH	DNT-454-04
CPP-28 (8-56'), 79 (44-60')	E0510402601AV-01	VOCs	DMG-322-04
CPP-28 (8-56'), 79 (44-60')	E0510402601RH-01	Radiochem (RH)	SOS-TL380-04R1
CPP-28 (8-56'), 79 (44-60')	E0510402601RN-01	Radiochem (RN)	SOS-TL379-04
CPP-28 (8-56'), 79 (44-60')	E0510402601TV-01	TCLP VOCs	DMG-320-04
CPP-31	E05104036013A-01	Total Metals (TAL)	DNT-438-04
CPP-31	E05104036013A-02	TCLP SVOCs	DMG-293-04
CPP-31	E05104036013A-03	TCLP Metals	DNT-440-04
CPP-31	E05104036019A-01	Nitrate/Nitrite pH	DNT-439-04
CPP-31	E0510403601AV-01	VOCs	DMG-332-04
CPP-31	E0510403601RH-01	Radiochem (all)	SOS-TL340-04R1
CPP-31	E0510403601TV-01	TCLP VOCs	DMG-292-04
CPP-31	E05104037013A-01	SVOCs	DMG-291-04
CPP-31 (16-18’)	E00905000013A-01	Total Mercury	DNT-203-05
CPP-31 (16-18’)	E00905000013A-02	Gamma Spec, Total Sr	SOS-TL131-05
CPP-79 (0-44')	E05104048013A-01	SVOCs	DMG-308-04
CPP-79 (0-44')	E05104048013A-02	TCLP SVOCs	DMG-307-04
CPP-79 (0-44')	E05104048013A-03	Total Metals (TAL)	DNT-442-04
CPP-79 (0-44')	E05104048013A-04	TCLP Metals	DNT-446-04
CPP-79 (0-44')	E05104048019A-01	Nitrate/Nitrite pH	DNT-445-04
CPP-79 (0-44')	E0510404801AV-01	VOCs	DMG-305-04
CPP-79 (0-44')	E0510404801RH-01	Radiochem (all)	BAM-008-05
CPP-79 (0-44')	E0510404801TV-01	TCLP VOCs	DMG-306-04
Rev 2 Reanalysis request	E0510402601RH-02	Pu-241 (6 samples)	SOS-TL385-04
Rev 3 Reanalysis request	E05104026013A-05	Zr (6 samples)	DNT-463-04
Rev 4 Reanalysis request	E0510403001RH-01	Radiochem re-analysis (4)	BAM-004-05R1

H-5.1 Field Quality Assurance/Quality Control

Several types of QC checks were performed in parallel with field sampling activities. As defined in the SAP, QC checks included duplicate samples and an equipment rinsate blank. The frequency and type of QC sample collection were dictated by the SAP (DOE-ID 2004b).

Field duplicates are defined as two independent samples collected in such a manner that they are equally representative of the variables of interest at a given point in space and time. Field duplicates provide an estimate of the field precision as indicated by the calculated relative percent difference (RPD) between duplicate results. The frequency of collection as implemented by the SAP is 5% of the total number of samples collected or 1 field duplicate for every 20 samples. Three individual field duplicates were collected for this field sampling event.

Equipment rinsate samples are defined as a sample of the final analyte-free water rinse collected from equipment decontaminated during a sampling event. Rinsates consist of certified-clean water poured through the sampling equipment, transferred into the sample bottle, and sent to the laboratory for analysis. Results from the rinsate samples are used to evaluate the sampling equipment and containers for contamination. Results provide an indicator of the field accuracy. Because sampling equipment was not reused for this project, the equipment rinsate sample was collected once all samples had been collected and consisted of rinsing with deionized water several assembled unused core barrels with the core catchers and tubes inserted. The water from the rinse was collected and composited and sent to the laboratory for analysis. One composite rinsate sample was collected for the project.

H-5.1.1 Field Precision

Field precision is a measure of the variability not caused by laboratory or analytical methods. The three types of field variability (heterogeneity) are spatially within a data population, between individual samples, and within an individual sample. The variability between and within samples can be evaluated using duplicate samples or sample splits. Field precision will be calculated as the relative percent difference (RPD) between two measurements. For radiological results, field precision is evaluated using the mean difference calculation. The mean difference is a standard statistical method of assessing the difference between two radioactivity measurements and determining the significance of that difference.

The RPD is calculated for every contaminant for which field duplicates exist. If both sample concentrations were not detected (below the minimum detection limit), then the RPD was not calculated. If one sample concentration is less than the detection limit, then one half of the minimum detection limit (MDL) was used in the RPD calculation.

The mean difference is calculated for every radiological contaminant for which field duplicates exist. If both concentrations were not detected, then the mean difference was not calculated. If one sample concentration was not detected, then one half of the contract required detection limit (CRDL) was used in the mean difference calculation.

As indicated earlier, three field duplicates were collected for this sampling event. The RPD between results was calculated as specified in the QAPjP (DOE-ID 2004c). Target acceptance levels for RPD were not defined in the SAP (DOE-ID 2004b) or QAPjP for detected analytes. For the purposes of this assessment, RPDs less than 50% and mean differences less than 3 were considered acceptable.

For sample number E0510402901 and its field duplicate E0510402902, only one calculation exceeded the acceptance level. The mean difference for strontium-90 was 4.53.

For sample number E0510404501 and its field duplicate E0510404502, several calculated results exceeded the acceptance level. The RPD for mercury was 124.32 using one-half the MDL in the RPD calculation since mercury was not detected in the original sample. The mean difference for Pu-238 was 4.21 using one-half the CRDL in the calculation since Pu-238 was flagged as a nondetect in the original sample. The mean difference for Tc-99 was 17.61.

For sample number E0510405901 and its field duplicate E0510405902, several calculated results exceeded the acceptance level. The RPD for arsenic was 116.64 using one-half the MDL in the RPD calculation because arsenic was not detected in the original sample. The RPD for nitrite-N was 82.53 using one-half the MDL in the RPD calculation since nitrite-N was not detected in the original sample. The mean difference for Pu-238 was 3.98.

Precision was acceptable for all other analytes in the duplicate samples. Given the heterogeneous nature of soils and that no one set of duplicate samples consistently indicated gross precision problems, precision of soil sampling in the field was acceptable.

H-5.1.2 Field Accuracy

Accuracy of field instrumentation can be maintained by calibrating all instruments used to collect data and cross checking with other independently collected data. Sources of field inaccuracy are sampling preservation and handling, field contamination, and the sample matrix. Sampling accuracy can be assessed by evaluating the results of field blanks, equipment rinsates, and/or trip blanks.

Contamination of the samples in the field or during shipment, by sources other than the contamination under investigation, would yield inaccurate results. One equipment blank was collected during this sampling activity to evaluate field accuracy. An equipment rinsate sample is obtained by rinsing sample collection equipment with analyte-free water, following decontamination, to evaluate field decontamination procedures.

Soil coring tools for this sampling activity were not reused between sample locations, and decontamination of the core tools was not required. However, the SAP required that equipment associated with sampling be thoroughly decontaminated prior to initial use. At the completion of sample collection activities, several unused soil core catchers were randomly selected. Clean water was poured over the core tools and captured in a container. Captured water was composited into a single container and sampled.

The equipment blank sample was identified as sample ID E0510406001, and was analyzed for radionuclides, pH, nitrate/nitrite, metals, VOCs, and SVOCs. Except for Cs-137, no other analytes were detected in the blank. For Cs-137, 167 pCi/L were detected in the sample. Given the fact that the sample was a composite from pouring water over several unused sample coring tools, one can only speculate as to the source of this contamination. Some of the sampling equipment stored on site was improperly stored on the ground (not wrapped in foil). Contamination may have originated from windblown dust on the sampling equipment, or the collection vessel used to collect the water after it was poured over the sampling equipment.

Even though Cs-137 was detected in the rinsate sample, this fact can have little bearing on the actual sample results. Soil core catchers were not reused between sample locations; therefore, cross contamination is not likely. Even if the contamination was common to all of the soil cores used to collect samples, this would only suggest that sample results might be slightly biased high.

It is possible to estimate how high the sample bias might be. The equipment blanks (E05104060) were collected from rinsing the unused Lexan sample liners. The liners were a single-use item. Total sample volume for the rinsate was 5 L of water. The equipment rinsate was shown to contain a concentration for Cs-137 of 167 pCi/L, (which meets the drinking water standard of 200 pCi/L). The total amount of Cs-137 removed from the sample tubes can be computed by multiplying the concentration by the volume: 167 pCi/L times 5 L. Therefore, the total amount of contamination found on the sample equipment is 835 pCi of Cs-137. The sample tubes are 2-5/8 in. in diameter by 2 ft long. The sample tubes hold approximately 0.075 ft^3 of soil when filled. Soil at INTEC averages approximately 135 lb/ft^3. Multiplying the volume of soil in the sample tube times the density gives a soil volume of 10.1 lb (22,227 g) in a filled sample. If all Cs-137 contamination found on the sample tube was mixed into a sample, then the contributed elevation of the Cs-137 content can be computed by dividing the total Cs-137 contamination by the volume of soil that it could contaminate: 835 pCi divided by 22,227 g indicates that each gram of soil may have picked up an additional 0.037 pCi of Cs-137. Because the risk-based level is 92 pCi/g (see Section 2 of the Feasibility Study, DOE-ID 2006), this small amount of contamination (0.037 pCi/g) is insignificant in determining whether the soil exceeds risk based levels or not.

The pH and nitrate/nitrite results were R-flagged by the independent validator during the validation process because the sample hold times were grossly exceeded. The pH hold time is 24 hours and the nitrate/nitrite hold time is 48 hours. Because radiological screening analysis had to be performed on the samples prior to off-Site shipment to comply with packaging and shipping requirements, it was impossible to get the samples to the laboratory in time to allow the laboratory to complete the analysis before the hold times expired. The screening analysis required several hours at a minimum to complete. Even though the hold times were exceeded, the results appear to be in line with the expected results for the rinsate sample.

The equipment rinsate data suggest a lessons learned scenario in that future similar sampling events should be conducted in such a way to protect sampling equipment from possible contamination due to wind-blown dust or other sources. In addition, for those analyses that have a short holding time, sampling personnel should make arrangements to perform the analysis at an on-Site laboratory to eliminate missing holding time requirements.

In general, based on the evaluation of the equipment rinsate, the accuracy of the field sampling event appears to be acceptable.

H-5.1.3 Field Completeness

Field completeness is a measure of the number of samples collected, expressed as a percentage of the number of samples planned to be collected. Field sampling completeness is affected by such factors as equipment and instrument malfunctions and insufficient sample recovery. The completeness goal for sampling activities as identified by the QAPjP (DOE-ID 2004c) is 90% for noncritical samples, and 100% for critical samples. Critical samples are those samples required to achieve project objectives or limits on decisions and errors.

Critical sample locations were identified in the SAP (DOE-ID 2004b). Every critical sampling interval was collected to the extent technically and administratively feasible. Where coreholes could not be installed due to infrastructure constraints, alternate locations were identified nearby where samples could be collected to address the data gaps. If a sampling interval could not be collected due to gamma radiation readings exceeding allowable levels, the decision was documented by the field team leader in the logbook.

For the CPP-15 sampling site, the sample rig was unable to advance the casing beyond 20 ft below the surface due to technical constraints. All samples were collected up to the 20-ft level for a completeness percentage of 100%.

For the CPP-27 sampling site, the sample rig was unable to advance the casing beyond 20 ft below the surface. All samples were collected up to 20 ft. However, the 14- to 16-ft interval did not contain enough volume after the sample collection for archiving. A nearby probe hole was installed a few days later, and the sample rig was able to advance the casing to 40 ft below the surface before refusal. Samples were collected from 20 to 36 ft. From 36 to 40 ft, no sample material was available for collection. Samples not collected beyond 36 ft were not included in the completeness calculation because technical constraints prevented the project from collecting samples beyond this point. Therefore, the completeness objective of 100% was accomplished for this site. Archive samples were considered noncritical samples, and the completeness objective of 90% for noncritical samples was also accomplished for this location.

All samples identified for collection and analysis at the CPP-28 site were collected to meet the completeness goal of 100%. For the 22 to 24-ft interval, insufficient sample remained after sample collection for archiving purposes. Because archive samples are considered noncritical samples, the completeness object of 90% for noncritical samples was accomplished for this site.

For the CPP-31 sampling site, the sample casing was pushed to 40 ft below the surface and samples were collected from each interval for 100% completeness. For the 36 to 40-ft interval, there was insufficient sample to collect a portion for archive. Because archive samples were considered noncritical, the 90% completeness objective was also accomplished for this site.

For sampling from the CPP-79 site, the sample casing was advanced to 46 ft below the ground surface and samples were collected from each interval. A second probe hole was installed nearby and advanced to 59 ft below the ground surface. Samples were collected from this second hole between 48 and 59 ft. There was insufficient volume in the 36 to 38-ft, 44 to 46-ft, 48 to 52-ft, 52 to 56-ft, and 56 to 59-ft intervals to collect archive samples. In addition, there was insufficient volume in the last three intervals (48 to 59 ft) for collection of the volatiles sample aliquots. Therefore, for the CPP-79 site, only 13 of 16 samples were able to be analyzed for Appendix IX volatile organic compounds for a completeness goal of 81% for this particular analysis.

Overall, 57 intervals were sampled, and only 3 intervals contained insufficient volume to perform all of the requested analyses. Given the number of analyses performed on each sample and the fact that all analyses were completed except for the volatile analysis of 3 samples, the completeness percentage for critical samples was 99% overall and 95% for volatile analysis.

Nine of the 57 intervals sampled, did not contain sufficient volume for an archive sample. Archive samples are considered noncritical samples. Therefore, the completeness percentage for archive samples overall was 84%.

While the completeness objectives established by the QAPjP (DOE-ID 2004c) were not met due to technical and administrative feasibility constraints, there were no impacts to the usability of the data.

H-5.1.4 Representativeness

Representativeness expresses the degree to which sample data accurately and precisely represent a characteristic of an environmental site. In essence, representativeness is a qualitative parameter that addresses whether the sampling program was properly designed to meet the project data needs. The

sampling locations, frequencies, analytical methods, and procedures used for this sampling event were chosen based on filling the existing data gaps. The QA objectives for representativeness were achieved.

H-5.1.5 Comparability

Comparability is a qualitative measure of the confidence with which one data set can be compared to another. For field aspects of the sampling program, data comparability is established using standard methods of sample collection and handling. The QA objectives for comparability were achieved for this field project.

H-5.2 Laboratory Quality Assurance/Quality Control

The internal laboratory QC checks, including the type and frequency of QC samples and calculation of data quality indicators, are described in ER-SOW-394, which is prepared by the SAM program. The laboratory master task subcontract contains specific acceptance limit criteria for the QC check measurements required by the methods and required corrective action when these limits are exceeded. Quality control measurements may include method blanks, matrix and surrogate spikes, and calibration checks.

Laboratory QA/QC evaluation focused on determining whether the laboratory QA objectives were achieved for the data set. As shown in Table H-3, thirty-nine SDGs were delivered from the laboratory to report the data generated from analyses performed on the samples. The first phase of the QA/QC evaluation was to review the individual laboratory QC elements (i.e., calibration, spike recovery, serial dilution) and the effects these may have had on the sample results. To accomplish this, each SDG underwent Level A validation as defined in Guide Document (GDE) -7003 “Levels of Analytical Method Data Validation.”

The Level A validation process consisted of data confirmation, data clarification, and data appraisal. Validation of each SDG included a check of completeness including chain-of-custody, requested versus reported analyses, analysis holding times, method blank analyses, MS/MSD analyses, duplicate analyses, internal standards areas, and review of the raw data. Where QA/QC parameters exceeded limits established by the SAM, validation flags were assigned to the data to indicate the usefulness of the data. Limitations and validation reports were issued for each SDG documenting the validation process and flags assigned to the data. Appendix G contains complete analytical results for the tank farm soil sampling event along with validation flags assigned to the data during the validation process. Specific explanation for the assignment of validation flags is contained in the referenced L&V reports.

H-5.2.1 Laboratory Precision

Precision is a measurement of the reproducibility of a measurement under a given set of conditions. Laboratory precision is calculated as defined in the QAPjP (DOE-ID 2004c). The goal is to meet the objectives of the QC limits specified in the analytical method, thus indicating that precision in the analysis has been achieved. In most analytical methods, precision is stated in terms of the RPD. Laboratory duplicates and MSD samples were predominantly used as the means to assess precision. For metals results, serial dilution percent differences were also used. The method for comparing radioactive duplicate samples involved the calculated mean difference between the sample and its duplicate. The applicable precision measurements and explanation of the validation flags can be found in the referenced validation reports.

H-5.2.2 Laboratory Accuracy

Accuracy is a measure of the closeness of an individual measurement to the true value. The laboratory objective for accuracy is to equal or exceed the accuracy demonstrated for those analytical methods on similar sample matrices. Laboratory accuracy for organic analysis is assessed by evaluating the MS percent recovery. Accuracy for inorganic analysis is assessed through the use of laboratory control samples and MSs. Blank samples are also used as a means to verify accuracy. Laboratory accuracy for radiological analysis is assessed through laboratory control samples, radiometric tracers, and chemical carriers. The referenced validation reports contain a detailed explanation of the validator's evaluation of laboratory accuracy.

H-5.2.3 Laboratory Completeness

Laboratory completeness is measured by comparing the number of acceptable analytical results obtained against the number of analytical results that were deemed unusable based on the validation process. Analytical completeness is affected if a sample is not analyzed before its holding time expires; if a sample is damaged during handling, shipping, unpacking, or storage; or if the laboratory data cannot be validated and the sample cannot be reanalyzed. Completeness is primarily affected by the laboratories failure to meet the QC limits as specified in the analytical methods. The individual validation reports contain explanations of the validated data and its usefulness.

H-5.2.4 Laboratory Representativeness and Comparability

Representativeness is a qualitative parameter that addresses the proper design of the analysis program. Comparability is the confidence with which one data set can be compared to another and is promoted by the use of standard analytical methods and validation guidelines. Representativeness and comparability objectives for this project have been achieved.

H-6. DATA ISSUES

Upon receipt of the validated data packages, project personnel conducted extensive review of the data to ensure the data was correct and there were no further issues. As a result of this project review, several issues were identified and resolved. This section identifies the various data issues for discussion.

H-6.1 Radioanalytical Data

Numerous data issues of note were identified in the radioanalytical data packages. Individual validation reports should be referenced to determine the specific explanation for the assignment of various data flags.

Several tritium hits were detected for samples in SDG E0510404801RH. This particular SDG contained analysis of samples taken from the CPP-79 site. The identification of tritium in these samples was unusual because these were the only samples from the whole sampling project where tritium was identified. The analytical laboratory was contacted to re-examine the tritium data. The lab spectroscopist reviewed the samples' liquid scintillation counter spectrum and determined that there was no characteristic tritium peaks in the regions of interest. Therefore, the tritium results in question were flagged "UJ" to indicate the results are a false positive.

In reviewing samples E0510403001RH and E0510403101RH, it was noted that uranium isotopic data did not appear to match the other results for the two locations. The results indicated more uranium contamination present in the former sample, and less in the latter. Other radioanalytical results were

opposite indicating the contamination resided in the latter sample. Project personnel suspected the samples might have been inadvertently switched at the laboratory. A review of the applicable paperwork at the lab did not reveal any problems. Therefore, re-analysis was requested using remaining sample material for the two samples. Re-analysis results verified project suspicions. It appeared that the two samples had been switched. The project rejected and flagged the original results. Results of the re-analysis are recorded in Appendix G and in the applicable validation report (BAM-004-05R1). For data use, only the re-analysis results should be used.

In reviewing samples E0510405601RH and E0510406301RH, it was noted that the Np-237, Pu-238, and Pu-239/240 results were not within the ranges expected by the project. A review of the paperwork associated with these analyses did not reveal any analysis anomalies or discrepancies. Therefore, the project requested re-analysis using remaining sample material from these two samples. The Np-237 result for E0510405601RH was 468 pCi/g from the original analysis and 48.5 pCi/g from the re-analysis. The latter result appeared to be more in line with project knowledge of the sampling site. However, re-analysis for Pu-238 and Pu-239/240 on both samples, and Np-237 on the second sample did not produce conclusive differences from the original analysis. Considering the inhomogenous nature of a soil matrix, both results may be valid. Therefore, both results are reported in Appendix G, 2004 Laboratory Data Tables.

Several samples collected from various sites contained elevated radionuclide contamination. Due to laboratory radiological handling restrictions, smaller sub-samples had to be taken for some analyses. This action impacts the calculation of the minimum detectable activity (MDA) causing the MDA to be relatively high. While this is not a problem if there are large amounts of the radionuclide present in the sample above the MDA, elevated MDAs can impact the data usability where the radionuclides cannot be detected above the MDA. If the analyte is not detected in the sample above the MDA, the data user may use the MDA level itself as a conservative estimate of how much is present in the sample. If the MDA is inflated due to the small size of the sample aliquot analyzed, the data user may experience a high bias in his or her calculations. Every effort was made by the laboratory to achieve the lowest possible MDA for each analysis. Separations techniques were also used by the laboratory to eliminate potential interferences.

Only one result in the radiochemical set of analyses was “R” flagged during the validation process. For sample E0510402601RH, the Am-241 result was rejected by the validator because the analytical yield was 169%. This was well outside the acceptance range of 30-110% specified in the validation procedure, GDE-205. Analytical yield is a measure of the efficiency of the radiochemical separation process. It is determined by adding a known amount of radioactive tracer to the sample prior to sample preparation and analysis and measuring the analytical yield at the completion of the analytical measurement process. It is used to measure and correct for losses that may have occurred during sample processing, separation, and quantification of the analyte. Abnormally high yields might be indicative of inappropriate separation methods for certain matrix interferences, instrument problems, calibration errors, or errors in the preparation of the tracer or carrier. While the exact reason for this abnormally high yield is not known, review of the data indicates that this was an isolated analytical anomaly. The analytical yields for the other samples were well within the acceptance range.

Upon delivery of the first radioanalytical data package E0510400001RH, it was noted that the laboratory only reported the Cs-137 and Eu-154 results from the gamma scan analysis. Even though the gamma scan analysis checks for numerous gamma-emitting radioisotopes, the lab only reported these 2 analytes because the project had specifically requested it. Project personnel determined that a full list of radioisotopes should be reported for this SDG, and for all other radioanalytical SDGs for this project. In response to this request, the laboratory issued a supplemental gamma scan package for E0510400001RH. The supplemental gamma scan package contained all of the gamma scan results including the Cs-137 and

Eu-154 results. Therefore, these 2 analytes were listed in both the original SDG and the supplemental SDG. In the preparation of this report, it was noted that the uncertainties for the Cs-137 and Eu-154 gamma scan results did not match in both data packages. The lab was contacted, and it was determined that the uncertainty calculations for the supplemental gamma package were incorrect. A revision to the report was issued (BAM-009-05). It was further noted that even after the revision was issued, the Cs-137 result for E0510401201RH did not match. The reported value in the supplemental data package was much lower than the value in the original SDG. The supplemental SDG case narrative stated "that in some cases the reporting software for gamma spec calculated the sample activity as greater than the MDA even though no photopeak was identified. To eliminate the potential misinterpretation of a false positive result, the sample activity was replaced with a value of -1.00E-03" (BAM-009-05). Since the supplemental data package superseded the original data package for gamma scan results, the Cs-137 result from the supplemental data package should be used. This result is included in the Appendix G, 2004 Laboratory Data Tables.

After the samples were collected and analyzed, the project determined that some samples needed to be analyzed for Pu-241. The purpose of this analysis was to aid the project in determining the source of the contamination and approximate time the contamination occurred. Six samples were identified by the project for Pu-241 analysis. Separate SDG and validation reports were issued for this analysis (SOS-TL385-04).

Sample E00905000013A was collected remotely from the archived 16-18 ft soil core in March 2005. The sample analysis was performed at the on-Site analytical facility. The on-Site analytical lab does not have an approved method for strontium-90. Per the agreed contract, the laboratory performed total strontium analysis of the sample. While total strontium analysis results would include both strontium-89 and strontium-90, the half-life of strontium-89 is 50.5 days. Given the age of the sample material, total strontium and strontium-90 would be considered equivalent for this sample.

H-6.2 Inorganic Data

As previously noted under the field accuracy discussion, pH, nitrite and nitrate results for the equipment blank sample E05104060019A, were qualified with an "R" during data validation suggesting the data should be rejected. The holding time for pH analysis as prescribed by EPA Method 150.1 is 24 hours from the time of sample collection. The analytical laboratory received the sample outside the hold time. Nitrate and nitrite was not extracted and analyzed until five days after collection. Even though the laboratory received the samples just 24 hours after sample collection, the nitrate and nitrite analysis was performed outside of the 48-hour holding time prescribed by EPA SW-846 Method 9056. The laboratory did not provide any explanation as to why the hold times were exceeded for nitrate and nitrite. However, impact to the project and the soil sample results is negligible. In the future, projects could consider having analyses with short holding times performed on-Site to ensure holding times are met.

After the samples were collected and analyzed, the project determined that some samples needed to be analyzed for zirconium. The purpose of this analysis was to aid the project in determining the source of the contamination and approximate time the contamination occurred. Six samples were identified by the project for zirconium analysis. Separate SDG and validation reports were issued for this analysis (DNT-463-04). It was noted in the L&V report that the laboratory analyzed the laboratory control sample from an aqueous matrix. Normally the laboratory control sample is supposed to resemble the matrix of the associated samples. The lab provided no explanation as to why this choice was made. However, the resulting impact to the data was negligible since the percent recovery for the MSD was above the established control limits. For the purposes of the project, the data results were sufficient to answer the question of the source of contamination.

To further aid the project in determining the source of contamination and time the contamination occurred, it was decided that the same six samples should be analyzed for fluoride. When the laboratory determines nitrate and nitrite, the same method yields fluoride results. Therefore, it was not necessary to perform the analysis again to obtain fluoride determinations. However, because fluoride was not requested originally, the QA/QC requirements did not apply to the fluoride determination. For compliant fluoride data, the lab would have to redo the analysis. Because the project determined that the need for fluoride analysis was not required to make environmental decisions, but rather as a tool to aid them in determining the source and age of the contamination in the soil, it was decided that the data from the original analysis (without QA/QC) was sufficient. Because of this, the fluoride data were not reported in Appendix G, 2004 Laboratory Data Tables. Table H-4 contains the fluoride results.

No other general data issues regarding inorganic data are discussed herein. Individual validation reports should be referenced to determine the specific explanation for the assignment of various data flags.

Table H-4. Table identifying fluoride results for select samples.

Sample Location	Sample Number	Compound	Result (mg/kg)
CPP-28, 8-12 ft	E05104026019A	Fluoride	< 1 mg/kg (wet)
CPP-28, 28-32 ft	E05104031019A	Fluoride	5.2 mg/kg (wet)
CPP-28, 52-56 ft	E05104065019A	Fluoride	< 1 mg/kg (wet)
CPP-79, 16-20 ft	E05104052019A	Fluoride	1.5 mg/kg (wet)
CPP-79, 32-36 ft	E05104056019A	Fluoride	1.7 mg/kg (wet)
CPP-79, 56-60 ft	E05104063019A	Fluoride	4.85 mg/kg (wet)

H-6.3 Organic Data

In general, there were no major data issues for organic data. Individual validation reports should be referenced to determine the specific explanation for the assignment of various data flags.

Samples E0510402601AV, E0510402701AV, and E0510402801AV were analyzed one day outside of the 14-day hold time from the collection of the sample. This was because there was a delay in the project providing the required DOE Form 741 information to the laboratory. The form information is required prior to the samples being made available to the laboratory for analysis. Due to the missed hold time, nondetects were qualified as undetected estimated quantities (UJ). Positive results were qualified as estimated (J).

The laboratory also noted in several of its organic data packages that the samples submitted as part of this project caused significant instrument problems. The response factor for vinyl chloride was high. Internal standard areas were low on many of the samples. MS/MSD recoveries were high for several samples. Continuing calibration percent recovery failures were noted. The lab took several troubleshooting measures, but recoveries seemed to deteriorate after several samples were run. Due to holding time constraints and scheduling difficulties, it was determined to run the samples anyway. However, this resulted in numerous qualifier flags being assigned to the data. Reference the applicable validation reports for specific information.

H-7. REFERENCES

40 CFR 262.30, 2005, "Packaging," Code of Federal Regulations, Office of the Federal Register, March 2005.

49 CFR 171, 2005, "General Information, Regulations, and Definitions," Code of Federal Regulations, Office of the Federal Register, January 2005.

49 CFR 172, 2005, "Hazardous Materials Table, Special Provisions, Hazardous Materials Communications, Emergency Response Information, and Training Requirements," Code of Federal Regulations, Office of the Federal Register, January 2005.

49 CFR 173, 2005, "Shippers-General Requirements for Shipments and Packagings," Code of Federal Regulations, Office of the Federal Register, January 2005.

49 CFR 174, 2005, "Carriage by Rail," Code of Federal Regulations, Office of the Federal Register, January 2005.

49 CFR 175, 2005, "Carriage by Aircraft," Code of Federal Regulations, Office of the Federal Register, January 2005.

49 CFR 176, 2005, "Carriage by Vessel," Code of Federal Regulations, Office of the Federal Register, January 2005.

49 CFR 177, 2005, "Carriage by Public Highway," Code of Federal Regulations, Office of the Federal Register, January 2005.

49 CFR 178, 2005, "Specifications for Packagings," Code of Federal Regulations, Office of the Federal Register, January 2005.

DOE-ID, 2004a, *Operable Unit 3-14 Tank Farm Soil and Groundwater Remedial Investigation/Feasibility Study Work Plan*, DOE/ID-10676, Rev. 1, U.S. Department of Energy Idaho Operations Office, June 2004.

DOE-ID, 2004b, *Tank Farm Soil and Groundwater Field Sampling Plan for the Operable Unit 3-14 Remedial Investigation/Feasibility Study*, DOE/ID-10764, Rev. 1, U.S. Department of Energy Idaho Operations Office, June 2004.

DOE-ID, 2004c, *Quality Assurance Project Plan for Waste Area Groups 1, 2, 3, 4, 5, 6, 7, 10, and Deactivation, Decontamination, and Decommissioning*, DOE/ID-10587, Rev. 8, U.S. Department of Energy Idaho Operations Office, March 2004.

DOE-ID, 2006, *Operable Unit 3-14 Tank Farm Soil and Groundwater Feasibility Study*, DOE/ID-11247, Rev. 0, U.S. Department of Energy Idaho Operations Office, May 2006.

ER-143-2004, 2004, " Sample Logbook – Project: ESP-051-04 - OU 3-14 Tank Farm Soil Characterization —August 9, 2004–September 30, 2004 (08/09/04–09/30/04)," Idaho National Engineering and Environmental Laboratory, October 2004.

ER-SOW-394, 2005, "Sample and Analysis Management Statement of Work for Analytical Services," Rev. 3, Idaho National Laboratory, March 2005.

ER-TOS-A2359, "Abbreviated Task Order Statement of Work (A-TOS) – ESP-051-04, Operable Unit 3-14 Tank Farm Soil Characterization," Rev. 0, Idaho National Engineering and Environmental Laboratory, July 29, 2004.

ER-TOS-S2528, "Analyses of Samples Collected in Support of the ESP-009-05, OU 3-14 Tank Farm Soils Archive Sampling of CPP-31," Rev. 0, Idaho National Laboratory, February 7, 2005.

GDE-205, 2004, "Radioanalytical Data Validation," Rev. 1, Idaho National Engineering and Environmental Laboratory, May 11, 2004.

GDE-7003, 2005, "Levels of Analytical Method Data Validation," Rev. 3, Idaho National Engineering and Environmental Laboratory, March 24, 2005.

D. M. Grigg letter to D. R. Kirchner, Transmittal of the Semivolatiles Limitations and Validation (L&V) Report for ESP-051-04, OU 3-14 Tank Farm Soil Characterization, SDG # E05104048013A, November 11, 2004, DMG-307-04.

D. M. Grigg letter to D. R. Kirchner, Transmittal of the Semivolatiles Limitations and Validation (L&V) Report for ESP-051-04, OU 3-14 Tank Farm Soil Characterization, SDG # E05104048013A, November 15, 2004, DMG-308-04.

D. M. Grigg letter to D. R. Kirchner, Transmittal of the Semivolatiles Limitations and Validation (L&V) Report for ESP-051-04, OU 3-14 Tank Farm Soil Characterization, SDG # E05104026013A, November 29, 2004, DMG-321-04.

D. M. Grigg letter to D. R. Kirchner, Transmittal of the Semivolatiles Limitations and Validation (L&V) Report for ESP-051-04, OU 3-14 Tank Farm Soil Characterization, SDG # E05104026013A, November 30, 2004, DMG-323-04

D. M. Grigg letter to D. R. Kirchner, Transmittal of the Semivolatiles Limitations and Validation (L&V) Report for ESP-051-04, OU 3-14 Tank Farm Soil Characterization, SDG # E05104000013A, October 20, 2004, DMG-265-04.

D. M. Grigg letter to D. R. Kirchner, Transmittal of the Semivolatiles Limitations and Validation (L&V) Report for ESP-051-04, OU 3-14 Tank Farm Soil Characterization, SDG # E05104000013A, October 20, 2004, DMG-267-04.

D. M. Grigg letter to D. R. Kirchner, Transmittal of the Semivolatiles Limitations and Validation (L&V) Report for ESP-051-04, OU 3-14 Tank Farm Soil Characterization, SDG # E05104036013A, November 2, 2004, DMG-293-04.

D. M. Grigg letter to D. R. Kirchner, Transmittal of the Semivolatiles Limitations and Validation (L&V) Report for ESP-051-04, OU 3-14 Tank Farm Soil Characterization, SDG # E05104037013A, November 2, 2004, DMG-291-04.

D. M. Grigg letter to D. R. Kirchner, Transmittal of the Volatiles Limitations and Validation (L&V) Report for ESP-051-04, OU 3-14 Tank Farm Soil Characterization, SDG # E0510404801AV, November 11, 2004, DMG-305-04.

D. M. Grigg letter to D. R. Kirchner, Transmittal of the Volatiles Limitations and Validation (L&V) Report for ESP-051-04, OU 3-14 Tank Farm Soil Characterization, SDG # E0510404801TV, November 11, 2004, DMG-306-04.

D. M. Grigg letter to D. R. Kirchner, Transmittal of the Volatiles Limitations and Validation (L&V) Report for ESP-051-04, OU 3-14 Tank Farm Soil Characterization, SDG # E0510402601TV, November 23, 2004, DMG-320-04.

D. M. Grigg letter to D. R. Kirchner, Transmittal of the Volatiles Limitations and Validation (L&V) Report for ESP-051-04, OU 3-14 Tank Farm Soil Characterization, SDG # E0510402601AV, November 29, 2004, DMG-322-04.

D. M. Grigg letter to D. R. Kirchner, Transmittal of the Volatiles Limitations and Validation (L&V) Report for ESP-051-04, OU 3-14 Tank Farm Soil Characterization, SDG # E0510400001AV, October 20, 2004, DMG-266-04.

D. M. Grigg to D. R. Kirchner, Transmittal of the Volatiles Limitations and Validation (L&V) Report for ESP-051-04, OU 3-14 Tank Farm Soil Characterization, SDG # E0510403601TV, November 2, 2004, DMG-292-04.

D. M. Grigg to D. R. Kirchner, Transmittal of the Volatiles Limitations and Validation (L&V) Report for ESP-051-04, OU 3-14 Tank Farm Soil Characterization, SDG # E0510403601AV, December 8, 2004, DMG-332-04.

B. A. McIlwain letter to D. R. Kirchner, Transmittal of Revised L&V Report for ESP-051-04, OU 3-14 Tank Farm Soil Characterization, SDG # E0510400001RH, February 11, 2005, BAM-009-05.

B. A. McIlwain letter to D. R. Kirchner, Revised Table in Transmittal of L&V Report in Support of ESP-051-04, OU 3-14 Tank Farm Soil Characterization, SDG # E0510403001RH, BAM-004-05R1.

B. A. McIlwain letter to D. R. Kirchner, Transmittal of Revised L&V Report for ESP-051-04, OU 3-14 Tank Farm Soil Characterization, SDG # E0510404801RH, February 9, 2005, BAM-008-05.

MCP-1194, 2003, "Logbook Practices for ER and D&D&D Projects," Rev. 1, Idaho National Engineering and Environmental Laboratory, May 14, 2003.

MCP-2752, 2006, "Shipments and Receipts of Nuclear Materials," Rev. 8, Idaho National Engineering and Environmental Laboratory, March 16, 2006.

S. Shinn letter to D. R. Kirchner, Revised Radiological Limitations and Validation (L&V) Report for the ESP-051-04, OU 3-14 Tank Farm Soil Characterization, SDG # E0510402601RH, November 29, 2004, SOS-TL380-04R1.

S. Shinn letter to D. R. Kirchner, Revised Radiological Limitations and Validation (L&V) Report for ESP-051-04 OU 3-14 Tank Farm Soil Characterization, SDG # E0510403601RH, December 16, 2004, SOS-TL340-04R1.

S. Shinn letter to D. R. Kirchner, Revised Radiological Limitations and Validation (L&V) Report for ESP-051-04 OU 3-14 Tank Farm Soil Characterization, SDG # E0510400001RH, December 17, 2004, SOS-TL330-04R3.

S. Shinn letter to D. R. Kirchner, Transmittal of the Organic Limitations and Validation (L&V) Report for ESP-051-04, OU 3-14 Tank Farm Soil Characterization, SDG # E0510400001TV, October 22, 2004, SOS-TL320-04.

S. Shinn letter to D. R. Kirchner, Transmittal of the Radiological Limitations and Validation (L&V) Report for ESP-051-04, OU 3-14 Tank Farm Soil Characterization, SDG # E0510402601RH, December 2, 2004, SOS-TL385-04.

S. Shinn letter to D. R. Kirchner, Transmittal of the Radiological Limitations and Validation (L&V) Report for the ESP-051-04, OU 3-14 Tank Farm Soil Characterization, SDG # E0510402601RN, November 29, 2004, SOS-TL379-04.

S. Shinn letter to D. R. Kirchner, Transmittal of the Radiological Limitations and Validation (L&V) Report for ESP-009-05, OU 3-14 Tank Farm Archive Samp CPP-31, SDG # E00905000013A, May 24, 2005, SOS-TL131-05.

D. N. Thompson letter to D. R. Kirchner, Transmittal of the Inorganic Limitations and Validation (L&V) Report for ESP-051-04, OU 3-14 Tank Farm Soil Characterization, SDG # E05104048013A, November 3, 2004, DNT-442-04.

D. N. Thompson letter to D. R. Kirchner, Transmittal of the Inorganic Limitations and Validation (L&V) Report for ESP-051-04, OU 3-14 Tank Farm Soil Characterization, SDG # E05104048013A, November 15, 2004, DNT-446-04.

D. N. Thompson letter to D. R. Kirchner, Transmittal of the Inorganic Limitations and Validation (L&V) Report for ESP-051-04, OU 3-14 Tank Farm Soil Characterization, SDG # E05104048019A, November 15, 2004, DNT-445-04.

D. N. Thompson letter to D. R. Kirchner, Transmittal of the Inorganic Limitations and Validation (L&V) Report for ESP-051-04, OU 3-14 Tank Farm Soil Characterization, SDG # E05104026013A, December 6, 2004, DNT-463-04.

D. N. Thompson letter to D. R. Kirchner, Transmittal of the Inorganic Limitations and Validation (L&V) Report for ESP-051-04, OU 3-14 Tank Farm Soil Characterization, SDG # E05104026013A, November 30, 2004, DNT-455-04.

D. N. Thompson letter to D. R. Kirchner, Transmittal of the Inorganic Limitations and Validation (L&V) Report for ESP-051-04, OU 3-14 Tank Farm Soil Characterization, SDG # E05104026019A, November 30, 2004, DNT-454-04.

D. N. Thompson letter to D. R. Kirchner, Transmittal of the Inorganic Limitations and Validation (L&V) Report for ESP-051-04, OU 3-14 Tank Farm Soil Characterization, SDG # E05104026013A, December 3, 2004, DNT-462-04.

D. N. Thompson letter to D. R. Kirchner, Transmittal of the Inorganic Limitations and Validation (L&V) Report for ESP-051-04, OU 3-14 Tank Farm Soil Characterization, SDG # E05105000013A, October 27, 2004, DNT-432-04.

D. N. Thompson letter to D. R. Kirchner, Transmittal of the Inorganic Limitations and Validation (L&V) Report for ESP-051-04, OU 3-14 Tank Farm Soil Characterization, SDG # E05104000019A, October 27, 2004, DNT-429-04.

D. N. Thompson letter to D. R. Kirchner, Transmittal of the Inorganic Limitations and Validation (L&V) Report for ESP-051-04, OU 3-14 Tank Farm Soil Characterization, SDG # E05104000013A, November 2, 2004, DNT-441-04.

D. N. Thompson letter to D. R. Kirchner, Transmittal of the Inorganic Limitations and Validation (L&V) Report for ESP-051-04, OU 3-14 Tank Farm Soil Characterization, SDG # E05104036013A, November 2, 2004, DNT-438-04.

D. N. Thompson letter to D. R. Kirchner, Transmittal of the Inorganic Limitations and Validation (L&V) Report for ESP-051-04, OU 3-14 Tank Farm Soil Characterization, SDG # E05104036013A, November 2, 2004, DNT-440-04.

D. N. Thompson letter to D. R. Kirchner, Transmittal of the Inorganic Limitations and Validation (L&V) Report for ESP-051-04, OU 3-14 Tank Farm Soil Characterization, SDG # E05104036019A, November 2, 2004, DNT-439-04.

D. N. Thompson letter to D. R. Kirchner, Transmittal of the Inorganic Limitations and Validation (L&V) Report for ESP-009-05, OU 3-14 Tank Farm Archive Sampling for CPP-31, SDG # E00905000013A, May 2, 2005, DNT-203-05.

TPR-7463, 2004, "OU 3-14 Tank Farm Soil Characterization Core Sampling," Rev. 1, Idaho National Engineering and Environmental Laboratory, August 2, 2004.

Appendix I

Soil Sampling Data Tables For Risk Assessment

Michael L. Abbott
Robin L. VanHorn

CONTENTS

TABLES

Appendix I

Soil Sampling Data Tables For Risk Assessment

I-1. SAMPLING DATA TABLES

Table I-1. 0 to 4-ft soil sampling results for soils inside the tank farm boundary.

Location	Sample Depth (ft)	Sample Number	Date Sampled	Compound	Lab Results (pCi/g)	Concentration 2004 (pCi/g)
CPP-33-1	1	CPP-33-01-R-1-1	10/1/1990	Am-241	2.04	1.995
CPP-26-3	1.8-2.7	30700801	1/1/1992	Am-241	1.34	1.313
CPP-26-3	1.8-2.7	30700901	1/1/1992	Am-241	0.639	0.626
CPP-26-1	3.8-4.7	30700101	1/1/1992	Am-241	0.574	0.562
CPP-20/25	1-1.5	3CS01001EH	6/28/1995	Am-241	0.17	0.168
CPP-20/25	1-1.5	3CS00201EH	6/28/1995	Am-241	0.06	0.059
CPP-28-1	2-3	E0510402401RH	8/18/2004	Am-241	0.0965	0.096
CPP-31	0-4	E0510403601RH	8/24/2004	Am-241	0.622	0.622
CPP-79	2-4	E0510404801RH	9/7/2004	Am-241	0.0362	0.036
CPP-20/25	1 - 1.5	3CS00201EH	6/28/1995	Co-60	0.090	0.0268
CPP-20/25	1 - 1.5	3CS01101EH	6/28/1995	Cs-134	0.190	0.009
CPP-20/25	1 - 1.5	3CS00201EH	6/28/1995	Cs-134	0.130	0.006
CPP-26-3	1.0-1.8	30700701	1/1/1992	Cs-137	108	80.6
CPP-26-3	1.8-2.7	30700801	1/1/1992	Cs-137	259	193
CPP-26-3	1.8-2.7	30700901	1/1/1992	Cs-137	176	131
CPP-26-1	3.8-4.7	30700101	1/1/1992	Cs-137	6460	4823
CPP-32E-1	1.4-2.3	30701001	1/1/1992	Cs-137	277	207
CPP-32E-1	2.2-2.9	30701101	1/1/1992	Cs-137	151	113
CPP-32E-1	2.2-2.9	30701201	1/1/1992	Cs-137	133	99.3
CPP-27-3	2-4	30801701	9/22/1992	Cs-137	0.739	0.561

Table I-1. (continued)

Location	Sample Depth (ft)	Sample Number	Date Sampled	Compound	Lab Results (pCi/g)	Concentration 2004 (pCi/g)
CPP-27-1	2-4	30800101	9/23/1992	Cs-137	4.62	3.51
CPP-20/25	1-1.5	3CS00101EH	6/28/1995	Cs-137	3.81	3.08
CPP-20/25	1-1.5	3CS00301EH	6/28/1995	Cs-137	15.2	12.3
CPP-20/25	1-1.5	3CS00501EH	6/28/1995	Cs-137	73.4	59.4
CPP-20/25	1-1.5	3CS01001EH	6/28/1995	Cs-137	32.8	26.5
CPP-20/25	1-1.5	3CS01101EH	6/28/1995	Cs-137	29.3	23.7
CPP-20/25	1-1.5	3CS00901EH	6/28/1995	Cs-137	11.4	9.22
CPP-20/25	1-1.5	3CS00701EH	6/28/1995	Cs-137	36.4	29.4
CPP-20/25	1-1.5	3CS00801EH	6/28/1995	Cs-137	25.9	21.0
CPP-20/25	1-1.5	3CS00201EH	6/28/1995	Cs-137	114	92.2
CPP-20/25	1-1.5	3CS00401EH	6/28/1995	Cs-137	9.6	7.8
CPP-20/25	1-1.5	3CS00601EH	6/28/1995	Cs-137	22	18
CPP-31	0-4	E0510403601RH	8/24/2004	Cs-137	214	214
CPP-27	0-4	E0510401201RH	8/12/2004	Cs-137	0.0482	0.048
CPP-28	0-4	E0510402401RH	8/18/2004	Cs-137	1070	1069
CPP-79	2-4	E0510404801RH	9/7/2004	Cs-137	29.8	29.8
CPP-32E-1	2.2-2.9	30701101	1/1/1992	Eu-154	0.811	0.298
CPP-32E-1	2.2-2.9	30701201	1/1/1992	Eu-154	0.535	0.197
CPP-32E-1	1.4-2.3	30701001	1/1/1992	Eu-154	0.456	0.168
CPP-26-3	1.0-1.8	30700701	1/1/1992	Eu-154	0.163	0.060
CPP-26-3	1.8-2.7	30700801	1/1/1992	Eu-154	0.652	0.240
CPP-26-3	1.8-2.7	30700901	1/1/1992	Eu-154	0.613	0.226
CPP-26-1	3.8-4.7	30700101	1/1/1992	Eu-154	10.7	3.94
CPP-20/25	1 - 1.5	3CS00201EH	6/28/1995	Eu-154	0.48	0.233
CPP-28-1	2-3	E0510402401RH	8/18/2004	Eu-154	0.852	0.848
CPP-20/25	1-1.5	3CS00101EH	6/28/1995	Np-237	0.16	0.16
CPP-20/25	1-1.5	3CS00301EH	6/28/1995	Np-237	0.14	0.14
CPP-20/25	1-1.5	3CS01001EH	6/28/1995	Np-237	0.1	0.10

Table I-1. (continued)

Location	Sample Depth (ft)	Sample Number	Date Sampled	Compound	Lab Results (pCi/g)	Concentration 2004 (pCi/g)
CPP-20/25	1-1.5	3CS01101EH	6/28/1995	Np-237	0.11	0.11
CPP-20/25	1-1.5	3CS00901EH	6/28/1995	Np-237	0.1	0.10
CPP-20/25	1-1.5	3CS00701EH	6/28/1995	Np-237	0.11	0.11
CPP-20/25	1-1.5	3CS00801EH	6/28/1995	Np-237	0.17	0.17
CPP-33-1	1	CPP33-01-1-1	10/1/1990	Pu-238	0.46	0.41
CPP-26-3	1.8-2.7	30700801	1/1/1992	Pu-238	3.09	2.80
CPP-26-3	1.8-2.7	30700901	1/1/1992	Pu-238	0.838	0.76
CPP-26-1	3.8-4.7	30700101	1/1/1992	Pu-238	3.58	3.24
CPP-20/25	1-1.5	3CS00301EH	6/28/1995	Pu-238	0.18	0.17
CPP-20/25	1-1.5	3CS00501EH	6/28/1995	Pu-238	0.18	0.17
CPP-20/25	1-1.5	3CS01001EH	6/28/1995	Pu-238	0.14	0.13
CPP-20/25	1-1.5	3CS01101EH	6/28/1995	Pu-238	0.43	0.40
CPP-20/25	1-1.5	3CS00701EH	6/28/1995	Pu-238	0.19	0.18
CPP-20/25	1-1.5	3CS00801EH	6/28/1995	Pu-238	0.11	0.10
CPP-20/25	1-1.5	3CS00201EH	6/28/1995	Pu-238	0.35	0.33
CPP-20/25	1-1.5	3CS00401EH	6/28/1995	Pu-238	0.11	0.10
CPP-20/25	1-1.5	3CS00601EH	6/28/1995	Pu-238	0.29	0.27
CPP-28-1	2-3	E0510402401RH	8/18/2004	Pu-238	0.200	0.20
CPP-79	2-4	E0510404801RH	9/7/2004	Pu-238	0.137	0.14
CPP-33	1	CPP33-01-1-1	10/1/1990	Pu-239/240	0.340	0.340
CPP-26-3	1.8-2.7	30700801	1/1/1992	Pu-239/240	0.159	0.159
CPP-26-3	1.8-2.7	30700901	1/1/1992	Pu-239/240	0.0963	0.096
CPP-26-1	3.8-4.7	30700101	1/1/1992	Pu-239/240	0.841	0.841
CPP-20/25	1-1.5	3CS00301EH	6/28/1995	Pu-239/240	0.050	0.050
CPP-20/25	1-1.5	3CS00201EH	6/28/1995	Pu-239/240	0.090	0.090
CPP-28-1	2-3	E0510402401RH	8/18/2004	Pu-239/240	0.0304	0.030
CPP-20/25	1-1.5	3CS00201EH	6/28/1995	Sr-90	330	265
CPP-20/25	1-1.5	3CS00501EH	6/28/1995	Sr-90	95	76.3

Table I-1. (continued)

Location	Sample Depth (ft)	Sample Number	Date Sampled	Compound	Lab Results (pCi/g)	Concentration 2004 (pCi/g)
CPP-20/25	1-1.5	3CS01001EH	6/28/1995	Sr-90	62.1	49.9
CPP-20/25	1-1.5	3CS01101EH	6/28/1995	Sr-90	40.6	32.6
CPP-20/25	1-1.5	3CS00801EH	6/28/1995	Sr-90	33.2	26.7
CPP-20/25	1-1.5	3CS00601EH	6/28/1995	Sr-90	32.6	26.2
CPP-20/25	1-1.5	3CS00701EH	6/28/1995	Sr-90	16.4	13.2
CPP-20/25	1-1.5	3CS00901EH	6/28/1995	Sr-90	11.6	9.3
CPP-20/25	1-1.5	3CS00301EH	6/28/1995	Sr-90	11.3	9.1
CPP-20/25	1-1.5	3CS00401EH	6/28/1995	Sr-90	8.1	6.5
CPP-20/25	1-1.5	3CS00101EH	6/28/1995	Sr-90	6.6	5.3
CPP-28-1	2-3	E0510402401RH	8/18/2004	Sr-90	78.3	78.2
CPP-79	2-4	E0510404801RH	9/7/2004	Sr-90	19.8	19.8
CPP-20/25	1-1.5	3CS00101EH	6/28/1995	Tc-99	1.2	1.2
CPP-20/25	1-1.5	3CS00301EH	6/28/1995	Tc-99	2.2	2.2
CPP-20/25	1-1.5	3CS00501EH	6/28/1995	Tc-99	1.1	1.1
CPP-20/25	1-1.5	3CS01001EH	6/28/1995	Tc-99	1.7	1.7
CPP-20/25	1-1.5	3CS01101EH	6/28/1995	Tc-99	1	1.0
CPP-20/25	1-1.5	3CS00901EH	6/28/1995	Tc-99	1.6	1.6
CPP-20/25	1-1.5	3CS00701EH	6/28/1995	Tc-99	1.4	1.4
CPP-20/25	1-1.5	3CS00801EH	6/28/1995	Tc-99	1.6	1.6
CPP-20/25	1-1.5	3CS00201EH	6/28/1995	Tc-99	2.1	2.1
CPP-20/25	1-1.5	3CS00401EH	6/28/1995	Tc-99	1.3	1.3
CPP-20/25	1-1.5	3CS00601EH	6/28/1995	Tc-99	0.9	0.9
CPP-79	2-4	E0510404801RH	9/7/2004	Tc-99	3.41	3.41
CPP-33-1	3	CPP33-01-3-2	10/1/1990	U-234	0.15	0.15
CPP-33-1	1	CPP33-01-1-1	10/1/1990	U-234	0.09	0.09
CPP-20/25	1-1.5	3CS00101EH	6/28/1995	U-234	0.80	0.80
CPP-20/25	1-1.5	3CS00301EH	6/28/1995	U-234	0.80	0.80
CPP-20/25	1-1.5	3CS00501EH	6/28/1995	U-234	0.70	0.70

Table I-1. (continued)

Location	Sample Depth (ft)	Sample Number	Date Sampled	Compound	Lab Results (pCi/g)	Concentration 2004 (pCi/g)
CPP-20/25	1-1.5	3CS01001EH	6/28/1995	U-234	1.00	1.00
CPP-20/25	1-1.5	3CS01101EH	6/28/1995	U-234	0.80	0.80
CPP-20/25	1-1.5	3CS00901EH	6/28/1995	U-234	0.80	0.80
CPP-20/25	1-1.5	3CS00701EH	6/28/1995	U-234	0.50	0.50
CPP-20/25	1-1.5	3CS00801EH	6/28/1995	U-234	0.80	0.80
CPP-20/25	1-1.5	3CS00201EH	6/28/1995	U-234	0.70	0.70
CPP-20/25	1-1.5	3CS00401EH	6/28/1995	U-234	0.80	0.80
CPP-20/25	1-1.5	3CS00601EH	6/28/1995	U-234	0.90	0.90
CPP-26-3	1.8-2.7	30700801	1/1/1992	U-234	2.21	2.21
CPP-26-3	1.8-2.7	30700901	1/1/1992	U-234	1.42	1.42
CPP-26-1	3.8-4.7	30700101	1/1/1992	U-234	1.16	1.16
CPP-31	0-4	E0510403601RH	8/24/2004	U-234	1.32	1.32
CPP-27	2-4	E0510401201RH	8/12/2004	U-234	0.471	0.471
CPP-28-1	2-3	E0510402401RH	8/18/2004	U-234	0.514	0.514
CPP-79	2-4	E0510404801RH	9/7/2004	U-234	1.81	1.81
CPP-26-3	1.8-2.7	30700801	1/1/1992	U-235	0.104	0.104
CPP-26-3	1.8-2.7	30700901	1/1/1992	U-235	0.0497	0.0497
CPP-26-1	3.8-4.7	30700101	1/1/1992	U-235	0.0454	0.0454
CPP-27	2-4	E0510401201RH	8/12/2004	U-235	0.0215	0.0215
CPP-28-1	2-3	E0510402401RH	8/18/2004	U-235	0.0214	0.0214
CPP-79	2-4	E0510404801RH	9/7/2004	U-235	0.0577	0.0577
CPP-20/25	1-1.5	3CS00301EH	6/28/1995	U-238	0.9	0.9
CPP-20/25	1-1.5	3CS00501EH	6/28/1995	U-238	0.6	0.6
CPP-20/25	1-1.5	3CS01001EH	6/28/1995	U-238	0.9	0.9
CPP-20/25	1-1.5	3CS01101EH	6/28/1995	U-238	0.9	0.9
CPP-20/25	1-1.5	3CS00701EH	6/28/1995	U-238	0.7	0.7
CPP-20/25	1-1.5	3CS00801EH	6/28/1995	U-238	1.0	1.0
CPP-20/25	1-1.5	3CS00201EH	6/28/1995	U-238	0.8	0.8

Table I-1. (continued)

Location	Sample Depth (ft)	Sample Number	Date Sampled	Compound	Lab Results (pCi/g)	Concentration 2004 (pCi/g)
CPP-20/25	1-1.5	3CS00401EH	6/28/1995	U-238	0.7	0.7
CPP-20/25	1-1.5	3CS00601EH	6/28/1995	U-238	1.0	1.0
CPP-31	0-4	E0510403601RH	8/24/2004	U-238	1.02	1.02
CPP-27	2-4	E0510401201RH	8/12/2004	U-238	0.498	0.498
CPP-28-1	2-3	E0510402401RH	8/18/2004	U-238	0.496	0.496
CPP-79	2-4	E0510404801RH	9/7/2004	U-238	0.797	0.797

Table I-2. CPP-15 0 to 10-ft soil sampling results.

Location	Sample Depth (ft)	Sample Number	Date Sampled	Compound	Lab Results (pCi/g)	Concentration 2004 (pCi/g)
CPP-15	1.4-2.8	E0510400001RH	8/9/2004	Am-241	0.0401	0.0401
CPP-15	4.2-5.7	E0510400101RH	8/10/2004	Am-241	0.0724	0.0724
CPP-15	7.1-8.5	E0510400201RH	8/10/2004	Am-241	0.0781	0.0781
CPP-15	9.9-11.3[a]	E0510400301RH	8/10/2004	Am-241	187	187
CPP-15	4.2-5.7	E0510400101RH(1)	8/10/2004	Co-60	0.222	0.22
CPP-15	7.1-8.5	E0510400201RH(1)	8/10/2004	Co-60	0.0957	0.096
CPP-15	9.9-11.3[a]	E0510400301RH(1)	8/10/2004	Co-60	1.39	1.39
CPP-15	1.4-2.8	E0510400001RH	8/9/2004	Cs-137	58.7	59
CPP-15	4.2-5.7	E0510400101RH	8/10/2004	Cs-137	89.9	90
CPP-15	7.1-8.5	E0510400201RH	8/10/2004	Cs-137	84.7	85
CPP-15	9.9-11.3[a]	E0510400301RH	8/10/2004	Cs-137	47000	46917
CPP-15	7.1-8.5	E0510400201RH	8/10/2004	Eu-154	0.134	0.133
CPP-15	9.9-11.3[a]	E0510400301RH	8/10/2004	Eu-154	38.7	38.5
CPP-15	7.1-8.5	E0510400201RH	8/10/2004	Np-237	0.0224	0.0224
CPP-15	9.9-11.3[a]	E0510400301RH	8/10/2004	Np-237	1.63	1.63
CPP-15	1.4-2.8	E0510400001RH	8/10/2004	Pu-238	0.326	0
CPP-15	4.2-5.7	E0510400101RH	8/10/2004	Pu-238	0.107	0
CPP-15	7.1-8.5	E0510400201RH	8/10/2004	Pu-238	0.178	0
CPP-15	9.9-11.3[a]	E0510400301RH	8/10/2004	Pu-238	1080	1079
CPP-15	1.4-2.8	E0510400001RH	8/9/2004	Pu-239/240	0.0337	0.0337
CPP-15	4.2-5.7	E0510400101RH	8/10/2004	Pu-239/240	0.0156	0.0156
CPP-15	7.1-8.5	E0510400201RH	8/10/2004	Pu-239/240	0.0284	0.0284
CPP-15	9.9-11.3[a]	E0510400301RH	8/10/2004	Pu-239/240	213	213
CPP-15	1.4-2.8	E0510400001RH	8/9/2004	Sr-90	26.7	26.6
CPP-15	4.2-5.7	E0510400101RH	8/10/2004	Sr-90	11.5	11.5
CPP-15	7.1-8.5	E0510400201RH	8/10/2004	Sr-90	21.3	21.3
CPP-15	9.9-11.3[a]	E0510400301RH	8/10/2004	Sr-90	7180	7167
CPP-15	4.2-5.7	E0510400101RH	8/10/2004	Tc-99	4.34	4.34

Table I-2. (continued).

Location	Sample Depth (ft)	Sample Number	Date Sampled	Compound	Lab Results (pCi/g)	Concentration 2004 (pCi/g)
CPP-15	7.1-8.5	E0510400201RH	8/10/2004	Tc-99	11.1	11.1
CPP-15	9.9-11.3 [a]	E0510400301RH	8/10/2004	Tc-99	15	15
CPP-15	1.4-2.8	E0510400001RH	8/9/2004	U-234	0.588	0.588
CPP-15	4.2-5.7	E0510400101RH	8/10/2004	U-234	0.795	0.795
CPP-15	7.1-8.5	E0510400201RH	8/10/2004	U-234	0.787	0.787
CPP-15	9.9-11.3 [a]	E0510400301RH	8/10/2004	U-234	99.4	99.4
CPP-15	1.4-2.8	E0510400001RH	8/9/2004	U-235	0.0391	0.0391
CPP-15	4.2-5.7	E0510400101RH	8/10/2004	U-235	0.0397	0.0397
CPP-15	7.1-8.5	E0510400201RH	8/10/2004	U-235	0.0281	0.0281
CPP-15	1.4-2.8	E0510400001RH	8/9/2004	U-238	0.647	0.647
CPP-15	4.2-5.7	E0510400101RH	8/10/2004	U-238	0.754	0.754
CPP-15	7.1-8.5	E0510400201RH	8/10/2004	U-238	0.473	0.473

a. The Agencies (conference call October 5, 2005) agreed not to use the values in the 9.9- to 11.3-ft range in the risk assessment because the site was remediated to a 10-ft depth.

Table I-3. CPP-58 0 to 10-ft soil sampling results.

Location	Sample Depth (ft)	Sample Number	Date Sampled	Compound	Lab Results (pCi/g)	Concentration 2004 (pCi/g)
CPP-58E-1	8-10	30805001	9/17/1992	Am-241	0.101	0.0991
CPP-58E-1	6-8	30804901	9/17/1992	Cs-137	43.2	32.8
CPP-58E-2	6-8	30806001	9/16/1992	Cs-137	9.8	7.4
CPP-58E-1	8-10	30805001	9/17/1992	Cs-137	48.5	36.8
CPP-58E-2	8-10	30806101	9/16/1992	Cs-137	20.7	15.7
CPP-58E-2	8-10	30806101	9/16/1992	Eu-154	0.154	0.0599
CPP-58E-1	8-10	30805001	9/17/1992	Pu-238	0.295	0.2684
CPP-58E-1	8-10	30805001	9/17/1992	Pu-239/240	0.0403	0.0403
CPP-58E-1	6-8	30804901	9/17/1992	Sr-90	33.4	33.4
CPP-58E-2	6-8	30806001	9/16/1992	Sr-90	5.86	5.86
CPP-58E-1	8-10	30805001	9/17/1992	Sr-90	33	33
CPP-58E-2	8-10	30806101	9/16/1992	Sr-90	3.8	3.8
CPP-58E-1	8-10	30805001	9/17/1992	U-234	1.13	1.13
CPP-58E-1	8-10	30805001	9/17/1992	U-235	0.0679	0.0679

Table I-4. Summary statistics for CPP-15, 0 to 10-ft depth (samples taken at 1.4- to 2.8-ft, 4.2- to 5.7-ft, and 7.1- to 8.5-ft depth intervals).

			Soil Concentration (pCi/g)			
COPC[a]	Number of Detects	Number of Samples	Minimum Detected	Maximum Detected	INL Background[b]	Less than Background?
Am-241	3	3	0.04	0.08	0.011	No
Co-60	2	2	0.10	0.22	N/A	N/A
Cs-137	3	3	59	90	0.82	No
Eu-154	1	1	0.13	0.13	N/A	N/A
Np-237	1	1	0.02	0.02	N/A	N/A
Pu-238	3	3	0.11	0.33	0.0049	No
Pu-239/-240	3	3	0.02	0.03	0.10	No
Sr-90	3	3	12	27	0.49	No
Tc-99	2	2	4.3	11	N/A	N/A
U-234	3	3	0.59	0.80	1.44	No
U-235	3	3	0.03	0.04	N/A	No
U-238	3	3	0.47	0.75	1.40	Yes

a. Only radiological contaminants are included. Nonradiological contaminants (mostly nondetect) were screened from further analysis in Table I-7.
b. 95% UTL from Rood, Harris, and White (1996).
N/A = not applicable.

Table I-5. Summary of 0 10-ft data for nonradionuclides for CPP-15 (contaminants with detects are highlighted).

Contaminant	Number of Detects	Number of Samples	Min Concentration (µg/kg)	Max Concentration (µg/kg)
1,1,1,2-Tetrachloroethane	0	4	9	11
1,1,1-Trichloroethane	0	4	9	11
1,1,2,2-Tetrachloroethane	0	4	9	11
1,1,2-Trichloroethane	0	4	9	11
1,1-Dichloroethane	0	4	9	11
1,1-Dichloroethene	0	4	9	11
1,2,3-Trichloropropane	0	4	9	11
1,2,4,5-Tetrachlorobenzene	0	4	309	347
1,2,4-Trichlorobenzene	0	4	309	347
1,2-Dibromo-3-chloropropane	0	4	9	11
1,2-Dibromoethane	0	4	9	11
1,2-Dichlorobenzene	0	8	9	347
1,2-Dichloroethane	0	4	9	11
1,2-Dichloropropane	0	4	9	11

Table I-5. (continued).

Contaminant	Number of Detects	Number of Samples	Min Concentration (µg/kg)	Max Concentration (µg/kg)
1,3,5-Trinitrobenzene	0	4	309	347
1,3-Dichlorobenzene	0	8	9	347
1,3-Dinitrobenzene	0	4	309	347
1,4-Dichlorobenzene	0	8	9	347
1,4-Dioxane	0	4	90	110
1,4-Naphthoquinone	0	4	309	347
1,4-Phenylenediamine	0	4	309	347
1-Naphthylamine	0	4	309	347
2,2'-Oxybis(1-chloropropane)	0	4	309	347
2,3,4,6-Tetrachlorophenol	0	4	309	347
2,4,5-Trichlorophenol	0	4	309	347
2,4,6-Trichlorophenol	0	4	309	347
2,4-Dichlorophenol	0	4	309	347
2,4-Dimethylphenol	0	4	309	347
2,4-Dinitrophenol	0	4	309	347
2,4-Dinitrotoluene	0	4	309	347
2,6-Dichlorophenol	0	4	309	347
2,6-Dinitrotoluene	0	4	309	347
2-Acetylaminofluorene	0	4	309	347
2-Amino-4-nitrotoluene	0	4	309	347
2-Butanone	1	4	9	52.9
2-Chloronaphthalene	0	4	309	347
2-Chlorophenol	0	4	309	347
2-Hexanone	0	4	9	11
2-Methylnaphthalene	0	4	309	347
2-Methylphenol	0	4	309	347
2-Naphthylamine	0	4	309	347
2-Nitroaniline	0	4	309	347
2-Nitrophenol	0	4	309	347
2-Picoline	0	4	309	347
2-sec-Butyl-4,6-dinitrophenol	0	4	309	347
3,3'-Dichlorobenzidine	0	4	309	347
3,3'-Dimethylbenzidine	0	4	309	347
3-Methylcholanthrene	0	4	309	347
3-Methylphenol	0	4	309	347
3-Nitroaniline	0	4	309	347
4,6-Dinitro-2-methylphenol	0	4	309	347
4-Aminobiphenyl	0	4	309	347
4-Bromophenyl phenyl ether	0	4	309	347
4-Chloro-3-methylphenol	0	4	309	347
4-Chloroaniline	0	4	309	347

Table I-5. (continued).

Contaminant	Number of Detects	Number of Samples	Min Concentration (µg/kg)	Max Concentration (µg/kg)
4-Chlorophenyl phenyl ether	0	4	309	347
4-Dimethylaminoazobenzene	0	4	309	347
4-Methyl-2-pentanone	0	4	9	11
4-Methylphenol	0	4	309	347
4-Nitroaniline	0	4	309	347
4-Nitrophenol	0	4	309	347
4-Nitroquinoline-1-oxide	0	4	309	347
7,12-Dimethylbenz(a)anthracene	0	4	309	347
Acenaphthene	0	4	309	347
Acenaphthylene	0	4	309	347
Acetone	3	4	10	103
Acetonitrile	0	4	90	110
Acetophenone	0	4	309	347
Acrolein	0	4	90	110
Acrylonitrile	0	4	90	110
Allyl chloride	0	4	9	11
Aniline	0	4	309	347
Anthracene	0	4	309	347
Arsenic	4	4	5430	14300
Benzene	0	4	9	11
Benzo(a)anthracene	0	4	309	347
Benzo(a)pyrene	0	4	309	347
Benzo(b)fluoranthene	0	4	309	347
Benzo(g,h,i)perylene	0	4	309	347
Benzo(k)fluoranthene	0	4	309	347
Benzyl alcohol	0	4	309	347
Bis(2-Chloroethoxy) methane	0	4	309	347
bis(2-Chloroethyl) ether	0	4	309	347
bis(2-Ethylhexyl) phthalate	4	4	89.5	132
Bromodichloromethane	0	4	9	11
Bromoform	0	4	9	11
Bromomethane	0	4	9	11
Butylbenzylphthalate	0	4	309	347
Carbon disulfide	0	4	9	11
Carbon tetrachloride	0	4	9	11
Chlorobenzene	0	4	9	11
Chlorodibromomethane	0	4	9	11
Chloroethane	0	4	9	11
Chloroform	0	4	9	11
Chloromethane	0	4	9	11
Chloroprene	0	4	9	11

Table I-5. (continued).

Contaminant	Number of Detects	Number of Samples	Min Concentration (µg/kg)	Max Concentration (µg/kg)
Chromium	4	4	21000	28300
Chrysene	0	4	309	347
cis-1,2-Dichloroethene	0	4	9	11
cis-1,3-Dichloropropene	0	4	9	11
Dibenz(a,h)anthracene	0	4	309	347
Dibenzofuran	0	4	309	347
Dibromomethane	0	4	9	11
Dichlorodifluoromethane	0	4	9	11
Diethylphthalate	0	4	309	347
Dimethyl phthalate	0	4	309	347
Di-n-butylphthalate	0	4	309	921
Di-n-octyl phthalate	0	4	309	347
Diphenylamine	0	4	309	347
Ethyl methacrylate	0	4	9	11
Ethyl methanesulfonate	0	4	309	347
Ethylbenzene	0	4	9	11
Famphur	0	4	309	347
Fluoranthene	0	4	309	347
Fluorene	0	4	309	347
Hexachlorobenzene	0	4	309	347
Hexachlorobutadiene	0	4	309	347
Hexachlorocyclopentadiene	0	4	309	347
Hexachloroethane	0	4	309	347
Hexachlorophene	0	4	309	347
Hexachloropropene	0	4	309	347
Indeno(1,2,3-cd)pyrene	0	4	309	347
Iodomethane	0	4	9	11
Isobutyl alcohol	0	4	90	110
Isophorone	0	4	309	347
Isosafrole	0	4	309	347
Mercury	4	4	68	532
Methapyrilene	0	4	309	347
Methyl methacrylate	0	4	9	11
Methyl methanesulfonate	0	4	309	347
Methylacrylonitrile	0	4	90	110
Methylene chloride	0	4	9	11
Naphthalene	0	4	309	347
Nitrate as Nitrogen	4	4	3240	3640
Nitrite as Nitrogen	0	4	760	760
Nitrobenzene	0	4	309	347
N-Nitrosodiethylamine	0	4	309	347

Table I-5. (continued).

Contaminant	Number of Detects	Number of Samples	Min Concentration (µg/kg)	Max Concentration (µg/kg)
N-Nitrosodimethylamine	0	4	309	347
N-Nitroso-di-n-butylamine	0	4	309	347
N-Nitroso-di-n-dipropylamine	0	4	309	347
N-Nitrosodiphenylamine	0	4	309	347
N-Nitrosomethylethylamine	0	4	309	347
N-Nitrosomorpholine	0	4	309	347
N-Nitrosopiperidine	0	4	309	347
N-Nitrosopyrrolidine	0	4	309	347
O,O,O-Triethyl phosphorothioate	0	4	309	347
o-Toluidine	0	4	309	347
Pentachlorobenzene	0	4	309	347
Pentachloroethane	0	4	309	347
Pentachloronitrobenzene	0	4	309	347
Pentachlorophenol	0	4	309	347
Phenacetin	0	4	309	347
Phenanthrene	3	4	32.4	342
Phenol	1	4	52.4	347
Pronamide	0	4	309	347
Propionitrile	0	4	90	110
Pyrene	0	4	309	347
Pyridine	0	4	309	347
Safrole	0	4	309	347
Styrene	0	4	9	11
Tetrachloroethene	0	4	9	11
Thionazin	0	4	309	347
Toluene	0	4	9	11
trans-1,2-Dichloroethene	0	4	9	11
trans-1,3-Dichloropropene	0	4	9	11
trans-1,4-Dichloro-2-butene	0	4	9	11
Trichloroethene	1	4	1	11
Trichlorofluoromethane	0	4	9	11
Vinyl acetate	0	4	9	11
Vinyl chloride	0	4	9	11
Xylene	0	4	9	11

Table I-6. Summary of 0 to 10-ft data for soils inside the tank farm boundary (contaminants with detections are highlighted).

Contaminant	Number of Detects	Number of Samples	Min Concentration	Max Concentration
Radionuclides			**pCi/g**	**pCi/g**
Am-241	25	30	-0.00721	2.91
C-14	0	12	-0.282	4.93
Ce-144	0	12	-19.6	0.631
Co-60	3	17	-0.001	6.15
Cs-134	0	17	-0.0229	0.1
Cs-137	44	48	-0.00104	6,730
Eu-152	0	12	-0.0695	1.43
Eu-154	22	34	-0.119	535
Eu-155	0	12	-2.13	0.0531
I-129	0	12	-0.0653	5.03
K-40[c]	9	9	16.8	6,460
Mn-54	0	12	-0.804	0.12
Np-237	2	17	-0.0378	0.5(.011)[b]
Pu-238	24	31	0.0165	5.85
Pu-239	7	9	0.0132	0.841
Pu-239/240	11	22	0.000971	0.614
Pu-241	1	1	6.96	6.96
Pu-242	9	9	0	0
Ru-106	0	17	-1.42	1.61
Sb-125	0	12	-3.38	5.37
Ag-108m	0	12	-0.0934	0.326
Ag-110m	0	12	-0.141	0.216
Sr-90	38	40	-2.19	32,600
Tc-99	4	12	-1.35	16.1
H-3	0	12	-9.4	19.6
U-233/234	12	12	0.46	1.81
U-234	19	19	0.09	2.21
U-235	19	31	0.00739	0.532
U-238	30	31	0.09	1.25
Zn-65	0	10	-0.0687	1.95
Metals			**mg/kg**	**mg/kg**
Arsenic	6	12	8.02	13(12.4)[b]
Chromium	21	21	10.3	60.3
Fluoride	9	9	1.58	2.09
Manganese	9	9	127	238
Mercury	12	20	0.009	0.3

Table I-6. (continued).

Contaminant	Number of Detects	Number of Samples	Min Concentration	Max Concentration
Nickel	9	9	11.2	19.4
Nitrate	21	21	0.033	3.55
Nitrite	0	21	0.076	0.76
Organics			**ug/kg**	**ug/kg**
1,1,1,2-Tetrachloroethane	0	12	9.7	11.1
1,1,1-Trichloroethane	0	12	9.7	11.1
1,1,2,2-Tetrachloroethane	0	12	9.7	11.1
1,1,2-Trichloroethane	0	12	9.7	11.1
1,1-Dichloroethane	0	12	9.7	11.1
1,1-Dichloroethene	0	11	9.7	11.1
1,2,3-Trichloropropane	0	12	9.7	11.1
1,2,4,5-Tetrachlorobenzene	0	10	340	417
1,2,4-Trichlorobenzene	0	11	340	417
1,2-Dibromo-3-chloropropane	0	12	9.7	11.1
1,2-Dibromoethane	0	12	9.7	11.1
1,2-Dichlorobenzene	0	23	9.7	417
1,2-Dichloroethane	0	12	9.7	11.1
1,2-Dichloropropane	0	12	9.7	11.1
1,3,5-Trinitrobenzene	0	11	340	417
1,3-Dichlorobenzene	0	23	9.7	417
1,3-Dinitrobenzene	0	11	340	417
1,4-Dichlorobenzene	0	23	9.7	417
1,4-Naphthoquinone	0	11	340	417
1-Naphthylamine	0	11	340	417
2,2'-Oxybis(1-chloropropane)	0	11	340	417
2,3,4,6-Tetrachlorophenol	0	11	340	417
2,4,5-Trichlorophenol	0	11	340	417
2,4,6-Trichlorophenol	0	11	340	417
2,4-Dichlorophenol	0	11	340	417
2,4-Dimethylphenol	0	11	340	417
2,4-Dinitrophenol	0	11	340	417
2,4-Dinitrotoluene	0	11	340	417
2,6-Dichlorophenol	0	11	340	417
2,6-Dinitrotoluene	0	11	340	417
2-Acetylaminofluorene	0	11	340	417
2-Amino-4-nitrotoluene	0	11	340	417
2-Butanone	0	12	9.7	11.1
2-Chloronaphthalene	0	11	340	417
2-Chlorophenol	0	11	340	417

Table I-6. (continued).

Contaminant	Number of Detects	Number of Samples	Min Concentration	Max Concentration
2-Hexanone	0	12	9.7	11.1
2-Methylnaphthalene	0	11	340	417
2-Methylphenol	0	11	340	417
2-Naphthylamine	0	11	340	417
2-Nitroaniline	0	11	340	417
2-Nitrophenol	0	11	340	417
2-Picoline	0	11	340	417
2-sec-Butyl-4,6-dinitrophenol	0	11	340	417
3,3'-Dichlorobenzidine	0	11	340	417
3,3'-Dimethylbenzidine	0	11	340	417
3-Methylcholanthrene	0	11	340	417
3-Methylphenol	0	11	340	417
3-Nitroaniline	0	11	340	417
4,6-Dinitro-2-methylphenol	0	11	340	417
4-Aminobiphenyl	0	11	340	417
4-Bromophenyl phenyl ether	0	11	340	417
4-Chloro-3-methylphenol	0	11	340	417
4-Chloroaniline	0	11	340	417
4-Chlorophenyl phenyl ether	0	11	340	417
4-Dimethylaminoazobenzene	0	11	340	417
4-Methyl-2-pentanone[a]	1	12	3.3	11.1
4-Methylphenol	0	11	340	417
4-Nitroaniline	0	11	340	417
4-Nitrophenol	0	11	340	417
4-Nitroquinoline-1-oxide	0	1	370	370
7,12-Dimethylbenz(a)anthracene	0	11	340	417
Acenaphthene	0	11	340	417
Acenaphthylene	0	11	340	417
Acetone[a]	2	12	9.7	25.3
Acetophenone	0	11	340	417
Acrylonitrile	0	9	97.3	111
Allyl chloride	0	12	9.7	11.1
Aniline	0	11	340	417
Anthracene[a]	1	11	42.1	379
Aramite	0	3	357	370
Benzene	0	12	9.7	11.1
Benzo(a)anthracene	0	11	340	417
Benzo(a)pyrene[a]	1	11	67.5	379
Benzo(b)fluoranthene	0	11	340	417

Table I-6. (continued).

Contaminant	Number of Detects	Number of Samples	Min Concentration	Max Concentration
Benzo(g,h,i)perylene	0	11	340	417
Benzo(k)fluoranthene	0	11	340	417
Benzyl alcohol	0	11	340	417
Bis(2-Chloroethoxy) methane	0	11	340	417
bis(2-Chloroethyl) ether	0	11	340	417
bis(2-Ethylhexyl) phthalate[a]	2	11	55.5	4,170(5,550)[b]
Bromodichloromethane	0	12	9.7	11.1
Bromoform	0	12	9.7	11.1
Bromomethane	0	12	9.7	11.1
Butylbenzylphthalate	0	11	340	417
Carbon disulfide	0	12	9.7	11.1
Carbon tetrachloride	0	12	9.7	11.1
Chlorobenzene	0	12	9.7	11.1
Chlorodibromomethane	0	12	9.7	11.1
Chloroethane	0	12	9.7	11.1
Chloroform	0	12	9.7	11.1
Chloromethane	0	12	9.7	11.1
Chloroprene	0	12	9.7	11.1
Chrysene	0	11	340	417
cis-1,2-Dichloroethene	0	12	9.7	11.1
cis-1,3-Dichloropropene	0	12	9.7	11.1
Dibenz(a,h)anthracene	0	11	340	417
Dibenzofuran	0	11	340	417
Dibromomethane	0	12	9.7	11.1
Dichlorodifluoromethane	0	12	9.7	11.1
Diethylphthalate	0	11	340	417
Dimethyl phthalate	0	11	340	417
Di-n-butylphthalate	0	11	340	417
Di-n-octyl phthalate	0	11	340	417
Diphenylamine	0	11	340	417
Ethyl methacrylate	0	12	9.7	11.1
Ethylbenzene	0	12	9.7	11.1
Famphur	0	11	340	417
Fluoranthene	0	11	340	417
Fluorene	0	11	340	417
Hexachlorobenzene	0	11	340	417
Hexachlorobutadiene	0	11	340	417
Hexachlorocyclopentadiene	0	11	340	417
Hexachloroethane	0	11	340	417

Table I-6. (continued).

Contaminant	Number of Detects	Number of Samples	Min Concentration	Max Concentration
Hexachloropropene	0	11	340	417
Indeno(1,2,3-cd)pyrene	0	11	340	417
Iodomethane	0	12	9.7	11.1
Isophorone	0	11	340	417
Isosafrole	0	11	340	417
Methapyrilene	0	11	340	417
Methyl methacrylate	0	12	9.7	11.1
Methyl methanesulfonate	0	11	340	417
Methylacrylonitrile	0	12	97.3	111
Methylene chloride[a]	1	12	9.7	23.4
Naphthalene	0	11	340	417
Nitrobenzene	0	11	340	417
N-Nitrosodiethylamine	0	11	340	417
N-Nitrosodimethylamine	0	11	340	417
N-Nitroso-di-n-butylamine	0	11	340	417
N-Nitroso-di-n-dipropylamine	0	11	340	417
N-Nitrosodiphenylamine	0	11	340	417
N-Nitrosomethylethylamine	0	11	340	417
N-Nitrosomorpholine	0	11	340	417
N-Nitrosopiperidine	0	11	340	417
N-Nitrosopyrrolidine	0	11	340	417
O,O,O-Triethyl phosphorothioate	0	11	340	417
o-Toluidine	0	11	340	417
Pentachlorobenzene	0	11	340	417
Pentachloroethane	0	11	340	417
Pentachloronitrobenzene	0	11	340	417
Pentachlorophenol	0	11	340	417
Phenacetin	0	11	340	417
Phenanthrene	0	11	340	417
Phenol[a]	4	11	39.6	417
Pronamide	0	11	340	417
Pyrene	0	11	340	417
Pyridine	0	11	340	417
Safrole	0	11	340	417
Styrene	0	12	9.7	11.1
Tetrachloroethene	0	12	9.7	11.1
Thionazin	0	11	340	417
Toluene[a]	4	21	1	11.1
trans-1,2-Dichloroethene	0	12	9.7	11.1

Table I-6. (continued).

Contaminant	Number of Detects	Number of Samples	Min Concentration	Max Concentration
trans-1,3-Dichloropropene	0	12	9.7	11.1
trans-1,4-Dichloro-2-butene	0	12	9.7	11.1
Trichloroethene	0	12	9.7	11.1
Trichlorofluoromethane	0	12	9.7	11.1
Vinyl acetate	0	12	9.7	11.1
Vinyl chloride	0	12	9.7	11.1
Xylene	0	12	9.7	11.1

a. Organics are not considered a COPC at this site. All detections are below INL Site ecologically based screening levels (EBSLs) or not available (NA). See Section 7 of the main document for a discussion of EBSLs.

b. The highest value is a nondetect. The value in parenthesis is the maximum detection.

c. K-40 is a natural occurring radionuclide and was not assessed further.

Table I-7. Screening[a] of 2004 nonradionuclides data for human health at CPP-15 and tank farm soils.

Detected Contaminants	Max Source Concentration (mg/kg)	Background Concentration[b] (mg/kg)	Max Concentration > Background?	1E-06 or HQ>1.0 PRG[c] (mg/kg)	Max Concentration > PRG?	Remains a COPC for HHRA
CPP-15						
Arsenic	1.43E+01	5.80E+00	Yes	3.90E-01	Yes	Yes (No)[d]
Chromium	2.83E+01	3.30E+01	No	2.10E+02	No	No
Mercury	5.32E-01	5.00E-02	Yes	2.30E+00	No	No
Nitrate	3.64E+00	NA	NA	No PRG	No PRG	No PRG
Thallium[e]	4.85E+00	NA	NA	5.20E+00	No	No
Zirconium	1.40E+01	NA	NA	No PRG	No PRG	No[f]
2-Butanone	5.29E-02	NA	NA	7.30E+02	No	No
Acetone	1.03E-01	NA	NA	1.60E+03	No	No
bis(2-Ethylhexyl)phthalate	1.32E-01	NA	NA	3.50E+01	No	No
Phenanthrene	3.62E-02	NA	NA	No PRG	No PRG	No PRG
Phenol	5.24E-02	NA	NA	3.70E+03	No	No
Trichloroethene	1.00E-03	NA	NA	5.30E-02	No	No
Tank Farm Soils						
4-Methyl-2-pentanone	1.11E-02	NA	NA	7.90E+01	No	No
Acetone	2.53E-02	NA	NA	1.60E+03	No	No
Anthracene	3.79E-01	NA	NA	2.20E+03	No	No
Benzo(a)pyrene	3.79E-01	NA	NA	6.20E-02	Yes	Yes (No)[g]
bis(2-Ethylhexyl)phthalate	4.17E-01	NA	NA	3.50E+01	No	No
Methylene chloride	2.34E-02	NA	NA	9.10E+00	No	No
Phenol	4.17E-01	NA	NA	3.70E+03	No	No
Toluene	1.11E-02	NA	NA	5.20E+02	No	No
Arsenic	1.24E+01	5.80E+00	Yes	3.90E-01	Yes	Yes (No)[d]
Chromium	6.03E+01	3.30E+01	Yes	2.10E+02	No	No

Table I-7. (continued).

Detected Contaminants	Max Source Concentration (mg/kg)	Background Concentration[b] (mg/kg)	Max Concentration > Background?	1E-06 or HQ>1.0 PRG[c] (mg/kg)	Max Concentration > PRG?	Remains a COPC for HHRA
Fluoride	2.09E+00	NA	NA	No PRG	No PRG	No PRG
Manganese	2.38E+02	4.90E+02	No	1.80E+02	Yes	No
Mercury	3.00E-01	5.00E-02	Yes	2.30E+00	No	No
Nickel	1.94E+01	3.50E+01	No	1.60E+02	No	No
Nitrate	3.55E+00	NA	NA	No PRG	No PRG	No PRG

No PRG = no risk-based value available.
NA = not applicable.
a. Screening is performed based on the approach discussed in Section 5.2 of the OU 3-13 RI/FS (DOE-ID 1997) but using Region 9 PRGs.
b. Background was taken from Rood, Harris, and White (1996) for composite samples.
c. Preliminary remediation goals are the lowest of either provided for residential and industrial soils in the EPA Region 9 PRGs Table (http://www.epa.gov/region09/waste/sfund/prg/whatsnew.htm).
d. The maximum concentration of arsenic at CPP-15 and Tank Farm Soils sampling was over the background developed by Rood, Harris, and White (1996). Natural arsenic concentrations in soil at the INL Site are known to vary greatly based on soil genesis; therefore, the arsenic values presented in Rood, Harris, and White (1996) are not always applicable at many of the waste area group sites. As discussed in detail in Appendix K of the OU 10-04 Comprehensive RI/FS (DOE-ID 2001), soil type and soil characteristics found at the INL Site vary greatly, depending on location. Because of sampling issues (as discussed in Appendix K of DOE-ID 2001), Rood, Harris, and White (1996) could use only the data from the New Production Reactor (NPR) study to calculate background values for arsenic for risk assessment purposes. A limiting factor is that the NPR study only collected soil samples from one soil type—sands over basalt, which generally underestimates the concentration of arsenic found in other INL Site soil types (Appendix K1, DOE-ID 2001). INTEC is located on the alluvial plain on the Big Lost River. The topography surrounding the facility is relatively flat. The soils surrounding the facilities are comprised primarily of Typic-Camborthids-Typic Calciorthids (TCC) and Typic Torrifluvents (TTF) soils (Olson, Jeppsen, and Lee 1995). Both TCC and TTF soils are alluvium, which are deposited by the Big Lost River. The TCC soils are loams or silty loams over gravelly or sandy loams, and the surface is frequently hardened due to alkaline conditions. As identified in Table K1-1 (DOE-ID 2001), the range of arsenic concentrations from soil with this type of deposition range from 2.1–27.0. The arsenic values found at CPP-15 are within this range. As these arsenic concentrations are also below the EPA Region 9 soil screening levels of 29 mg/kg for migration to groundwater and below the 1E-04 PRG (39 mg/kg) for this site. (Most cleanup goals for human health at INL Site are based on these PRGs). Arsenic is eliminated as a concern in this evaluation.
e. Thallium value is maximum detection from pre-2004 sampling.
f. Rood, Harris, and White (1996) provided no background value for zirconium (Zr). However, the average Zr content calculated for various soils of the U.S. averages 224 ppm (Kabata-Pendias and Pendias (1985), which is well above the maximum concentration detected (32 mg/kg). Therefore, it is concluded that this concentration is representative of the normal tank farm soil background.
g. Benzo(a)pyrene at the Tank Farm Soils is a carcinogen, and the risk is expressed as a probability. Benzo[a]pyrene is not manufactured and has no industrial uses. It is ubiquitously distributed throughout the environment as a consequence of its formation during the combustion of organic matter. The sampling at the Tank Farm Soils resulted in 1 detection out of 11 soil samples analyzed (0.357 mg/kg). This maximum concentration of benzo(a)pyrene (0.357 mg/kg) exceeded the residential soil 1E-06 PRG (0.062 mg/kg) and the industrial soil 1E-06 PRG (0.21 mg/kg). As discussed in VanHorn and Stacey (2004), if less than 10 contaminants remain after screening against 1E-06 PRGs, it is possible to screen these contaminants against a less stringent level. If the maximum concentration for a given radionuclide is less than or equal to 1E-05, it can be eliminated as a concern (if less than 10 contaminants remain). This is because the INL Site typically sets cleanup goals at 1E-04 based on the scenario. The maximum concentration of benzo(a)pyrene (0.357 mg/kg) is almost 6 times less than the 1E-05 PRG (2.1 mg/kg). This maximum concentration is also below the EPA Region 9 soil screening levels for migration to groundwater. Therefore, this COPC was eliminated as a concern.

I-2. REFERENCES

DOE-ID, 1997, *Comprehensive RI/FS for the Idaho Chemical Processing Plant OU 3-13 at the INEEL-Part B, FS Report (Final)*, DOE/ID-10572, U.S. Department of Energy Idaho Operations Office, November 1997.

DOE-ID, 2001, *Comprehensive Remedial Investigation/Feasibility Study for Waste Area Groups 6 and 10 Operable Unit 10-04*, DOE/ID-10807, Rev. 0, U.S. Department of Energy Idaho Operations Office, August 2001.

Kabata-Pendias, A. and H. Pendias, 1985, "Trace Elements in Soils and Plants," Boca Raton, Florida: CRC Press Inc., 1985.

Olson, G. L., D. J. Jeppesen, and R. D. Lee, 1995, *The Status of Soil Mapping for The Idaho National Engineering Laboratory*, INEL-95/0051, Lockeed Idaho Technologies Company, January 1995.

Rood, S. M., G. A. Harris, and G. J. White, 1996, *Background Dose Equivalent Rates and Surficial Soil Metal and Radionuclide Concentrations for the Idaho National Engineering Laboratory*, INEL-94/0250, Rev. 1, Lockheed Martin Idaho Technologies Company, August 1996.

VanHorn, R. L., and S. Stacey, 2004, *Risk-Based Screening and Assessment Approach for Waste Area Group 1 Soils*, INEEL/EXT-03-00540, Rev. 0, Idaho Completion Project, Idaho National Engineering and Environmental Laboratory, May 2004.

Appendix J

Evaluation of Sr-90: Hydrogeochemical Simulation of the CPP-31 Release from the Alluvium, Inclusion of Other Sources, Sensitivity, and Implications

Annette Schafer
Larry Hull

TABLE OF CONTENTS

LIST OF FIGURES

LIST OF TABLES

EVALUATION OF Sr-90: HYDROGEOCHEMICAL SIMULATION OF THE CPP-31 RELEASE FROM THE ALLUVIUM, INCLUSION OF OTHER SOURCES, SENSITIVITY, AND IMPLICATIONS

Annette Schafer and Larry Hull

J-1 INTRODUCTION AND OVERVIEW

Sources of Sr-90 include the: tank farm sources (18,100 Ci), OU 3-13 soil sources (918 Ci), CPP-02 abandoned french drain (33.8 Ci), CPP-3 injection well failure (8.0 Ci), and percolation ponds (0.3 Ci). In addition, 16 Ci of Sr-90 were injected directly into the aquifer in well CPP-03 as service waste. The primary sources of Sr-90 in the tank farm were associated with sites CPP-31 (15,900 Ci), and CPP-79 deep (874 Ci). Current Sr-90 found in the aquifer is thought to originate primarily from the discharge of service waste in CPP-03, and from rapid transport of Sr-90 originating in CPP-79 and CPP-31.

In order to quantitatively assess the evolution of Sr-90 as it was transported through the alluvium, into and through the vadose zone, and its subsequent migration in the aquifer, a series of models were used. Of these different models, a traditional advective-dispersive multiphase transport simulation approach was adopted to represent the transport from sites CPP-79, CPP-03 (and its failure), CPP-02, the percolation ponds, and the OU 3-13 soil sources. For these sites, the model used is described in detail in Appendix A. Deviations from this model consist of the parameterization (and justification) of interbed K_ds which are discussed in Section J-6.

A more detailed geochemical approach was taken to represent the release of very high ionic strength sodium bearing waste that occurred at Site CPP-31. In 1972, 15,000 Ci of Sr-90 were released into the surficial alluvial material along with 18,600 gal of sodium-bearing waste. This highly acidic, very high ionic strength sodium bearing waste from the concentrate of the Process Equipment Waste Evaporator is responsible for the majority of contaminants currently in the alluvium and underlying vadose zone at INTEC. Three key observations have lead to the use of a comprehensive hydrogeochemical simulation approach. These are

- Previous efforts to evaluate the fate of the Sr-90 originating at Site CPP-31 have used numerical models with a constant K_d parameter to simulate reactive transport. In order to match observed high concentrations of Sr-90 in the northern upper shallow perched water, a relatively low adsorption coefficient was required (K_d=0.25 mL/g). In these models, the low K_d was applied throughout the simulation period, resulting in all of the Sr-90 leaving the alluvium relatively rapidly. Soil concentrations obtained in one well suggest that Sr-90 still exists in the alluvium at fairly high concentrations. It is difficult to explain the very low K_d and its difference to measured Sr-90 K_d data at INL.
- Justification of the low K_d was made by Cooper (Appendix D), based on a simple analysis of the CPP-31 release. He also simulated the transport of Sr-90 as it migrated through a one-dimensional column, with the model incorporating the chemistry of the released fluid, and measured soil geochemistry (personal communication). In this simulation, it was assumed that the vertical flow occurred under saturated conditions, and a representative cross-sectional area was computed to allow saturated conditions to exist. The resultant area was on the order of a half-meter in diameter. In addition to determining the area available for flow, this area also determines the volume of minerals available for reaction with the influxing fluid. The small area, and small volume resulted in all of the Sr-90 rapidly leaving the alluvium.
- Co-released cesium has been inferred to be spread over an aerially extensive region near CPP-31 based on measured gamma readings (discussed below). Transported Sr-90 would have moved initially with the cesium. This implies that the area (and volume of minerals) contacted by the influxing fluid is much larger than that assumed in the one-dimensional column study of Cooper. In addition to affecting the hydrologic transport of the release, the geochemical conditions would be different, and would likely lead to a larger effective adsorption for Sr-90.

Although use of a constant K_d could be used to simulate the initial rapid migration of Sr-90 from the alluvium, it makes it improbable that Sr-90 would be retained in the alluvial soils. In order to account for the rapid release over an area thought to represent the actual release, and in order to more accurately assess the relevant processes, a detailed geochemical analysis of the CPP-31 release was conducted, and is presented in Sections J-2 through J-5.

In this appendix, the following information is presented:

- An overview of the CPP-31 Release and of the geochemical processes involved.
- An overview of the parameters needed to implement the geochemical model
- Verification of the geochemical model by comparison to experimental data
- Application of the geochemical model in a one-dimensional column to explain the coupled transport and geochemical phenomena
- A discussion of the geochemistry of the sedimentary interbeds including estimates of partitioning coefficients
- Parameterization of the full 3-dimensional model for site-specific application to INTEC
- Simulations in 3-dimensions for Sr-90 migration through the alluvium, vadose zone, and aquifer including all sources of Sr-90 using the most plausible parameters for use in the RI/BRA.
- Simulations in 3-dimensions for Sr-90 from land surface to the aquifer using mid-range parameters for use as the basis of the complete sensitivity analysis
- A detailed evaluation of where the Sr-90 comes from that is predicted to arrive in the aquifer
- A sensitivity analysis to the geochemical parameters as perturbations of the RI/BRA model
- A sensitivity analysis to hydrologic conditions and parameters as perturbations of the RI/BRA model
- A discussion of the resultant vadose zone and aquifer calibration for the various parameterizations
- A review of the data included in this model and recommendations for additional data collection

followed by an overview of the implications with respect to long-term aquifer concentrations.

J-2 CPP-31 RELEASE: OVERVIEW OF GEOCHEMICAL PROCESSES

In 1972, 15,000 Ci of Sr-90 in 18,600 gal of sodium-bearing waste were released to surficial alluvium in the tank farm at INTEC. This highly acidic, very high ionic strength sodium bearing waste from the concentrate of the Process Equipment Waste Evaporator is responsible for the majority of contaminants currently in the alluvium and underlying vadose zone at INTEC. Released radionuclides are currently being investigated under the CERCLA process and are the primary focus of the RI/BRA/FS. Previous efforts to evaluate the fate of the Sr-90 have used numerical models with a constant K_d parameter to simulate reactive transport. The use of K_d values to simulate sorption is only strictly valid in a system that is at complete steady state from a geochemical perspective (Reardon 1981). In the case of the acidic sodium-bearing waste release at the INTEC tank farm, the chemistry of the pore water in the vadose zone underwent extreme changes in chemistry. To address the highly dynamic evolution of the fluid released from CPP-31 as it was transported through the vadose zone, a more robust approach was needed, and is presented in Sections J-2 through J-5.

A geochemical conceptual model was used to identify the important system components and processes that will alter/control the transport of strontium resulting from the CPP-31 release. The processes considered to be important are based on the high ionic strength of the acidic sodium-bearing waste. First, minerals will be dissolved by the strong acid in the sodium-bearing waste, consuming hydrogen ion from the released solution which will result in an increase of the pH of the acidic solution and decrease in pH of the native pore water. As the pH of the acidic fluid rises, the solution may become supersaturated with other minerals that will precipitate. Second, the high concentration of cations released in the sodium-bearing waste, and generated by dissolution of minerals, will compete for exchange sites on clay minerals in the sediment. The complex interaction between dissolved mineral species and competition for exchange sites ultimately dictates the evolution of the individual solution species. In order to develop a quantitative representation of this system, it is necessary to consider the alluvial sediments, chemistry of the native pore water and infiltrating solution, and the background hydrologic system including natural recharge. A general overview of the interactions between solid and aqueous phases are discussed below, with details of the geochemical model presented in the following section.

The alluvial sediment is a mixture of quartz, calcite, alumino-silicate minerals, and clays. The reaction of calcite with the initial sodium-bearing waste will release carbon dioxide gas into the pore space of the unsaturated alluvium and will release calcium into the pore water. This dissolution of calcite will occur rapidly in strong acid, allowing use of an equilibrium model for this process. Alumino-silicate minerals will dissolve more slowly, and if the pH is rapidly neutralized by the calcite, these minerals can be considered inert. However, as the pH of the sodium-bearing waste increases, the solubility of individual sodium-bearing waste components will change. Of particular interest is the aluminum, which is a major component of the sodium-bearing waste (0.5 M). The precipitation of aluminum as gibbsite, or its inclusion in secondary clay minerals may play a role in buffering the pH. Buffering the pH of the pore water will, in turn, alter the concentrations of competing species. In contrast, even though the activity of the individual radionuclides is elevated in the sodium-bearing waste, the molal quantities of the radionuclides are low. As a result, the radionuclide mobility will most likely be controlled by sorption to mineral surfaces as opposed to being controlled by the precipitation of secondary minerals.

The sorption to mineral surfaces will be controlled by competition for ion exchange sites by the various cations in solution. Initially, ion exchange sites in the alluvium are expected to be mainly filled with calcium. The sodium-bearing waste has a very high initial concentration (1.5 M) of sodium, and upon contact with this solution, the sodium will replace most of the calcium on the exchange sites. The high sodium will also compete with other cations, such as strontium (Sr-90) and cesium (Cs-134 and Cs-137), for exchange sites. Both strontium and cesium are cations characterized by low ionic potential (valence / ionic radius), and weak hydration. As a result, the primary mode of interaction of Cs and Sr with mineral surfaces is ion exchange (Appelo and Postma 1996). In ion exchange, the cation forms an outer sphere complex with a mineral surface to balance fixed charge deficit caused by ionic substitution within the mineral lattice. Clays are the predominant source of cation exchange capacity in most sediments, although manganese minerals can also provide some cation exchange capacity. Strontium exchanges with planar sites on clays. Cesium, however, can

exchange both with planar sites and with frayed edge sites on clays (Zachara, et al. 2002). The binding to the frayed edge sites is much stronger than to the planar ion exchange sites. As a result, Cs shows a very strong binding to clays at low concentrations, with weaker binding at higher concentrations. At least two ion exchange sites (and sometimes more) are commonly used to model the sorption of cesium to clay minerals (Zachara, et al. 2002; Steefel, et al. 2003). As a final point, ion exchange reactions involving Cs and Sr are relatively rapid, and can be represented using an equilibrium model as opposed to occurring over long time periods requiring a kinetic approach.

J-2.1 Geochemical Model Overview

For relatively large alkali-earth cations with low hydrated ionic charge density, such as strontium, sorption to soil surfaces will mainly occur through formation of outer-sphere complexes at fixed-charge sites on the planer surfaces of clay minerals. The formation of these outer-sphere complexes is described by cation exchange theory. A general expression for the cation exchange reaction is (Appelo and Postma 1996)

$$Z_j S_i^{+Z_i} + Z_i S_j X_{Z_j} \leftrightarrow Z_i S_j^{+Z_j} \tag{J-2-1}$$

Where S_i and S_j are cations i and j with charges z_i and z_j, and X is a the cation exchange site. For example, the exchange of strontium for sodium on cation exchange sites is given by:

$$Sr^{2+} + 2NaX \leftrightarrow 2Na^{+} + SrX_2 \tag{J-2-2}$$

Because strontium has a charge of +2, it displaces two sodium ions and occupies two ion exchange sites. The activity of the cations on the ion exchange sites follows the Gains-Thomas convention and is given by the equivalent fraction. The equilibrium equation based on the law of mass action is:

$$K_{Sr/Na} = \frac{a_{Na}^2 \left[\frac{2m_{SrX_2}}{X_T}\right]}{a_{sr}\left[\frac{m_{NaX}}{X_T}\right]^2} \tag{J-2-3}$$

Where:

$K_{Sr/Na}$	=	selectivity coefficient for Sr - Na exchange
m	=	molality of surface exchange species (mole/L)
X_T	=	cation exchange capacity (mole/L)
a	=	free ion activity of the cation

When strontium is present in low concentrations relative to sodium, it is sometimes assumed that the aqueous and sorbed concentrations of sodium do not change significantly during the sorption process allowing Equation J-2-3 to be simplified to

$$K_{Sr/Na}\frac{\left[\frac{m_{NaX}}{X_T}\right]^2 \gamma_{Sr}}{a_{Na}^2}\frac{X_T}{2}\frac{\rho}{\theta} = \frac{C_{Sr-sol}}{C_{sr-dis}} = K_d \tag{J-2-4}$$

Where:

γ	=	activity coefficient for strontium in solution
ρ	=	bulk density of solid (kg/L)
θ	=	water content (L/L)
$C_{Sr\text{-}sol}$	=	concentration sorbed to solid (mole/kg)
$C_{Sr\text{-}dis}$	=	concentration dissolved in solution (mole/L)

All the terms moved to the left side of Equation 4 indicate the wide range of parameters that are implicitly assumed constant to apply a K_d approach to reactive transport.

For the leak of sodium-bearing waste at CPP-31, the aqueous concentration of sodium changes several orders of magnitude so that both the aqueous concentration and the equivalent fraction of sodium on the ion exchange sites undergo significant changes. In conjunction, there are parallel reactions taking place, particularly with calcium being released by dissolution of calcite, and the resultant competition for the same ion exchange sites. Using the cation exchange modules in TOUGHREACT (Xu, et al. 2004), we can explicitly include competitive cation exchange reactions in the transport simulation in addition to including the precipitation/dissolution processes. In adopting this mechanistic approach to simulating the evolution of the released sodium-bearing waste, the first-order equilibrium K_d is explicitly not considered.

J-3 CATION EXCHANGE MODEL PARAMETERS

To implement competitive cation exchange in TOUGHREACT, the following information must be known or estimated.

- cation exchange capacity
- selectivity coefficients for all significant cations
- pore water and infiltration water chemistry
- composition of cations occupying the exchange sites on the sediment

This list is not independent. Given the pore water composition and the selectivity coefficients, the composition of the exchange assemblage will be fixed. We therefore only need to know two of the last three items to complete the model. The following sections review existing data to determine if representative value or values for each parameter can be determined.

J-3.1 Cation Exchange Capacity

Because of internal lattice substitutions in clay minerals, the minerals have a net negative surface charge that is independent of pH. Additional negative surface charge may develop along the edges of the clay plates as pH rises, but this is usually not a significant fraction of total surface charge for illite and smectite clays (McBride 1994), which are the predominant clays in INL alluvial sediments (Bartholomay, et al. 1989). Cations are sorbed to the clay mineral surface by electrostatic attraction based on this charge. The total negative charge present to bind cations is termed the cation exchange capacity (CEC).

J-3.1.1 Analytical Method Comparability

To measure CEC, a soil sample is placed in contact with a solution containing a high concentration of one cation, usually sodium or ammonium. This contacting solution is replaced several times until all of the exchange sites on the soil are occupied by a single type of cation. Then, the soil is placed in contact with a solution containing a different cation, such as potassium, which exchanges for the first cation. The amount of the first cation in the solution following exchange gives the CEC of the sediment.

The most common method analysis during the 1950s used ammonium-acetate buffered at pH 7 for the initial solution to saturate the exchange sites (McBride 1994). For calcareous soils, such as the Big Lost River gravels, this may result in dissolution of calcite. Calcium released by dissolution will compete with the ammonium for exchange sites on the clays during the saturation step. As a result, the method can be biased low for total CEC. An improved method is to buffer the solution at pH 8.2, as is included in EPA method SW 9081. Dissolution of soil carbonate minerals will be minimized, decreasing the potential for calcium to prevent complete saturation of exchange sites by sodium.

J-3.1.2 Existing Data Sources

Review of the INL literature and the Environmental Data Warehouse showed three primary periods of sampling for analysis of CEC on Big Lost River sediments in the vicinity of INTEC. The first round of sampling was conducted during the initial assessment of the National Reactor Testing Station (now the Idaho National Laboratory) in the mid 1950s by the U. S. Geological Survey. The second round was conducted in the mid 1960s, and the third round was conducted in the early 2000s for ecological risk assessment. Excavation of the alluvium during construction of the tank farm would have mixed the material and destroyed any layering from original deposition. Photographs taken during construction of the tanks show evidence that materials were not sorted or size segregated before being backfilled into the excavation. During construction projects, additional material has been added to the tank farm from nearby gravel pits when backfill was needed. Because

of this, we conclude that alluvial material in the tank farm will have the same average geochemical properties as Big Lost River alluvium outside the tank farm. Mixing sediments with higher than average CEC or lower than average CEC will have been mixed with material with average CEC. As a result, tank farm backfill may show a wider a range of properties than undisturbed alluvium, but these properties will be relatively uniformly distributed.

The USGS collected surface sediment samples as part of the initial INL site characterization (Nace, et al. 1956). The method used to determine the CEC is not explicitly stated. Lacking specific information, we may assume that the method used ammonia-acetate buffered at pH 7. The CEC results may be biased low because of calcium released by dissolution of calcite, but there is insufficient information to be certain. There is an extensive discussion of the distribution of CEC with grain size, and the authors state “it is believed that the exchange values reported... are in the correct order of magnitude for the total exchange capacity of the gross parent samples.” Based on this, we conclude that the mass of large particles separated before determination of the CEC was then added back to correct the CEC measurements to total bulk sample mass.

The data have been divided into INTEC specific CEC measurements, and CEC measurements from the general central INL area (Table J-3-1). The box around INTEC in Figure J-3-1 shows the locations that are considered INTEC specific. Locations at the southern end of the map are near the CFA landfills. All of the locations on the map are located in alluvial gravel of the Big Lost River based on geologic maps of the area. The Big Lost River has been fed from the same source area during the entire period that the alluvium was being deposited, and shows similar mineralogy (Bartholomay, et al. 1989). Given similar source area, mineralogy, grain-size distribution, and depositional environment for the area depicted in Figure J-3-1, we conclude that sediment samples throughout this region would be representative of gravels at INTEC and within the tank farm.

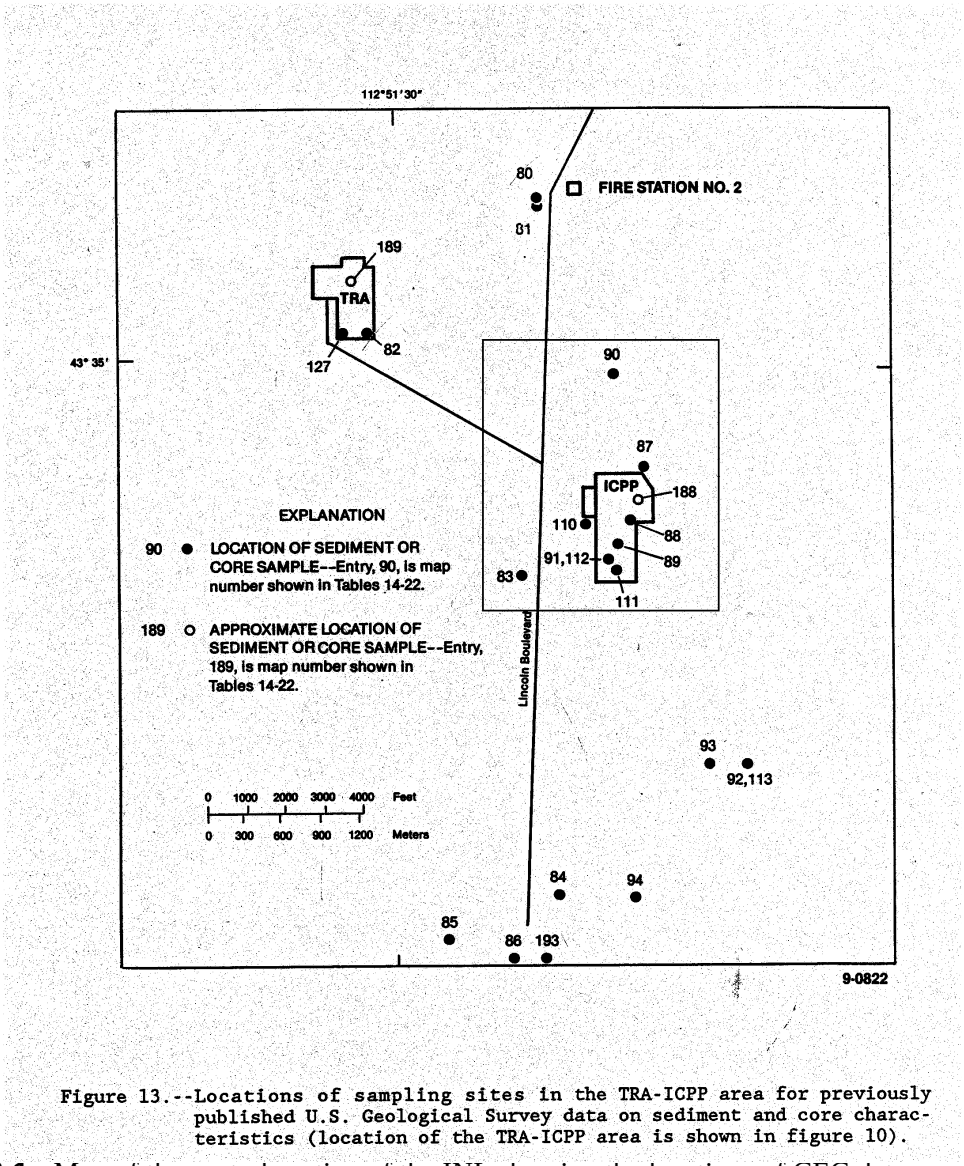

Figure 13.--Locations of sampling sites in the TRA-ICPP area for previously published U.S. Geological Survey data on sediment and core characteristics (location of the TRA-ICPP area is shown in figure 10).

Figure J-3-1. Map of the central portion of the INL showing the locations of CEC data samples. Numbers correspond to location numbers in Table J-3-1. Map from Bartholomay et al. (1989)

Table J-3-1. CEC measurements from alluvium in the central portion of the INL shown in Figure J-3-1

CEC (meq/100 g)/100 g)	Map Location	Sample Level Top (ft)	Sample Level Bottom (ft)	INTEC or Area
1.8	83	8	8	INTEC
2.2	87	12	12	INTEC
3.4	88			INTEC
2.7	89	43	44	INTEC
2.9	90	6	7	INTEC
2.0	91	10	10	INTEC
4.5	91	12	12	INTEC
2.0	112			INTEC
4.5	112			INTEC
3.1	80	5	5.5	Area
2.9	80	10	10.5	Area
3.6	81	3	3.5	Area
3.4	82	12	12	Area
2.3	82	14	14	Area
2.5	84	5	5	Area
3.7	85	5	5	Area
3.9	86	5	5	Area
3.7	92	4	5	Area
3.2	93	1	2	Area
2.1	94	5	5	Area
3.7	113			Area

Data from the U. S. Geological Survey characterization studies are compiled in Table 14 of Bartholomay (Bartholomay, et al. 1989). Cross referencing data in Table 14 with the map in Bartholomay's Figure 13, twenty-one CEC measurements for Big Lost River alluvium from the INTEC vicinity can be identified. Nine of the samples are from the INTEC facility and an additional 12 samples from the general area near INTEC. Samples of alluvium for CEC measurements come from a range of depths from 1 ft to 44 ft (Table J-3-1). CEC data at INTEC range from 1.8 meq/100 g to 4.5 meq/100 g. Outside the INTEC “box”, the CEC ranges from 2.1 meq/100 g to 3.9 meq/100 g. The means are 2.9 meq/100 g for INTEC and 3.2 meq/100 g for the area, and are not significantly different at the 90% confidence level. Because the data at INTEC and the data in the central INL area overlap, and the means are not significantly different, we group the data and calculate over all statistics for the samples. The mean is 3.05 meq/100 g with a 95% confidence range from 2.71 to 3.40 meq/100 g. Twenty-one samples from a rather large area of the central portion of the INL, all representing alluvium of the Big Lost River, show little variation in CEC. The total range is from about 2 to 4.5 meq/100 g with a mean of 3.0 meq/100 g. The USGS data are generally representative of Big Lost River alluvium *in situ*, with a possibility of a slight low bias depending on the method of measurement used.

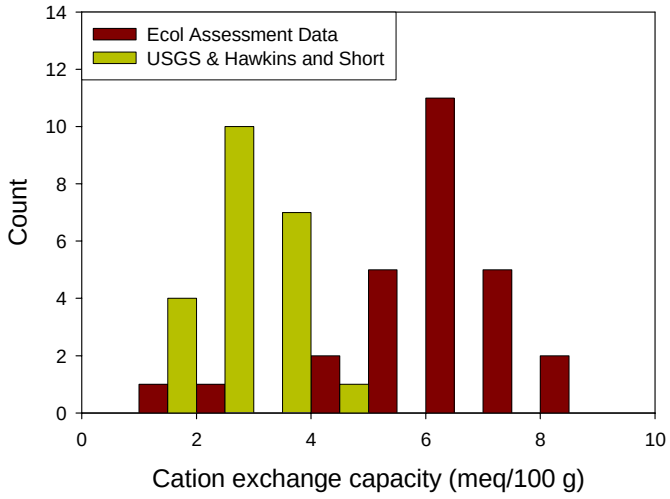

Figure J-3-2. Histogram of measured cation exchange capacity for Big Lost River alluvium near INTEC. Data for the 2000+ sampling period were adjusted by a factor of 0.4 to account for the estimated grain-size discrimination during sample collection. USGS data are from 1956 and are not adjusted. Hawkins and Short CEC measurements are adjusted based on measured grain-size analyses.

An early investigation into the sorption of Sr and Cs by sediments at the INL was conducted by Hawkins and Short (Hawkins and Short 1965). They measured CEC on alluvial sediments collected in the vicinity of INTEC and Reactor Technology Complex. Three different methods were used to measure CEC, and all methods gave good agreement. Solutions were not buffered, so calcite dissolution would have been minimized. Multiple measurements of CEC on the same material using the same method gave quite variable results ranging from 3.2 to 7.8 meq/100 g. CEC for Sr ranged from 7.9 to 12 meq/100 g, and for Cs ranged from 4.3 to 8.3 meq/100 g. Different exchange capacities for different ions is not uncommon (Zachara, et al. 2002), however, the TOUGHREACT code can only handle a single CEC. Hawkins and Short sieved the alluvium to remove material larger than 2 mm. Sieve analyses of the Big Lost River alluvium from which the samples used by Hawkins and Short were taken are reported by Hawkins and Foster (Hawkins and Foster 1963). The sieve analyses indicate that 75% to 77% of the alluvium in the samples was greater than 2 mm. If the Sr CEC for the Hawkins and Short samples are adjusted by a factor of 0.24 to include the weight of the total alluvium assuming the > 2 mm fraction has zero CEC, then the results are on the order of 2 to 3 meq/100 g. Based on the agreement among different methods of CEC measurement, and the ability to correct the CEC results to bulk alluvium using measured grain size analyses, the Hawkins and Short data are considered comparable to the earlier USGS results.

The sampling locations where the alluvium samples were collected are shown in Hawkins and Foster (Hawkins and Foster 1963). The samples come from gravel pits just north of CFA, just east of INTEC, and near Fire Station No. 2. Two samples collected north-west of RTC may not be from Big Lost River alluvium and were not considered here. The remaining samples are from Big Lost River alluvium in similar depositional environments as the alluvium at INTEC, and are therefore considered representative.

During recent remedial investigations, 27 samples of surficial alluvium were collected just outside the INTEC fence to the north, east, south and west of the facility. The samples were composites and were collected either at the ground surface or between depths of 0 to 24 in. below the surface. In the field during sample collection, samples were screened though a #9 wire mesh with a reported particle size discrimination of 3.7 mm[1]. Grain-size distribution was not measured on these samples, so the fraction of sample weight removed cannot be calculated. CEC was determined by EPA method SW9081. In this method, exchange sites are saturated with sodium in a solution buffered at pH 8.2. By buffering the solution at pH 8.2, dissolution of soil carbonate minerals will be minimized, decreasing the potential for calcium to prevent complete saturation of exchange sites by sodium. The sodium is subsequently displaced by ammonium acetate solution, and the CEC calculated from the amount of displaced sodium. CEC measurements from these samples range from 4.3 to 20.3 meq/100 g with a median of 15.9 meq/100 g.

These numbers are significantly higher than earlier USGS measurements. Because of the particle size discrimination during sampling, these results are not representative of Big Lost River alluvium. The measured values cannot be corrected because grain-size information on the samples is lacking. The screen used does not match the size of sieves used for particle size analysis, and so a direct comparison between the screen size and other data on grain size analyses cannot be made. A statistical summary of grain-size properties of Big Lost River alluvium (Bartholomay, et al. 1989) indicate a wide range in the percent of material greater than 2 mm. For Big Lost River channel deposits (Bartholomay et al. Table 7) the screening could have removed from as little as 15% of the sample material to as much as 80% of the sample material. In Bartholomay et al. Table 3, grain-size data from samples collected closest to INTEC are more uniform and suggest an average weight percent greater than 2 mm of about 60% (Bartholomay, et al. 1989). Based on an assumption that 60% of the alluvial material would have been removed by screening, the 2000 - 2004 data were adjusted with a factor of 0.4 to estimate *in situ* Big Lost River alluvium CEC (Figure J-3-2). The analytical method used to measure CEC should give comparable and representative data, the sample locations from INTEC provide representative material. Because of sample handling before analysis, however, the analytical data are neither representative nor comparable. An approximate correction can be made for this handling, however the uncertainty in the final data is something like ±20% based on the uncertainty in the size fraction analyzed.

Based on all available data, alluvial CEC in the tank farm will be low, on the order of a few meq/100 g. Data from the USGS collected in 1956 and from Hawkins and Short are representative of the CEC of bulk alluvium. Data from the two studies are in agreement even though the method of CEC measurement is different. Data collected for the Ecological Risk Assessment are not representative of bulk alluvium properties. A correction can be made to adjust for removal of gravel, but uncertainty remains ±20% for these measurements. CEC measurements range from about 2 to about 8 meq/100 g (Figure J-3-2), with the most reliable data falling between 2 and 5 meq/100 g.

J-3.2 Selectivity Coefficients

There is a distinct preference for certain cations on ion exchange sites, with preference given to those cations with larger *hydrated* ionic potentials (Appelo and Postma 1996). This order of preference is given in lyotropic series presented by a number of authors.

$$Cs^+ > Sr^{2+} > Ca^{2+} > Mg^{2+} > K^+ > NH_4^+ > Na^+ > H^+$$

The order of preference in these series show widespread agreement (McBride 1994; Appelo and Postma 1996; Sparks 2003) indicating that selectivity coefficients show a consistent order of preference across a range of sediment materials. The consistent order of selectivity indicates that cation properties are more important for determining ion selectivity than are material properties. We conclude from this that ion exchange selectivity coefficients taken from the literature will provide a good starting point for the ion exchange model. In the results presented here, ion exchange selectivity coefficients were taken from Table 5.5 on page 160 of Appelo

1. This is not a 9-mesh Tyler screen, but a commercial wire screen. Personal communication, August 31, 2005, Tom Haney, Field Team Leader for sampling.

and Postma (Appelo and Postma 1996) because this table provides a fairly comprehensive set of exchange coefficients that are comparable, and includes all the components of primary interest for the tank farm. These coefficients are given for the Gaines-Thomas convention and written in terms of one sodium ion reacting. The coefficients are, therefore, in the same form as used in TOUGHREACT. Ion exchange selectivity coefficients adopted for the model are shown in Table J-3-2. Hydrogen ion was adopted from Appelo (Appelo 1994). Because the hydrogen ion is so tightly hydrated, it has a very low hydrated ionic potential, and does not compete readily for ion exchange sites (McBride 1994). Because of the low pH of the sodium-bearing waste, however, there may be appreciable concentrations of hydrogen ion and so it is included in the model.

Table J-3-2. Ion exchange selectivity coefficients from Appelo and Postma (1996) or Appelo (1994) used in the validation of the ion exchange model.

Ion +1	$K_{Na/i}$	Ion +2	$K_{Na/i}$
H	7.7E+5	Mg	0.50
Na	1.00	Ca	0.40
NH_4	0.25	Sr	0.35
K	0.20		
Cs	0.08		

No measurements of site-specific ion exchange selectivity coefficients have been made for Big Lost River alluvium. There have been many measurements of partition coefficients for Sr (K_d values). Some of these even included testing the effects of competing cations on the K_d value (Hawkins and Short 1965; Bunde, et al. 1997; Liszewski, et al. 1997; Bunde, et al. 1998; Liszewski, et al. 1998). Only Hawkins and Short report the CEC value associated with the sediments used in the experiments. Therefore, the Hawkins and Short data can be used to evaluate applicability of these exchange coefficients (Table J-3-2) to Big Lost River alluvium. This evaluation will be reported in a later section of this report.

J-3.3 Pore Water Chemistry and Solid Phases

Parameterization of the remainder of the geochemical model includes the incorporation of sodium-bearing waste chemistry, pore water and recharge water chemistry, and solid phase geochemical properties.

J-3.3.1 Sodium-bearing Waste Composition

The composition of the sodium-bearing waste is taken from a memo prepared by Don Rhodes in 1972 (Rhod-4-72) for tank WM-181. The components of sodium-bearing waste important for strontium transport are given in Table J-3-3. Hydrogen ion is important because it will dissolve calcite and release calcium. Hydrogen and sodium are possible competitors with strontium and cesium for exchange sites. Nitrate provides charge balance, but can also form soluble complexes with strontium at high nitrate concentrations, which increases strontium mobility. Aluminum will primarily play a role in lowering the pH by forming aluminum hydroxide minerals that require hydrogen. These aluminum hydroxide minerals will subsequently precipitate.

Table J-3-3. Components of sodium-bearing waste included in reactive transport model. Other components were present at concentrations much less than these and were not considered in the model.

Component	Concentration (reported)[1]	units	Concentration (mole/L)[2]	Activity (Ci/L)
H^+	1.4	M	1.5	na
NO_3-	4.38	M	4.5	na
Na^+	36.6	g/L	1.5	na
Al^{+++}	0.56	M	0.5	na
Cs-134	3.74E+04	dps/mL	5.834E-09	1.01E-03
Cs-137	8.81E+06	dps/mL	2.016E-05	2.38E-01
Cs (tot)			2.019E-05	na
Sr-90	7.91E+06	dps/mL	1.74E-05	2.14E-1

1. Rhodes (1972), sodium-bearing waste chemical analysis WM-181
2. used in model

J-3.3.2 Pore Water and Recharge

The geochemistry of perched water at INTEC has been reported in Roddy (Roddy 2005). The chemistry of the perched water is highly variable (Table J-3-4) because there are multiple sources of recharge contributing to the perched water. In spite of the range in chemical composition, the perched zone waters are close to saturation with respect to calcite in equilibrium with a soil gas phase at a partial pressure of carbon dioxide of around 10^{-2} atm. These two geochemical constraints were placed on the composition of the pore water. We then took the minimum sodium and chloride concentrations in perched water (0.3 mmol/L) for background electrolyte. This set of parameters allows all the significant components of the sodium-bearing waste and all the significant chemical reactions in the geochemical model to be incorporated into the model. One final condition was set on the pore water with the aluminum concentration set by equilibrating the water with gibbsite. Minimizing the number of components in the system, we set the initial pore water and recharge to be a low molality sodium chloride solution saturated with respect to calcite at a partial pressure of CO2(g) of 10^{-2} atm. This reflects an increase in carbon dioxide over atmospheric from microbial activity in the subsurface. The resulting chemical composition alluvium pore water is shown in Table J-3-5. The same water composition was used for the pore water at the start of the simulation, as well as the composition of the recharge water. Note that this pore water contains stable natural strontium. One of the sensitivity analysis presented here evaluates the effect of including or excluding the natural strontium from the geochemical model on the transport of radioactive Sr-90.

Table J-3-4. Summary statistics for perched water in the vadose zone at the north end of INTEC (Roddy 2005).

Parameter	Unit	Maximum	Minimum	Mean	# of Samples
Ca	mmol/l	2.92	0.75	1.61	62
Na	mmol/l	4.65	0.32	1.72	62
K	mmol/l	0.54	0.05	0.15	62
Mg	mmol/l	1.77	0.07	0.74	62
Sr	mmol/l	0.007	0.003	0.004	15
Cl	mmol/l	5.78	0.33	1.41	67
SO4	mmol/l	0.69	0.02	0.32	67
HCO3	mmol/l	8.87	0.39	3.53	65
Temp	°C	20.50	9.60	15.36	16
pH		8.10	7.02	7.51	20
log P_{CO2}	atm	-1.67	-2.95	-2.26	21
Saturation index for calcite		0.51	-0.31	0.03	21
Saturation index for strontianite		-1.41	-1.88	-1.70	7

Table J-3-5. Pore water and recharge water composition. This water is a low ionic strength sodium-chloride solution saturated with respect to calcite at a partial pressure of carbon dioxide of 0.01 atm.

Component	Concentration (mmol/L)
H^+	5.369E-05
pH	7.30
Ca^{+2}	1.64
Sr^{2+}	0.007
Na^+	0.33
Cl^-	0.33
HCO_3^-	3.64

J-3.3.3 Solid Phase Geochemical Properties and Parameters

The tank farm was constructed by excavating the alluvium at INTEC to bedrock, building the tanks, and then backfilling around the tanks. The alluvium at INTEC contains both Big Lost River channel deposits, and Big Lost River overbank deposits, which during construction would have been well homogenized. We adopt an assumption that the backfill material is homogeneous, and is representative of typical Big Lost River alluvium. Big Lost River alluvium in the vicinity of INTEC has been characterized for selected geochemical characteristics (Hawkins and Short 1965; Bartholomay, et al. 1989; Del Debbio and Thomas 1989; Liszewski, et al. 1997; Liszewski, et al. 1998; Rosentreter, et al. 1999). Table J-3-6 summarizes the mineralogic composition

.

Table J-3-6. Mineralogy of Big Lost River channel and overbank deposits. Values are weight percent.

	Channel deposits[1] (n = 11)		Overbank deposits[1] (n = 5)		INTEC alluvium[2] (n = 3)
Mineral	**Range**	**Median**	**Range**	**Median**	**Range**
Quartz	32 - 45	38	27 - 37	33	41 - 56
Plagioclase	16 - 30	23	11 - 19	16	18 - 21
K-feldspar	6 - 18	12	9 - 15	12	0 - 13
Calcite	0 - 6	3	3 - 12	7	3 - 12
Pyroxene	8 - 14	12	5 - 10	8	0 - 14
Dolomite	0 - 3	0	3 - 7	6	0 - 0
Clays	8 - 14	10	14 - 27	19	0 - 22

1. (Bartholomay, et al. 1989)
2. (Liszewski, et al. 1997)

Clay minerals identified in the field samples are dominantly illite, smectite, and mixed-layer illite/smectite with smaller amounts of kaolinite (Bartholomay, et al. 1989). Calcite is common. Dolomite is less common, and would be much slower to react with acid. We leave dolomite out of the model so that Mg can be left out of the model for simplification. Considering the mixing that took place, a range of calcite contents of 3 to 7 weight% would be expected in the alluvium, with a value of 5 weight% identified as the midpoint. Del Debbio and Thomas (Del Debbio and Thomas 1989) characterized INTEC alluvium as part of a K_d investigation, and determined calcite to be 5.6 weight%, which is in agreement with the USGS data. For a site-wide investigation of strontium adsorption to surficial sediment, Liszewski et al. (Liszewski, et al. 1997) measured mineralogy of INTEC alluvium for three samples (Table J-3-6). The mineralogy of these samples, including calcite, correspond to other measurements of mineralogy in INTEC alluvium. Table J-3-7 gives mineral parameters needed to convert among weight percent, moles, and volume percent. The specific gravity of alluvium grains is very consistent at 2.725 ± 0.022 (2 std. dev) g/cm^3. Five wt% calcite in the alluvium solids converts to 5.03 volume% of calcite in the alluvium solids (cm^3 calcite / cm^3 alluvium). Other values adopted for the alluvium are bulk density of 1.8 g/cm and porosity of 0.33 cm^3/cm^3.

Mass balance calculations indicate that sufficient calcite is present in the alluvium to react with (i.e. neutralize) the acid in the sodium-bearing waste. However, depending on the distribution of flow, significant acidity could remain if flow was concentrated along a few flow paths. If significant acidity remains unbuffered after calcite is consumed, then other minerals can be included in the model to dissolve more slowly by a kinetic reaction and provide additional pH buffer capacity.

Table J-3-7. Mineral properties for converting between mass and volume.

Mineral	Molar volume (cm^3/mole)	Molecular weight (g/mole)	Mineral density (g/cm^3)
Calcite	36.934	100.087	2.710
Gibbsite	31.956	78.004	2.441

J-3.4 Equilibrium Exchange Assemblage

The ratio of cations on ion exchange sites on a clay is related to the ratio of cations in solution by the selectivity coefficients. Once the selectivity coefficients and pore water chemistry are defined, the initial exchange assemblage on the clays is fixed. Using the pore water chemistry defined in Table J-3-5 and the selectivity coefficients defined in Table J-3-2, the surface exchange assemblage can be calculated and is shown in Table J-3-8.

Table J-3-8. Surface exchange assemblage for clay minerals calculated in equilibrium with pore water.

Exchange Species	Concentration (mole/L)	Equivalent fraction
CaX_2	0.196	0.994
SrX_2	0.00063	0.003
NaX	0.0012	0.003
Total	0.198	1.000

No measurements of equilibrium exchangeable cations have been made on sediments from INTEC. Measurements have been made on sediments from the SDA (Table J-4-1). Divalent cations, calcium plus magnesium, make up about 95% of the exchangeable cations with monovalent cations consisting of about 5%. This is in general agreement with the values calculated here, and so the equilibrium exchange assemblage shown in Table J-3-8 is adopted for the model of the alluvium.

J-4 VERIFICATION OF THE ION EXCHANGE MODEL

Because ion exchange depends on the ionic potential of the hydrated ion, much of the ionic selectivity is due to the aqueous ion and not the surface. Therefore, as an initial starting point, selectivity coefficients from the literature are appropriate. However, verification of the ion exchange parameters would enhance the level of confidence in the geochemical model. The investigation conducted by Hawkins and Short (Hawkins and Short 1965) provides a dataset that can be used to verify the model. These authors measured the effect of competing ions including calcium, magnesium, sodium, potassium, ammonium, and hydrogen on the sorption of Sr and Cs to INTEC alluvial sediments. Strontium and cesium adsorption data were digitized from graphs presented in Hawkins and Short, and experimental solution chemistry was taken from water compositions given in the report. The cation exchange capacity of the sediment used in these calculations was 8 meq/100 g, which is intermediate between their high and low exchange capacity sediments. Their experiments consisted of 25 mL solutions contacted with 1 g of sediment. Scaling this to 1 L of solution gives 1000/25 or 40 g/L and results in 40 g of sediment and 8 meq/100 g of CEC in a single liter of test solution. This gives 3.2 mM of exchange sites per experiment.

Table J-4-1. Hawkins and Short solution chemistry and calculated composition of the cation exchange sites using the Appelo and Postma selectivity coefficients. Measured equivalent fractions from the SDA are shown for comparison.

Component	Dissolved (mg/L)	Dissolved (mmol/L)	Sorbed (mmol/L)	Equivalent fraction (model)	Equivalent fraction (measured SDA)
Na	163	7.09	0.156	0.049	0.02
K	25	0.64	0.070	0.022	0.03
NH_4	25	1.39	0.116	0.036	--
Ca	125	3.12	1.100	0.696	0.75
Mg	31	1.28	0.311	0.196	0.20

To perform the verification calculations, the exchanging mineral surface was first equilibrated with the test solution containing all cations at the primary concentration. This equilibration gives a total moles of each cation in the system, which is summed over the dissolved species and the cation exchange sites. The equivalent fraction (modeled) column in J-4-1 shows the equivalent fraction for each ion on the soil surface calculated using the Appelo and Postma selectivity coefficients. Measured equivalent fractions for SDA interbed sediments (Leecaster and Hull 2003) are shown in the final column. While these materials are interbeds from a different facility, the relative magnitude of the calculated values are close to the measured values. Calcium dominates the CEC sites, with the other predominant divalent cation, Mg, filling the second largest number of sites.

In the Hawkins and Short Sr experiments, radioactive Sr-85 was added to the solutions at a concentration of 50 μCi/L. Converting 50 μCi/L of Sr-85 gives 2.48E-11 mole/L of Sr. This is the value of Sr used in modeling the adsorption experiments. Cs adsorption experiments were run at 5 mg/L total Cs. Radioactive Cs was used as a tracer.

J-4.1 Comparison of the Ion Exchange Model to the Hawkins and Short Strontium Experiments

The Hawkins and Short strontium ion exchange experiments were simulated using the Appelo and Postma selectivity coefficients. Hydrogen ion was added using a selectivity coefficient from Appelo (Appelo 1994). All of the Hawkins and Short Sr adsorption experiments (Figure J-4-2 A to D) were matched very well with no modifications to the CEC or the selectivity coefficients (Figure J-4-1). The hydrogen ion is very strongly hydrated and has a relatively small charge. As a result, it is not very competitive for exchange sites. There is very little effect of pH on Sr exchange (Figure J-4-2).

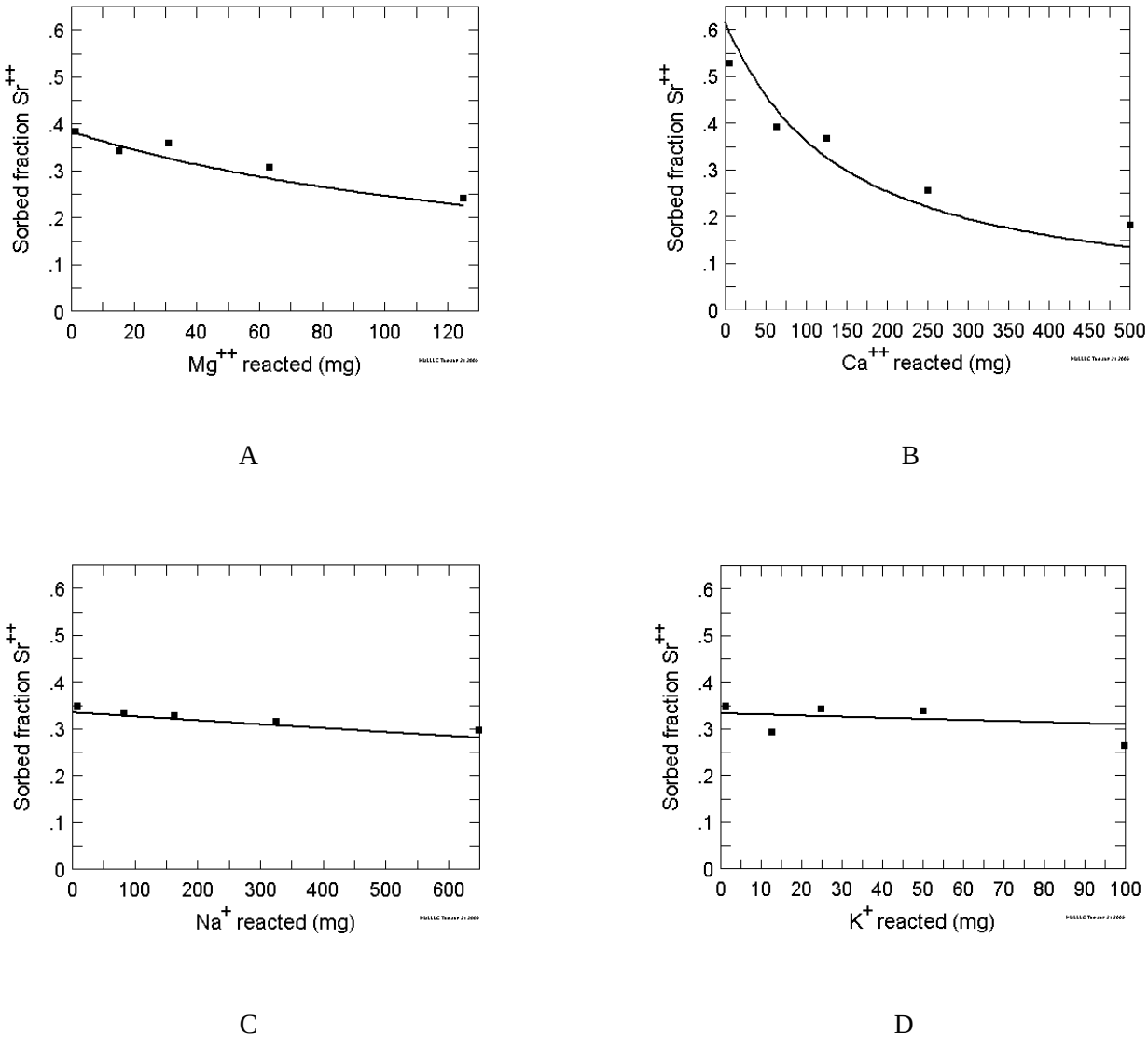

Figure J-4-1. Plot of sorbed Sr fraction as a function of competing cation concentration in solution. The amount of metal reacted is the concentration of the competing cation (mg/L) in solution. Points are measured values from Hawkins and Short (1965). Line is a model using selectivity coefficients from Appelo and Postma (1997).

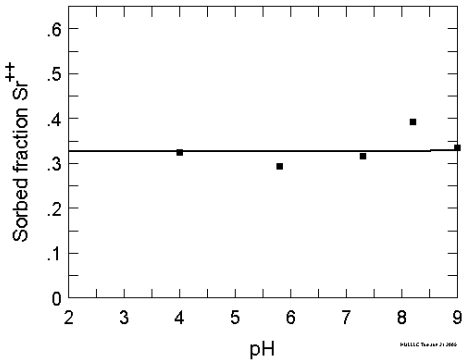

Figure J-4-2. Plot of sorbed Sr fraction as a function of pH of solution. Points are measured values from Hawkins and Short. Line is a model using selectivity coefficients from Appelo and Postma. For H+, the selectivity coefficient is 7.7E+05.

The selectivity coefficients take from Appelo and Postma do an excellent job of matching the sorption of strontium to INTEC sediments. The resultant ion exchange model is given below.

Monovalent

>X:Na+ + Na+	= >X:Na + Na+	Selectivity coef = 1.00
>X:NH4 + Na+	= >X:Na + NH4+	Selectivity coef = 0.25
>X:K + Na+	= >X:Na + K+	Selectivity coef = 0.20
>X:H + Na+	= >X:Na + H+	Selectivity coef = 7.7E+05

Divalent

0.5 >X2:Mg + Na+	= >X:Na + 0.5 Mg++	Selectivity coef = 0.50
0.5 >X2:Ca + Na+	= >X:Na + 0.5 Ca++	Selectivity coef = 0.40
0.5 >X2:Sr + Na+	= >X:Na + 0.5 Sr++	Selectivity coef = 0.35

J-4.2 Comparison of the Ion Exchange Model to the Hawkins and Short Cesium Experiments

Cesium ion exchange has frequently been found to be more complicated that strontium. Zachara et al. (Zachara, et al. 2002) show that Cs is not only sorbed by ion exchange to planar sites on the surfaces of clay minerals, but by ion exchange to frayed edge sites. Ion exchange is considered to be the mechanism for both sites, because Zachara et al found no evidence for pH effects on Cs adsorption to clays. Two ion exchange sites were needed to fit the Hawkins and Short data for Cs. For the planar sites, the selectivity coefficients for the ions other than Cs are the same as used for Sr. Cs exchange is much stronger than indicated by the Appelo and

Postma selectivity coefficient (Table J-3-2), and the CsX exchange coefficient was significantly increased (Table J-4-2). The first plot matched was the plot of Cs sorption as a function of Cs concentration. To achieve the high sorbed fraction at low Cs concentrations, the strong exchange frayed-edge site was needed in the model. The frayed edge site was estimated by fitting the data visually. The CEC for the frayed edge site is 3.25E-03 meq/100 g. The properties for the site are:

>F:Na + Na+	= >F:Na + Na+	Selectivity coef = 1.00
>F:K + Na+	= >F:Na + K+	Selectivity coef = 0.006
>F:Cs + Na+	= >F:Na + Cs+	Selectivity coef = 2E-07

This gives a reasonable good match to the Hawkins and Short data, but the plot in Hawkins and Short is limited in terms of the range of conditions covered. The fit is shown in linear and logarithmic forms (Figure J-4-3) to show that the values of selectivity coefficient selected for formation of this species do not seem to overly estimate adsorption at low Cs concentrations. Hawkins and Short experiments were mostly run at 5 mg/L total Cs concentration.

The selectivity coefficient for Cs in Appelo and Postma was not strong enough to match the data. More sorption of Cs to INTEC sediments was measured by Hawkins and Short than is calculated using the Appelo and Postma coefficient of 0.08. The selectivity coefficient was estimated by fitting the Hawkins and Short data by visual inspection. The low capacity CEC data were used in the fitting exercise. The final selectivity coefficient for planer ion exchange sites adopted for INTEC sediment is 0.0063.

.

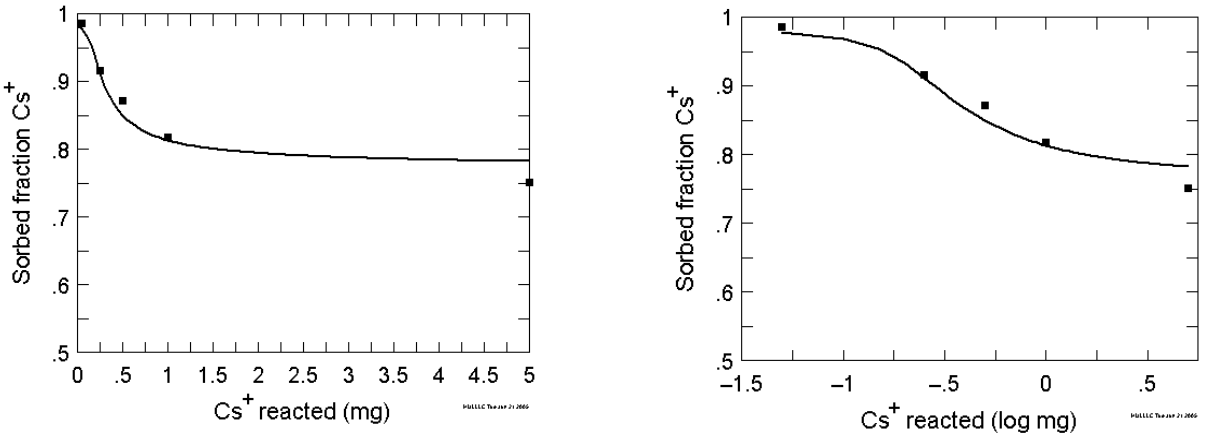

A B

Figure J-4-3. Plot of sorbed Cs fraction as a function of total Cs added to solution. There is relatively strong sorption of Cs at low concentrations, which decreases as Cs concentrations increase. This is modeled as a strong frayed edge site present at low concentrations that is filled first, followed by ion exchange on a planar site. Planar site CEC = 3.2 mM. Frayed edge site CEC = 1.3E 03

..

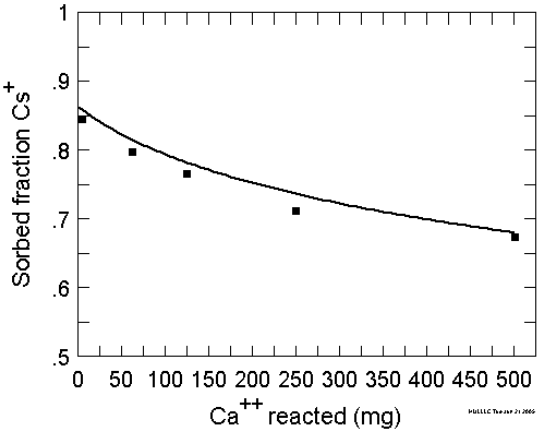

A

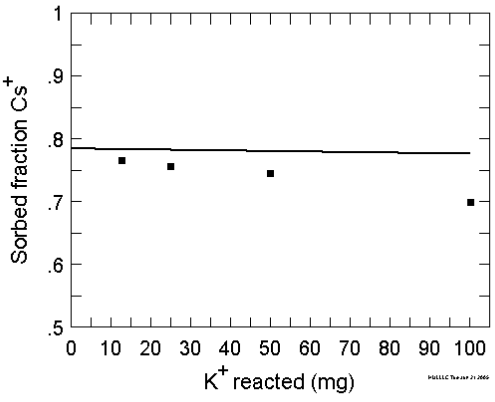

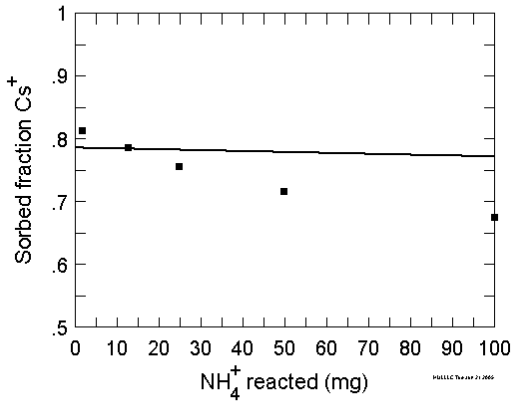

B C

Figure J-4-4. Plot of sorbed Cs fraaction as a function of A) Ca, B) K and C) NH4 ion concentration in solution. The amount of metal reacted is the concentration of the competing cation (mL/g) in solution. Points are measured values from Hawkins and Short. Line is a model using selectivity coefficients from Appelo and Postma except for Cs.

.

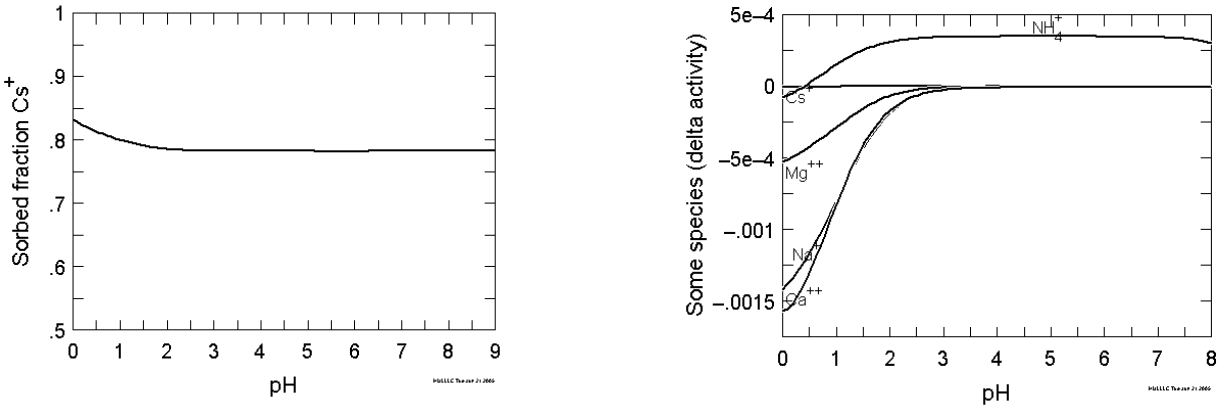

A B

Figure J-4-5. Panel A is a plot of sorbed Cs fraction as a function of pH in solution. Hawkins and Short did not measure the effect of pH on Cs sorption. Line is a model using selectivity coefficients from Appelo and Postma except for Cs. Panel B shows the change in ion activity due to the increase in ionic strength as pH approaches 0. Cs, being a small monovalent ion, changes much less than the divalent cation resulting in a change in solution activity ratios even though the concentration ratios do not change.

Elevated concentrations of K and NH_4 decrease the sorption of Cs to clays to a greater extent than the model predicts (Figure J-4-4). This is the poorest fit obtained, and the model underestimates the selectivity for Cs and NH_4. However, changing the NH_4 selectivity coefficient would also change the Sr plot, which showed a good match. Given the low likelihood of significant NH_4 concentrations in the tank farm sediments, this is not considered a problem.

Hawkins and Short did not measure the change in Cs partitioning with pH. However, Cs sorption is little affected by changes in pH (Zachara, et al. 2002). The calculated change in sorbed fraction is very small over the pH range 0 to 9 (Figure J-4-5). The increase in sorbed fraction at low pH can be attributed to changes in the ion activities in solution as ionic strength gets large near pH 0.

The TOUGHREACT code only has provision for one type of CEC site. Therefore, the two-site model cannot be directly implemented in the code. This only affects cesium sorption, and not strontium sorption. The total cesium concentration from the sodium-bearing waste is on the order of 2E-05 molar (Table J-3-3). The estimated number of frayed edge sites in the alluvium ranges from 1.7E-04 to 5.8E-04 molar, depending on the moisture content of the alluvium. Therefore, we do not anticipate that the frayed edge sites will become saturated with cesium. We can adjust the selectivity coefficient to the planer sites to mimic the adsorption of Cs to the frayed edge sites. The partition coefficient is the product of the number of sites and the selectivity coefficient (Hull, et al. 2004). Because the number of planer sites is much greater than the number of frayed edge sites, the selectivity coefficient has to be decreased by the ratio of the number of planer sites to frayed edge sites. This gives a final selectivity coefficient for Cs on planer sites of 0.0006 (Table J-4-2).

Selectivity coefficients for cation exchange are primarily dependent on ionic properties rather than sediment properties. The general agreement in the relative order of cation selectivity among numerous authors indicates general wide agreement on the relative magnitudes of selectivity coefficients. Hawkins and Short conducted experiments on competitive adsorption of Sr and Cs on sediments representative of INTEC alluvium, and provide sufficient data to determine that their results are comparable to *in situ* alluvium conditions. Based on the ability to match the Hawkins and Short strontium and cesium adsorption experiments, we conclude that, except for cesium, the selectivity coefficients selected from Appelo and Postma are applicable to INTEC alluvial sediments.

Table J-4-2. Ion exchange selectivity coefficients from Appelo and Postma used in the validation of the ion exchange model.

Ion +1	$K_{Na/i}$	Ion +2	$K_{Na/i}$
H	7.7E+5	Ca	0.40
Na	1.00	Sr	0.35
K	0.20	Mg	0.50
Cs	0.0006		
NH_4	0.25		

J-4.3 Comparison of the Ion Exchange Model to Measured Alluvium K_d Values

A second set of data that can be used to test the ion exchange model and the model parameterization was collected by the USGS and Idaho State University (Liszewski, et al. 1998). In this study, samples of alluvium and sedimentary interbeds from wells USGS-121 and USGS-123 were tested for a wide range of physical properties and were used to determine strontium K_d values. Of interest for the source release model are the measurements made in surficial alluvium.

Well 121 is just north of the INTEC facility and well 123 is just south of the INTEC facility. Samples of alluvium were collected from a number intervals from land surface to 29 ft in well 121 and from land surface to a depth of 26 ft in well 123. A total of 21 samples were analyzed for K_d values. The top two or three intervals in each well consisted of finer grained material than the deeper samples. This difference will be seen in the measured K_d values. The two wells tested are adjacent to INTEC and samples were collected from a range of depths in the alluvium. Therefore, we conclude that the samples are representative of alluvium at INTEC and are comparable to materials likely to be in the tank farm.

Samples for K_d measurements were sieved to remove the size fraction greater than 4.7 mm. The remaining material was crushed until all of the material passed through a 2 mm sieve. Grain size distributions were measured and reported, so that measured K_d values can be corrected for the mass of material removed. Freundlich isotherms were fit to the experimental data. However, the “n” parameter in the Freundlich equation for all samples was very close to one. Therefore, the Freundlich isotherms are essentially linear, and the Freundlich K can be interpreted as a K_d parameter. Sample depths, gravel fractions, and corrected K_d values for alluvium are shown in Table J-4-3. The samples near the surface have K_d values significantly greater than samples collected from greater depths. This reflects a fine-grained layer of loess deposited on top of the alluvial gravels. Average values for the deeper samples are shown that do not include the near-surface material (near surface material not included in the average is shown in italics in Table J-4-3. In well 121 the average K_d was 20 mL/g and in well 123 the average K_d is 23 mL/g.

Table J-4-3. Measured K_d values from Liszewski et al. (1998).

Well 121 Surficial sediments				
Freundlich K	**Freundlich n**	**% > 4.7 mm**	**Depth (ft)**	**Corrected K_d (mL/g)**
93	1.0	0.0	2.3	93
145	1.1	0.0	4.3	145
144	1.0	0.0	6.2	144
61	0.97	75.5	13.1	15
61	0.99	74.2	15.1	16
56	0.99	68.0	17.1	18
57	1.1	74.4	19.0	15
59	1.0	76.5	21.0	14
70	1.0	57.2	23.0	30
62	1.1	68.1	26.9	20
73	0.93	57.2	28.9	31
			average	20
Well 123 Surficial sediments				
Freundlich K	**Freundlich n**	**% > 4.7 mm**	**Depth (ft)**	**Corrected K_d (mL/g)**
112	1.1	36.8	2.0	71
52	0.89	59.7	4.3	21
40	0.92	55.7	5.9	18
48	1.1	54.7	9.8	22
48	1.1	69.6	12.1	15
57	0.84	66.0	14.1	19
61	1.1	62.4	16.1	23
58	0.92	50.0	18.0	29
85	0.96	54.6	21.0	39
70	1.3	65.2	25.6	24
			average	23

Unfortunately, one of the parameters that was not measured on these samples was the cation exchange capacity. Therefore we cannot use PHREEQC to model these experiments to validate the cation exchange model. One thing we can do, however, is to use PHREEQC in an inverse manner. Using the water chemistry used in the K_d experiments, and the measured K_d value, we can use PHREEQC to calculate what the CEC of the sediments must have been to get the measured K_d value. This is not an independent verification of the cation exchange model, because we do not have the CEC of the samples. However, it will provide an estimate of the CEC of the samples which can be compared to measured values of CEC from other studies.

A plot of alluvium K_d values measured by Liszewski et al. (1998) against the CEC values calculated from the measurements using PHREEQC is shown in Figure J-4-6. The correlation is perfect because there is a functional relation between the two variables, with no independent measurements. However, the calculated CEC values can be compared to measurements of CEC from alluvium. The calculated CEC values are shown in Table J-4-4. The calculated CEC values range from 1.4 meq/100 g to 14.5 meq/100 g with an average of 3.9 meq/100 g. It is clear from the plot in Figure J-4-6 that only a few values are greater than 5 meq/100 g. From the table, it is clear that these high CEC samples are associated with the near-surface fine-grained sediments, not the river alluvium. Therefore, from these calculations we find that the Liszewski et al. (1998) measured K_d values are consistent with alluvium of the Big Lost River having a narrow range in CEC values, and that the range is between 1.5 meq/100 g and 4 meq/100 g. These numbers are very similar to the range of CEC values measured by the USGS in 1956. The water chemistry and the solid to solution ratio used in the Liszewski experiments are very different than the water chemistry and solid to solution ratio used in the TOUGHREACT simulation of the alluvium. PHREEQC was used to calculate the expected K_d value for alluvium based on the alluvium pore water chemistry, a water saturation of 0.1 and a bulk density of 1.8 g/cm^3. The calculated K_d values (Figure J-4-6) appropriate for the range of anticipated alluvium CEC are from about 5 to 20 mL/g.

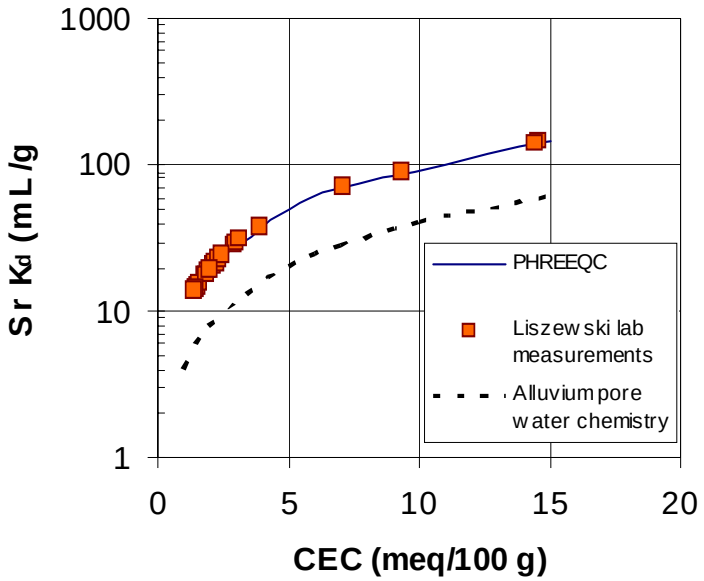

Figure J-4-6. Plot of correlation between K_d values measured by Liszewski et al (1998) and CEC values calculated from the measured Kd values using PHREEQC. Dashed line shows calculated Sr Kd values for pore water chemistry used in the TOUGHREACT simulation. Given the CEC values consistent with the Liszewski lab measurements, we expect the Kd value in the alluvium to be between 5 and 20 mL/g depending on the CEC of the alluvium.

Table J-4-4. CEC values for surficial alluvium calculated from measured K_d values in Liszewski et al. (1998).

Depth (ft)	Corrected K_d (mL/g)	CEC (meq/100 g)
2.0	70.8	7.1
2.3	93.0	9.3
4.3	145.0	14.5
4.3	21.0	2.1
5.9	17.7	1.8
6.2	144.0	14.4
9.8	21.7	2.2
12.1	14.6	1.5
13.1	14.9	1.5
14.1	19.4	1.9
15.1	15.7	1.6
16.1	22.9	2.3
17.1	17.9	1.8
18.0	29.0	2.9
19.0	14.6	1.5
21.0	13.9	1.4
21.0	38.6	3.9
23.0	30.0	3.0
25.6	24.4	2.4
26.9	19.8	2.0
28.9	31.2	3.1
	Mean	3.9
	Maximum	14.5
	Minimum	1.4

Comparing the K_d values calculated with PHREEQC (dashed line in Figure J-4-6) to the K_d values measured by Liszewski et al. (1998) show that the calculated K_d values are smaller than the measured K_d values at a given CEC. This difference is because the water used in the Liszewski laboratory experiments was mixed to emulate water discharged to the percolation ponds, not pore water or perched water at the north end of INTEC. The percolation pond water contained much lower concentrations of divalent cations than the vadose zone water at the north end of INTEC and the water composition used in the TOUGHREACT simulations. The average measured K_d value of about 20 mL/g (Table J-4-3) from Liszewski is about what is calculated for a CEC of 4 meq/100 g using alluvium pore water chemistry. As CEC decreases below 4 meq/100 g, the K_d will decrease linearly, with a value of about 5 mL/g when CEC is 1 meq/100 g. Using the competitive cation exchange model for strontium adsorption has allowed us a much better understanding of the partitioning of strontium to alluvium, and the effects the geochemical environment has on the partitioning. The lower alluvium K_d values from 5 to 20 mL/g better reflect the in situ geochemical conditions expected in the alluvium at the tank farm.

J-5 COUPLED TRANSPORT AND GEOCHEMICAL PHENOMENA: ONE-DIMENSIONAL SIMULATIONS

This section provides an overview of Sr-90 transport from the sodium-bearing waste release using a one-dimensional representation of the tank farm alluvium. The purpose of this section is to provide an overview of the relative transport rates of various dissolved species, changes in pH and mineral composition of the sediments, and a discussion of partitioning between sediment and pore water. This will provide a basic understanding of the processes that are taking place in the alluvium as the sodium-bearing waste is neutralized, and migrates downwards. We also evaluate the sensitivity of the predicted Sr-90 migration to the natural background strontium concentration in the pore water.

For the one-dimensional simulation, the leak and the alluvium are represented as a single column of alluvium with x and y dimensions of 60 m by 30 m (200 ft by 100 ft). The alluvium is divided into 36 cells each 0.5 m (1.64 ft) in height. Vertical locations in the alluvium are given as elevation above the basalt contact. To avoid problems with boundary conditions at the sediment-basalt interface, 10 cells were defined as basalt to allow the alluvium to drain freely. A constant vertical flux from infiltration was applied at the surface. Pore water, recharge, and sodium-bearing waste compositions are the same as for the three-dimensional model discussed below. A cation exchange capacity of 5 meq/100 g (midpoint of distribution in Figure J-3-2) was used in the one-dimensional model.

In the first few steps of the computer simulation, the flux of water and the water content of the alluvium are allowed to come to steady state, resulting in a water saturation of about 30%. The leak was then simulated to occur in cell 33 (depth of 1.25 m), and the sodium-bearing waste was allowed to react with the alluvium and to be washed downwards by recharge from the surface. Acidic sodium-bearing waste reacts with calcite in the alluvium consuming hydrogen ion from the waste and releasing carbon dioxide.

$$CaCO_3 + 2\ HNO_3 \Leftrightarrow Ca^{2+} + CO_2(g) + 2\ NO_3^- + H_2O \qquad \text{(J-5-1)}$$

While the sodium-bearing waste is neutralized by the calcite reaction, sufficient hydrogen ion remains to lower the pH of pore water. TOUGHREACT is a multiphase flow simulator, allowing the transport of CO_2 as a gas and also as a constituent dissolved in water. Figure J-5-1 shows the volume fraction of calcite in the alluvium 1 week and 1 year after the leak. One week corresponds to the maximum drop in pH in the release cell. The volume fraction of calcite is quickly reduced from the original quantity of 0.050 to 0.049 in the cell where the sodium-bearing waste was released. There is some additional dissolution of calcite in the release cell and in the

cell immediately below the release point over the next year. The total amount of calcite dissolved is a small fraction of the total available calcite so there should be adequate buffer capacity in the alluvium.

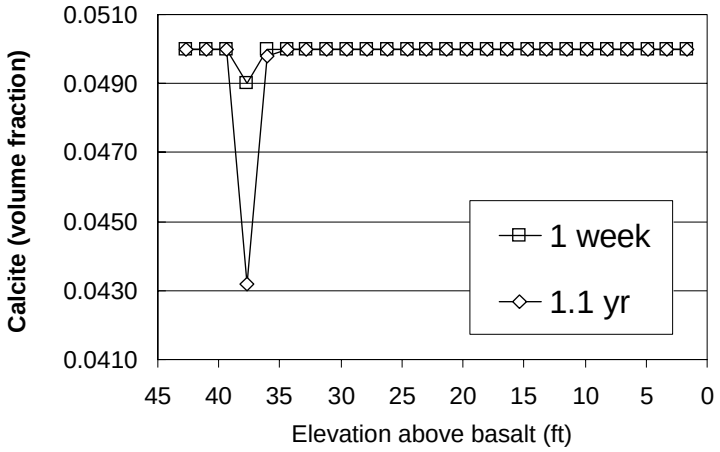

Figure J-5-1. Volume fraction of calcite at 1 week and 1 year after release of sodium-bearing waste.

The pH of pore water in the release cell drops quickly reaching a minimum value of 5.7 one week after release (Figure J-5-2). The pH of the water moving downward from the cell where the leak occurred remains less than the initial pore water pH of 7.3 because of the increased CO_2 partial pressure from calcite dissolution. The increased partial pressure of CO_2 dissolves a small amount of calcite in the cells immediately below the release depth. The model indicates that the calcite in the alluvium rapidly buffers the pH of the sodium-bearing waste so that extreme pH values are not observed in the pore water. There will be a transient pH drop from the release of carbon dioxide from calcite dissolution, but this dissipates within a matter of weeks. The minimum pH of pore water after the initial calcite dissolution is about 6.5, and this pH-minimum moves down through the alluvium over a period of about 4 years. As the peak concentrations of the sodium-bearing waste move downward, the cation ratio in the pore water changes back to natural levels. Calcium in the recharge water replaces sodium from the ion exchange sites. As a result the pore water becomes undersaturated with respect to calcite, and some calcite dissolves. The dissolution of calcite to replace the calcium lost to ion exchange sites raises the pH in the pore water to about 7.5. Once the excess sodium has been replaced by calcium on the ion exchange sites, the pore water pH will return to about 7.3.

In the immediate vicinity of the release, 0.0012 volume fraction of gibbsite is formed as the sodium-bearing waste is neutralized (not shown). This small amount will not affect hydraulic properties of the media. Because the lowest pH predicted by the model is 5.7, the amount of dissolution of alumino-silicate minerals, such as feldspars, will be relatively minor and does not need to be included in the model.

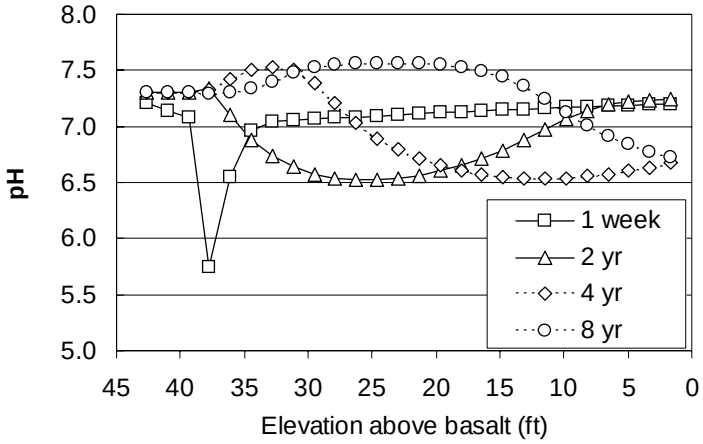

Figure J-5-2. Vertical profiles in alluvium pore-water pH.

The mobility of the major ionic species will depend on reactions with ion exchange sites on the clay minerals. Cations will react with ion exchange sites, and may migrate slower than nitrate, which is considered a conservative species. The distribution of major dissolved species after 2.03 years is shown in Figure J-5-3. Peak nitrate concentrations have been reduced from 4.5 M to 0.4 M by mixing with pore water in the alluvium. Nitrate and calcium have migrated the farthest and move at about the same rate as indicated by the coincident rise in concentrations of both components between elevations above the basalt interface of 10 to 20 ft. Nitrate is from the sodium-bearing waste and calcium is generated by the dissolution of calcite by nitric acid. Because calcium is essentially saturated on exchange sites in the alluvium, there is little loss by ion exchange and no discernible retardation. Sodium, on the other hand, is significantly retarded relative to nitrate and calcium. Most of the ion exchange sites in the alluvium are initially filled with calcium, and so the high sodium concentrations in the sodium-bearing waste drive exchange reactions where sodium knocks calcium off the clays. Calcium, therefore, is kept in solution, but some of the sodium is removed.

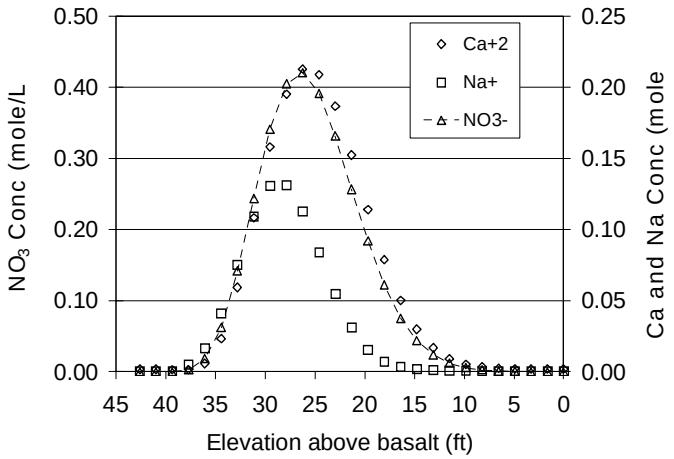

Figure J-5-3. Vertical distribution of calcium, sodium, and nitrate in the alluvium pore water 2.03 yr after the leak.

Initial concentrations of Sr in the sodium-bearing waste are on the order of $2X10^{-5}$ M. At two years, there is a strontium peak migrating at about the same rate as the peaks in major cations, and showing similar retardation as sodium relative to the migration of calcium (Figure J-5-4). The retardation of strontium relative to calcium indicates that strontium does interact with ion exchange sites on the clays. Two factors however, inhibit strontium adsorption, which keeps more strontium in solution than would be predicted by a constant K_d model. One factor is the competition for ion exchange sites, and the second factor is the formation of aqueous complexes of strontium in solution.

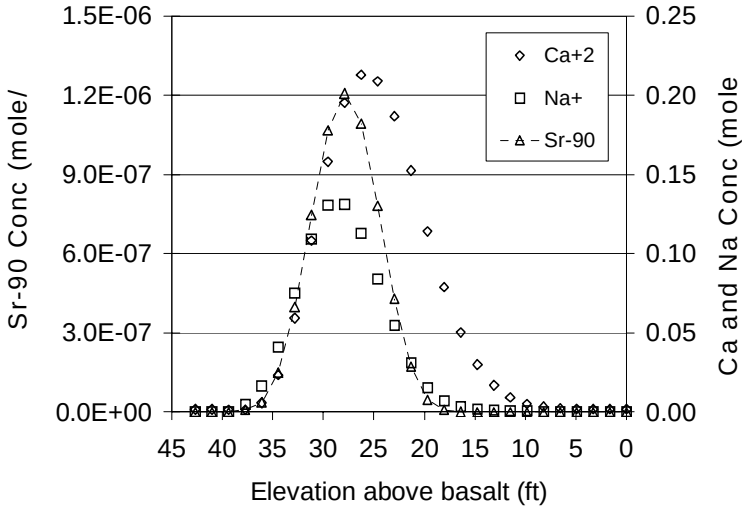

Figure J-5-4. Vertical distribution of strontium, sodium, and calcium in the alluvium pore water at 2.03 years after the leak.

The distribution of strontium between aqueous species and ion exchange sites shows significant variations with depth that are correlated to the peaks in the major chemical components in the sodium-bearing waste (Figure J-5-9). In normal pore water, 98.6% of the strontium is on exchange sites, and only 1.4% in solution. In the sodium-bearing waste solution, however, only about 30% of the strontium is on the ion exchange sites and 70% in aqueous solution. This partitioning to the aqueous phase is responsible for the more rapid migration of strontium. There are two factors that decrease strontium partitioning to clays. The first factor is the formation of soluble aqueous complexes of strontium with nitrate ion. About 24% of the strontium is in the form of aqueous nitrate complexes, and therefore is sequestered in solution and will not adsorb as strongly on clays (Figure J-5-5). There is also a decrease in partitioning of strontium ion (Sr^{2+}) to clays with free strontium in solution increasing from 1.4% to 44%. The decrease in partitioning is the result of increased competition for ion exchange sites by elevated calcium and sodium concentrations in solution. Both competitive cation exchange and formation of aqueous complexes are needed to accurately predict the transport of strontium from the sodium-bearing waste leak.

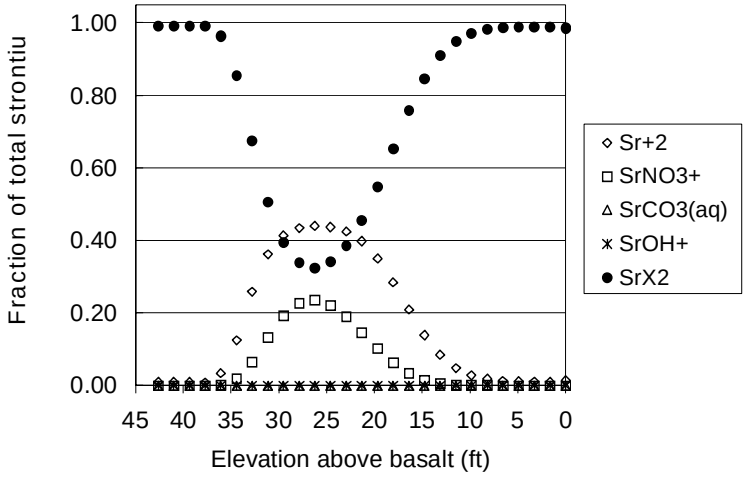

Figure J-5-5. Distribution of strontium among aqueous species and ion exchange sites at 2.03 years after release.

The replacement of calcium on ion exchange sites by sodium is well illustrated in Figure J-5-6, where the concentrations of the exchangeable cation species are shown. The exchangeable calcium concentration is at a minimum where the sodium maximum is located at an elevation of about 30 ft 2.03 years after the release. As the sodium peak migrates downwards through the alluvium, some of the strontium is left behind on ion exchange sites (Figure J-5-6 B, between 35 and 40 ft elevation). Thus, the elevated cation concentrations from the sodium-bearing waste spill enhance the transport of the strontium through the alluvium. However, once those peak concentrations have migrated downwards, the preferential partitioning of strontium over calcium to cation exchange sites results in a much less mobile fraction of strontium. Also, the decrease in nitrate concentration decreases the formation of soluble aqueous complexes of strontium.

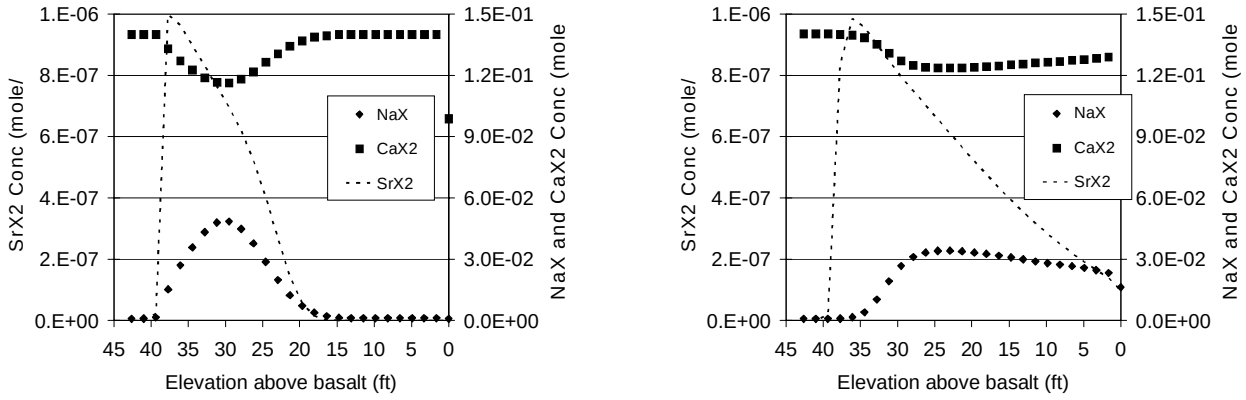

Figure J-5-6. Distribution of exchangeable cations with depth in the alluvium 2.03 (A) and 8.05 (B) years after the leak.

.

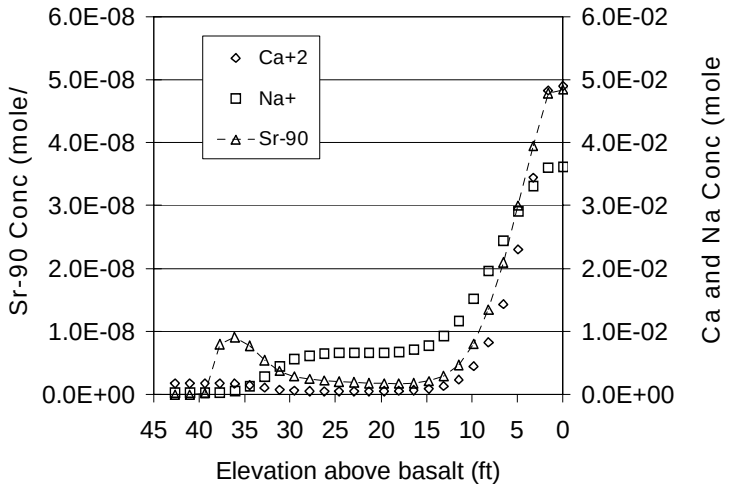

Figure J-5-7. Concentration of cations in solution at 8.05 years.

The elevated aqueous strontium concentration near the sediment - basalt interface (elevation 0 ft) at 8.05 years (Figure J-5-7) is not matched by an elevated concentration of strontium on ion exchange sites at the corresponding time and elevation (Figure J-5-6 B). However, the elevated aqueous concentrations of strontium at 8.05 years at an elevation of 35 to 40 ft does correspond to an elevated concentration on exchange sites where the aqueous sodium and calcium concentrations have returned to near normal levels. Translating this information into a time history of release for strontium-90 (Figure J-5-8) shows that there will be about a

two-order of magnitude higher release of strontium-90 because of the competition of exchange sites from sodium and calcium. Peak releases from the alluvium to the underlying basalt are calculated (in the one-dimensional model) to take place between about 4 and 12 years after release. Once the cation peak has passed, there will be a steady release of strontium, which is similar to what would be predicted with a K_d model.

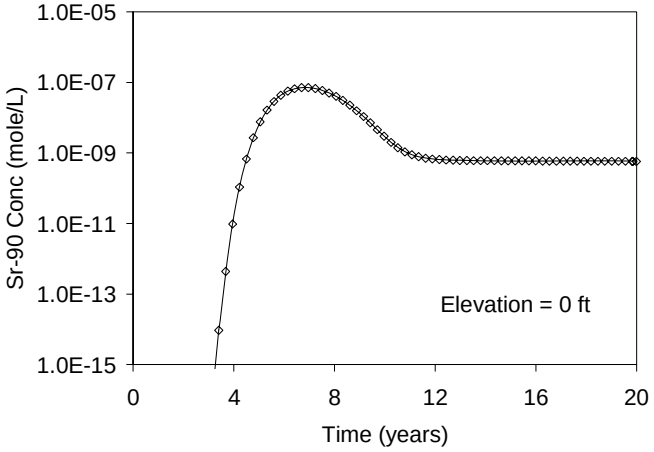

Figure J-5-8. Concentration of Sr-90 in pore water at the sediment-basalt interface.

Two factors enhance the transport of strontium through alluvium immediately after the leak. Some strontium forms complexes with nitrate at the very high concentrations in the sodium-bearing waste and is prevented from sorbing to clays. In addition, high sodium and calcium concentrations inhibit the sorption of strontium to ion exchange sites. After 8.05 years (Figure J-5-7), there is a peak of strontium migrating downwards in conjunction with the peak concentrations in sodium, calcium, and nitrate. The initial

breakthrough fronts of nitrate and calcium move more rapidly because these two species are not retarded (Figure J-5-3). Significant strontium remains on ion exchange sites behind the sodium peak, and there is a continuous slow release of strontium from these exchange sites. Including the high ion concentrations from the sodium-bearing waste leak results in a variable partitioning of strontium to the ion exchange sites from aqueous complexation and competitive ion exchange.

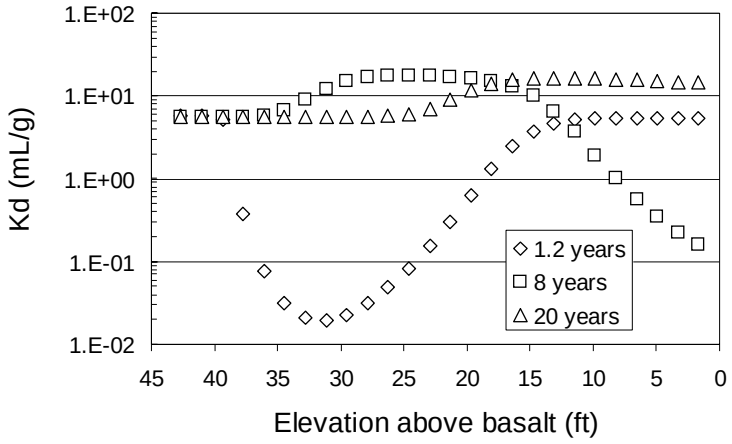

Figure J-5-9. Distribution of strontium between aqueous and solid phases with depth between 1.2 years, 8 years, and 20 years after the leak.

The changes in partitioning with depth corresponding to changes in the bulk water chemistry can be illustrated by calculating a local effective K_d value at each depth. This is calculated from the predicted sorbed concentration and the predicted aqueous concentration by:

$$K_d = \frac{C_{ads}}{C_{sol}} \frac{S_l \theta}{\rho} \qquad \text{(J-5-2)}$$

where:

C_{ads} = adsorbed concentration (mol/L)

C_{sol} = dissolved concentration (mol/L)

S_l = saturation (cm^3 of water/cm^3 of rock)

θ = porosity (0.32 cm^3/cm^3)

ρ = bulk density (1.8 g rock/cm^3 of rock)

Using Equation J-5-2 and the parameter values given with it, predicted solid and aqueous concentrations of strontium can be used to calculate K_d values. These values are shown in Figure J-5-9 for 1.2, 8, and 20 years after the leak. In the native pore water, the strontium K_d is predicted to be about 6 mL/g at a water saturation of 0.32. During the leak, when calcium and sodium concentrations in pore water are at their peak values, strontium K_d values can drop to about 0.02 mL/g. As the water moves downward through the alluvium, and mixes with native pore water, peak concentrations of sodium and calcium decrease, resulting in an increase in K_d values for strontium (Figure J-5-9). For a brief period around 8 years after the leak, most ion exchange sites are filled with sodium rather than calcium. Because strontium can more easily replace sodium than calcium, the K_d value actually increases above the value under natural conditions. By 20 years, effects of the sodium-bearing waste leak are almost gone, and partitioning of strontium has returned to normal.

One side effect of linking of K_d to solution concentrations, is that there will be a bimodal transport of strontium through the vadose zone. Strontium traveling with the sodium peak will move faster than strontium that falls behind the sodium peak (see Figure J-5-7). Thus, some strontium could move downward out of the alluvium relatively rapidly. Strontium remaining in the alluvium would migrate very slowly, because the pore water chemistry would have changed substantially.

J-5.1 Presence of Stable Strontium

Pore water in the alluvium will have stable strontium. This strontium will also compete for ion exchange sites, and will have the same selectivity as radioactive strontium 90. Therefore, this strontium may have an effect on the partitioning of Sr-90. The effect of stable strontium was evaluated using the one-dimensional transport model. Calculations were performed after adding a second strontium species to the TOUGHREACT database with exactly the same chemical properties as radioactive Sr-90. The concentration of stable strontium was selected as 0.007 mmol/L (Table J-3-4). This is the highest concentration measured in perched water wells by Roddy (2003), and will give the highest likely amount of competition for exchange sites in alluvium.

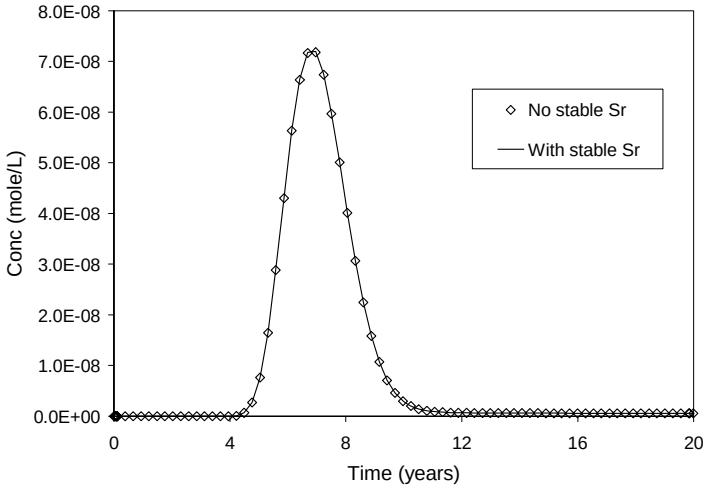

Figure J-5-10. Simulated Sr-90 concentrations with and without natural, stable strontium at a concentration of 0.007 mmolar at the sediment - basalt interface.

The peak strontium-90 concentration at the sediment-basalt interface (Figure J-5-10) occurs 7 years after the leak. Without stable strontium in the system, the peak concentration is predicted to be 7.183E-08 mole/L. With 0.007 mmol/L stable strontium, the peak release concentration increases to 7.196E-08 mole/L, or a change of 0.18%. Based on this comparison, we conclude that the inclusion of stable strontium does not make a significant change in the predicted release of Sr-90 from the alluvium. We therefore, did not include stable strontium in the three-dimensional simulations to decrease the size of the chemical matrix that needed to be solved.

Based on this analysis, we can conclude that the ion exchange model adequately represents the chemical evolution of the CPP-31 release. This one-dimensional analysis is useful in developing an understanding of initial rapid transport of strontium through the alluvium and into the underlying basalt followed by a slow-delayed release of strontium from the alluvium under pseudo-static geochemical conditions. Evaluation of the site-specific applicability requires (a) parameterization of the full alluvium,

vadose zone, and aquifer models for Sr-90, comparison of known field data to geochemical model predictions, and an analysis of the predictive sensitivity to model parameter uncertainty. Parameterization of the alluvium model follows from the previous discussion, and parameterization of the vadose zone and aquifer models follow the presentation contained in Appendix A, Section 5.1. The noted exception is the geochemical properties of interbed sediments for Sr-90. These specifically include the partitioning coefficient (K_d) which is discussed below in Section J-6. The site-specific application is presented in Sections J-7 through J-12.

J-6 ESTIMATE OF K_d IN THE SEDIMENTARY INTERBEDS

The geochemical reactions responsible for retardation of Sr-90 in the alluvium were discussed above, and are largely similar to those affecting the migration of Sr-90 through the vadose zone interbeds. However, the lithologic descriptions of these materials (Liszewski et al. 1998) are very different than lithologic descriptions of surface alluvium. The alluvium is characterized as gravel and sandy-gravel. Interbeds, on the other hand, are commonly described as muddy-sand, sandy-mud, or muddy-sandy-gravel. These descriptions imply significantly more fine-grained sediment and clay minerals in the interbeds. Thus, different K_d values may be applicable in the interbeds than in the alluvium. In the remainder of this section, we evaluate appropriate K_d values for sedimentary interbeds at INTEC.

Strontium K_d values in sedimentary interbeds at INTEC were estimated three different ways from existing information for use in this work. They are:

1. Strontium K_d values were measured on samples collected from sedimentary interbeds at INTEC (Liszewski et al. 1998). After review of the laboratory procedures used to collect these K_d values, we conclude that they are biased high because of the water chemistry used during the measurements. Therefore, the measured values may not be representative of the geochemical conditions in the interbeds.
2. Hawkins and Short (1965) developed an equation to predict the K_d value of strontium for INTEC alluvium after measuring the partitioning of strontium as a function of water chemistry. This equation includes a term for cation exchange capacity (called saturation capacity). However, all Hawkins and Short measurements were made at one CEC value, and so the sensitivity of the calculated K_d to CEC was never validated. Entering water analyses for perched zone wells compiled by Roddy (2005), the Hawkins and Short equation can be used to calculate a strontium K_d for each water analysis.
3. Finally, we used the PHREEQC geochemical code and selectivity coefficients for a cation exchange geochemical model to calculate strontium K_d values using the Roddy water analyses. One difficulty with the latter two calculations is that no CEC values have been measured on interbeds at INTEC. CEC values have been measured on interbeds at other facilities at the INL, particularly at the Subsurface Disposal Area (Barraclough et al., 1976; Rightmire 1984; Leecaster and Hull 2003). USGS investigations have shown that the interbeds across the southern INL (including the Subsurface Disposal Area, Reactor Technology Complex, and INTEC) all contain sediment from the Big Lost River derived from mountains to the north (Bartholomay, 1990). Because the sediments are derived from the same source areas, and therefore will have a common mineralogy, the geochemical properties will be similar. This does not permit us to determine specific CEC values for specific wells at INTEC, but does provide a good indication of the range of CEC values to be expected for interbed materials derived from Big Lost River deposits. We use the summary statistics (range and average) of the Subsurface Disposal Area CEC data in the calculations for INTEC.

Liszewski et al. (1998) collected cores of sedimentary interbed material for measurement of strontium K_d values. The cores came from well USGS-121, just north of INTEC, and well USGS-123, just south of INTEC. The material tested was from the 110 ft, the 140 ft, and the 380 ft interbeds. The well locations are close to INTEC and the material used in the experiments is representative of the subsurface under the INTEC facility. Grain-size analyses were conducted on the material, and 100% of the interbed material was smaller than 4.7 mm (Table J-6-1). Material between 2.0 mm and 4.7 mm was crushed to pass through a 2 mm sieve. Therefore, all of the sedimentary interbed material was used in the experiments, and no gravel adjustment is necessary. K_d experiments were conducted using a synthetic water made-up to emulate discharge to the percolation ponds. This water is essentially Snake River Plain Aquifer water with sodium and chloride added from regeneration of water softeners and ion exchange columns. The water chemistry is shown in Table J-6-2. Strontium partitioning was fit using a Freundlich isotherm model rather than a K_d model. However, the n values for the Freundlich equation were all very close to 1.0. Therefore, the Freundlich K is essentially a K_d value. The measured Freundlich K / K_d values are shown in Table J-6-1 along with summary statistics. One K_d value

measured in well 123 at a depth of 155.8 ft is 60 mL/g, while the remaining K_d values range from 131 to 240 mL/g. The overall mean of all the data is 168 ± 50 mL/g.

The water used in the Liszewski experiments is high in sodium, but very low in calcium and magnesium relative to perched water at the north end of INTEC. This can be seen from the data in Table J-6-2. Liszewski used a calcium concentration of 20 mL/g, where most perched zone wells have from 50 to 80 mL/g calcium. Liszewski used 4 mL/g magnesium, where most perched zone wells have from 12 to 25 mL/g magnesium. The low concentrations of divalent cations in the test solutions will permit more strontium to exchange onto the ion exchange sites, thus over estimating K_d values. Additional calculations shown later in this section will explain this in more detail. Therefore, the measured K_d values from Liszewski are probably higher than K_d values that would be applicable to perched water zones at the north end of INTEC, even though these are site-specific measurements on representative material.

Table J-6-1. Measured Sr-90 K_d values for sedimentary interbeds at INTEC from Liszewski et al. (1998).

Well 121 Interbeds				Well 123 Interbeds			
Freundlich K	**% > 4.7 mm**	**Depth (ft)**	**Corrected K_d (mL/g)**	**Freundlich K**	**% > 4.7 mm**	**Depth (ft)**	**Corrected K_d (mL/g)**
140	0	401.1	140	131	0	107.3	131
163	0	401.5	163	238	0	109.6	238
210	0	402.8	210	240	0	112.5	240
167	0	404.8	167	60	0	155.8	60
158	0	410.0	158	204	0	157.8	204
154	0	413.3	154	155	0	161.0	155
		Mean	165			Mean	171
		Minimum	140			Minimum	60
		Maximum	210			Maximum	240

Hawkins and Short (1965) measured the partitioning of strontium to a composite sample of INTEC alluvium over a range of water chemistry.These authors varied calcium, magnesium, sodium, potassium, ammonia, and pH. There was no effect of pH on the partitioning of strontium. The cations calcium and magnesium where the most important cations, with significant decreases in strontium adsorption with increasing concentrations of the divalent cations. From the laboratory experiments, Hawkins and Short used multiple regression to develop an equation to predict strontium K_d from the concentrations of cations in the water and the cation exchange capacity. We used this equation to calculate K_d values for perched water zones at the north end of INTEC for water chemistry given in Roddy (2005). There are no measurements of the CEC of interbed materials at INTEC. There are, however, numerous measurements of interbed CEC from the Subsurface Disposal Area (Barraclough et al. 1976; Rightmire 1984; Leecaster and Hull 2003). Using the average CEC of 21 meq/100 g from Leecaster and Hull, we calculated the range of K_d values for INTEC perched zone water chemistry (Table J-6-2). The calculated K_d values range from 19 to 40 mL/g with an average of 31 mL/g. The range of values is much lower than the measured K_d values from Liszewski. The lowest K_d values are calculated for well MW-1 with the highest calcium concentrations (about 100 mL/g). Water from well 33-3 is not included in these summary statistics, because water from this well is contaminated from a brine pit (Table J-6-2), and is not considered representative of perched water at INTEC. The K_d value calculated for well 33-3 is negative, illustrating that statistically derived regression equations cannot be used to extrapolate beyond the conditions under which they were derived.

Hawkins and Short's equation was developed from measurements made at one CEC. Therefore, the sensitivity of the predictions to other CEC values was not quantified when the equation was developed. We evaluated the sensitivity of the calculated K_d values to CEC, because CEC is not known for the INTEC interbeds. CEC was varied over the range of CEC values for Subsurface Disposal Area interbeds, from 1 meq/100 g to 45 meq/100 g. Over that range, the average calculated K_d value ranged from 22 to 52 meq/100 g (Table J-6-3).

Table J-6-2. Cation composition of perched zone monitoring wells from Roddy (2005), and Sr-90 K_d values calculated using the Hawkins and Short regression equation with a CEC of 21 meq/100 g. The CEC of 21 meq/100 g is the average CEC reported by Leecaster and Hull (2003) for interbeds at the Subsurface Disposal Area.

Well ID	Sampling Date	CEC (meq / 100g)	pH	K (mg/L)	Na (mg/L)	Ca (mg/L)	Mg (mg/L)	NH4-N (mg/L)	K_d (mL/g)
	Liszewski	21.0	8.0	2.0	100	20.	4.	0.0	59
33-3	2/12/2004	21.0	7.28	18.2	853	328	101	0.20	-3
33-2	9/23/2003	21.0	7.38	7.31	46.30	54.50	14.40	0.20	37
33-2	2/11/2004	21.0	7.74	4.25	48.90	52.10	14.00	0.20	38
33-2	7/12/2004	21.0	7.43	5.77	45.00	48.60	12.80	0.20	40
33-2	10/4/2004	21.0	7.80	3.91	54.20	52.90	14.30	0.19	38
33-4-1	9/17/2003	21.0	7.50	3.08	13.80	57.30	15.20	0.20	37
33-4-1	2/24/2004	21.0	7.26	2.69	12.40	59.30	15.70	0.20	35
37-4	9/10/2003	21.0	7.49	4.56	49.60	87.40	28.30	0.20	23
37-4	5/18/2004	21.0	7.61	3.99	37.60	87.80	25.90	0.33	24
55-06	9/16/2003	21.0	7.50	6.72	39.10	75.40	22.60	0.20	28
55-06	2/19/2004	21.0	7.71	4.59	30.60	61.50	18.60	0.20	24
MW-1-4	9/18/2003	21.0	7.31	6.35	34.20	105.00	31.50	0.20	19
MW-1-4	5/25/2004	21.0	7.29	8.83	30.40	95.10	28.40	0.92	22
MW-2	2/19/2004	21.0	7.29	5.03	49.20	76.60	21.00	0.20	28
MW-20-2	9/16/2003	21.0	7.40	8.51	26.50	65.60	17.40	0.20	33
MW-20-2	2/25/2004	21.0	7.78	7.55	29.40	73.70	21.30	2.88	29
MW-5-2	9/15/2003	21.0	7.50	3.99	30.30	66.30	17.60	0.20	32
MW-5-2	2/18/2004	21.0	7.29	3.28	24.10	53.90	14.60	0.20	37
								Mean[1]	31
								Minimum	19
								Maximum	40

1. Summary statistics exclude well 33-3 and the water chemistry used by Liszewski et al (1998).

Table J-6-3. Sensitivity of the average calculated interbed K_d value to the CEC used in the Hawkins and Short equation. The range of CEC values is based on the range of CEC values for sedimentary interbeds at the Subsurface Disposal Area (Barraclough et al. 1976; Rightmire 1984; Leecaster and Hull 2003).

CEC (meq/100 g)	Average K_d (mL/g)
1	22
5	23
15	28
21	31
25	34
35	42
45	52

The third approach to estimating K_d values in the INTEC sedimentary interbeds was to use the PHREEQC geochemical code to calculate strontium partitioning using an ion exchange model. The concentrations of strontium on ion exchange sites and the strontium remaining in solution were then used to calculate a K_d. The PHREEQC code implements an ion exchange model similar to the model used in the TOUGHREACT code, and results of these calculations are comparable using the two codes.

To perform the calculations, inputs to the model include perched zone water chemistry, cation exchange capacity, and selectivity coefficients for cations. These concepts are discussed in more detail in Section J-3. Verification of the cation exchange model using the Hawkins and Short laboratory experiments is discussed in Section J-4. As discussed above, no data on CEC of sedimentary interbeds at INTEC are available. Calculations were performed for a range of perched zone water chemistry from Table J-6-2. A range of CEC was used to evaluate the possible range of K_d values that might be expected. The lab K_d experiments of Liszewski were also simulated. No direct comparison can be made between the Liszewski lab data and the K_d values calculated with PHREEQC because no CEC values are available. Therefore, the PHREEQC model, cannot be verified with the Liszewski et al. (1998) lab experiments.

Results of the simulations are presented in Table J-6-4 and displayed graphically in Figure J-6-1. Strontium K_d values calculated as a function of CEC using the water chemistry used in the laboratory experiments of Liszewski et al. (1998) range from 50 to 454 mL/g. With the one exception of 60 mL/g, the bulk of K_d values measured by Liszewski et al. ranged from 130 to 240 mL/g. From Table J-6-4, this range in calculated K_d values corresponds to a range in CEC values from about 12 meq/100 g to 25 meq/100 g. This range is very typical of fine-grained interbeds at the Subsurface Disposal Area, and seems reasonable for fine-grained interbeds at INTEC as well. Using water analyses from monitoring wells MW-1, MW-2, and 33-2, which cover the range from lowest to highest concentrations of divalent cations in perched zone water, K_d values were calculated for interbed materials. Focusing on the range of K_d values from 15 to 25 meq/100 g, the calculated K_d values range from 28 to 103 mL/g (Table J-6-4). The K_d value for MW-2, with an intermediate cation concentration, at a median CEC of 20 meq/100 g, is 52 mL/g. K_d values were also calculated using the perched water chemistry from well 33-3. This well has been contaminated by brine, and is not representative of perched water under INTEC. High concentrations of brine can, however, significantly affect the partitioning of strontium to sediments as shown by the very low K_d values for well 33-3 in Table J-6-4.

Table J-6-4. Calculated K_d values as a function of CEC using the ion exchange model in PHREEQC and water analyses from Table J-6-2

	K_d (mL/g)				
CEC (meq/100 g)	**MW-1**	**MW-2**	**33-2**	**33-3**	**Liszewski**
5	9.4	13.0	20.6	2.5	50.4
10	18.8	26.0	41.2	5.1	100.7
15	28.3	39.1	61.8	7.6	151.2
20	37.6	52.1	82.4	10.1	201.5
25	47.1	65.2	103.1	12.6	252.1
35	66.0	91.2	144.3	17.7	352.9
45	84.8	117.3	185.5	22.7	453.7

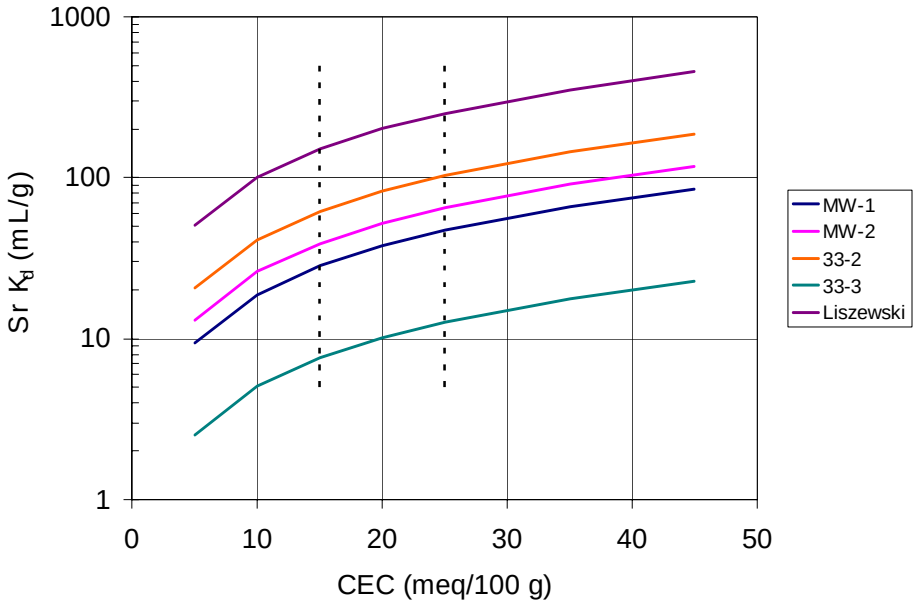

Figure J-6-1. Range of strontium K_d values calculated for INTEC interbeds using perched zone water chemistry from vadose zone monitoring wells. Kd values calculated using the water chemistry used in the lab experiments of Liszewski et al. (1998) are also shown. Vertical dashed lines show the 95% confidence interval for the average cation exchange capacity calculated from the measured Kd values.

Three methods were used to evaluate the range of likely K_d values in INTEC sedimentary interbeds. The three methods were:

- measured K_d values from Liszewski et al (1998) on INTEC sedimentary interbed materials
- calculated K_d values using INTEC perched zone water chemistry and an empirical regression equation developed by Hawkins and Short (1965)
- calculated K_d values using INTEC perched zone water chemistry and the cation exchange geochemical model in PHREEQC.

The measured Liszewski et al. K_d values match K_d values calculated for the laboratory water chemistry using the PHREEQC code if the CEC of the samples is in the range of 12 to 25 meq/100 g. This range of CEC values is typical for Subsurface Disposal Area interbeds, and seems reasonable for fine-grained interbeds at INTEC. The PHREEQC simulations show that the Liszewski et al. K_d values are biased high because of the low divalent cations present in the laboratory water used in the experiments. K_d values calculated using INTEC perched zone water chemistry and the Hawkins and Short equation and the PHREEQC code are in agreement. The Hawkins and Short equation, at a CEC of 21 meq/100 g, yields K_d values ranging from 19 to 40 mL/g with an average of 31 mL/g. The PHREEQC code, at a CEC of 20 meq/100 g, yields K_d values ranging from 37.6 to 83.4 mL/g with a midpoint of 52.1 mL/g.

Strontium K_d in interbeds is sensitive to both CEC and water chemistry. At a constant CEC of 20 meq/100 g, the difference in water chemistry between wells MW-1 and 33-2 changes the calculated K_d value from 37.6 to 83.4 mL/g (Table J-6-4). This same magnitude of change in K_d value for constant water chemistry in MW-1 is calculated if the CEC increases from 20 to 45 meq/100 g; or for well 33-2 if CEC decreases from 20 to 10 meq/100 g. Given the range in water chemistry of the perched water at INTEC, and the fact that CEC will show spatial variation in the interbeds, a range of K_d values from 22 to 78 was used in the simulated transport of strontium to the aquifer. Within this range, a value near 50 mL/g probably represents the best estimate of an average K_d value for interbeds.

J-7 SITE-SPECIFIC APPLICATION

Evaluation of (a) model applicability, (b) data sufficiency, and (c) model sensitivity for the CPP-31 release was performed as a three-step process. In the first step, site-specific field data were compiled for use in direct model to data comparison. In the second step, the one-dimensional model was re-configured into a three-dimensional system more representative of the physical conditions during the CPP-31 release. The three-dimensional model was then run, and model predictions were compared to the field data. The third step analyzed the overall model sensitivity to input parameters. This final step was necessary in order to evaluate whether or not the available data are sufficient to draw conclusions about strontium risk from the alluvium. It involves determination of the sensitivity of predicted results to uncertainty in the input parameters. Even if parameters are poorly constrained, if the final result is relatively insensitive to the parameter, collecting additional data to reduce uncertainty may not be justified. In this last section, we consider sensitivity to the geochemical parameters including (a) uncertainty in the cation exchange capacity, (b) uncertainty in the selectivity coefficient for strontium, and (c) uncertainty to pore water chemistry; and to the uncertainty in hydrologic conditions that includes (a) uncertainty in infiltration conditions, (b) uncertainty in sediment distributions, and (c) uncertainty in hydraulic properties.

J-7.1 Data for Site-Specific Model Parameterization

Site-specific simulation of the CPP-31 release requires parameterization of the hydraulic conditions and model verification by comparison to field data. Hydraulic conditions include the properties of the alluvium, recharge rates, and conditions surrounding the release. The soil hydraulic properties were initially taken from the base-grid model used to estimate the vertical migration of other surface releases (Appendix A, Section 5.1). These final calibrated parameters were presented in Appendix A, Section 6, and correspond to a course-highly transmissive-and low capillarity medium. These soil properties result in essentially vertical transport through the alluvium with very little lateral spreading due to capillary forces. This is appropriate because construction activities near CPP-31 have resulted in well mixed sediments with insignificant layering that would result in subhorizontal migration of fluid introduced near land surface. As a result, we assume that the alluvium is homogeneous with respect to hydraulic conductivity, soil-moisture characteristics, and dispersivity. As in the TETRAD-based simulations of the other contaminants, it is assumed that the recharge rate occurring at land surface is steady-state and 18 cm/yr. Unlike the other large-scale simulations, it is assumed that the bottom boundary condition in this model is steady-state, is representative of a saturated condition occurring in the perched water underlying the upper basalt unit, and is not influenced by the transient infiltration resulting from the Big Lost River or Percolation Pond discharges. The remaining hydrologic condition that is specific to site CPP-31 pertains to the conditions surrounding the release location. It is known that there is a subsurface enclosed conduit that underlies the actual point of release. This conduit is tens of meters long (X-direction), several meters wide (Y-direction), and on the order of 2 meters high (Z-direction), and exists at a depth of roughly 5 m below the point of release. This conduit is felt to be responsible for the horizontal distribution of the released sodium bearing waste as evidenced by high concentrations of gamma radiation observed in well and boreholes throughout the tank farm area. It is this gamma radiation that will be used to determine the initial release configuration, in addition to supplying some measure of model verification.

J-7.1.1 Cesium and Strontium Field Data

As shown in Section J-5, because of the high selectivity for cesium, it is rapidly adsorbed onto the exchange sites in the INTEC alluvium, and after a very brief period of initial migration, essentially becomes a non-mobile contaminant. This lack of mobility can be used as an indicator of how the initial relatively high-volumetric flow was dispersed in the alluvium. Quantifying this initial distribution is important because it determines the amount of mineral contacted during the initial rapid buffering period as the calcite is dissolved.

In Section J-5, a 1-Dimensional model was used to illustrate the coupled hydrogeochemical transport of competing cations in an ion exchange model. Those 1-Dimensional simulations were based on a horizontal dimension of 60 m X 30 m, which means that the CPP-31 release was applied uniformly over this dimension. In those simulations, there was adequate calcium to rapidly buffer the pH of the infiltrating solution. As this areal extent is changed, the dynamics of the geochemical evolution will change.

In order to constrain the horizontal dimension for the site-specific application of this model, we have relied on the field collected gamma data. Gamma radiation near CPP-31 is due predominately to the presence of cesium. In the initial release, Cs-134 (1.01e-3 Ci/L, half-life of 2.1 years) and Cs-137 (2.38e-01 Ci/L, half life of 30.2 years) were both present and at early times would have contributed to measured gamma emissions, while at late times, the gamma emissions would be primarily attributable to Cs-137. CERCLA site CPP-31 within the INTEC tank farm has been surveyed to obtain the gamma distribution during four different time periods: 1975, 1983, 1992, and 2004. The 1975 data were collected from 32 locations to depths of 25 ft. Gamma radiation was measured by lowering a radiation detector down the well or exploratory hole, and because of the instruments used, the measurements are not comparable to the current acceptable methods. In addition, these early measurements would have been influenced by both Cs-137 and Cs-134, requiring that data be available to convert the gamma readings to soil concentrations in order to use this data. As a result, this data was not combined with data collected during more recent surveys for use here. The 1983 data were collected from 24 locations to depths of up to 30 ft. The only record of these gamma radiation measurements is a paper copy reporting results, and lacks method details. As with the 1975 data, the 1983 data was not used. The 1992 data were collected from 10 wells at every other foot of depth up to 24 ft. All of these wells were re-logged in 2004 when a more complete survey was conducted. The 2004 data (See Appendix F of this document for details) were collected from 50 wells using a AMP-100 and AMP-50 downhole gamma loggers to depths of up to 56 ft. Additionally, there were 14 boreholes within CPP-31 surveyed to depths of up to 39 ft. In order to correlate the gamma readings with soil concentrations, the 2004 effort also included taking core samples from Sites CPP-28, CPP-31, and CPP-79 at locations associated with the highest gamma radiation, and sending these cores for laboratory analysis of soil concentrations.

There was a positive correlation between the natural log of gamma radiation (mR/hr) and natural log of Cs-137 soil concentrations (pCi/g) across the range of values. The zero mR/hr down-hole gamma readings were considered non-detects and were removed from consideration in this analysis. Also, the gamma readings between 0 and 1 mR/hr were not correlated to the Cs-137 results, so the data sets used to derive the correlations were reduced to contain only gamma readings greater than or equal to 1 mR/hr. A regression was fit to the natural log of Cs-137 and natural log of gamma readings, using indicators for data from the three sites. The possibility of significant differences in intercept or slope was incorporated into the regression equation through indicator variables (Z). The full model was:

$$\ln Y = \beta_0 + \beta_1 \ln X + \beta_2 Z_1 + \beta_3 Z_2 + \beta_4 Z_1 \ln X + \beta_5 Z_2 \ln X + \varepsilon \qquad \text{(J-7-1)}$$

where,

Y	=	Cs-137 soil concentrations (pCi/g)
X	=	gamma reading (mR/hr)
Z1	=	indicator of data from Site CPP-28
Z2	=	indicator of data from Site CPP-31
β_i	=	parameter coefficients to be estimated
ε	=	unknown error

The indicator variables equaled one for data from that site and zero otherwise. The main effect Z terms represented possible differences in model intercepts among the CPP sites. The interaction terms (Z×ln(X)) represented possible differences in model slopes among CPP sites. If the corresponding coefficients were significantly different than zero, then significant differences exist. Insignificant terms were removed, leaving

only site-terms that significantly differed. Removal of insignificant terms (Z1, Z1×ln(X), and Z2×ln(X)) resulted in the following model

$$\ln Y = 5.02 + 1.43 \ln X - 1.85 Z_2 \quad \text{(J-7-2)}$$

The CPP-31 (Z_2=1) regression equation used to convert the gamma radiation (mR/hr) to Cs-137 (pCi/g) was:

$$\ln Y = 3.17 + 1.43 \ln X \quad \text{(J-7-3)}$$

For ease of comparison to the transient ToughReact predictions of Cs-137 soil concentrations, the field soil concentrations were un-decayed from 2004 to the release year of 1972.

After conversion of the data to 1972 pCi/g activity, the values were Krigged to predict Cs-137 over the area of interest within CPP-31 (Figure J-7-2). The krigging was done using automated algorithms within EVS (Ctech, Inc.). The predictions were made with a maximum allowable predicted activity of 5E7 pCi/g. The uniformly gridded soil concentrations were then used to estimate the initial activity at the time of release:

$$Ci_{total} = \sum_{i = 1, ngrids} \rho_{Bulk} Y_i V \quad \text{(J-7-4)}$$

where

ρ_{bulk} = 1300 kg/m^3 is the bulk density

Y_i = predicted soil concentration in each grid

V = volume of each grid (2.1 x 1.5 x 1.1 = 3.5 m^3)

This resulted in an initial release activity of 14,500 Ci of Cs-137, about 10% below the assumed source term of 16,000 Ci. The difference between the Cs estimated to be on the soil and the assumed source arises because the calculation neglects Cs existing in the aqueous phase. The resulting distribution of soil concentration for Cs-137 shown in Figure J-7-2 suggests that the high-volumetric rate of release was not dominated by gravity, and instead flowed along the top of the conduit resulting in a nearly uniform distribution along the 40 m length. There is less spreading of the higher concentrations transverse to the axial direction, and less vertical migration. Figure J-7-1 presents a summary of this distribution, and shows that the bulk of soil is contaminated between concentrations of 1E5 and 1E7 pCi/g. The region contaminated at the 1E8 level is much smaller.

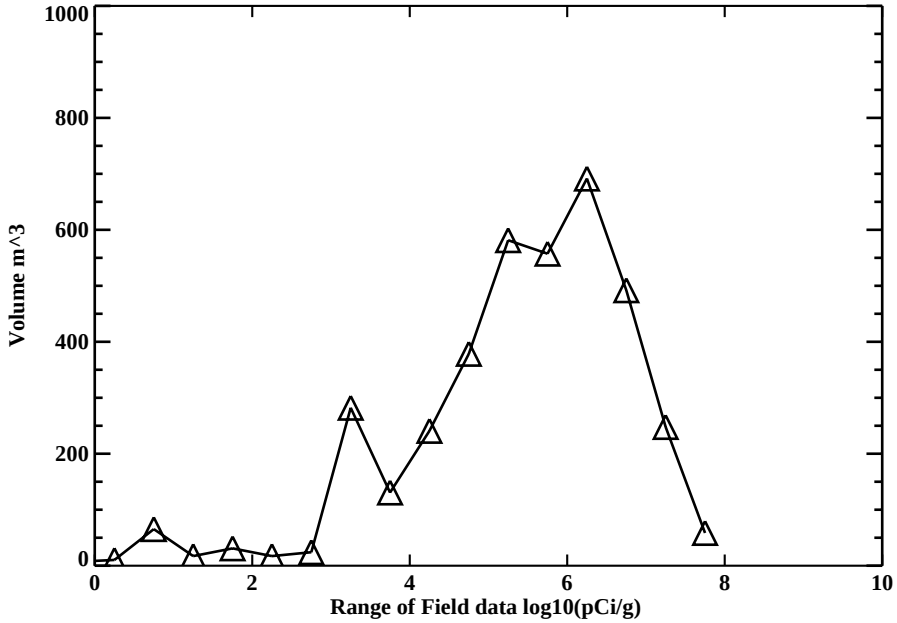

Figure J-7-1. Volume of Cs-137 contaminated soil plotted as a function of soil concentration as (log10(Cs pCi/L)). This figure is the histogram of soil-concentration normalized by the volume occupied.

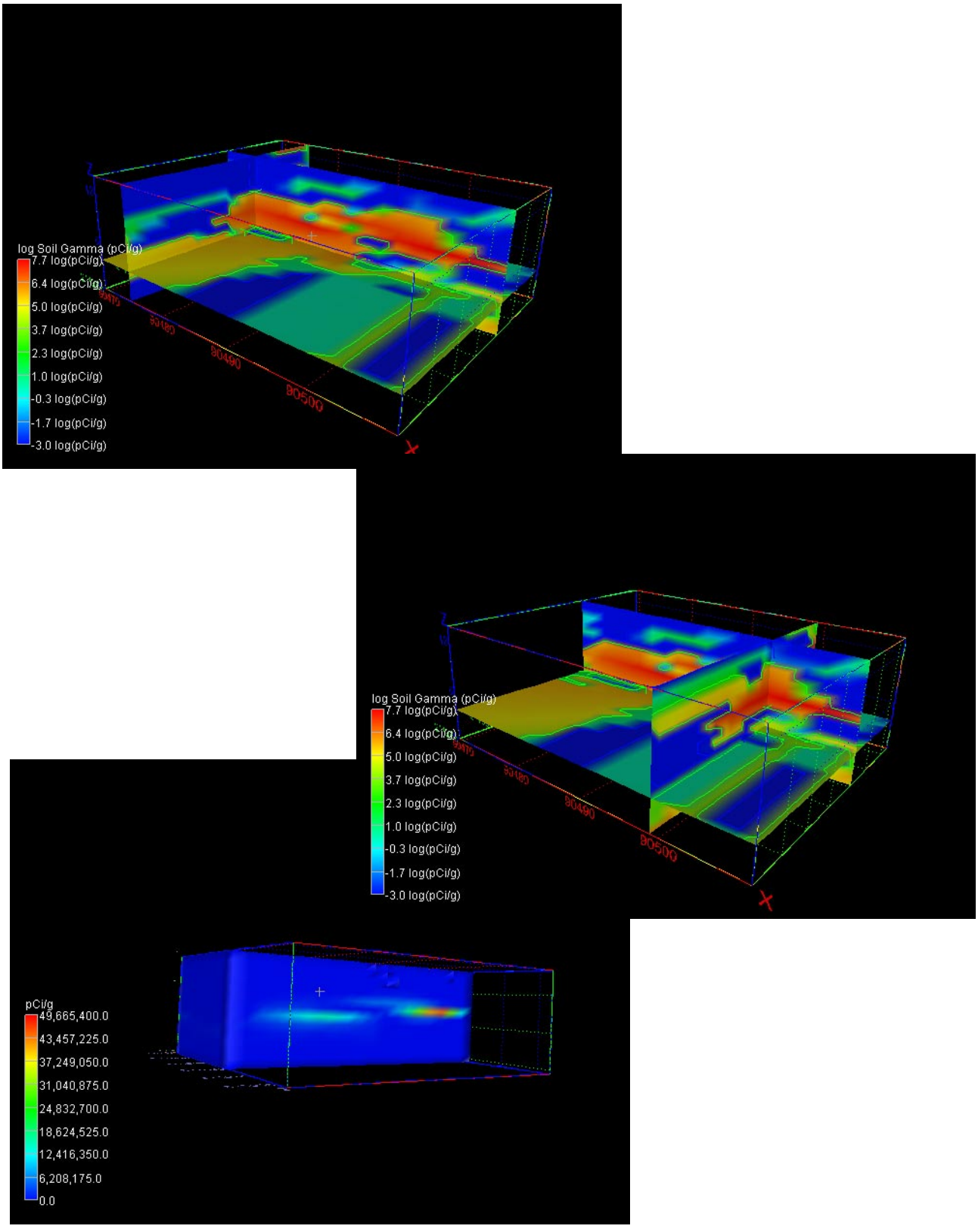

Figure J-7-2. Krigged Cs-137 soil concentrations decayed to 1972 (log10 in pCi/g). Dimensions are 40 m X 32 m X 14 m.

This analysis suggests that the initial fluid containing the highly adsorbed cesium was distributed along an axial distance of roughly 40 m and a transverse distance of 15 m (area of 600 m^2). The vertical transport would have been dominated by gravitational forces, and controlled by the cation exchange process discussed in Section J-5. In the absence of the barrier, and given the hydrologic properties currently assumed for the alluvium, this release would have migrated vertically from the point of failure and would have spanned a much smaller areal extent. To accomplish this spreading, the following simulations for the CPP-31 release do not use a "point release", but include the barrier in addition to distributing the release over a representative area of 600 m^2.

J-7.2 Site-Specific Configuration for CPP-31

The base model used in this analysis is a three-dimensional representation of the CPP-31 release. Beginning with the previously parameterized 1-dimensional hydrogeochemical model, the horizontal plane (X-Y plane) was subdivided into 20x5 grid blocks each 3x6 m^2 in area. This results in a final discretization of 20x5x36 blocks over a volumetric extent of 60x30x18 meters oriented in the x-y-z directions. Under the release location, a low-permeability, low-porosity, geochemically inert barrier was placed at a depth of 5 m. This barrier represents the plumbing conduit that underlies the CPP-31 release location. It is thought that the released fluid flowed along this barrier, and was distributed horizontally under capillary and dispersive forces prior to being transmitted vertically through the alluvium. The barrier is represented by one grid block in both the Y- and Z- directions, and extends 54 m in the X-direction. In an attempt to reproduce as much of the actual hydrologic condition present at the time of release, the leak was simulated to occur over a period of 5 days, and was initially released in a single grid block. The released liquid flowed across the top of the barrier, and leaked over the edges into the next two adjacent grid blocks in the horizontal plane. After only 50 days, the water saturation in the vicinity of the barrier stabilized, achieving pseudo-steady state with respect to water potential and saturation. When the leak chemistry was included in this initial simulation, the numerical solution became unstable, and chemical mass balance was lost. The loss of mass balance is a function of the manner in which TOUGHREACT accounts for liquid volume in each cell as the saturation changes in time. In order to achieve numerical stability, the sodium-bearing waste was released in the model over a time-period of 50 days (rather than 5 days). The resulting saturation profiles are similar at the end of the 50 days, indicating that this modification was insignificant from the perspective of area contacted by the infiltrating fluid. The model was then run for a twenty year time period, to obtain the activity of cesium and strontium leaving the alluvium and to obtain the effective K_d for the activity remaining in the alluvium.

For consistency with the presentation of the fate and transport of other contaminants considered in this RI/BRA, we have selected a parameter set that will be the base-case against which other parameterizations will be compared. The base-case presented below assumes a cation exchange capacity of 7 meq/100 g, background infiltration of 18 cm/yr, release duration of 50 days, and release area of 600 m^2. Sensitivity to geochemical parameters and hydrologic conditions will follow the presentation of base-case results. Following the sensitivity, a discussion of implications will be presented for the various parameterizations. This differs from the format of presentation for the other contaminants considered in this RI/BRA because the implications with respect to the amount of Sr-90 remaining in the alluvium, its mobility, and the amount and mobility of Sr-90 entering the interbeds of the alluvium will ultimately play a key role in determining the end-state of the contaminated soils at INTEC. The discussion of implications requires an understanding of the complete hydrogeochemical system.

Results presented and discussed in the following sections consider the evolution of constituents released at Site CPP-31 in the alluvium, the state of strontium remaining in the alluvium, the flux rate of activity leaving the alluvium in the first 20 years (explained below), and the downward migration of strontium as it passes from the alluvium and enters the aquifer. To accomplish this, the geochemical model is first run for a given parameterization to obtain the spatio-temporal distributions of 1) aqueous phase strontium species in the alluvium, 2) strontium sorbed to the solid phase, 3) effective adsorption coefficient computed as an activity-weighted average, and 4) the flux of strontium activity leaving the alluvium. This activity flux becomes the source-release term that is input into the base grid model (Appendix A, Section 5.1.1) of the vadose zone, which in turn, becomes the source-term for the complete vadose zone transport model for Sr-90.

The Sr-90 activity that is remaining in the alluvium was also put into the base grid model as a source term, located at the location of highest measured soil concentrations in 2004. The effective K_d was then applied to the base grid model alluvium. As a result of this process, there is a different activity-release function for each parameterization that accounts for the initial transient sorption process which approaches a pseudo-steady state after about 20 years of evolution. As with the prediction of other contaminant aquifer concentrations, the activity flux from the vadose zone is then input into the aquifer model (Appendix A, Section 5) and the spatio-temporal distribution of aquifer concentrations are computed.

J-8 RI/BRA MODEL RESULTS

Based on an analysis of the available CEC data for the alluvium, the operational range spans 2-15 meq/100 g, and based on a review of available interbed adsorption characteristics, the range spans 20-85 mL/g. Within these ranges, the most probable values for INTEC materials are a CEC in the alluvium of 2 meq/100 g, and an interbed K_d=50 mL/g. These parameters form the basis of the risk predictions contained in the summary of Sr-90 in Appendix A. Results using these parameters are presented in the following sections for the migration of Sr-90 through the alluvium, vadose zone, and aquifer. Throughout this document, these results are referred to as the RI/BRA model results.

J-8.1 Geochemical Evolution in the Alluvium

ToughReact was parameterized using a CEC=2 meq/100 g, an infiltration rate through the tank farm of 18 cm/yr, and the previously discussed hydrogeochemical properties of the alluvial material. This model was used to compute the resultant water saturation and the distribution of chemical species through time.

Figure J-8-1 presents the time-evolution of water saturation as intersecting perpendicular slices through the model domain. The initial saturation is 31% throughout the bulk of the region, with lower initial saturations directly under the barrier, and 100% saturation along the bottom of the modeling domain representing the perched water. The region of high saturation near the center-top of the domain, and extending 54 m in the X-direction, and 6 m in the Y-direction corresponds to that of the barrier. It has a porosity of 0.1%, and hydraulic conductivity 1/100th that of the surrounding alluvium. Although the saturations in the barrier are 100%, the relative volume is small. The low barrier permeability results in a lower saturation directly under the barrier by diverting the background infiltration water originating from precipitation. This halo effect will be observed in all of the subsequent plots of concentration as the released liquid flows along the barrier, and spills over the sides. High transmissivity of the alluvium retards lateral migration away from the line-source of release, allowing nearly vertical transport of the sodium bearing waste. Perched water is represented in this figure in the bottom grid block (red), and the lower saturations just above the perched water are a consequence of the basalt units underlying the alluvium. These basalts are much thicker in the full vadose-zone model, but the effect of the capillary break imposed by their presence is captured here. The open flow bottom boundary allows contaminants to exit the system without having to impose a geochemical boundary condition.

The time-evolution of saturation shown in Figure J-8-1 illustrates the small increase in saturation resulting from the CPP-31 release and its relatively rapid re-equilibration. Although seemingly large, 18600 gallons is equivalent to 70 m^3. It is distributed over the 600 m^2 area corresponding to the horizontal cross-sectional area impacted by the gamma radiation. This results in a small increase in saturation over that area, which coupled with the high permeability, low capillarity alluvium hydraulic properties, is rapidly transported downward along nearly vertical flow paths. The pseudo-steady state saturation prior to the CPP-31 release is 31%, and the porosity is 32%, resulting in a residual moisture content of 10%.

The overall transport of the sodium bearing waste follows the geochemical processes discussed in Section J-5, with the Sr-90 transported downward as either SrNO3, Sr+, SrCO3, and SrOH (listed in order of abundance). The remaining non-aqueous phase Sr-90 is held in place on the cation exchange sites. The most abundant aqueous species, SrNO3, is rapidly transported through the alluvium as shown in Figure J-8-2 at 4, 12, and 18 months after the initial release. The next abundant species, Sr+ ion, is as mobile as the SrNO3 as shown in Figure J-8-3. This figure shows that the Sr+ ion reaches the basalt-alluvium interface after roughly 3 years. In both cases, the Sr+ ion and SrNO3 move basically as pulses of contaminant with a very small residual remaining near the barrier. SrCO3 migrates more slowly, is much less abundant (Figure J-8-4), and is more uniformly distributed over the vertical direction. This indicates that it is continually replenished with changing geochemical conditions. Migration patterns for SrOH are given in Figure J-8-5, and the very small abundance of this species is indicated in the color key. Its migration pattern indicates that, like Sr+ and SrNO3, it basically moves as a pulse.

The combined aqueous-phase Sr-90 is given in Figure J-8-6. This distribution is similar to that for Sr+ and SrNO3, the primary species in solution. From this figure, it is difficult to discern the bimodal transport of Sr-90 that was apparent in the 1-dimensional analysis presented in Section J-5. However, it is readily apparent in the summary plot of flux leaving the alluvium shown in Figure J-8-9. There mobilities of SrNO3, Sr+, SrCO3, SrOH, are given in Figure J-8-9 (A-D). For ease in comparison, the subspecies are overplotted in Subplot E and are combined as total Sr-90 continually being transferred into the aqueous phase from the exchange sites in Subplot F. Figure J-8-9 (G) shows the cumulative Sr-90 that has been transported out of the bottom alluvium plane, and Figure J-8-9 (H) presents the rate at which the activity leaves the alluvium. There are three primarily different flux rates shown in the latter subplot, corresponding to the different mobilities of SrNO3, Sr+, SrCO3, SrOH, and to the Sr-90 that is continually being transferred into the aqueous phase from the exchange sites. It is key to note that after 5, 10, 15, and 20 years, the total Sr-90 that has entered the vadose zone under the alluvium is 5187 , 12272, 12310, and 12336 Curies, respectively. From this, it is readily apparent that there is an initial rapid release of Sr-90 within the first 5 years, followed by a slow-steady release that occurs at a much retarded rate dictated by the cation exchange process.

The distribution of Sr-90 on exchange sites (adsorbed) shown in Figure J-8-7. Initially, there is no Sr-90 on the exchange sites, with all of the Sr-90 existing in the aqueous-phase. Even after six months, there is very little Sr-90 on the exchange sites below 6 m in depth. However, after roughly 5 years (Figure J-8-9-I) the distribution of Sr-90 on the exchange sites (solids) is essentially constant. As the aqueous-phase Sr-90 moved through the alluvium, the lateral distribution was quite small, with very little of the Sr-90 migrating directly beneath the barrier, and with very little overall transverse dispersion.

The ratio of adsorbed to aqueous-phase activity is reflected in the transient nature of effective adsorption coefficient (given by Equation J-5-2) and is shown in Figure J-8-8. This figure illustrates that even after 16 months (4/1973), the strontium mobility was essentially unretarded. After 7 years (1979), the effect of adsorbing Sr-90 onto the exchange sites begins to become apparent, resulting in an increase in the activity-weighted K_d. After 19 years, the adsorption coefficient is nearly constant, but still spatially variable and ranges within the plume between 0.7 and 6 mL/g. An activity-averaged K_d value was computed for each time using:

$$\overline{K_d} = \frac{\sum C_{solid}(pCi/g)K_d}{\sum C_{solid}} \qquad \text{(J-8-1)}$$

where C_{solid} (pCi/g) is the concentration of the Sr-90 on exchange sites in each grid block, K_d (mL/g) is the adsorption coefficient computed at each grid block, and the sum is restricted to those grid blocks where the solids concentration is non-zero. Clearly, this average K_d is evolving in time, but as shown in Figure J-8-9 (j), it eventually approaches a pseudo-steady value of 2 mL/g. After 20 years, there are 3564 Ci remaining in the alluvium, with most of that existing on the exchange sites (as opposed to being in the pore water).

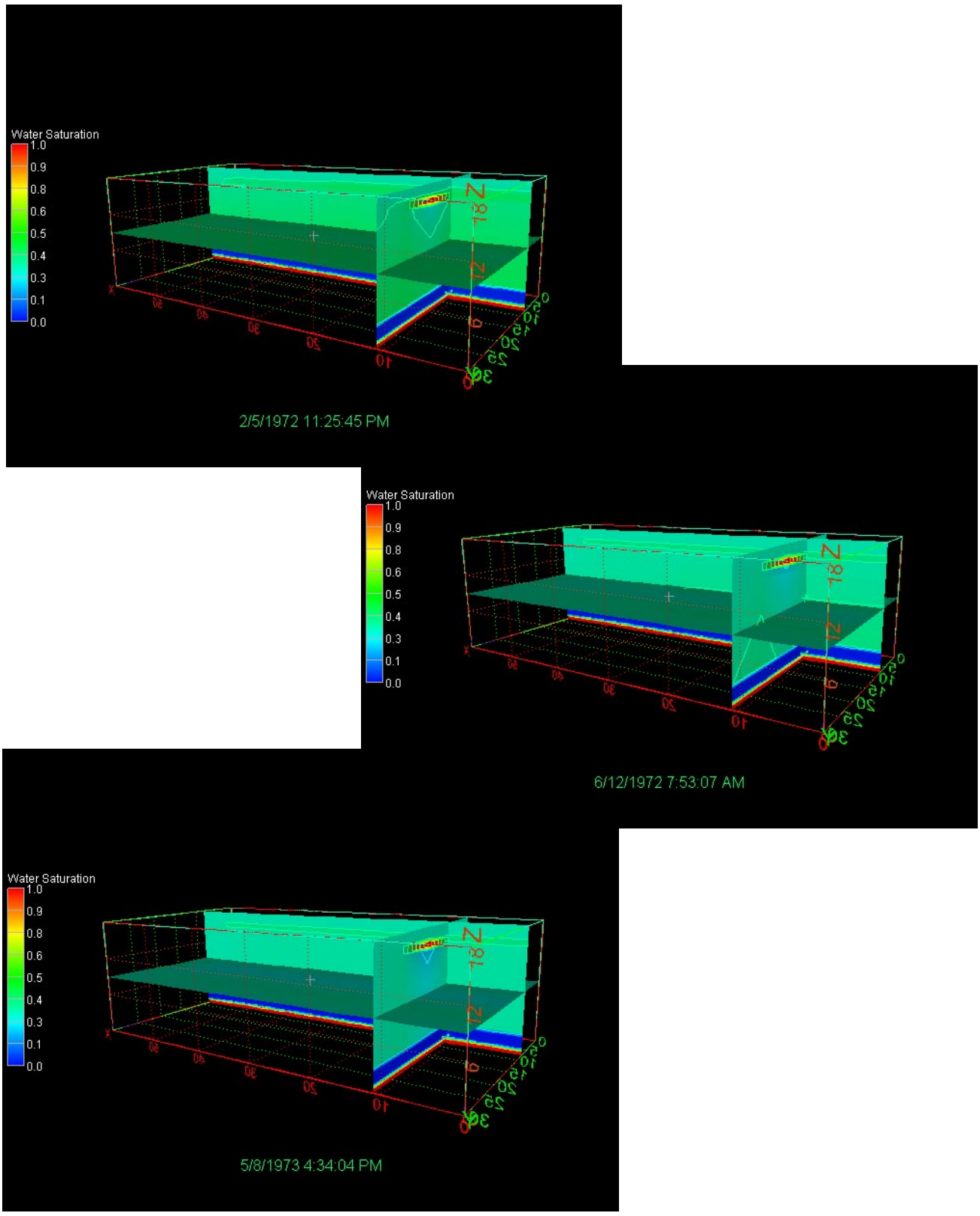

Figure J-8-1. RI/BRA base case: water saturation 1, 5, and 17 months after CPP-31 release showing rapid re-equilibration in saturation and small net increase in saturation.

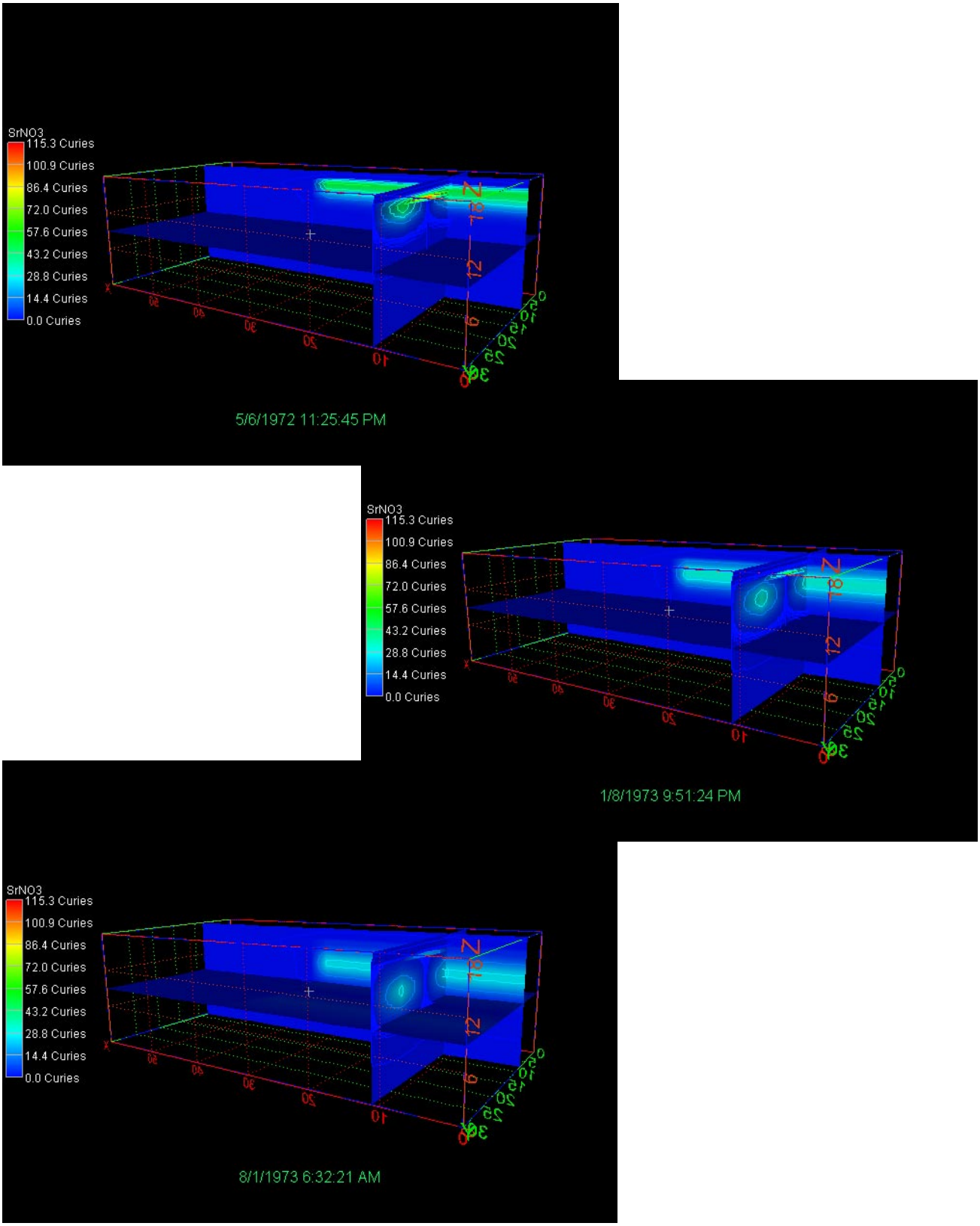

Figure J-8-2. RI/BRA base case: SrNO3 4, 12, and 18 months after CPP-31 release.

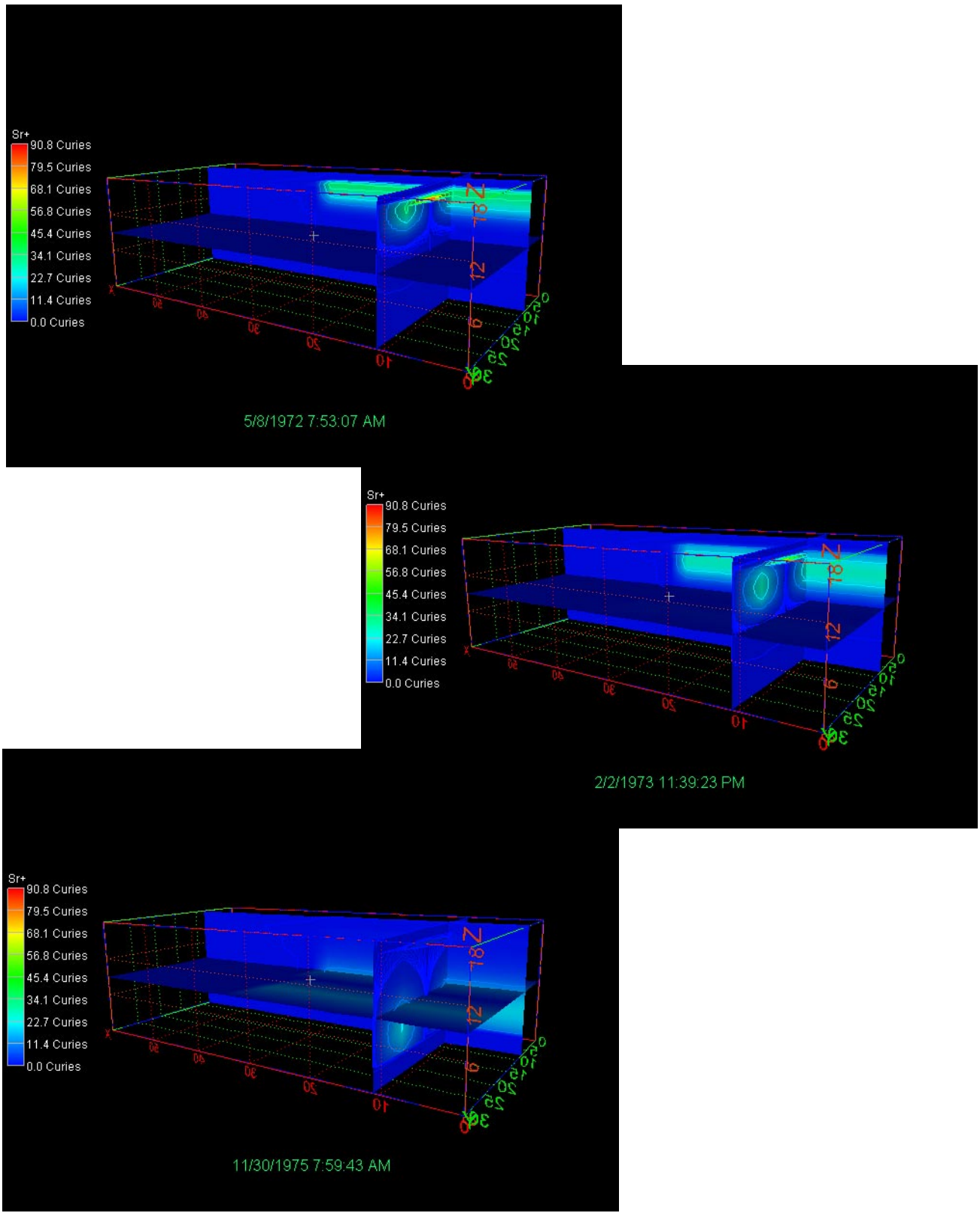

Figure J-8-3. RI/BRA base case: Sr+ the aqueous phase 4, 13, and 48 months after CPP-31 release.

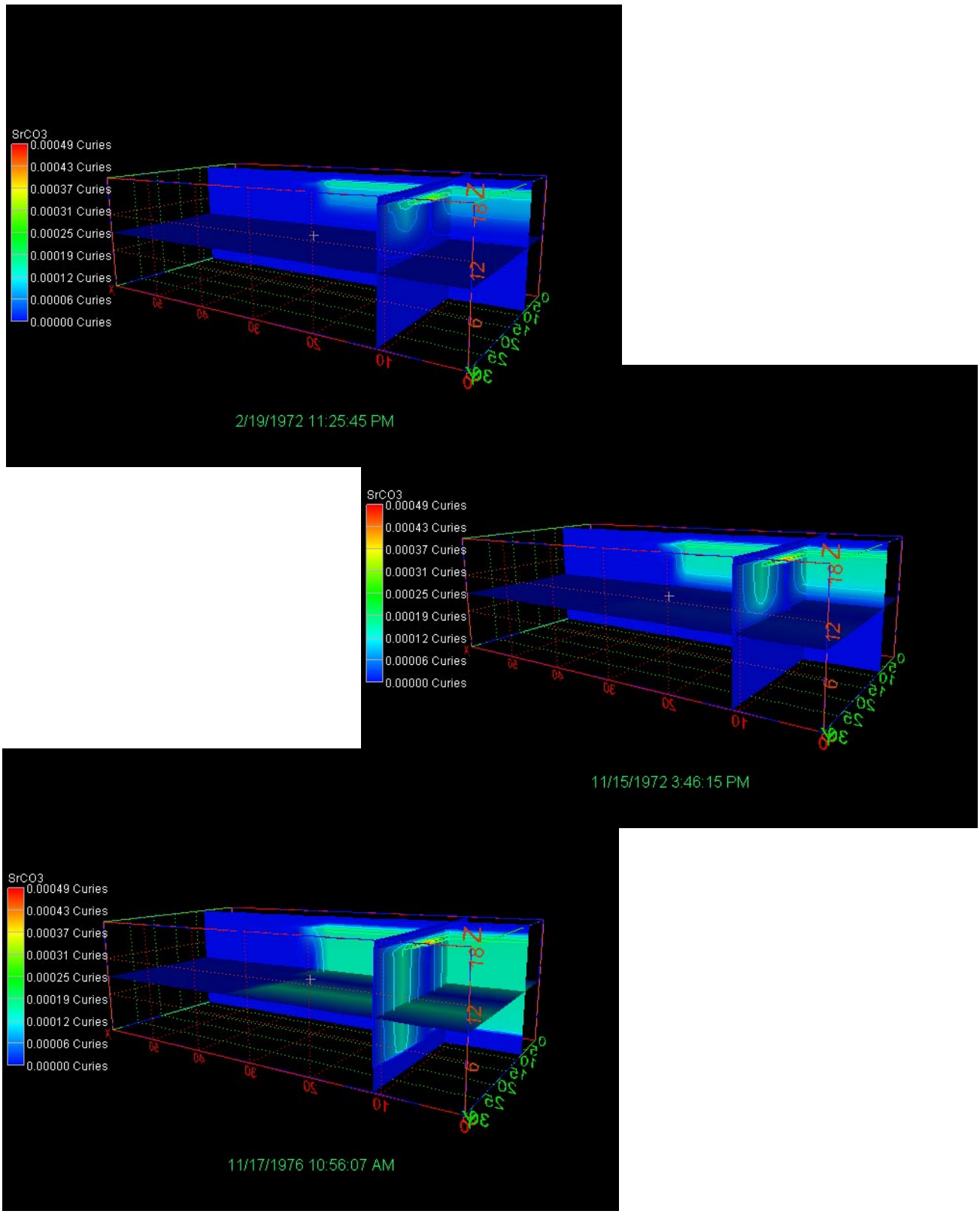

Figure J-8-4. RI/BRA base case: SrCO3 1 month, 10 months, and 5 years after CPP-31 release.

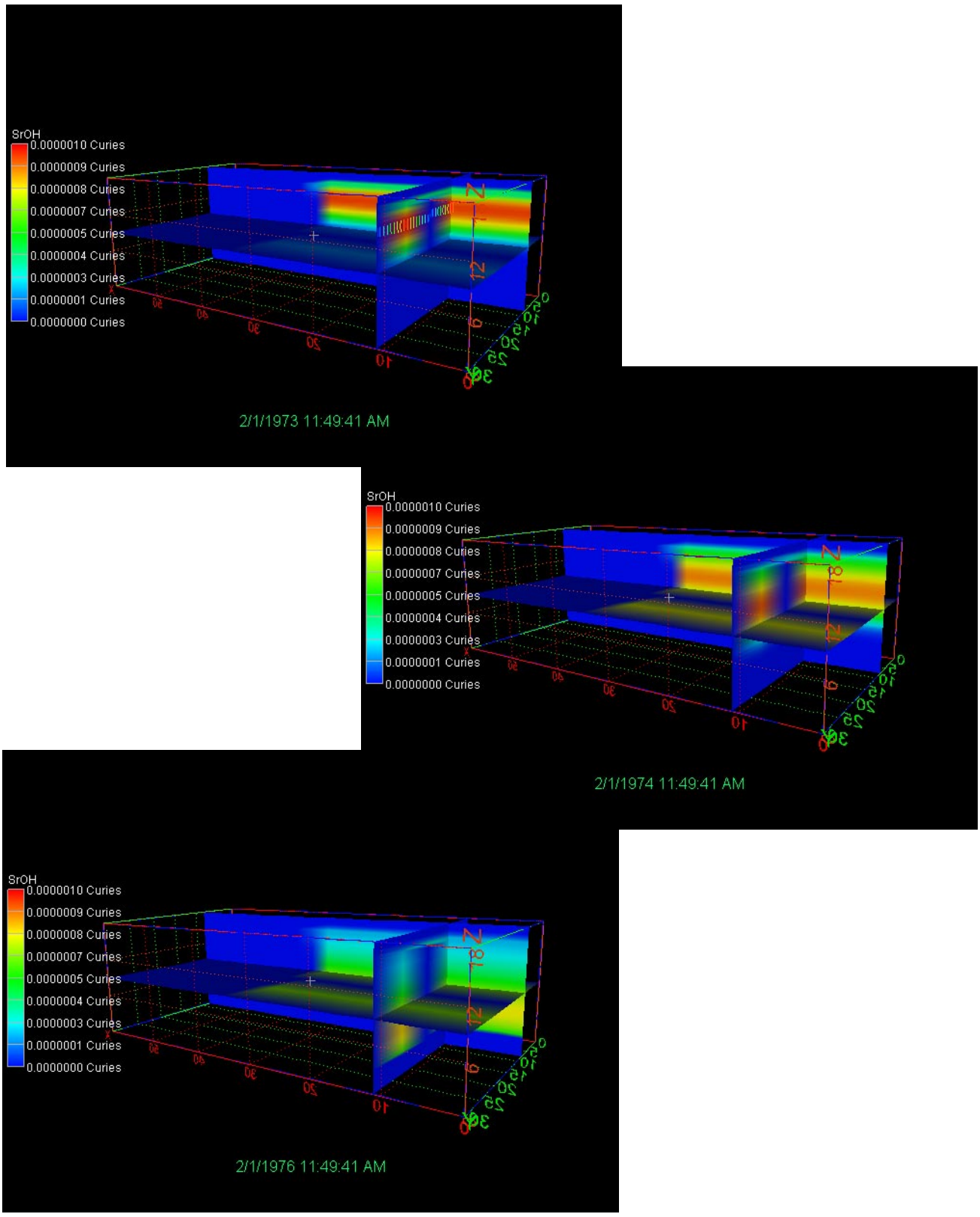

Figure J-8-5. RI/BRA base case: SrOH 13, 24, and 48 months after CPP-31 release.

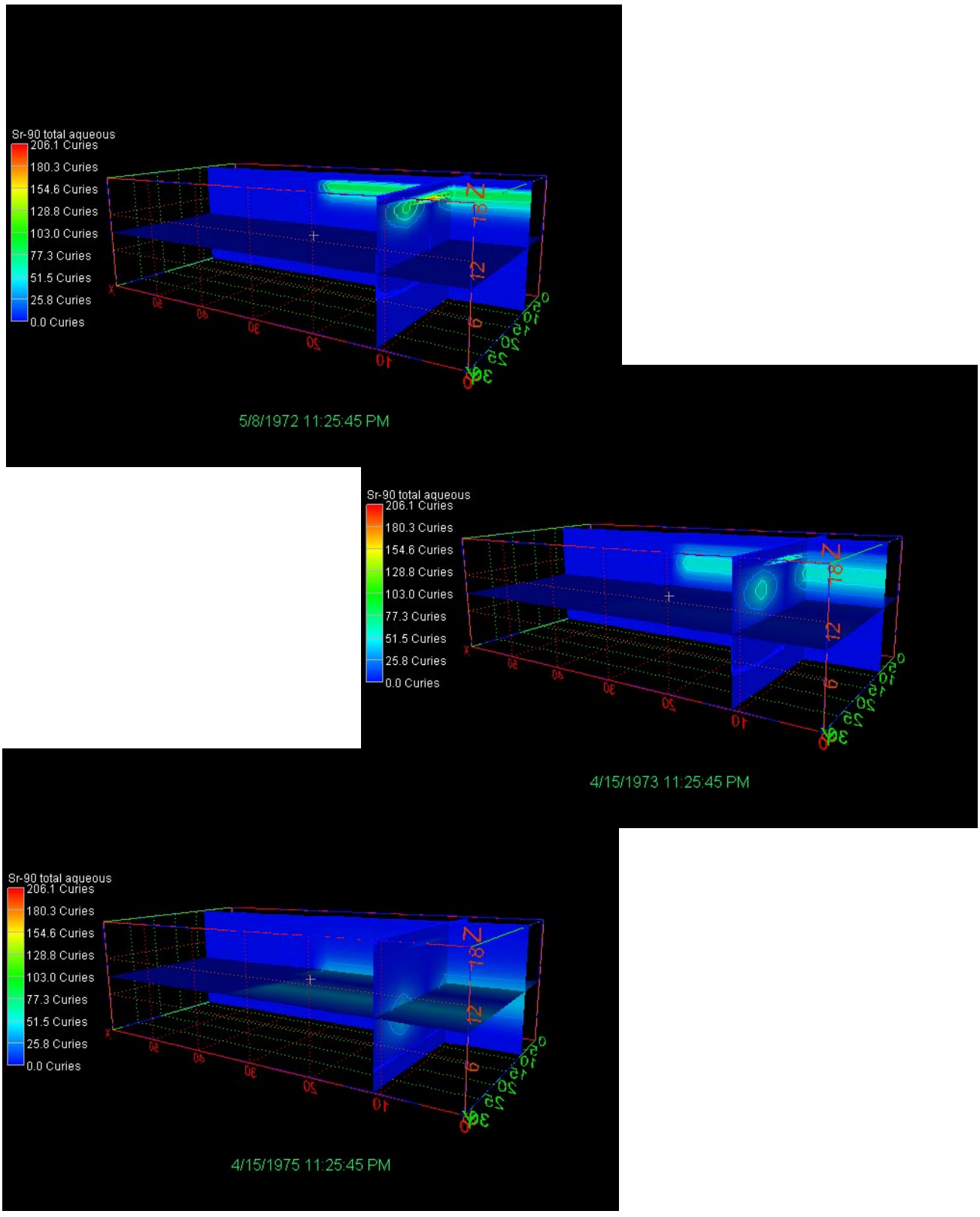

Figure J-8-6. RI/BRA base case: total aqueous-phase Sr-90 0.5, 1.5, and 3 years after CPP-31 release.

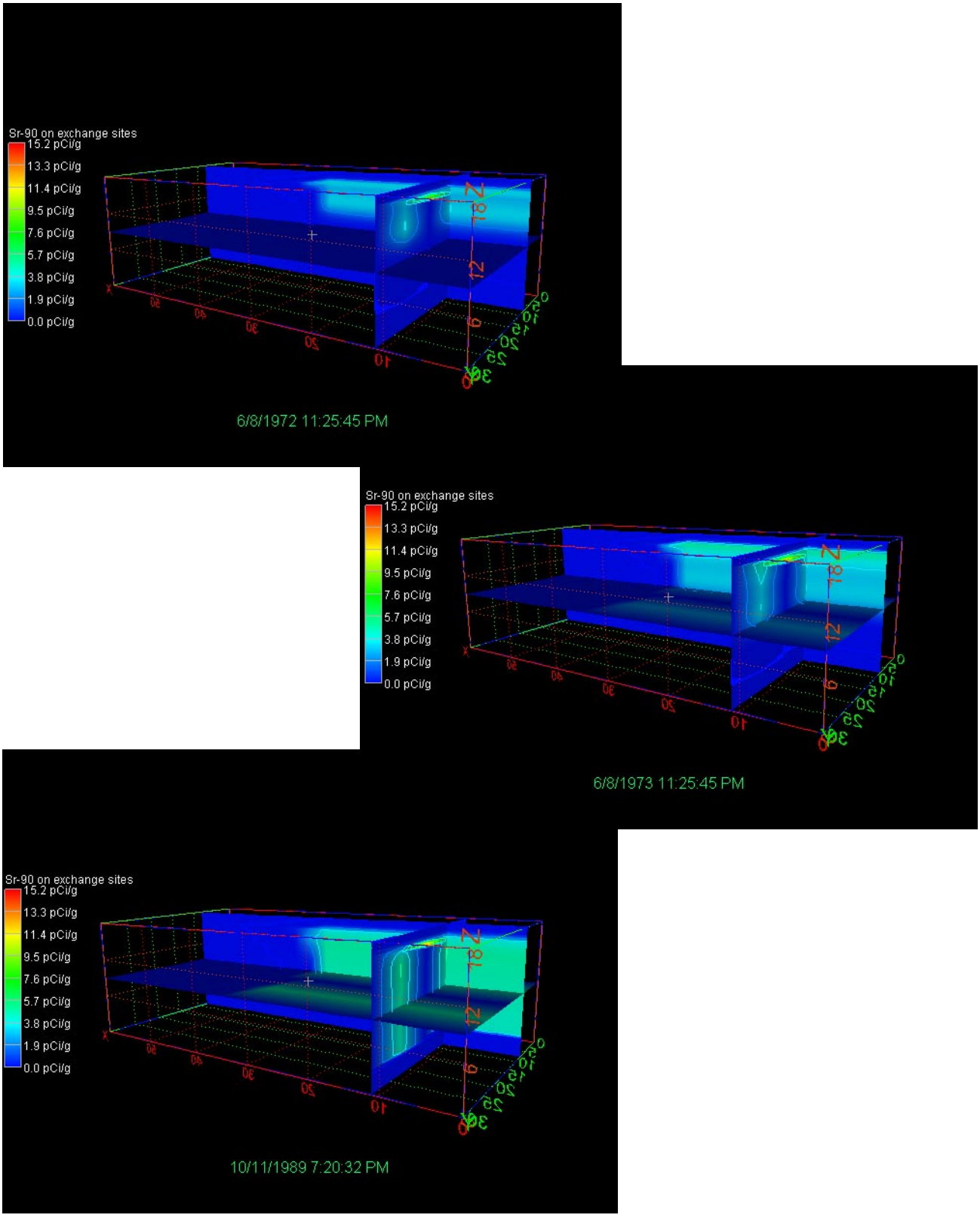

Figure J-8-7. RI/BRA base case: Sr90 on the exchange sites 1,2, and 3 years after the CPP-31 release.

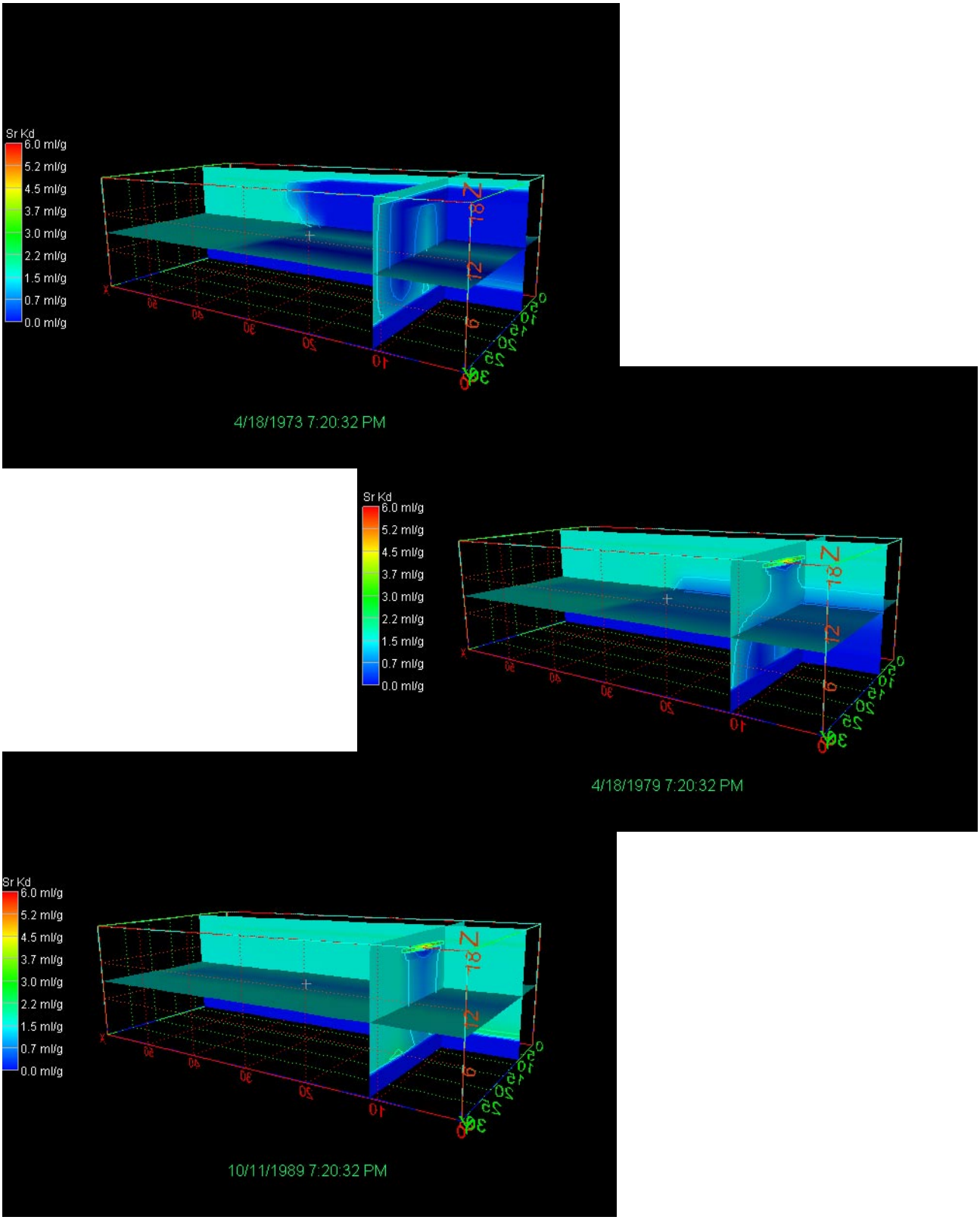

Figure J-8-8. RI/BRA base case: effective partitioning between aqueous and solid-phase Sr-90 0.5, 1.5, and 17.5 years after CPP-31 release.

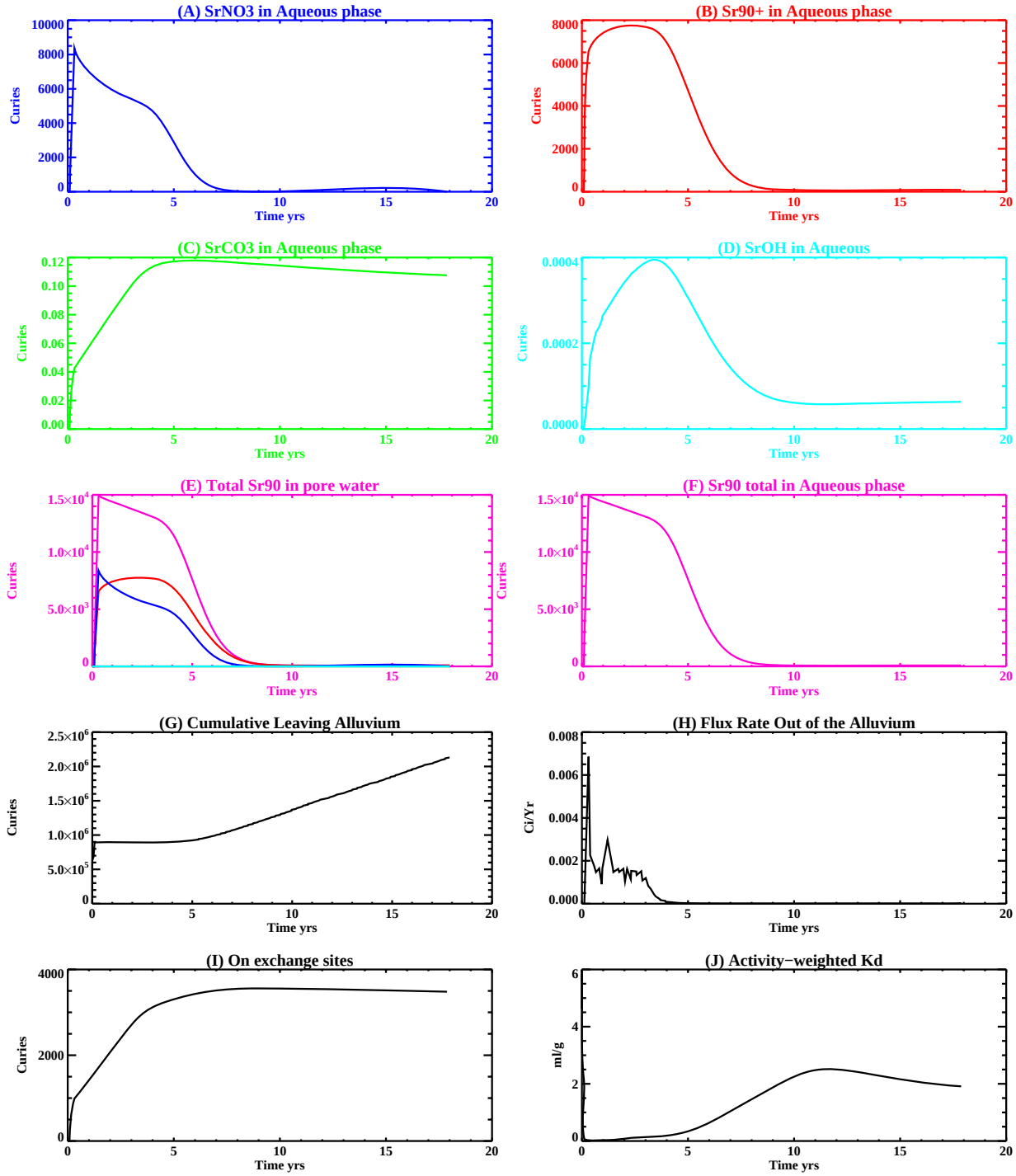

Figure J-8-9. RI/BRA base case: summary figure illustrating the speciation of Sr-90 in the aqueous phase (A-F), total Sr-90 in the pore-water of the alluvium (E), cumulative curies of Sr-90 having left the alluvium (G), flux rate leaving the alluvium (H), Sr-90 on the exchange sites (I), and effective partitioning coefficient (Kd) (J).

J-8.2 Vadose Zone Sr-90 Simulation Results

All sources of Sr-90 were considered in the vadose zone simulations. These included: (1) tank farm sources at 1.81e+4 Ci, (2) OU 3-13 soil sources at 9.18e+2 Ci, (3) CPP-02 abandoned french drain at 33.8 Ci, (4) CPP-3 injection well failure at 8.3 Ci, and (5) the percolation pond at 0.3 Ci. The Sr-90 released directly into the aquifer from the injection well operation was 16.0 Ci. Representation of these sources in the model are as follows:

- 15900 Ci from CPP-31 release in the tank farm were represented using (a) the activity-release function shown in Figure J-8-9 (H) for the 12336 Ci released during the first 20 years, and placing this activity flux directly above the basalt interface of the base model (Appendix A, Section 5.1)). and (b) distributing the remaining 3564 Ci through the alluvium scaled to the measured soil concentrations obtained during the 2004 sampling cycle (Appendix G and Table 5-32). This mapping allowed most of the activity to be placed at the elevation of the highest measured soil concentrations, with less activity located deeper. To simulate the transport of the activity remaining in the alluvium, an effective K_d of 2 mL/g was used (Figure J-8-8 (J)) for the alluvium sediments.
- transport of Sr-90 from sources other than CPP-31 originating in the alluvium, whose location is spanned by the submodel (Appendix A, Section 5.1), were simulated using the submodel. Because these source locations were outside the influence of the high ionic strength, acidic CPP-31 release, a K_d of 20 mL/g was used in the submodel alluvium.
- transport of Sr-90 from sources located outside of the submodel horizontal extent were also placed in the base model used to simulate the transport of the CPP-31 remaining in the alluvium. Because of model limitations, the effective K_d for the alluvium underlying these source locations was also set to the value used to simulate the transport of Sr-90 predicted to remain in the alluvium after 20 yrs (first bullet). The relative magnitude of these sources are small relative to the residual Sr-90 predicted to remain in the alluvium after 20 yrs. In this case, the K_d is smaller than that used to simulate the transport of Sr-90 from sources within the submodel boundary which will result in a slight overprediction of peak aquifer concentrations.

Figures J-8-10 through J-8-13 illustrate the horizontal and vertical distribution of the Sr-90 in the vadose zone through the year 2293. The concentration isopleths on those plots are for 80., 8.0, and 0.8 pCi/L levels as thin red, thick red, and black lines, respectively. These contours represent the concentration of Sr-90 in the pore water in the alluvium in addition to representing the concentration of Sr-90 in the perched water. Even though the anthropogenic water is removed in year 2095, the pore water does not completely dry up. The Sr-90 in the pore water will continue to exist until it decays away, or is transported out of the vadose zone, or the pore water evaporates.

Sr-90 arrival in key perched water wells is presented in Figure J-8-14 and is presented for all of the perched water wells in Section J-12. In the key wells presented here, the mismatch (Figure J-8-15) is generally less than a factor of 10, (log RMS<1., defined in Appendix A, Section 6), with the exception of wells MW-6, 33-4-1, MW-10-2, and USGS-050. The mismatch in MW-06 is associated with one very high measurement in the early 2000s relative to the much lower concentrations observed in the 1990s. Well 33-4-1 is well north of the tank farm, and has much lower concentrations overall. Well MW-10-2 is south east of the tank farm. The overall character of field data is replicated by the model, but the predicted concentration response is over exaggerated. The worst match occurs for well USGS-050, where concentrations are overpredicted by a factor of 400 ($380=10^{2.58}$), and are overpredicted in all of the simulations that follow. As discussed in Appendix A, Section ,6.3.2.1 the casing in this well has historically allowed downward migration of contaminants from higher elevations. The highest concentrations in the vadose zone pore water occur in the shallow interbeds with

lowest concentrations appearing deeper. By allowing rapid migration through this well, the pore water near USGS-050 has much higher concentrations than observed in other deep wells. This leakage has not been accounted for in any of the vadose zone simulations presented here. In most of the key perched water wells, the difference between predicted and observed concentrations differs by less than a factor of 5 (log RMS< 0.76), which is very good given the overall complexity of the vadose zone at INL.

Peak vadose zone concentrations through time are given in Figure J-8-16 and are above 2,000 pCi/L for the entire period. Initial high concentrations in 1968 are a result of the failed injection well. Smaller peaks occurring around year 2000 result from increased flows in the Big Lost River as the fluxes drive higher concentrations from the deeper perched zones into the aquifer. Highest concentrations (1.1E9 pCi/L) in the vadose zone are predicted to occur in 1978 as the initial fast release of activity from CPP-31 arrives in the vadose zone and combines with that released at site CPP-79 deep.

The rate at which this activity enters the aquifer for the RI/BRA base case is shown in Figure J-8-17. The combined releases of Sr-90 originating at land surface result in extensive contamination across the entire INTEC vadose zone. The half-life of Sr-90 is 28.7 years, and is roughly equal to the travel time for surface water to reach the aquifer. Sr-90 retardation in the interbed sediments should increase the Sr-90 travel time to several half-lives, allowing much of the Sr-90 to decay en route to the aquifer. Even with this decay, a significant amount of Sr-90 is still predicted to reach the aquifer with the bulk of the Sr-90 arriving prior to the year 2005. In Figure J-8-17, the CPP-3 injection well failure is responsible for the early fluxes into the aquifer, with Sr-90 originating at land surface arriving after year 2000. Retardation in the alluvium and interbeds coupled with decay greatly reduces the flux of Sr-90 out of the alluvium after year 2010. For a detailed discussion of specific contributors to fluxes through the vadose zone, the reader is referred to Section J-9.

Figure J-8-10. RI/BRA base case: Sr-90 vadose zone concentration (horizontal contours) (pCi/L) (MCL = thick red line, 10*MCL = thin red line, MCL/10 = black line).

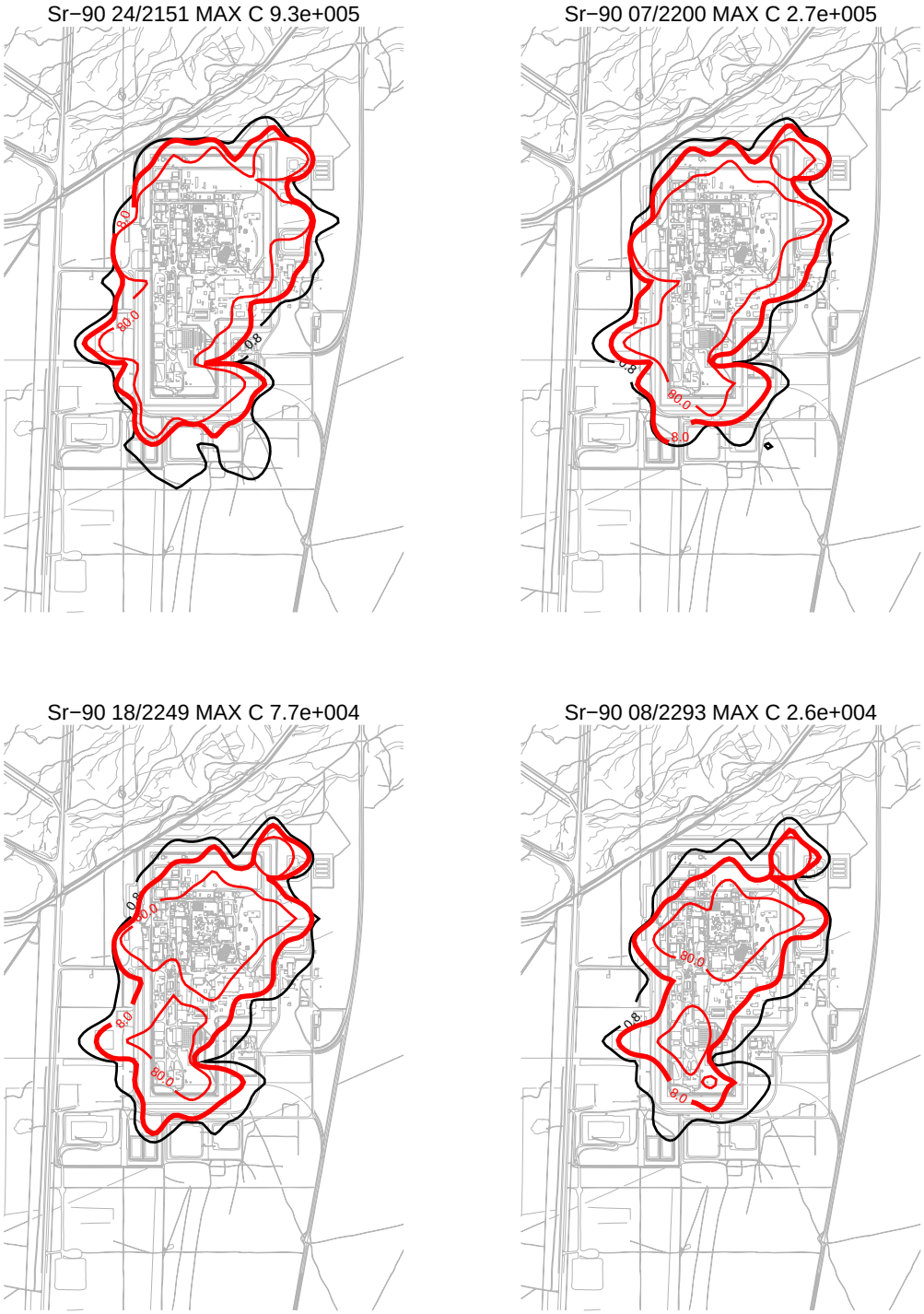

Figure J-8-11. RI/BRA base case: Sr-90 vadose zone concentration (horizontal contours) (pCi/L) (MCL = thick red line, 10*MCL = thin red line, MCL/10 = black line).

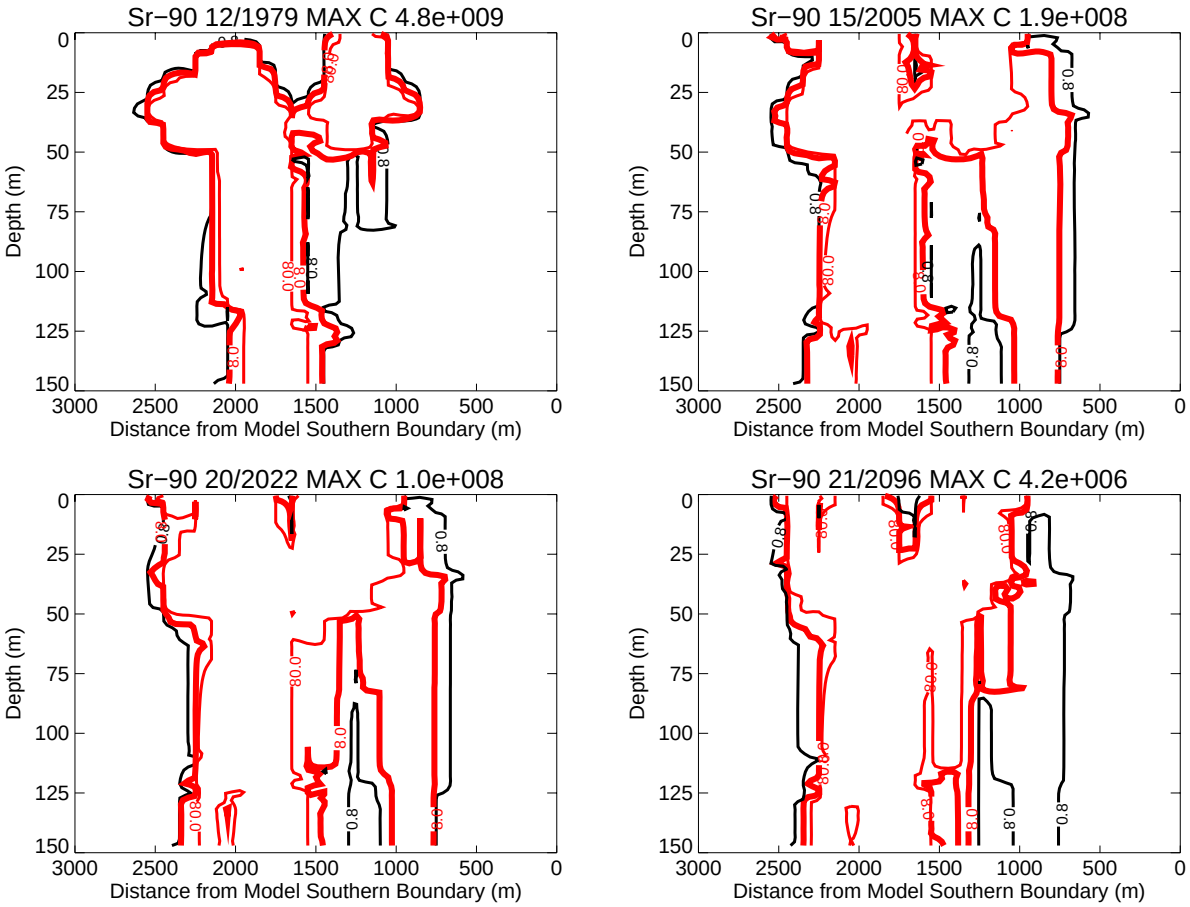

Figure J-8-12. RI/BRA base case: Sr-90 vadose zone concentrations (vertical contours) (pCi/L) (MCL = thick red line, 10*MCL = thin red line, MCL/10 = black line).

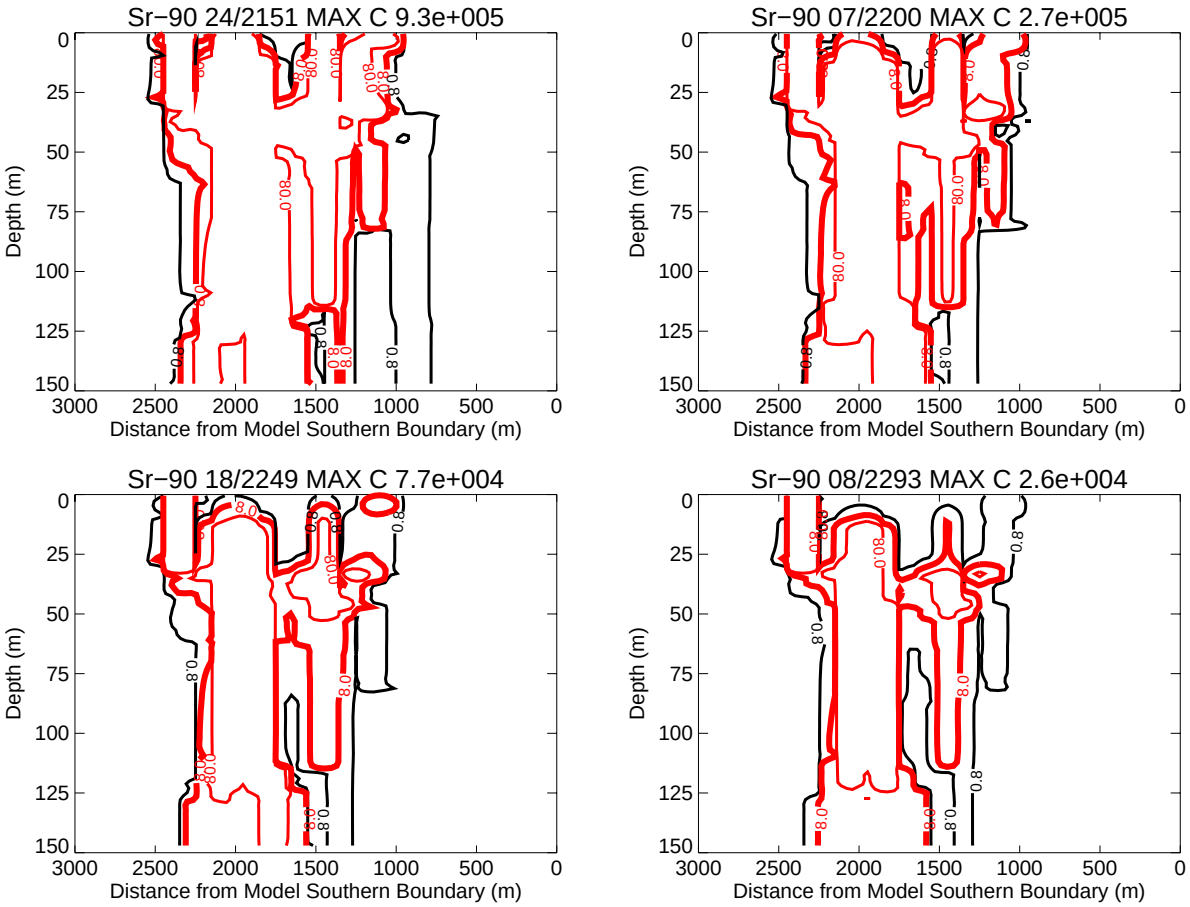

Figure J-8-13. RI/BRA base case: Sr-90 vadose zone concentrations (vertical contours) (pCi/L) (continued) (MCL = thick red line, 10*MCL = thin red line, MCL/10 = black line).

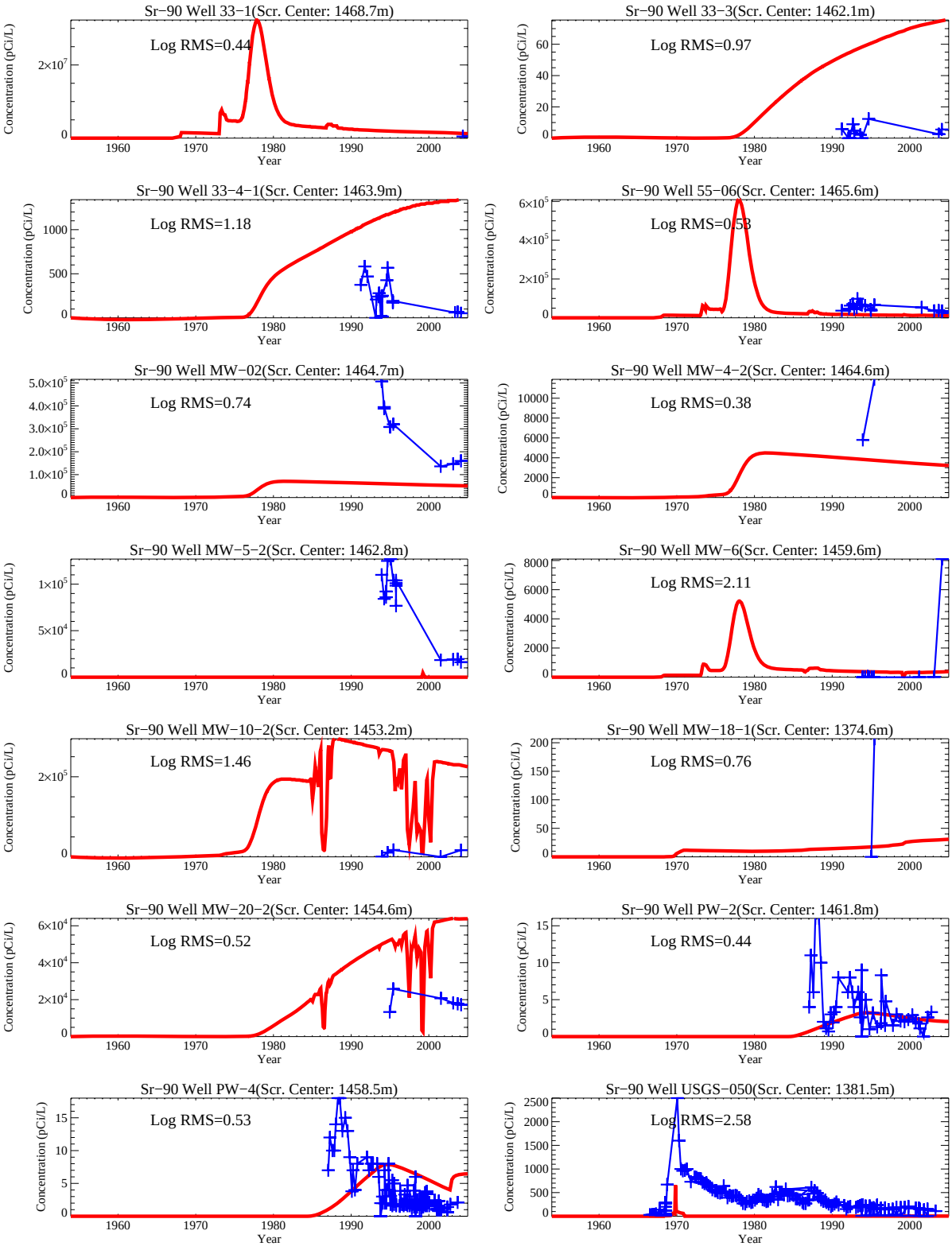

Figure J-8-14. RI/BRA base case: Sr-90 concentration in perched water wells (pCi/L) (Measured values = blue crosses, red = model at screen center).

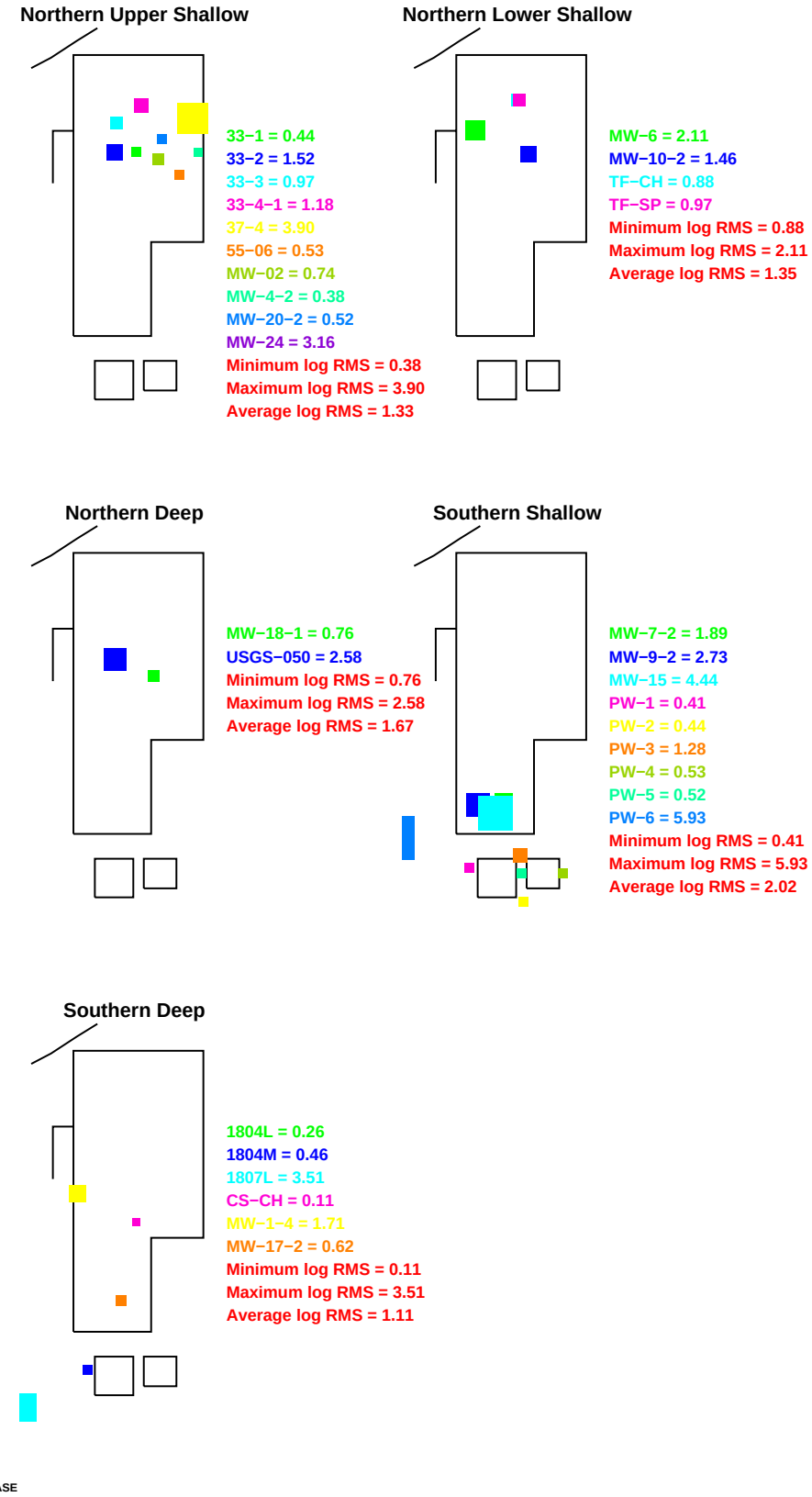

Figure J-8-15. RI/BRA base case: Log 10 Root mean square error (RMS) by depth and northing.

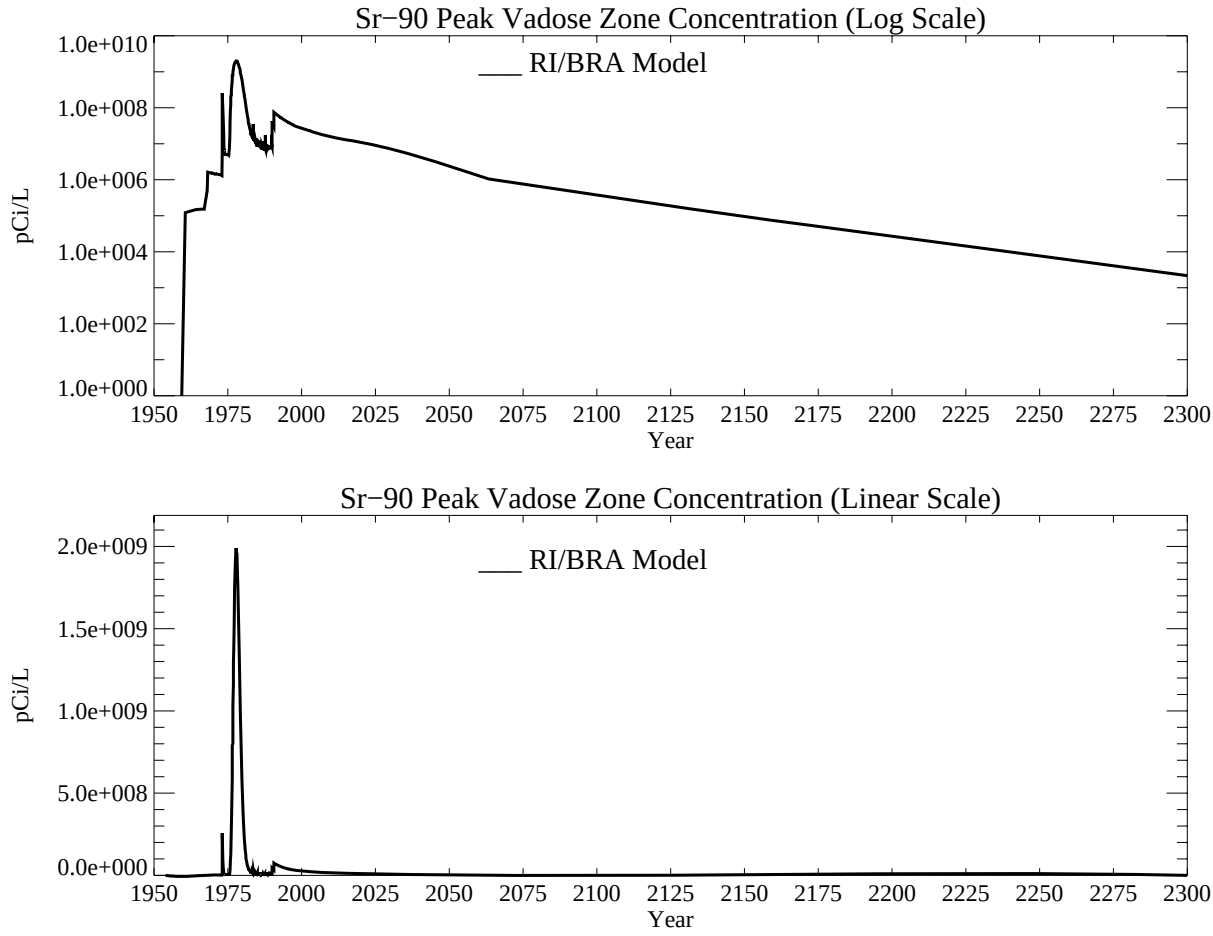

Figure J-8-16. RI/BRA base case: Sr-90 peak vadose zone concentrations (pCi/L).

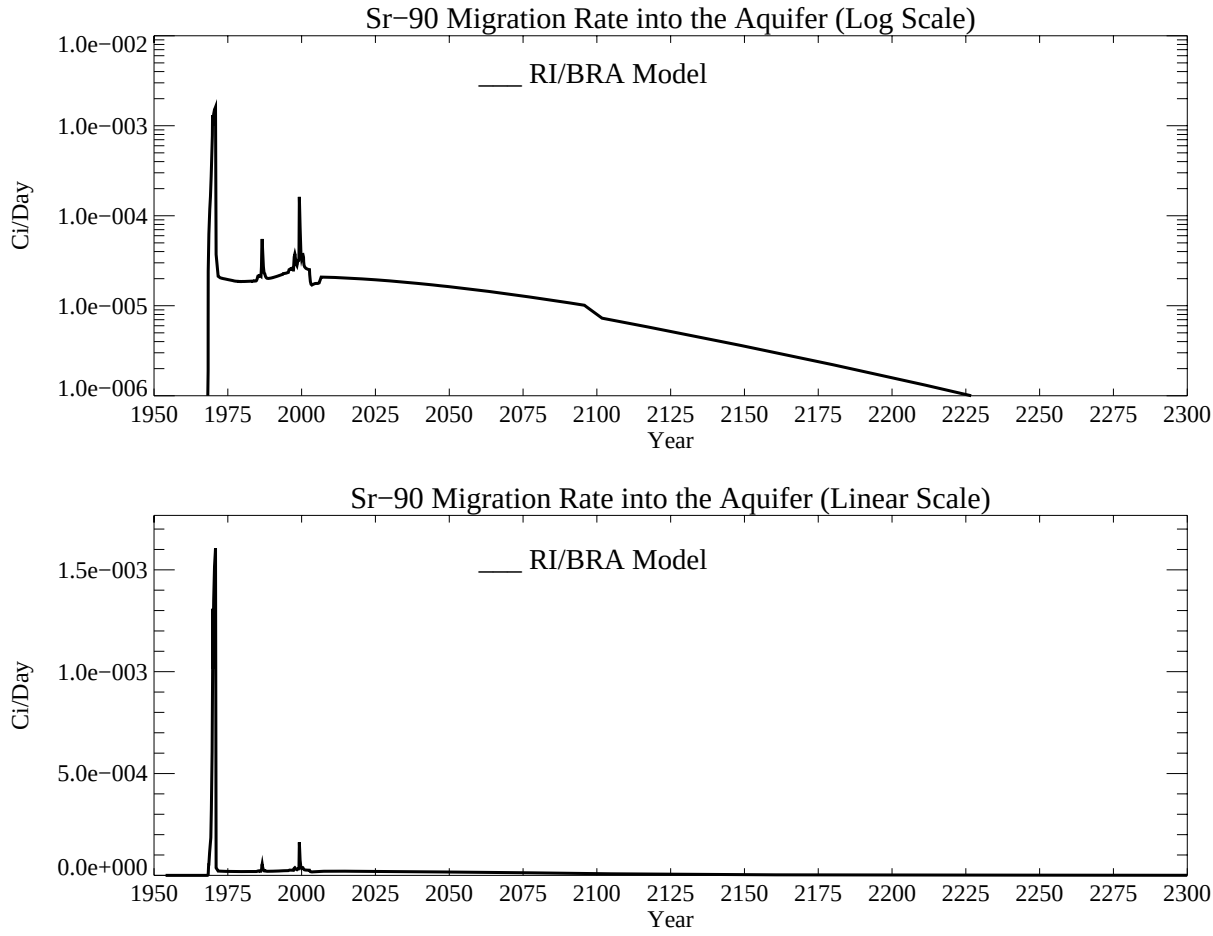

Figure J-8-17. RI/BRA base case: Sr-90 activity flux into the aquifer (Ci/day).

J-8.3 Aquifer Sr-90 Simulation Results

Predicted spatial distribution in the aquifer is shown in Figures J-8-18 and J-8-19 by concentration isopleths presented at 0.8, 8.0, and 80 pCi/L. The resultant peak aquifer concentrations are given in Figure J-8-20.

The peak aquifer Sr-90 concentration was predicted to be 5761 pCi/L in 1965 and is the result of the CPP-3 injection well. The simulated Sr-90 concentrations remained above the MCL from 1960 through year 2129. Sr-90 concentrations in the aquifer are predicted to decline after the year 2000 with a step decrease in concentration following the removal of anthropogenic water at land surface in 2095.

The current Sr-90 contamination in the aquifer near the INTEC is most likely derived from the CPP-3 injection well, because the bulk of the Sr-90 from the tank farm has not yet reached the aquifer. The predicted peak Sr-90 concentration in the year 2095 is 18.6 pCi/L. This concentration exceeds the MCL by a factor of 2.3, with the majority of the long-term impact originating from the initial rapid release of Sr-90 from the tank farm in combination from that from CPP-79 deep. For a detailed discussion of specific contributors to aquifer concentrations, the reader is referred to Sections J-9.

The Sr-90 contour plots presented in Figures J-8-18 are based on the Sr-90 concentrations obtained on the coarse grid for years 2005, 2022, 2077, and 2096. The distribution in years 2049, 2077, 2096, and 2151 are given for the fine grid results in Figure J-8-19. There is some overlap in the times in these figures to allow representation of the 2095 distribution should it extend south of the percolation ponds in the sensitivity results presented in Sections J-10 and J-11. The large-scale figures show that Sr-90 may just now be reaching the CFA and that percolation pond recharge may have reduced aquifer concentrations in the southern INTEC. The small-scale results show that although concentrations are predicted to exceed the MCL after 2095, the area impacted by Sr-90 is between the INTEC fence line and the region directly under the tank farm by year 2049.

Data collected for Sr-90 in the aquifer was obtained throughout the period of INTEC operations. As shown in the following sections, the majority of the Sr-90 appearing in aquifer monitoring wells originates from the CPP-03 injection well. Model predictions in the aquifer prior to about 1990 reflect this origin, implying that the comparison of model predictions to measured data will be independent of the parameters used in the vadose zone. On the other hand, the comparison of model predictions to measured data obtained in the vadose zone perched water wells is highly dependant on the model parameterization. To avoid replicating the comparison to field data, the aquifer calibration is presented after all of the sensitivity simulations in Section J-12.

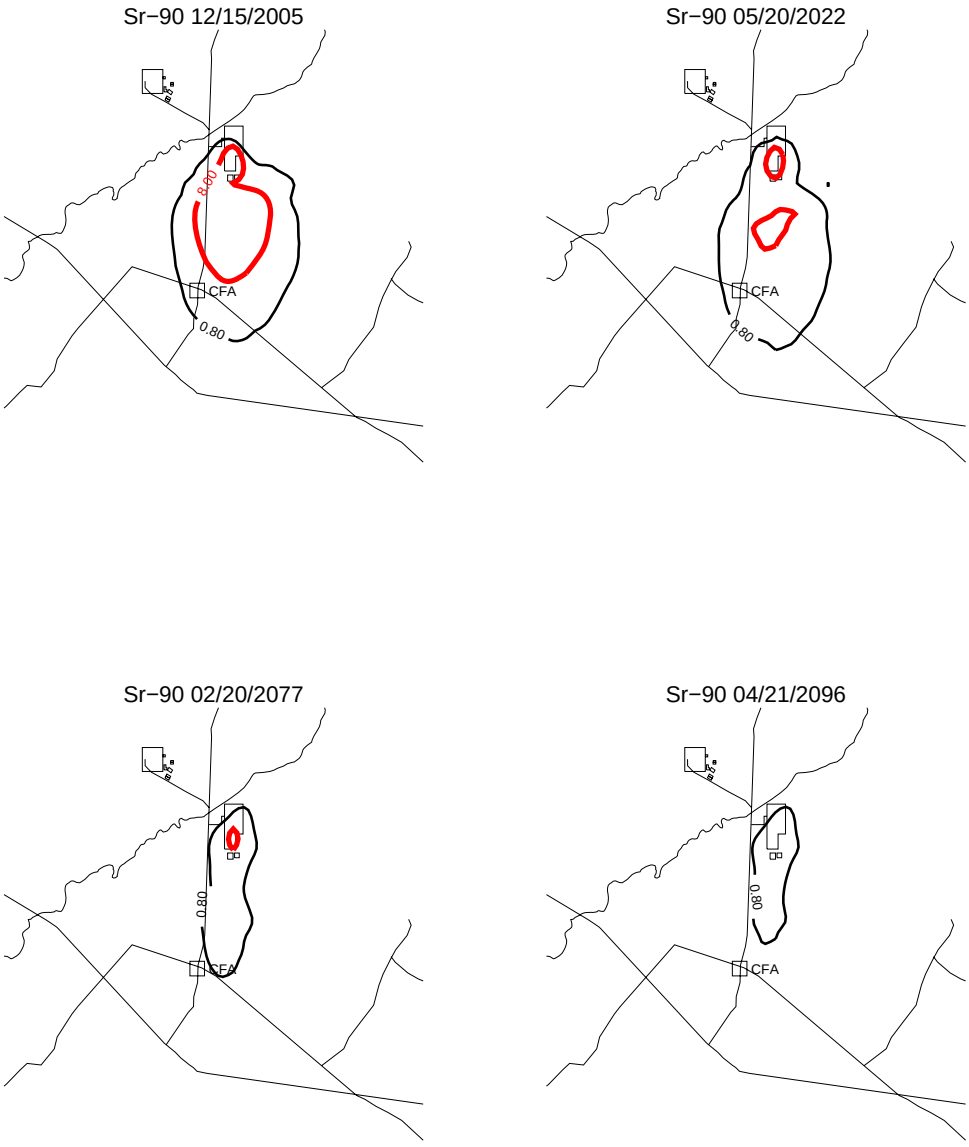

Figure J-8-18. RI/BRA base case: Sr-90 aquifer concentration contours (pCi/L) (MCL = thick red line, 10*MCL = thin red line, MCL/10 = black line). Corresponding contours in fine-scale are shown in Figure J-8-19.

Figure J-8-19. RI/BRA base case: Sr-90 aquifer concentration contours (pCi/L) (continued) (MCL = thick red line, 10*MCL = thin red line, MCL/10 = black line).

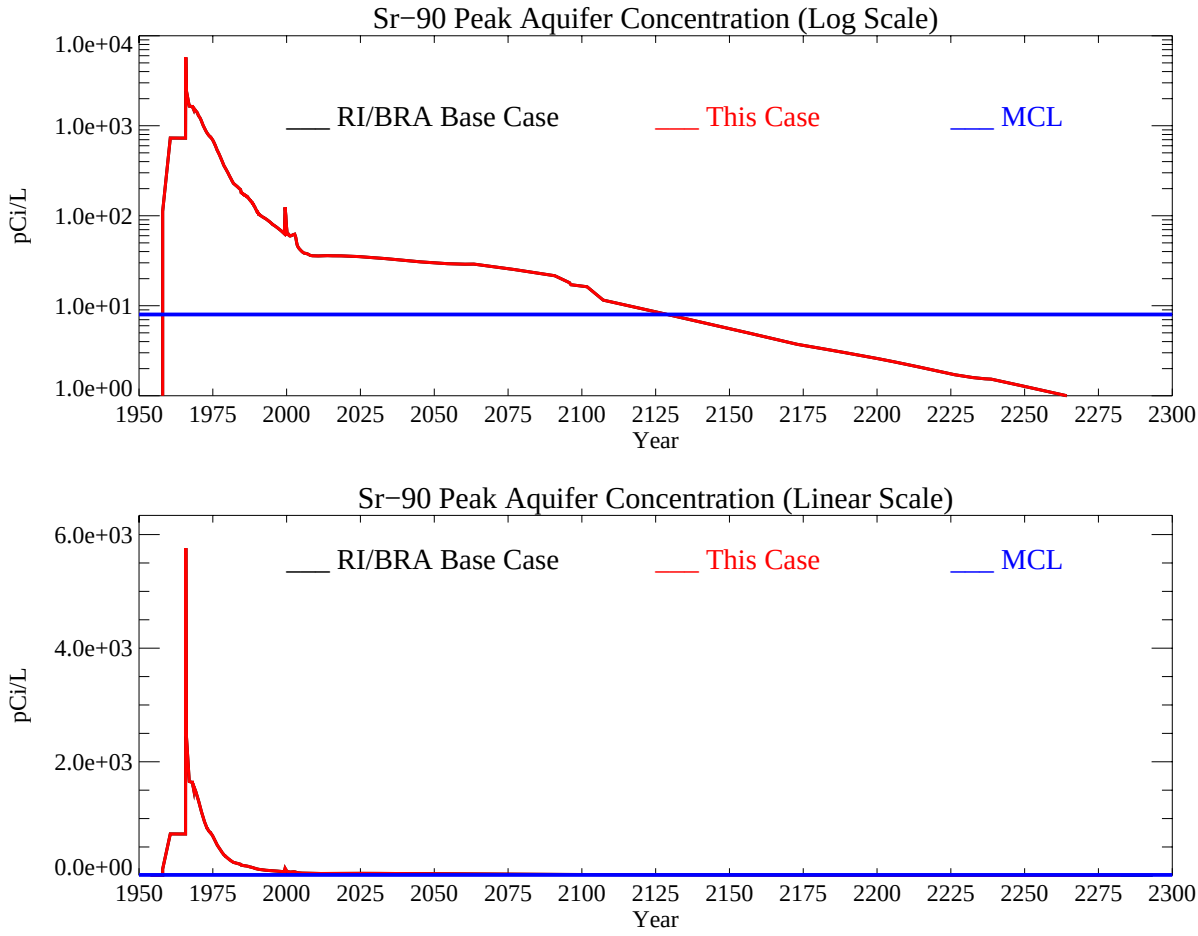

Figure J-8-20. RI/BRA base case: Sr-90 peak aquifer concentrations (pCi/L) with the MCL in blue.

J-9 EVALUATION OF SR-90 PEAK AQUIFER CONCENTRATION BY SOURCE

Sources of Sr-90 included in the sensitivity and RI/BRA base simulations included the: tank farm sources (18,100 Ci), OU 3-13 soil sources (918 Ci), CPP-02 abandoned french drain (33.8 Ci), CPP-3 injection well failure (8.0 Ci), and percolation ponds (0.3 Ci). In addition, 16 Ci of Sr-90 were injected directly into the aquifer in well CPP-03 as service waste. The primary sources of Sr-90 in the tank farm were associated with CPP-31 (15,900 Ci) and CPP-79 deep (874 Ci), with the remaining Sr-90 originating from the OU 3-13 soil sites and from the failed injection well. The following analysis presents the evolution of Sr-90 as it migrates through the vadose zone and into the aquifer from CPP-79, CPP-31, and all other sources. In all three cases, the source geochemical model is that presented in Section J-8.

J-9.1 Contribution From All Sources of Sr-90 Excluding CPP-31 and CPP-79 Deep

The following results are presented to analyze the contribution from the sources of Sr-90 not including CPP-31 and CPP-79 deep. These sources of Sr-90 include all of the OU 3-13 Group 3 soil sites, and all of the OU 3-14 sites except CPP-31 and CPP-79 deep. These results are a subset of the model predictions presented in Section J-8, where it was assumed that the OU 3-13 Group 3 soil sites were outside the influence of acidic releases and the K_d applied in the alluvium in the base grid was 20 mL/g.

J-9.1.1 Vadose Zone Sr-90 Simulation Results

The spatial distribution of Sr-90 in the vadose zone is presented in Figures J-9-1 through J-9-4 through the year 2293. The profiles of vertical concentration show the contribution from (a) the percolation ponds and southern OU 3-13 soil sources in southern INTEC, (b) OU 3-13 soil sources and CPP-79 shallow in northern INTEC, and (c) the influence of the failed injection well at early times deep in the vadose zone (at about 1750 m from the southern boundary). The horizontal distribution shows the extensive early contribution from the failed injection well, and an isolated contribution from CPP-37B to the northeast of the tank farm. This latter contribution is probably overestimated here as discussed in Appendix A, Section 5. In fact, the source activities for most of the OU 3-13 soil sources were probably overestimated and many of those contaminated soil sources have been the target of remedial actions. Given that the activities of Sr-90 at these sites is small compared to CPP-31 and CPP-79, these source activities were not re-evaluated, and the remedial actions are not accounted for in this RI/BRA.

Peak vadose zone concentrations from these sources are represented by the red line in Figure J-9-5. Initial high concentrations between 1968 and 1990 are a result of the failed injection well. The increase in concentration occurring around year 2000 is a result of increased flows in the Big Lost River. Increasing the flow in the Big Lost River drives higher concentrations from the 380 ft interbed into the aquifer. In this plot, the highest concentrations (4.6E6 pCi/L) in the vadose zone are predicted to occur in 1990 and are (a) between the 380 ft interbed and aquifer and (b) between land surface and the lower northern perched water.

In addition to the contribution from these sources shown in red, the RI/BRA base case which included all of the Sr-90 sources is shown in black. The largest deviation occurs after 1986. These deviations represents the combined influence of CPP-31 and CPP-79 deep. At later times, the source of the deviation is the same, but the differences between predicted concentration histories are more damped, illustrating the effect of dispersive downward transport from CPP-31 and CPP-79 deep.

The rate at which the activity leaves the vadose zone and enters the aquifer is shown in Figure J-9-6. and can be compared directly to the RI/BRA base case (shown in black). The similarity of results represented by the black and red lines prior to about year 2000 shows that the majority of the total flux simulated in the RI/BRA base case (black line) originates from sites other than CPP-31 and CPP-79 deep. The very small difference in the flux magnitude between 1980 and 2000 (difference between the red and black lines) is a reflection of the early arrival from those two large activity sources.

Figure J-9-1. Sr-90 vadose zone concentration excluding CPP-31 and CPP-79 (horizontal contours) (pCi/L) (MCL = thick red line, 10*MCL = thin red line, MCL/10 = black line).

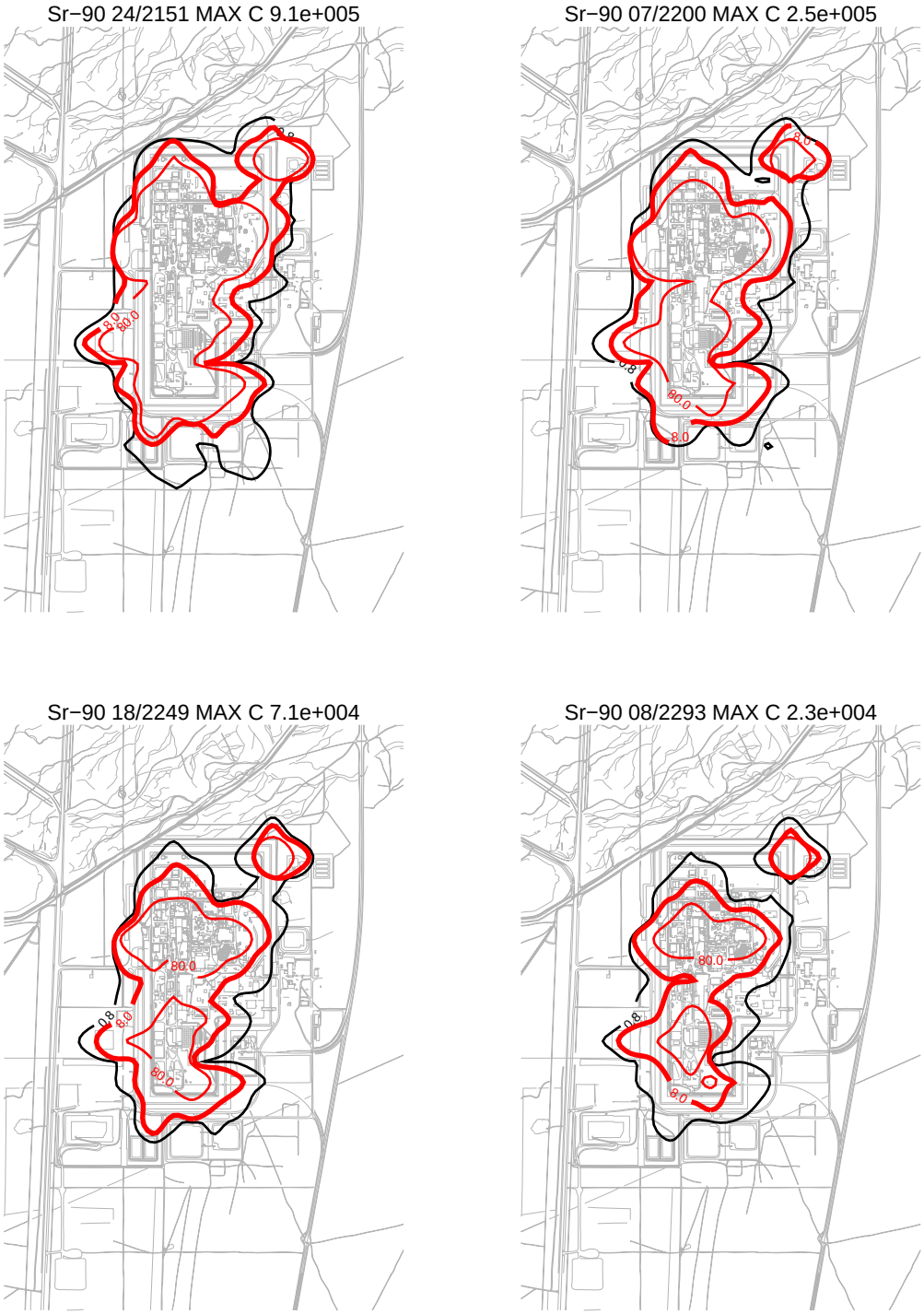

Figure J-9-2. Sr-90 vadose zone concentration excluding CPP-31 and CPP-79 (horizontal contours) (pCi/L) (MCL = thick red line, 10*MCL = thin red line, MCL/10 = black line).

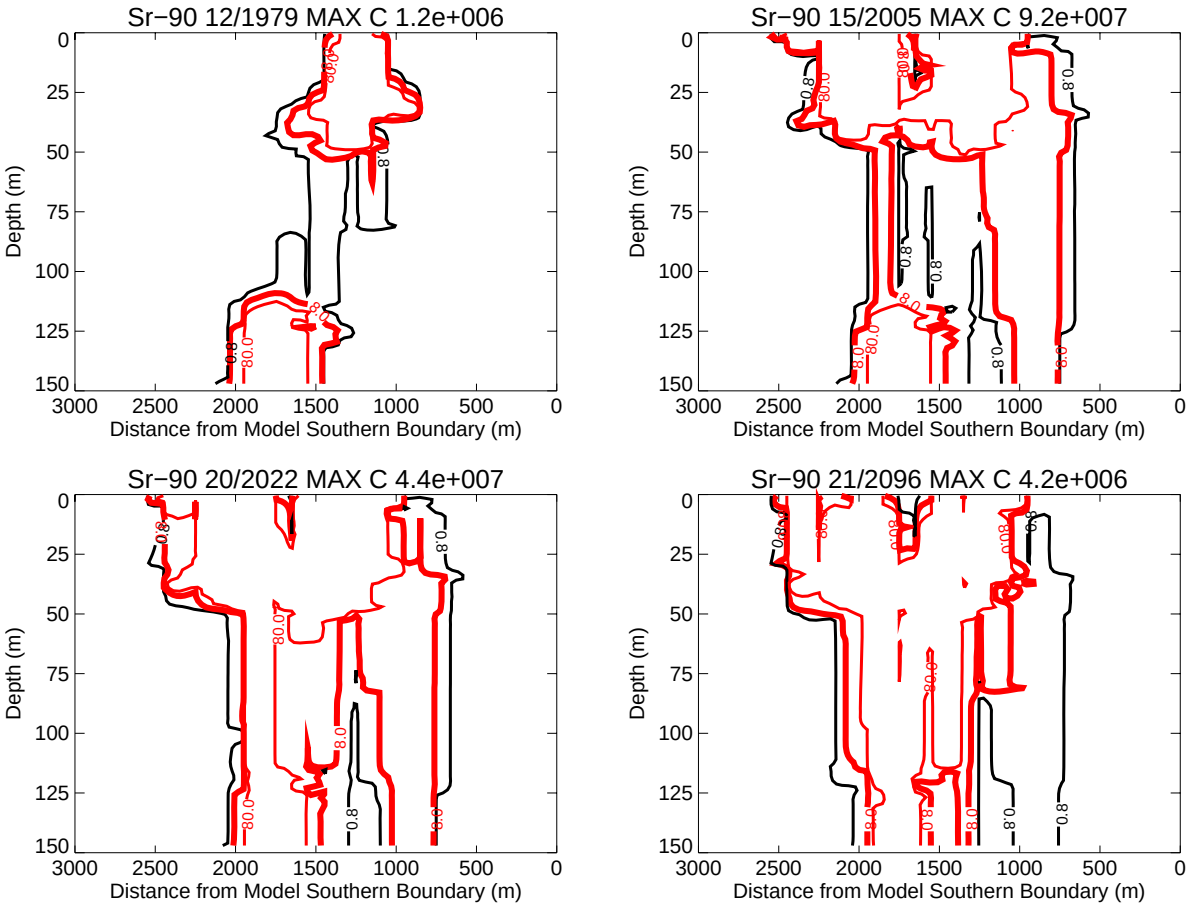

Figure J-9-3. Sr-90 vadose zone concentrations excluding CPP-31 and CPP-79 (vertical contours) (pCi/L) (MCL = thick red line, 10*MCL = thin red line, MCL/10 = black line).

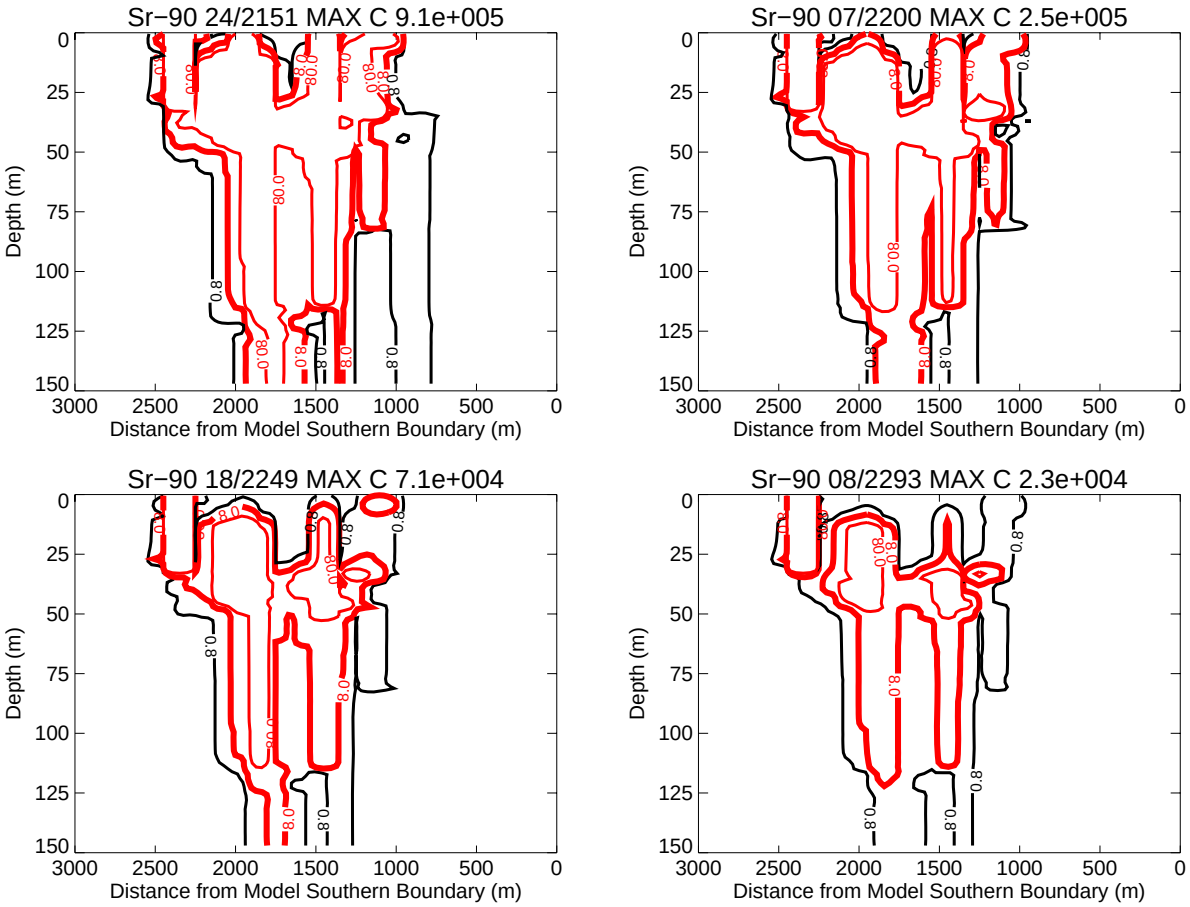

Figure J-9-4. Sr-90 vadose zone concentrations excluding CPP-31 and CPP-79 (vertical contours) (pCi/L) (continued) (MCL = thick red line, 10*MCL = thin red line, MCL/10 = black line).

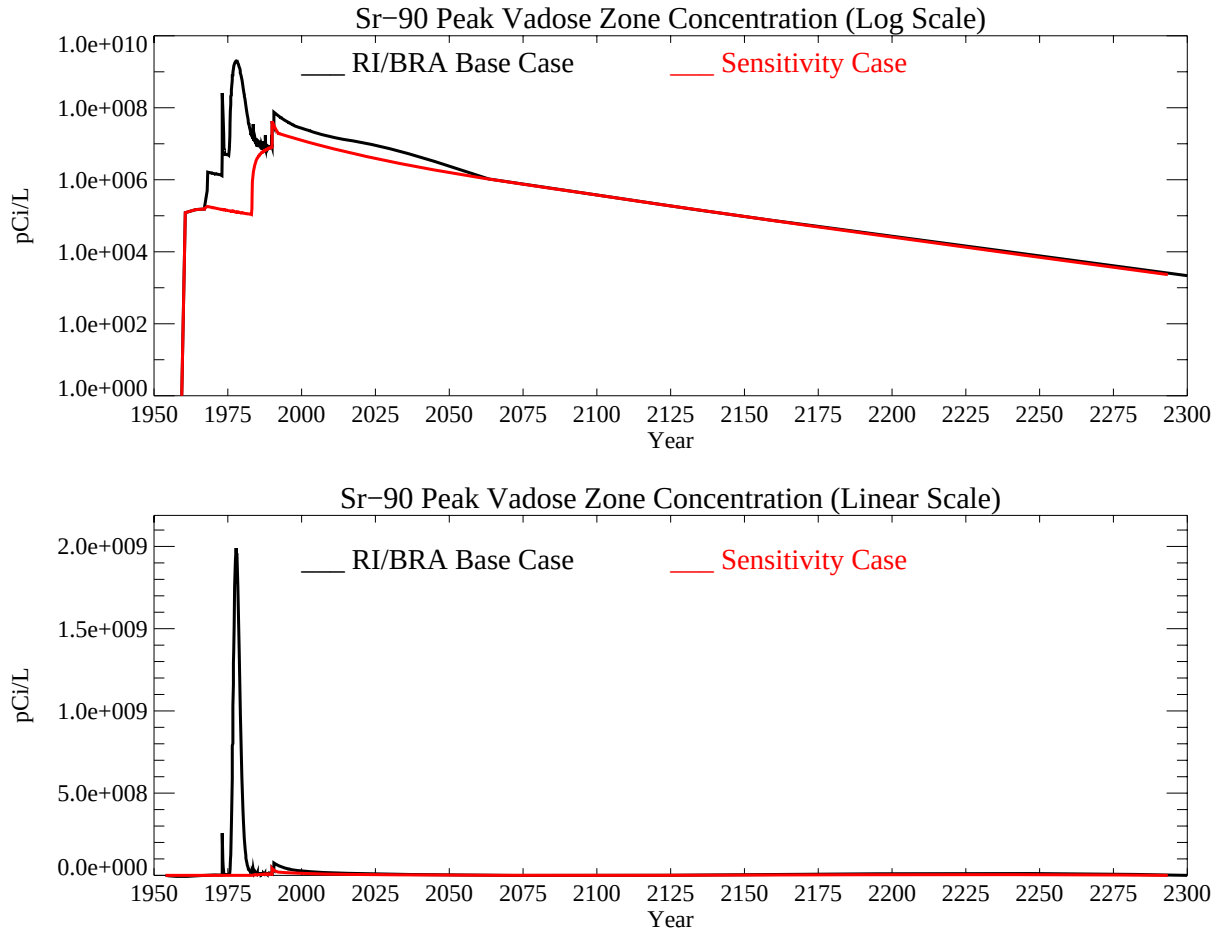

Figure J-9-5. Sr-90 peak vadose zone concentrations excluding CPP-31 and CPP-79 (pCi/L) with the RI/BRA model in black and these sources only in red.

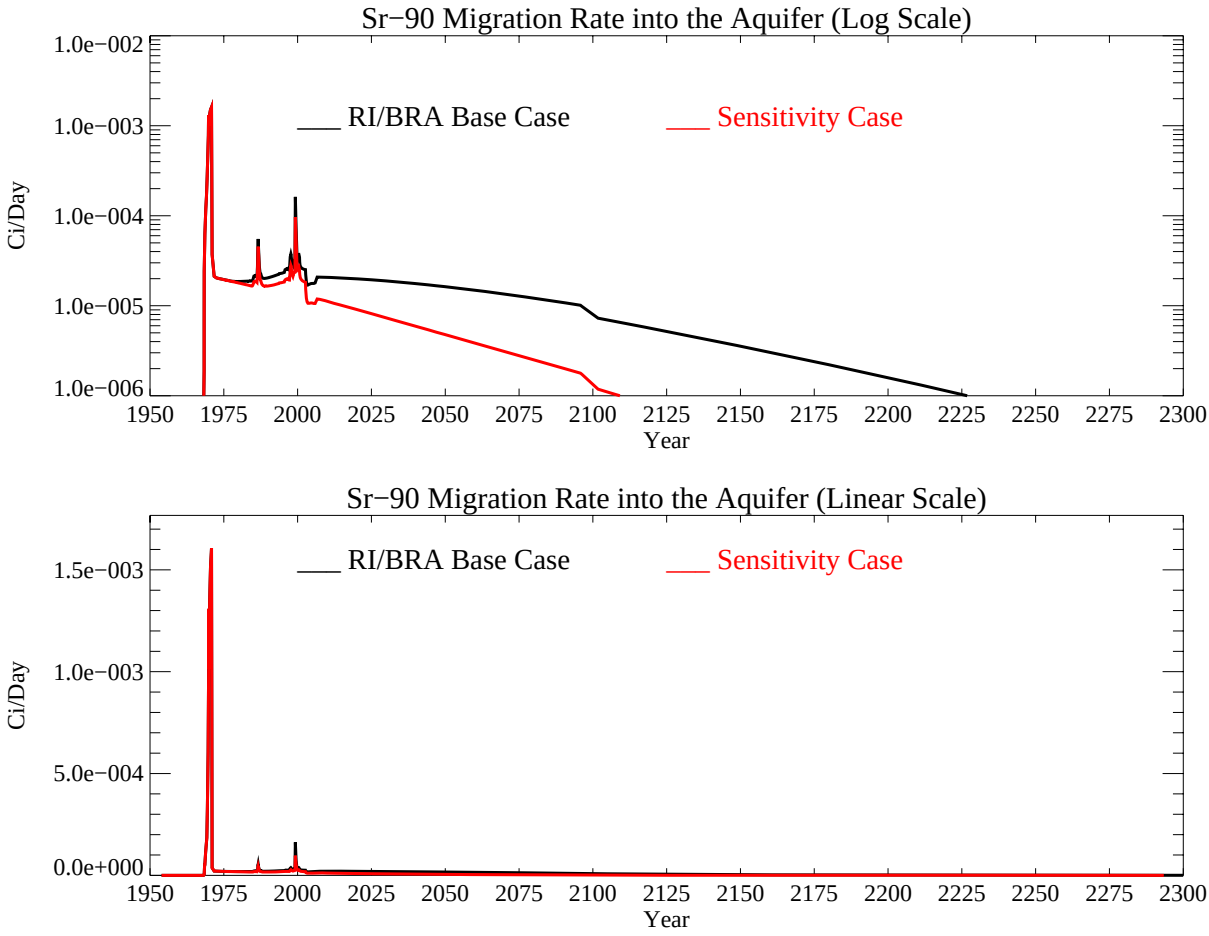

Figure J-9-6. Sr-90 activity flux into the aquifer excluding CPP-31 and CPP-79 (Ci/day) with the RI/BRA model in black, and these sources only in red.

J-9.1.2 Aquifer Sr-90 Simulation Results

The horizontal distribution of Sr-90 in the aquifer for the time period spanning 1979-2096 in the course grid is given in Figure J-9-7, and on the fine grid spanning 2096-2249 in Figure J-9-8. As with the vadose zone plots, these concentration isopleths are presented at 0.8, 8.0, and 80 pCi/L. The distribution prior to 2095 (Figure J-9-7) can be compared to that obtained considering all sources (Figure J-8-18), and shows that current aquifer concentrations primarily originate from these sources. At later times (Figures J-9-8 and J-8-19), there are significant differences illustrating the contribution from the major tank farm sources.

The resultant peak aquifer concentrations are given in Figure J-9-9. The peak aquifer Sr-90 concentration was predicted to be 5761 pCi/L in 1965 and is the result of the CPP-3 well. Simulated Sr-90 concentrations were predicted to remain above the MCL from 1960 through year 2047 from these sources and were predicted to decline after the year 2000. As shown in the RI/BRA model, there is a significant step decrease in concentration following the removal of anthropogenic water at land surface in 2095.

The predicted peak Sr-90 concentration here in the year 2095 is 3.2 pCi/L, about 17% of that predicted considering all of the sources (black line). This concentration is less than half of the MCL, underlining the importance of the vadose zone contributions. Considering these sources alone, concentrations are predicted to fall below the MCL in 2047.

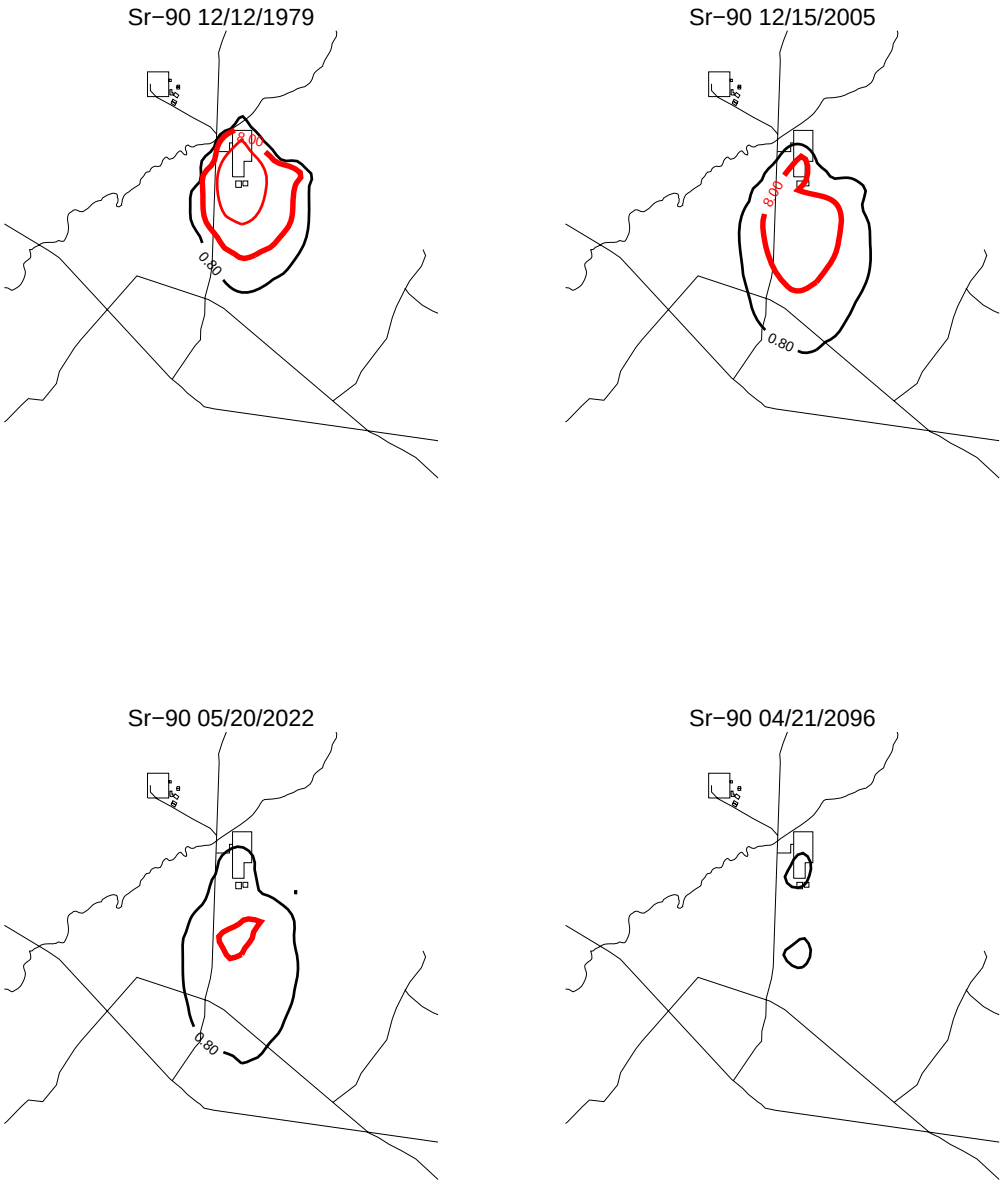

Figure J-9-7. Sr-90 aquifer concentration contours (pCi/L) (MCL = thick red line, 10*MCL = thin red line, MCL/10 = black line).

Figure J-9-8. Sr-90 aquifer concentration contours (pCi/L) (continued) (MCL = thick red line, 10*MCL = thin red line, MCL/10 = black line).

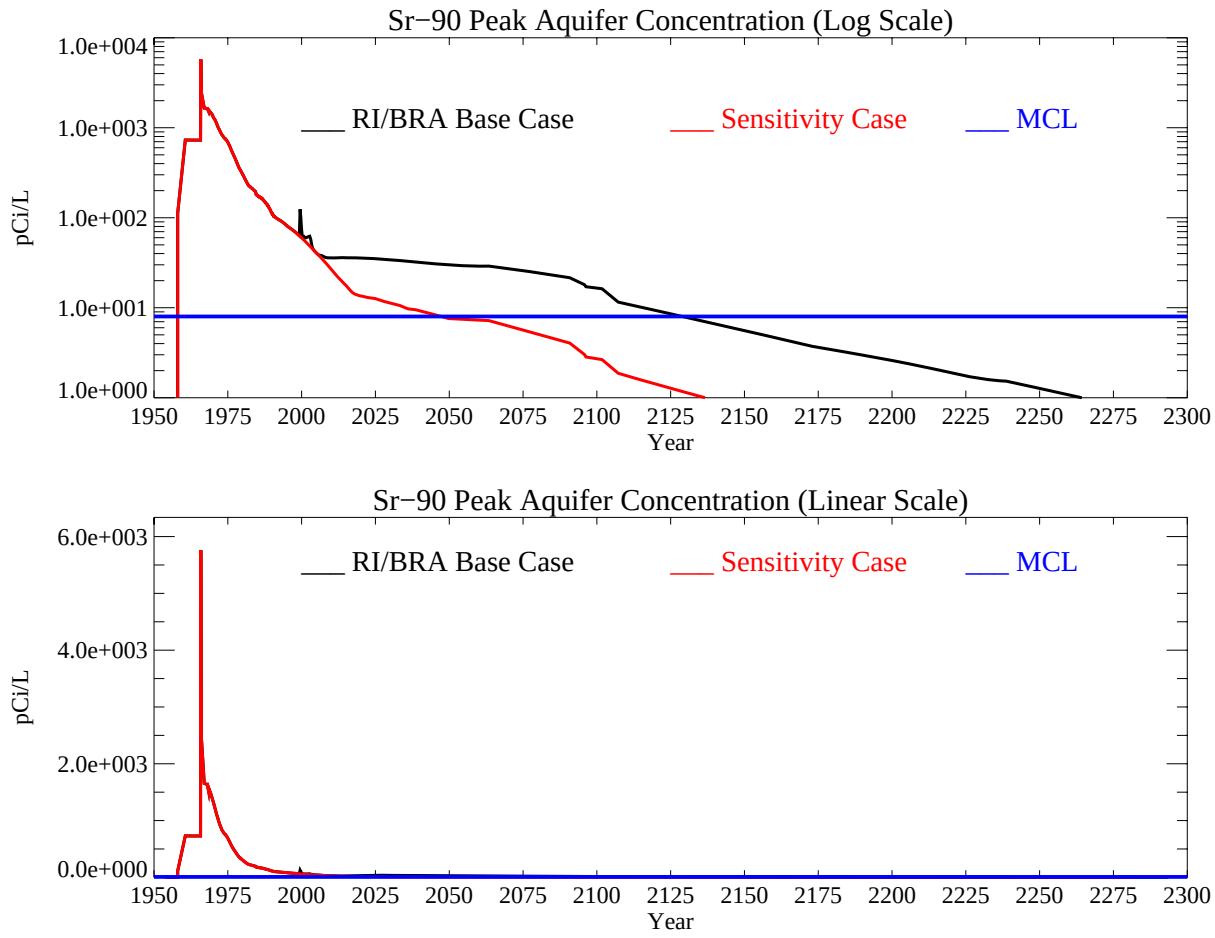

Figure J-9-9. Sr-90 peak aquifer concentrations (pCi/L) with the MCL in blue, RI/BRA model in black and these sources only in red.

J-9.2 Contribution from CPP-79 Deep

The following results are presented to analyze the contribution from just CPP-79 Deep for the RI/BRA model predictions presented in Section J-8.

J-9.2.1 Vadose Zone Sr-90 Simulation Results

The Sr-90 spatial distribution through year 2293 from CPP-79 deep is given in Figures J-9-10 through J-9-13. These can be compared to the distribution predicted for theRI/BRA base case which were presented in Figures J-8-10 through J-8-13. The vertical distribution of Sr-90 from Site CPP-79 Deep in year 1979 extends from land surface to the aquifer. This very early arrival of Sr-90 in very high pore water concentrations is a reflection of dispersive transport, and is not reflective of the advective transport that occurs at a much reduced rate. Even though the vertical profiles suggest that flow is primarily vertical, the horizontal contour plots show that the lateral extent impacted by CPP-79 in the vadose zone is extensive.

Peak vadose zone concentrations through time are given by the red line in Figure J-9-14 and are slightly below 100 pCi/L in year 2300. The step increases in concentrations are the result of the two different releases in that occurred in 1968 and again in 1973. The early arrival deep in the vadose zone is a function of (a) the CPP-79 Deep release occurring just above the basalt-alluvium interface, and (b) the vertical driving force presented by the 2500 gallon release that occurred just above CPP-79 Deep in Site CPP-79 shallow. There was actually very little water associated with CPP-79 Deep itself (only about 400 gallons). These concentrations can be compared to those obtained when all sources of Sr-90 are considered (shown in black). Although Sr-90 originating from CPP-79 deep is distributed throughout the vadose zone, the concentrations from this source are only a small percentage of the other peak concentrations. This is an artifact of the high pore water concentration that exists in the alluvium rather than an indication of whether or not CPP-79 is a major contributor to aquifer concentrations.

The rate at which the CPP-79 deep activity enters the aquifer is shown by the red line in Figure J-9-15, and can be compared directly to the RI/BRA model including all sources (shown as black). This comparison illustrates that about 10% of the activity leaving the alluvium after year 2000 originated from CPP-79 deep. This suggests that there is a significant overlapping contribution from non-CPP-31 and CPP-31during the 1990-2010 time period, and that the fluxes arriving in the aquifer after about 2010 are primarily associated with CPP-31 and CPP-79. The results showing the CPP-31 contributions are presented in Section J-9.3 and J-9.4.

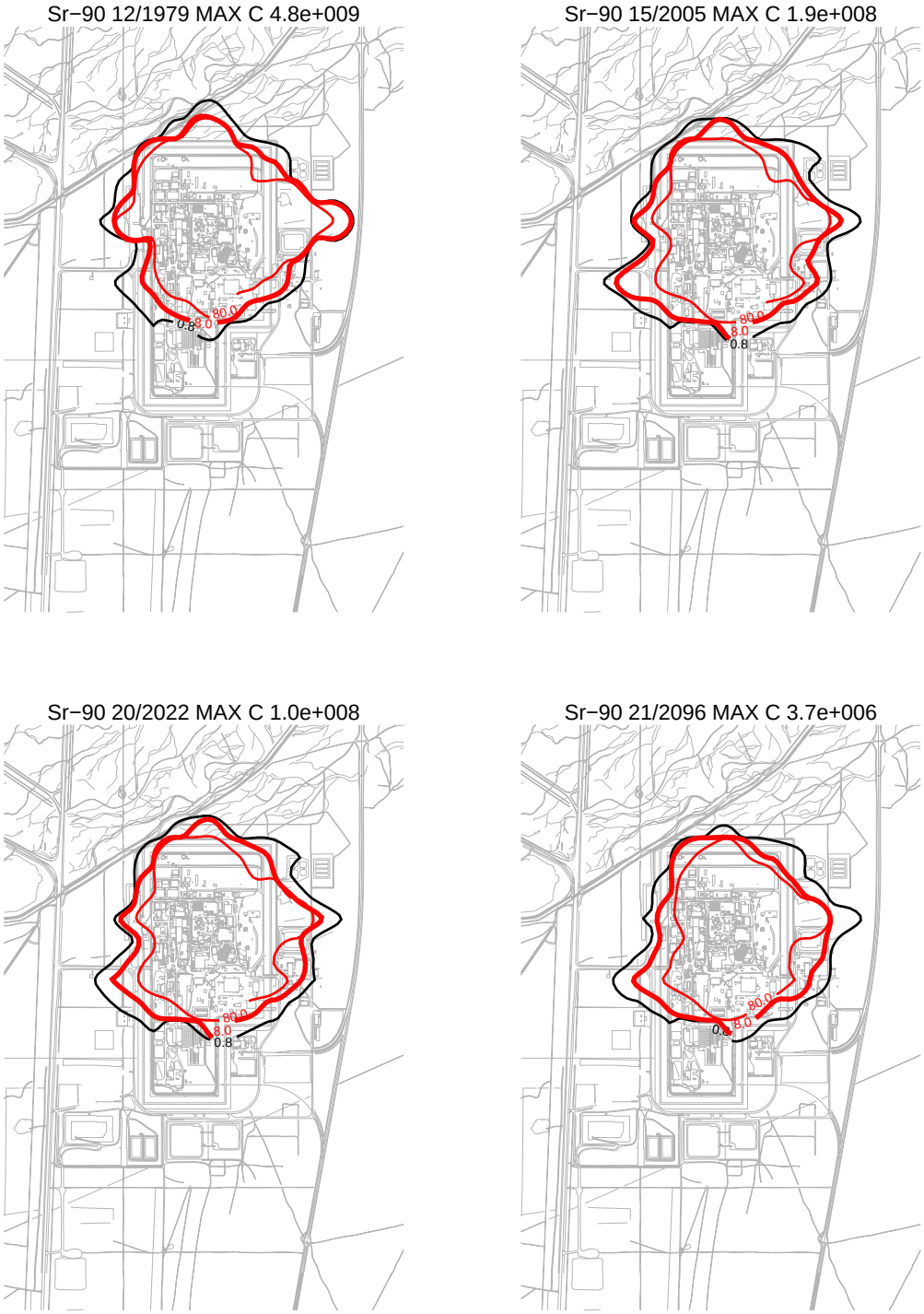

Figure J-9-10. Sr-90 vadose zone concentration from CPP-79 deep (horizontal contours) (pCi/L) (MCL = thick red line, 10*MCL = thin red line, MCL/10 = black line).

Figure J-9-11. Sr-90 vadose zone concentration from CPP-79 deep (horizontal contours) (pCi/L) (MCL = thick red line, 10*MCL = thin red line, MCL/10 = black line).

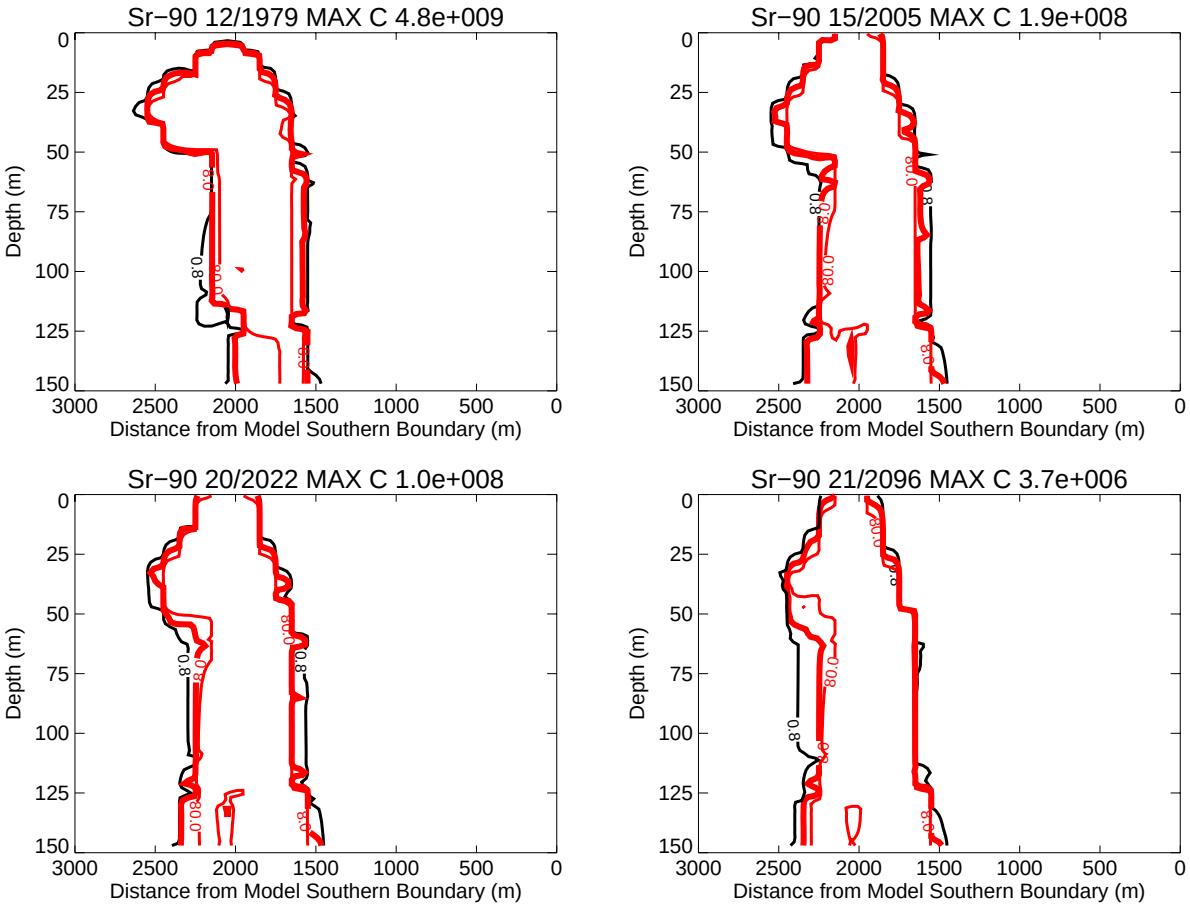

Figure J-9-12. Sr-90 vadose zone concentrations from CPP-79 deep (vertical contours) (pCi/L) (MCL = thick red line, 10*MCL = thin red line, MCL/10 = black line).

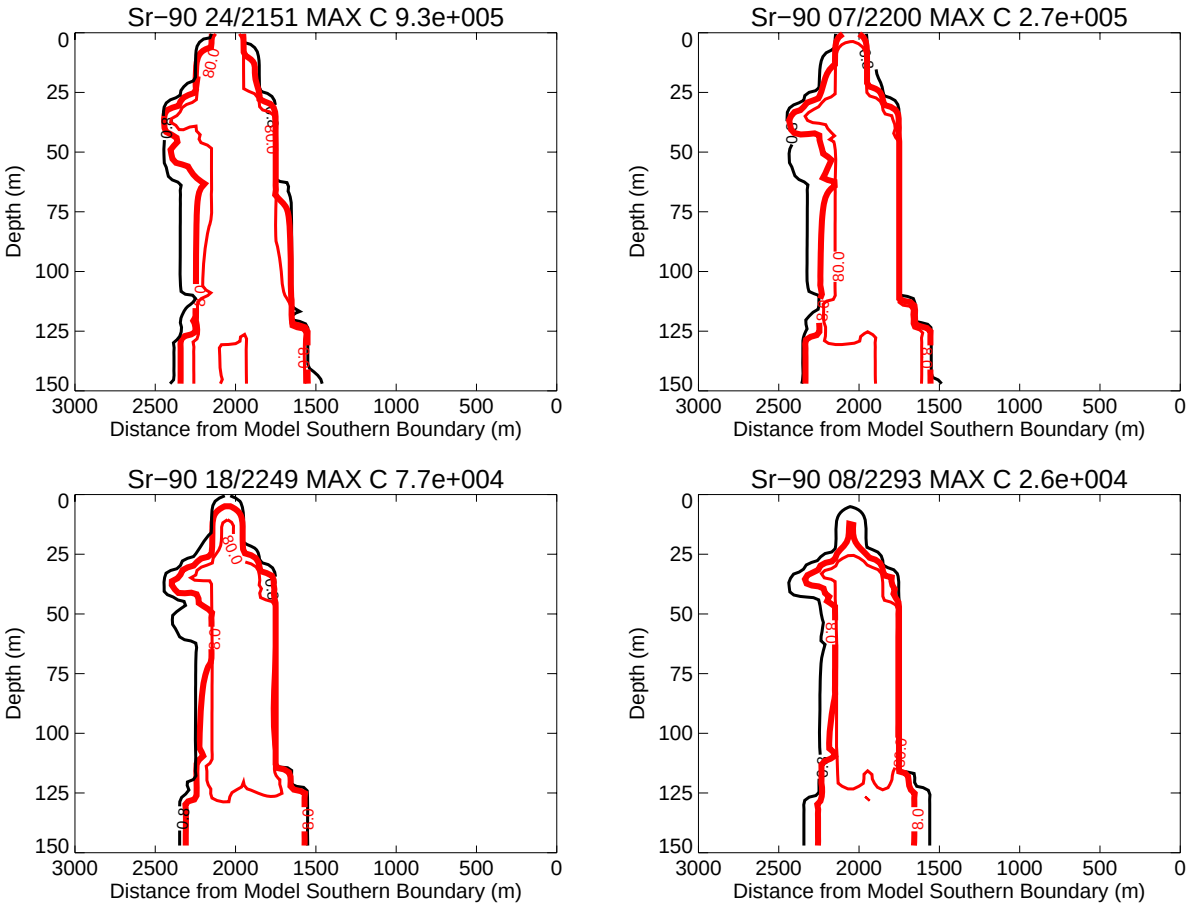

Figure J-9-13. Sr-90 vadose zone concentrations from CPP-79 deep (vertical contours) (pCi/L) (continued) (MCL = thick red line, 10*MCL = thin red line, MCL/10 = black line).

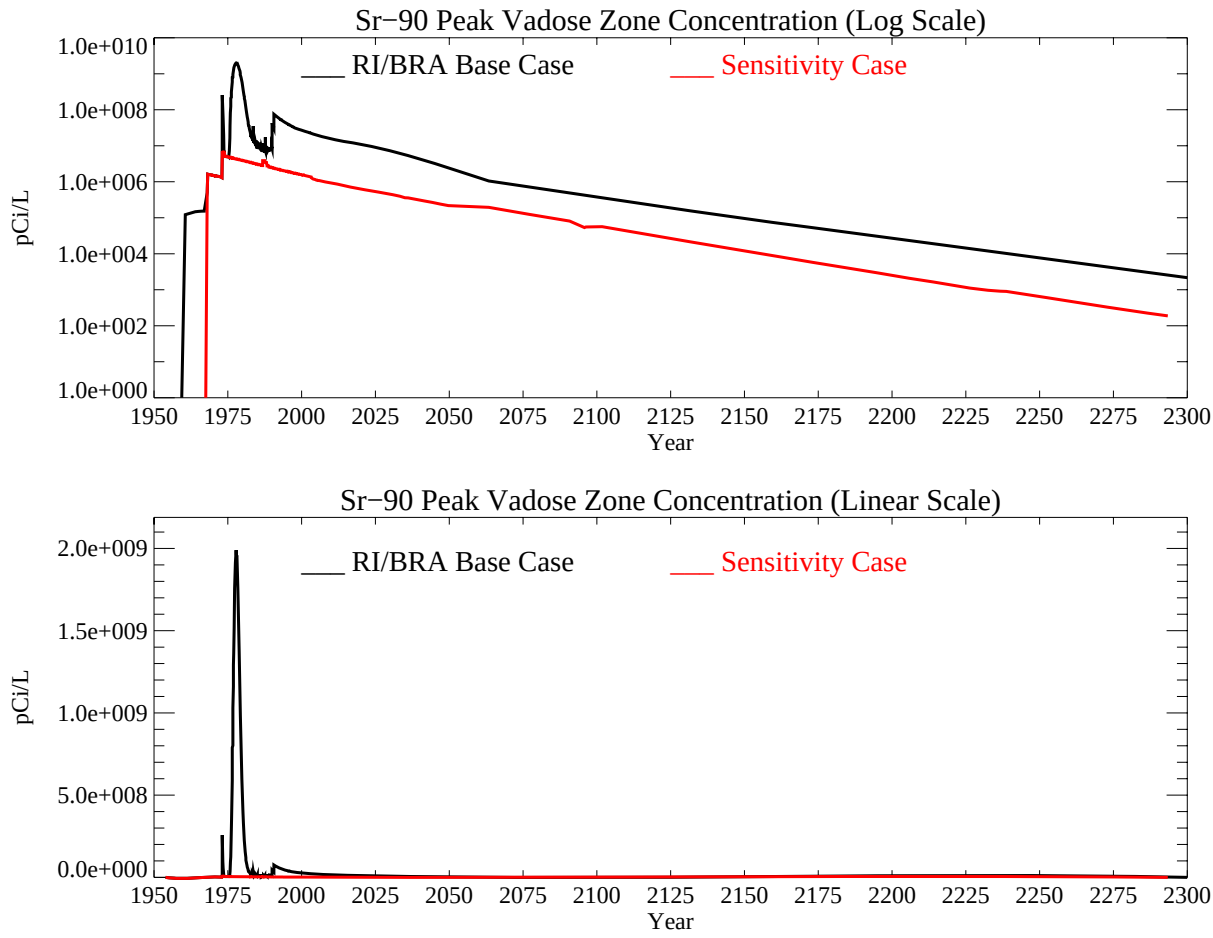

Figure J-9-14. Sr-90 peak vadose zone concentrations from CPP-79 deep (pCi/L) with the RI/BRA model in black and the CPP-79 deep source in red.

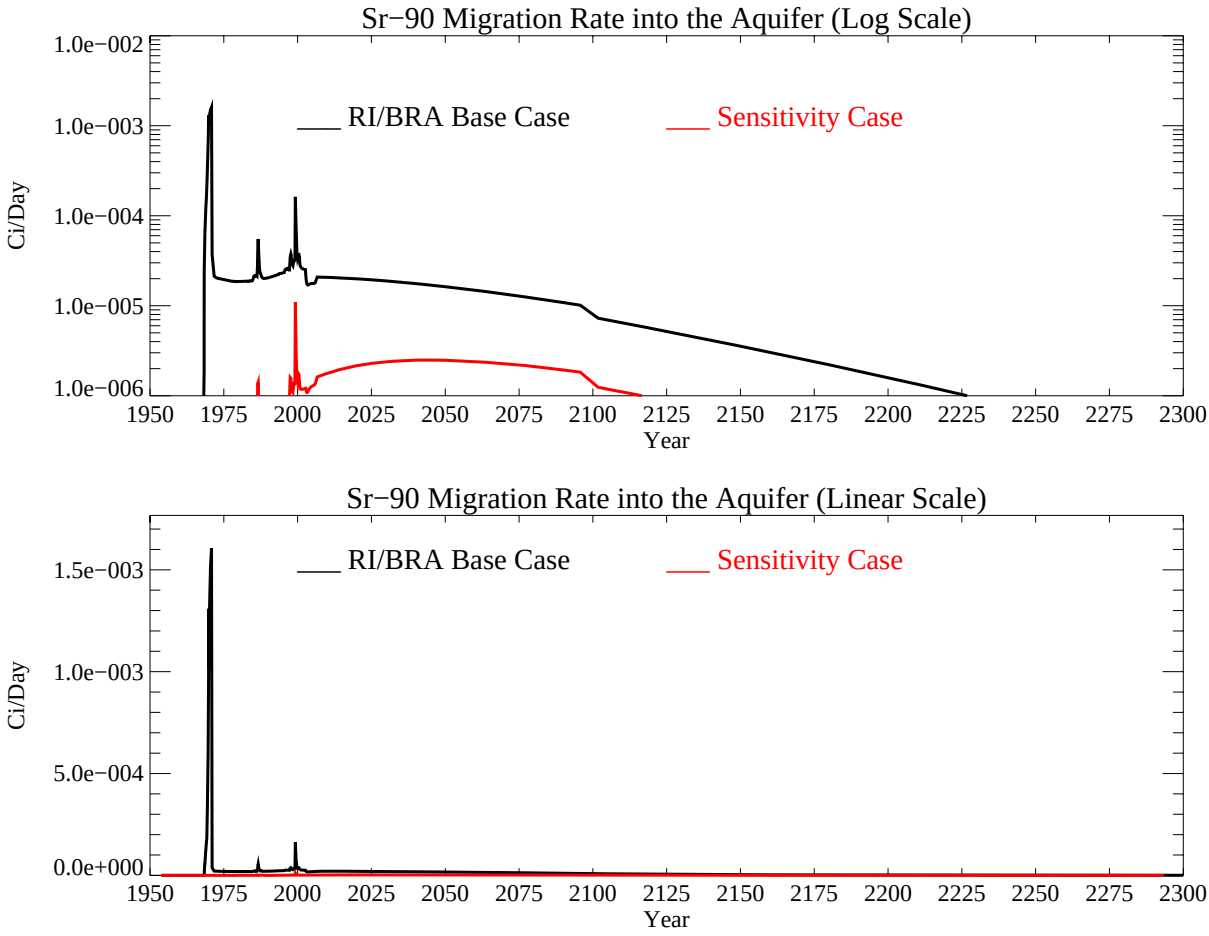

Figure J-9-15. Sr-90 activity flux into the aquifer from CPP-79 deep (Ci/day) with the RI/BRA model in black, and the CPP-79 deep source in red.

J-9.2.2 Aquifer Sr-90 Simulation Results

The distribution of Sr-90 in the aquifer for the time period spanning 1979-2096 is shown in the far-field in Figure J-9-16, and in the near-field in Figure J-9-17 for the 2096-2249 time period. The isopleths for year 2005 are provided to indicate that the aquifer is currently being impacted by Site CPP-79 deep. The area predicted to be impacted by CPP-79 deep is considerably smaller than that impacted by the injection well, the failure of the injection well, and other Sr-90 sources.

As shown in Figure J-9-18, the largest aquifer impact occurs in the 2000-time frame, with concentrations in the aquifer approaching 13 pCi/L. The predicted peak Sr-90 concentration in the year 2095 is 4.6 pCi/L, about equal to that of the contribution from non-tank farm sources, and about one quarter of the total aquifer impact in 2095. Although the concentrations from this source are not predicted to be less than the MCL by 2000, the area impacted by CPP-79 above the MCL by itself is small. It is the overlap of this area with that caused by CPP-31 that contributes to aquifer concentrations exceeding the MCL over a larger area.

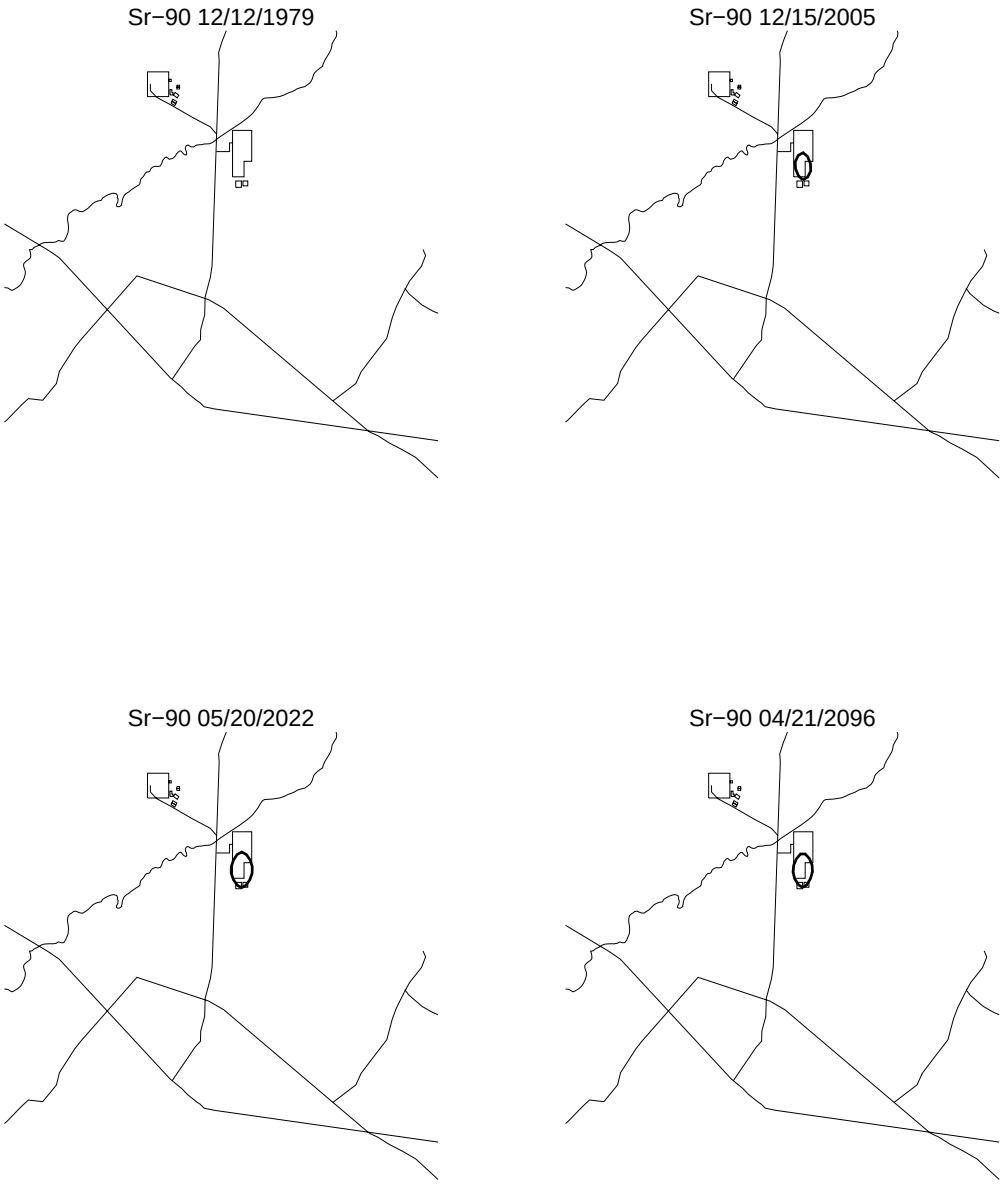

Figure J-9-16. Sr-90 aquifer concentration contours from CPP-79 deep (pCi/L) (MCL = thick red line, 10*MCL = thin red line, MCL/10 = black line).

Figure J-9-17. Sr-90 aquifer concentration contours from CPP-79 deep (pCi/L) (continued) (MCL = thick red line, 10*MCL = thin red line, MCL/10 = black line).

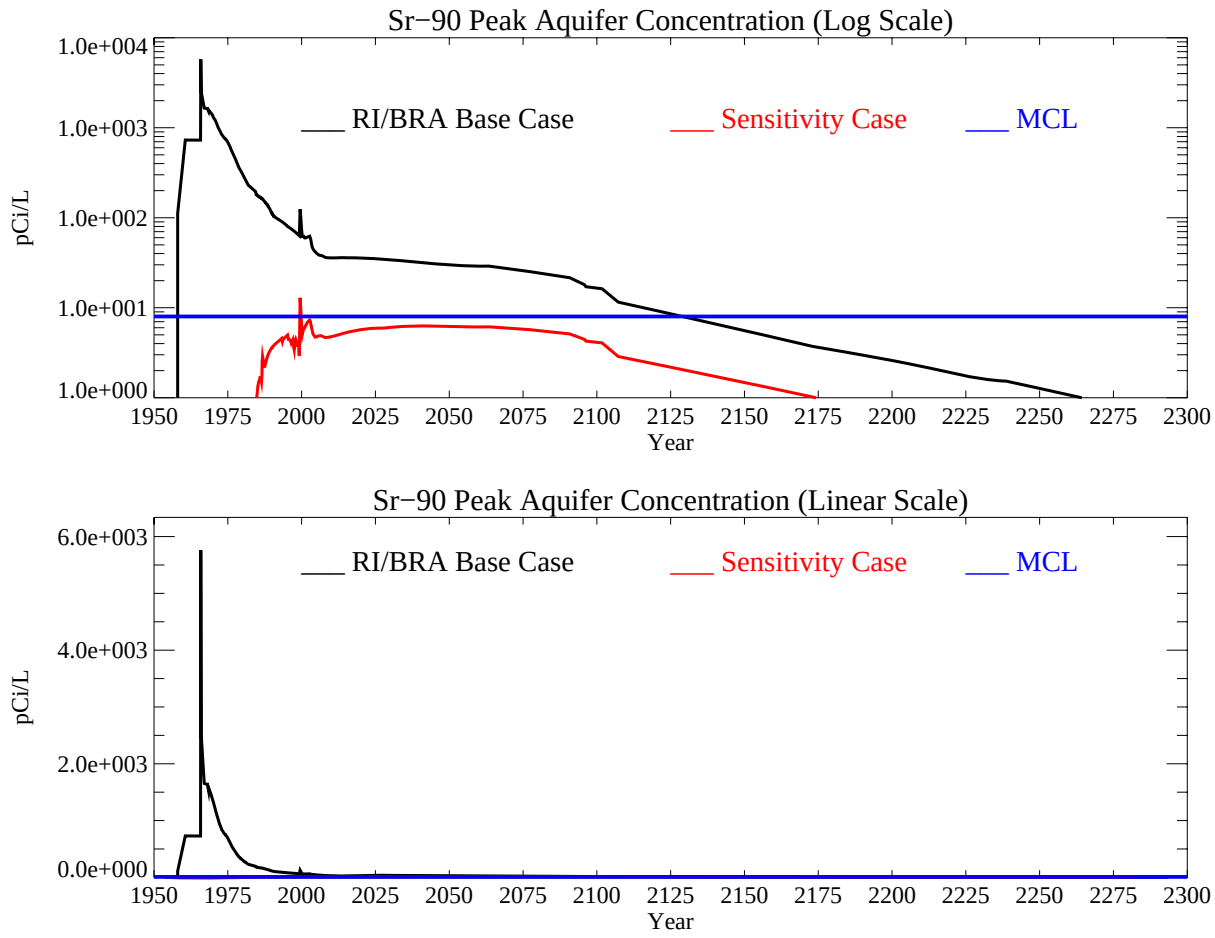

Figure J-9-18. Sr-90 peak aquifer concentrations from CPP-79 deep (pCi/L) with the MCL in blue, RI/BRA model in black and the CPP-79 deep source in red.

J-9.3 Contribution from CPP-31

The following results are presented to analyze the contribution from CPP-31 for the model predictions presented in Section J-8.

J-9.3.1 Vadose Zone Sr-90 Simulation Results

The spatial distribution of Sr-90 originating at site CPP-31 is shown in Figures J-9-19 through J-9-22. These vadose zone contours include the affects from the initial rapid release of 12336 Ci in addition to the slow release from the alluvium of the residual 3564 Ci. In comparison to the distribution obtained for the Site CPP-79 deep release, (Figures J-9-10 through J-9-13), they are remarkably similar. This similarity occurs because 1) the significant activity released from the alluvium for CPP-31 occurred over a relatively small time frame (0-7 years), followed by an insignificant additional release throughout the remaining time period, and 2) the activity released in CPP-79 was placed just above the basalt-alluvium interface, followed by a relatively large volume of water just above the source location. In the case of CPP-31, the initial mobile activity is on the order of 12336 Ci, and in the case of CPP-79 deep, the activity is about 1000 Ci. The release history accounts for the similarity in time required to reach the perched water, and close release locations at land surface account for much of the spatial similarity. The vertical distribution of Sr-90 from Site CPP-31 in year 1979 extends from land surface to the aquifer. This very early arrival of Sr-90 in relatively high pore water concentrations is a result of dispersive transport. Even though the vertical profiles suggest that flow is primarily vertical, the horizontal contour plots show that the lateral extent impacted by CPP-31 is extensive.

Peak vadose zone concentrations for the CPP-31 source through time are shown in black in Figure J-9-23 and are slightly below 10,000 pCi/L in year 2300. The three separate arrivals of Sr-90 in the vadose zone are a reflection of the relative mobility of SrNO3, Sr+ ion, and SrOH. Peak concentrations in the vadose zone for the RI/BRA base case (black) and those from this simulation are nearly identical and are a reflection of the pore water concentration in the alluvium.

The rate at which this activity enters the aquifer is given in Figure J-9-24 (shown in red), and can be compared directly to the RI/BRA model including all of the sources (shown in black). Compared to the flux originating from site CPP-79, it is apparent that most of the post 2000 contribution will have originated from site CPP-31. In consideration of the results shown in Section J-9.4, it is clear that this activity originated with the initial early release from CPP-31, and is not coming from the Sr-90 remaining in the alluvium after 1993.

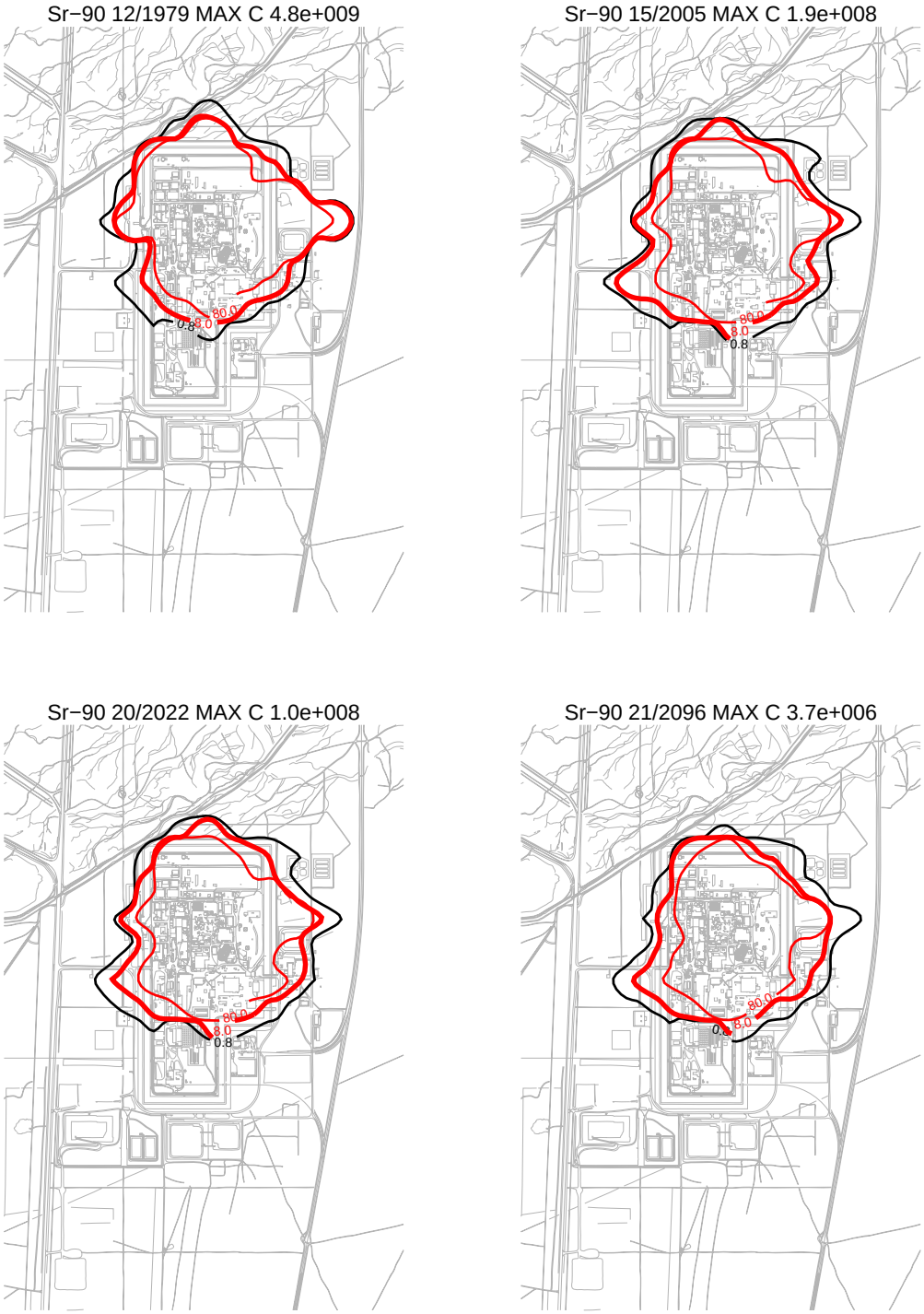

Figure J-9-19. Sr-90 vadose zone concentration from CPP-31 (horizontal contours) (pCi/L) (MCL = thick red line, 10*MCL = thin red line, MCL/10 = black line).

Figure J-9-20. Sr-90 vadose zone concentration from CPP-31 (horizontal contours) (pCi/L) (MCL = thick red line, 10*MCL = thin red line, MCL/10 = black line).

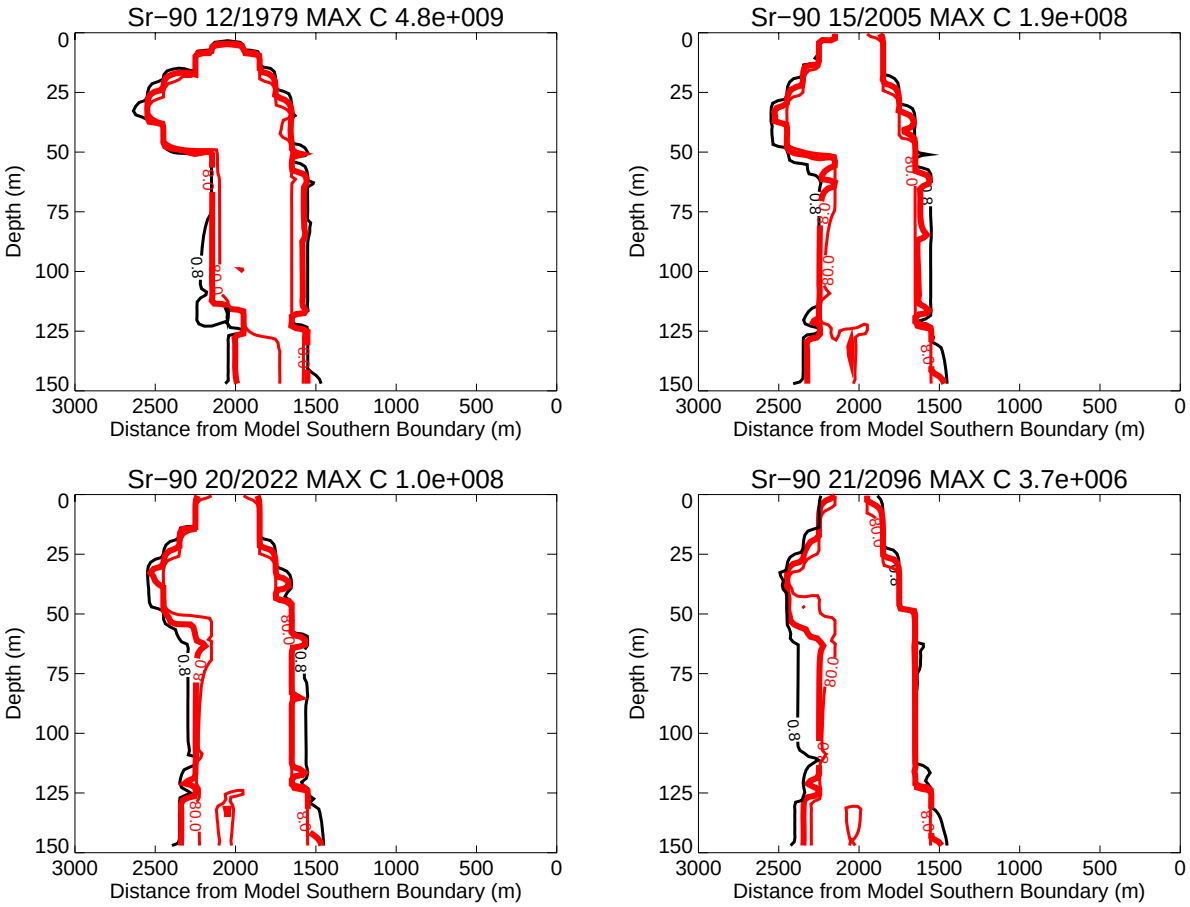

Figure J-9-21. Sr-90 vadose zone concentrations from CPP-31 (vertical contours) (pCi/L) (MCL = thick red line, 10*MCL = thin red line, MCL/10 = black line).

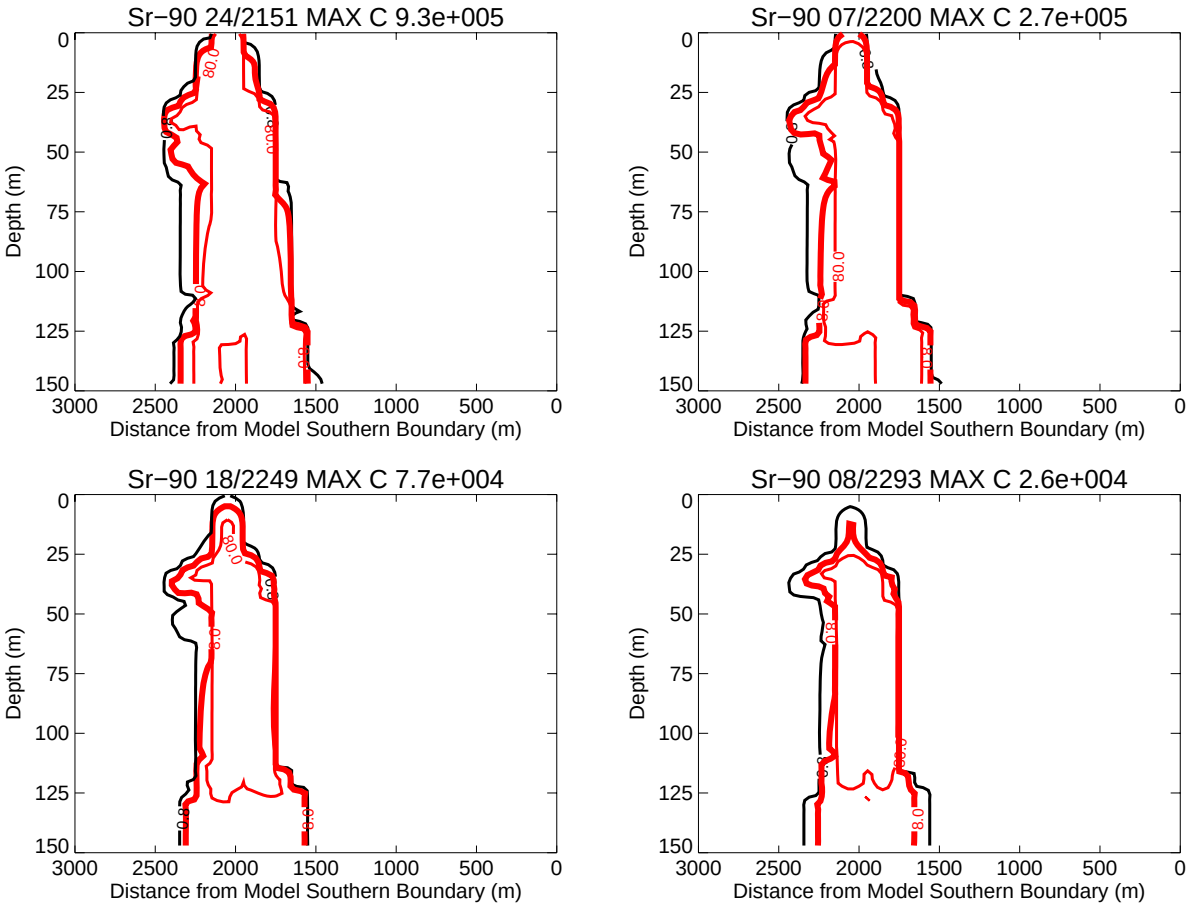

Figure J-9-22. Sr-90 vadose zone concentrations from CPP-31 (vertical contours) (pCi/L) (continued) (MCL = thick red line, 10*MCL = thin red line, MCL/10 = black line).

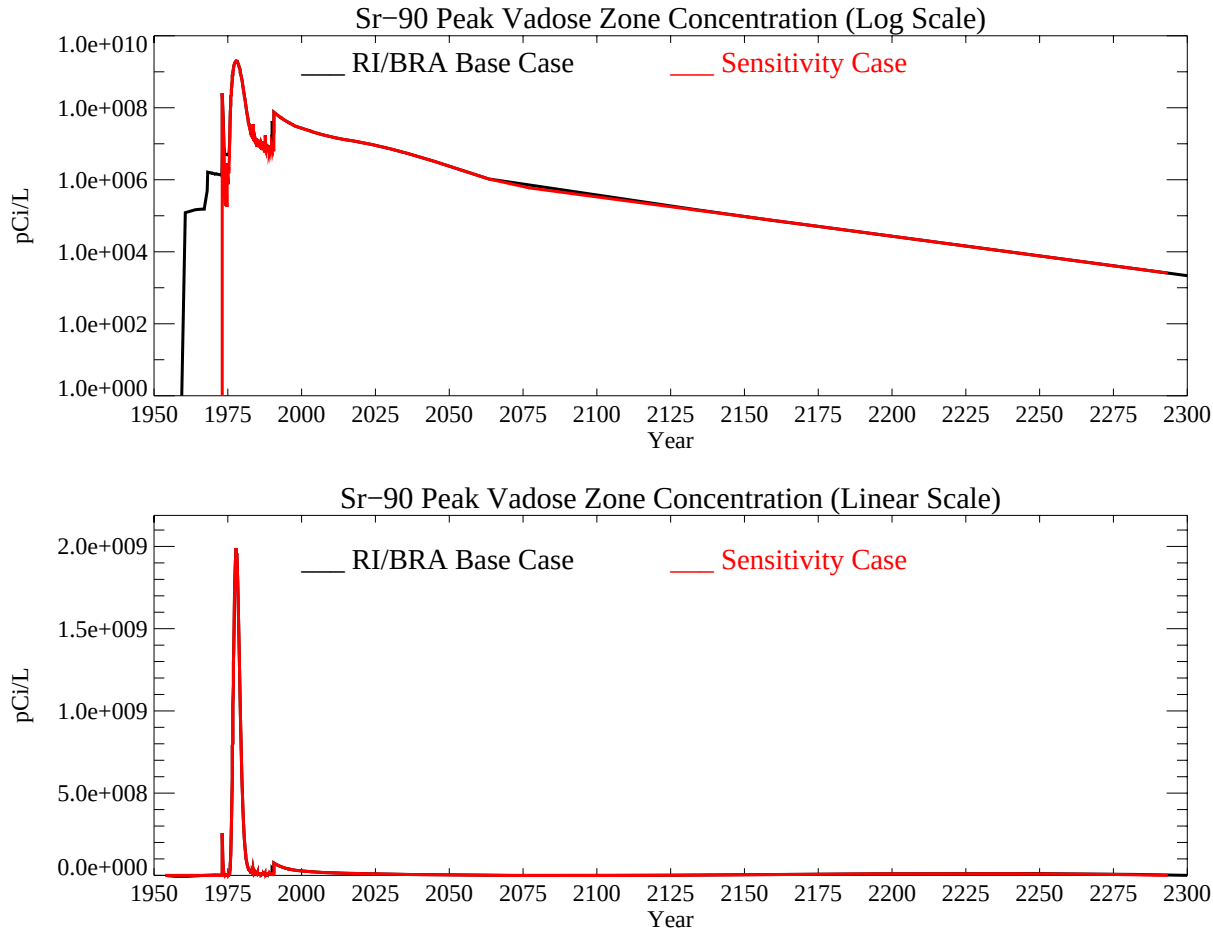

Figure J-9-23. Sr-90 peak vadose zone concentrations from CPP-31 (pCi/L) with the RI/BRA model in black and the CPP-31 source in red.

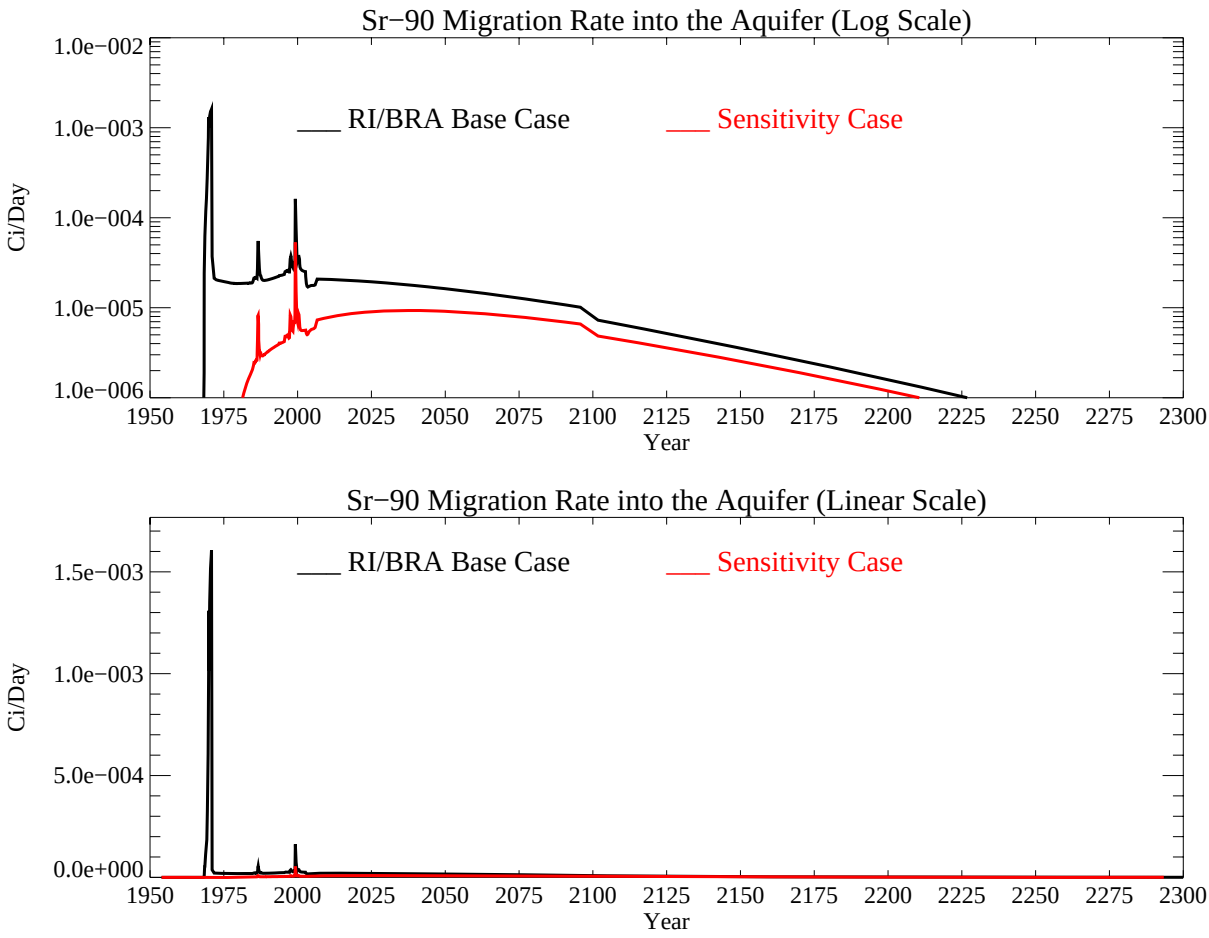

Figure J-9-24. Sr-90 activity flux into the aquifer from CPP-31 (Ci/day) with the RI/BRA model in black, and the CPP-31 source in red.

J-9.3.2 Aquifer Sr-90 Simulation Results

The distribution of Sr-90 in the aquifer for the time period spanning 1979-2096 is given for the far-field in Figure J-9-25. Near-field results representative of the fine-grid are shown for the 2096-2249 time period in Figure J-9-26. The contours for year 2005 indicate that the aquifer is currently being impacted by Site CPP-31. Contours for years 2095-2200 indicate that the highest concentrations occur to the south of INTEC with an extension to the north, consistent with predictions for Tc-99. This differs from the impact of CPP-79 which occurs further south and west. Differences in north-south flow patterns arise as a result of the interbed topology that creates an apparent divide close to directly below INTEC. The area impacted by CPP-31 is considerably smaller than that predicted to be impacted by other Sr-90 sources combined through year 2022, but is larger after year 2096. Sr-90 concentrations are predicted to remain above the MCL during the 1986-2107 time period. This is apparent in the peak aquifer concentration plot given in Figure J-9-27. By comparing the contribution from CPP-79, the impact of CPP-31 is much longer in duration with concentrations predicted to fall below 8 pCi/L for CPP-79 in year 2107.

At a maximum, the highest aquifer impact occurs in the 2000-time frame, with concentrations in the aquifer approaching 61.5 pCi/L. This is larger than the 12.9 pCi/L contribution from CPP-79. In contrast, the predicted peak Sr-90 concentration from CPP-31 in the year 2095 is 4.6 pCi/L, which is about equal to that from CPP-79 and to that from non-CPP-79 and non-CPP-31 sources. The area impacted by CPP-31 above the 0.8 pCi/L level mimics the area impacted above the MCL when all sources were considered in the RI/BRA model. This indicates that the majority of impact at times beyond 2095 is a result of the Sr-90 released into the perched water.

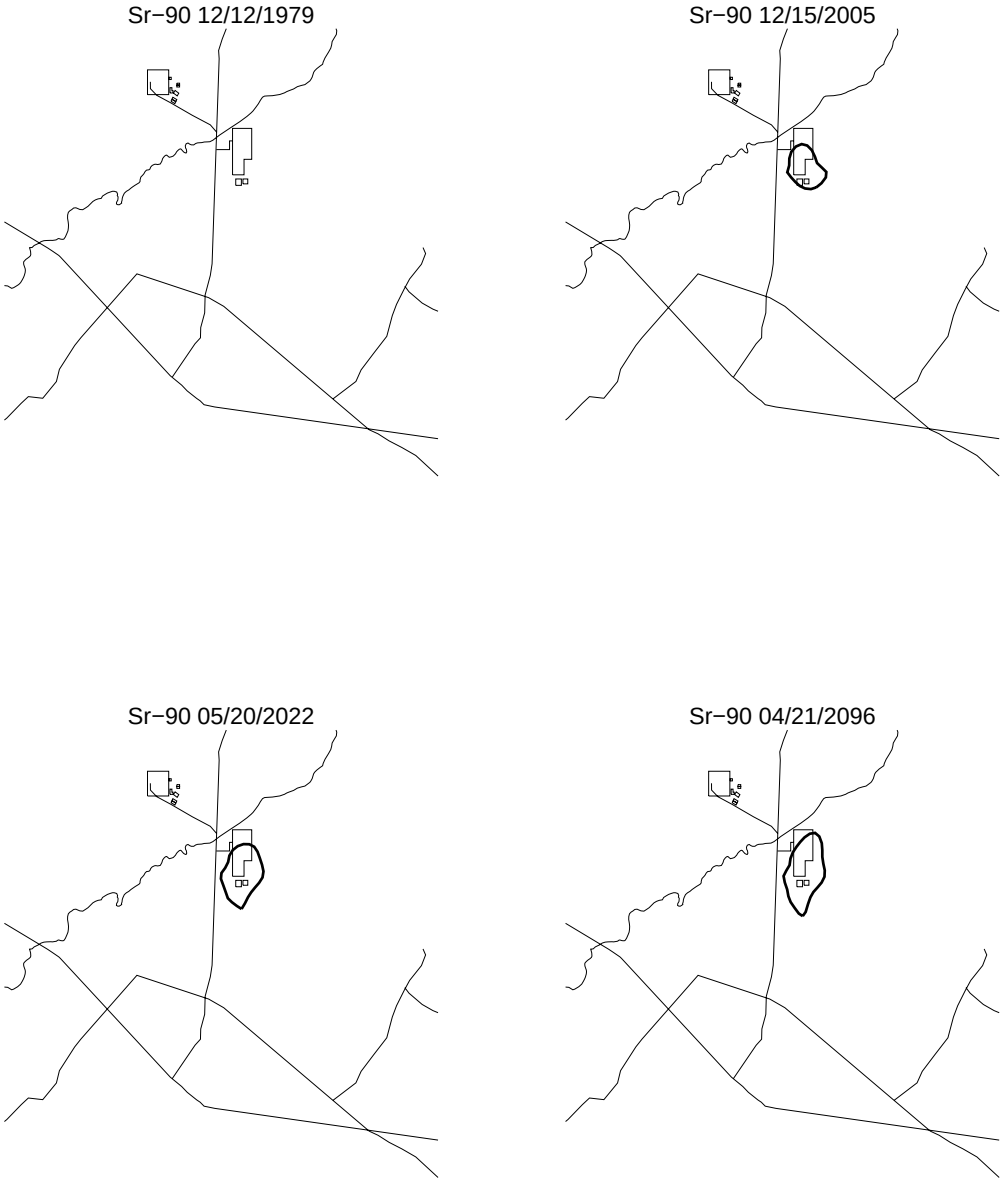

Figure J-9-25. Sr-90 aquifer concentration contours from CPP-31 (pCi/L) (MCL = thick red line, 10*MCL = thin red line, MCL/10 = black line).

Figure J-9-26. Sr-90 aquifer concentration contours from CPP-31 (pCi/L) (continued) (MCL = thick red line, 10*MCL = thin red line, MCL/10 = black line).

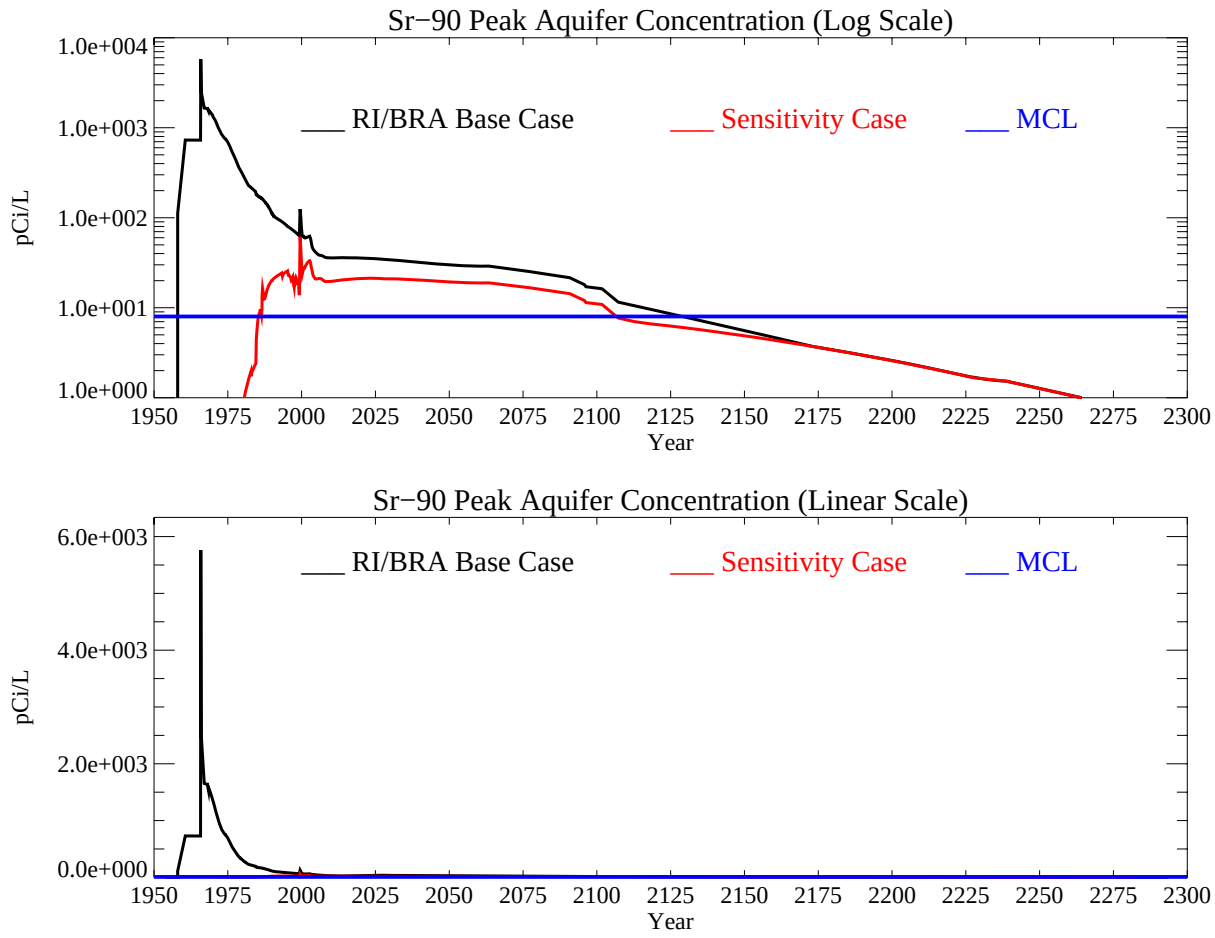

Figure J-9-27. Sr-90 peak aquifer concentrations from CPP-31 (pCi/L) with the MCL in blue, the RI/BRA model in black, and the CPP-31 source in red.

J-9.4 Contribution By Sr-90 Remaining in the Alluvium at CPP-31

In the model results presented in Sections J-8.2, J-8.3, and J-9.3, it was not clear whether or not the Sr-90 thought to remain in the alluvium after year 1992 was contributing significantly to predicted aquifer concentrations. The bulk of this residual Sr-90 would be associated with CPP-31, and would consist of the 3564 Ci distributed throughout the alluvium. It would not include much, if any, of the original 874 Ci from CPP-79 deep because that release occurred just above the alluvium-basalt interface. The later CPP-79 shallow release occurred above CPP-79 deep, contained fewer curies of Sr-90, and was accompanied by 25,000 gallons of water. That later release would have rapidly flushed most of the Sr-90 from CPP-79 deep into the northern upper shallow perched water, leaving very little in the alluvium. The following simulation results evaluate the contribution to aquifer concentrations from the 3564 Ci of Sr-90 thought to remain in the alluvium after year 1972. In this simulation, only the 3564 Ci source was considered.

J-9.4.1 Vadose Zone Sr-90 Simulation Results

In this simulation, 3564 Ci of Sr-90 were distributed vertically in the alluvium in year 1993. As in the RI/BRA base case (considering all sources of Sr-90), this 3564 Ci was distributed vertically through the alluvium, with the activity distribution scaled to the measured soil concentrations obtained during the 2004 sampling (Appendix G, and Table 5-32). This mapping allows most of the activity to be placed at the elevation of the highest measured soil concentrations, with less activity located deeper. To simulate the transport of the activity remaining in the alluvium, an effective K_d of 2 mL/g was used (Figure J-8-9 (J)) for the alluvium sediments.

Figures J-9-28 through J-9-31 illustrate the distribution of Sr-90 in the vadose zone through the year 2293. The concentration isopleths on those plots are for 80., 8.0, and 0.8 pCi/L levels as thin red, thick red, and black lines, respectively. These contours represent the concentration of Sr-90 in the pore water in the alluvium in addition to representing the concentration of Sr-90 in the perched water. The horizontal distribution of Sr-90 in the vadose zone pore water is confined to a much smaller area compared to that obtained considering all of the CPP-31 release (compare Figures J-9-19 and J-9-28). The downward transport allows some Sr-90 to reach the vadose zone-aquifer interface by year 2005 in concentrations just above 8 pCi/L, and by 2096, there is a very small area at this interface where concentrations of 80 pCi/L exist. However, by year 2200, the region above 80 pCi/L has receded upward and is above the 380 ft interbed where it remains through year 2293. After these concentrations reach the aquifer, they will be diluted, and will be much lower than they are predicted to be in the vadose zone.

Peak vadose zone concentrations through time are given in Figure J-9-32. The highest value occurs in 1990, and is 7.5e7 pCi/L. Concentrations are highest in the alluvium, and decrease with depth as the Sr-90 is diluted by influxing water from anthropogenic sources, precipitation infiltration, and from the Big Lost River.

The rate at which this activity enters the aquifer is shown by the red line in Figure J-9-33. For comparison, the rate at which Sr-90 enters the aquifer in the RI/BRA base case is included as the black line. This figure clearly indicates that the flux of Sr-90 entering the aquifer from the residual amount remaining at site CPP-31 in the alluvium is about 10% of that predicted to arrive from other sources. This flux occurs at about 1E-6 Ci/day during a relatively brief period between years 2060 and 2100. This forty year period is much shorter than that the period impacted by the other sources combined. The impact of this relatively small contribution to aquifer concentrations is shown in Figure J-9-34.

Figure J-9-28. SR-90 remaining in the alluvium from CPP-31: vadose zone concentration (horizontal contours) (pCi/L) (MCL = thick red line, 10*MCL = thin red line, MCL/10 = black line).

Figure J-9-29. Sr-90 remaining in the alluvium from CPP-31: vadose zone concentration (horizontal contours) (pCi/L) (MCL = thick red line, 10*MCL = thin red line, MCL/10 = black line).

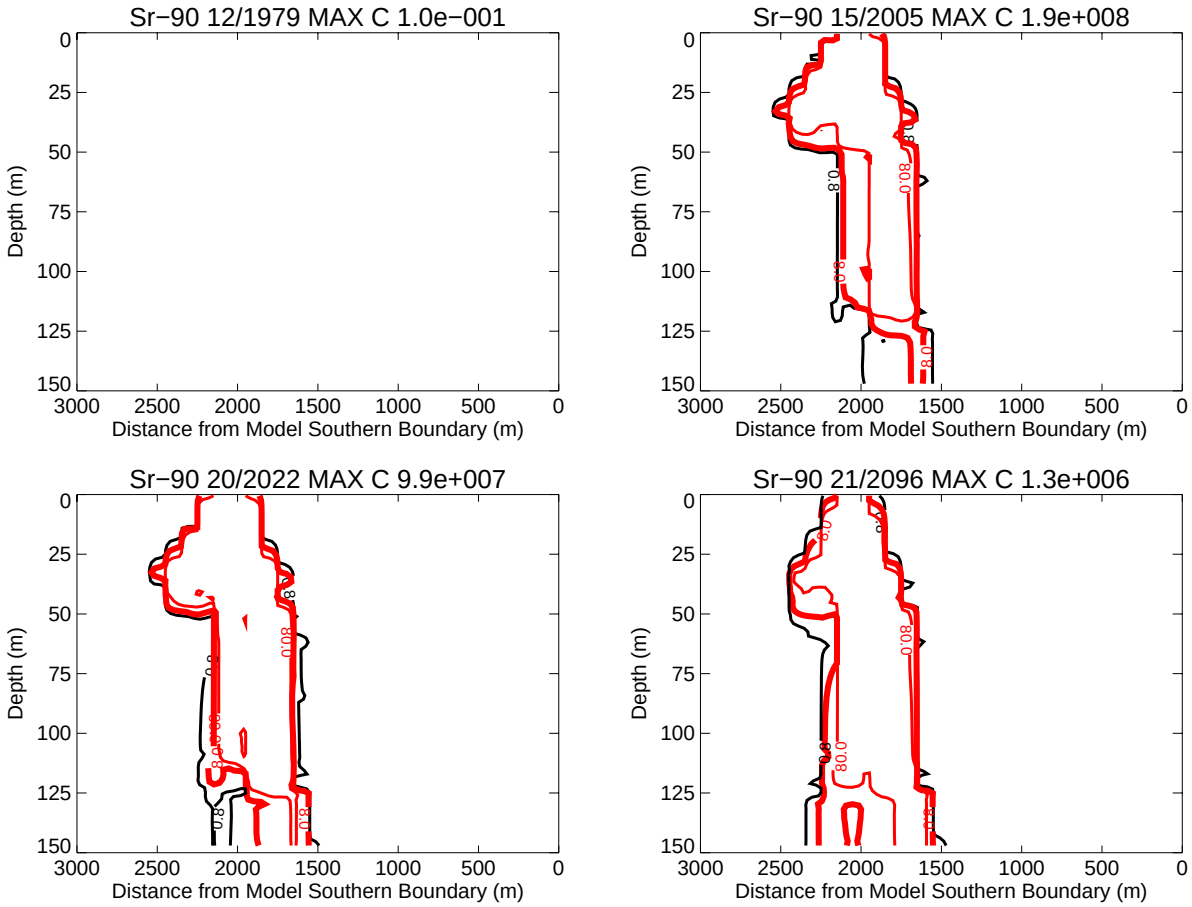

Figure J-9-30. Sr-90 remaining in the alluvium from CPP-31: vadose zone concentrations (vertical contours) (pCi/L) (MCL = thick red line, 10*MCL = thin red line, MCL/10 = black line).

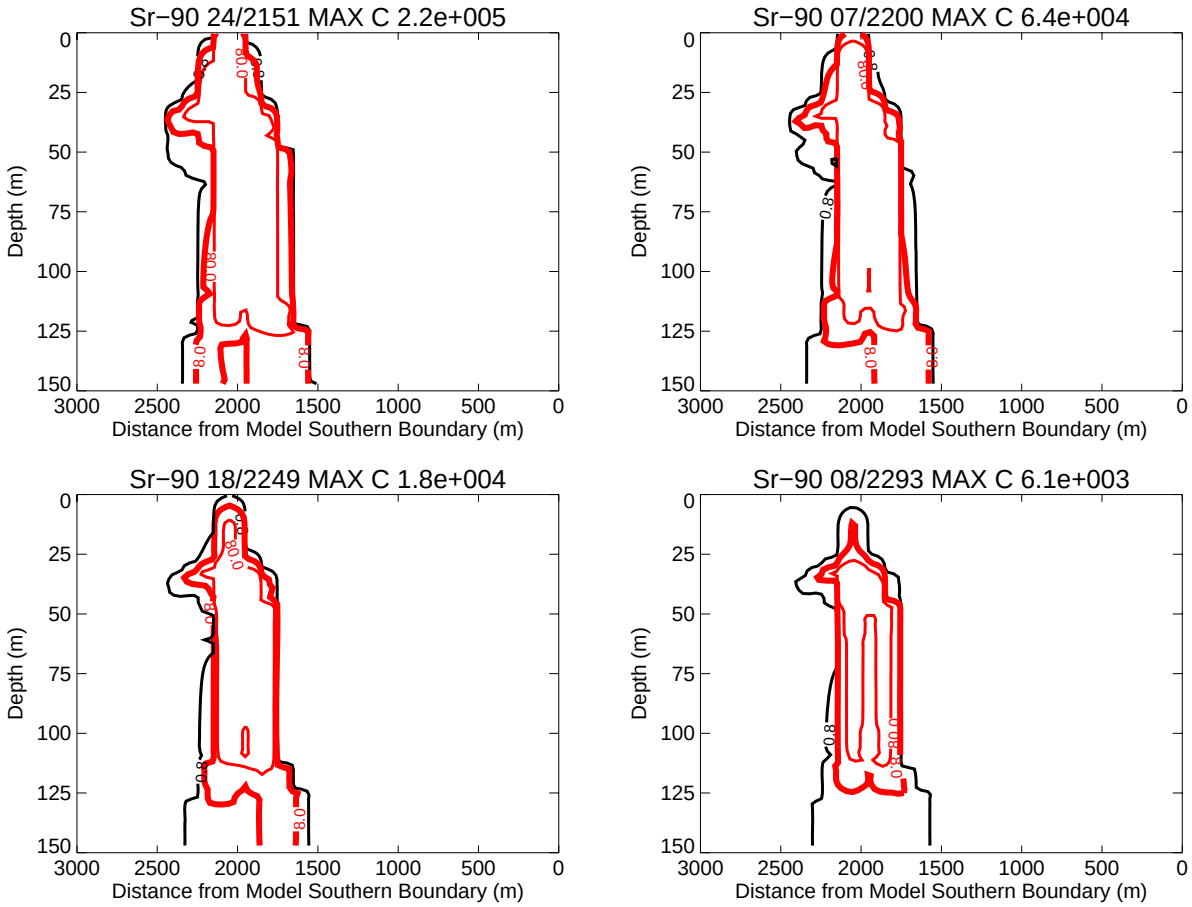

Figure J-9-31. Sr-90 remaining in the alluvium from CPP-31:vadose zone concentrations (vertical contours) (pCi/L) (continued) (MCL = thick red line, 10*MCL = thin red line, MCL/10 = black line).

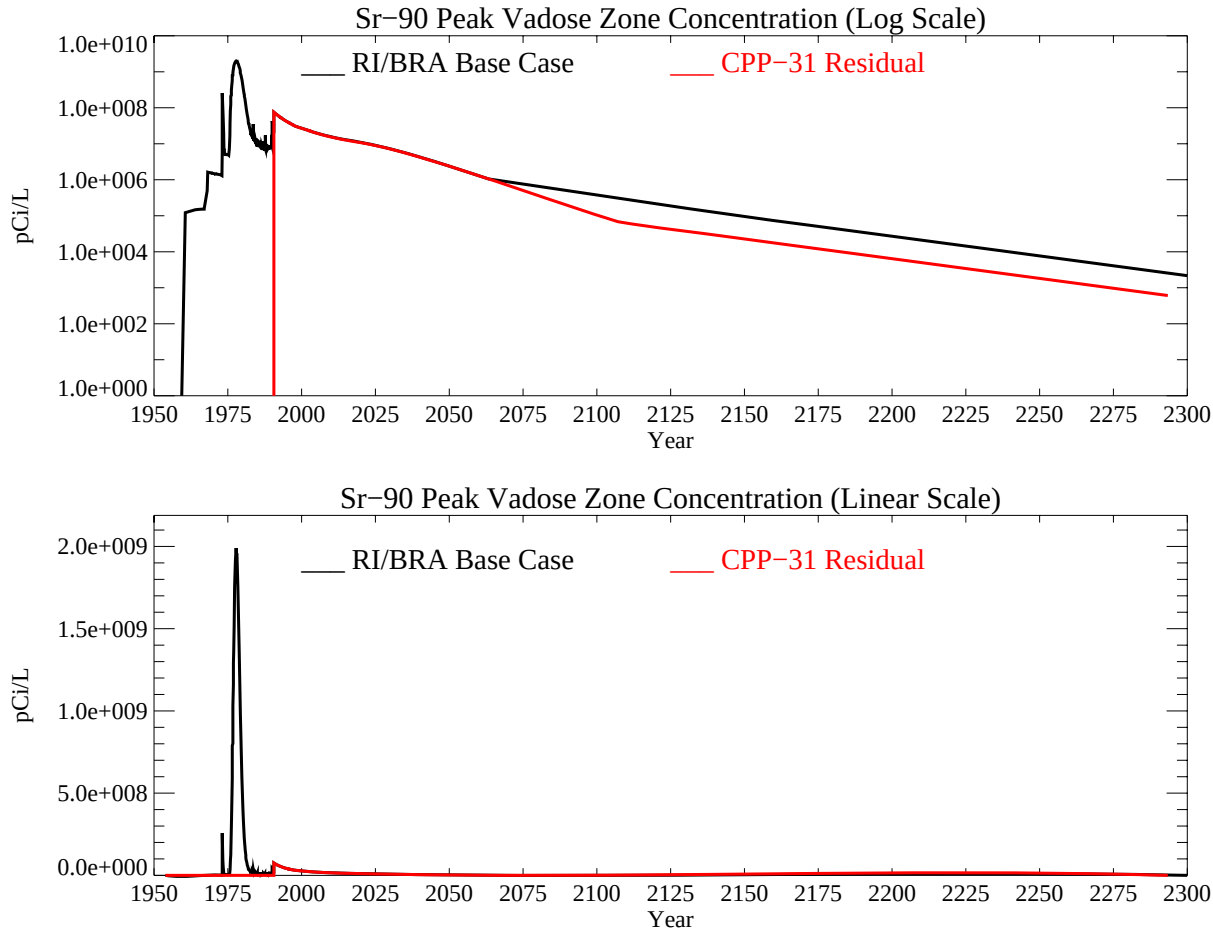

Figure J-9-32. Sr-90 remaining in the alluvium from CPP-31: peak vadose zone concentrations (pCi/L) with the RI/BRA model in black and this residual after 20 years from CPP-31 in red.

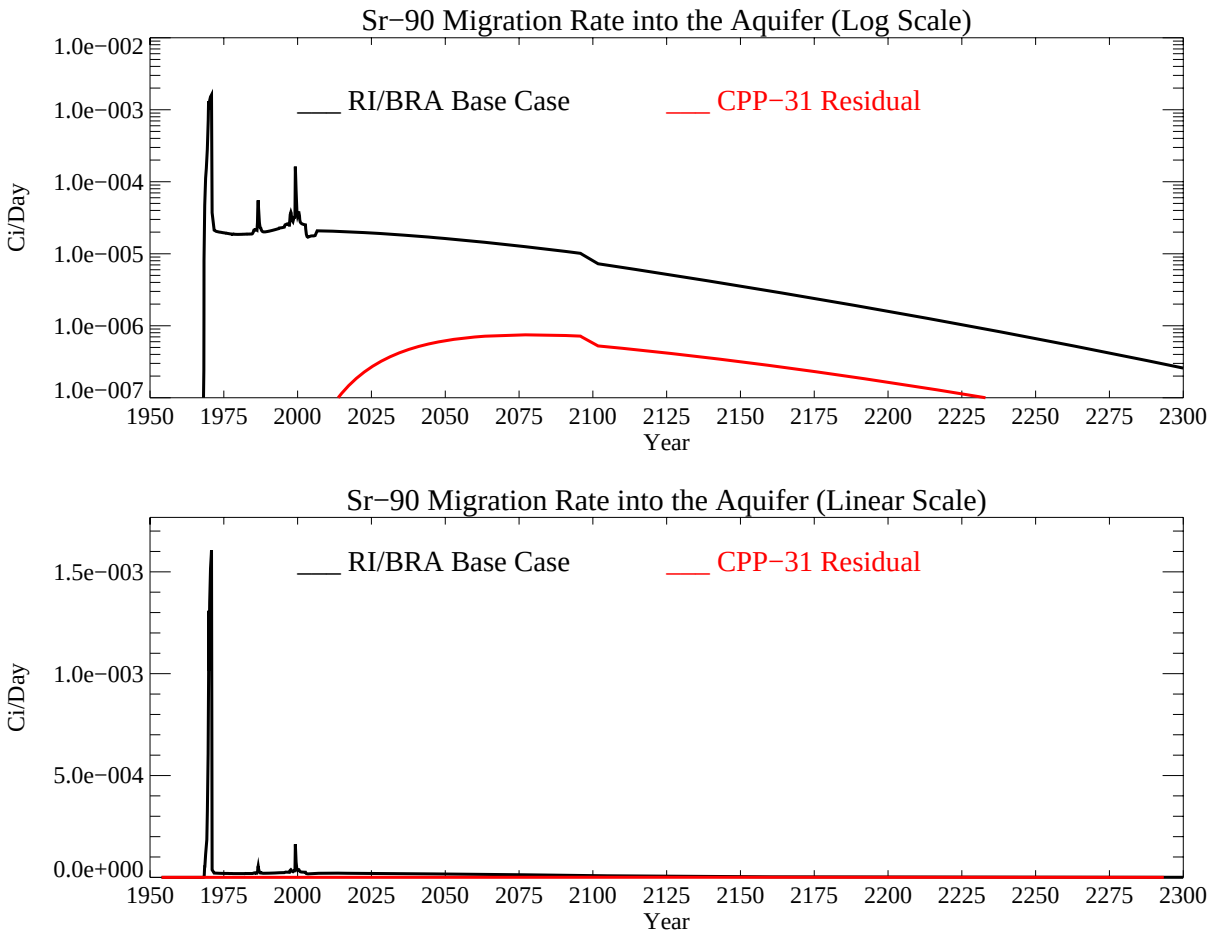

Figure J-9-33. Sr-90 remaining in the alluvium from CPP-31: activity flux into the aquifer (Ci/day) with the RI/BRA base case in black, and the CPP-31 residual in red.

J-9.4.2 Aquifer Sr-90 Simulation Results

The resultant peak aquifer concentration is given in Figure J-9-34. The highest predicted concentration from the CPP-31 residual source is 1.77 pCi/L, which occurs in year 2077. The predicted concentration in year 2095 is just slightly lower at 1.7 pCi/L. Concentrations are less than 1 pCi/L from this residual alluvial source after year 2110. On this figure, the peak concentration resulting from all source of Sr-90 is shown in black for the RI/BRA base simulation using these same model parameters. During the 2030 to 2150 time period, the peak concentration from all of the sources of Sr-90 exceeds 25 pCi/L. This means that less than 10% of the total is being supplied by the 3564 Ci of Sr-90 remaining in the alluvium after 1993.

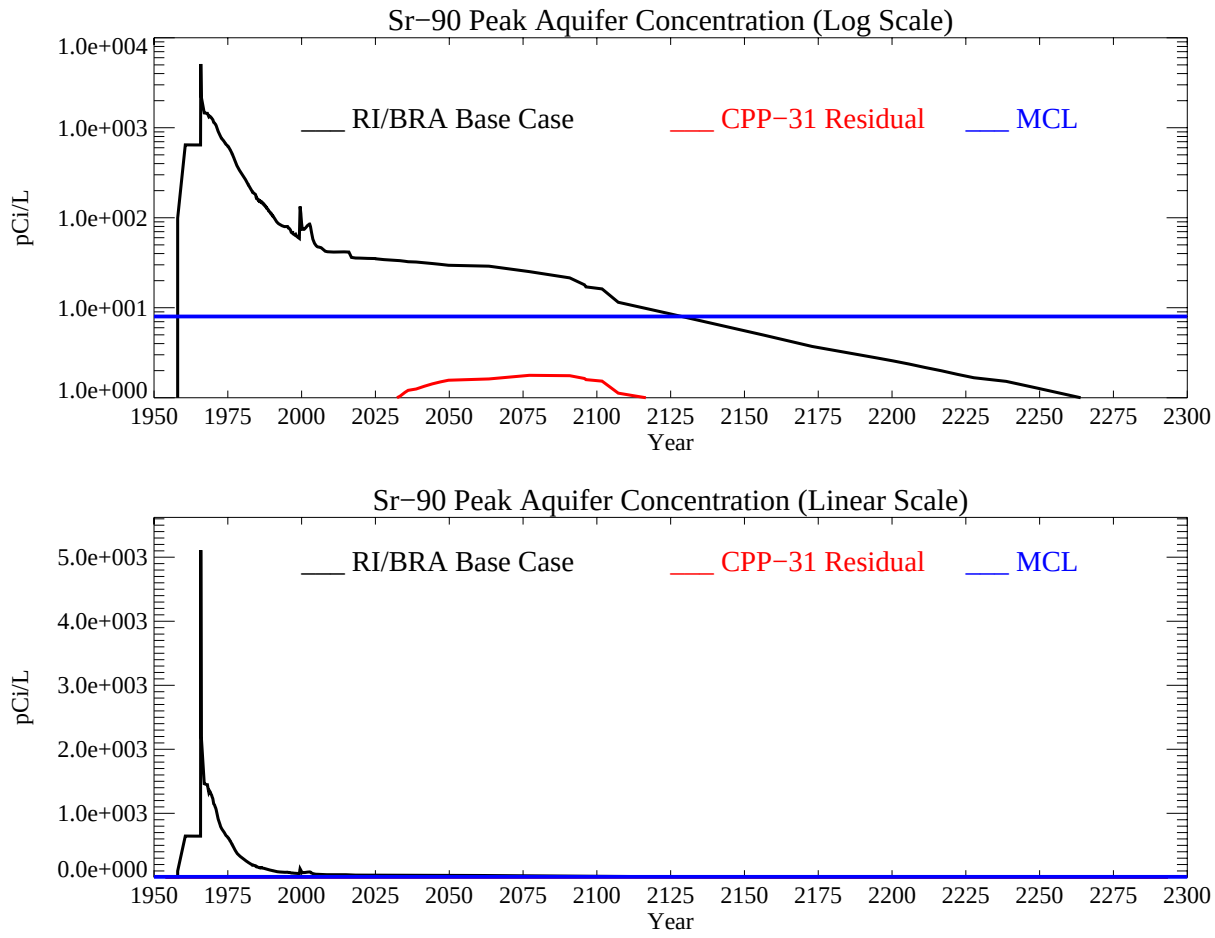

Figure J-9-34. Sr-90 remaining in the alluvium from CPP-31: peak aquifer concentrations (pCi/L) with the MCL in blue, RI/BRA model in black and this residual from CPP-31in red.

J-10 SENSITIVITY TO GEOCHEMICAL INPUTS

Primary geochemical parameters include alluvium properties: cation exchange capacity, selectivity coefficient for strontium, and background sodium concentration; and interbed K_d. Sensitivity to the cation exchange capacity and selectivity coefficients were determined through simulation using the base model discussed in Section J-8. In the following simulations a single parameter change was made. The simulation forming the basis of the sensitivity simulations used a CEC of 2 meq/100 g, a strontium selectivity coefficient of 0.35, a background sodium concentration of 3.3 mmol/L, and an interbed K_d of 22 mL/g. The sensitivity to cation exchange capacity includes simulations using a CEC of 3 meq/100 g, 5 meq/100 g, or 7 meq/100 g. The sensitivity to strontium selectivity coefficient ($K_{Na/Sr}$) used a range from 0.25 to 0.45. Sensitivity to background sodium concentration evaluated the effect of lowering pore water sodium concentrations to 0.22 mmol/L. Sensitivity to interbed K_d was also assessed, by raising the K_d from 22 mL/g to 78 mL/g (spanning the entire range). To assess model sensitivity, we have chosen to look at 1) total activity leaving the alluvium at periods of 5, 10, 15, and 20 yrs, 2) effective adsorption capacity (K_d) after 20 yrs, 3) the impact on the vadose zone, and 4) resultant aquifer concentrations. These results are summarized following the presentation of all simulation in Table J-10-1.

J-10.1 Alluvial CEC of 3 meq/100 g

The recommended CEC range for INTEC alluvial material is 2-8 meq/100 g. A value of 2 meq/100 g was used in the RI/BRA model, and a value of 3 meq/100 g is evaluated here. This simulation uses an infiltration rate from precipitation of 18 cm/yr applied across the INTEC facility, all of the anthropogenic water, and an interbed of K_d=50 mL/g as was used in the RI/BRA base case (Section J-8).

J-10.1.1 Geochemical Evolution in the Alluvium

Summary performance measures for the geochemical evolution of Sr-90 in the alluvium are presented in Figure J-10-1 and can be compared to the RI/BRA base case measures shown in Figure J-8-9. An increase from 2 meq/100 g to 3 meq/100 g has increased the amount of Sr-90 associated with the solid phase as shown by the amount of Sr-90 on exchange sites (subplot I) The total curies after 20 years adsorbed with a CEC of 2 meq/100 g is roughly 3500, compared to nearly 5000 in this scenario. As more of the Sr-90 is associated with exchange sites, it is removed from the aqueous solution. Subplots A-F show the significant decrease in SrNO3 and Sr+ ion, SrCO3, and SroH in the aqueous phase.

The relative abundance of SrNO3 is much larger than the other species, and a 5% decrease is significant. It results in only 10864 Ci leaving the alluvium relative to the 12336 Ci predicted in the RI/BRA base case. After 5, 10, 15, and 20 years, the total Sr-90 that has entered the vadose zone under the alluvium is 14239, 10820, 10842, and 10864 Curies, respectively as shown in Figure J-10-1-G. With this higher CEC, a larger fraction (5036 Ci vs. 3564 Ci) remains in the alluvium after 20 years (Figure J-10-1-I).

The largest difference in the distribution of Sr-90, relative to the base case, occurs in the adsorbed Sr-90. The effective K_d is essentially the ratio of activity on the exchange sites to that in the aqueous phase. As the exchanged activity increases, the aqueous phase Sr-90 concentrations decrease, and the effective K_d increases. The time evolution of this parameter is quite different than observed in the RI/BRA base case (Figure J-10-1 (J)). During the 7-15 year period, the effective K_d is almost double that in the RI/BRA base case. After 20 years, the effective K_d is approaching an average value of 3.75 mL/g.

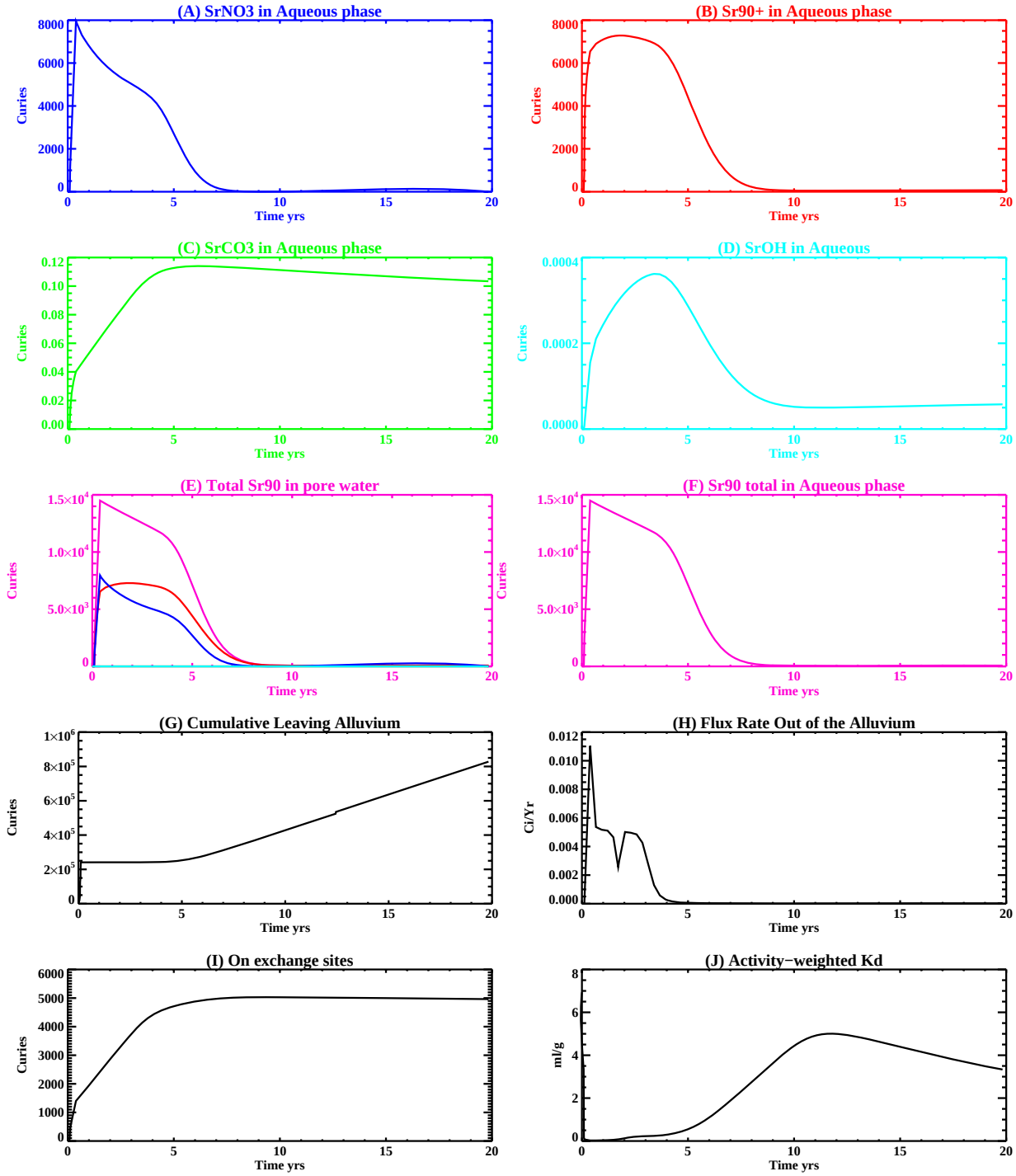

Figure J-10-1. Summary figure illustrating the speciation of Sr-90 in the aqueous phase (A-F), total Sr-90 in the pore-water of the alluvium (E), cumulative curies of Sr-90 having left the alluvium (G), flux rate leaving the alluvium (H), Sr-90 on the exchange sites (I), and effective partitioning coefficient (Kd) (J).

J-10.1.2 Vadose Zone Sr-90 Simulation Results

The release of Sr-90 in this simulation followed the same procedure as was used in the RI/BRA model:

- 15900 Ci from CPP-31 release in the tank farm were represented using (a) the activity-release function shown in Figure J-10-1 (H) for the 10864 Ci released during the first 20 years, and placing this activity flux directly above the basalt interface of the base model (Appendix A, Section 5.1); and (b) distributing the remaining 5036 Ci through the alluvium scaled to the measured soil concentrations obtained during the 2004 sampling cycle (Appendix G and Table 5-32). To simulate the transport of the activity remaining in the alluvium, an effective K_d of 3.75 mL/g was used (Figure J-10-1 (J)) for the alluvium sediments.
- transport of Sr-90 from sources other than CPP-31 originating in the alluvium, whose location is spanned by the submodel (Appendix A, Section 5.1), were simulated using the submodel. Because these source locations were outside the influence of the high ionic strength, acidic CPP-31 release, a K_d of 20 mL/g was used in the submodel alluvium.
- transport of Sr-90 from sources located outside of the submodel horizontal extent were also placed in the base model used to simulate the transport of the CPP-31 remaining in the alluvium. The effective K_d for the alluvium underlying these source locations was also set to the value used to simulate the transport of Sr-90 predicted to remain in the alluvium after 20 yrs (first bullet). The relative magnitude of these sources are small relative to the residual Sr-90 predicted to remain in the alluvium after 20 yrs. In this case, the K_d is much smaller than that used to simulate the transport of Sr-90 from sources within the submodel boundary. This conservativism might increase peak aquifer concentrations slightly.

The horizontal and vertical distribution of Sr-90 in the vadose zone is given in Figures J-10-2 through J-10-5 through the year 2293. Primarily because of the contour intervals provided (plus/minus one order of magnitude of the MCL), the differences relative to the RI/BRA base case are imperceptible in these figures.

One of the goals of this sensitivity study is to explain the choice of RI/BRA model, which is best accomplished by comparing the available field data to model predictions. The arrival of Sr-90 in key perched water wells is shown in Figure J-10-6 and is summarized by the RMS error for all perched water wells in Figure J-10-7. In this simulation, about 90% as much Sr-90 was initially released into the perched water relative to the RI/BRA base case, and the Sr-90 remaining in the alluvium will not have arrived to influence these calibration measures. Because of the timing, these results can be compared to the RI/BRA base case (Figures J-8-14 and J-8-15). In the RI/BRA base case, the model was overpredicting concentrations in northern perched water wells. By releasing less Sr-90 into the perched water, this model matches the data slightly better, but the differences are small. In southern INTEC, predicted concentrations in this case are slightly better. However, concentrations in the southern INTEC wells are orders of magnitude smaller than they are in northern INTEC. Bettering the match to those wells at the expense of a worse match in northern INTEC is not desirable. Overall, the relatively small difference in Sr-90 released into the perched water results in very similar perched water concentrations and very similar matches to the field data. A detailed comparison of the model fit to field data for both of these primary model parameter sets is presented in Section J-12 following the remainder of the sensitivity results. This similarity is reflected in the peak vadose zone concentrations through time presented in Figure J-10-8.

The rate at which Sr-90 enters the aquifer is given in Figure J-10-9, and can be compared directly to the RI/BRA model (black) results. Nearly doubling the amount of Sr-90 arriving in the perched water within the first 20 years following the CPP-31 release has not resulted in a commensurate increase in flux rate out of the vadose zone.

Figure J-10-2. Sr-90 vadose zone concentration assuming an alluvium CEC=3 meq/100 g (horizontal contours) (pCi/L) (MCL = thick red line, 10*MCL = thin red line, MCL/10 = black line).

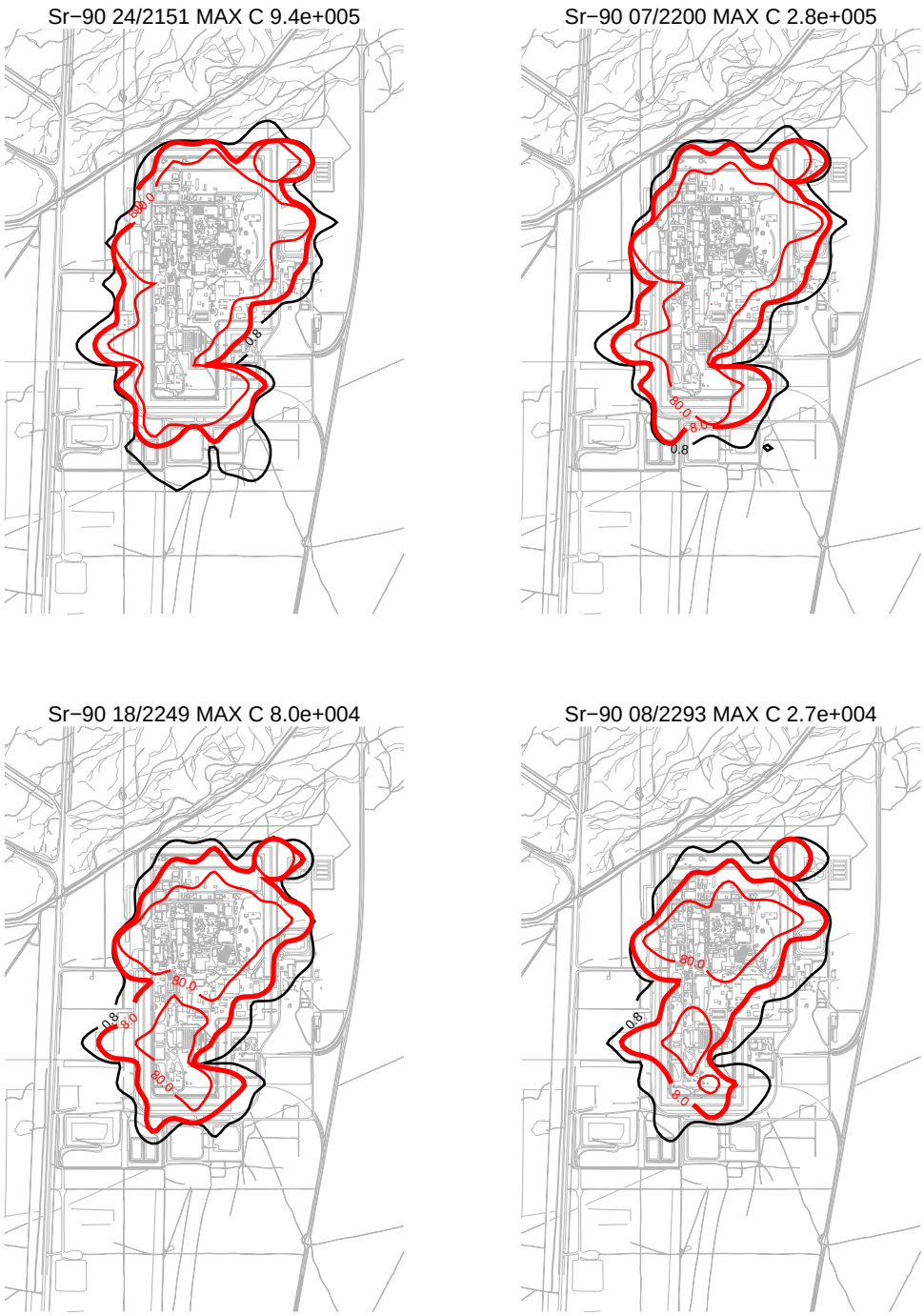

Figure J-10-3. Sr-90 vadose zone concentration assuming an alluvium CEC=3 meq/100 g (horizontal contours) (pCi/L) (MCL = thick red line, 10*MCL = thin red line, MCL/10 = black line).

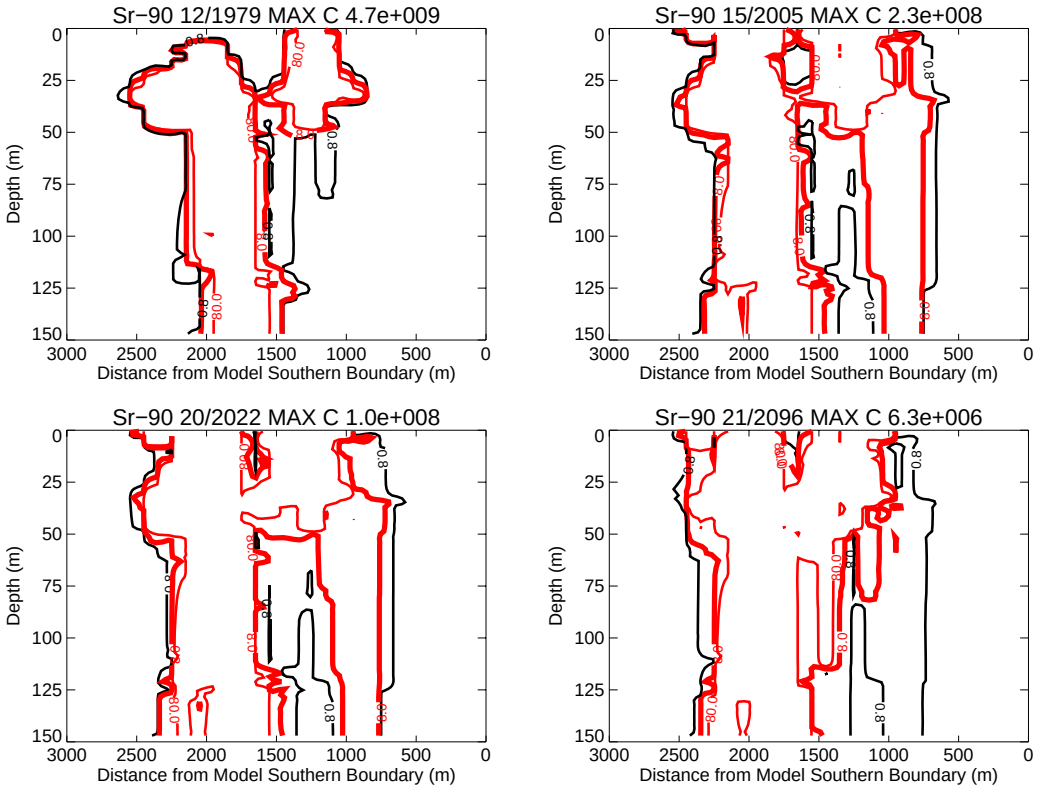

Figure J-10-4. Sr-90 vadose zone concentrations assuming an alluvium CEC=3 meq/100 g (vertical contours) (pCi/L) (MCL = thick red line, 10*MCL = thin red line, MCL/10 = black line).

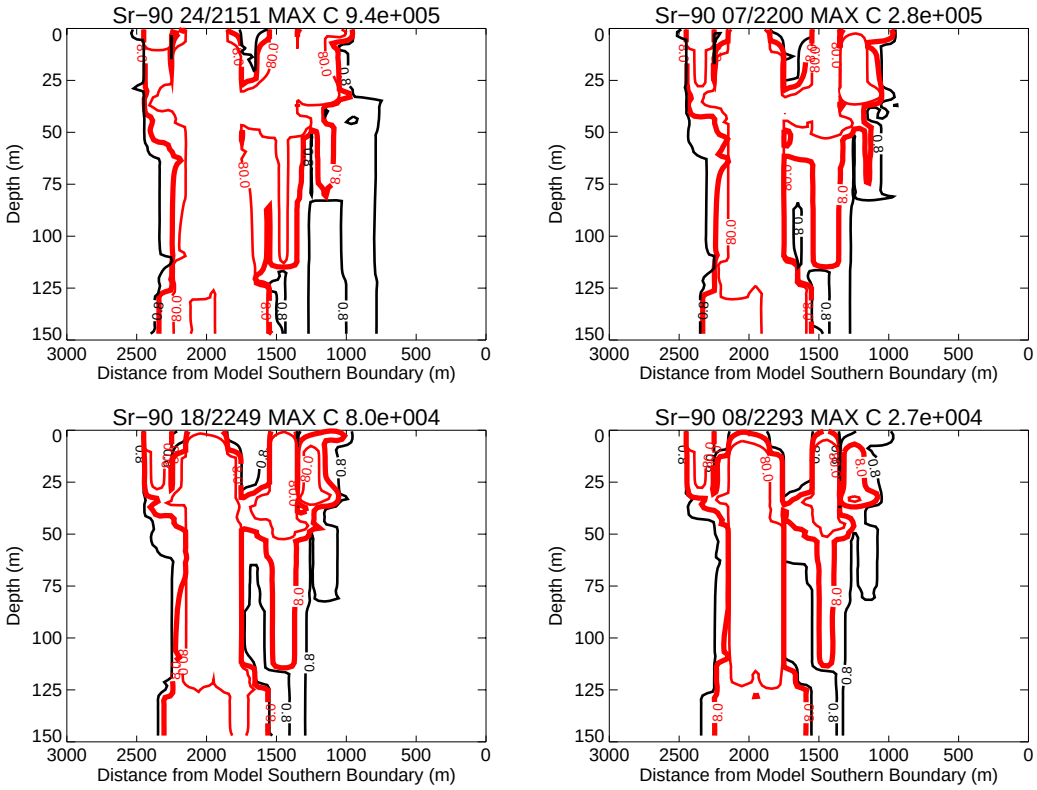

Figure J-10-5. Sr-90 vadose zone concentrations assuming an alluvium CEC=3 meq/100 g (vertical contours) (pCi/L) (continued) (MCL = thick red line, 10*MCL = thin red line, MCL/10 = black line).

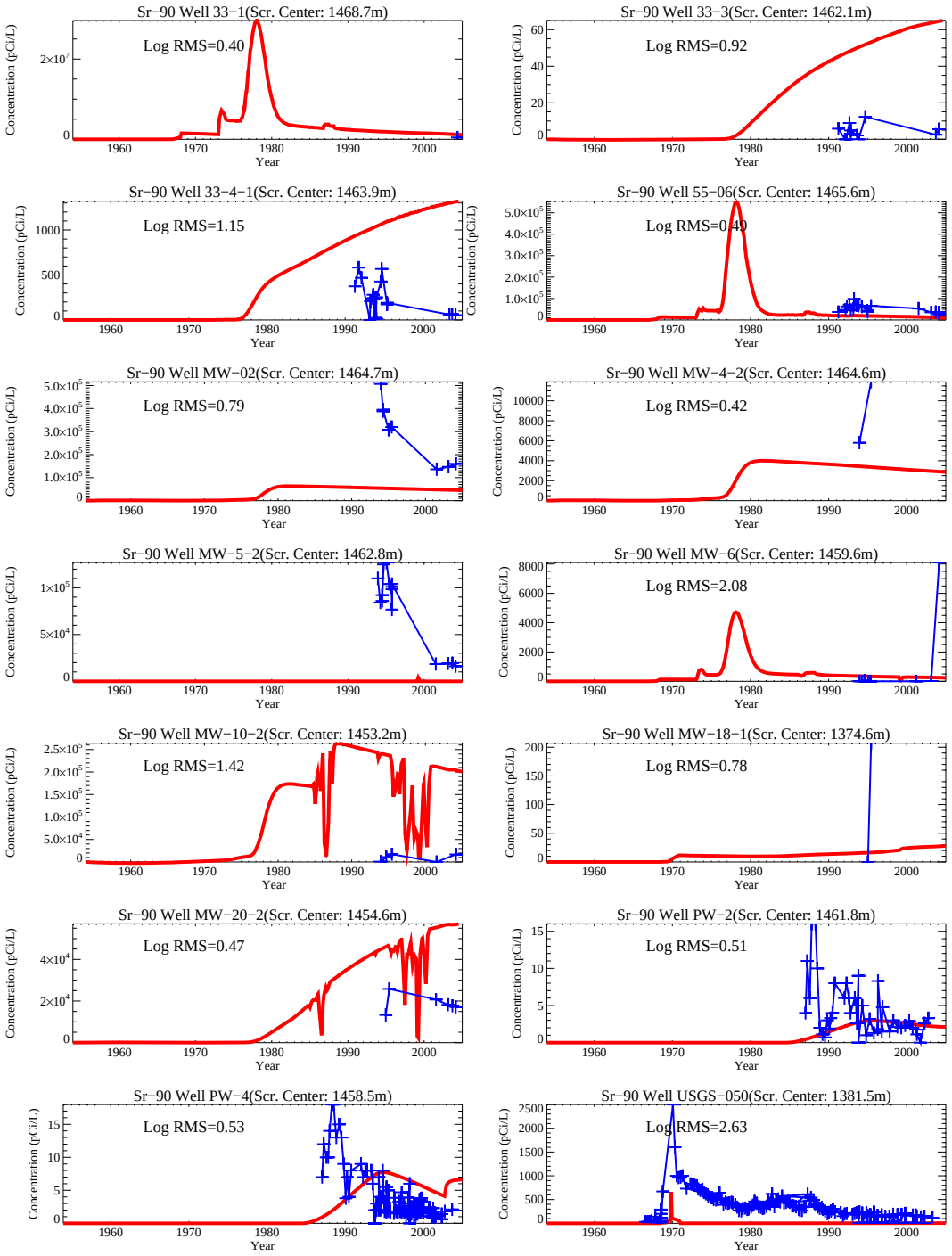

Figure J-10-6. Sr-90 concentration in perched water wells assuming an alluvium CEC=3 meq/100 g (pCi/L) (Measured values = blue crosses, red = model at screen center).

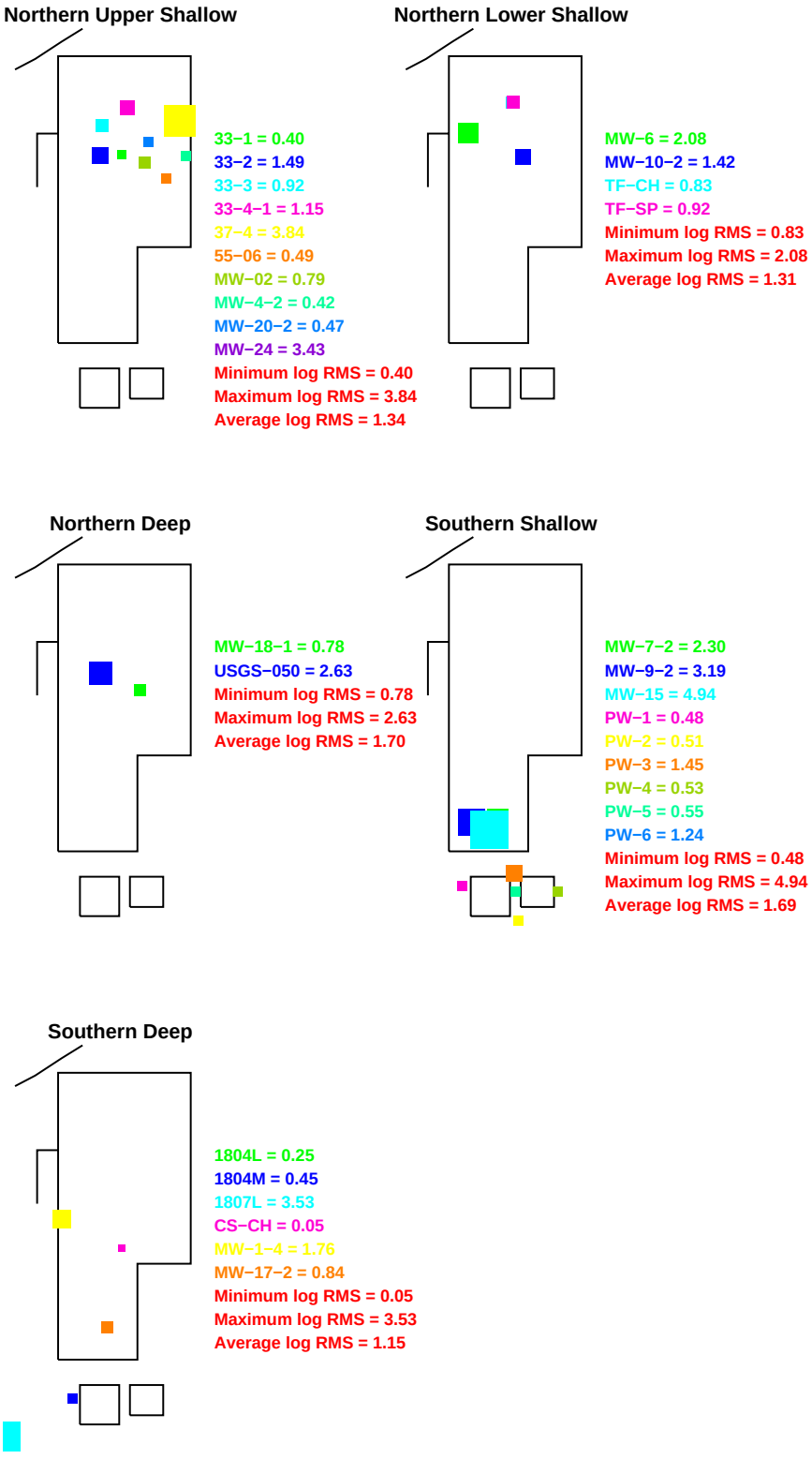

Figure J-10-7. Log 10 Root mean square error (RMS) by depth and northing assuming an alluvium CEC=3 meq/100 g.

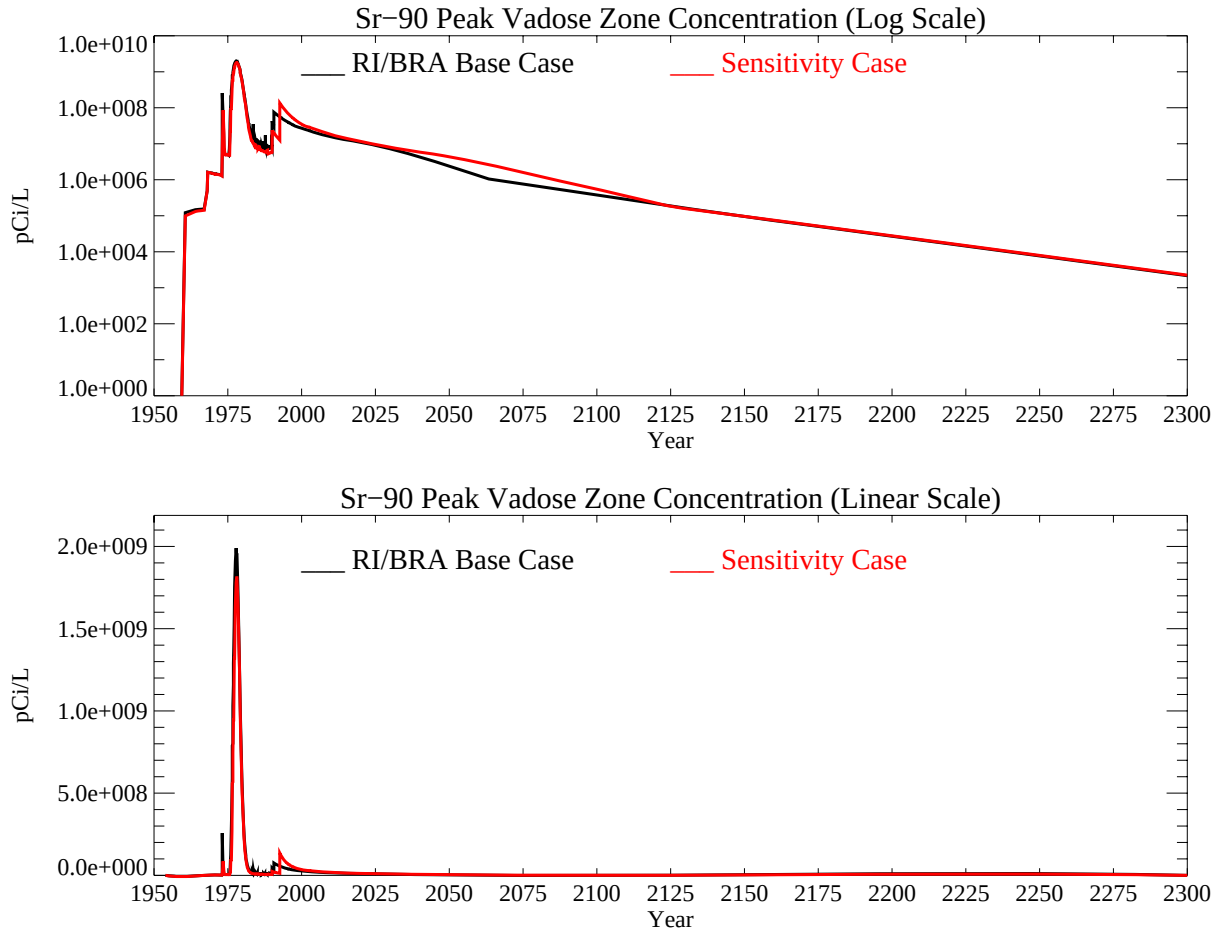

Figure J-10-8. Sr-90 peak vadose zone concentrations assuming an alluvium CEC=3 meq/100 g (pCi/L) with the RI/BRA model in black and this sensitivity run in red.

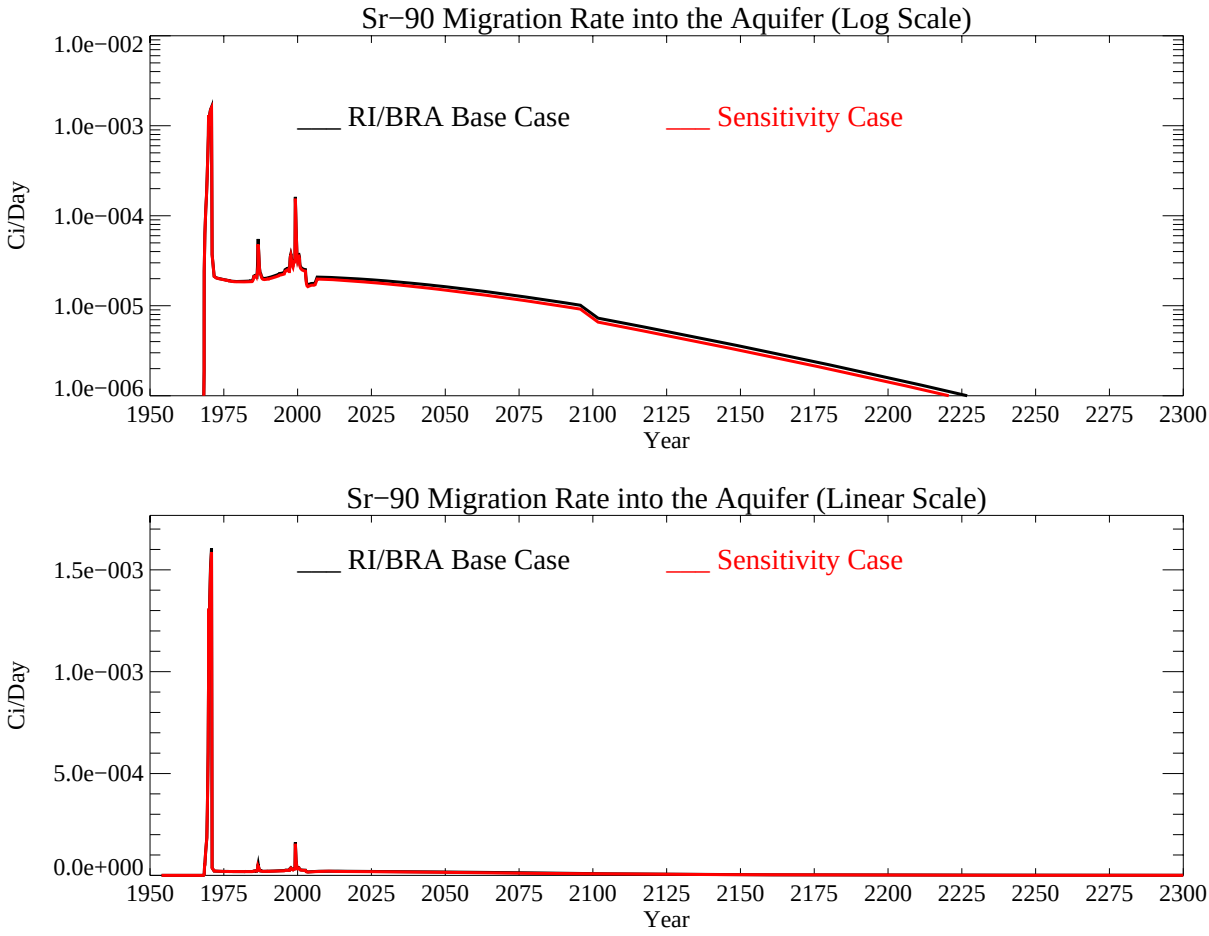

Figure J-10-9. Sr-90 activity flux into the aquifer assuming an alluvium CEC=3 meq/100 g (Ci/day) with the RI/BRA model in black, and this sensitivity run in red.

J-10.1.3 Aquifer Sr-90 Simulation Results

The distribution of Sr-90 in the aquifer for the time period spanning 2005-2096 on the course grid is given in Figure J-10-10. It is presented for the 2049-2151 time period on the fine grid in Figure J-10-11. Resultant peak aquifer concentrations are given in Figure J-10-12, with the red line representing the results of this simulation. Because the Sr-90 originating at land surface does not arrive in the aquifer until the late 1980's, comparisons to measured data are not presented for aquifer wells.

The three important performance measures are concentrations beyond 2095, the spatial extent of contamination, and the time period during which concentrations exceed the MCL. The predicted peak Sr-90 concentration in the year 2095 is 16.7 pCi/L, about 90% of that predicted in the RI/BRA model. This is in direct proportion to the amount of Sr-90 arriving in the perched water within 20 years of the CPP-31 release. This concentration is twice as high as the MCL. The peak concentration in year 2095 is insignificantly different from the RI/BRA base case compared to the overall model uncertainty.

The Sr-90 contour plots presented in Figures J-10-10 and J-10-11 illustrate that the predicted distribution in the aquifer does not differ greatly from that predicted in the RI/BRA model. They show that although concentrations are predicted to exceed the MCL beyond 2095, that the area impacted by Sr-90 above 8 pCi/L is between the INTEC fence and the former percolation ponds in 2095.

The third measure in this sensitivity result is the time during which the MCL is exceeded. A 20% reduction in the amount of Sr-90 released from the alluvium into the perched water allows the MCL to be reached only 6 years earlier than predicted in the RI/BRA base case. In this case, the simulated Sr-90 concentrations remain above the MCL from 1960 through year 2123, while in the RI/BRA base case it occurred by year 2129. Given the overall model uncertainty, this difference is insignificant.

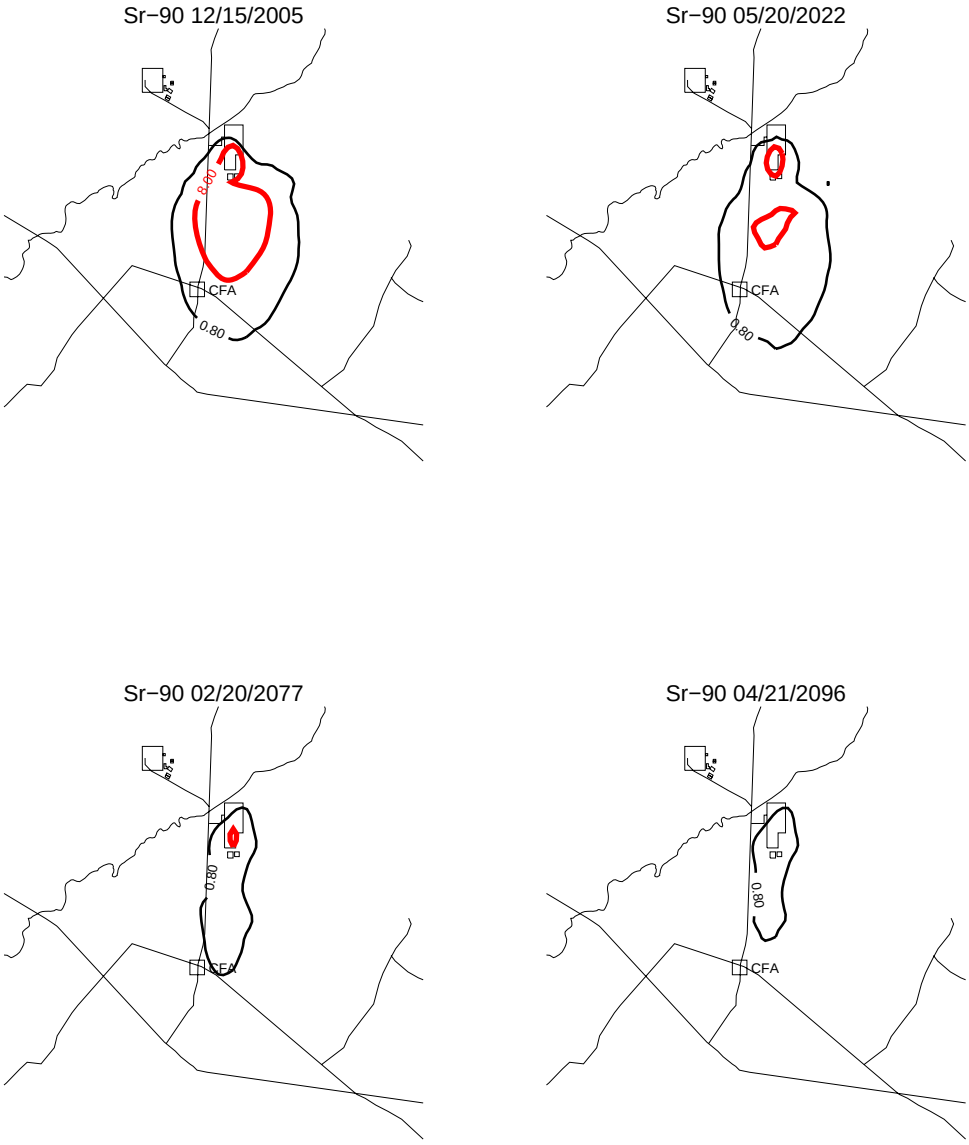

Figure J-10-10. Sr-90 aquifer concentration contours assuming an alluvium CEC=3 meq/100 g (pCi/L) (MCL = thick red line, 10*MCL = thin red line, MCL/10 = black line).

Figure J-10-11. Sr-90 aquifer concentration contours assuming an alluvium CEC=3 meq/100 g (pCi/L) (continued) (MCL = thick red line, 10*MCL = thin red line, MCL/10 = black line).

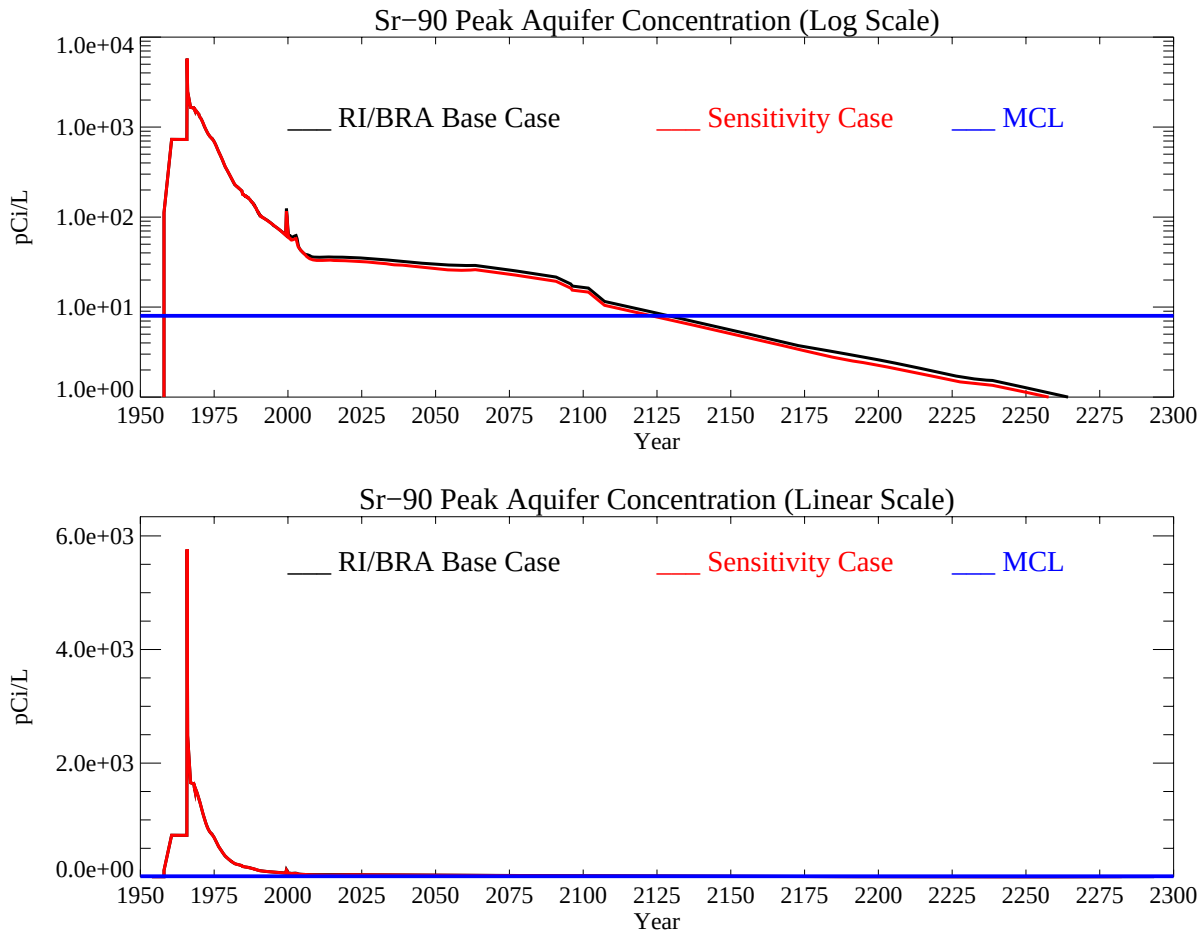

Figure J-10-12. Sr-90 peak aquifer concentrations assuming an alluvium CEC=3 meq/100 g (pCi/L) with the MCL in blue, RI/BRA model in black and this sensitivity run in red.

J-10.2 Higher Alluvial CEC of 7 meq/100 g

In order to evaluate the non-linearity of predicted response to CEC, the higher end of alluvium CEC was considered. This simulation was conducted to complete the alluvium CEC range from 2, 3, and 7 meq/100 g, and is based on the RI/BRA model presented in Section J-8.

J-10.2.1 Geochemical Evolution in the Alluvium

For comparison to the RI/BRA model, figures for the transport of total aqueous Sr, the amount of Sr-90 on exchange sites, and the resultant effective K_d are given in Figures J-10-13 through J-10-15. The aqueous phase concentrations are lower than predicted in the RI/BRA model in response to the higher CEC. Simultaneously, the total Sr-90 associated with exchange sites is slightly higher, with most of the Sr-90 existing on exchange sites at higher elevations in the alluvium. The resultant effective partition coefficient is significantly higher, with the highest values coinciding with the center of aqueous phase activity.

After 5, 10, 15, and 20 years, the total Sr-90 that has entered the vadose zone under the alluvium is 1773, 6378, 6393, and 6403 Curies, respectively as shown in Figure J-10-16. It is readily apparent that over the entire range of CEC expected to exist in the INTEC alluvium, the initial rapid release of Sr-90 occurs within the first 5 years. With the higher CEC, a larger fraction (9497 Ci vs. 3564 Ci) remains in the alluvium after 20 years as shown in the summary Figure J-10-16. Over the entire range examined here, the amount of transported Sr-90 (Figure J-10-13) is a nearly linear function of CEC.

The majority of Sr-90 remaining in the alluvium exists at shallow depths on the exchange sites as shown in Figures J-10-14 and J-10-16. The largest change in the distribution of Sr-90 on the exchange sites occurs soon after the CPP-31 release. During the first five years, the slightly mobile Sr-90 migrates from the initial release location and partitions onto the solids. As this redistribution occurs, there is an initial rise in effective K_d, reaching a peak value of 20 mL/g at 12 years, followed by a slow decrease in Sr-90 on the exchange sites as the other cations in solution leave the alluvium. Increasing the CEC has increased the effective K_d for the Sr-90 remaining in the alluvium to 17 mL/g compared to 2 mL/g in the base case as shown in Figures J-10-13 and J-10-16. The decrease in initial released activity and large increase in effective K_d is reflected in the resulting peak vadose zone and aquifer concentrations.

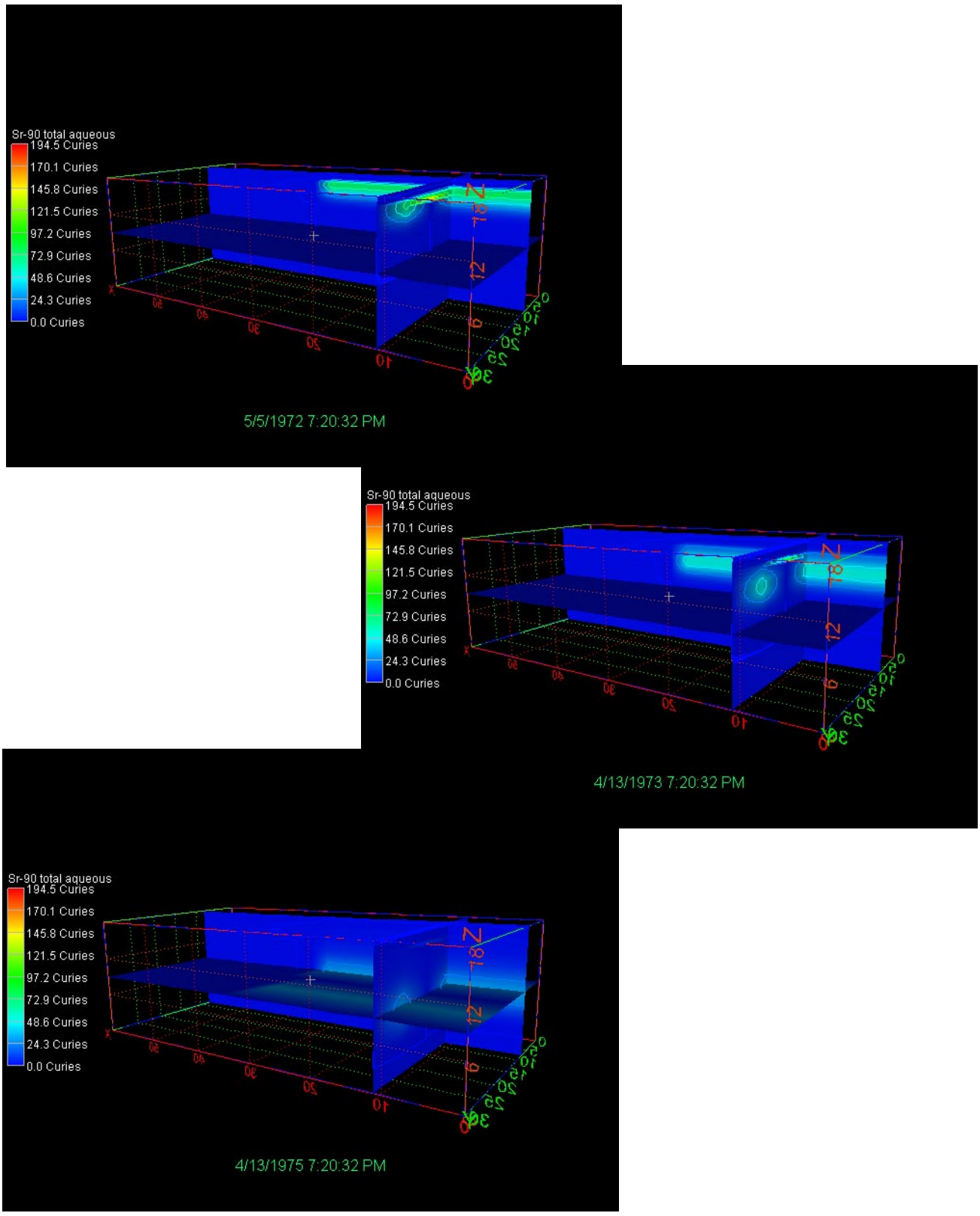

Figure J-10-13. Total aqueous-phase Sr-90 0.5, 1.5, and 3 years after CPP-31 release with CEC = 7 meq/100 g.

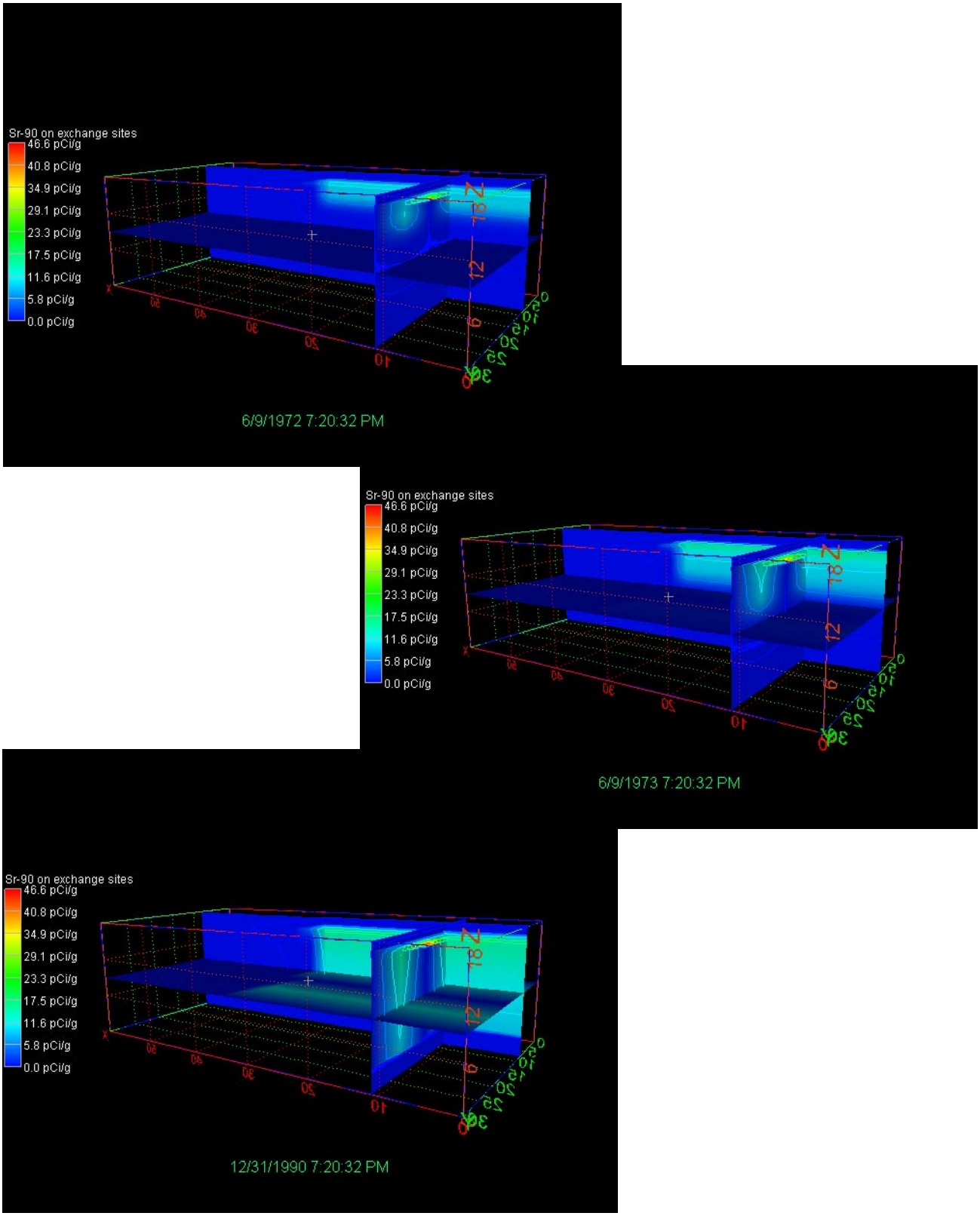

Figure J-10-14. Sr90 on the exchange sites 1,2, and 3 years after the CPP-31 release with CEC = 7 meq/100 g.

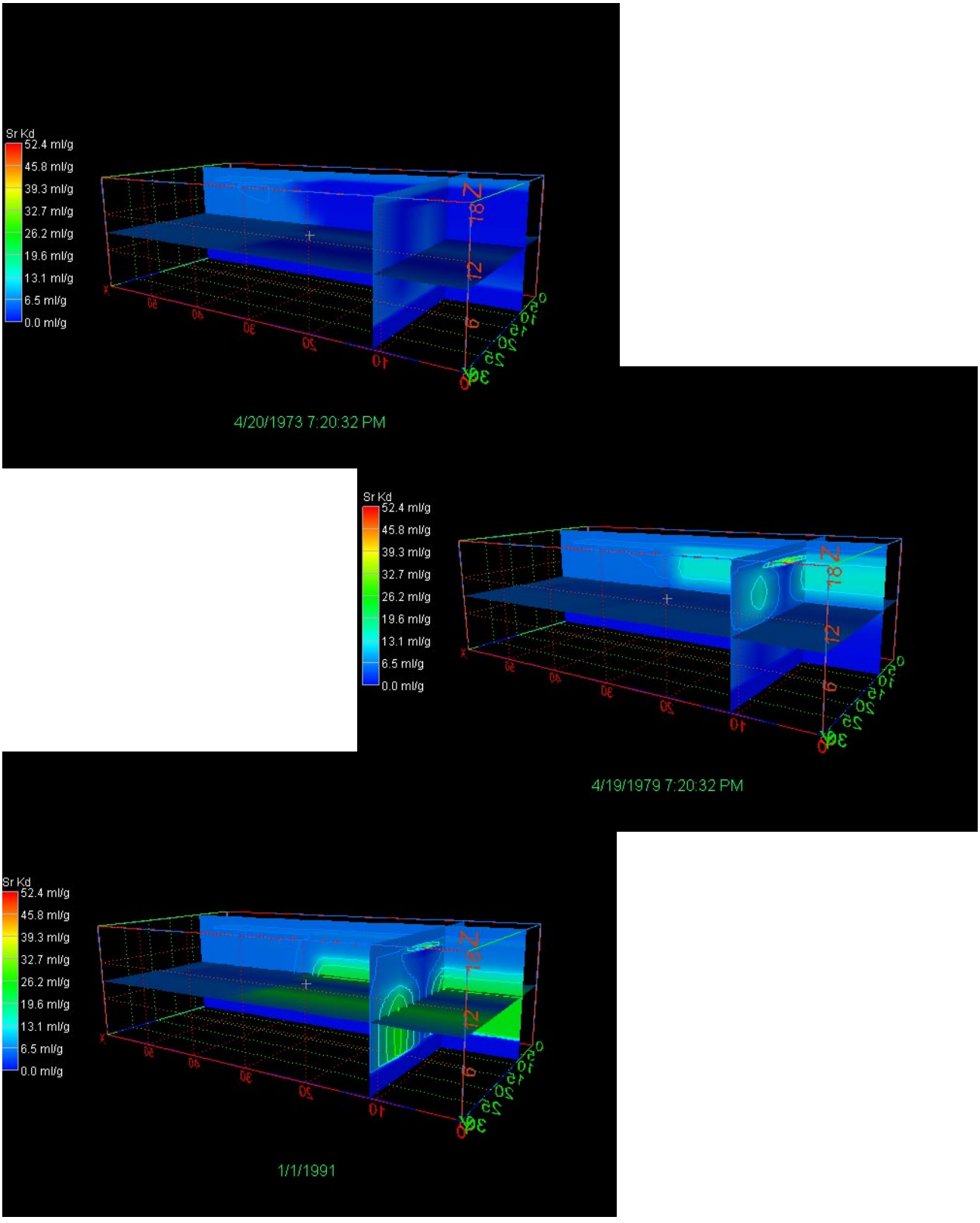

Figure J-10-15. Effective partitioning between aqueous and solid-phase Sr-90 0.5, 1.5, and 17.5 years after CPP-31 release with CEC = 7 meq/100 g.

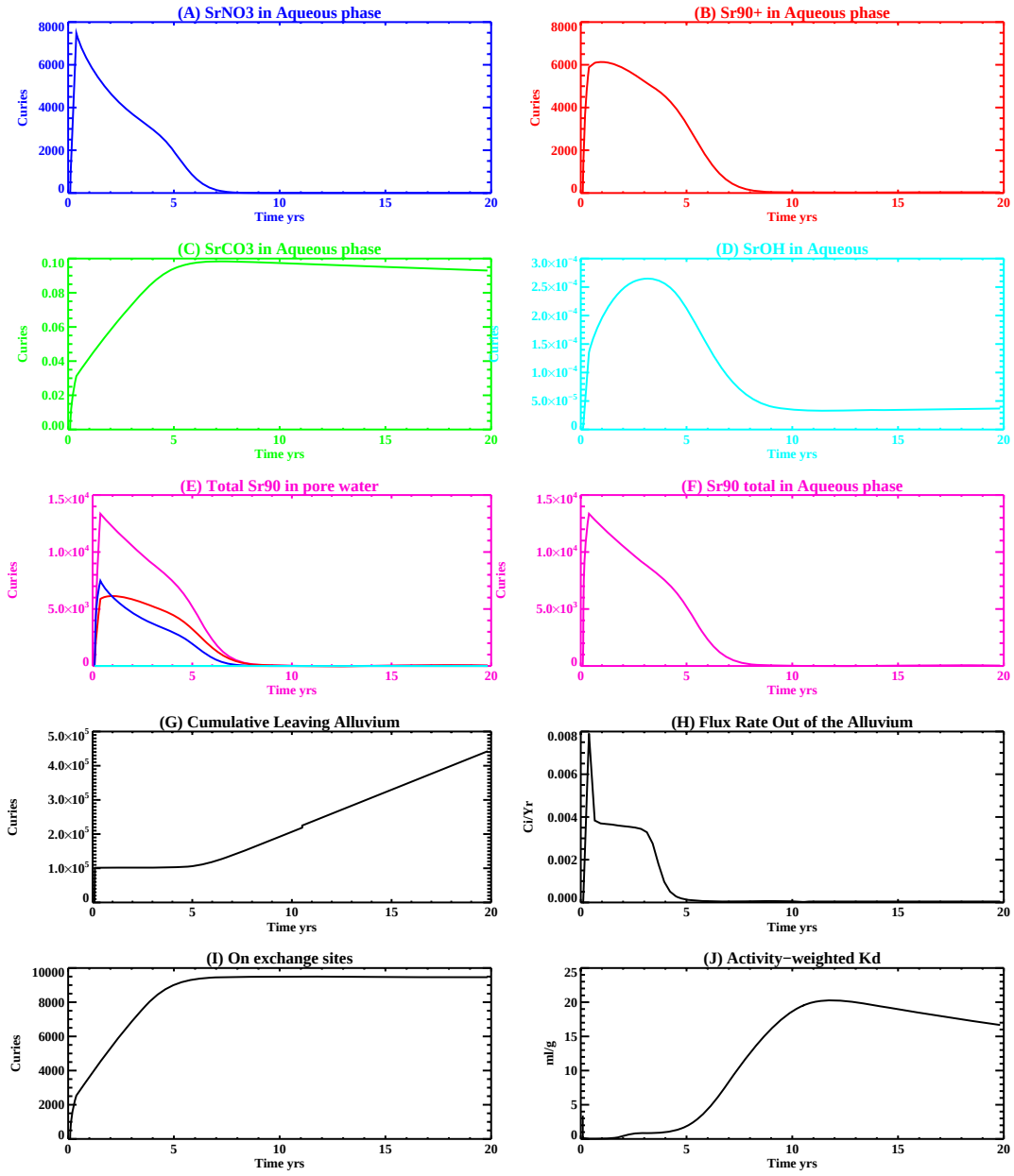

Figure J-10-16. Summary figure illustrating the speciation of Sr-90 in the aqueous phase (A-F), total Sr-90 in the pore-water of the alluvium (E), cumulative curies of Sr-90 having left the alluvium (G), flux rate leaving the alluvium (H), Sr-90 on the exchange sites (I), and effective partitioning coefficient (Kd) (J).

J-10.2.2 Vadose Zone Sr-90 Simulation Results

The release of Sr-90 in this simulation followed the same procedure as was used in the sensitivity base-case:

- 15900 Ci from CPP-31 release in the tank farm were represented using (a) the activity-release function shown in Figure J-10-16 (H) for the 6403 Ci released during the first 20 years, and placing this activity flux directly above the basalt interface of the base model (Appendix A, Section 5.1). The remaining 9497 Ci were distributed vertically through the alluvium scaled to the measured soil concentrations obtained during the 2004 sampling cycle (Appendix G and Table 5-32). To simulate the transport of the activity remaining in the alluvium, an effective K_d of 17 mL/g was used (Figure J-10-16 (J)) for the alluvium sediments.
- transport of Sr-90 from sources other than CPP-31 originating in the alluvium, whose location is spanned by the submodel (Appendix A, Section 5.1), were simulated using the submodel. Because these source locations were outside the influence of the high ionic strength, acidic CPP-31 release, a K_d of 20 mL/g was used in the submodel alluvium.
- transport of Sr-90 from sources located outside of the submodel horizontal extent were also placed in the base model used to simulate the transport of the CPP-31 remaining in the alluvium. The effective K_d for the alluvium underlying these source locations was also set to the value used to simulate the transport of Sr-90 predicted to remain in the alluvium after 20 yrs (first bullet). The relative magnitude of these sources are small relative to the residual Sr-90 predicted to remain in the alluvium after 20 yrs. In this case, the K_d is about equal to the value used to simulate the transport of Sr-90 from sources within the submodel boundary.

Figures J-10-17 through J-10-20 illustrate the distribution of the Sr-90 in the vadose zone through the year 2293 and the arrival of Sr-90 for key perched water wells is shown in Figure J-10-21. The subplots presented in Figure J-10-21 suggest that the model is predicting concentrations in the northern upper shallow wells quite well, however, concentrations in the northern lower shallow and northern deep perched water are not matched as well as they were in the RI/BRA base case. Specifically, comparisons to field data for wells near the former percolation ponds are much worse because of the increase in alluviul K_d (see Figure J-10-22). By comparing the predicted concentrations for wells near the percolation ponds obtained in simulations using 2, 3, and 7 meq/100g simulations, the better match to field data was obtained with the lower CEC values. Based on this observation, a reasonable K_d for the alluvium near the percolation ponds would be 2 mL/g which is consistent with the analyses of alluvial K_d presented in Section J-4.3, and suggests that the percolation pond water influences transport in that area.

Peak vadose zone concentrations through time are shown in red in Figure J-10-23 and are lower than the values predicted using the RI/BRA model (black) throughout most of the simulation time period. The largest deviations occur near the time of the highest vadose zone concentrations when they are 25% of those obtained in the RI/BRA model. It is apparent from this that the highest concentrations actually occur in the pore water of the alluvium.

The rate at which Sr-90 activity enters the aquifer is represented by the red line in Figure J-10-24, and can be compared directly to the RI/BRA model (black) results. Relative to the RI/BRA model, increasing the CEC has resulted in:

- 52% as much Sr-90 leaving the alluvium in the first 20 years (6403 vs. 12336)
- 267% as much Sr-90 remaining in the alluvium (9497 Ci vs. 3564 Ci)
- decreased mobility of Sr-90 due to an increase in K_d (17 mL/g vs. 2 mL/g)

The higher K_d used to simulate the transport of the Sr-90 remaining in the alluvium means that the peak aquifer concentrations can be attributed solely to the Sr-90 originating at non-CPP-31 sources added to those attributable to the 6403 Ci released during the first 5 years. This has important implications with respect to the fate of Sr-90 remaining in the alluvium, and suggests that although there is a larger source remaining in the

alluvium, that it does not appreciably increase the total activity leaving the vadose zone. This is apparent in Figure J-10-24 where the difference in the flux of activity into the aquifer between the base case and this simulation is primarily due to differences occurring during first 5 years.

Figure J-10-17. Sr-90 vadose zone concentration with an alluvial CEC=7 meq/100 g (horizontal contours) (pCi/L) (MCL = thick red line, 10*MCL = thin red line, MCL/10 = black line).

Figure J-10-18. Sr-90 vadose zone concentration with an alluvial CEC=7 meq/100 g (horizontal contours) (pCi/L) (MCL = thick red line, 10*MCL = thin red line, MCL/10 = black line).

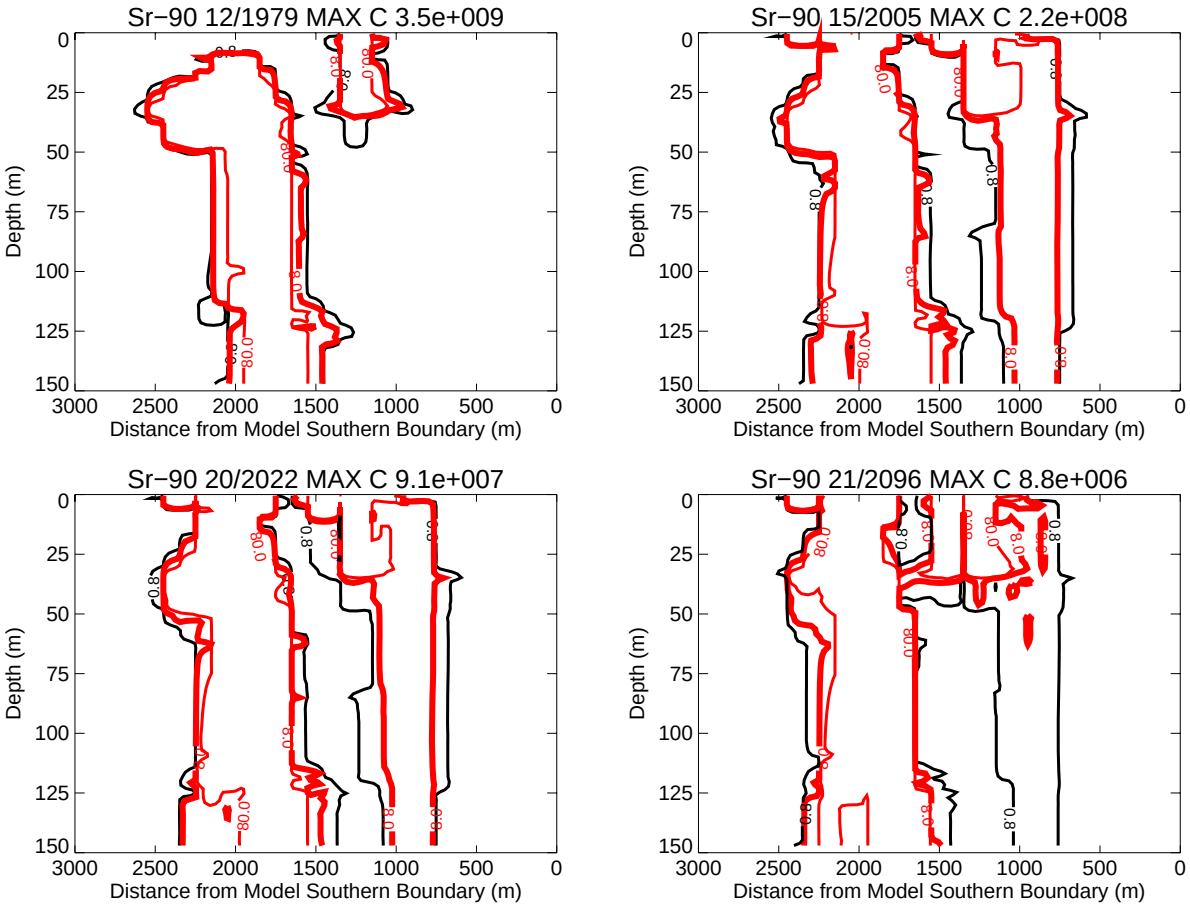

Figure J-10-19. Sr-90 vadose zone concentrations with an alluvial CEC=7 meq/100 g (vertical contours) (pCi/L) (MCL = thick red line, 10*MCL = thin red line, MCL/10 = black line).

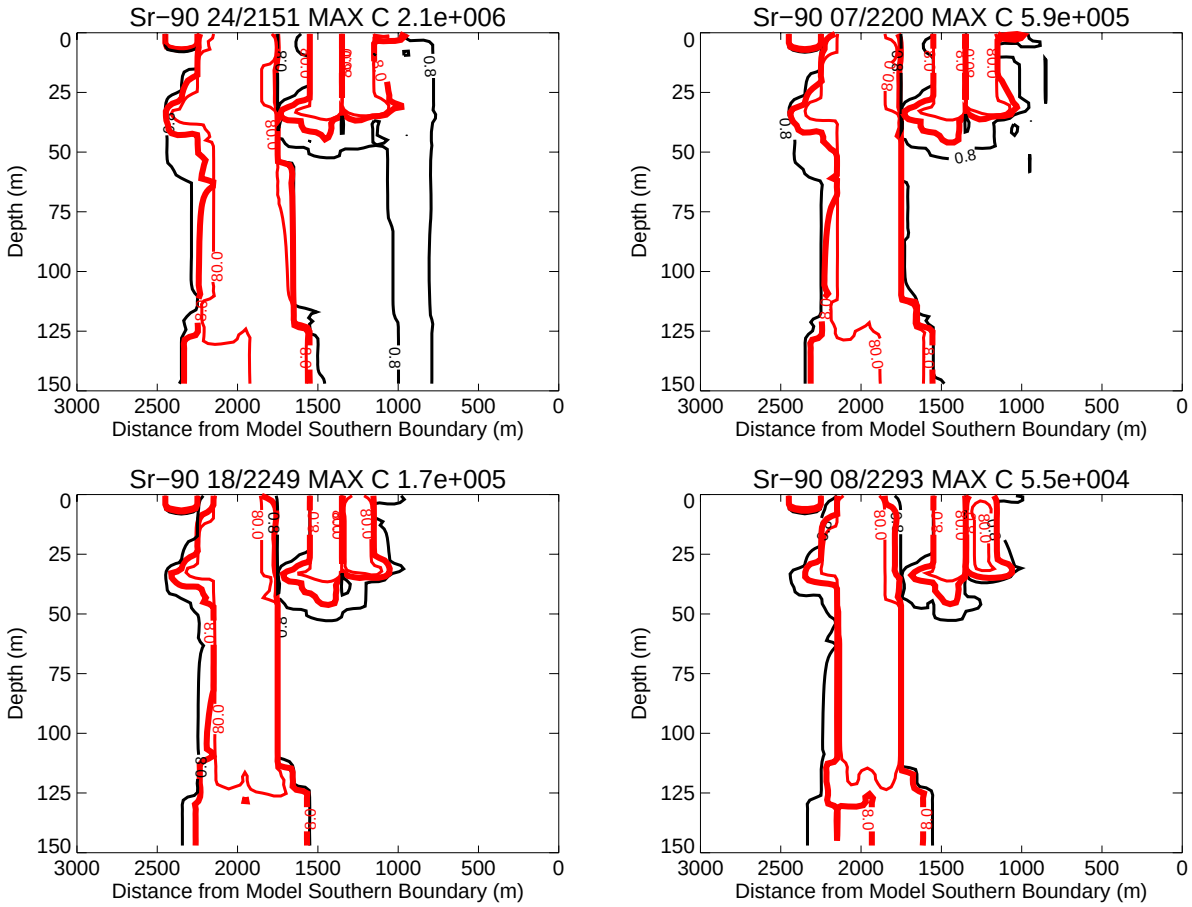

Figure J-10-20. Sr-90 vadose zone concentrations with an alluvial CEC=7 meq/100 g (vertical contours) (pCi/L) (continued) (MCL = thick red line, 10*MCL = thin red line, MCL/10 = black line).

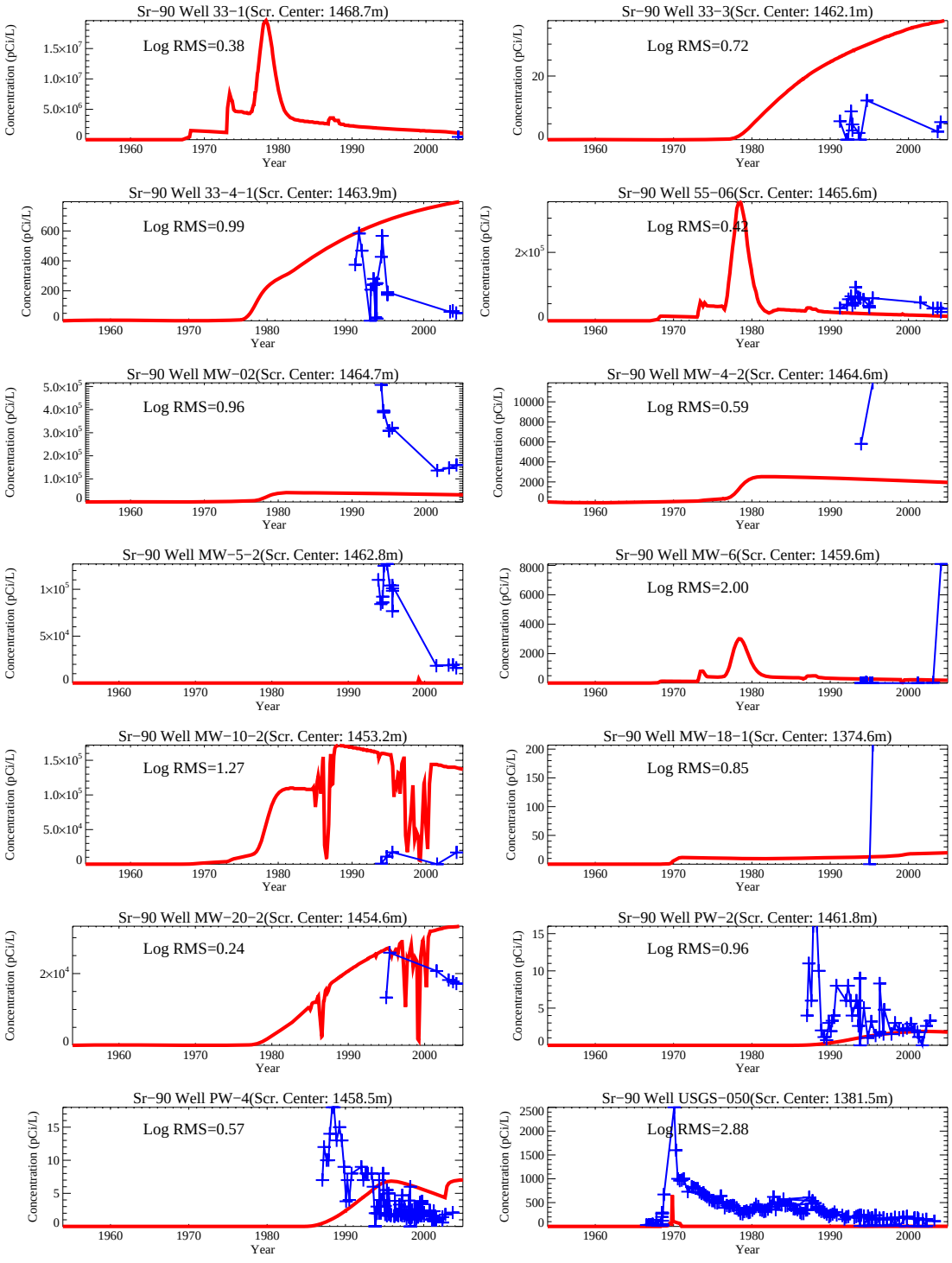

Figure J-10-21. Sr-90 concentration in perched water wells with an alluvial CEC=7 meq/100 g (pCi/L) (Measured values = blue crosses, red = model at screen center).

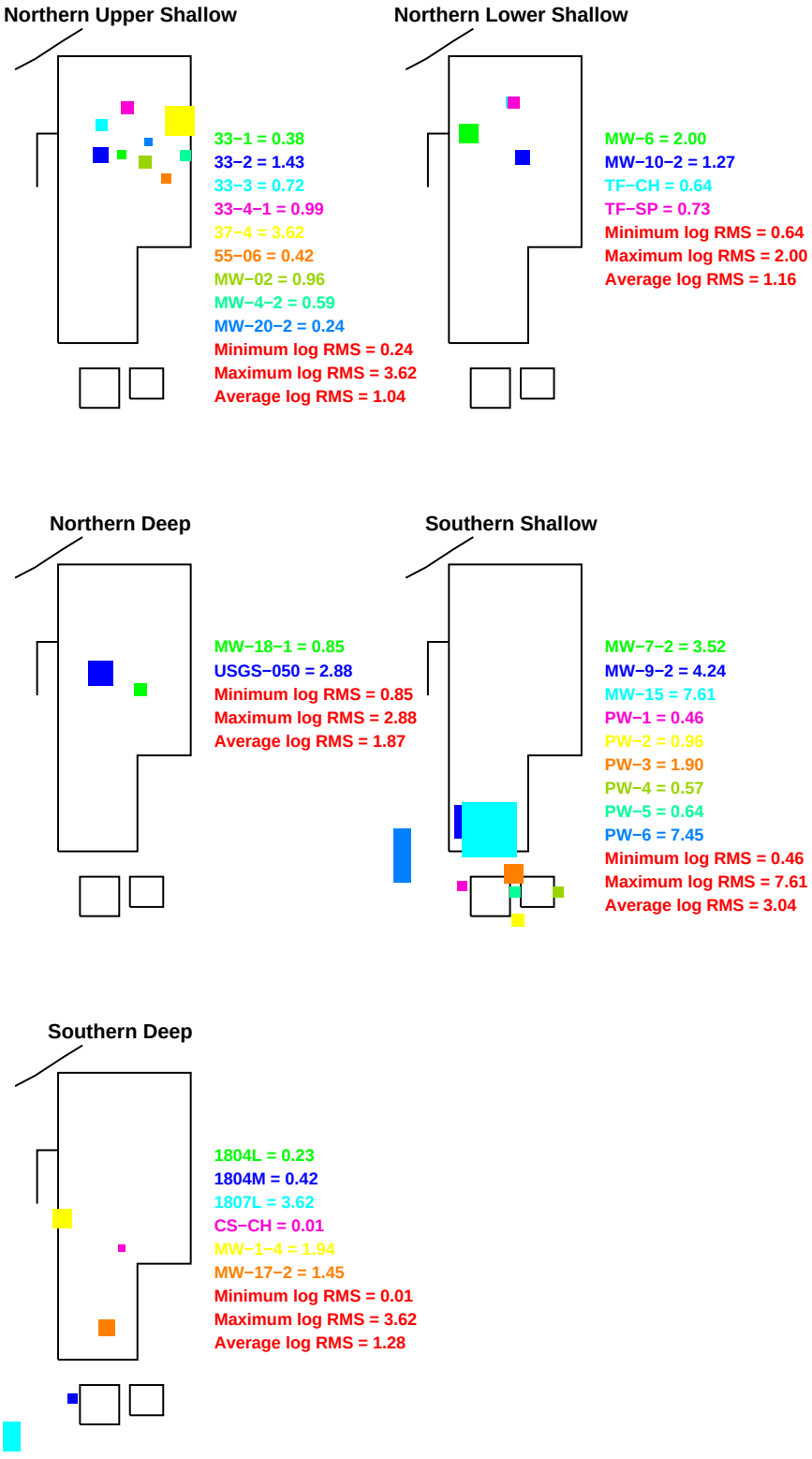

Figure J-10-22. Log 10 Root mean square error (RMS) by depth and northing with an alluvial CEC=7 meq/100 g.

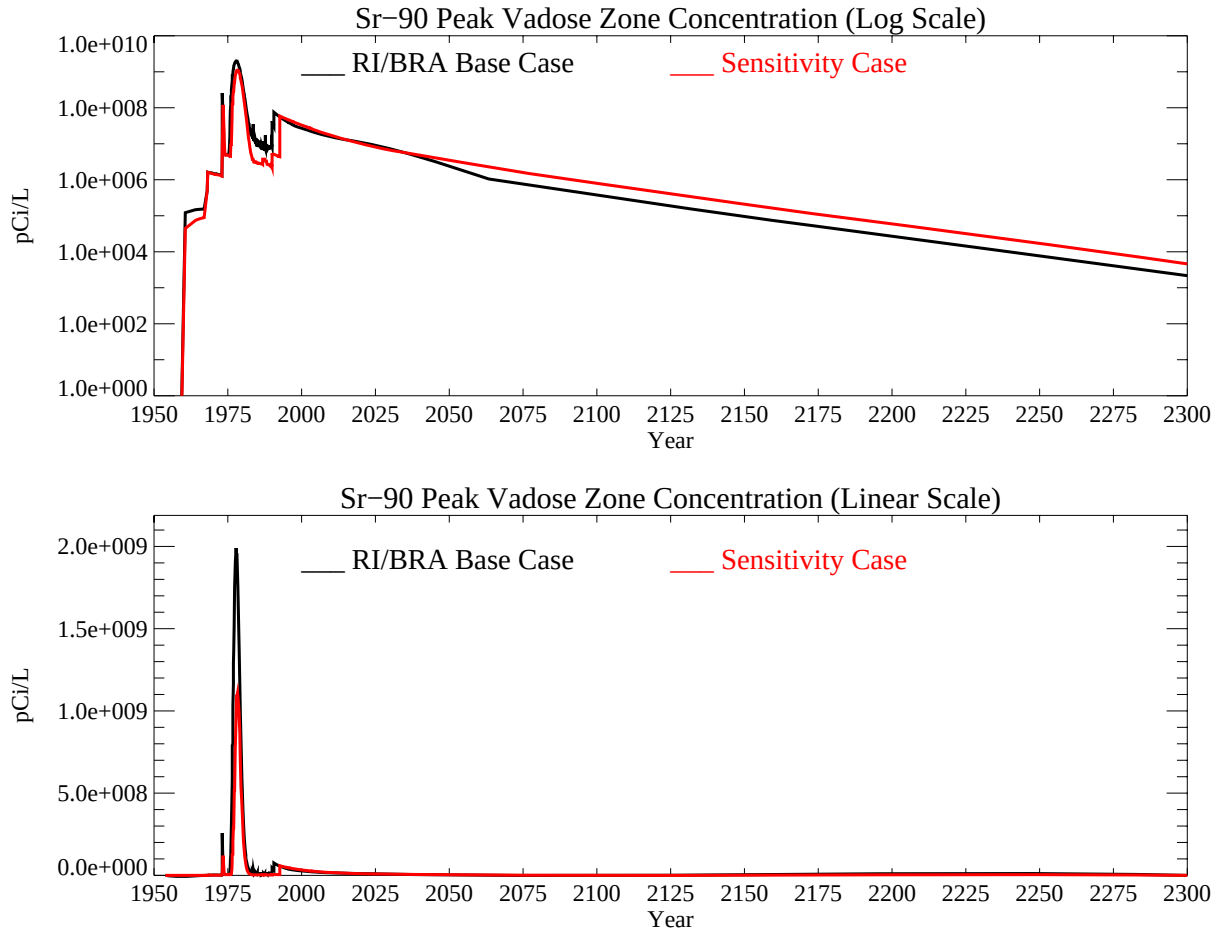

Figure J-10-23. Sr-90 peak vadose zone concentrations with an alluvial CEC=7 meq/100 g (pCi/L) with the RI/BRA model in black and this sensitivity run in red.

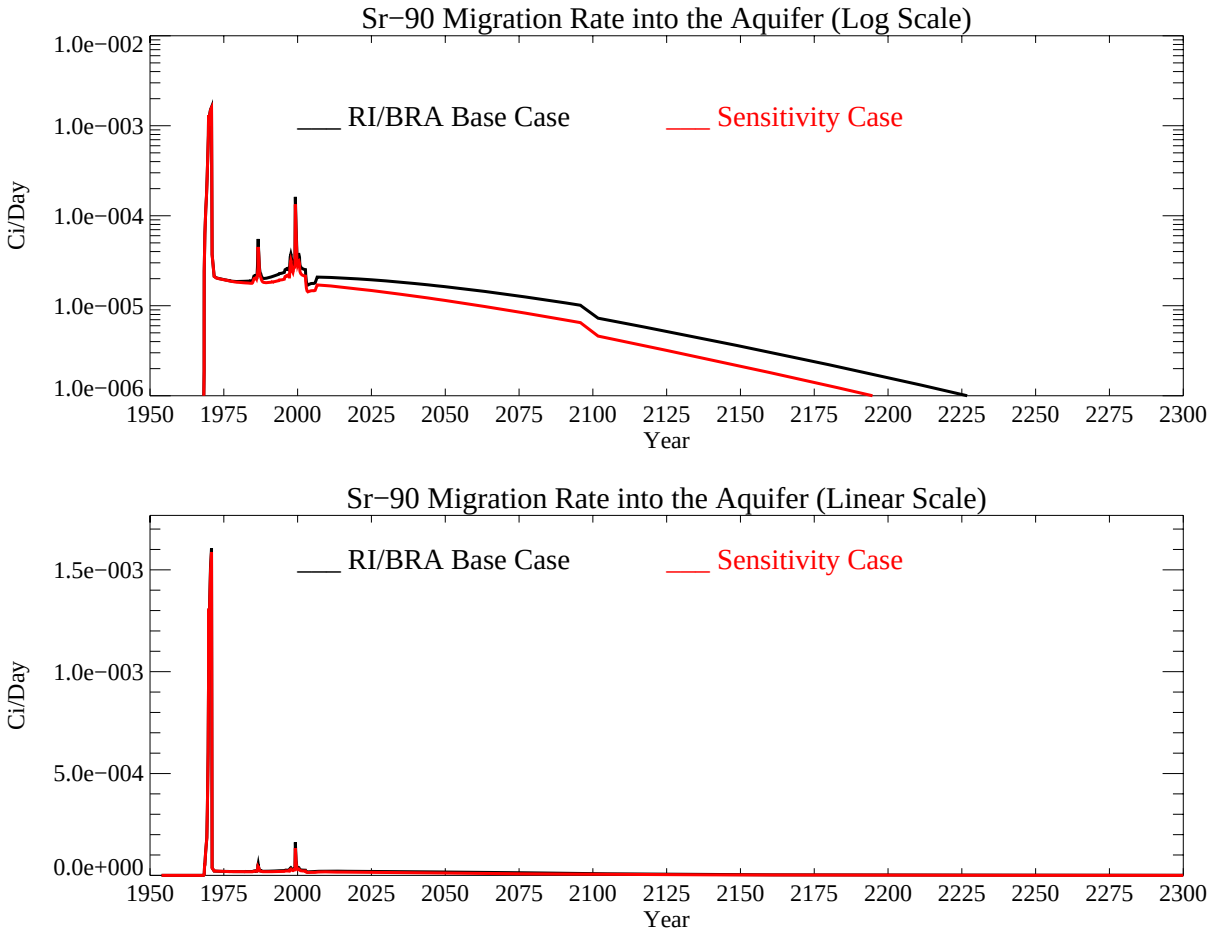

Figure J-10-24. Sr-90 activity flux into the aquifer with an alluvial CEC=7 meq/100 g (Ci/day) with the RI/BRA model in black, and this sensitivity run in red.

J-10.2.3 Aquifer Sr-90 Simulation Results

The distribution Sr-90 in the aquifer for the time period spanning 2005-2096 is given on the course grid in Figure J-10-25 and on the fine grid in Figure J-10-26 for times spanning 2049-2151. The resultant peak aquifer concentrations are given in Figure J-10-27. Because the Sr-90 originating in the vadose zone does not arrive in the aquifer until the mid 1980's, comparisons to measured data are not presented for aquifer wells.

The three important performance measures are concentrations beyond 2095, the spatial extent of contamination, and the time period during which concentrations exceed the MCL. The predicted peak Sr-90 concentration in the year 2095 is 11.5 pCi/L, 60% of that predicted in the RI/BRA model. This concentration exceeds the MCL by a factor of 1.5, with the majority of the long-term impact originating from the initial rapid release of Sr-90 from the tank farm. If there were a significant contribution from the larger activity remaining at the surface, the deviation between RI/BRA and this model peak concentrations would increase over time. The absence of increased deviation confirms that the Sr-90 remaining adsorbed to the alluvial sediments is not significantly contributing to aquifer concentrations later in time.

The Sr-90 contour plots presented in Figures J-10-25 and J-10-26 suggest that the predicted distribution in the aquifer after 2000 does not differ greatly from that predicted in the RI/BRA model. Although Sr-90 concentrations in the aquifer are predicted to exceed the MCL beyond 2095, the area impacted by Sr-90 above 8 pCi/L is well within the INTEC fence line by 2049.

The time during which the MCL is exceeded in this case (year 2105) is significantly sooner than obtained in the RI/BRA model (2129).

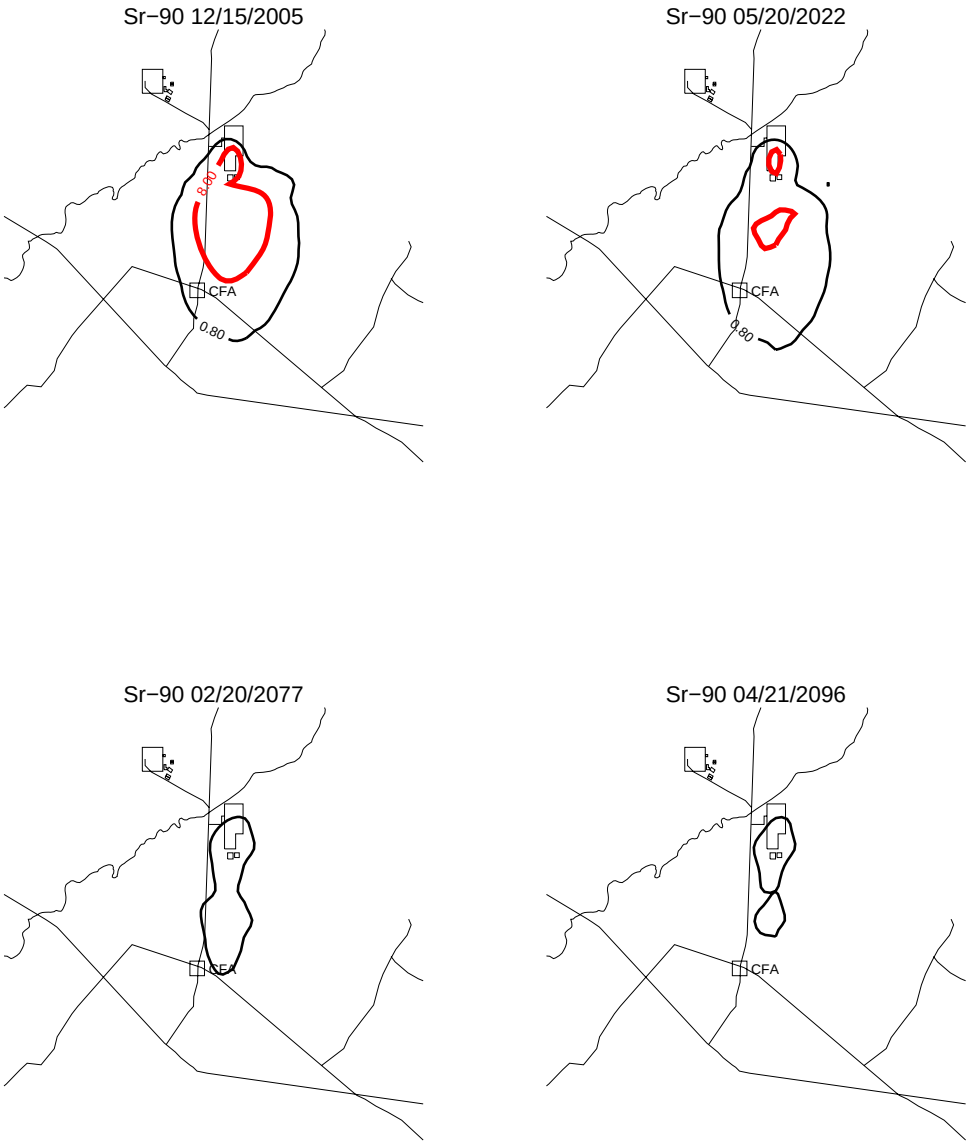

Figure J-10-25. Sr-90 aquifer concentration contours with an alluvial CEC=7 meq/100 g (pCi/L) (MCL = thick red line, 10*MCL = thin red line, MCL/10 = black line).

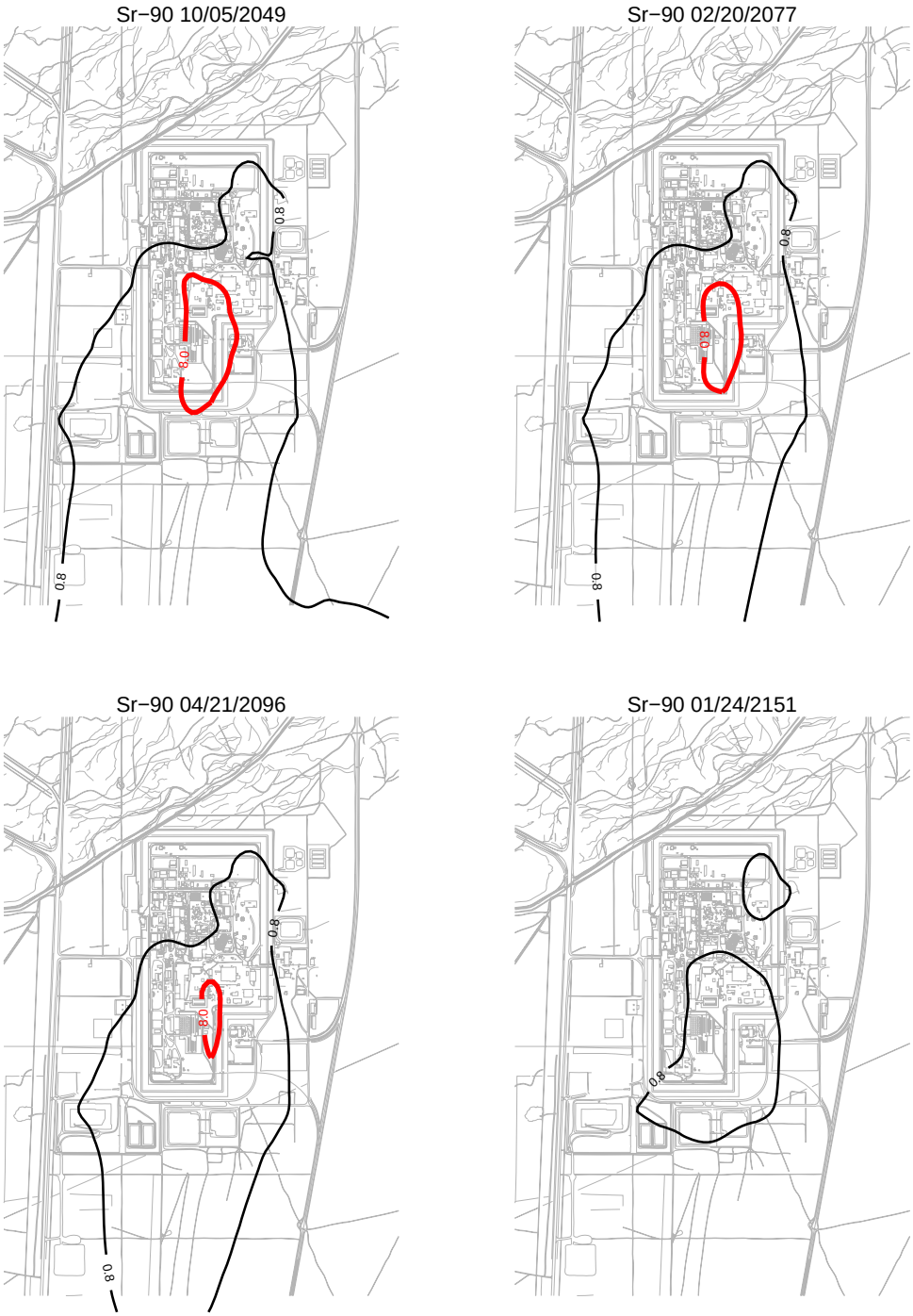

Figure J-10-26. Sr-90 aquifer concentration contours with an alluvial CEC=7 meq/100 g (pCi/L) (continued) (MCL = thick red line, 10*MCL = thin red line, MCL/10 = black line).

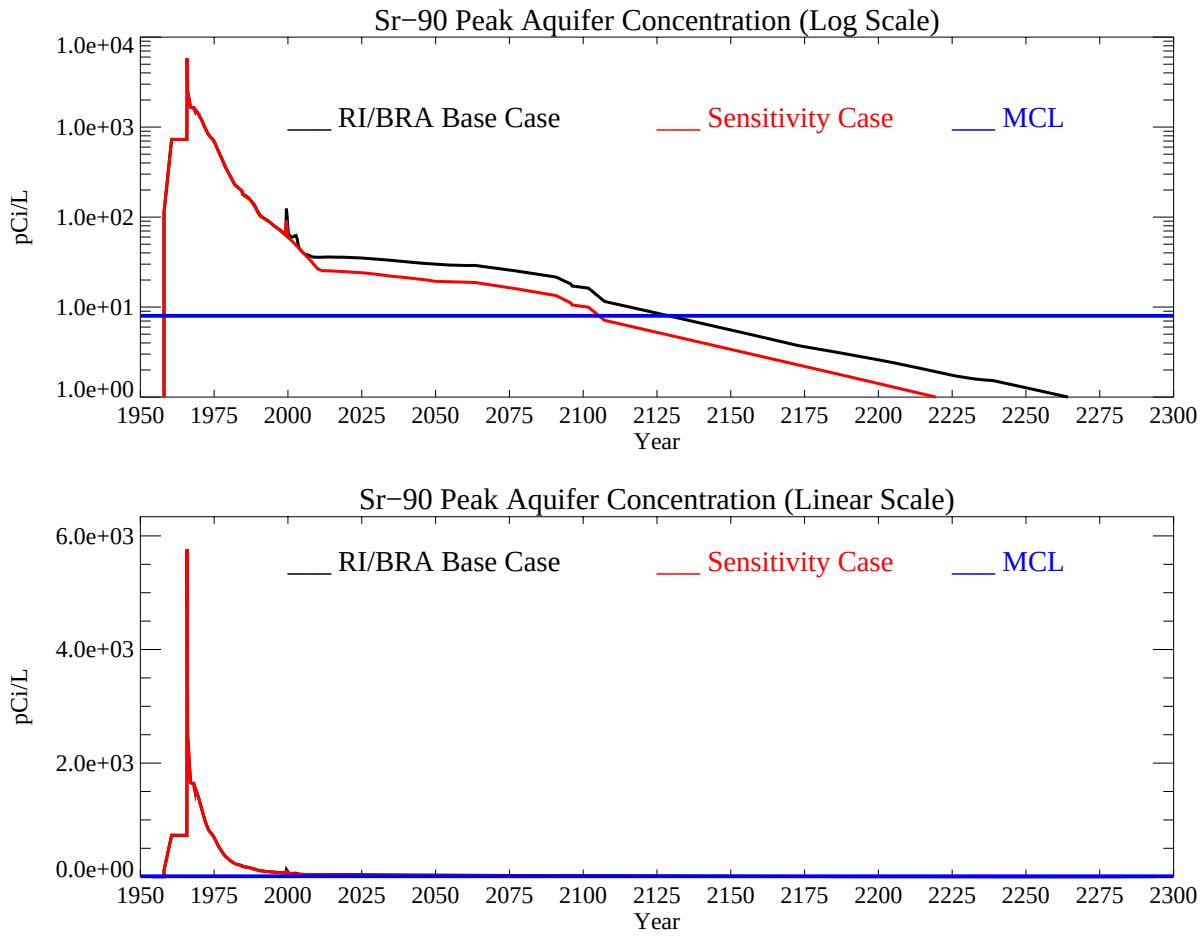

Figure J-10-27. Sr-90 peak aquifer concentrations with an alluvial CEC=7 meq/100 g (pCi/L) with the MCL in blue, RI/BRA model in black and this sensitivity run in red.

J-10.3 Decreased Interbed K_d of 22 mL/g

The previous two simulations examined the resulting uncertainty in predicted vadose zone and aquifer concentrations that are associated over the range of CECs in the alluvium. The interbed materials are also variable, with a smaller expected range in adsorptive capacity. Less variability occurs primarily as a result of a narrower size fractionation, with the material being much finer. As discussed in Section J-6, the K_d used in the RI/BRA model is representative of the mid-range K_d of 50 mL/g. This sensitivity study examines the impact of using a K_d on the low end of the expected range, with this value equal to 22 mL/g.

J-10.3.1 Geochemical Evolution in the Alluvium

This sensitivity simulation uses the geochemical results obtained for the RI/BRA base case simulation presented in Section J-8. In the RI/BRA model, 12336 Ci were released in the first 20 years, with 3564 Ci remaining in the alluvium with a K_d of 2 mL/g. The difference between this simulation and the sensitivity base case is solely due to the decreased interbed K_d.

J-10.3.2 Vadose Zone Sr-90 Simulation Results

The release of Sr-90 in this simulation followed the same procedure as was used in the RI/BRA model:

- 15900 Ci from CPP-31 release in the tank farm were represented using (a) the activity-release function shown in Figure J-8-9 (H) for the 12336 Ci released during the first 20 years, and placing this activity flux directly above the basalt interface of the base model (Appendix A, Section 5.1). The remaining 3564 Ci were placed roughly mid way through the alluvium, corresponding to the location of the peak measured soil concentrations obtained during the 2004 (Appendix G and Table 5-32) sampling cycle. To simulate the transport of the activity remaining in the alluvium, an effective K_d of 2 mL/g was used (Figure J-8-9 (J)) for the alluvium sediments.
- transport of Sr-90 from sources other than CPP-31 originating in the alluvium, whose location is spanned by the submodel (Appendix A, Section 5.1), were simulated using the submodel. Because these source locations were outside the influence of the high ionic strength, acidic CPP-31 release, a K_d of 20 mL/g was used in the submodel alluvium.
- transport of Sr-90 from sources located outside of the submodel horizontal extent were also placed in the base model used to simulate the transport of the CPP-31 remaining in the alluvium. The effective K_d for the alluvium underlying these source locations was also set to the value used to simulate the transport of Sr-90 predicted to remain in the alluvium after 20 yrs (first bullet). The relative magnitude of these sources are small relative to the residual Sr-90 predicted to remain in the alluvium after 20 yrs.

The distribution of Sr-90 in the vadose zone is shown through year 2293 in Figures J-10-28 through J-10-31. The arrival of Sr-90 in key perched water wells is compared to field data in Figure J-10-32, and is summarized for all wells in Figure J-10-33. The subplots presented in Figure J-10-32 suggest that the model is overpredicting concentrations in most of the higher concentration upper shallow perched water wells. The wells near the former percolation ponds also have a poorer match because of the decreased interbed K_d. The worst matches occur in the deeper wells because Sr-90 can migrate from the shallow higher concentration regions, resulting in general overprediction at depth.

Peak vadose zone concentrations through time are shown in red in Figure J-10-34 and are about equal to those predicted in the RI/BRA base case through year 2050. This is an indication that these high vadose zone concentrations are in the alluvium because the lower interbed K_d would allow perched water concentrations to increase above those predicted by the RI/BRA model.

The rate at which Sr-90 enters the aquifer (red) is given in Figure J-10-35, and can be compared directly to the RI/BRA model predictions (black). Clearly, decreasing the interbed K_d has had a significant impact on the expected migration of Sr-90 into the aquifer, with this impact occuring throughout the entire simulation period. The distribution coefficient is essentially the ratio of mass (activity) adsorbed on the exchange sites to that in the aqueous phase. As the K_d decreases, the aqueous phase concentration increases. Applying the smaller K_d to all of the interbed sediments allows less adsorption of total Sr-90 activity throughout the vadose zone, including the deeper interbeds affected by the failed CPP-03 injection well. The lower K_d increases the downward migration of Sr-90 and allows less decay to occur en route to the aquifer. The flux rate predicted using a K_d of 22 mL/g is much higher than predicted in the RI/BRA model.

Figure J-10-28. Sr-90 vadose zone concentration assuming an interbed K_d=22 mL/g (horizontal contours) (pCi/L) (MCL = thick red line, 10*MCL = thin red line, MCL/10 = black line).

Figure J-10-29. Sr-90 vadose zone concentration assuming an interbed K_d=22 mL/g (horizontal contours) (pCi/L) (MCL = thick red line, 10*MCL = thin red line, MCL/10 = black line).

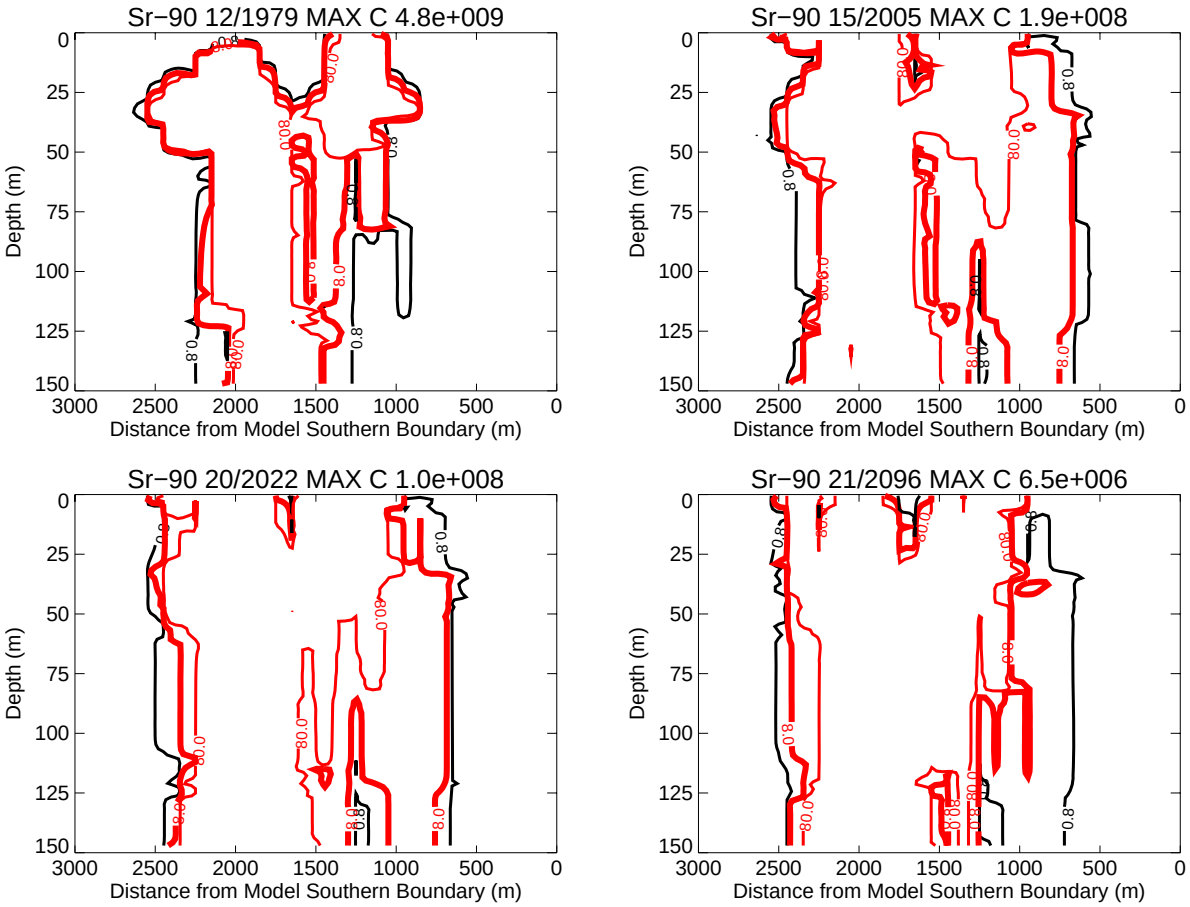

Figure J-10-30. Sr-90 vadose zone concentrations assuming an interbed K_d=22 mL/g (vertical contours) (pCi/L) (MCL = thick red line, 10*MCL = thin red line, MCL/10 = black line).

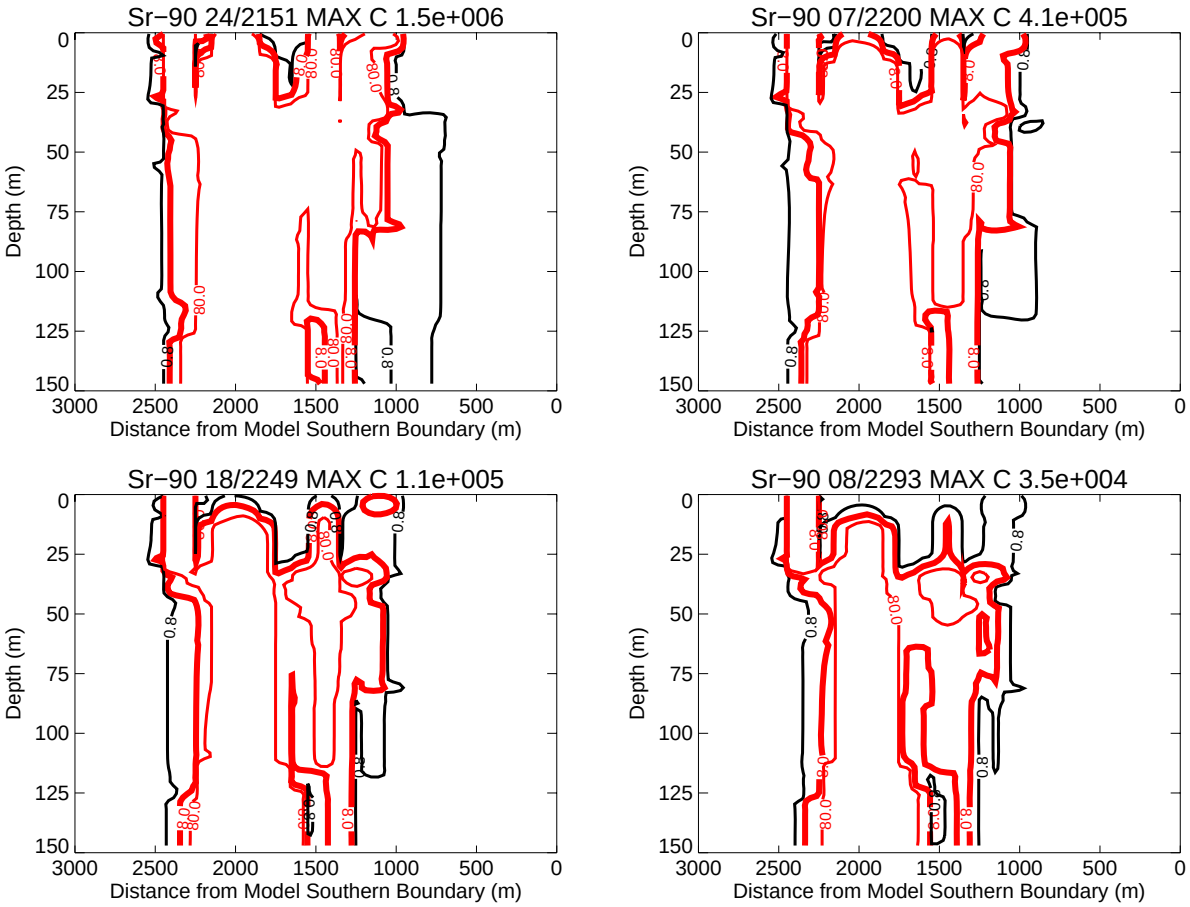

Figure J-10-31. Sr-90 vadose zone concentrations assuming an interbed K_d=22 mL/g (vertical contours) (pCi/L) (continued) (MCL = thick red line, 10*MCL = thin red line,

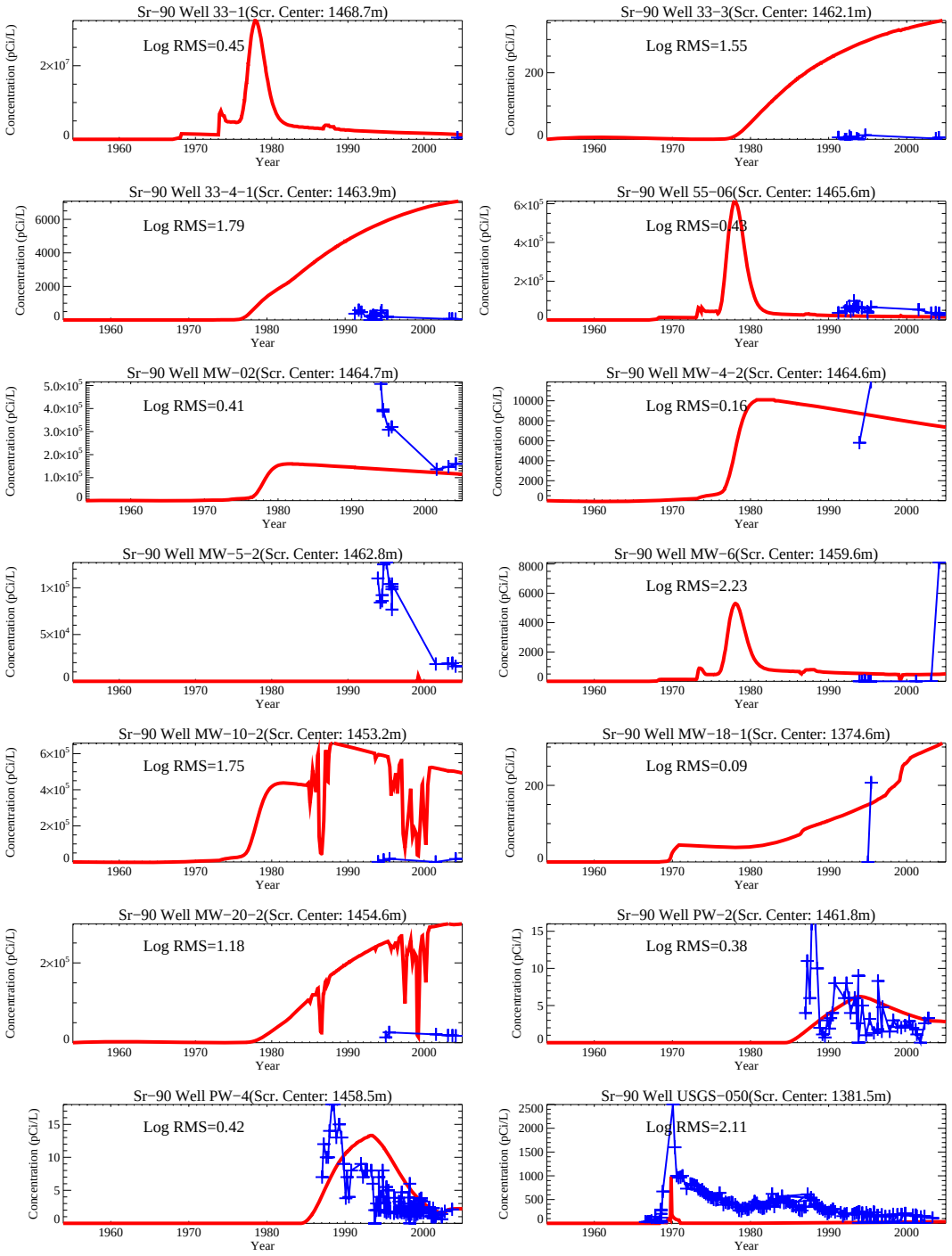

Figure J-10-32. Sr-90 concentration in perched water wells assuming an interbed K_d=22 mL/g (pCi/L) (Measured values = blue crosses, red = model at screen center).

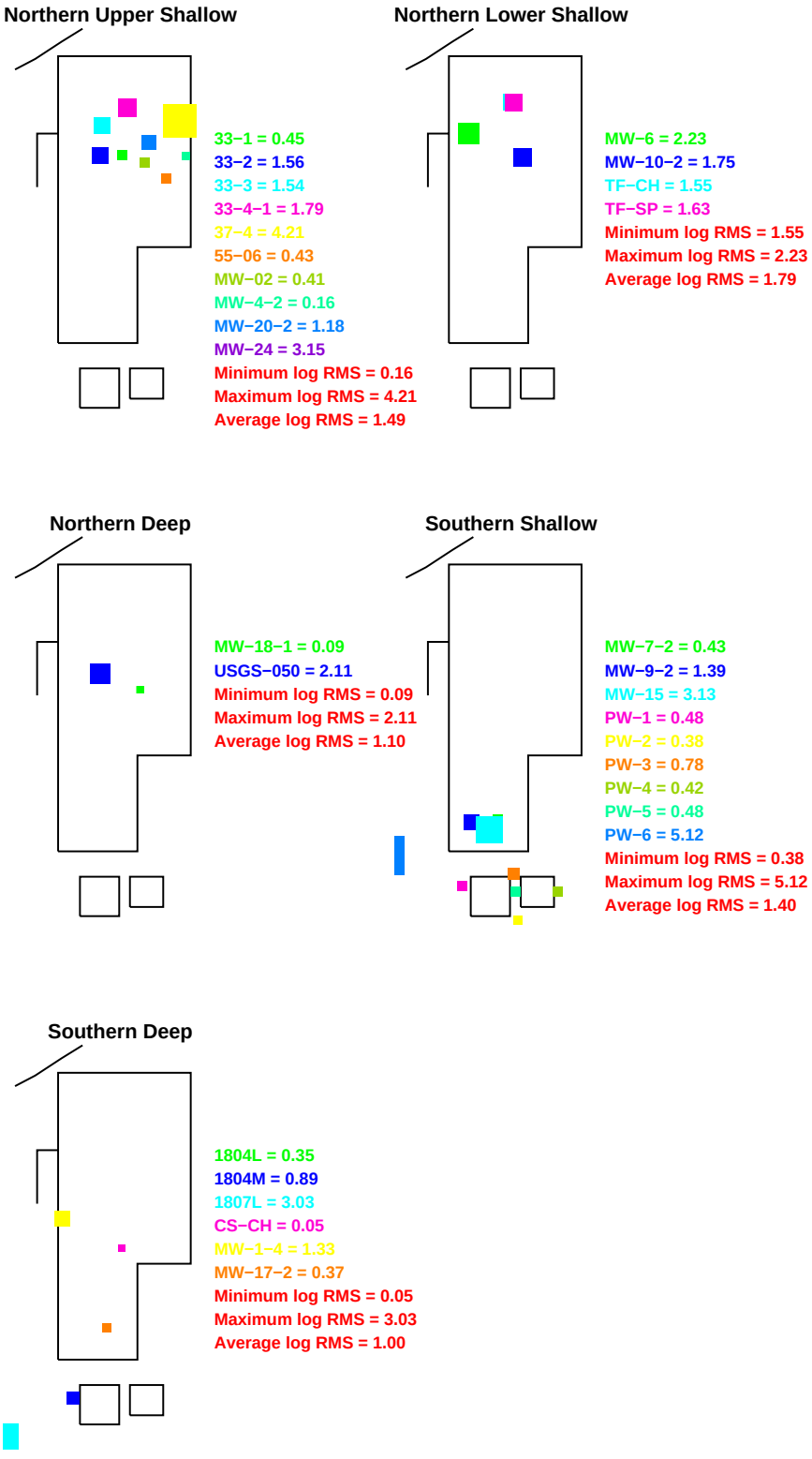

Figure J-10-33. Log 10 Root mean square error (RMS) by depth and northing assuming an interbed K_d=22 mL/g.

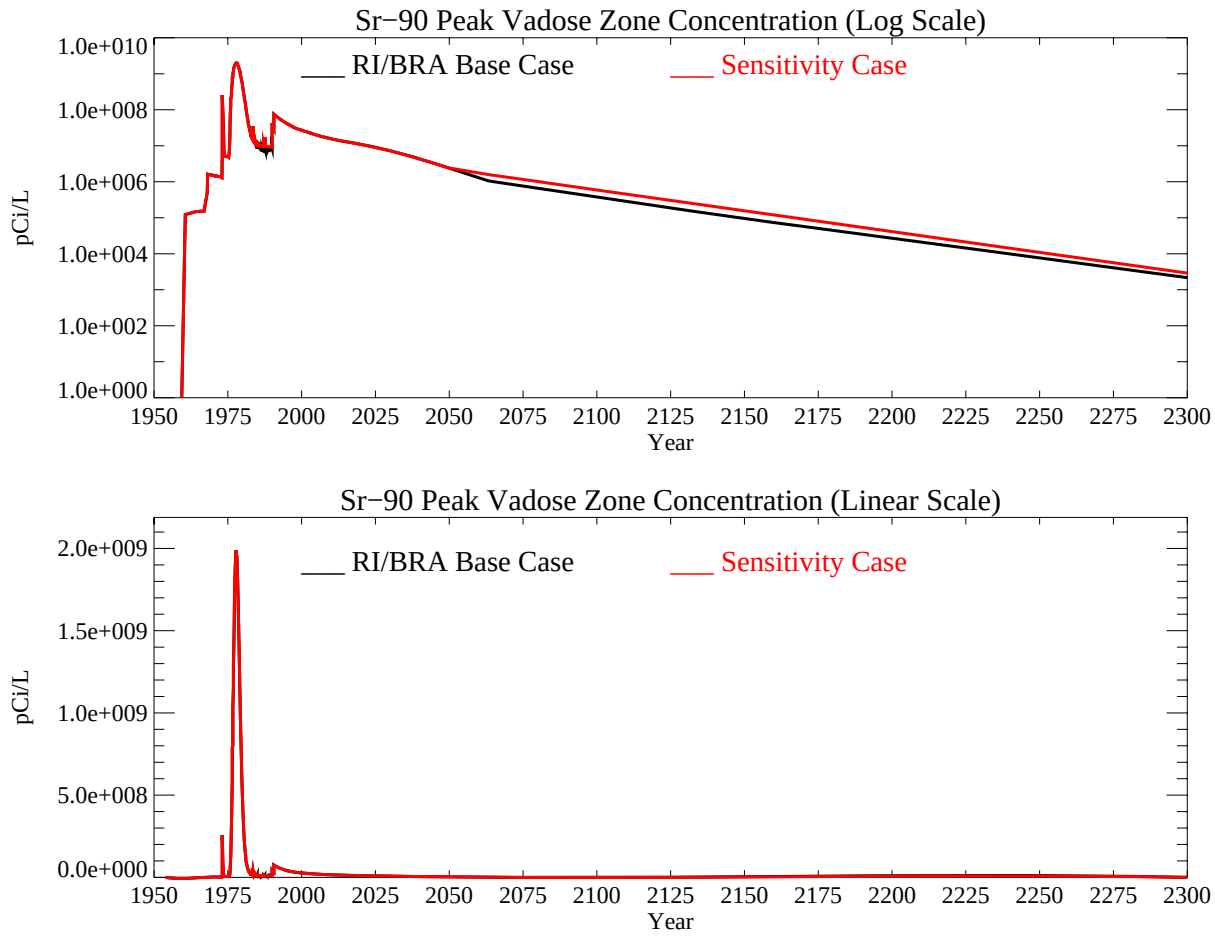

Figure J-10-34. Sr-90 peak vadose zone concentrations assuming an interbed K_d=22 mL/g (pCi/L) with the RI/BRA model in black and this sensitivity run in red.

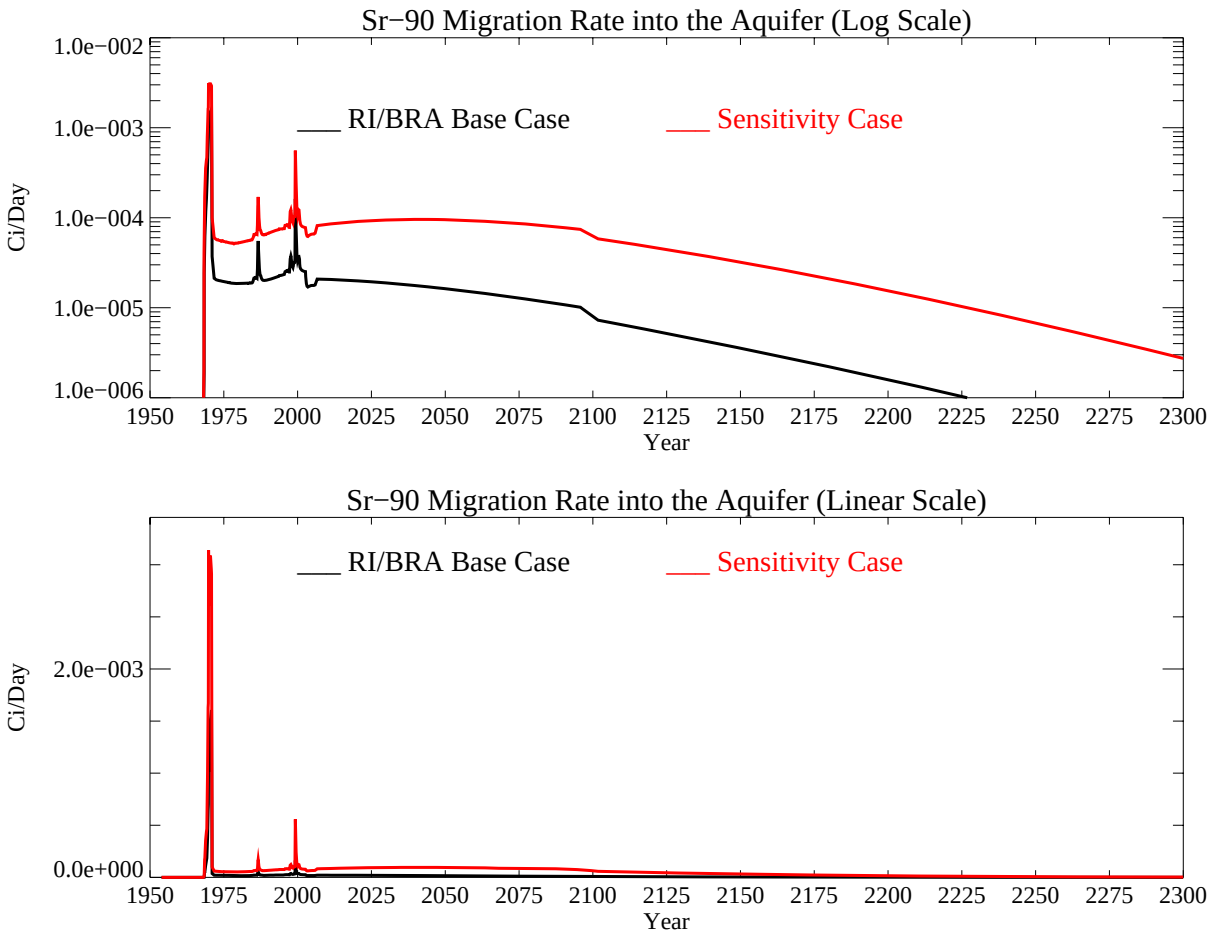

Figure J-10-35. Sr-90 activity flux into the aquifer assuming an interbed K_d=22 mL/g (Ci/day) with the RI/BRA base case in black, and this sensitivity run in red.

J-10.3.3 Aquifer Sr-90 Simulation Results

On the course grid, the distribution Sr-90 in the aquifer for the time period spanning 2005-2096 is given in Figure J-10-36. Figure J-10-37 contains the contours on the fine grid for the 2049-2151 time period. Resultant peak aquifer concentrations are given in Figure J-10-38. Because the Sr-90 originating in the vadose zone does not arrive in the aquifer until the mid 1980's, comparisons to measured data are not presented for aquifer wells.

The three performance measures are peak concentration in 2095, area impacted above the MCL, and time during which the MCL is exceeded. Decreasing the interbed Kd by a factor of 2.3 has increased the peak concentration in 2095 to 110.8 pCi/L, about six times that predicted for the sensitivity base case (18.6 pCi/L). The nonlinearity is caused by the combination of increased flux rate out of the alluvium and lack of decay enroute. This difference is significant given overall model uncertainty.

There are also significant differences in the spatial distribution of Sr-90. The Sr-90 contour plots presented in Figures J-10-36 and J-10-37 show that Sr-90 concentrations in the aquifer are predicted to be extensive through out the presented time interval. The concentration isopleth representing the MCL is not contained within the intec facility boundaries until about 2151. This means that the flux rate of Sr-90 coming from the vadose zone is much higher than the dilution, retardation, and decay rates in the aquifer.

The simulated Sr-90 concentrations with this lower adsorption in the interbeds remain above the MCL from 1960 through year 2263. In the RI/BRA base-case, peak concentrations were not reduced below the MCL until year 2129. Decreasing the K_d by a factor of 2.3 keeps predicted Sr-90 concentrations in the aquifer above the MCL for an additional 134 years.

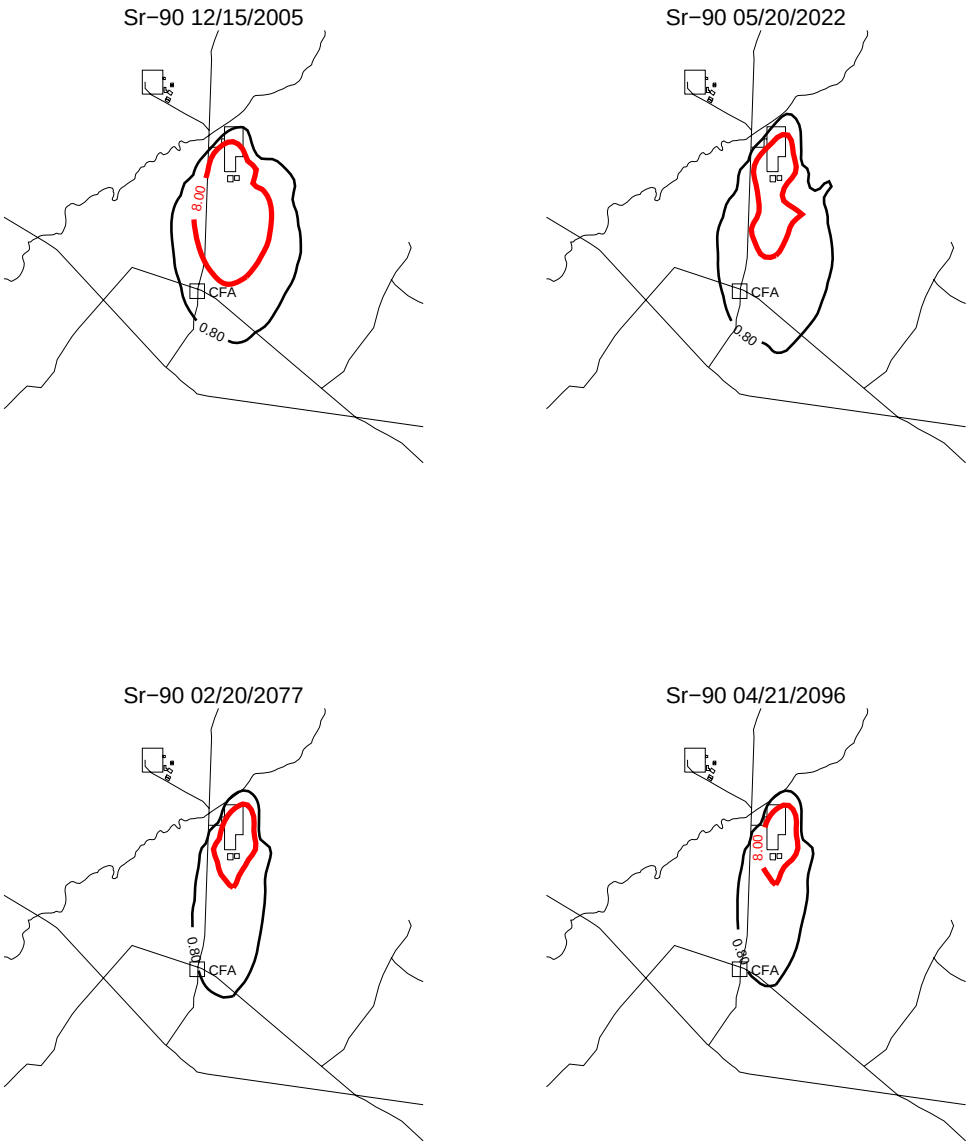

Figure J-10-36. Sr-90 aquifer concentration contours assuming an interbed K_d=22 mL/g (pCi/L) (MCL = thick red line, 10*MCL = thin red line, MCL/10 = black line).

Figure J-10-37. Sr-90 aquifer concentration contours assuming an interbed K_d=22 mL/g (pCi/L) (continued) (MCL = thick red line, 10*MCL = thin red line, MCL/10 = black line).

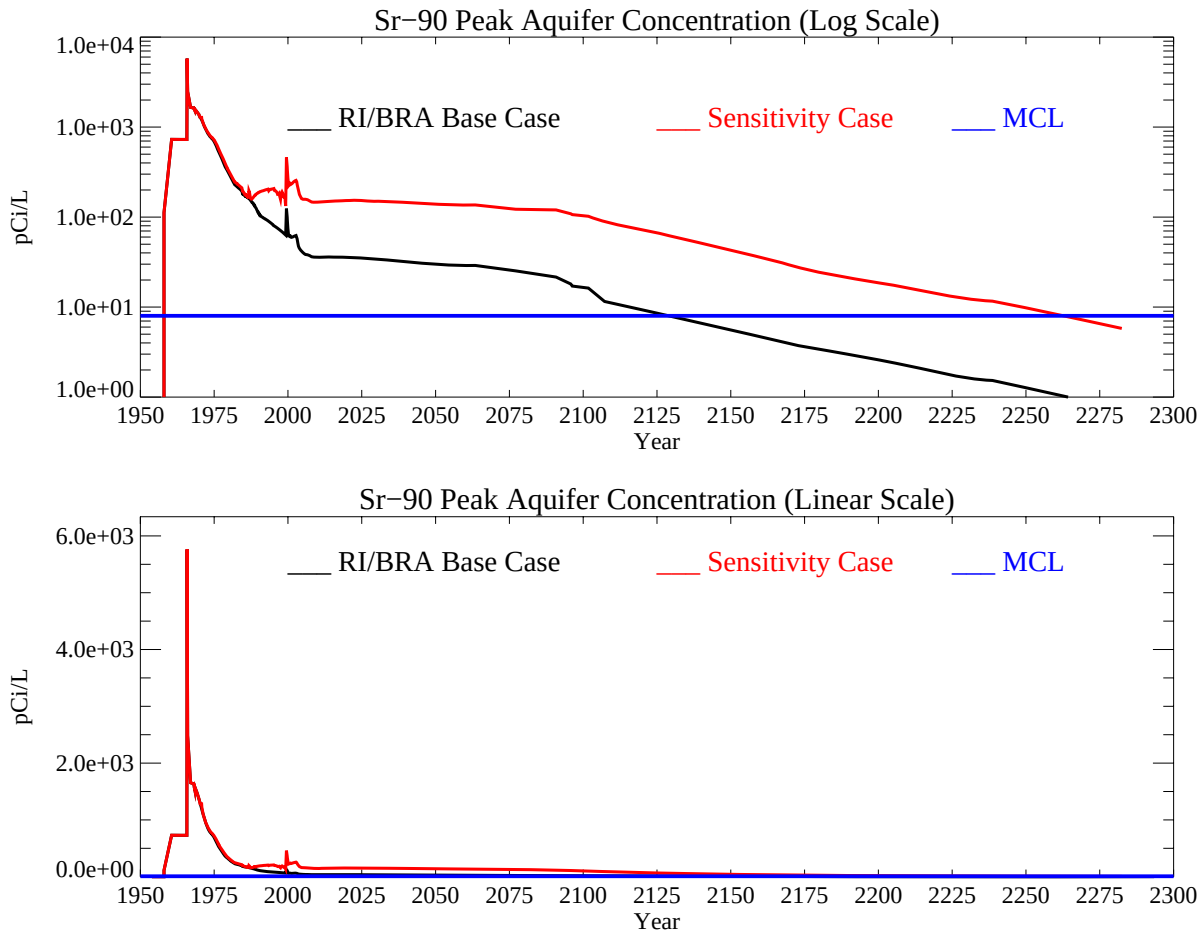

Figure J-10-38. Sr-90 peak aquifer concentrations assuming an interbed K_d=22 mL/g (pCi/L) with the MCL in blue, RI/BRA model in black and this sensitivity run in red.

J-10.4 Increased Interbed K_d of 78 mL/g

A mid-range interbed K_d of 50 mL/g was used in the RI/BRA model. As discussed in Section J-6, the expected interbed K_d range is 25-84 mL/g. The previous simulation presented in Section J-10.3 was presented to evaluate the low end of the range and used 22 mL/g. This sensitivity study examines the impact of using a K_d on the high end of the expected range, with this value equal to 78 mL/g.

J-10.4.1 Geochemical Evolution in the Alluvium

This sensitivity simulation uses the geochemical results obtained for the RI/BRA model presented in Section J-8. In the RI/BRA model, 12336 Ci were released in the first 20 years, with 3564 Ci remaining in the alluvium with a K_d of 2 mL/g. The difference between this simulation and the sensitivity base case is solely due to the increased interbed K_d, with this value equal to 78 mL/g.

J-10.4.2 Vadose Zone Sr-90 Simulation Results

The release of Sr-90 in this simulation followed the same procedure as was used in the RI/BRA model:

- 15900 Ci from CPP-31 release in the tank farm were represented using (a) the activity-release function shown in Figure J-8-9 (H) for the 12336 Ci released during the first 20 years, and placing this activity flux directly above the basalt interface of the base model (Appendix A, Section 5.1). The remaining 3564 Ci were placed roughly mid way through the alluvium, corresponding to the location of the peak measured soil concentrations obtained during the 2004 (Appendix G and Table 5-32) sampling cycle. To simulate the transport of the activity remaining in the alluvium, an effective K_d of 2 mL/g was used (Figure J-10-16 (J)) for the alluvium sediments.
- transport of Sr-90 from sources other than CPP-31 originating in the alluvium, whose location is spanned by the submodel (Appendix A, Section 5.1), were simulated using the submodel. Because these source locations were outside the influence of the high ionic strength, acidic CPP-31 release, a K_d of 20 mL/g was used in the submodel alluvium.
- transport of Sr-90 from sources located outside of the submodel horizontal extent were also placed in the base model used to simulate the transport of the CPP-31 remaining in the alluvium. The effective K_d for the alluvium underlying these source locations was also set to the value used to simulate the transport of Sr-90 predicted to remain in the alluvium after 20 yrs (first bullet). The relative magnitude of these sources are small relative to the residual Sr-90 predicted to remain in the alluvium after 20 yrs.

The distribution of Sr-90 in the vadose zone is shown in Figures J-10-39 through J-10-42 for the 1979-2293 time period. The arrival of Sr-90 in key perched water wells is compared to field data in Figure J-10-43, and is summarized for all wells in Figure J-10-44. The subplots presented in Figure J-10-43 shows that the model is still slightly overpredicting concentrations in the northern upper shallow perched wells. The match to wells in the south has been much improved. The match to field data worsens as the distance from the well to the tank farm, or the well from the percolation pond increases. This is because the higher K_d does not allow the Sr-90 to migrate outward from the higher concentration regions near these two source locations. It is likely that a very good match could be obtained with a slightly higher K_d and higher anthropogenic water losses in northern INTEC.

Peak vadose zone concentrations through time are shown in red in Figure J-10-45 and are about equal to those obtained using the RI/BRA model parameters (black). This is because the highest pore water concentrations are in the alluvium (and not affected by the interbed K_d), or that they are representative of the pore water in the basalts, which are also not affected by interbed K_d.

The rate at which Sr-90 enters the aquifer (red) is given in Figure J-10-46, and can be compared directly to the RI/BRA model results (black). As when the interbed K_d was assumed to be on the low end of the plausible range, using an interbed Kd on the high end of the range has had a significant impact on the expected migration rate of Sr-90 into the aquifer. Migration rates with this higher Kd are significantly higher throughout the entire simulation period. The distribution coefficient is essentially the ratio of mass (activity) adsorbed on the exchange sites to that in the aqueous phase. As the K_d increases, the aqueous phase concentration decreases. Applying the larger K_d to all of the interbed sediments allows much more adsorption of total Sr-90 activity throughout the vadose zone, including the deeper interbeds affected by the failed CPP-03 injection well. The higher K_d retards the downward migration of Sr-90 and allows more decay to occur en route to the aquifer. The flux rate predicted using a K_d of 78 mL/g is much lower than predicted in the RI/BRA model.

Figure J-10-39. Sr-90 vadose zone concentration assuming an interbed K_d=78 mL/g (horizontal contours) (pCi/L) (MCL = thick red line, 10*MCL = thin red line, MCL/10 = black line).

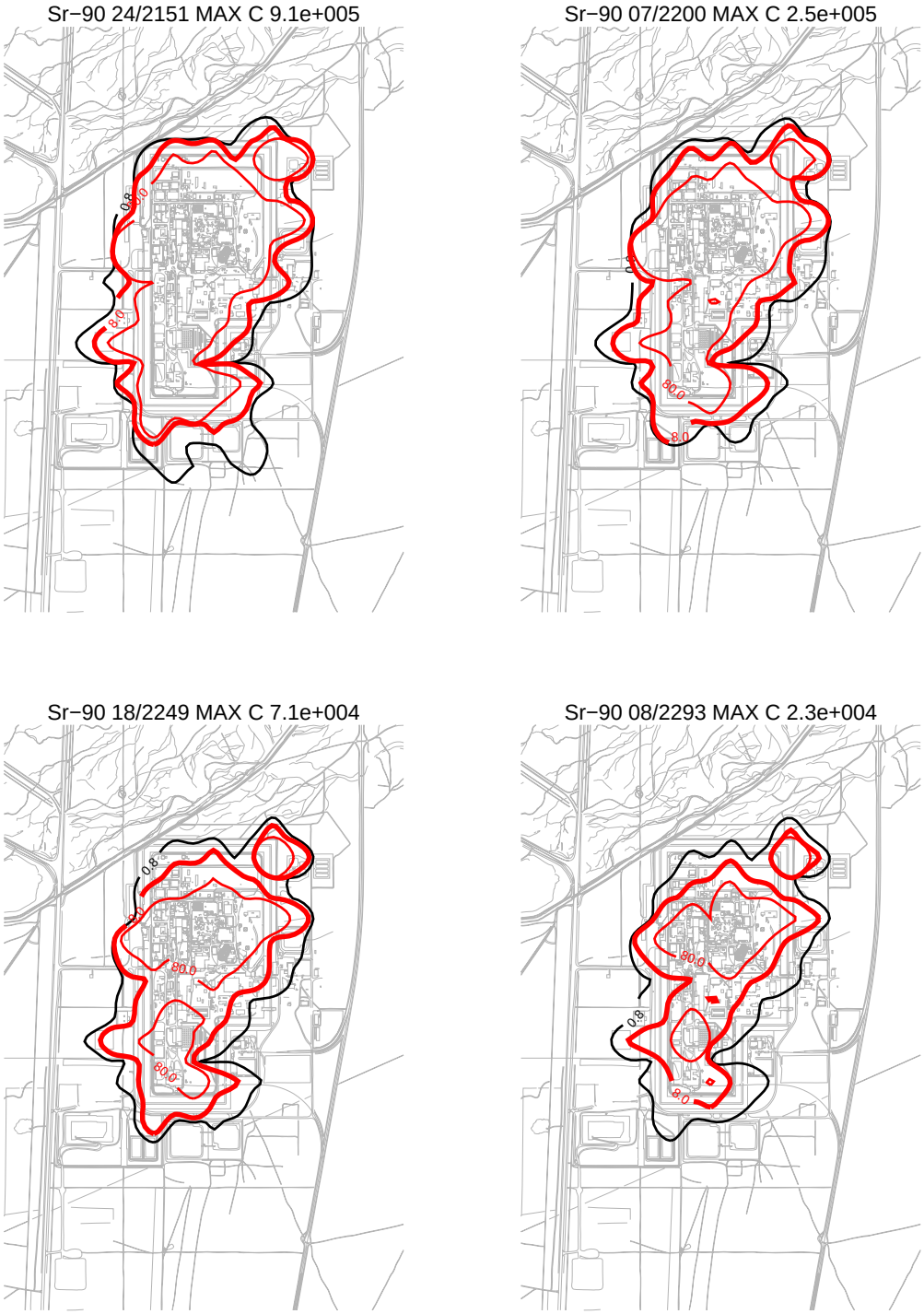

Figure J-10-40. Sr-90 vadose zone concentration assuming an interbed K_d=78 mL/g (horizontal contours) (pCi/L) (MCL = thick red line, 10*MCL = thin red line, MCL/10 = black line).

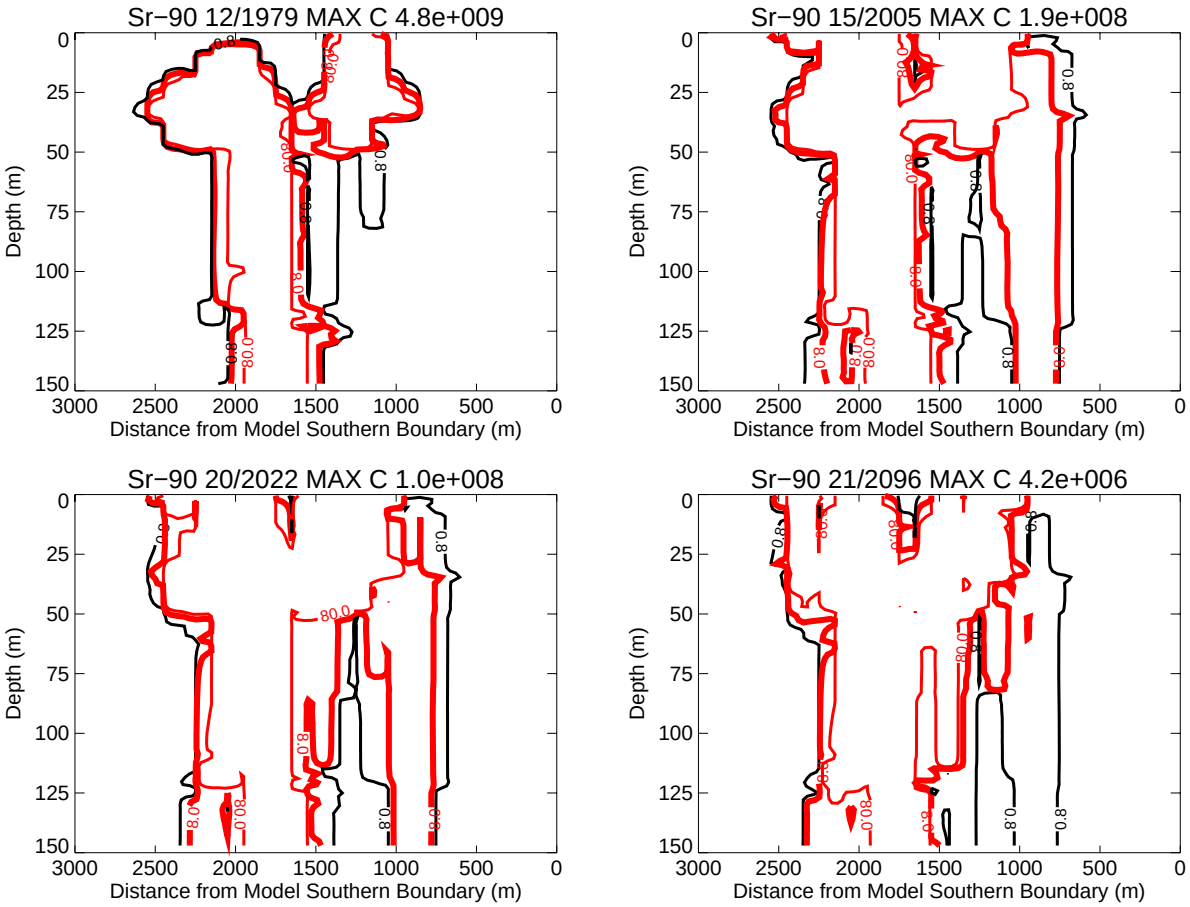

Figure J-10-41. Sr-90 vadose zone concentrations assuming an interbed K_d=78 mL/g (vertical contours) (pCi/L) (MCL = thick red line, 10*MCL = thin red line, MCL/10 = black line).

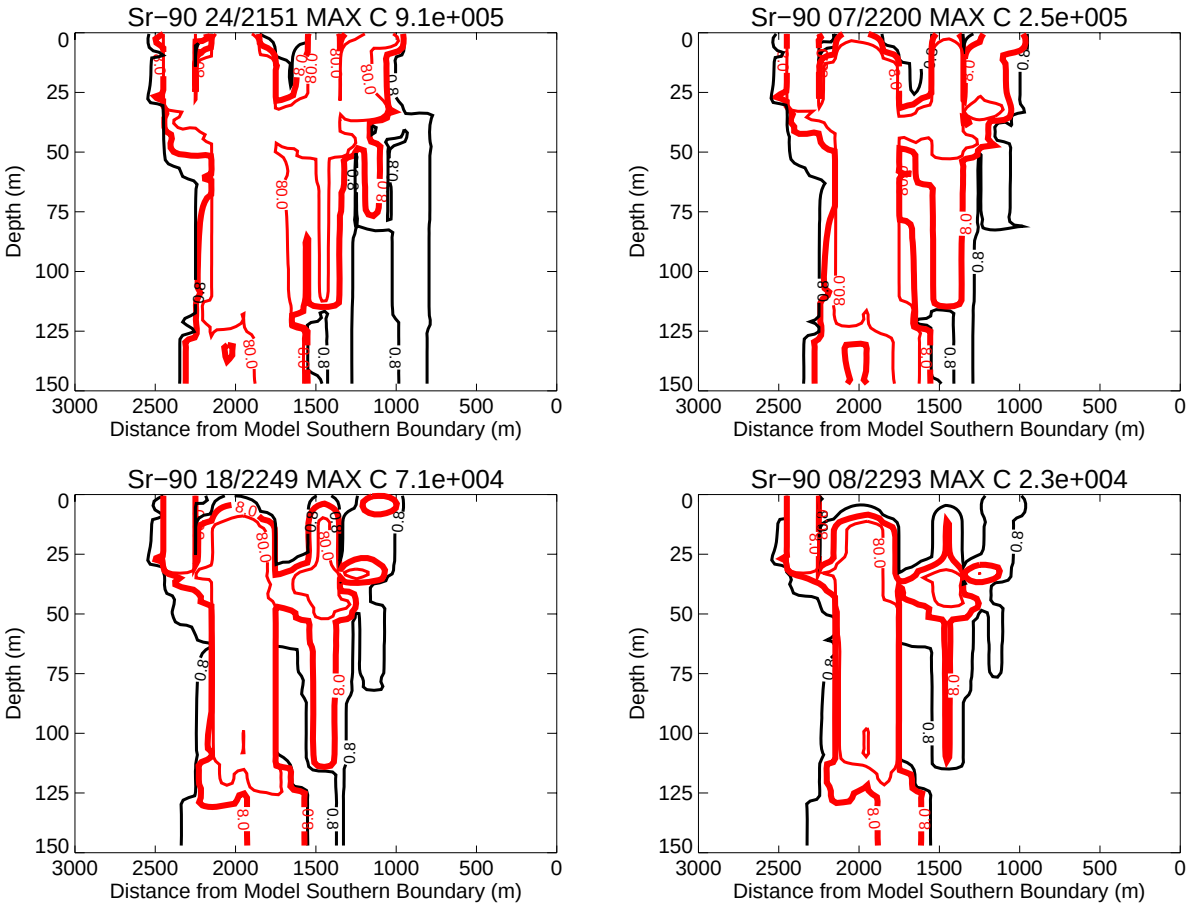

Figure J-10-42. Sr-90 vadose zone concentrations assuming an interbed K_d=78 mL/g (vertical contours) (pCi/L) (continued) (MCL = thick red line, 10*MCL = thin red line, MCL/10 = black line).

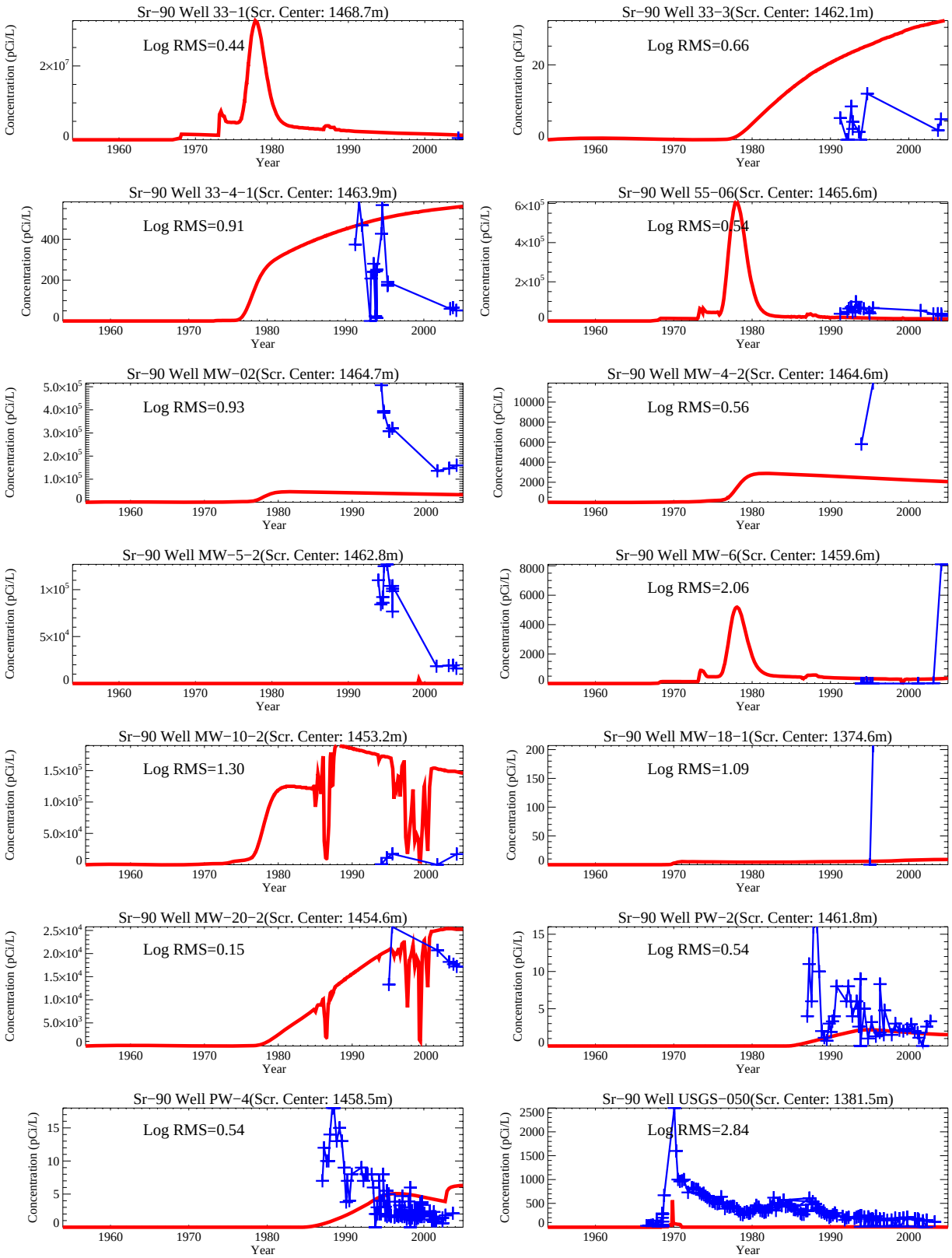

Figure J-10-43. Sr-90 concentration in perched water wells assuming an interbed K_d=78 mL/g (pCi/L) (Measured values = blue crosses, red = model at screen center).

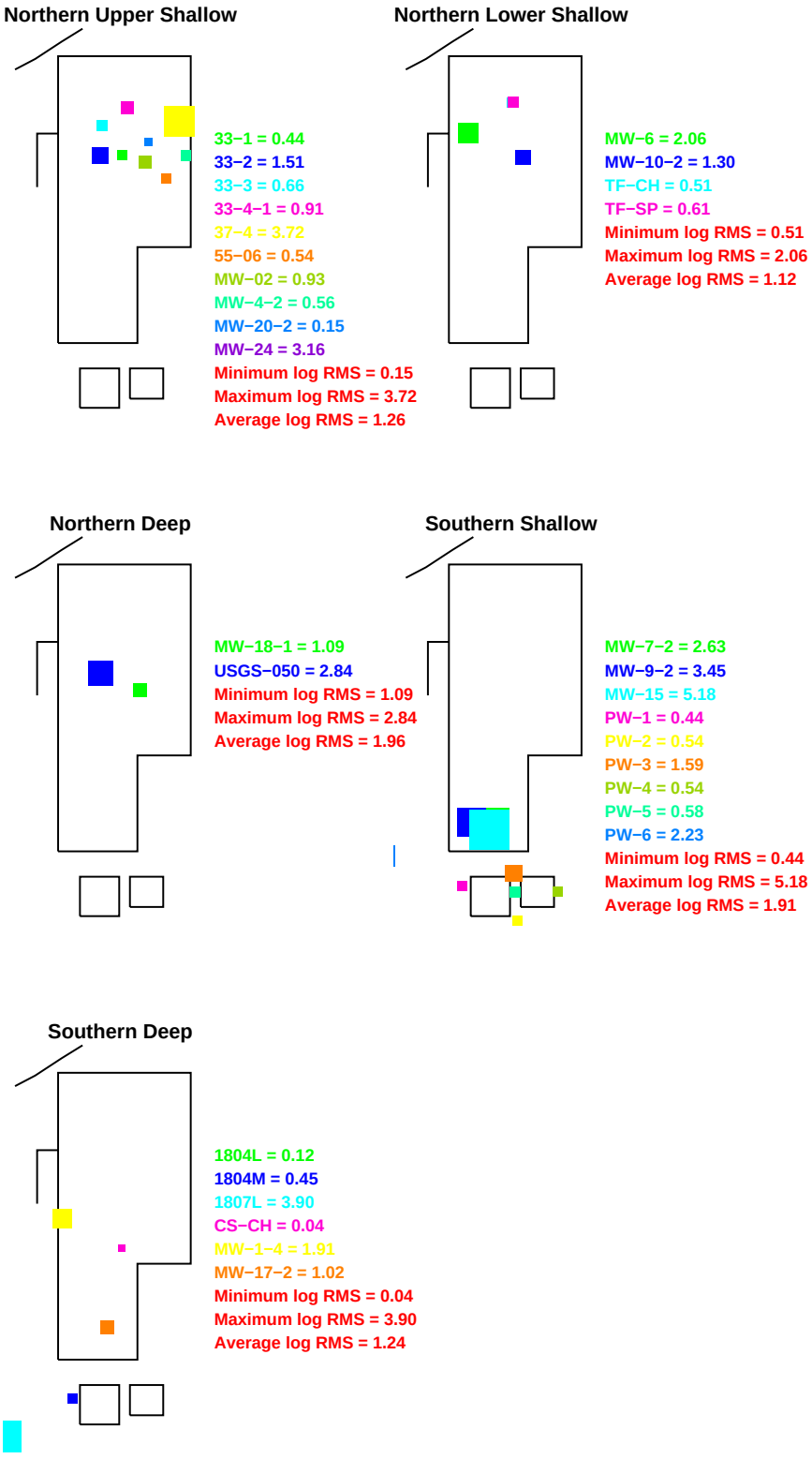

Figure J-10-44. Log 10 Root mean square error (RMS) by depth and northing assuming an interbed K_d=78 mL/g.

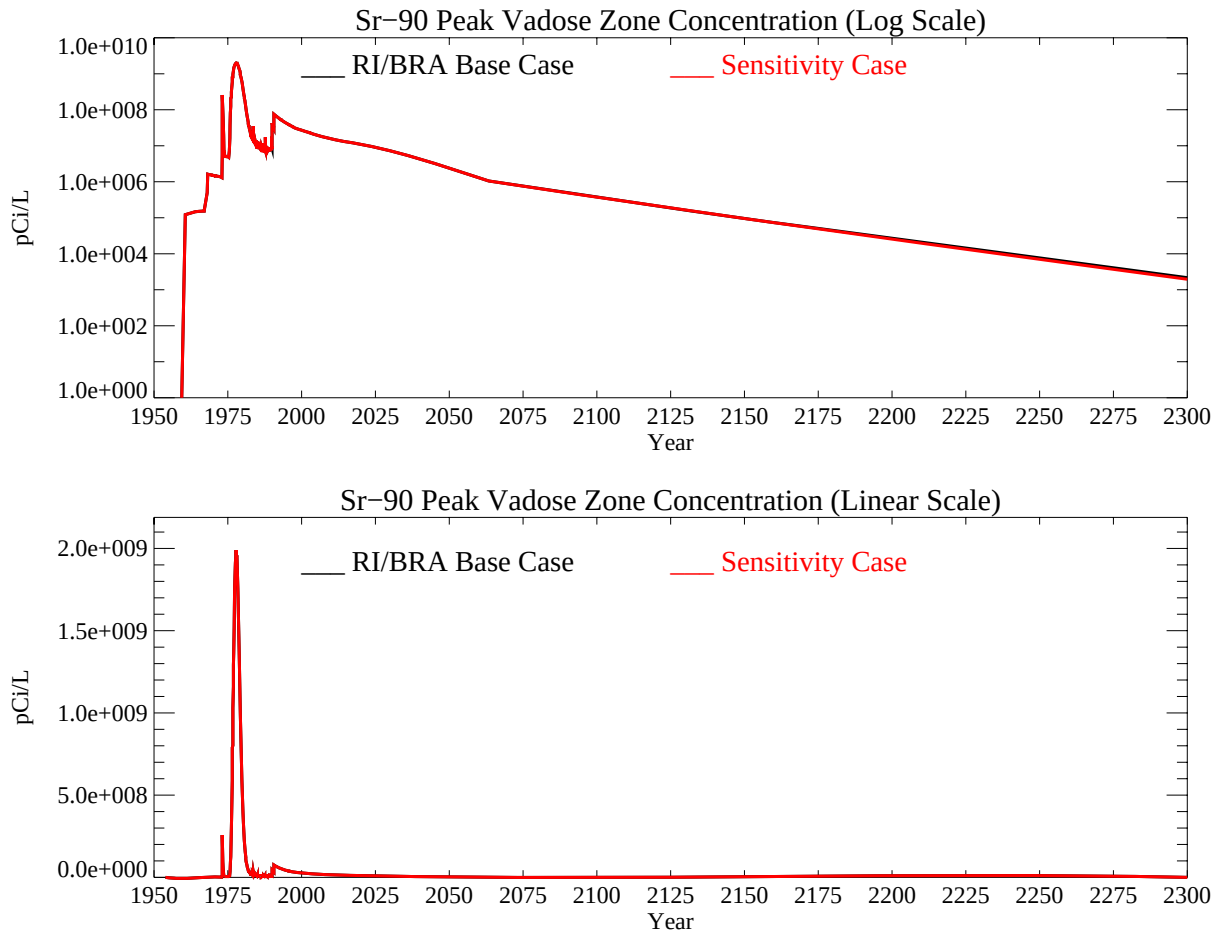

Figure J-10-45. Sr-90 peak vadose zone concentrations assuming an interbed K_d=78 mL/g (pCi/L) with the RI/BRA model in black and this sensitivity run in red.

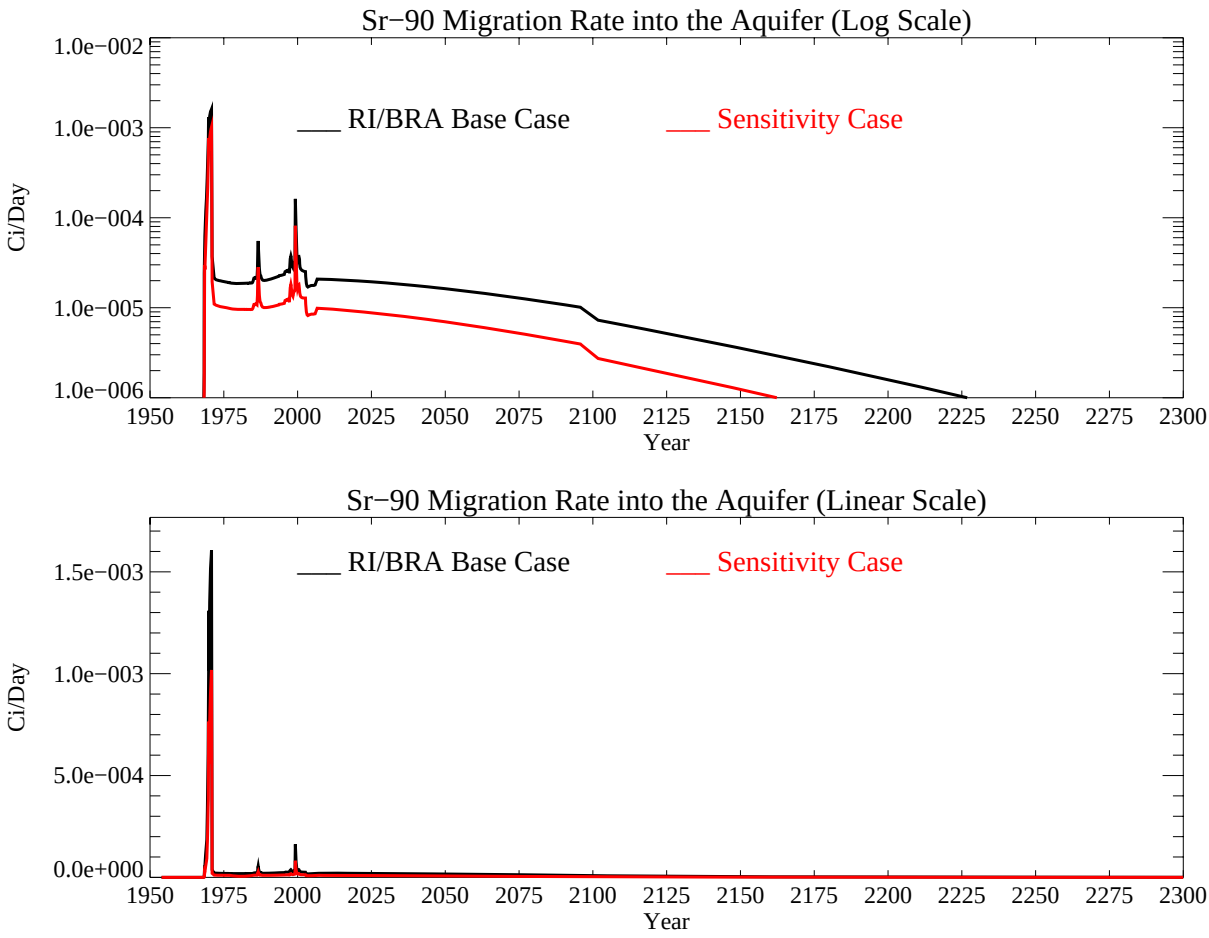

Figure J-10-46. Sr-90 activity flux into the aquifer assuming an interbed K_d=78 mL/g (Ci/day) with the RI/BRA base case in black, and this sensitivity run in red.

J-10.4.3 Aquifer Sr-90 Simulation Results

The distribution in Sr-90 in the aquifer for the time period spanning 2005-2096 is given on the course grid in Figure J-10-47. It is given for the 2049-2151 time period on the fine grid in Figure J-10-48. Resultant peak aquifer concentrations are given in Figure J-10-49. Because the Sr-90 originating in the vadose zone does not arrive in the aquifer until the mid 1980's, comparisons to measured data are not presented for aquifer wells.

The three performance measures are peak concentration in 2095, area impacted above the MCL, and time during which the MCL is exceeded. The peak concentration in 2095 is 8.1 pCi/L, about half that predicted for the RI/BRA base case (18.6 pCi/L). This difference is significant, but less than the difference predicted using a lower $K_{d.}$ given overall model uncertainty.

The more significant performance measure in this simulation is the spatial distribution of Sr-90. The Sr-90 contour plots presented in Figures J-10-47 and J-10-48 show that Sr-90 concentrations in the aquifer are predicted to exceed the MCL through year 2096. By year 2049, the region impacted by concentrations above the MCL are well within the INTEC fence line. This means that the flux rate of Sr-90 coming from the vadose zone is less than the dilution, retardation, and decay rate in the aquifer. It also implies that the source of Sr-90 south of INTEC in year 2022 is from the injection well or from earlier arrival of Sr-90 from the deep vadose zone impacted by that well's failure.

The simulated Sr-90 concentrations with this higher adsorption in the interbeds remain above the MCL from 1960 through year 2096. In the RI/BRA base-case, peak concentrations were not reduced below the MCL until year 2129.

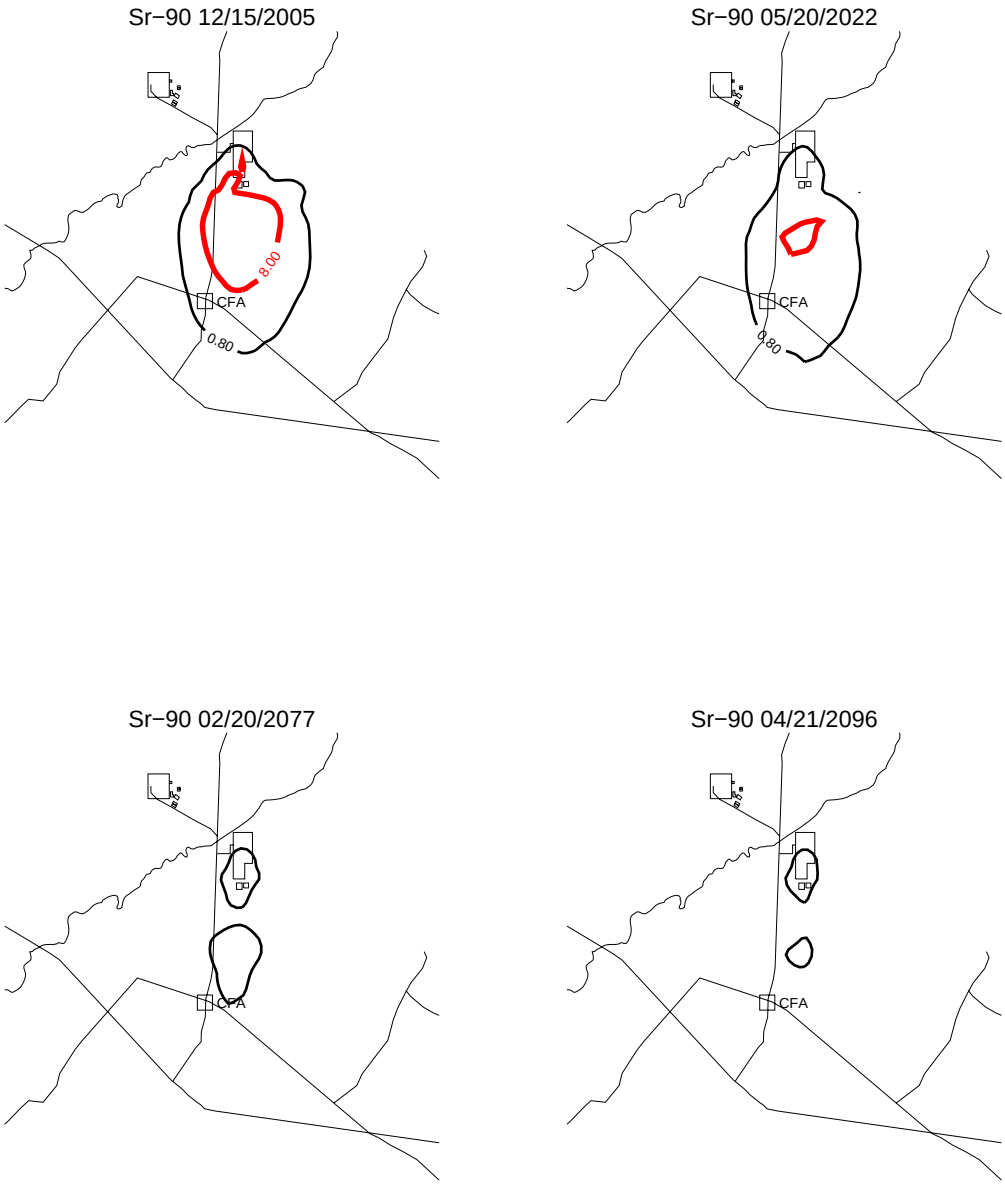

Figure J-10-47. Sr-90 aquifer concentration contours assuming an interbed K_d=78 mL/g (pCi/L) (MCL = thick red line, 10*MCL = thin red line, MCL/10 = black line).

Figure J-10-48. Sr-90 aquifer concentration contours assuming an interbed K_d=78 mL/g (pCi/L) (continued) (MCL = thick red line, 10*MCL = thin red line, MCL/10 = black line).

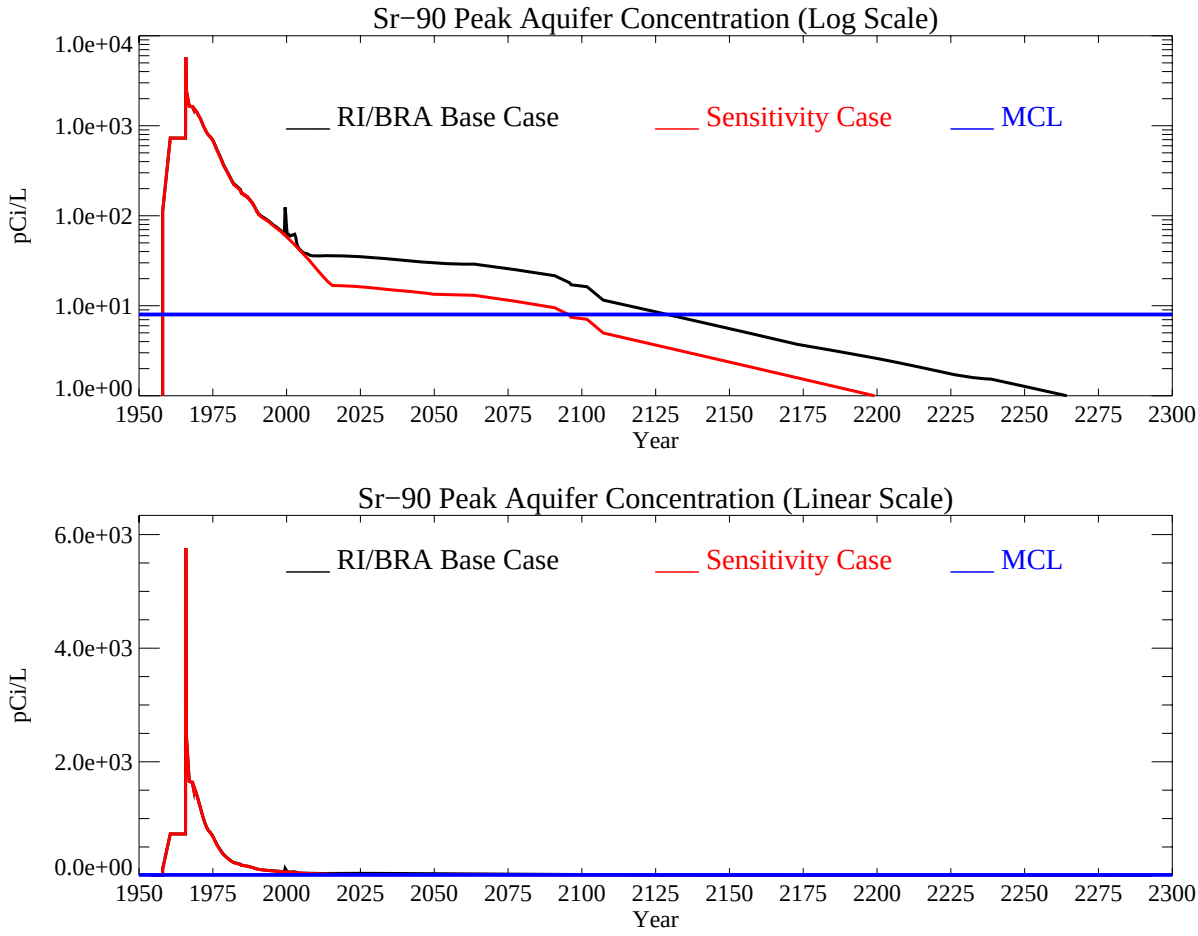

Figure J-10-49. Sr-90 peak aquifer concentrations assuming an interbed K_d=78 mL/g (pCi/L) with the MCL in blue, RI/BRA model in black and this sensitivity run in red.

J-10.5 Summary of Sensitivity to Geochemical Parameters

In the geochemical model, 15,900 Ci of Sr-90 were released to the alluvium by the CPP-31 leak. From the one-dimensional model, we saw that a fraction of the strontium moves relatively rapidly through the alluvium either complexed with nitrate ion, or because of inhibition of adsorption as a result of competition with elevated sodium and calcium concentrations in solution. Once the sodium-bearing waste peak has passed through the alluvium, the remaining strontium on the ion exchange sites is released much more slowly. With the parameters used in the model, the sodium-bearing waste pulse leaves the alluvium between 5 and 10 years after release. In all cases, we saw some fraction of the 15,900 Ci released within the first 10 years, with only a small incremental increase at 20 years (Table J-10-1).

In the 3-dimensional RI/BRA model, 12336 Ci of Sr-90 were released from the alluvium into the vadose zone after 20 years. As the CEC increases from 2 to 3 meq/100 g, the amount of Sr-90 released decreased slightly to 110864 Ci after 20 years. Increasing the CEC to 7 meq/100 g further decreased the amount of Sr-90 released at 20 years to 6403 Ci. From the simulated partitioning of strontium between liquid and solid phases we calculated K_d values (see Equation J-5-2) for the alluvium. There was quite a range in calculated partitioning coefficients (Table J-10-1). For CEC of 2 meq/100 g, K_d values are much lower than commonly considered applicable to alluvium. Higher K_d values at 7 meq/100 g were comparable to K_d values measured by the USGS.(Liszewski, et al. 1997; Liszewski, et al. 1998)

All of the CEC values used in the sensitivity runs were within the range of data obtained from the literature for INTEC alluvium. Changing the CEC produced two changes in model output. First, the fraction of the total Sr-90 released in the first 20 years was affected. Second, the steady-state K_d value after the leak has been flushed from the alluvium was affected. Decreasing the CEC resulted in more Sr-90 being flushed quickly from the alluvium. It also resulted in the remaining Sr-90 being more mobile. Higher CEC resulted in more Sr-90 being retained in the alluvium. However, the steady-state K_d value was higher so that this residual Sr-90 was less mobile. The amount of residual Sr-90 and the mobility of the residual Sr-90 are important for evaluating risk and remedial alternatives. The amount of Sr-90 released from the alluvium in the first 20 years affects perched water concentrations, and impacts the parameter values necessary for the vadose zone model to match measured Sr-90 concentrations in perched water.

The chemical composition of the pore water was estimated from measurements taken in perched water zones (Table J-3-4). These measurements reflect multiple sources of water, some of which contain contaminants or dissolved solids from plant water systems. Recharge in the alluvium is likely to be closer in composition to precipitation, and may have lower concentrations of sodium. Because sodium is one of the cations important in the competitive cation exchange reactions, the sensitivity of strontium transport to a lower sodium concentration in pore water/recharge was assessed. The other components in pore water are based on the assumption of calcite saturation at a partial pressure of carbon dioxide of 10^{-2} atm. This assumption fixes carbonate, pH, and calcium within a fairly narrow range. As a result, there is a limited range in uncertainty for calcium and pH and we did not test for sensitivity to these parameters.

The sodium concentration used in the pore water model is the lowest measured in perched water, and is equal to the concentration of sodium in the Snake River Plain aquifer. Precipitation may have a lower concentration. Sensitivity to sodium concentration was tested by dropping the sodium concentration to 0.22 mmol/L from 0.33 mmol/L in the base case. The change in sodium concentration resulted in a very slight increase in the release of Sr-90 at 20 years (Table J-10-1). The likely reason for this is that the lower background sodium concentrations increase the calcium saturation on the ion exchange sites. The greater fraction of calcium on the clays decreases the partitioning of strontium to ion exchange sites. This decrease is small and does not increase the release of Sr-90 significantly. Therefore, the Sr-90 release is not sensitive to background concentrations of sodium in the pore water and the estimated values used in the model do not need to be refined.

The third parameter evaluated for effect on Sr-90 release is the strontium selectivity coefficient. The selectivity coefficient is primarily related to the properties of the cation. Cations in solution are not equally sorbed to ion exchange sites on clays. Cations with greater hydrated ionic potential are preferentially sorbed. This means that divalent cations are more strongly bound than monovalent cations. Larger cations (greater atomic number) in a group are less strongly hydrated than smaller cations. As a result of the lower hydration, cations with greater atomic number have fewer waters of hydration and consequently a greater hydrated ionic potential. Thus, the order of preference for divalent alkaline earth cations is $Ba^{2+} > Sr^{2+} > Ca^{2+} > Mg^{2+}$. Strontium will be more strongly sorbed to ion exchange sites than calcium and magnesium as well as the monovalent cation sodium.

We varied the selectivity coefficient of strontium to be as low as calcium and as high as barium. Given the general consensus on the ordering of selectivity coefficients, this effectively brackets the total range over which the selectivity coefficient could range. We lowered the selectivity of strontium to a value (0.45) slightly lower than calcium. This increased the release of Sr-90 to 9,454 Ci because calcium and sodium were much more effective at competing for exchange sites with strontium. Raising the selectivity coefficient to a value more representative of barium decreased the release of Sr-90 to 3,369 Ci at 10 years. The calculated release of Sr-90 is sensitive to the selectivity coefficient for strontium. The range of selectivity coefficients tested exceeds the likely range in uncertainty in the selectivity coefficient because if the values selected were true, it would alter the selectivity sequence for cations. Furthermore, the selectivity coefficients used in the base case do a good job of matching laboratory measurements of strontium sorption to INTEC sediments. Therefore, we conclude that additional refinement of selectivity coefficients for INTEC specific materials is not likely to significantly impact the uncertainty in the calculated Sr-90 release from alluvium.

The final parameter investigated was the interbed K_d. Available field data suggests that a range of K_d in the interbeds would be appropriate. The range is dictated by soil textural and mineralogic characteristics in combination with water chemistry. Based on available data, this range spans 25 to 84 mL/g for sedimentary interbeds at the INL. At the low end of 22 mL/g, the RI/BRA model was used to predict peak concentrations of 110.8 pCi/L in year 2095, with concentrations falling below 8 pCi/L in year 2263. Near the high end of this range, a K_d of 78 mL/g results in a peak aquifer concentration of 8.1 pCi/L in 2095, with concentrations below 8 pCi/L by year 2096. Using the three performance measures of peak 2095 concentration, extent of the aquifer contaminated above the MCL, and the time during which concentrations exceed the MCL as a basis for comparison, the sensitivity of this model to interbed K_d is very high. Selecting a single value from the possible range helps bracket the endpoints of prediction, but in reality, a single value is unlikely to exist. Had spatially variable values been used, the peak concentration range would be narrower, converging to a value representative of the mean 50 mL/g K_d used in the RI/BRA model

Table J-10-1. Geochemical parametric sensitivity summary. All Sr-90 activities are undecayed.

	CEC=2 (meq/100 g)	CEC=3 (meq/100 g)	CEC=5 (meq/100 g)	CEC=7 (meq/100 g)	$K_{Na/Sr}$= 0.25	$K_{Na/Sr}$= 0.45	Na^+ = 0.22 (mmol/L)	CEC=2 (meq/100g) K_d=22 (mL/g)	CEC=2 (meq/100g) K_d=78 (mL/g)
Alluvium Statistics									
Years after CPP-31	**Activity Leaving Alluvium (Ci)**								
5 yrs	5187	4239	2793	1773	1658	3090	1921	5187	5187
10 yrs	12272	10820	8352	6378	3369	9454	6497	12272	12272
15 yrs	12310	10842	8368	6393	3373	9470	6509	12310	12310
20 yrs	12336	10864	8380	6403	3378	9480	6517	12336	12336
Activity Remaining in Alluvium (Ci)	3564	5036	7520	9497	12522	6420	9383	3564	3564
Effective K_d (mL/g) at 20 years	2	3.75	9.2	17	39	13		2	2
Vadose Zone Statistics									
Peak Concentration (pCi/L)	1.8E9	1.8E9	1.6E9	1.1E9				2.0E9	2.0E9
Year Peaked	1979	1979		1971				1978	1978
Aquifer Statistics									
Peak Concentration (pCi/L) in 2095	18.6	16.7		11.5				110.8	8.1
Year C is below 8 pCi/L	2129	2123		2105				2263	2096

shaded cells = RI/BRA base case

J-11 SENSITIVITY TO HYDROLOGIC CONDITIONS

Sensitivity to hydrologic conditions was determined through simulation using the base model discussed in Section J-8. In these sensitivity simulations a single parameter change was made. The RI/BRA base model was based on an alluvium CEC of 2 meq/100 g, a strontium selectivity coefficient of 0.35, a background sodium concentration of 3.3 mmol/L, an average infiltration rate of 18 cm/yr, and an interbed K_d of 50 mL/g.

- The first sensitivity to hydrologic conditions includes simulations using an initial infiltration rate of 18 cm/yr through the first 5 years after the CPP-31 release at which time, the infiltration rate was reduced to 2 cm/yr in order to account for the infiltration reducing liner that was placed on the tank farm in 1977.
- As discussed in Appendix A, Section 3.3 and in Appendix B, it is not clear that the liner is effective in reducing infiltration through the tank farm, and some of the monitoring results suggest that it may be increasing local recharge in that area. The second sensitivity simulation evaluates the transport using an infiltration rate of 39 cm/yr to account for that potential increase in infiltration rate. As with the first hydrologic sensitivity run, the rate was not changed until year 1977.
- In the base case simulations for all of the contaminants evaluated in this RI/BRA, it was assumed that the water losses due to anthropogenic activities were distributed throughout INTEC. It is likely that more of these water losses occur in northern INTEC in association with increased facility activity. The fourth sensitivity examines the effect of higher recharge in northern INTEC.
- The fifth hydrologic sensitivity is presented to examine the effect of removing the anthropogenic water altogether after year 2035. Clearly, the influence of recharge is large, as evidenced by the sharp reduction in flux rates into the aquifer from the vadose zone shortly after year 2095. This sharp reduction was apparent in each of the activity-flux into the aquifer plots presented thus far. There is an ongoing effort to reduce the anthropogenic water losses at INTEC. If this effort is effective, those losses will occur much earlier than the 2095 time-frame assumed for the base-case simulations. This simulation is presented to evaluate the importance accelerating actions to reduce anthropogenic water losses.
- The sixth sensitivity is presented to evaluate the potential land-use impact. In the RI/BRA, it was assumed that the land-use through year 2095 would require pumping water from the SRPA at current rates. This assumption is consistent with an industrial use scenario, where large water volumes would be necessary in order to sustain the commercial activities. If the land-use changes significantly, or if the current production wells are moved out of the influence of INTEC (i.e., further north or east), the draw-down currently observed in the aquifer would stop. Pumping is assumed to stop in year 2012, 2035, and 2096 in the three scenarios evaluated.
- The final sensitivity simulation examines the effect of increasing the interbed dispersivity in an attempt to better match concentrations in wells to the southeast of the tank farm. In most of the results presented this far, predicted concentrations in wells to the southeast have been lower than observed. Achieving the lateral migration necessary to move the Sr-90 toward those wells might be possible by increasing the lateral dispersivity.

These results are summarized in Table J-11-1 following the presentation of simulation results for each case.

J-11.1 Lower 3 cm/yr Infiltration Through The Tank Farm Liner

The RI/BRA model incorporated infiltration from precipitation at a rate of 18 cm/yr applied within the INTEC fence line including through area representing the tank farm. Five years after the CPP-31 release, an infiltration reducing liner was placed over the tank farm. In this simulation, we assume that from the beginning of the simulation period through 1976 the infiltration rate through the tank farm is 18 cm/yr. In 1977 and beyond, we assume that the liner is effective at reducing infiltration to 3 cm/yr in the four grid blocks representing the tank farm. This total 3 cm/yr implies that anthropogenic water leaks and precipitation infiltration are reduced by the presence of the liner.

J-11.1.1 Geochemical Evolution in the Alluvium

A decrease from 18 cm/yr to 3 cm/yr in infiltration rate occurring 5 years after the CPP-31 release has resulted in a rapid decrease in SrCO3 and SrOH in the aqueous phase, accompanied by an increase in Sr+ ion in the aqueous phase. The relative abundance of Sr+ ion is much larger than that of SrCO3 and SrOH, resulting in an increase in aqueous phase Sr-90 concentrations with the decrease in infiltration water. This is presumably a result of decreasing the incoming flux of Na, HCO3-, and Ca+2 ions that are contained in the infiltration water.

The amount of transported aqueous-phase Sr-90 is somewhat sensitive to this change in buffering capacity, and as a result, more Sr-90 leaves the alluvium in the first 20 years under this scenario than was predicted to occur in the absence of the tank farm liner. After 5, 10, 15, and 20 years, the total Sr-90 that has entered the vadose zone under the alluvium is 1342, 7243, 7845, and 8037 Curies, respectively as shown in Figure J-11-1. With this lower infiltration rate, a slightly smaller fraction (7863 Ci vs. 9497 Ci) remains in the alluvium after 20 years (Figure J-11-1). The flux rate shown in Figure J-11-1 (H) has an relatively high spike due to the numerical differentiation of the cumulative effluent shown in Figure J-11-1 (G) that is smoothed as the data is input into the vadose zone model.

The largest difference in the distribution of Sr-90, relative to the base case, occurs in the adsorbed Sr-90. Shortly after the decrease in infiltration rate, there is a rapid decline in Sr-90 on the exchange sites. The effective K_d is essentially the ratio of activity on the exchange sites to that in the aqueous phase. As the exchanged activity decreases, the aqueous phase Sr-90 concentrations increase, and the effective K_d decreases. The time evolution of this parameter is quite different than observed in the RI/BRA base case (Figure J-8-9 (J)). After 20 years, the effective K_d has not equilibrated to an average value as was observed in the other simulations, primarily because the decreased flux rate has not yet flushed the remaining sodium and calcium from the CPP-31 release out of the alluvium. Although not at a pseudo-steady state, at 20 years, the effective K_d is roughly 6.4 mL/g.

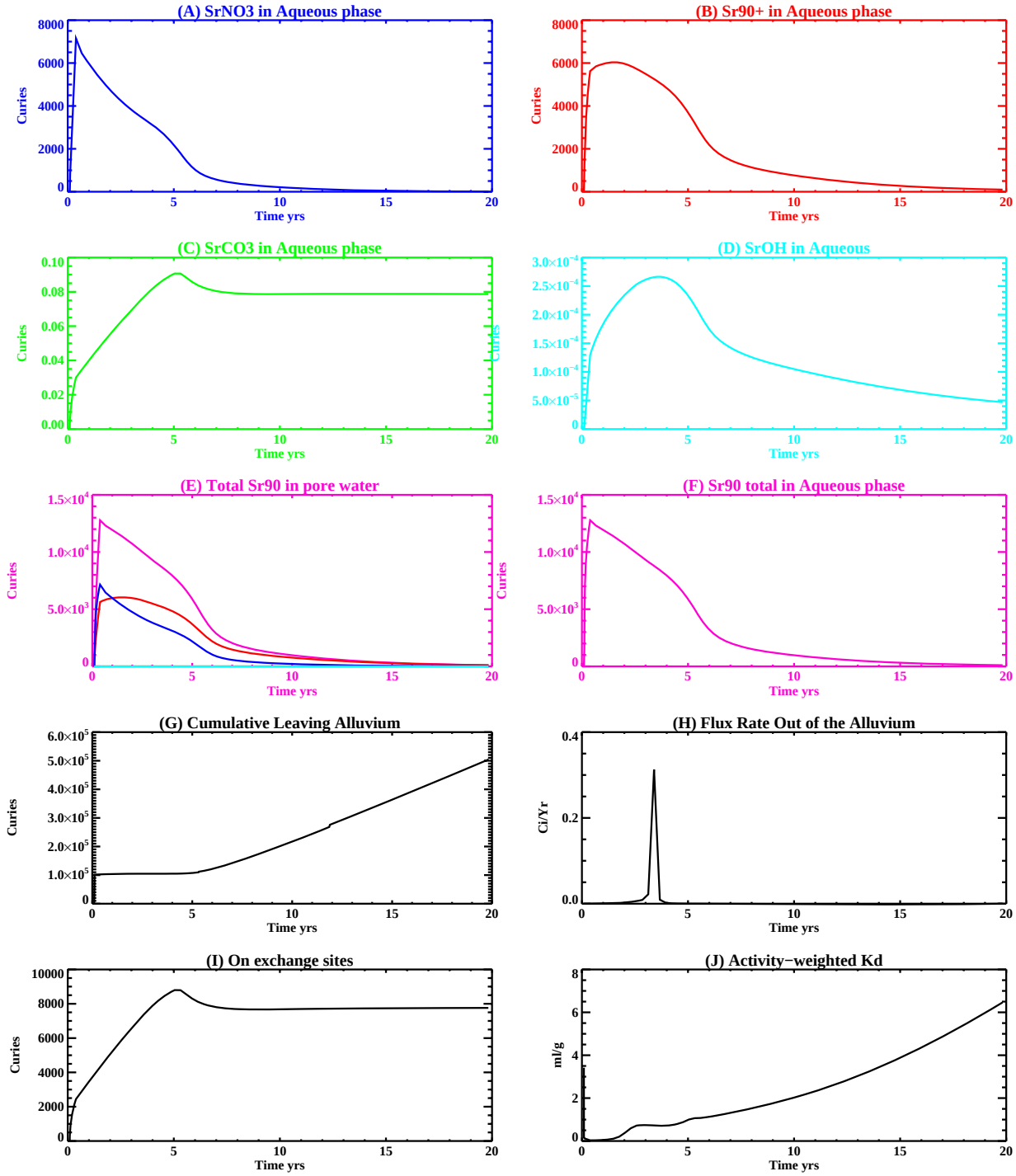

Figure J-11-1. Summary figure illustrating the speciation of Sr-90 in the aqueous phase (A-F), total Sr-90 in the pore-water of the alluvium (E), cumulative curies of Sr-90 having left the alluvium (G), flux rate leaving the alluvium (H), Sr-90 on the exchange sites (I), and effective partitioning coefficient (Kd) (J).

J-11.1.2 Vadose Zone Sr-90 Simulation Results

The release of Sr-90 in this simulation followed the same procedure as was used in the RI/BRA model:

- 15900 Ci from CPP-31 release in the tank farm were represented using (a) the activity-release function shown in Figure J-11-1 (H) for the 8037 Ci released during the first 20 years, and placing this activity flux directly above the basalt interface of the base model (Appendix A, Section 5.1). The remaining 7863 Ci were vertically through the alluvium, scaled to the measured soil concentrations obtained during the 2004 (Appendix G and Table 5-32) sampling cycle. To simulate the transport of the activity remaining in the alluvium, an effective K_d of 6.4 mL/g was used (Figure J-11-1 (J)) for the alluvium sediments.
- transport of Sr-90 from sources other than CPP-31 originating in the alluvium, whose location is spanned by the submodel (Appendix A, Section 5.1), were simulated using the submodel. Because these source locations were outside the influence of the high ionic strength, acidic CPP-31 release, a K_d of 20 mL/g was used in the submodel alluvium.
- transport of Sr-90 from sources located outside of the submodel horizontal extent were also placed in the base model used to simulate the transport of the CPP-31 remaining in the alluvium. The effective K_d for the alluvium underlying these source locations was also set to the value used to simulate the transport of Sr-90 predicted to remain in the alluvium after 20 yrs (first bullet). The relative magnitude of these sources are small relative to the residual Sr-90 predicted to remain in the alluvium after 20 yrs. In this case, the K_d is much lower than that used to simulate the transport of Sr-90 from sources within the submodel boundary. However, this should not effect the peak aquifer concentrations by more than 10%.

The distribution of Sr-90 is presented in Figures J-11-2 through J-11-5 for the 1979-2293 time period. The arrival in key perched water wells is compared to the field data in Figure J-11-6, and is summarized for all of the perched water wells in Figure J-11-7. The match to observed data in the key wells is quite similar to that obtained in the RI/BRA base case. In general, the match to field data with these parameters is slightly better in northern INTEC, and slightly worse in southern INTEC. The better match in northern INTEC results from the complex combination of reduced infliltration (anthropogenic and precipitation) causing less dilution and less Sr-90 being mobilized through the alluvium in the first 20 years following the CPP-31 release. Higher concentrations would be expected with less dillution, and lower concentrations would be expected with less Sr-90 present. In this case, the competing effects balance and allow the predicted concentrations in the perched water to be quite similar. The poorer match to southern wells is more informative. With an effecitve K_d higher than used in the RI/BRA base case, concentrations are less overpredicted. This is indicative of percolation pond water being of lower ionic strength, effectively raising the K_d from the base case value of 2 mL/g. It suggests that the effective K_d in southern INTEC should be in the 2-10 mL/g range.

Peak vadose zone concentrations through time are given in Figure J-11-8 in red, and are shown for the RI/BRA base case in black. As expected from the similarity in RMS, the peak concentrations are quite similar. The differences occur shortly after the liner emplacement, and are probably associated with pore water concentrations in the alluvium. The rate at which Sr-90 enters the aquifer from the vadose zone is given in Figure J-11-9 for this simulation in red, and can be compared directly to the RI/BRA base case (shown as black). It is interesting to note that the decrease in infiltration rate resulted in:

- 35% less Sr-90 leaving the alluvium in the first 20 years (8037 vs. 12336) following the alterations in chemical balance caused by reducing the influx of HCO_3 as discussed in Section J-11.1.1.
- twice as much Sr-90 remaining in the alluvium (7863 Ci vs.3564 Ci)
- decreased mobility of Sr-90 in the alluvium reflected by a larger K_d (6.4 mL/g vs. 2 mL/g)

The relatively low K_d used to simulate the transport of the Sr-90 remaining in the alluvium still allows most of the Sr-90 to remain in the alluvium. The small differences between flux rates into the aquifer for the RI/BRA base case and this simulation are due to the complex combination of reduced infliltration (anthropogenic and

precipitation reduced to 3 cm/yr) causing less dilution and less Sr-90 being mobilized through the alluvium in the first 20 years following the CPP-31 release. Higher concentrations would be expected with less dillution, and lower concentrations would be expected with less Sr-90 present. In this case, the competing effects balance and allow the predicted flux rates out of the vadose zone to be quite similar. The long-term persistence of the similarity is consistent with the results shown in Section J-9.4 where it was shown that with an alluvium K_d of 2 mL/g, leaving 3564 Ci of Sr-90 in the alluvium does not result in an appreciable increase the flux of activity leaving the vadose zone. In this case, the amount left in the alluvium after 20 years is only twice that amount, and the K_d in this case is three times higher.

Figure J-11-2. Sr-90 vadose zone concentration reducing infiltration in the tank farm to 3 cm/yr (horizontal contours) (pCi/L) (MCL = thick red line, 10*MCL = thin red line, MCL/10 = black line).

Figure J-11-3. Sr-90 vadose zone concentration reducing infiltration in the tank farm to 3 cm/yr (horizontal contours) (pCi/L) (MCL = thick red line, 10*MCL = thin red line, MCL/10 = black line).

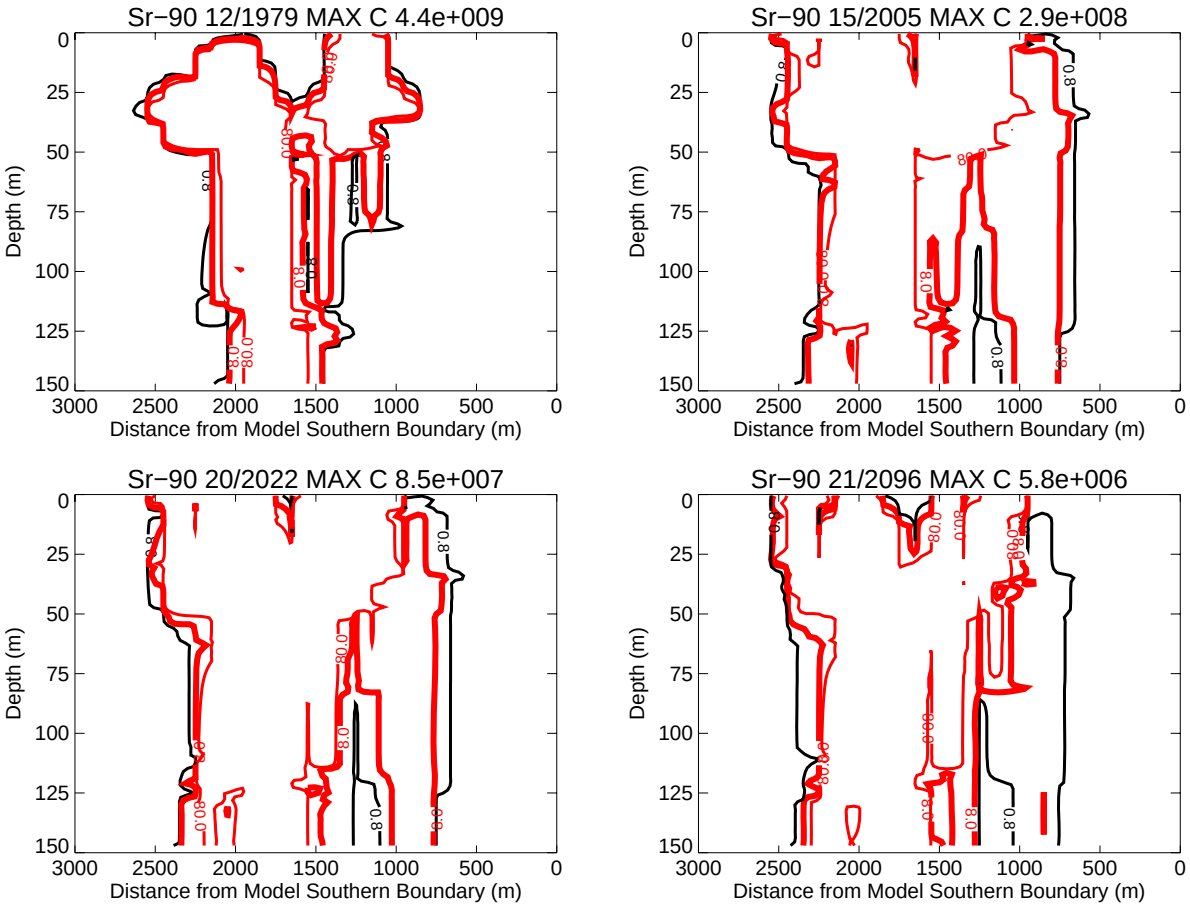

Figure J-11-4. Sr-90 vadose zone concentrations reducing infiltration in the tank farm to 3 cm/yr (vertical contours) (pCi/L) (MCL = thick red line, 10*MCL = thin red line, MCL/10 = black line).

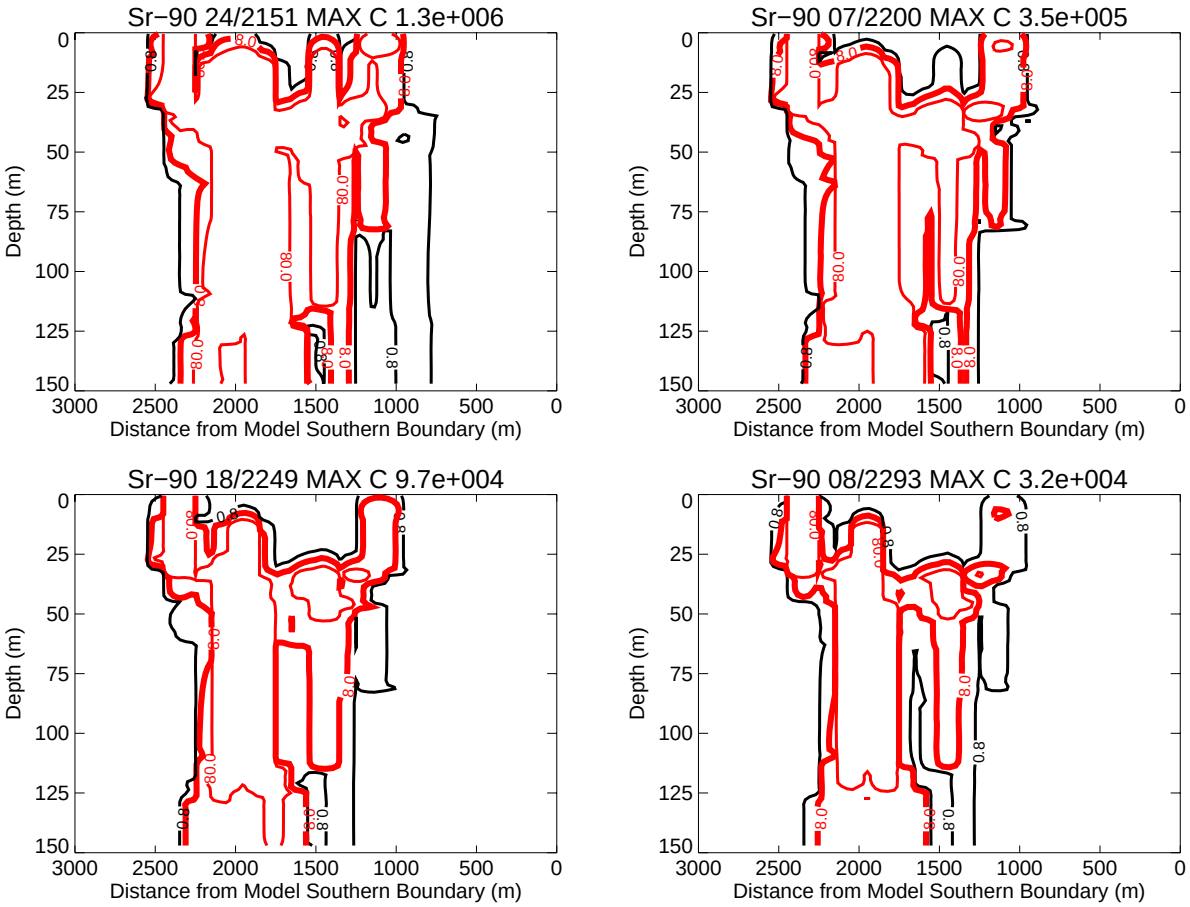

Figure J-11-5. Sr-90 vadose zone concentrations reducing infiltration in the tank farm to 3 cm/yr (vertical contours) (pCi/L) (continued) (MCL = thick red line, 10*MCL = thin red line, MCL/10 = black line).

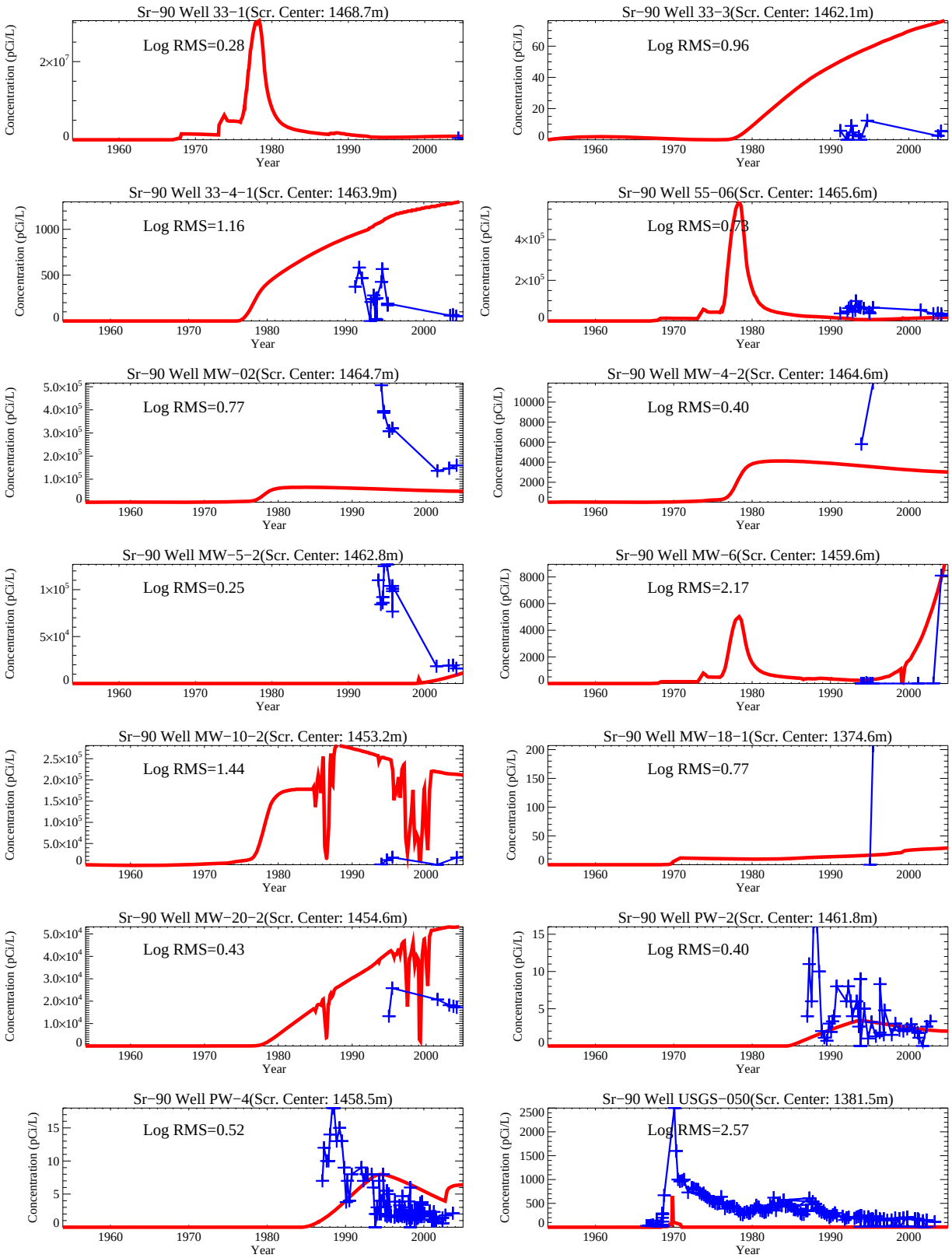

Figure J-11-6. Sr-90 concentration in perched water wells reducing infiltration in the tank farm to 3 cm/yr (pCi/L) (Measured values = blue crosses, red = model at screen center).

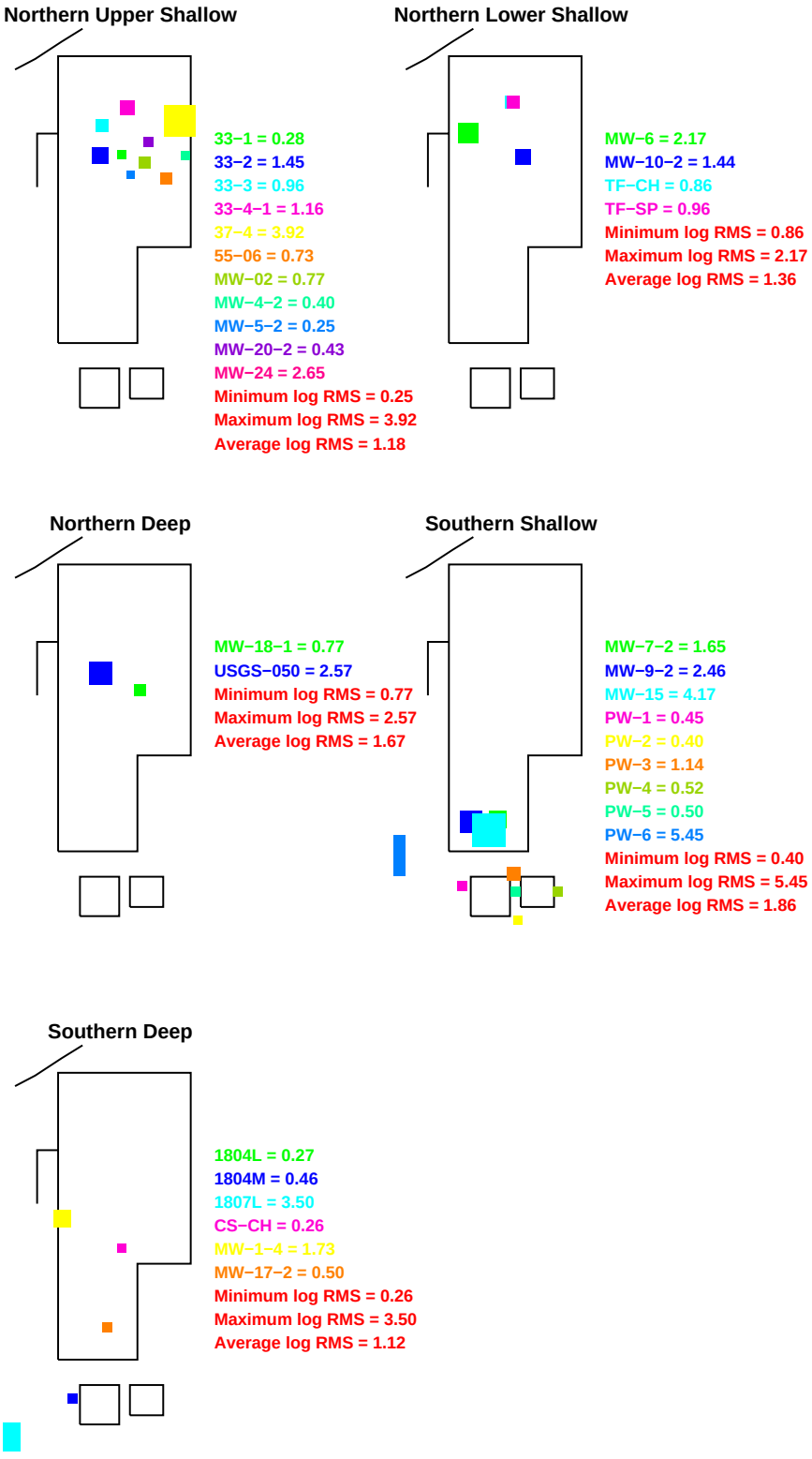

Figure J-11-7. Log 10 Root mean square error (RMS) by depth and northing reducing infiltration in the tank farm to 3 cm/yr.

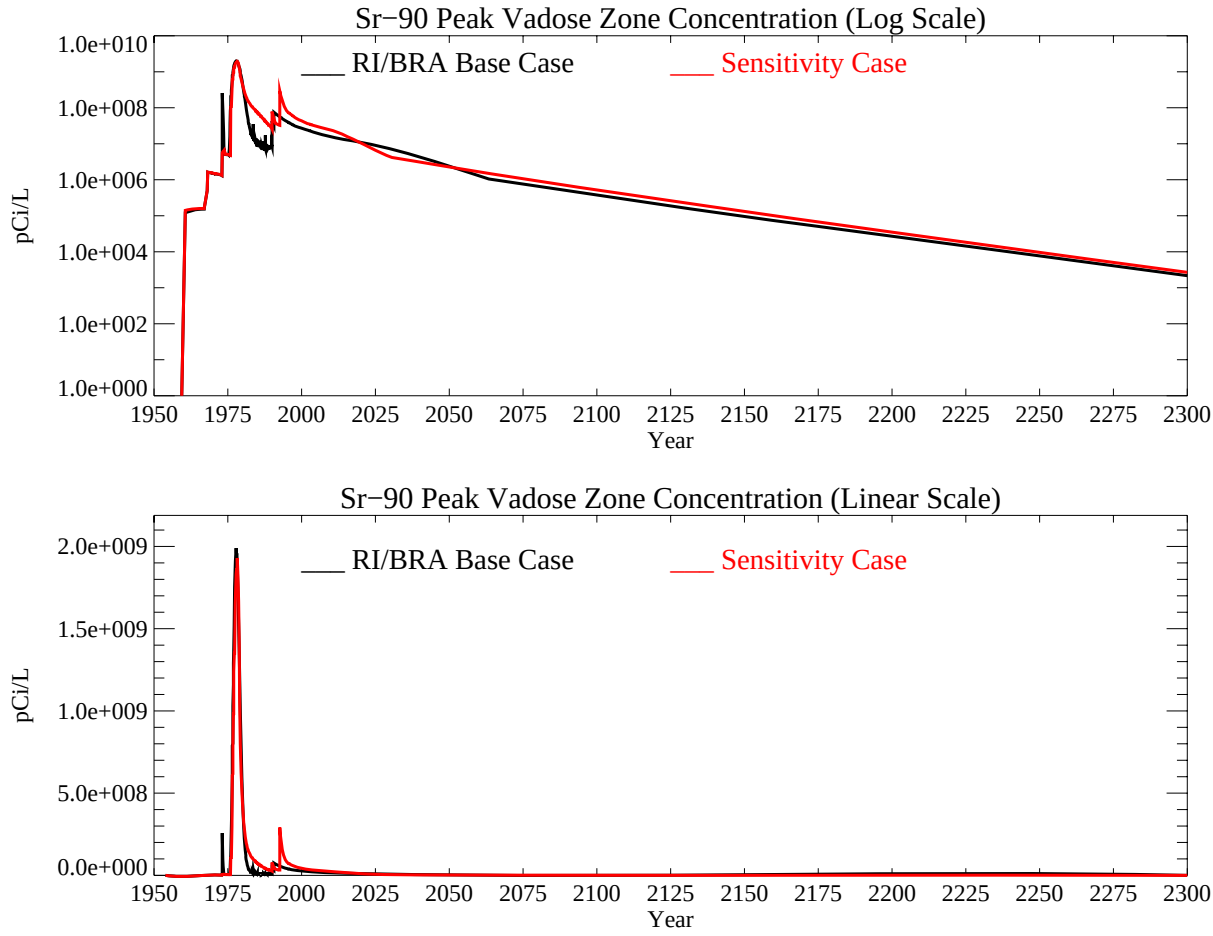

Figure J-11-8. Sr-90 peak vadose zone concentrations reducing infiltration in the tank farm to 3 cm/yr (pCi/L) with the RI/BRA model in black and this sensitivity run in red.

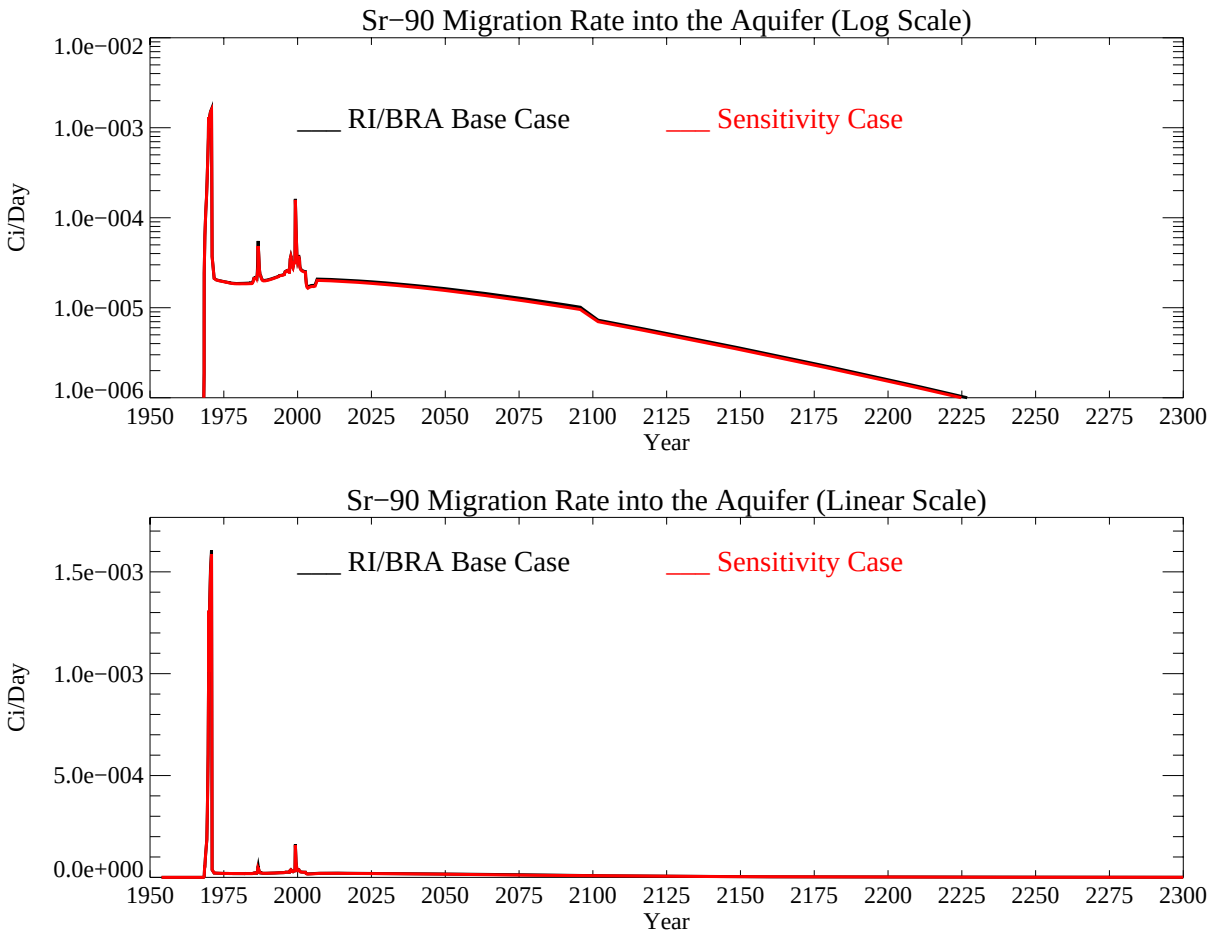

Figure J-11-9. Sr-90 activity flux into the aquifer reducing infiltration in the tank farm to 3 cm/yr (Ci/day) with the RI/BRA model in black and this sensitivity run in red.

J-11.1.3 Aquifer Sr-90 Simulation Results

The distribution of Sr-90 in the aquifer for the time period spanning 2005-2096 is given in Figure J-11-10 for the far-field with near-field results shown for the 2049-2151 time frame in Figure J-11-11. There are significant differences in the overall distribution of Sr-90 in the aquifer. This is apparent by comparing Figure J-8-19 to J-11-11 and noting that the decreased infiltration rate has reduced the spatial extent of Sr-90 in the 0.8 pC/L-8 pCi/L range north of the tank farm. As discussed in Appendix A, there is an apparent water divide near the tank farm in the 110 ft interbed. It slopes north nearer the Big Lost River, and slopes south near the tank farm. Reducing the overall infiltration in this case has prevented the higher Sr-90 concentrations from migrating to the north where they are driven downward by the high fluxes from the Big Lost River. Keeping the Sr-90 to the south where it moves slower allows it to decay more en route to the aquifer and has allowed the area above the MCL to be contained to a very small area just south of the tank farm in year 2095.

Peak aquifer concentrations for this simulation are shown in red and can be compared to the RI/BRA base case results shown in black on Figure J-11-12. The simulated Sr-90 concentrations were predicted to remain above the MCL from 1960 through year 2099. In the RI/BRA base case, the peaks in concentration that occur in the 2000-2005 time frame are a direct result of peak flows in the Big Lost River that drive Sr-90 from deep in the vadose zone. Those peaks are not present in this sensitivity case. However, in both cases, there is a noticeable step decrease in concentration that occurs following the removal of anthropogenic water at land surface in 2095. The predicted peak Sr-90 concentration in the year 2095 is 8.9 pCi/L, about twice as high as predicted for the RI/BRA base case (18.6 pCi/L).

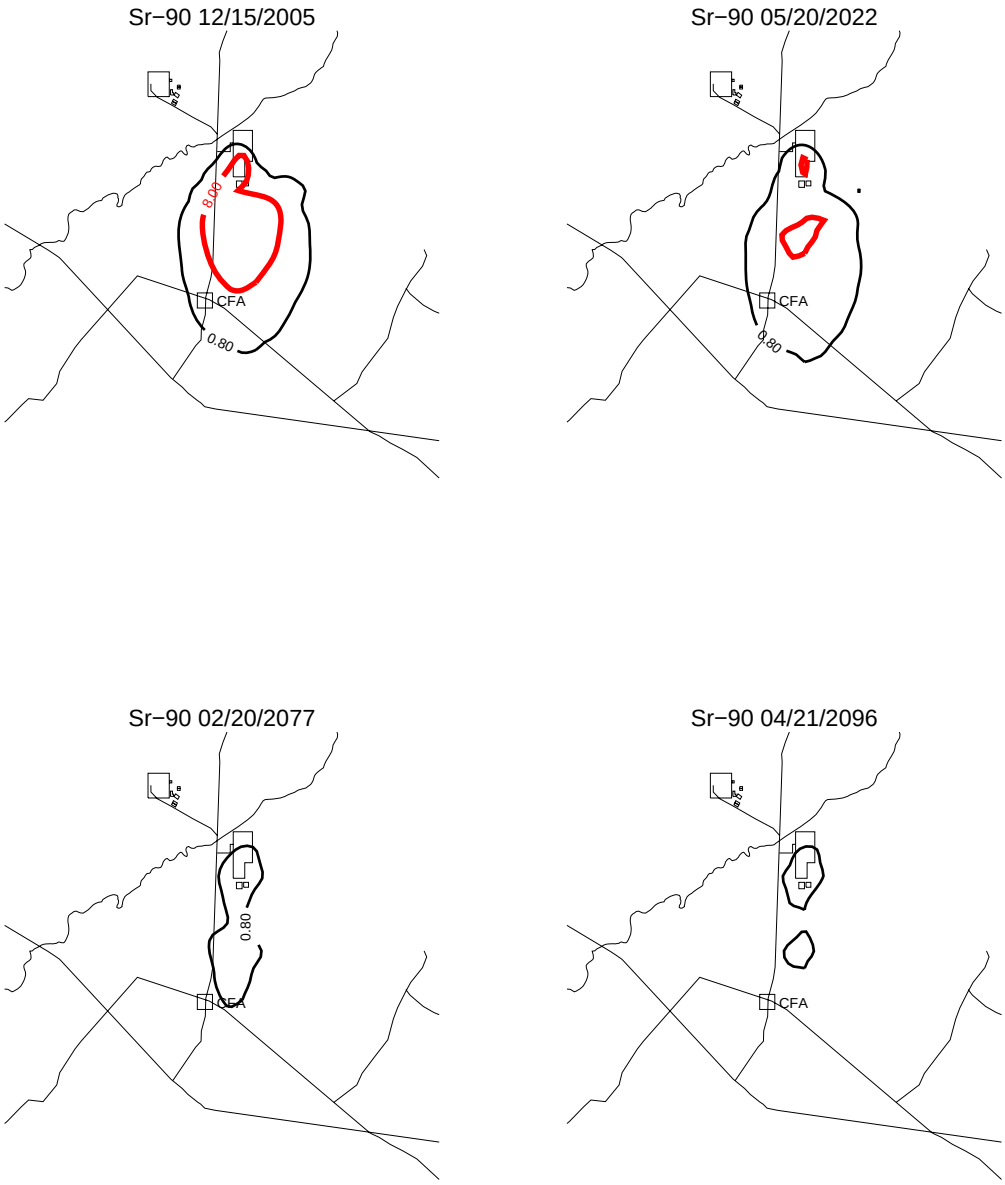

Figure J-11-10. Sr-90 aquifer concentration contours reducing infiltration in the tank farm to 3 cm/yr (pCi/L) (MCL = thick red line, 10*MCL = thin red line, MCL/10 = black line).

Figure J-11-11. Sr-90 aquifer concentration contours reducing infiltration in the tank farm to 3 cm/yr (pCi/L) (continued) (MCL = thick red line, 10*MCL = thin red line, MCL/10 = black line).

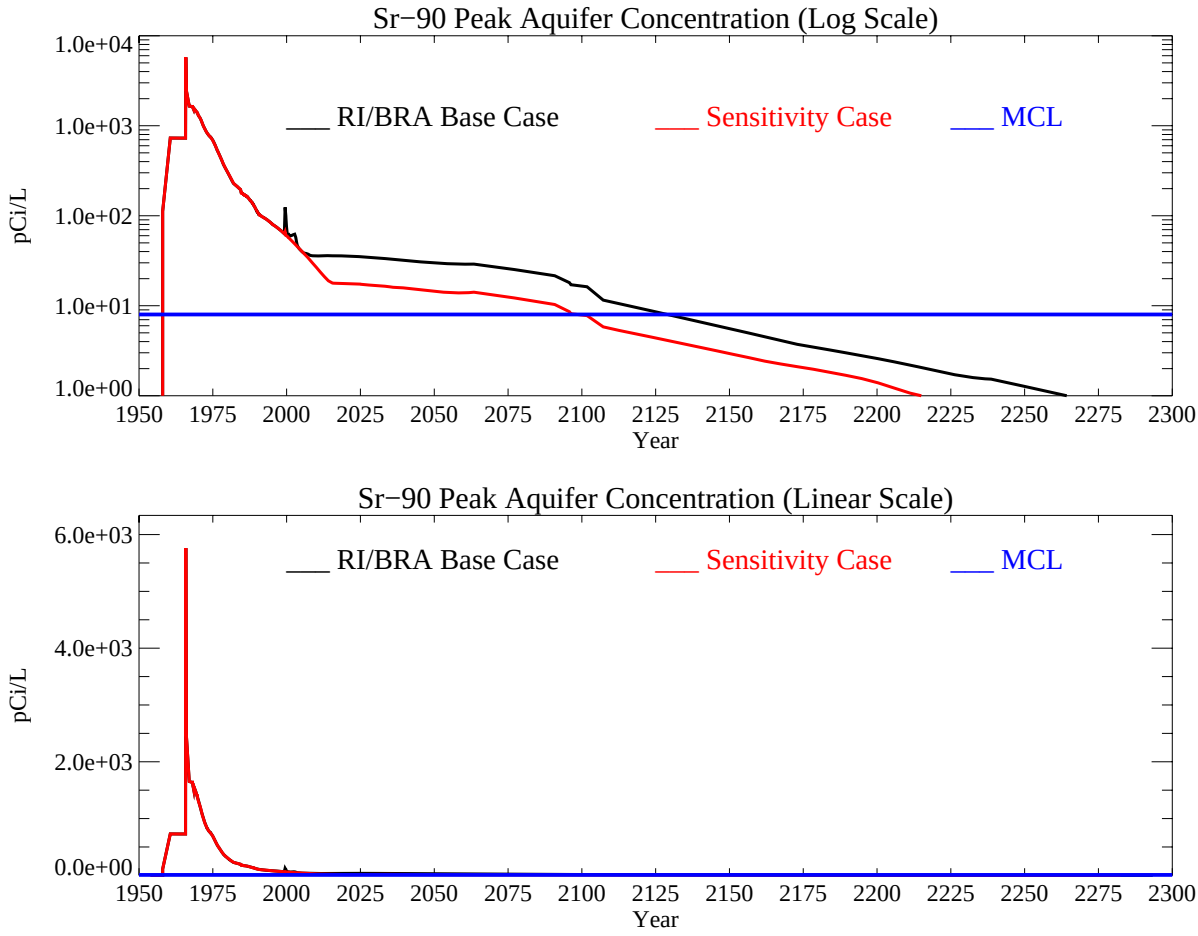

Figure J-11-12. Sr-90 peak aquifer concentrations reducing infiltration in the tank farm to 3 cm/yr (pCi/L) with the MCL in blue, RI/BRA model in black and this sensitivity run in red.

J-11.2 Higher 39 cm/yr Infiltration Through the Tank Farm Liner

It is not clear that the liner placed over the tank farm in 1977 is effective in reducing infiltration. As discussed in Appendix A, Section 3.3 and in Appendix B, some of the monitoring results suggest that it may be increasing local recharge in that area. This sensitivity simulation evaluates the transport assuming that 39 cm/yr infiltrates through the liner in the tank farm to account for that potential increase in infiltration rate. As with the first hydrologic sensitivity run, the rate was not changed until year 1977, and is representative of the total infiltration including that from anthropogenic losses and precipitation. The affected area corresponds to the 10 acres spanning the tank farm.

J-11.2.1 Geochemical Evolution in the Alluvium

An increase from 18 cm/yr to 39 cm/yr in infiltration rate after 1977 (5 years after the CPP-31 release) resulted in a rapid increase in SrCO3, and decrease in SrOH and Sr+ ion in the aqueous phase. The relative abundance of Sr+ ion is much larger than that of SrCO3 and SrOH, resulting in an overall decrease in aqueous phase Sr-90 concentrations with the increase in infiltration water. This is a result of increasing the incoming flux of Na, HCO3-, and Ca+2 ions that are contained in the infiltration water. Although, in the case of CPP-31, the competition effect for exchange sites resulted in more Sr-90 mobility, the influx of HCO3 results in increased buffer capacity. The pH of this resulting scenario is slightly higher than it was for the RI/BRA base case.

The amount of transported aqueous-phase Sr-90 (Figure J-11-13) is somewhat sensitive to this change in buffering capacity, and as a result, less Sr-90 leaves the alluvium in the first 20 years under this scenario than as predicted to occur in the absence of the slight increase in infiltration. After 5, 10, 15, and 20 years, the total Sr-90 that has entered the vadose zone under the alluvium is 1575, 5536, 5558, and 5580 Curies, respectively as shown in Figure J-11-13 (G). With this higher infiltration rate, a much larger fraction (10320 Ci vs. 3564 Ci) remains in the alluvium after 20 years as shown in the summary Figure J-11-13 (I).

The largest difference in the distribution of Sr-90, relative to the RI/BRA base case, occurs in the Sr-90 on the exchange sites and in the SrCO3 species. The change in Sr90 on exchange sites mirrors that in the SrCO3 species. Shortly after the increase in infiltration rate, there is a rapid increase in Sr-90 on the exchange sites. Because the majority of Sr-90 is in the adsorbed phase after the initial re-equilibration period, this increase is significant. The effective K_d is essentially the ratio of activity on the exchange sites to that in the aqueous phase. As the exchanged activity increases, and the aqueous phase Sr-90 concentrations decrease, the effective K_d increases. After 20 years, the effective K_d has approached an average value of 13 meq/L, which is much higher than that obtained in the RI/BRA base case.

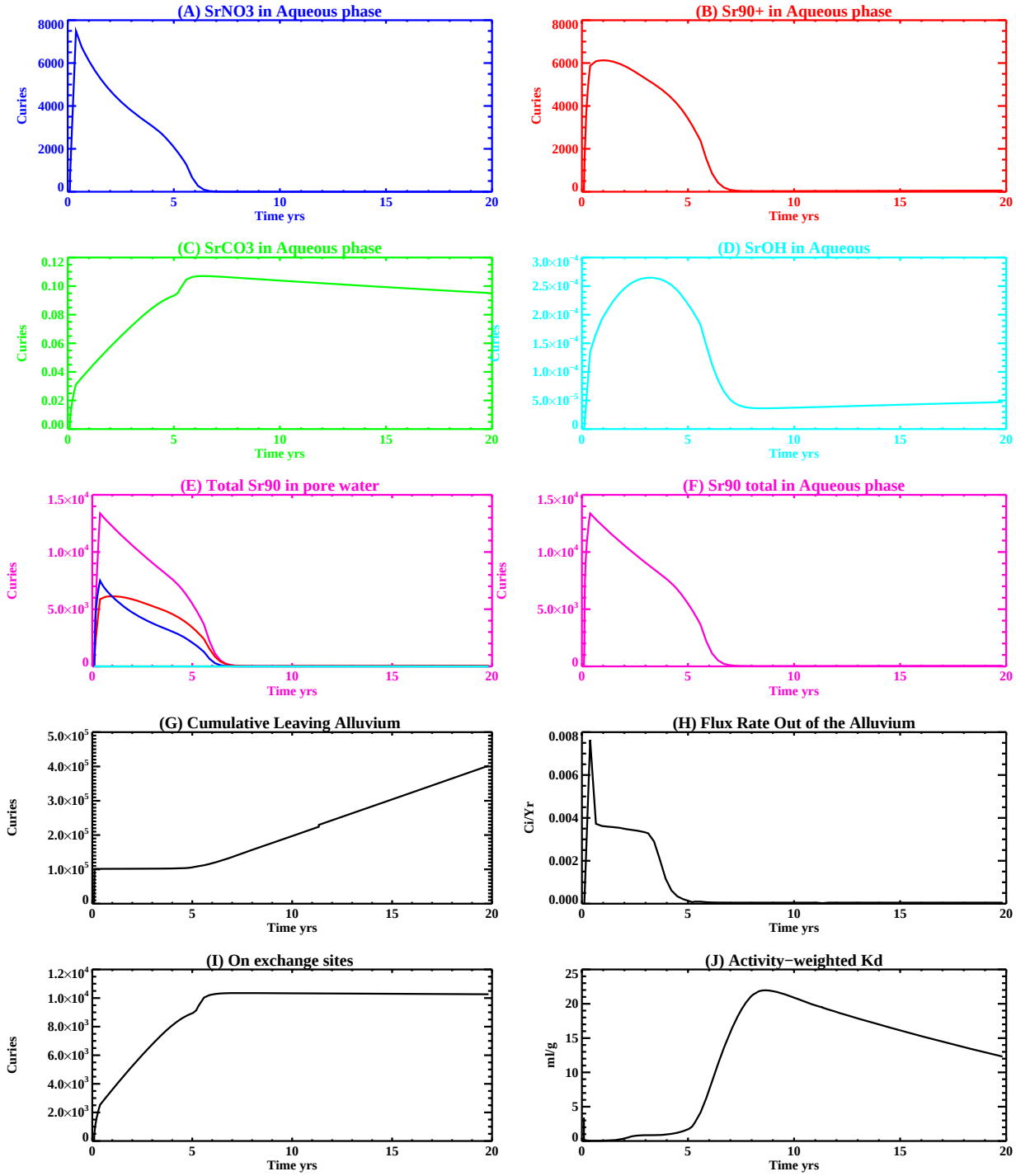

Figure J-11-13. Summary figure illustrating the speciation of Sr-90 in the aqueous phase (A-F), total Sr-90 in the pore-water of the alluvium (E), cumulative curies of Sr-90 having left the alluvium (G), flux rate leaving the alluvium (H), Sr-90 on the exchange sites (I), and effective partitioning coefficient (Kd) (J).

J-11.2.2 Vadose Zone Sr-90 Simulation Results

The release of Sr-90 in this simulation followed the same procedure as was used in the RI/BRA-case:

- 15900 Ci from CPP-31 release in the tank farm were represented using (a) the activity-release function shown in Figure J-11-13 (H) for the 5580 Ci released during the first 20 years, and placing this activity flux directly above the basalt interface of the base model (Appendix A, Section 5.1). The remaining 10320 Ci were placed vertically through the alluvium, scaled to the measured soil concentrations obtained during the 2004 (Appendix G and Table 5-32) sampling cycle. To simulate the transport of the activity remaining in the alluvium, an effective K_d of 13 mL/g was used (Figure J-11-13 (J)) for the alluvium sediments.
- transport of Sr-90 from sources other than CPP-31 originating in the alluvium, whose location is spanned by the submodel (Appendix A, Section 5.1), were simulated using the submodel. Because these source locations were outside the influence of the high ionic strength, acidic CPP-31 release, a K_d of 20 mL/g was used in the submodel alluvium.
- transport of Sr-90 from sources located outside of the submodel horizontal extent were also placed in the base model used to simulate the transport of the CPP-31 remaining in the alluvium. The effective K_d for the alluvium underlying these source locations was also set to the value used to simulate the transport of Sr-90 predicted to remain in the alluvium after 20 yrs (first bullet). The relative magnitude of these sources are small relative to the residual Sr-90 predicted to remain in the alluvium after 20 yrs. In this case, the K_d is slightly lower than that used to simulate the transport of Sr-90 from sources within the submodel boundary. However, this should not affect the peak aquifer concentrations by more than 10%.

Figures J-11-14 through J-11-17 give the distribution of the Sr-90 in the vadose zone through the year 2293. Figure J-11-18 illustrates Sr-90 arrival in key perched water wells, and the match to field data for all perched water wells is summarized in Figure J-11-19. There are no significant differences relative to the RI/BRA base case.

Peak vadose zone concentrations through time are given in Figure J-11-20 and are shown in red. Highest concentrations (3.0E9 pCi/L) in the vadose zone are predicted to occur in 1978 and are a combination of the initial fast release of activity from CPP-31 and the activity from CPP-79. The peak concentration in the vadose zone assuming an infiltration rate of 39 cm/yr is about 1.5 times that obtained in the RI/BRA base case (black) with 22 cm/yr (18 cm/yr precipitation + 4 cm/yr anthropogenic water) infiltration. Higher vadose zone concentrations occur in the pore water of the alluvium and are associated with the increased activity remaining in the alluvium.

The rate at which Sr-90 enters the aquifer is given in Figure J-11-21 in red, and can be compared directly to the RI/BRA base case (shown as black). Fluxes from the vadose zone into the aquifer are slightly higher than predicted in the base case. The higher fluxes are primarily associated with increased migration out of the deep vadose zone. This is apparent because the increase in infiltration rate has resulted in:

- half as much Sr-90 leaving the alluvium in the first 20 years (5580 vs. 12336)
- three times as much Sr-90 remaining in the alluvium (10320 Ci vs. 3564 Ci)
- a significant decrease in mobility of Sr-90 out of the alluvium due to an increase in K_d (13 mL/g vs. 2 mL/g)
- increased dillution in the vadose zone caused by the higher infiltration rate

In the upper vadose zone, this should translate into lower concentrations. However, in the deeper vadose zone it results in more rapid migration of the Sr-90 introduced into the vadose zone from the failed injection well.

Figure J-11-14. Sr-90 vadose zone concentration with higher 39 cm/yr infiltration through the tank farm (horizontal contours) (pCi/L) (MCL = thick red line, 10*MCL = thin red line, MCL/10 = black line).

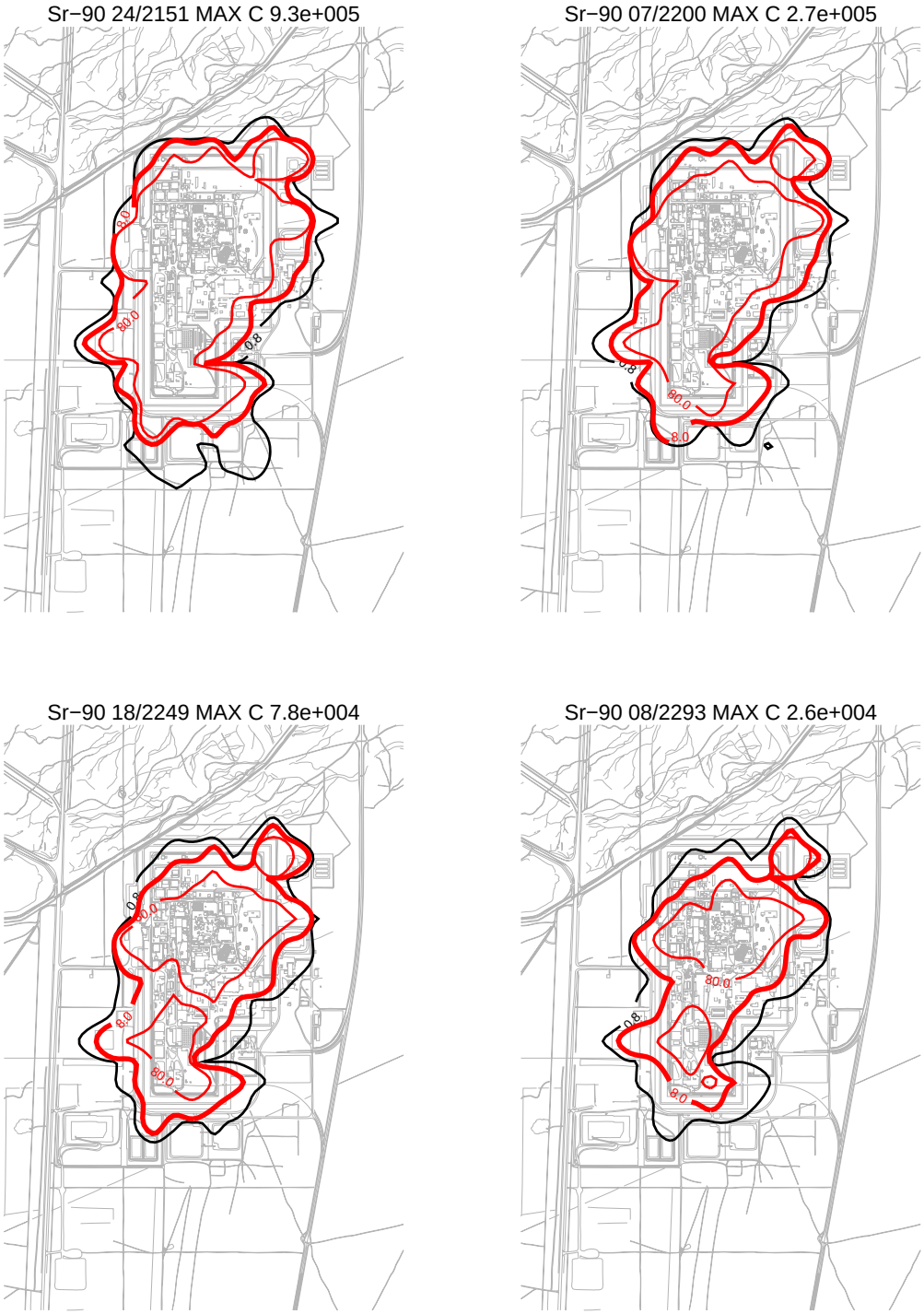

Figure J-11-15. Sr-90 vadose zone concentration with higher 39 cm/yr infiltration through the tank farm (horizontal contours) (pCi/L) (MCL = thick red line, 10*MCL = thin red line, MCL/10 = black line).

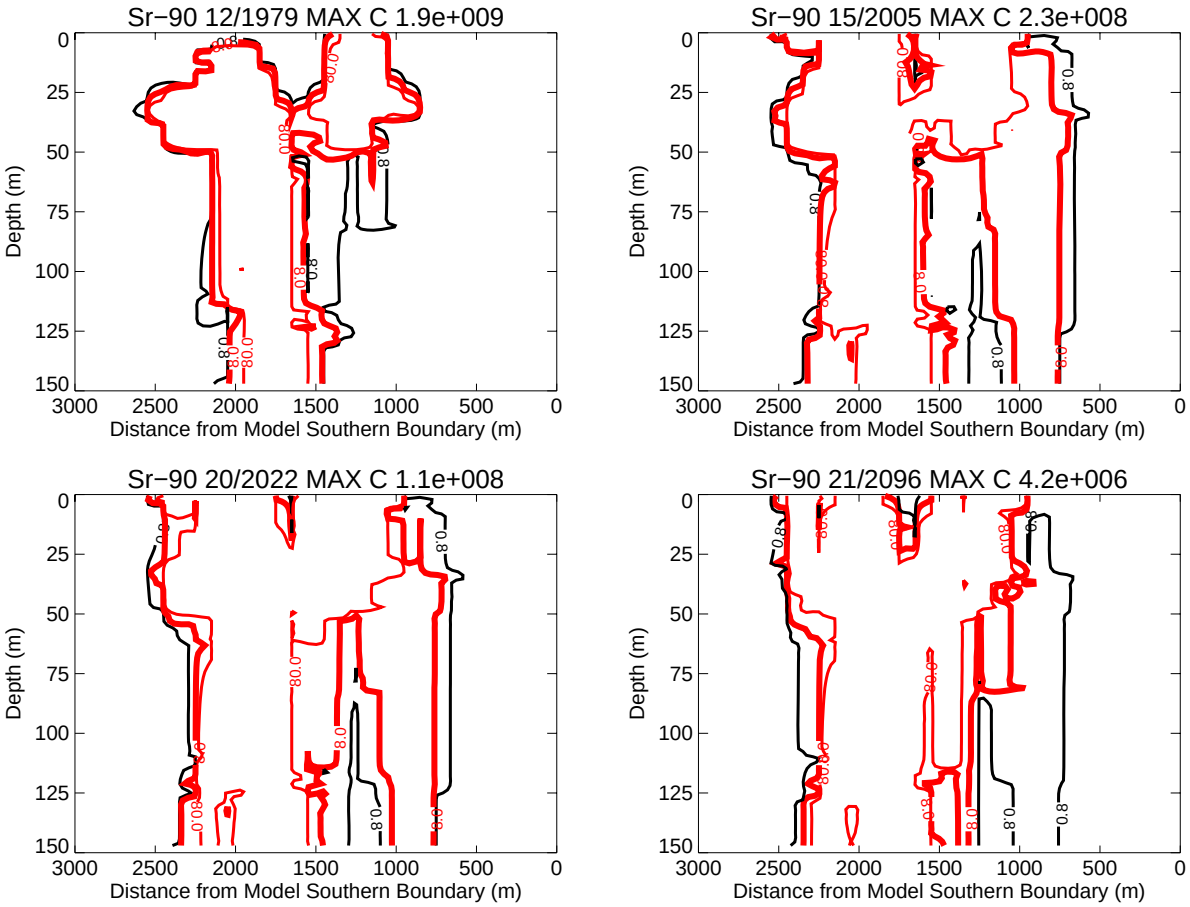

Figure J-11-16. Sr-90 vadose zone concentrations with higher 39 cm/yr infiltration through the tank farm (vertical contours) (pCi/L) (MCL = thick red line, 10*MCL = thin red line, MCL/10 = black line).

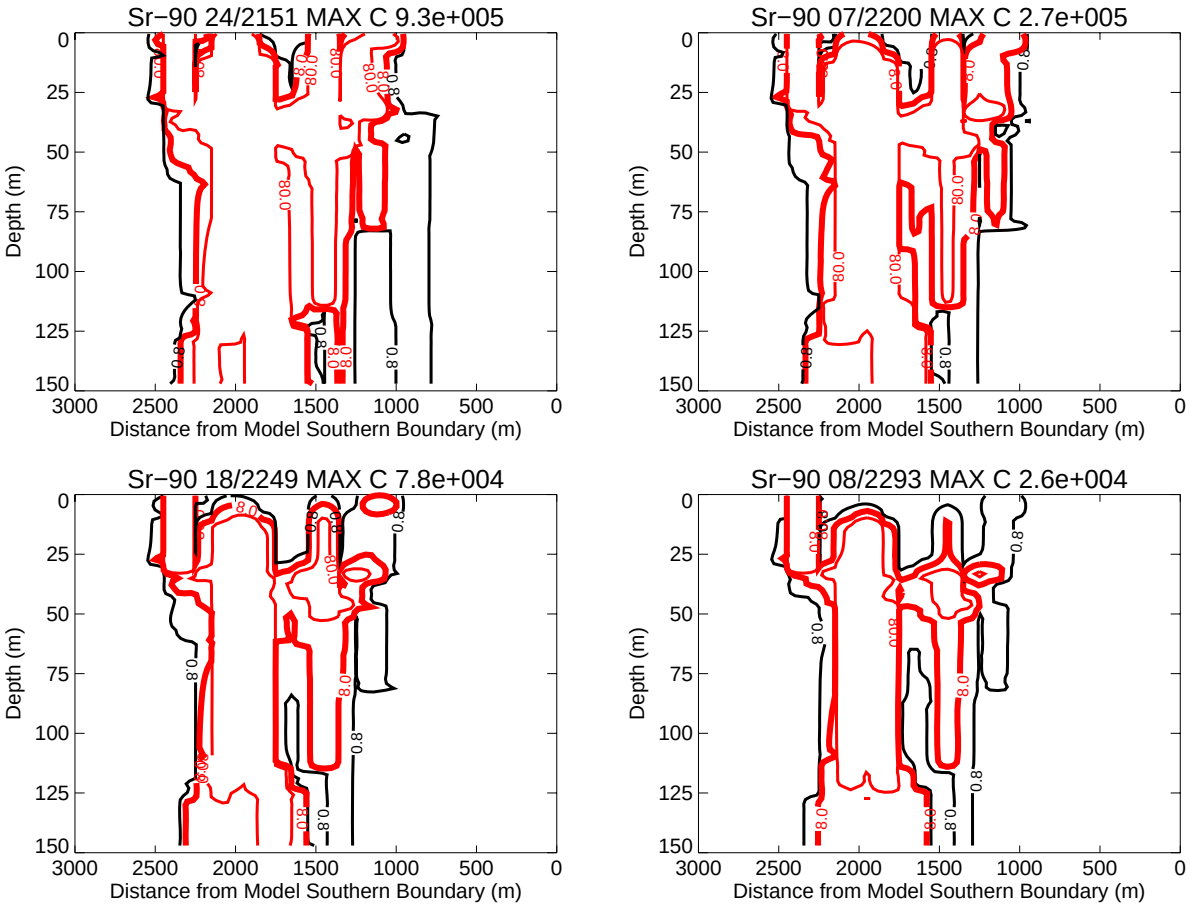

Figure J-11-17. Sr-90 vadose zone concentrations with higher 39 cm/yr infiltration through the tank farm (vertical contours) (pCi/L) (continued) (MCL = thick red line, 10*MCL = thin red line, MCL/10 = black line).

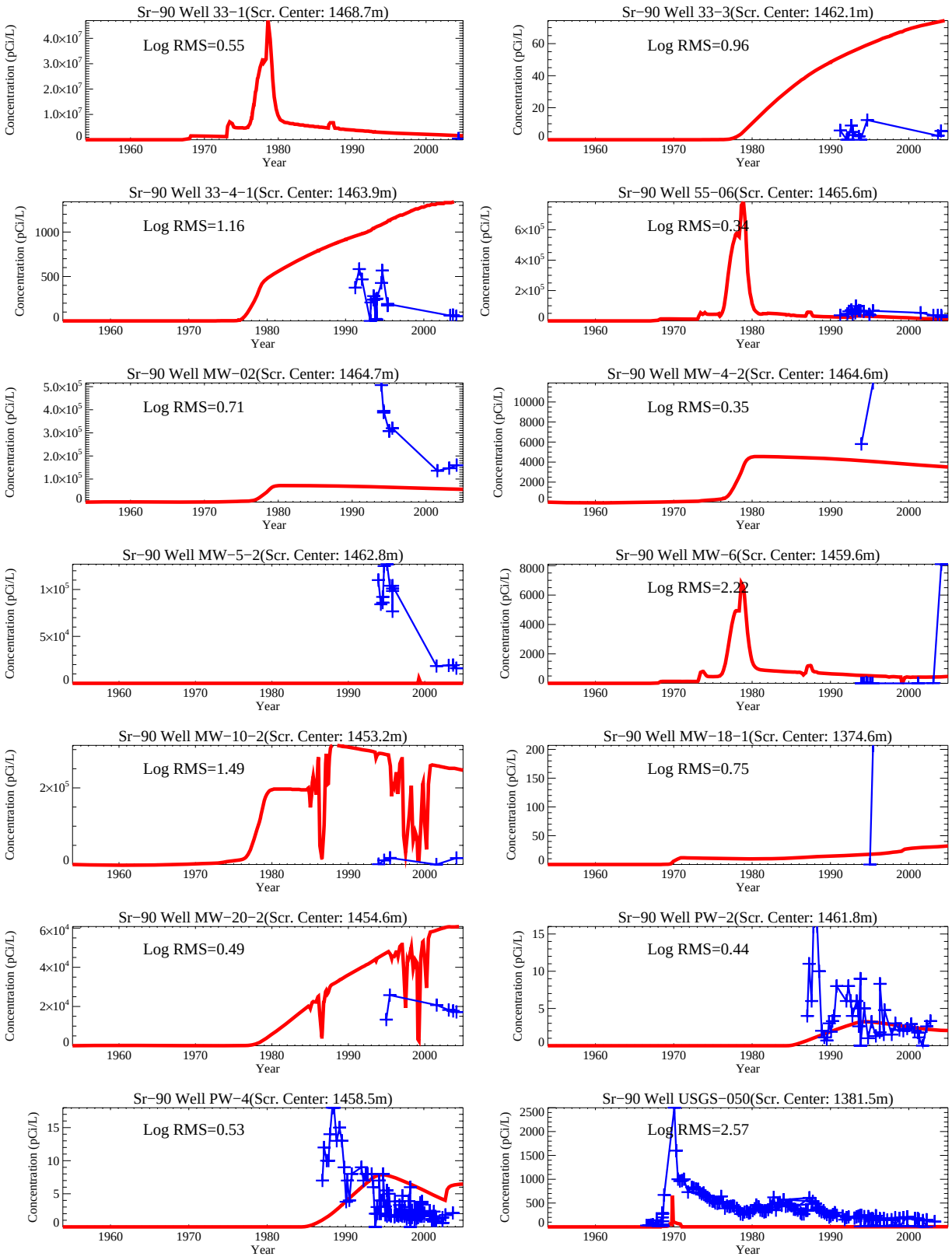

Figure J-11-18. Sr-90 concentration in perched water wells with higher 39 cm/yr infiltration through the tank farm(pCi/L) (Measured values = blue crosses, red = model at screen center).

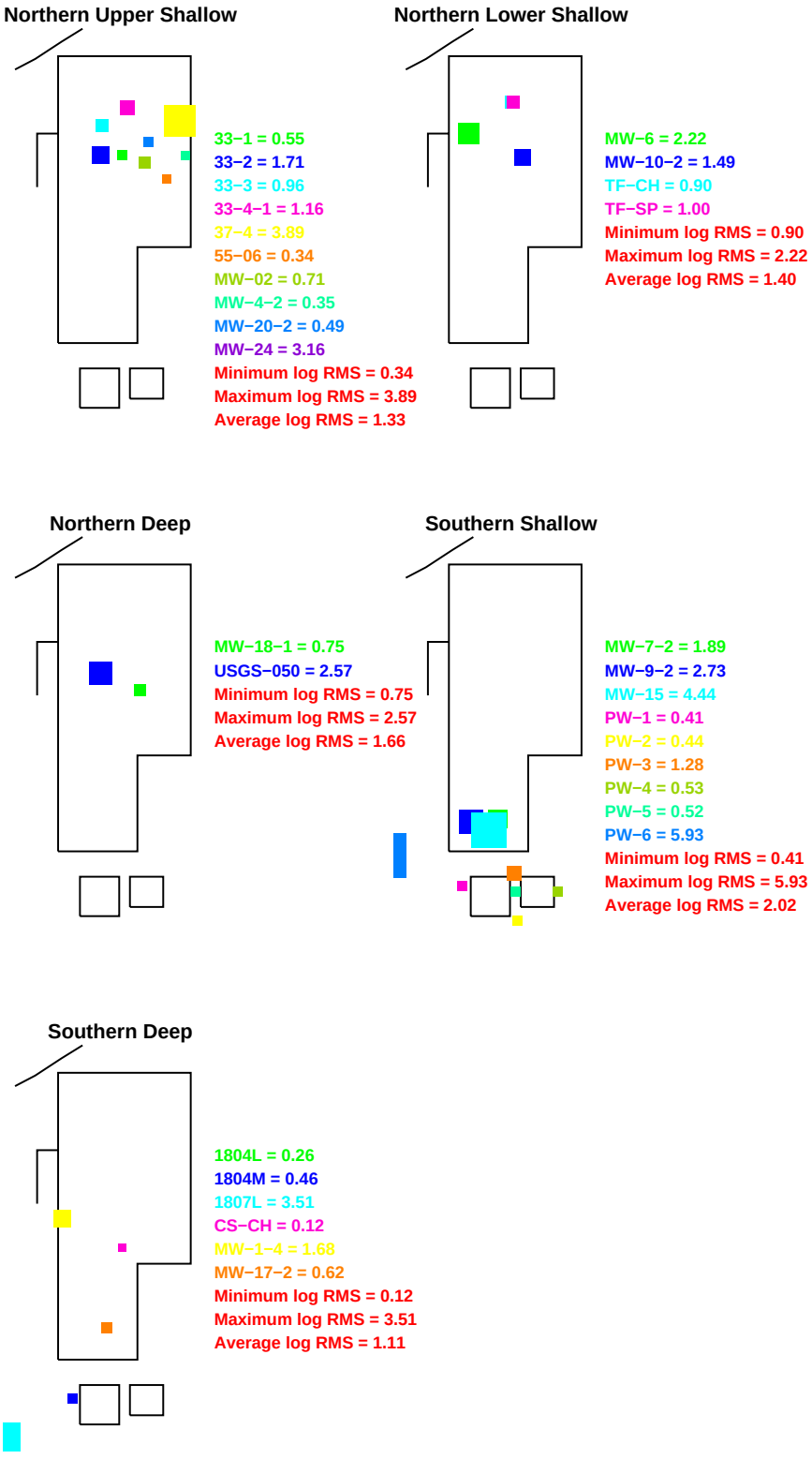

Figure J-11-19. Log 10 Root mean square error (RMS) by depth and northing with higher 39 cm/yr infiltration through the tank farm.

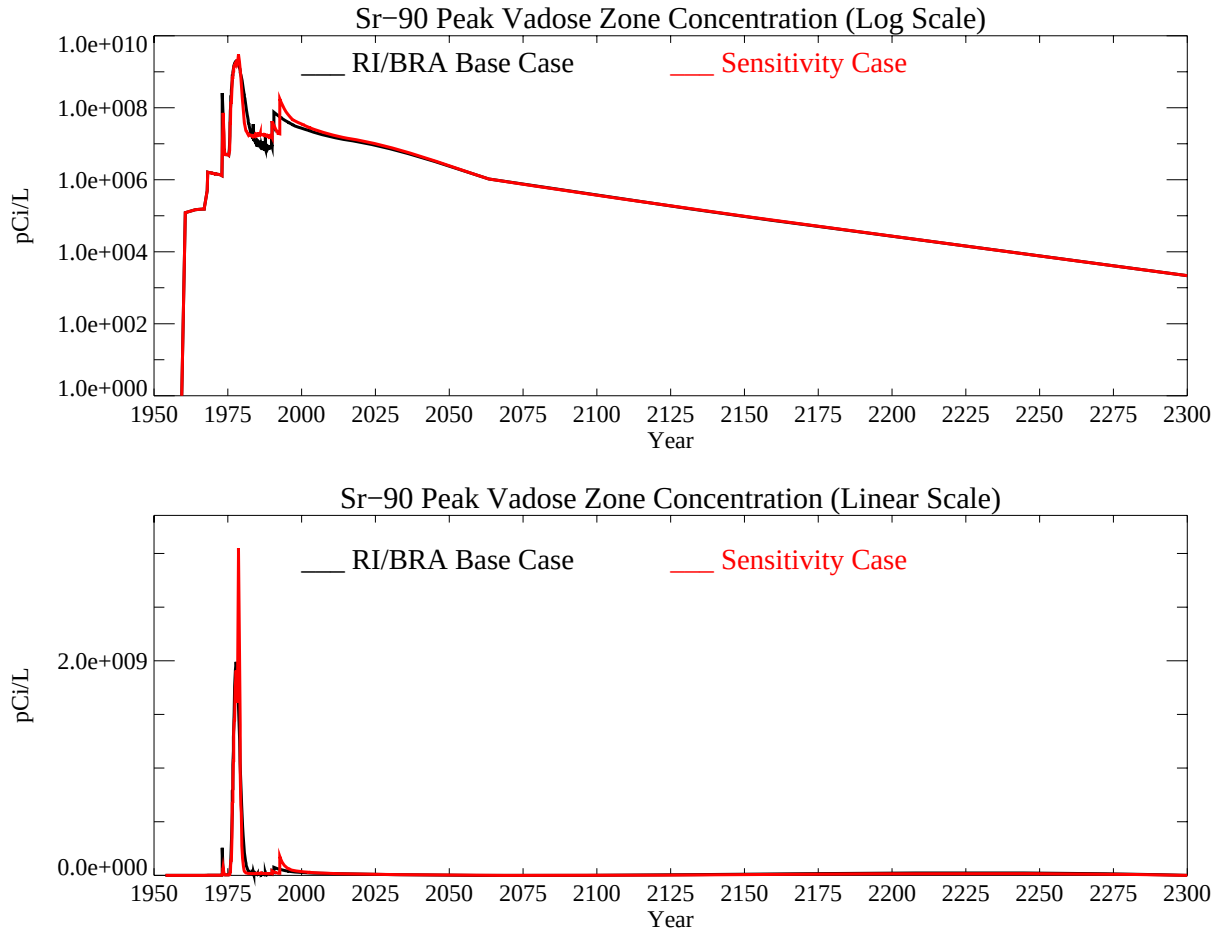

Figure J-11-20. Sr-90 peak vadose zone concentrations with higher 39 cm/yr infiltration through the tank farm. The RI/BRA model is shown in black and this sensitivity run in red.

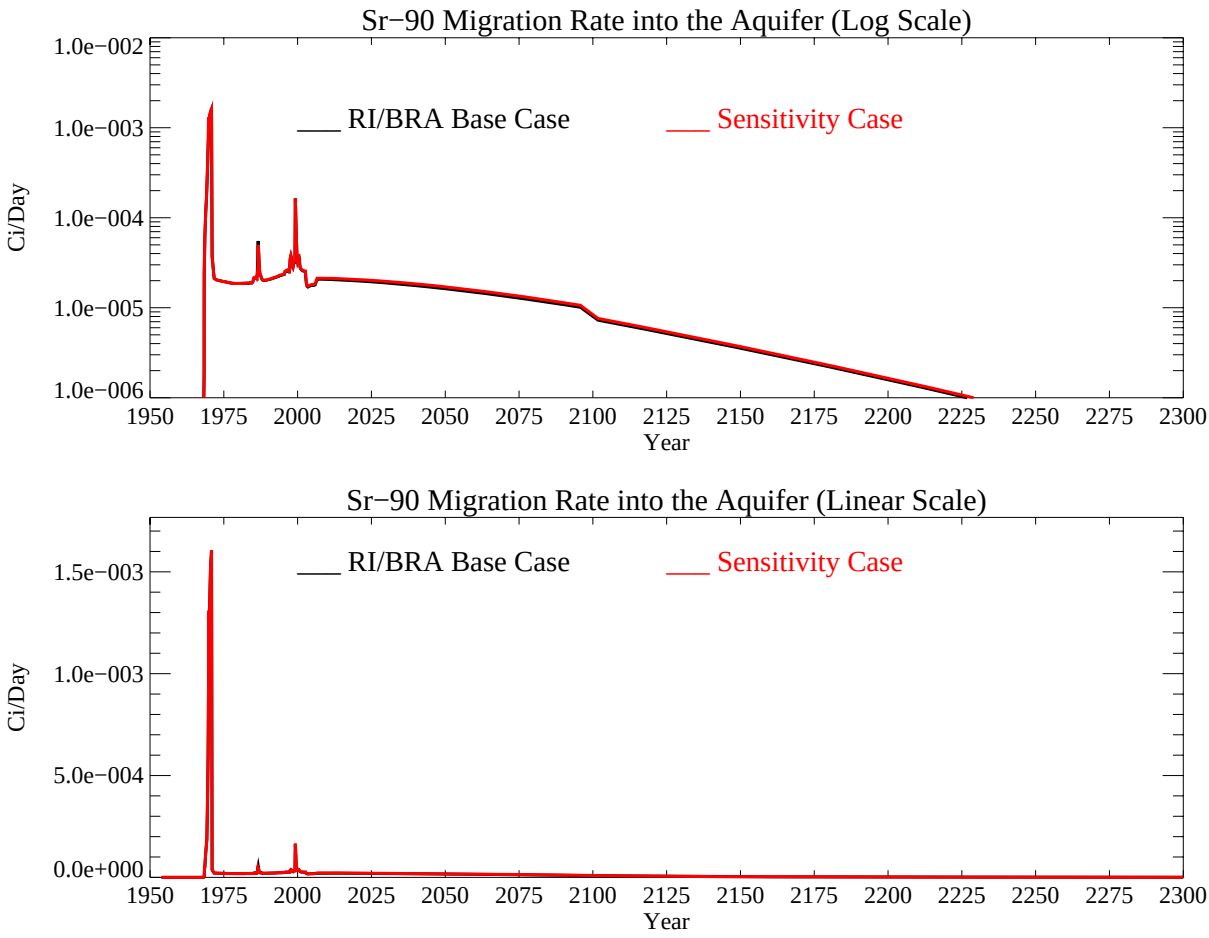

Figure J-11-21. Sr-90 activity flux into the aquifer (Ci/day) with higher 39 cm/yr infiltration through the tank farm. The RI/BRA model is shown in black and this sensitivity run in red.

J-11.2.3 Aquifer Sr-90 Simulation Results

The distribution of Sr-90 in the aquifer for the time period spanning 2005-2096 is given for the far-field in Figure J-11-22 with near-field results shown in Figure J-11-23 for the 2049-2151 time period. The resultant peak aquifer concentrations are given in Figure J-11-24. Because the Sr-90 originating in the vadose zone does not arrive in the aquifer until the mid 1980's, comparisons to measured data are not presented for aquifer wells.

Peak aquifer Sr-90 concentrations were predicted to be 5761 pCi/L in 1965 and are the result of the CPP-03 well. The simulated Sr-90 concentrations remained above the MCL from 1960 through year 2148. The Sr-90 concentrations in the aquifer are predicted to decline after the year 2000 with a step decrease in concentration following the removal of anthropogenic water at land surface in 2095. The predicted peak Sr-90 concentration in the year 2095 is 27.3 pCi/L, roughly 1.5 times higher than predicted for the base case (18.6 pCi/L).

Predicted aquifer concentrations for the year 2095 exceed the MCL by a factor of 3.4, with the majority of the long-term impact originating from the failed injection well. The Sr-90 contour plots presented in Figures J-11-22 and J-11-23 show the Sr-90 plume shrinking slowly in areal extent after the present time. Further, although Sr-90 concentrations in the aquifer are predicted to exceed the MCL through 2148, the area impacted by Sr-90 above 8 pCi/L is between the tank farm and the former percolation ponds by 2095, with a small area to the northeast of the tank farm. The extent is generally larger than predicted for the RI/BRA base case through the 2096 time period, but by 2151, the plumes are nearly identical.

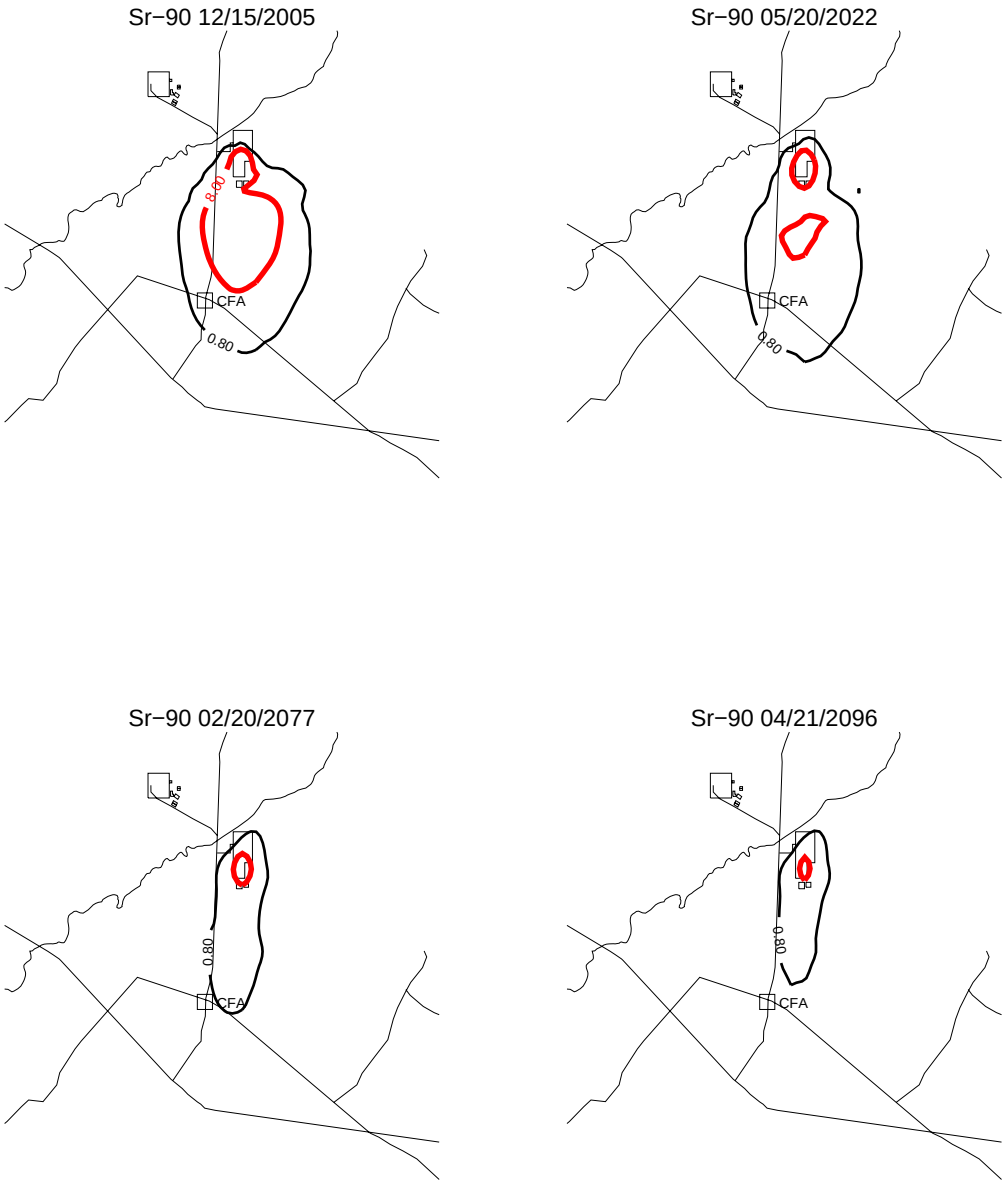

Figure J-11-22. Sr-90 aquifer concentration contours with higher 39 cm/yr infiltration through the tank farm (pCi/L) (MCL = thick red line, 10*MCL = thin red line, MCL/10 = black line).

Figure J-11-23. Sr-90 aquifer concentration contours with higher 39 cm/yr infiltration through the tank farm (pCi/L) (continued) (MCL = thick red line, 10*MCL = thin red line, MCL/10 = black line).

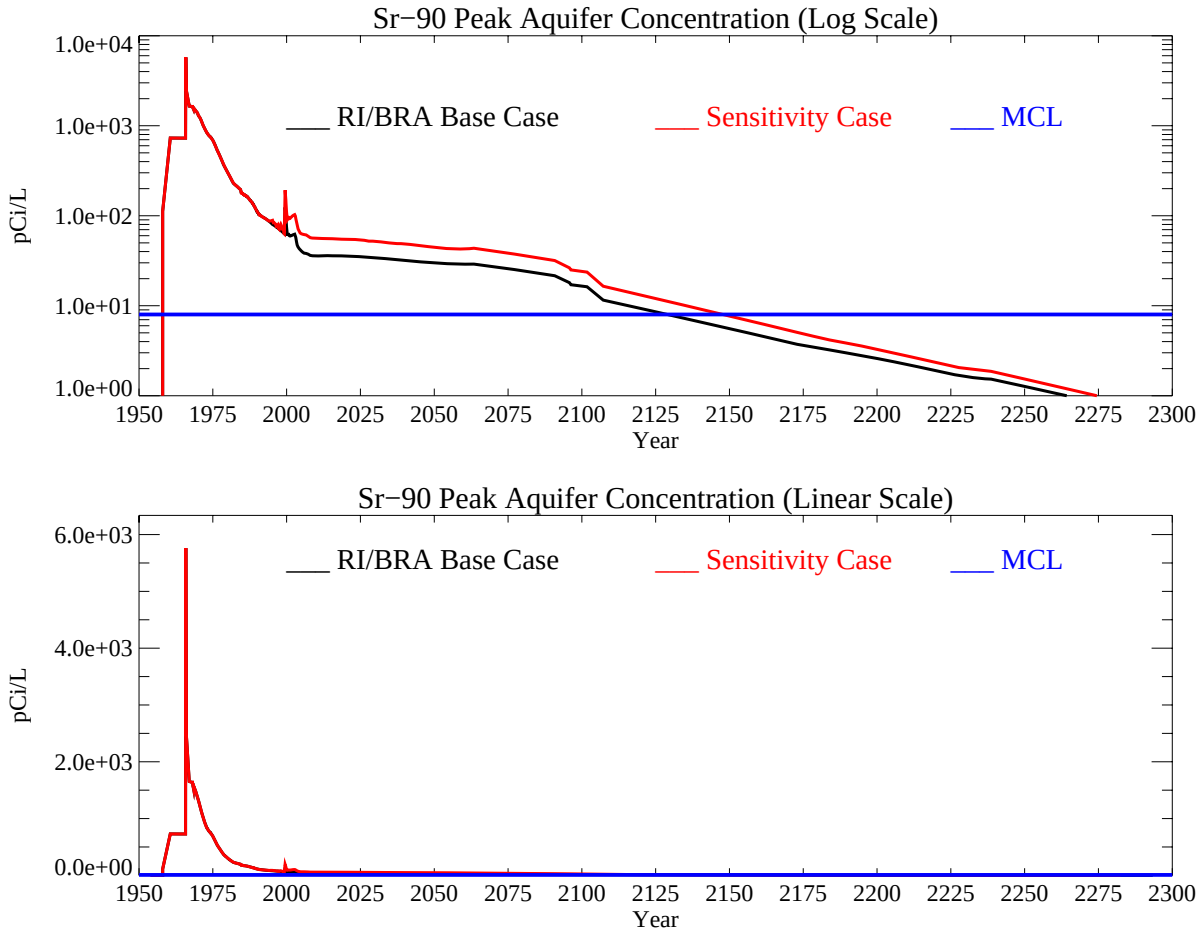

Figure J-11-24. Sr-90 peak aquifer concentrations with higher 39 cm/yr infiltration through the tank farm (pCi/L) with the MCL in blue, RI/BRA model in black and this sensitivity run in red.

J-11.3 Anthropogenic Water Focused in Northern INTEC

The sensitivity to higher anthropogenic recharge rates in northern INTEC was investigated by using a "worst case" infiltration scenario. The recharge rate used here was estimated from the imbalance between water production and known discharges to the percolation ponds. Recent records of the water production and final use at INTEC indicate that approximately 10 to 11 percent of the water produced is unaccounted for through existing metering. The total water usage in 2004 was approximately 495 million gallons and 10.5 percent of this volume is 52 million gallons. This volume of water represents metering inaccuracies, systems that are not metered (e.g., steam discharges, firewater testing, etc.), and other unintentional discharges. The density of utilities at the INTEC suggest that the discharge would be focused on the northern INTEC in an area of approximately 49 acres surrounding the tank farm.

In this infiltration scenario, the 52 million gallons were distributed across 49 acres, resulting in an anthropogenic recharge rate of 98 cm/year. This infiltration was in addition to the estimated recharge from precipitation of 18 cm/year, for a total of 116 cm/year. The simulated water was placed in the area surrounded by Palm Avenue, Hemlock street, Ash Avenue and the western INTEC security fence. The area beneath building 666 was also included. The area directly below the tank farm area was excluded from the higher water losses, and only 18 cm/year precipitation recharge was applied because most utilities do not run through the tank farm and the high and low tank farm infiltration sensitivity simulations assessed the sensitivity of tank farm contaminant mobility to recharge rate. The intent of this simulation was to investigate the movement of contaminants out of the perched water zones and to assess whether or not focusing the infiltration would result in complete saturation of the interbed regions. The high infiltration rate was applied for the entire assumed operational period of the INTEC (1954 through 2095). For comparison, the base case assumes that roughly 10 million gallons per year infiltrates over the entire developed INTEC facility (approximately 180 acres), equivalent to a rate of approximately 5 cm/year in addition to 18 cm/yr from precipitation.

Focusing this recharge outside of the tank farm allows the use of the activity-flux from the alluvium discussed in Section J-8.1, and therefore uses the RI/BRA flux of Sr-90 out of the alluvium.

J-11.3.1 Vadose Zone Sr-90 Simulation Results

The distribution of Sr-90 in the vadose zone is shown in Figures J-11-25 through J-11-28 through the year 2293. Compared to the RI/BRA base case, the horizontal extent of Sr-90 is further in the northern shallow vadose zone. This effect is more apparent in the comparison to field data presented in Figure J-11-29.

The predicted Sr-90 concentrations in perched water wells (Figures J-11-29 and J-11-30) show that observed concentrations in shallow well completions (MW-33-1 and MW-55-06) are better matched with these increased fluxes. This better match occurs because the higher fluxes push Sr-90 out laterally from directly beneath the tank farm through the upper portion of the shallow northern perched water. Concentrations in wells closer to the tank farm (MW-10-2 and MW-20-2) are over predicted because too much Sr-90 is being driven downward. In wells an intermediate distance from the tank farm, there is an overall slight decrease in perched water concentrations because of dilution in the upper shallow interbed. In addition, there is increased lateral movement toward wells MW-02, 55-06, 4-2, and 18-1. The wells near the former percolation ponds are not as affected because the percolation pond discharges are much higher than discharges in the RI/BRA model from other anthropogenic waters.

Peak vadose zone concentrations for this simulation are represented by the red line in Figure J-11-31 and are somewhat lower at late times relative to the RI/BRA base case shown in black. Highest concentrations 4.0E8 pCi/L) in the vadose zone are predicted to occur in 1978 as activity released during the first 20 years after the CPP-31 release combine with those from CPP-79 in the vadose zone.

The rate at which this activity enters the aquifer is given in Figure J-11-32 by the red line, and can be compared directly to the RI/BRA base case shown in black. The large difference in anthropogenic water results in a significant increase in flux leaving the vadose zone throughout the entire simulation period. In both cases, the anthropogenic water is removed in year 2095.

Figure J-11-25. Sr-90 vadose zone concentration with anthropogenic water focused in northern INTEC (horizontal contours) (pCi/L) (MCL = thick red line, 10*MCL = thin red line, MCL/10 = black line).

Figure J-11-26. Sr-90 vadose zone concentration with anthropogenic water focused in northern INTEC (horizontal contours) (pCi/L) (MCL = thick red line, 10*MCL = thin red line, MCL/10 = black line).

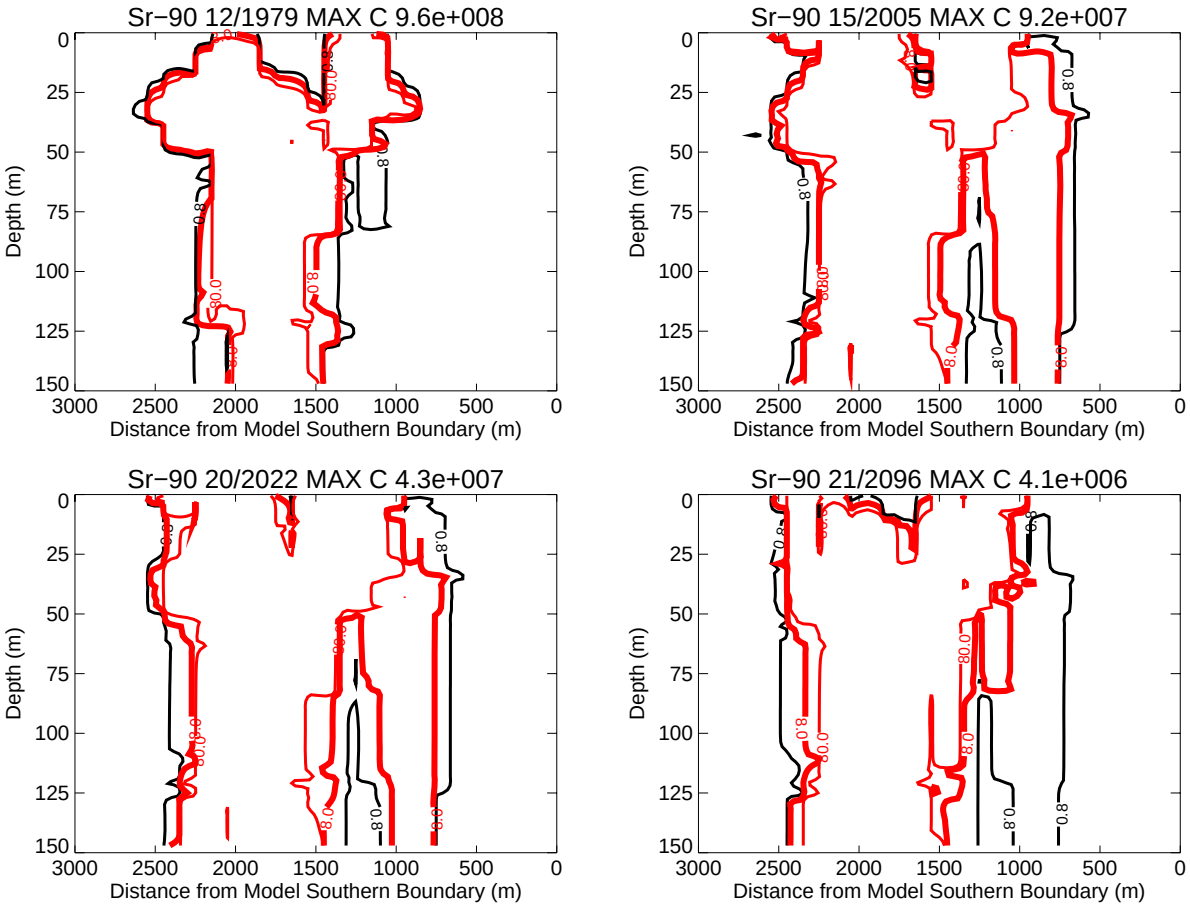

Figure J-11-27. Sr-90 vadose zone concentrations with anthropogenic water focused in northern INTEC (vertical contours) (pCi/L) (MCL = thick red line, 10*MCL = thin red line, MCL/10 = black line).

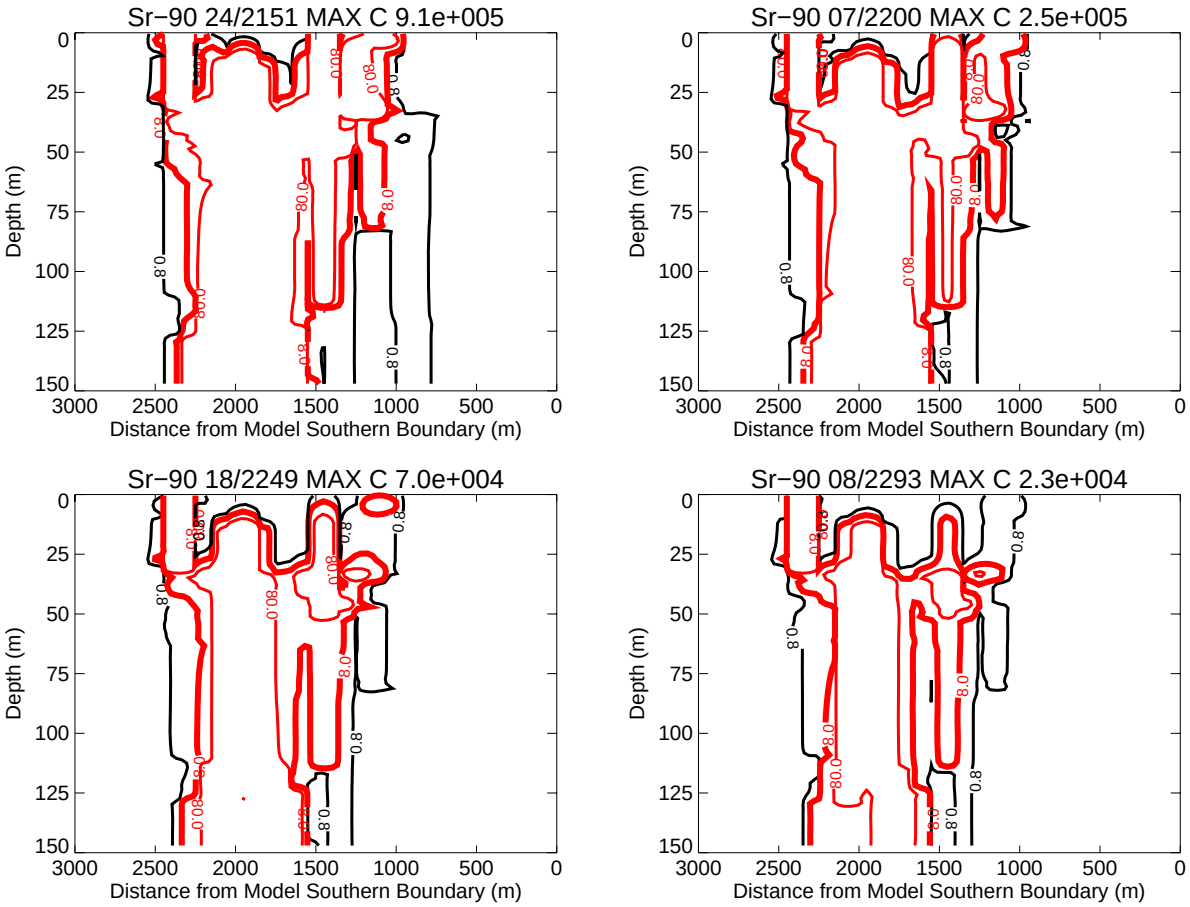

Figure J-11-28. Sr-90 vadose zone concentrations with anthropogenic water focused in northern INTEC (vertical contours) (pCi/L) (continued) (MCL = thick red line, 10*MCL = thin red line, MCL/10 = black line).

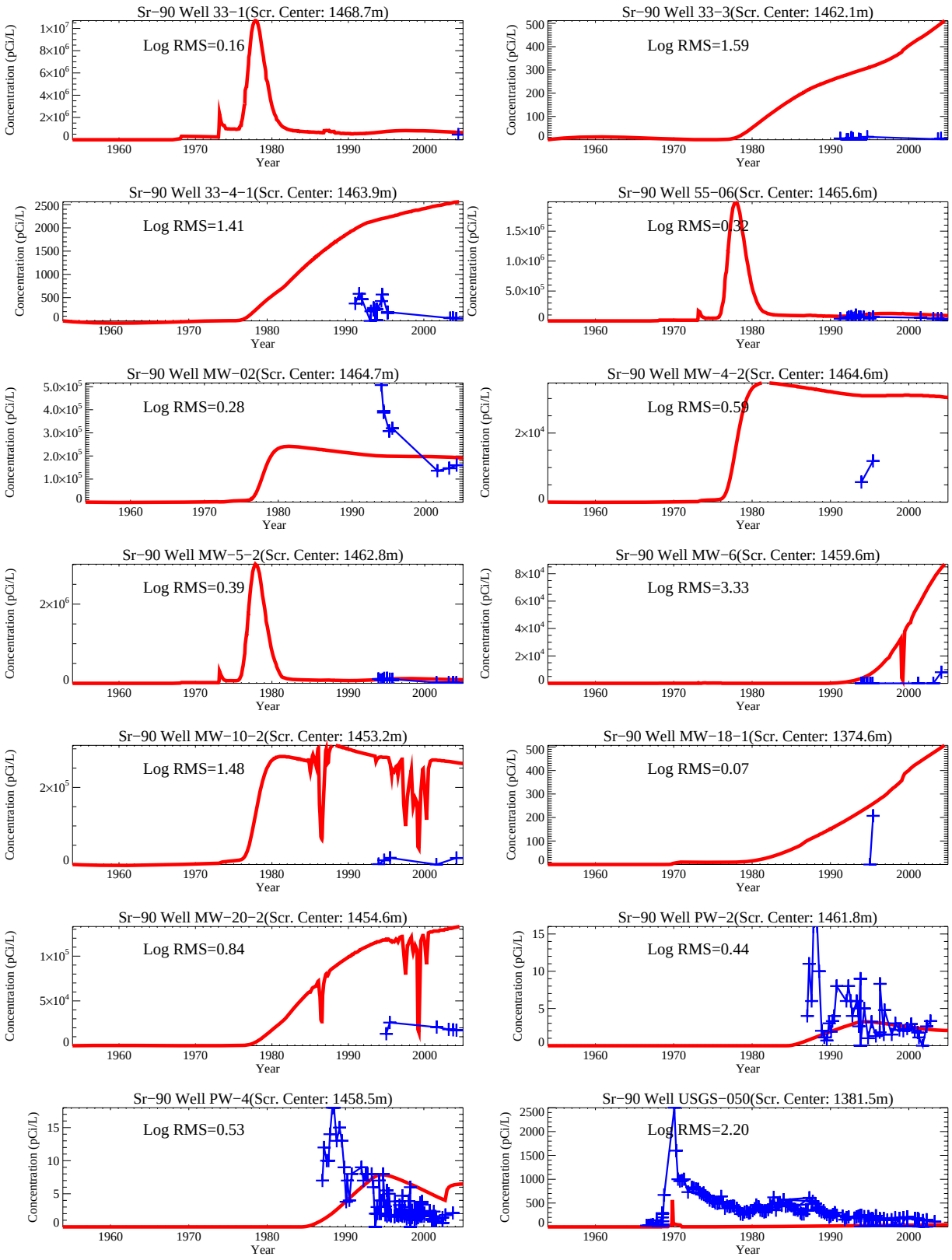

Figure J-11-29. Sr-90 concentration in perched water wells with anthropogenic water focused in northern INTEC (pCi/L) (Measured values = blue crosses, red = model at screen center).

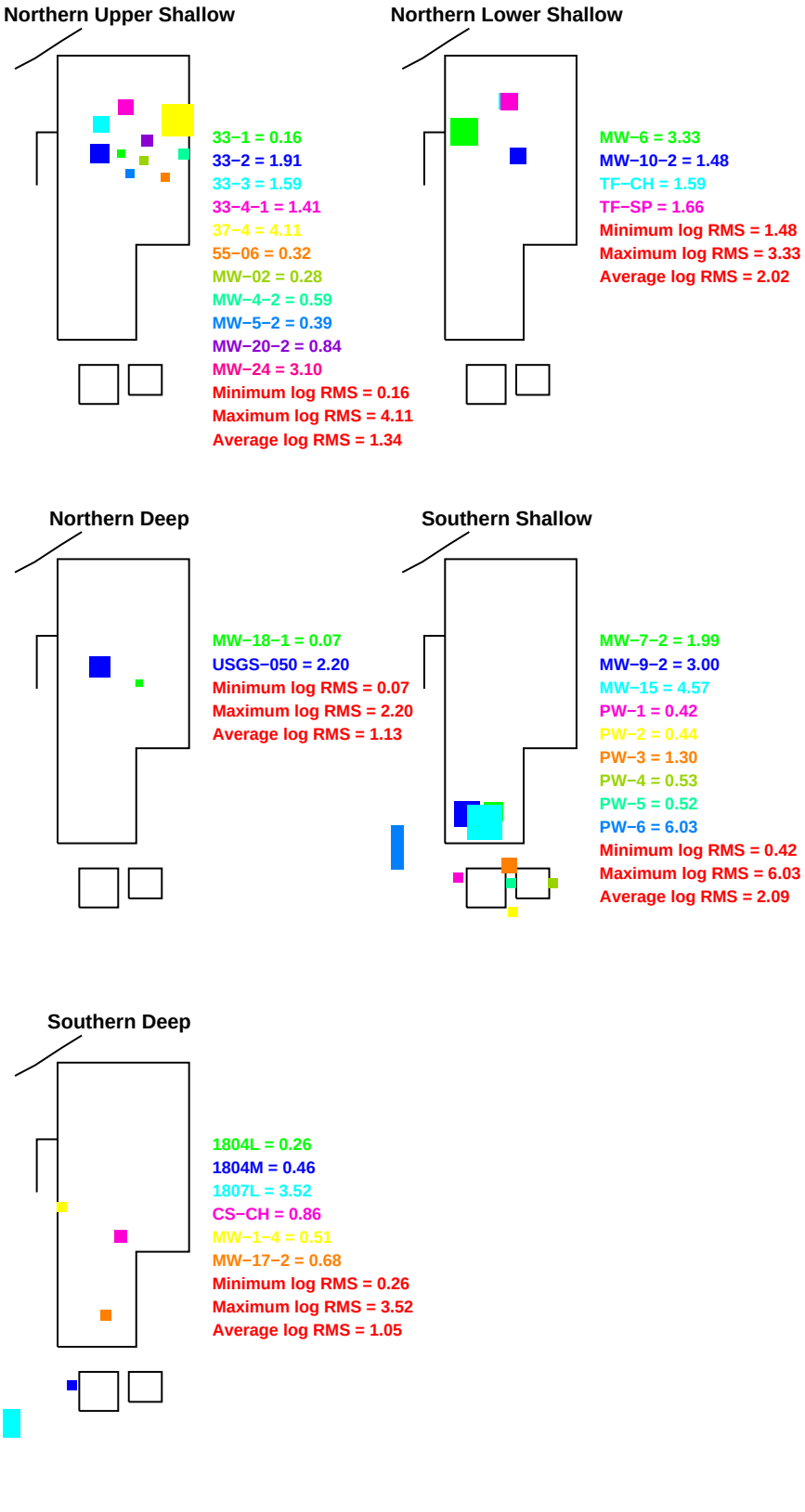

Figure J-11-30. Log 10 Root mean square error (RMS) by depth and northing with anthropogenic water focused in northern INTEC.

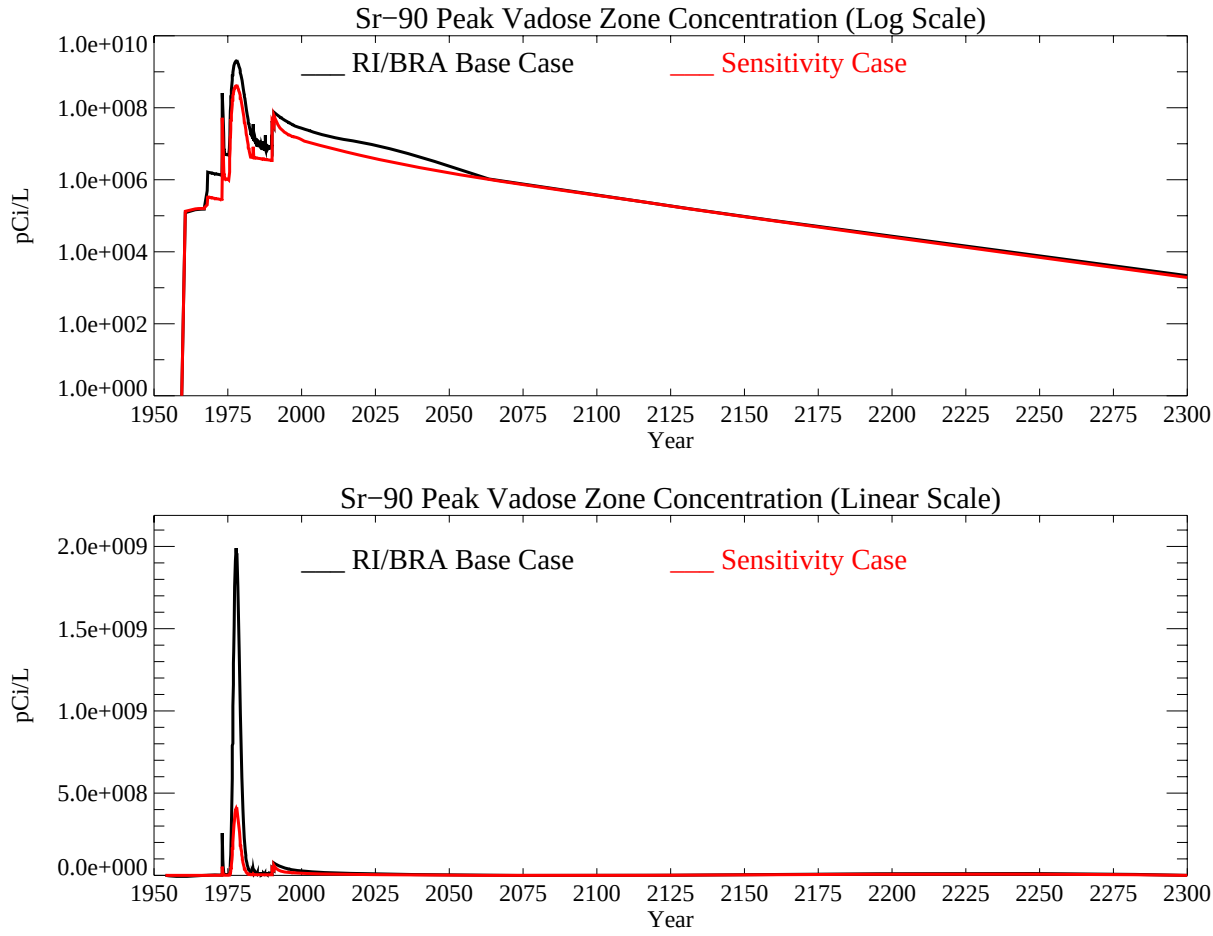

Figure J-11-31. Sr-90 peak vadose zone concentrations with anthropogenic water focused in northern INTEC (pCi/L). The RI/BRA model is shown in black and this sensitivity run in red.

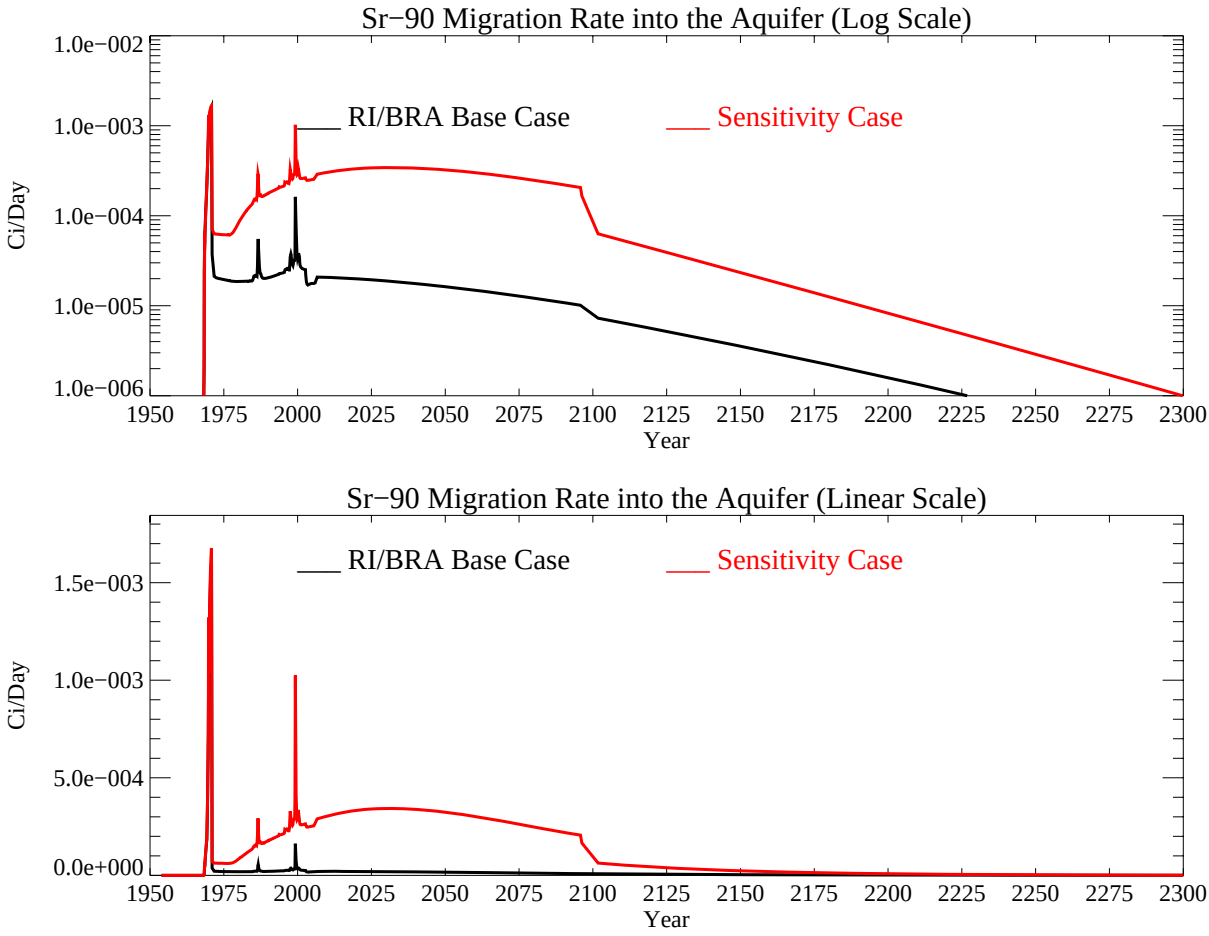

Figure J-11-32. Sr-90 activity flux into the aquifer (Ci/day) with anthropogenic water focused in northern INTEC. The RI/BRA model is shown in black and this sensitivity run in red.

J-11.3.2 Aquifer Sr-90 Simulation Results

The distribution Sr-90 in the aquifer for the time period spanning 2005-2096 is shown for the far field in Figure J-11-33 and in the near field in Figure J-11-34 for the 2049-2151 time period. The resultant peak aquifer concentrations are given in Figure J-11-35. Based on these results, in year 2095, the predicted peak concentration is 343 pCi/L, 18.5 times higher than predicted in the RI/BRA base case. This is much higher than predicted in the other simulations because the higher infiltration rate decreases the residence time in the vadose zone. As a result, Sr-90 is not allowed to decay while still in the vadose zone. Increasing the anthropogenic water in northern INTEC keeps simulated Sr-90 concentrations above the MCL from 1960 through year 2214. Further, the Sr-90 concentrations in the aquifer are not predicted to decline until after the year 2020. Compared to the RI/BRA base case, this is an additional 85 years during which remedial actions must be successful.

Available Sr-90 data in the aquifer does not support this infiltration rate. Measured data from the SRPA indicates that Sr-90 concentrations are currently declining in the aquifer with current values less than 40 pCi/L. With this infiltration rate, the peak concentration for year 2005 is approximately 672 pCi/L, 17 times higher than the observed data. Further, the predicted concentrations do not decline significantly until at least 2020. Higher flux rates from the alluvium are not attenuated naturally by aquifer water passing beneath the

tank farm, and this keeps the areal extent of Sr-90 above the MCL from shrinking. In all of the other sensitivity results obtained in this study, the Sr-90 plume was predicted be reduced in size after the present time which is consistent with measured data. All of other simulations show that there should be a significant reduction in plume size by 2010. If this scenario is correct, Sr-90 concentrations should just now be decreasing in the aquifer.

Calibration to Sr-90 data was performed separately in the vadose zone and in the aquifer. If observed data in the northern upper shallow perched water (100 ft) were used independently of the other perched water or aquifer results, it would suggest that more anthropogenic water is being discharged in northern INTEC than assumed in the RI/BRA base case. However, the match to field data in the northern lower upper shallow perched water (140 ft) and the match to aquifer data indicates that the infiltration rates here are too high. Because of this apparent discrepancy, it is important to recognize why the average RMS is lower in perched water wells in the northern upper shallow perched water in this case.

Standing free perched water above the 110 ft and 140 ft interbeds directly under the tank farm is not created using the base flux rates for any of the model simulations. As a result, lateral advection and dispersion in the model is forced to occur through the interbeds. While traveling through the interbeds, the transported Sr-90 is subjected to adsorption which lowers the concentrations and retards lateral movement. Increasing the flux rates allows more advection to occur high in the interbed and just below the basalt-interbed contact. The lateral migration of Sr-90 in this simulation accounts for the better match to field data for wells in the 110 ft interbed. However, this high infiltration rate also drives more Sr-90 deeper into the 140 ft interbed, resulting in overpredicting observed concentrations in the northern lower shallow perched water and a worse match to field data.

Simultaneously matching observed aquifer concentrations, concentrations in the 140 ft interbed, and the higher concentrations to the southeast of the tank farm in the northern upper shallow perched water might be accomplished by lowering the permeability of the 110 ft interbed and using a slightly higher K_d.

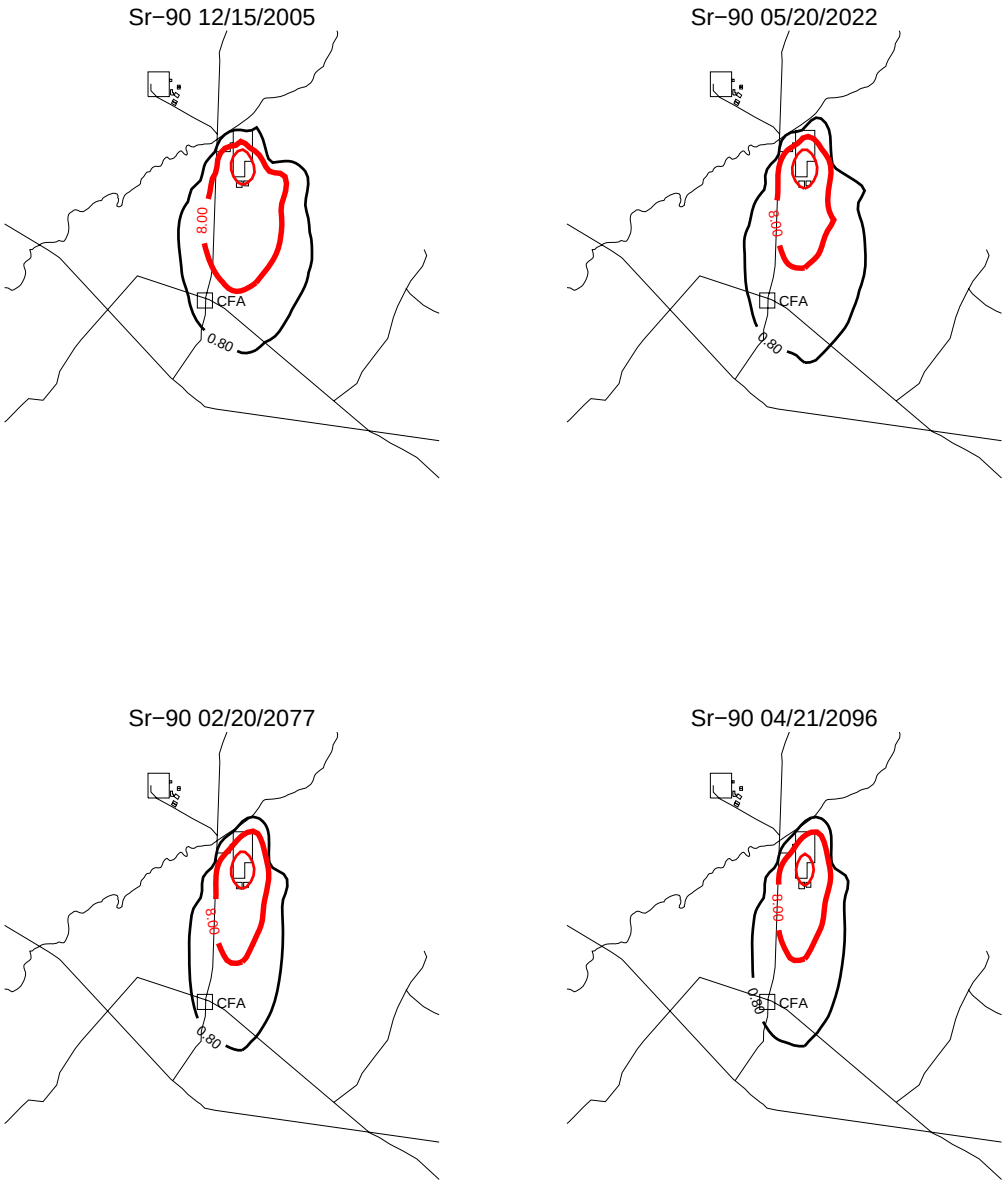

Figure J-11-33. Aquifer concentration contours with anthropogenic water focused in northern INTEC (pCi/L) (MCL = thick red line, 10*MCL = thin red line, MCL/10 = black line).

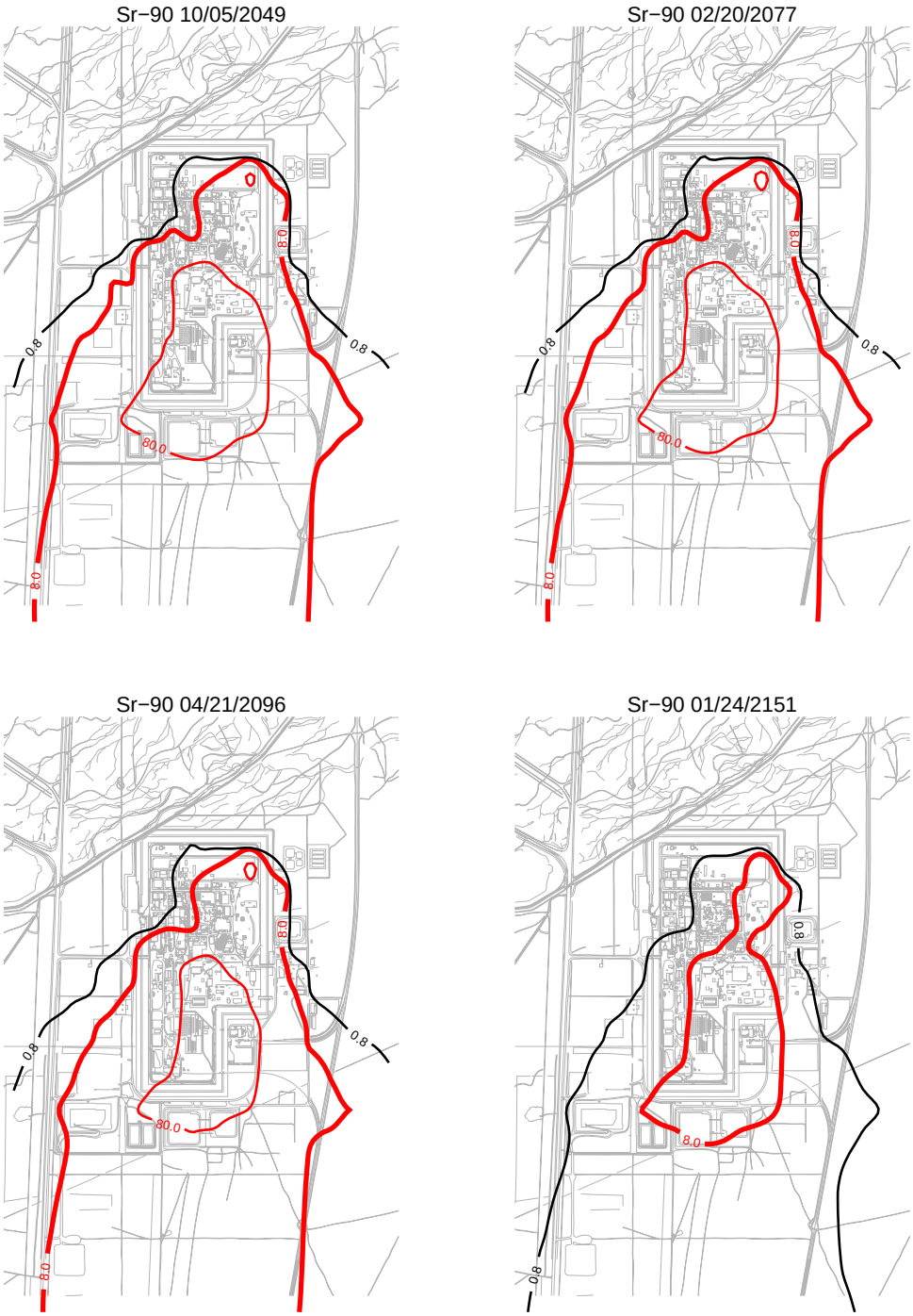

Figure J-11-34. Sr-90 aquifer concentration contours with anthropogenic water focused in northern INTEC (pCi/L) (continued) (MCL = thick red line, 10*MCL = thin red line, MCL/10 = black line).

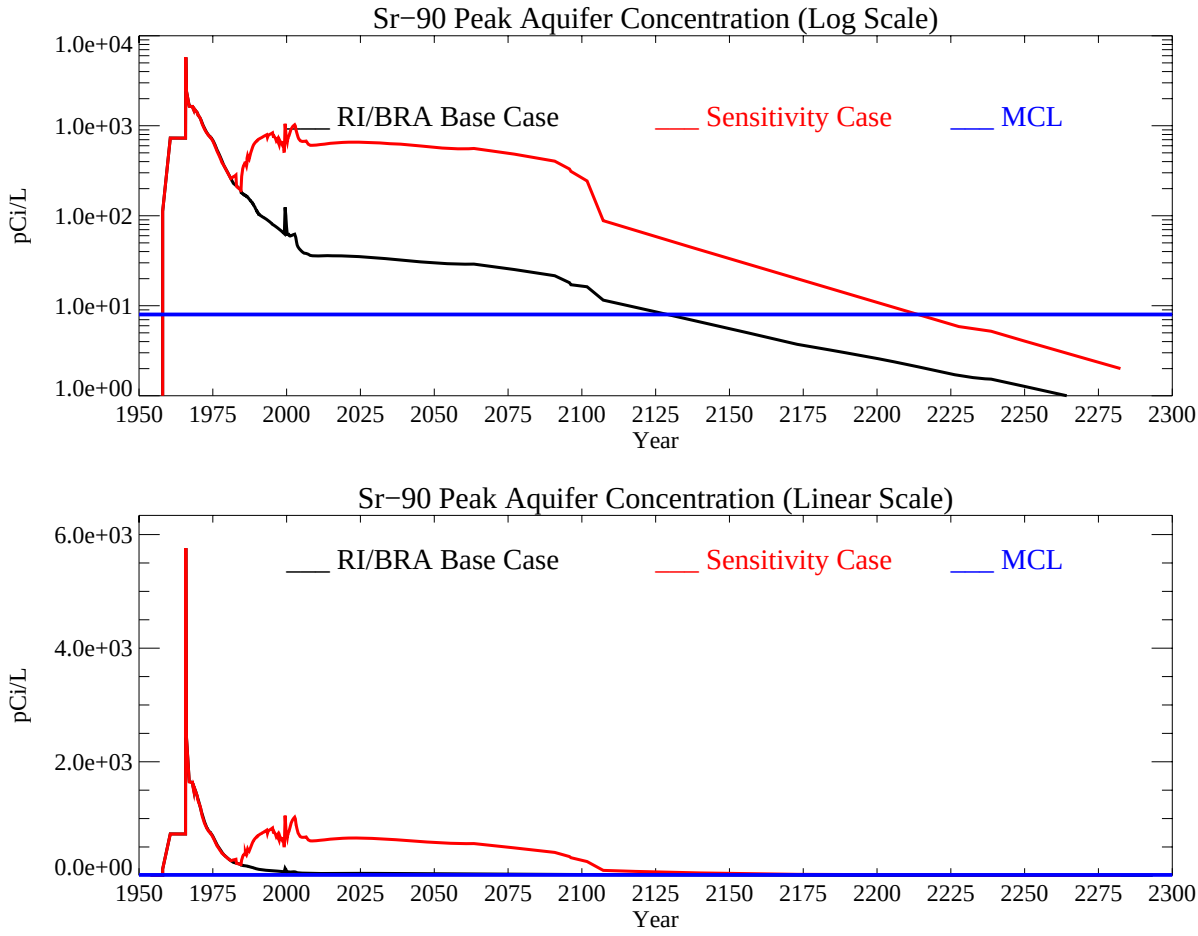

Figure J-11-35. Sr-90 peak aquifer concentrations with anthropogenic water focused in northern INTEC (pCi/L) with the MCL in blue, RI/BRA model in black and this sensitivity run in red.

J-11.4 Stopping Anthropogenic Water Losses In Year 2035

Each of these sensitivity simulations has suggested that anthropogenic water contributes to the downward movement of Sr-90 from the perched water regions. This has been apparent in the step-decrease in activity leaving the vadose zone and the corresponding decrease in aquifer concentrations following the removal of anthropogenic water in 2095. INTEC operations is in the process of reducing their anthropogenic water losses through a series of activities. If these activities are successful, or if operations at INTEC are significantly reduced, there will be a commensurate decrease in anthropogenic water losses to the vadose zone. This sensitivity analysis examines the impact on the transport of Sr-90 assuming anthropogenic water losses cease in year 2035, as opposed to continuing through year 2095 as assumed in the RI/BRA base case.

J-11.4.1 Vadose Zone Sr-90 Simulation Results

This simulation uses the activity-flux from the alluvium corresponding to the RI/BRA base case discussed in Section J-8. Figures J-11-36 through J-11-39 illustrate the horizontal and vertical distribution of the Sr-90 in the vadose zone through the year 2293. Figure J-11-40 illustrates Sr-90 arrival in key perched water wells, and the comparison to field data for all perched water wells is shown in Figure J-11-41. The first 3 subplots in Figure J-11-36 are identical to the base case as are the comparisons to field data because the anthropogenic water was not removed until 2035. The later-time subplots presented in Figure J-11-39 are also not significantly different than those presented for the RI/BRA base case.

Predicted peak vadose zone concentrations through time are given in Figure J-11-42 and are not significantly different than those presented for the base case. The highest concentration is 2.0E9 pCi/L which is equal to that obtained in the base case. The rate at which this activity enters the aquifer is given in Figure J-11-43, and can be compared directly to the base case (shown as black). Note that decreasing anthropogenic water in year 2035 relative to decreasing it in year 2095 results in a modest change in flux rates out of the aquifer only during the 2035-2095 time period.

Figure J-11-36. Sr-90 vadose zone concentration stopping anthropogenic water losses in 2035 (horizontal contours) (pCi/L) (MCL = thick red line, 10*MCL = thin red line, MCL/10 = black line).

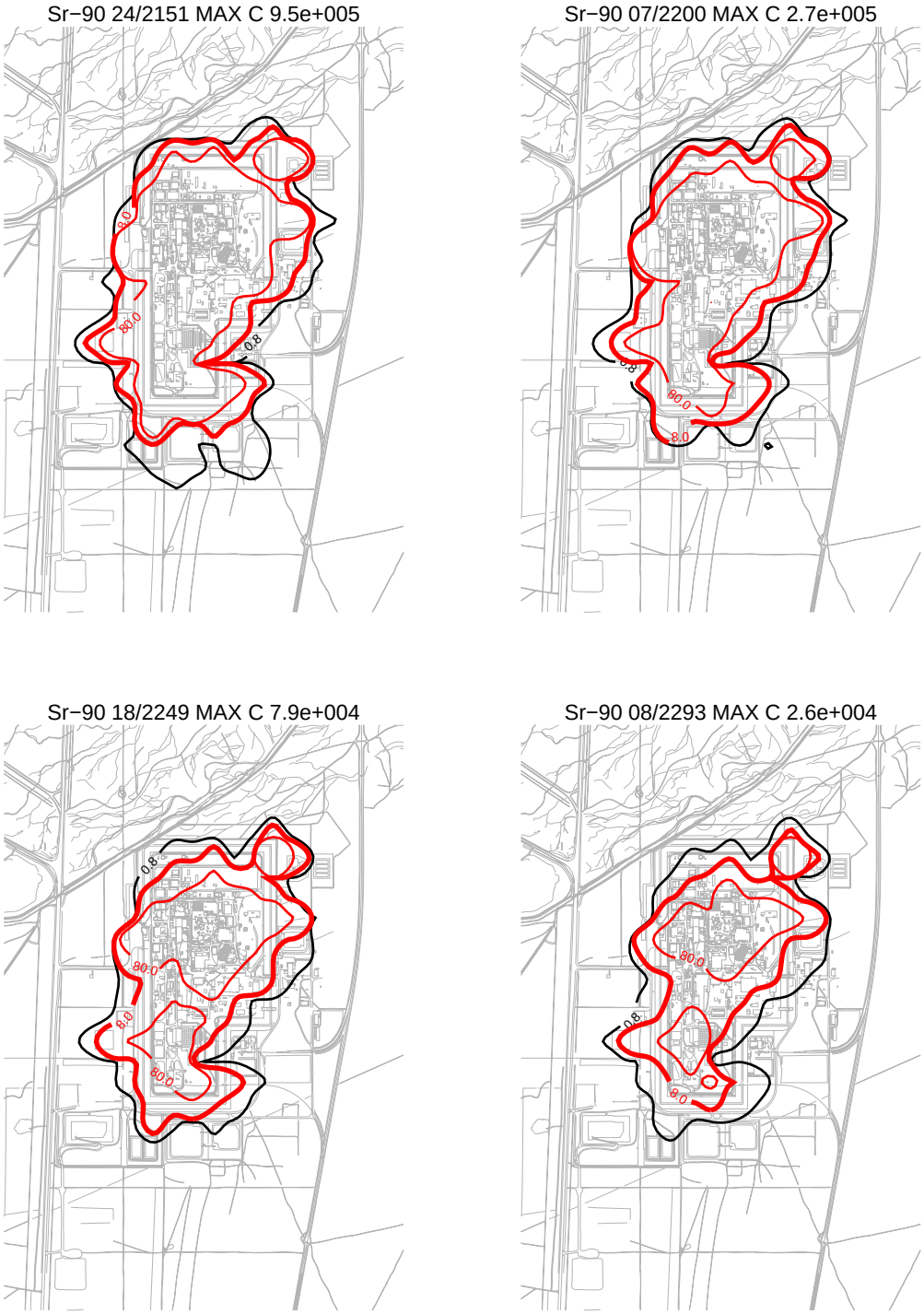

Figure J-11-37. Sr-90 vadose zone concentration stopping anthropogenic water losses in 2035 (horizontal contours) (pCi/L) (MCL = thick red line, 10*MCL = thin red line, MCL/10 = black line).

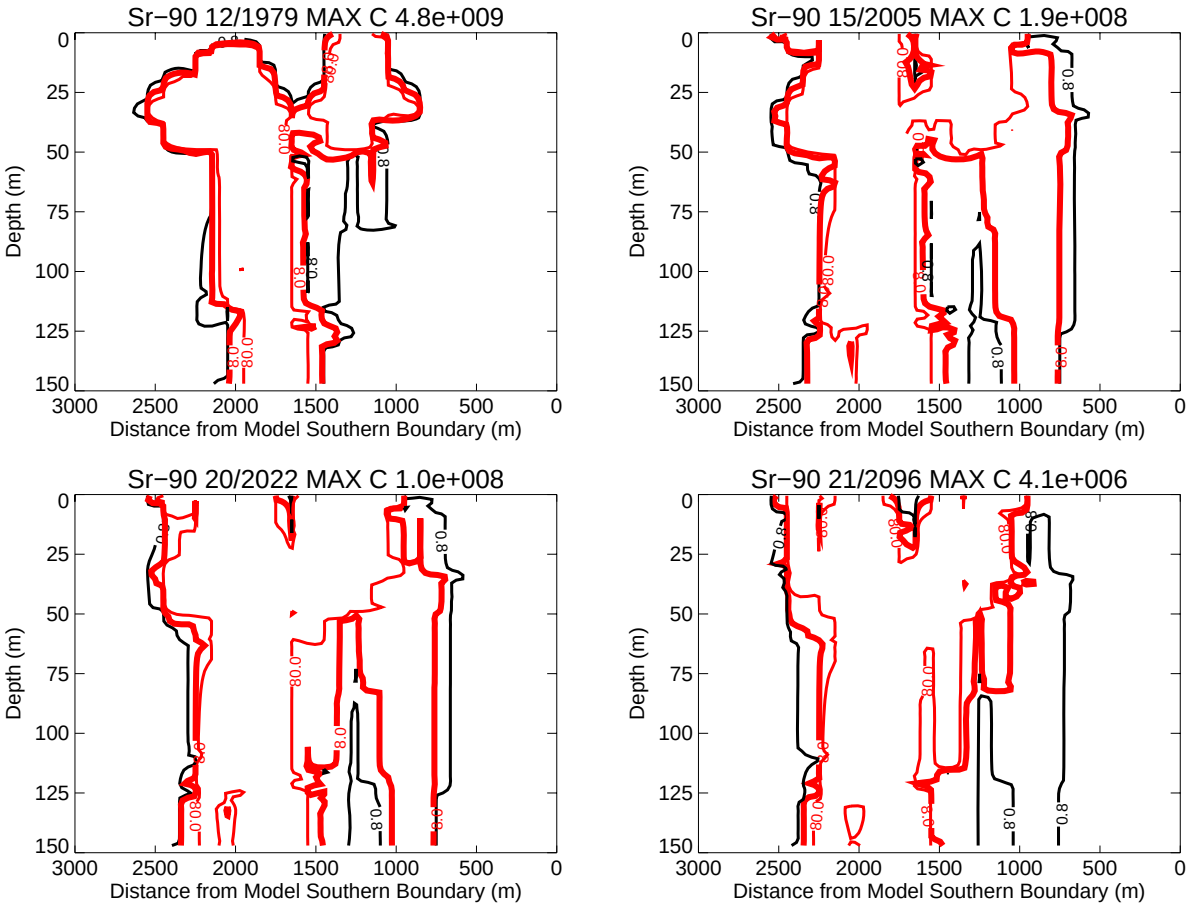

Figure J-11-38. Sr-90 vadose zone concentrations stopping anthropogenic water losses in 2035 (vertical contours) (pCi/L) (MCL = thick red line, 10*MCL = thin red line, MCL/10 = black line).

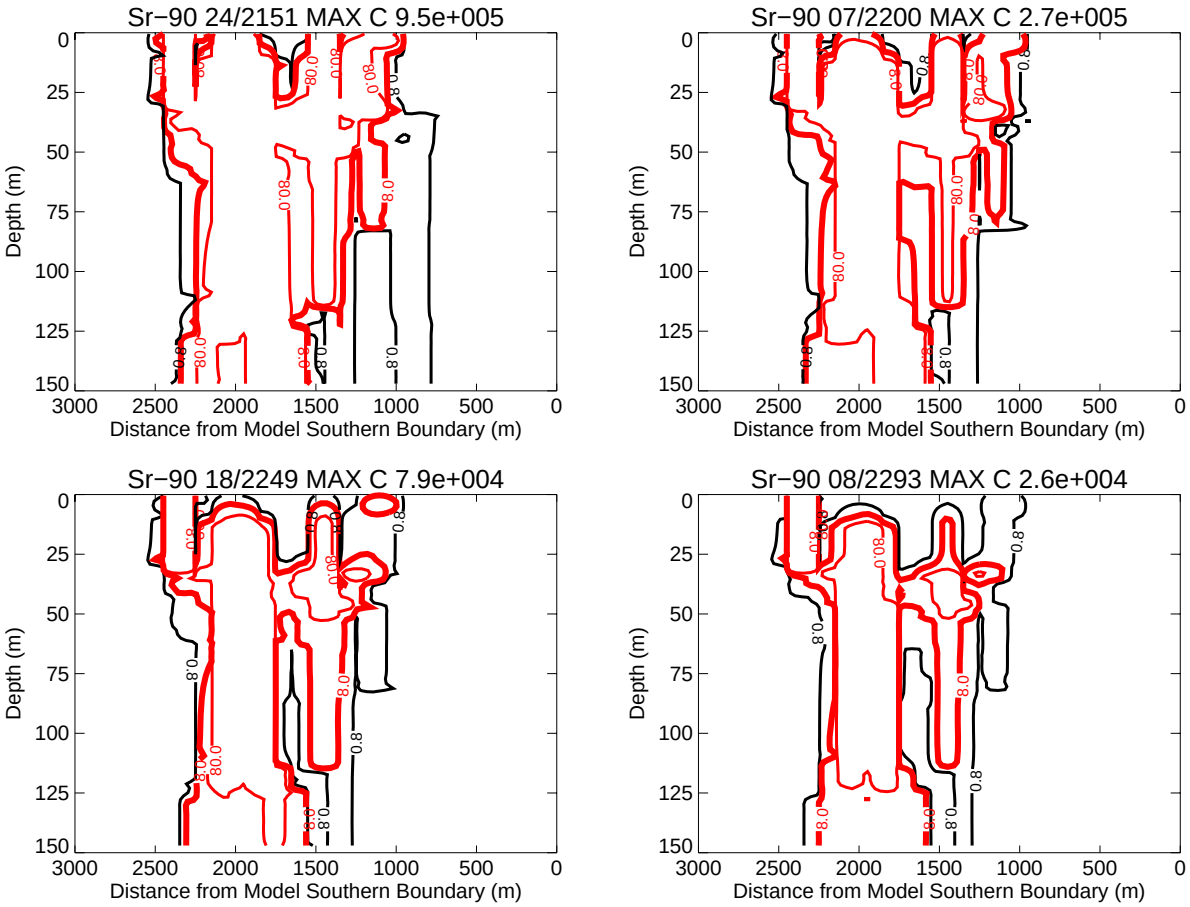

Figure J-11-39. Sr-90 vadose zone concentrations stopping anthropogenic water losses in 2035 (vertical contours) (pCi/L) (continued) (MCL = thick red line, 10*MCL = thin red line, MCL/10 = black line).

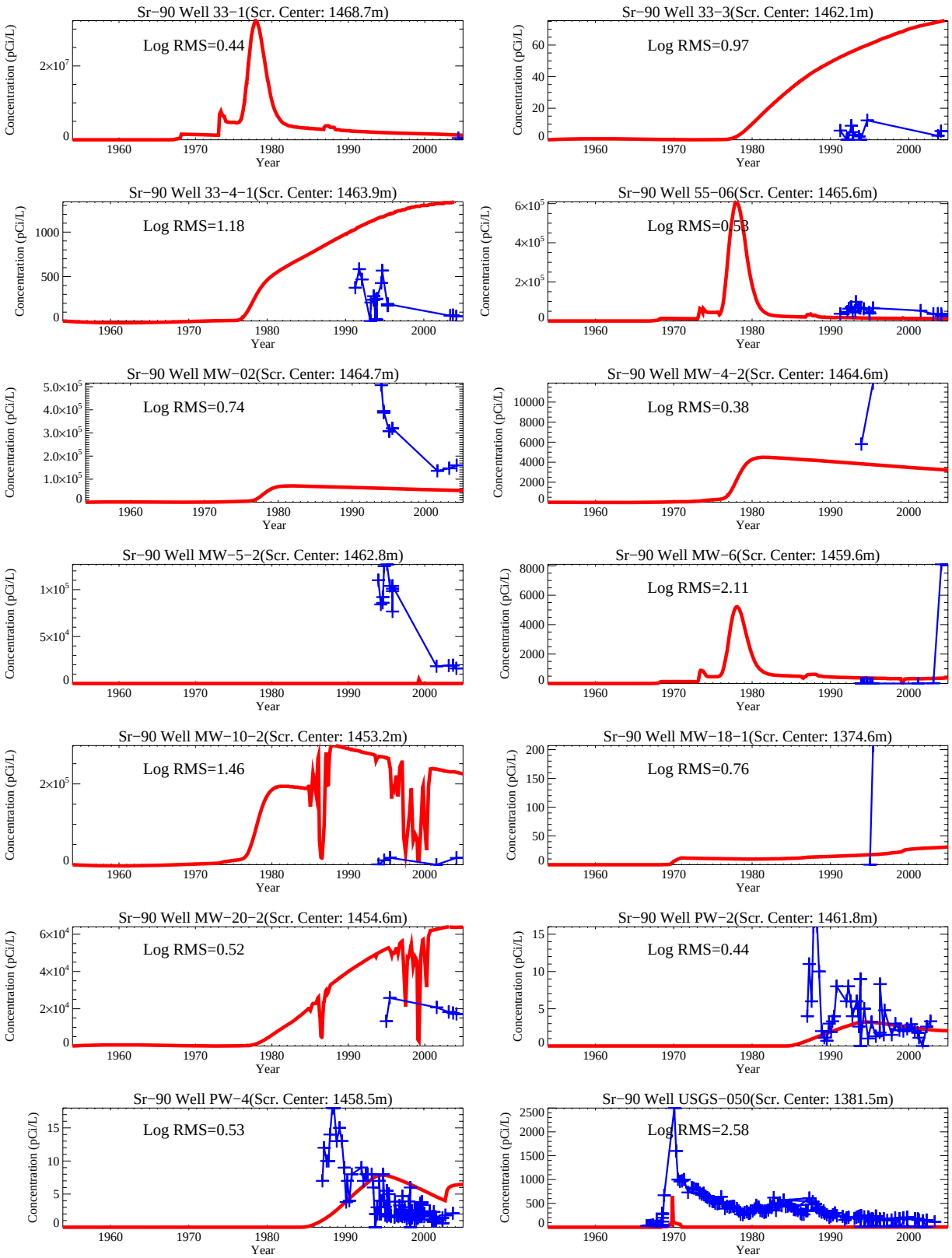

Figure J-11-40. Sr-90 concentration in perched water wells stopping anthropogenic water losses in 2035 (pCi/L) (Measured values = blue crosses, red = model at screen center).

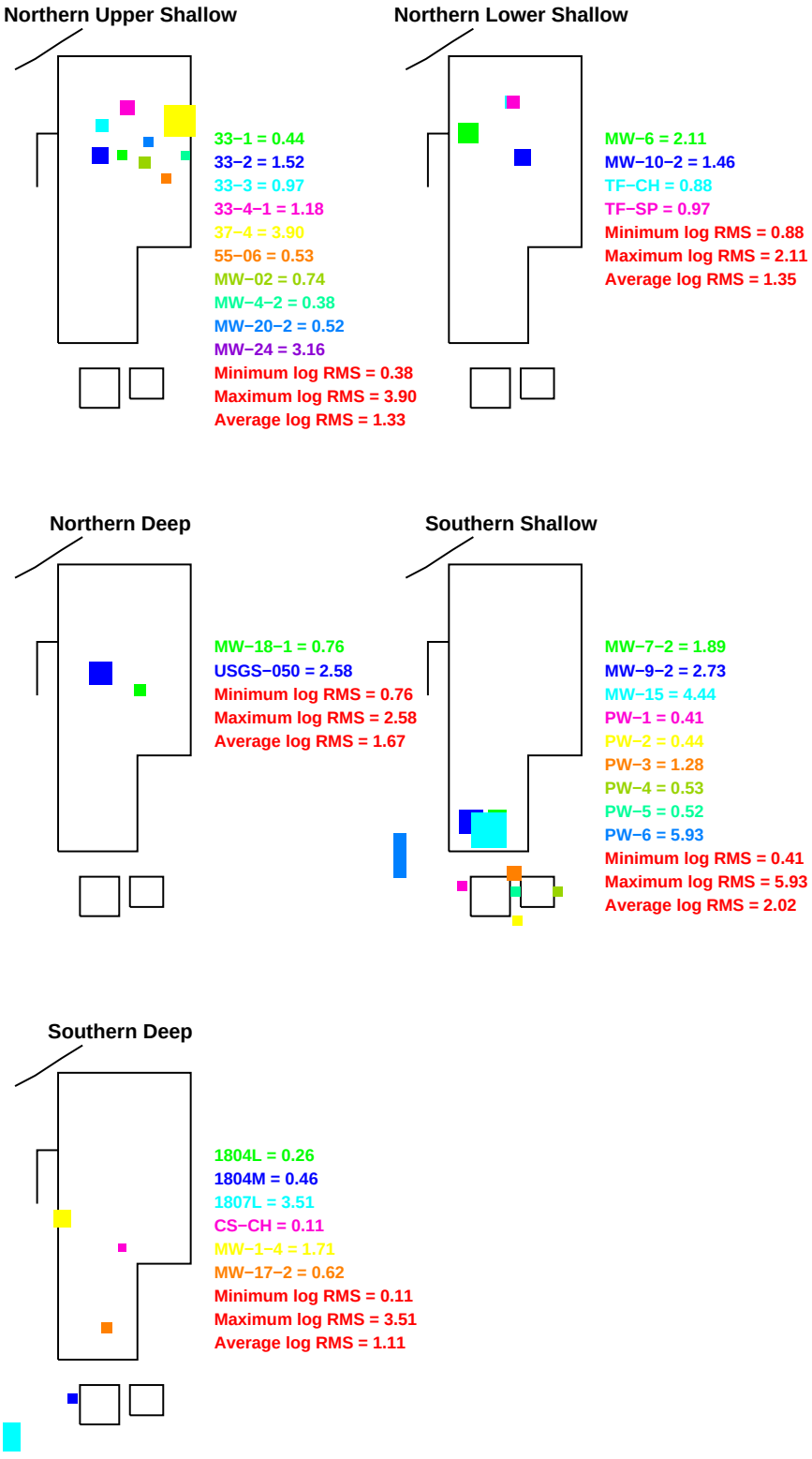

Figure J-11-41. Log 10 Root mean square error (RMS) by depth and northing stopping anthropogenic water losses in 2035.

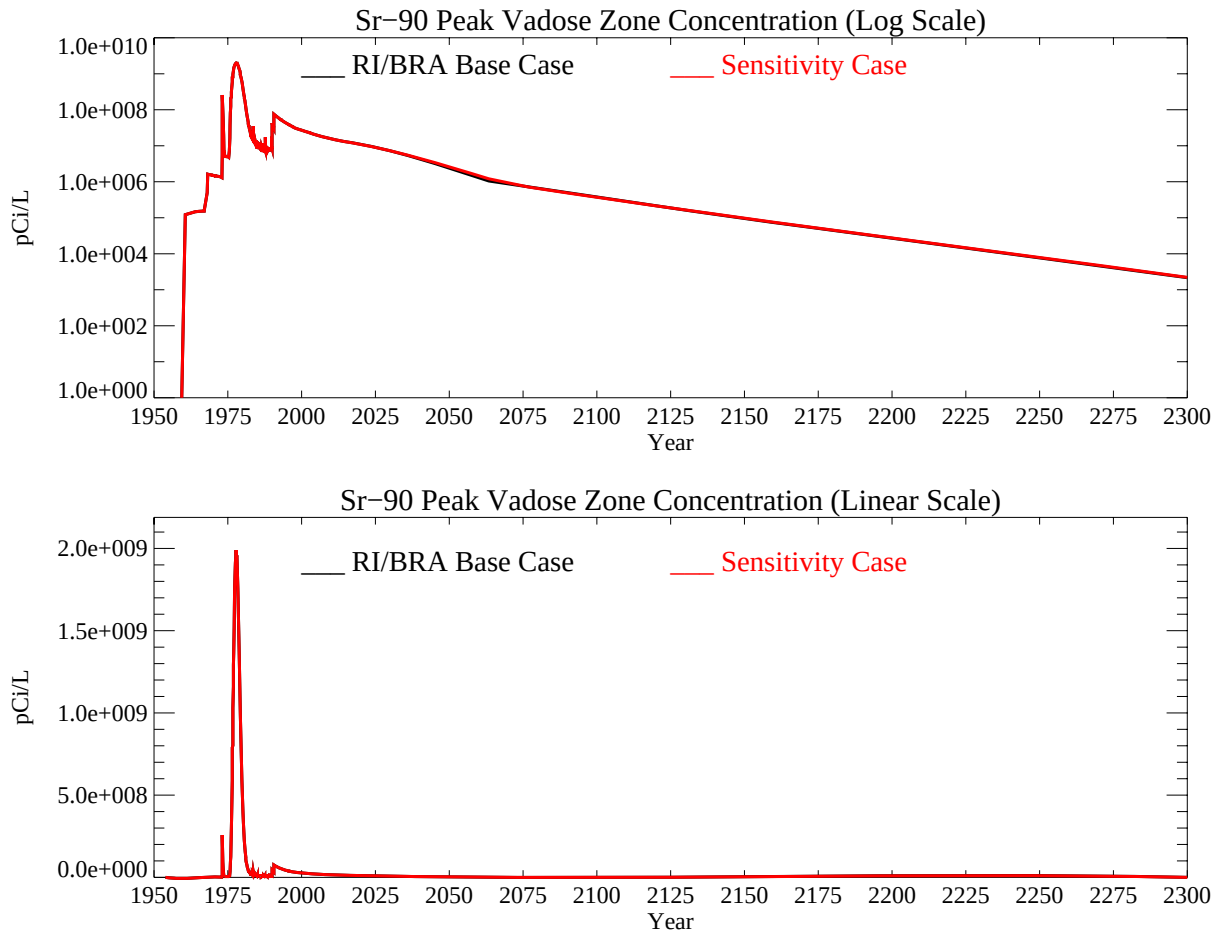

Figure J-11-42. Sr-90 peak vadose zone concentrations stopping anthropogenic water losses in 2035 (pCi/L) with the RI/BRA model in black and this sensitivity run in red.

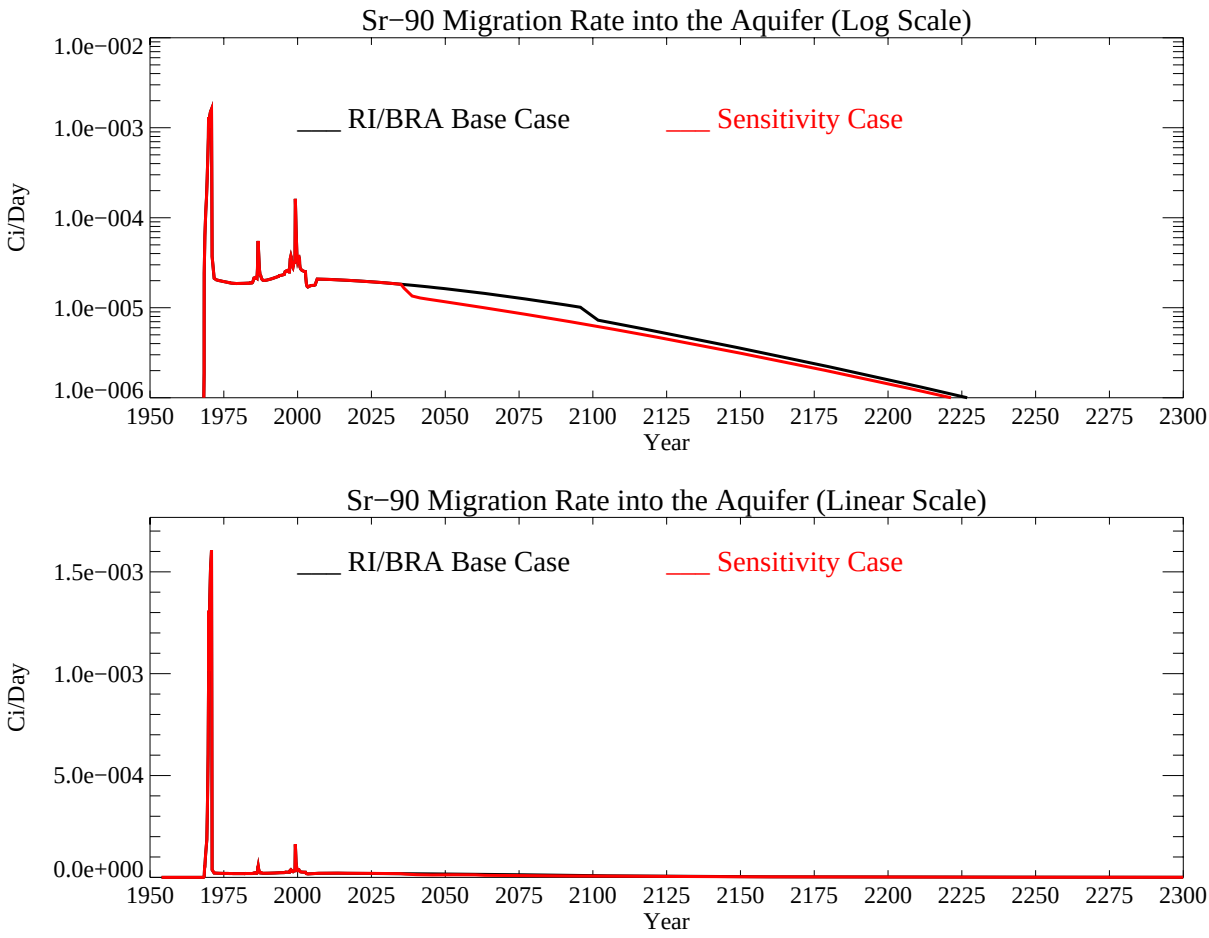

Figure J-11-43. Sr-90 activity flux into the aquifer stopping anthropogenic water losses in 2035 (Ci/day) with the RI/BRA model shown in black, and this sensitivity run in red.

J-11.4.2 Aquifer Sr-90 Simulation Results

The distribution of Sr-90 in the aquifer for the time period spanning 2005-2096 is presented for the far-field in Figure J-11-44 with near-field results given for the 2049-2151 time period in Figure J-11-45. The resultant peak aquifer concentrations are given in Figure J-11-46. Because the Sr-90 originating in the vadose zone does not arrive in the aquifer until the mid 1980's, comparisons to measured data are not presented for aquifer wells.

The peak aquifer Sr-90 concentrations mimic the behavior of the flux out of the vadose zone. As a result, they are identical prior to 2035, and converge back to the RI/BRA predicted concentrations after about year 2125. The simulated Sr-90 concentrations remained above the MCL from 1960 through year 2121, with a predicted peak concentration in year 2095 of 12 pCi/L. This concentration exceeds the MCL by a factor of 1.5. The Sr-90 contour plots presented in Figures J-11-44 and J-11-45 illustrate that although Sr-90 concentrations in the aquifer are predicted to exceed the MCL beyond 2095, the area impacted by Sr-90 above 8 pCi/L is between the tank farm and former percolation ponds in 2096.

The relative insensitivity to early removal of the anthropogenic water was based on the average INTEC water losses of 5 cm/yr. If the anthropogenic water losses are actually focused in northern INTEC, as simulated in Section J-11.3, these results might be quite different.

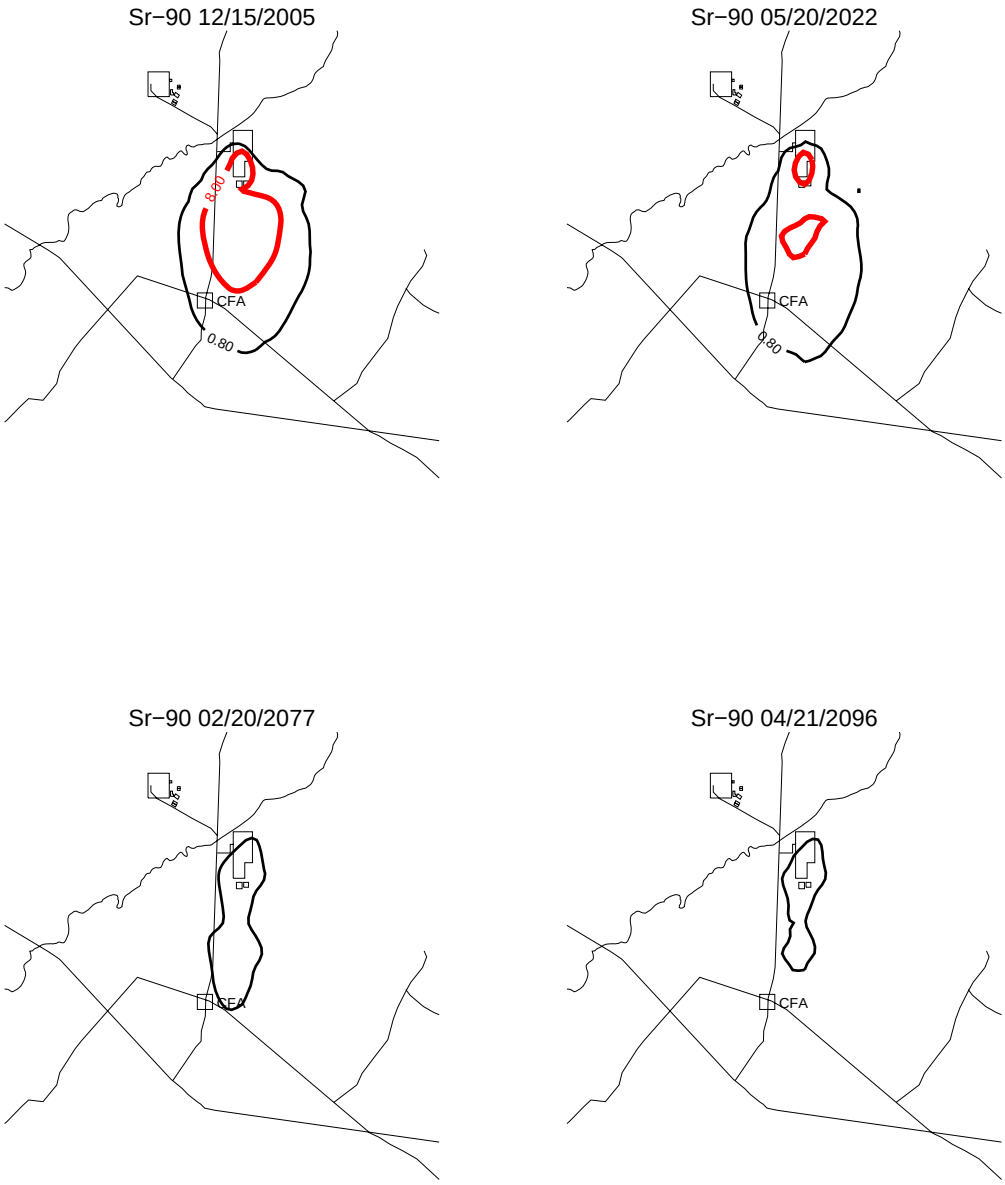

Figure J-11-44. Sr-90 aquifer concentration contours stopping anthropogenic water losses in 2035 (pCi/L) (MCL = thick red line, 10*MCL = thin red line, MCL/10 = black line).

Figure J-11-45. Sr-90 aquifer concentration contours stopping anthropogenic water losses in 2035 (pCi/L) (continued) (MCL = thick red line, 10*MCL = thin red line, MCL/10 = black line).

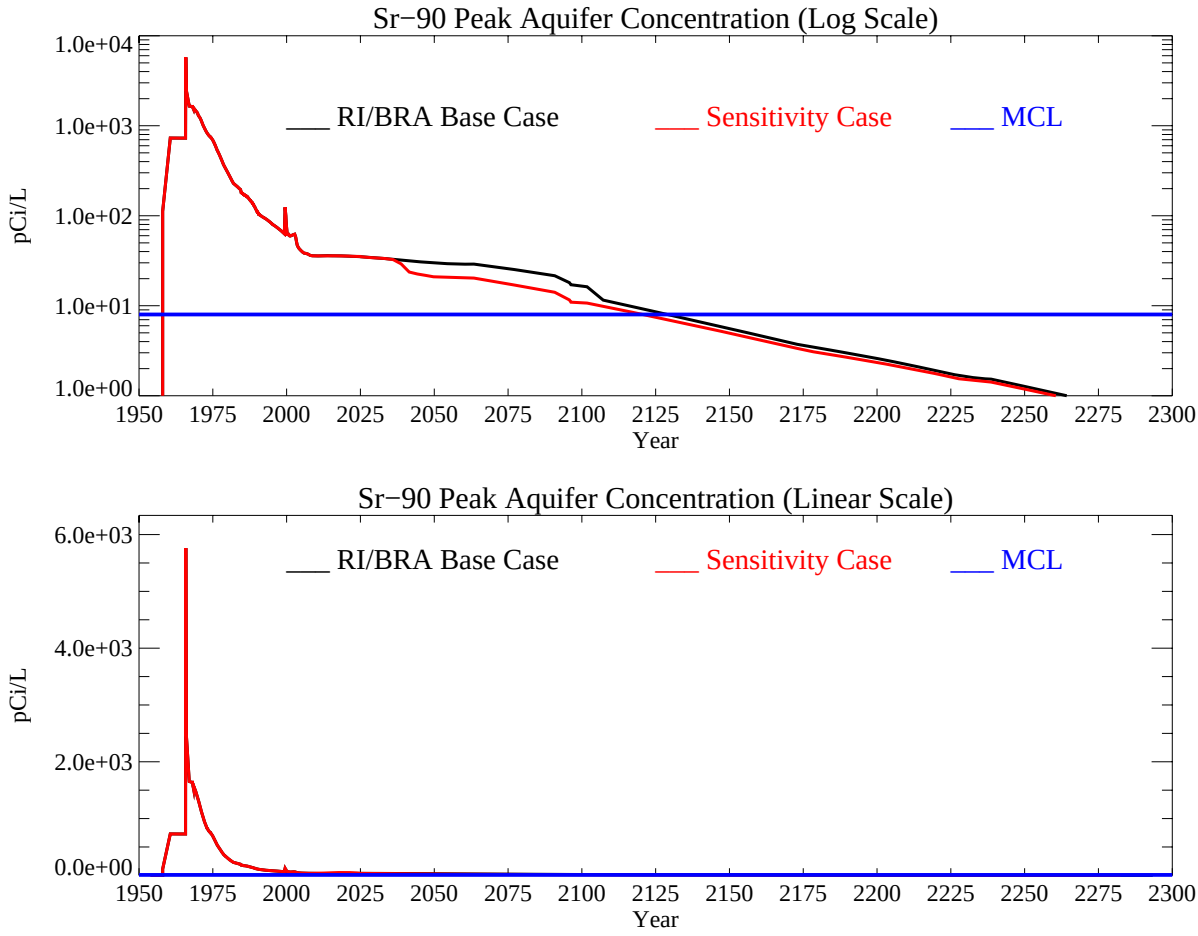

Figure J-11-46. Sr-90 peak aquifer concentrations stopping anthropogenic water losses in 2035 (pCi/L) with the MCL shown in blue, the RI/BRA model in black and this sensitivity run in red.

J-11.5 Removing the Production Wells

The following simulations are presented to evaluate the potential land-use impact which affects the amount of water required and the time-frame during which it is required. In the RI/BRA, it was assumed that the land-use through year 2095 would require pumping water from the SRPA at current rates. This assumption is consistent with an industrial use scenario, where large water volumes would be necessary in order to sustain the commercial activities. If the land-use changes significantly, or if the current production wells are moved out of the influence of INTEC (i.e., further north or east), the draw-down currently observed in the aquifer would stop. The influence of the production wells will be shown relative to the drawdown predicted for the RI/BRA base case in year 2010 (Figure J-11-47). Important features in Figure J-11-47 include the (a) locations of the CPP-2 and CPP-1 production wells just south of the INTEC fence line, (b) position of the 1356.4 m and 1356.6 m contour lines, and the very flat head distribution between them, and (c) the head gradient overall represented by the density of contours drawn at 0.1 m contour intervals.

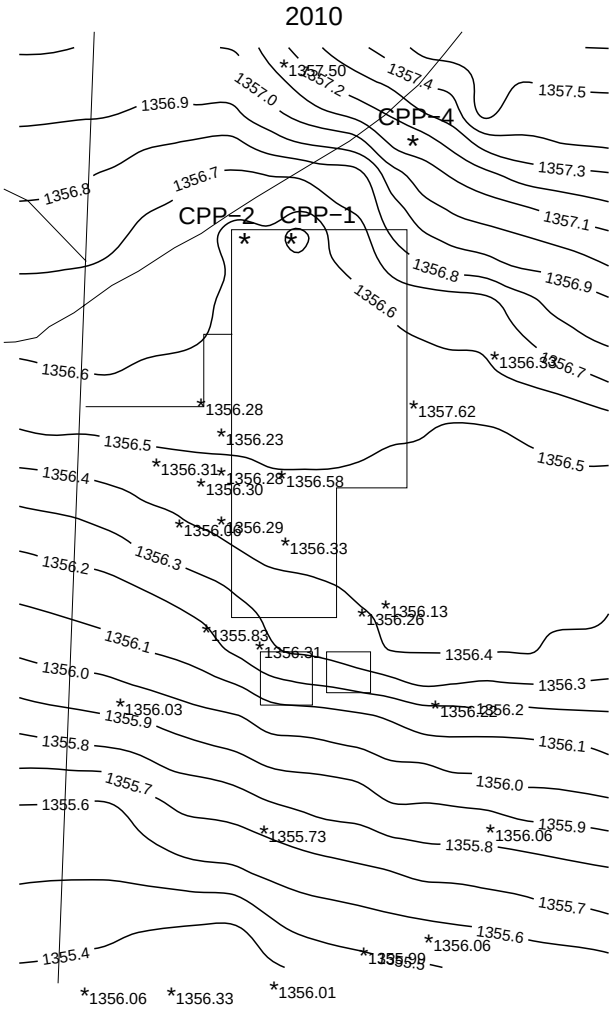

Figure J-11-47. Head (m) distribution predicted for the RI/BRA base case in year 2010.

J-11.5.1 Removing the Production Wells in 2012.

In the simulation presented below, pumping from CPP-1 and CPP-2 is assumed to stop in year 2012. Because the land-use scenario remains potentially industrial, the anthropogenic water losses were not reduced in this simulation, making this simulation representative of relocating the production wells outside of the INTEC viscinity. This simulation uses the activity-flux from the alluvium corresponding to the RI/BRA base case discussed in Section J-8.1, and also uses the RI/BRA flux of Sr-90 out of the vadose zone. As a result, the differences between the RI/BRA model predictions and those presented below are the sole consequence of production in the CPP-1 and CPP-2 wells.

J-11.5.1.1 Aquifer Sr-90 Simulation Results

After removal of the production wells, the hydraulic head almost immediately returns to pre-pumping conditions. The affect of the production wells on the hydraulic head is apparent through the comparison of Figures J-11-47 and J-11-48. The hydraulic influence of the production wells is obvious. Important features to note include the

- shift southward of the 1356.4 m and 1356.6 m contour lines. In the RI/BRA model, the 1356.6 m level occurred north of the two production wells, and the 1356.4 m contour level was south of the CPP-3 injection well. After removing the production wells, the lower contour passes just north of the former percolation ponds, and the 1356.6 m contour level is about where the 1356.5 m contour level was in the RI/BRA model. This implies that the region of influence of the pumping wells extends well south of the former percolation ponds. Differences in contour levels exist well north of the production wells.
- absence of the very flat head distribution in central INTEC. Removing the production wells has greatly increased the gradient in the region containing the highest predicted concentrations in the INTEC facility boundary. This means that the velocity in that region will be proportionally higher.
- drawdown north of the tank farm toward CPP-1 and CPP-2. It is known that the production wells are capturing contaminants (ICP 2004). In the 110-ft interbed, there is a water divide caused by a change in slope that occurs very near the tank farm. North of the tank farm, the interbed slopes toward the Big Lost River, and South of the tank farm, the slope is to the south. It is likely that contaminants being produced in CPP-1 and CPP-2 are coming from the vadose zone, and that those produced contaminants are associated with flow to the north of the divide.
- width of the area affected by the production wells near CPP-1 and CPP-2. Pumping alternates between CPP-1 and CPP-2. This switching contributes to northwestward movement of water and contaminants, increased dispersion, intermittant southward transport, and very slow transport in the aquifer of contaminants arriving from the vadose zone northeast of the tank farm.
- head gradient overall. The gradient northeast of the production wells and the gradient south of the former percolation ponds is very similar in both models. This suggests that the migration of Sr-90 currently in the SRPA and south of the former percolation ponds will not be affected by removing the production wells. However, it is clear that there will be some influence within the facility boundaries.

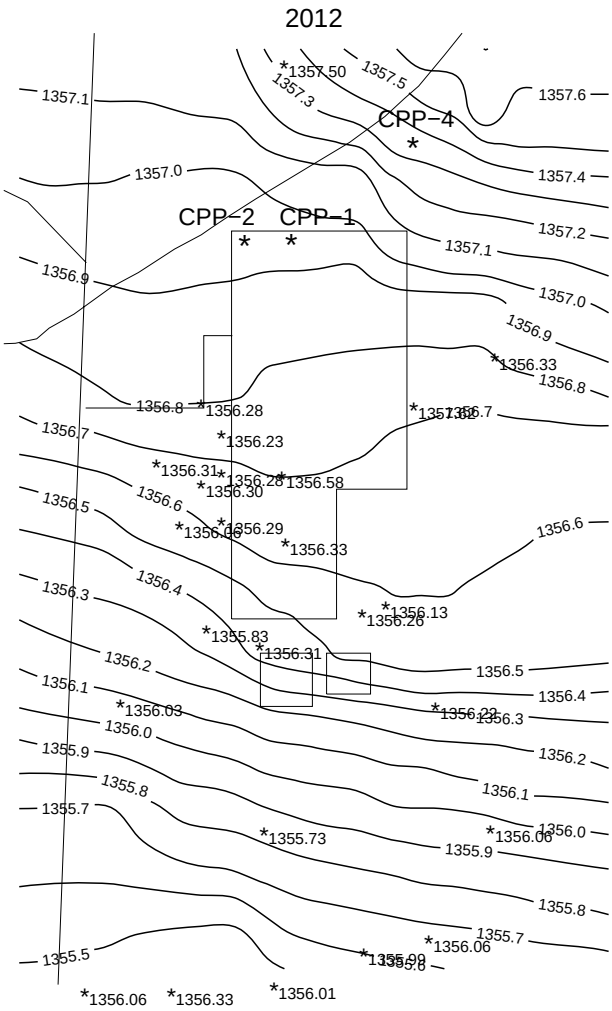

Figure J-11-48. Head (m) distribution predicted after removing the production wells in year 2012.

The influence on Sr-90 transport is shown in the far-field for the time period spanning 2005-2096 in Figure J-11-49. The near-field distribution is shown in Figure J-11-50 for the 2049-2151 time period, and resultant peak aquifer concentrations are given in Figure J-11-51. Comparing the far-field distribution of Sr-90 shows that removing the production wells has little effect on the distribution of Sr-90 downgradient of INTEC through year 2022. This is primarily because the Sr-90 currently in the aquifer was introduced in well CPP-03 which is in the region of the aquifer least affected by the imposed pumping gradients. In the near-field, the area impacted above the MCL is much smaller in central INTEC by year 2049. Increased velocity through central INTEC allows for more dilution and increased dispersion. Although natural attenuation is increased, it still is not sufficient to completely counter the incoming fluxes from the vadose zone. To the northeast of the tank farm, a small region above the MCL has developed. The increase in concentrations near the production wells is a result of (a) decreasing the dispersion that was being caused by switching production between the two wells, and (b) removing the slight remediation that occurs during the pumping operations.

Peak aquifer concentration decreases immediately after pumping ceases from the production wells. However, the peak concentrations are again very similar by year 2150. The convergance of peak concentration occurs because the location of the peak concentration is different with and without the production wells present. By year 2108, predicted concentrations are below the MCL, and by year 2095, the peak concentration is 11.9 pCi/L. Relocating the production wells has reduced the time during which the MCL is exceeded by 20 years. This is significant from the perspective of contingent pump and treat alternatives being evaluated in the feasibility study.

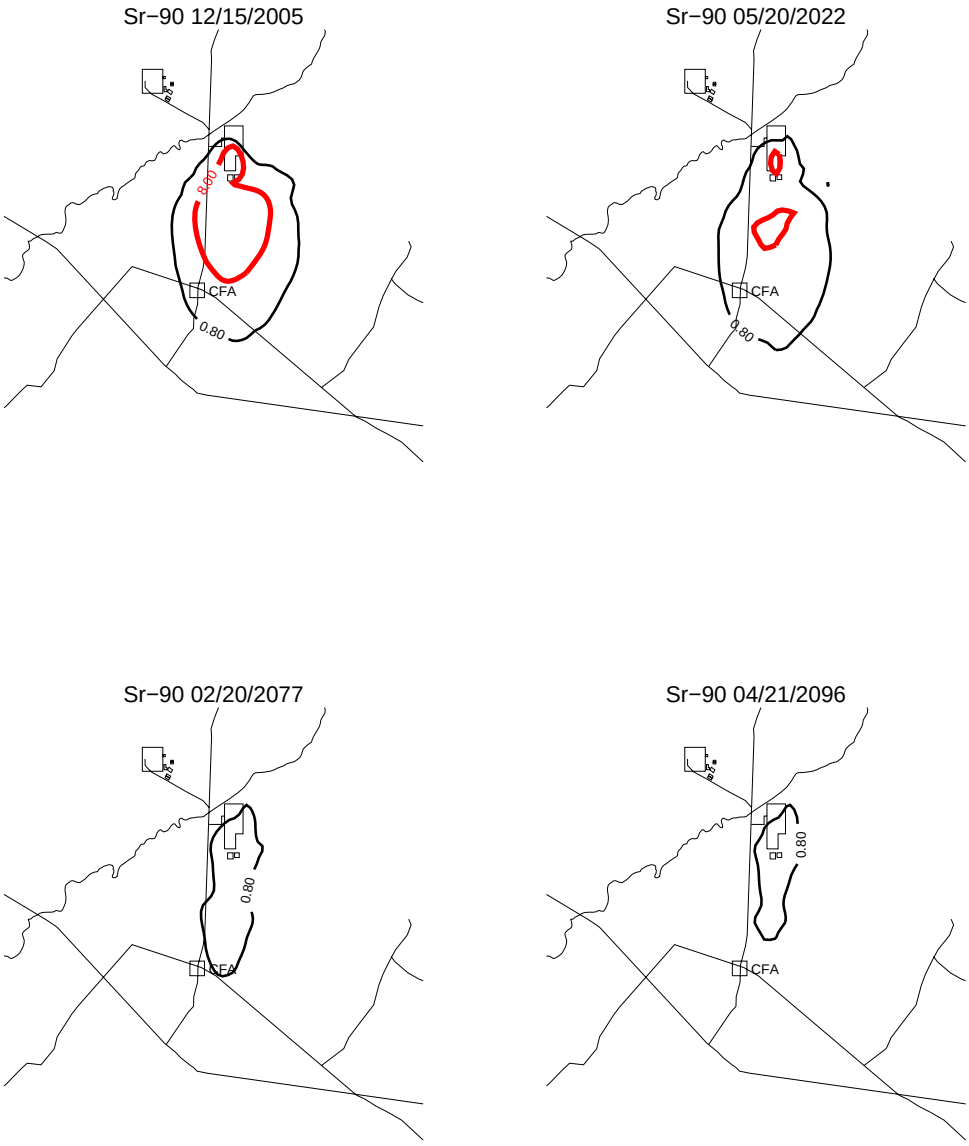

Figure J-11-49. Sr-90 aquifer concentration contours removing production wells in 2012 (pCi/L) (MCL = thick red line, 10*MCL = thin red line, MCL/10 = black line).

Figure J-11-50. Sr-90 aquifer concentration contours removing production wells in 2012 (pCi/L) (continued) (MCL = thick red line, 10*MCL = thin red line, MCL/10 = black line).

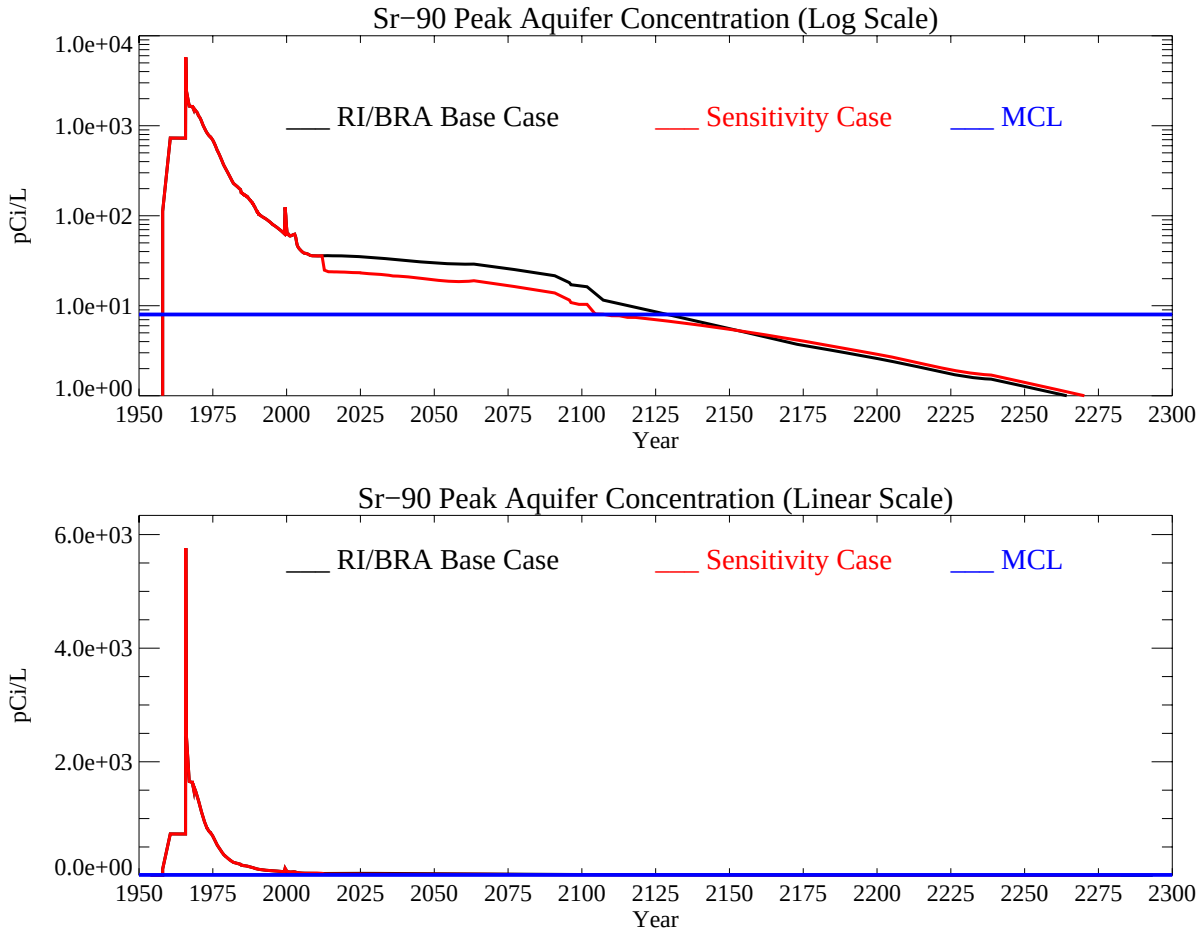

Figure J-11-51. Sr-90 peak aquifer concentrations removing production wells in 2012 (pCi/L) with the MCL shown in blue, the RI/BRA model in black and this sensitivity run in red.

J-11.5.2 Removing the Production Wells In Year 2035

In the simulation presented below, pumping is assumed to stop in year 2035. This simulation uses the activity-flux from the alluvium corresponding to the RI/BRA base case discussed in Section J-8.1, and also uses the RI/BRA flux of Sr-90 out of the vadose zone. Because the land-use scenario remains potentially industrial, the anthropogenic water losses were not reduced. Thus, this simulation is representative of relocating the production wells outside of the INTEC viscinity.

J-11.5.2.1 Aquifer Sr-90 Simulation Results

The effect of the production wells in year 2035 is very similar to that in year 2012. This is apparent by comparing the hydraulic head in Figures J-11-48 and J-11-52. The similar hydraulic influence occurs because:

- steady-state Big Lost River recharge is assumed to start in year 2005, and was in effect prior to year 2012 and through the end of the simulation period.
- precipitation recharge is steady-state throughout the simulation period.
- transient fluxes equilibrated prior to year 2012 after the percolation ponds were relocated.
- the equilibration period in the aquifer is extremely short after the production wells are turned off.

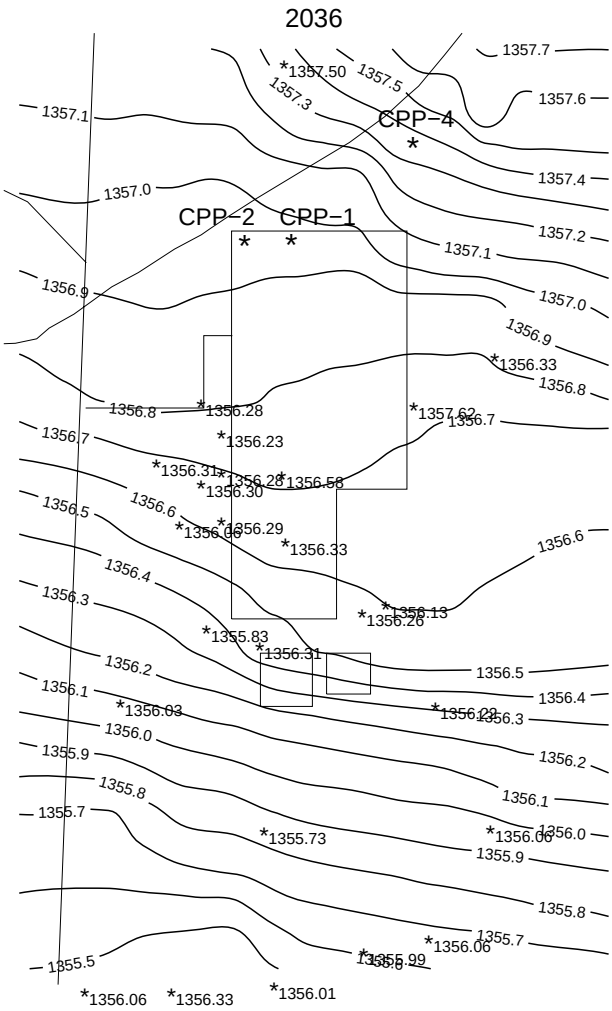

Figure J-11-52. Head (m) distribution predicted after removing the production wells in year 2035.

The influence on Sr-90 transport is shown in the far-field for the time period spanning 2005-2096 in Figure J-11-53 with the near-field distribution shown in Figure J-11-54 for the 2049-2151 time period. Resultant peak aquifer concentrations are given in Figure J-11-55. Because the water flux from the vadose zone is steady-state after year 2012, the incoming fluxes are exactly the same in all of the production well sensitivity simulations. The continual arrival from the vadose zone is being attenuated in the aquifer at rate sufficient to keep the Sr-90 plume within the INTEC fence regardless of whether or not the production wells are in use. Removing the production wells 20 years earlier allowed those fluxes to be attenuated for a longer period of time, but the continued arrival keeps concentrations above the MCL through year 2107 in either case, and the peak concentrations (11.9 pCi/L) in year 2095 are nearly identical.

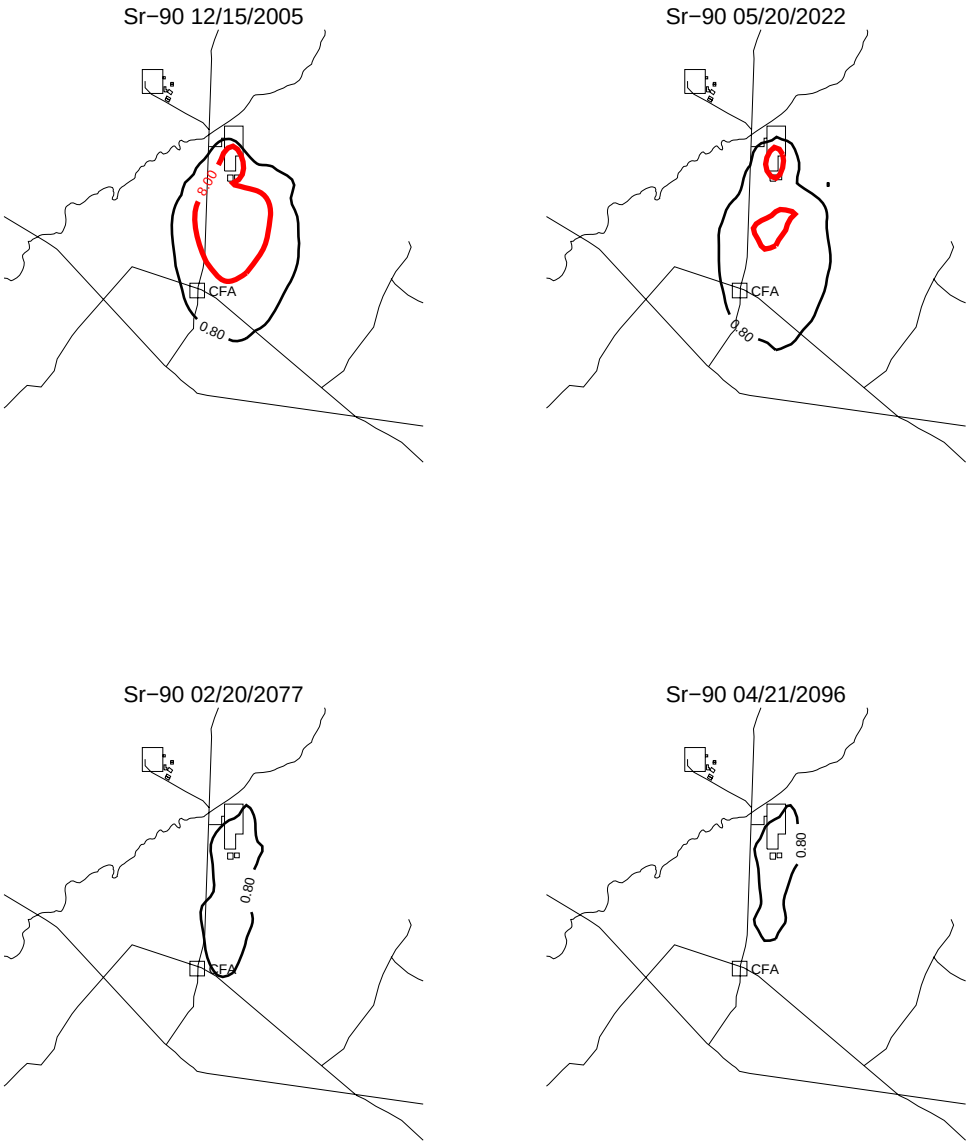

Figure J-11-53. Sr-90 aquifer concentration contours removing the production wells in 2035 (pCi/L) (MCL = thick red line, 10*MCL = thin red line, MCL/10 = black line).

Figure J-11-54. Sr-90 aquifer concentration contours removing the production wells in 2035 (pCi/L) (continued) (MCL = thick red line, 10*MCL = thin red line, MCL/10 = black line).

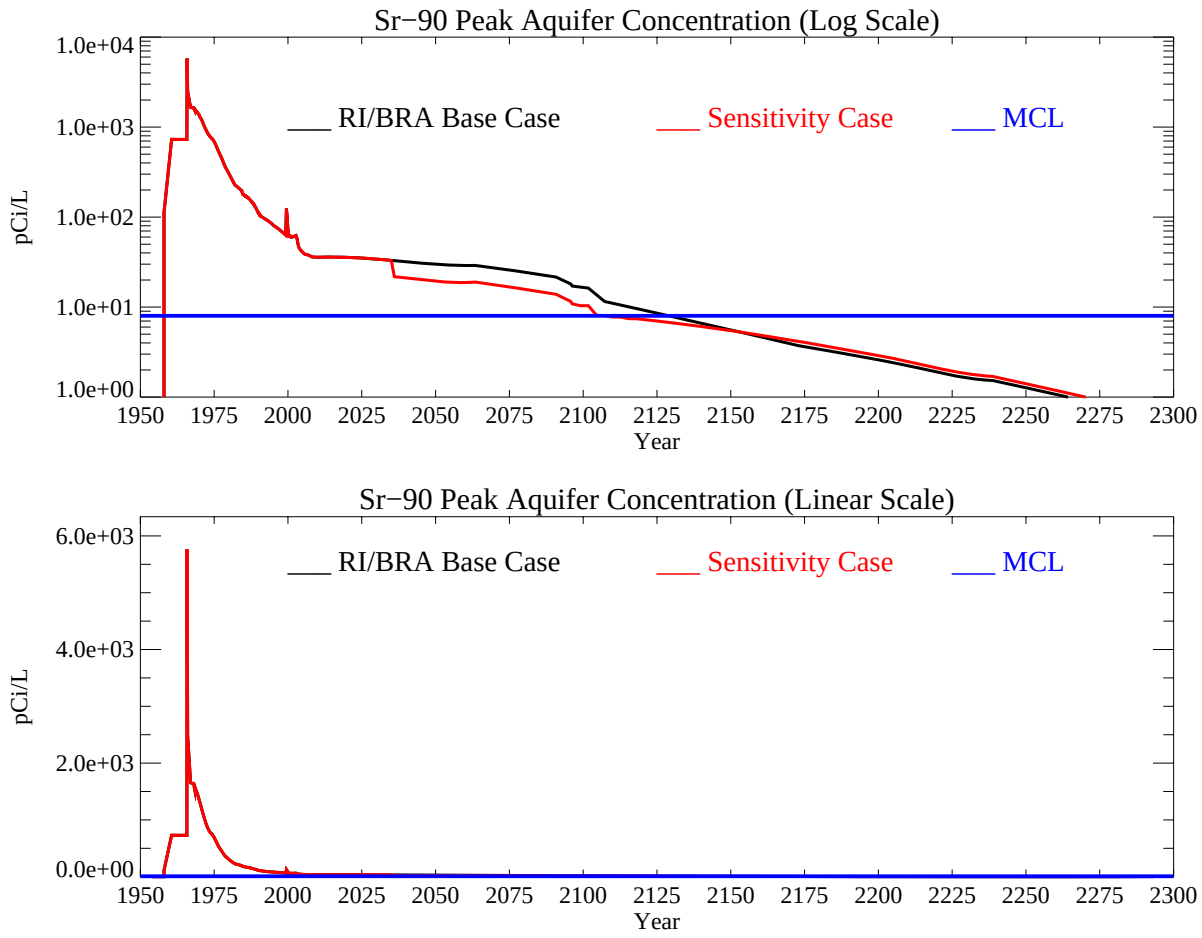

Figure J-11-55. Sr-90 peak aquifer concentrations removing the production wells in 2035 (pCi/L) with the MCL shown in blue, the RI/BRA model in black and this sensitivity run in red.

J-11.5.3 Removing the Production Wells In Year 2096

In the simulation presented below, pumping is assumed to stop in year 2096. This simulation uses the activity-flux from the alluvium corresponding to the RI/BRA base case discussed in Section J-8.1, and also uses the RI/BRA flux of Sr-90 out of the vadose zone. Because the land-use scenario remains potentially industrial, the anthropogenic water losses were not reduced. Thus, this simulation is representative of relocating the production wells outside of the INTEC viscinity.

J-11.5.3.1 Aquifer Sr-90 Simulation Results

After removal of the production wells, the hydraulic head almost immediately returns to pre-pumping conditions. The affect of the production wells in year 2096 is again very similar to that in years 2012 and 2035. This is apparent by comparing the hydraulic head in Figures J-11-48, J-11-52, and J-11-56. The similarity in hydraulic influence occurs because:

- steady-state Big Lost River recharge is assumed to start in year 2005, and was in effect prior to year 2012 and through the end of the simulation period.
- precipitation recharge is steady-state throughout the simulation period.
- transient fluxes equilibrated prior to year 2012 after the percolation ponds were relocated.
- the equilibration period in the aquifer is extremely short after the production wells are turned off.

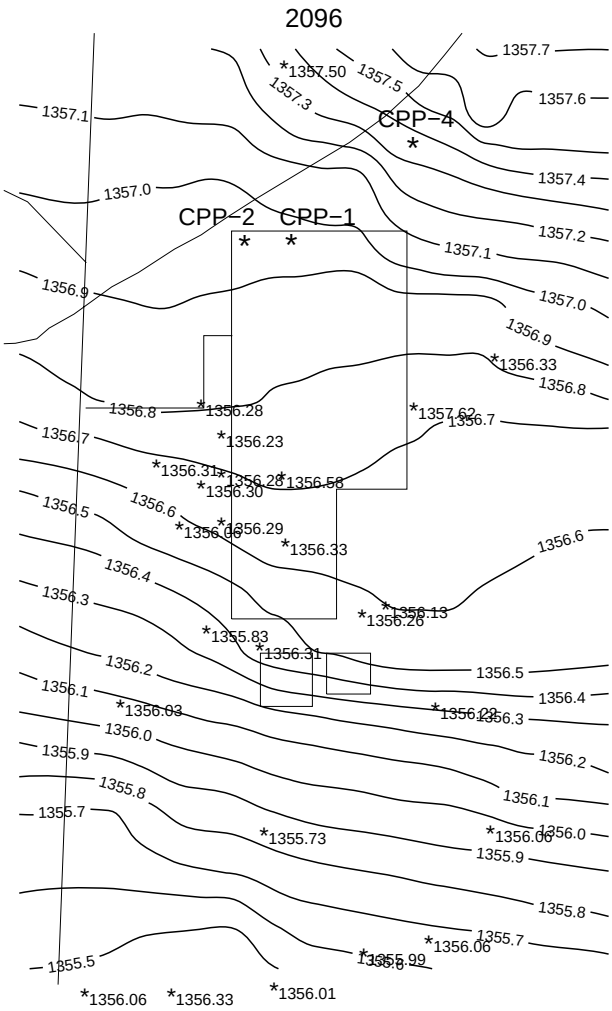

Figure J-11-56. Head (m) distribution predicted after removing the production wells in year 2096.

The influence on Sr-90 transport is shown in the far-field for the time period spanning 2005-2096 in Figure J-11-57 with the near-field distribution shown in Figure J-11-58 for the 2049-2151 time period. Resultant peak aquifer concentrations are given in Figure J-11-59. Waiting until year 2097 to remove the production wells has a slight impact on the distribution of Sr-90 above the MCL. Removing the production wells in either 2012 or 2035 allowed earlier natural attenuation of Sr-90 to occur in central INTEC, but keeping the production wells on-line through year 2096 prevents concentrations above the MCL from occurring in northeast INTEC. Because the water flux from the vadose zone is steady-state after year 2012, the incoming fluxes are exactly the same in all of the production well sensitivity simulations. Removing the production wells earlier allows those fluxes to be attenuated for a longer period of time. However, the peak aquifer concentration still exceeds the MCL through year 2108 and is 18.6 pCi/L in year 2096.

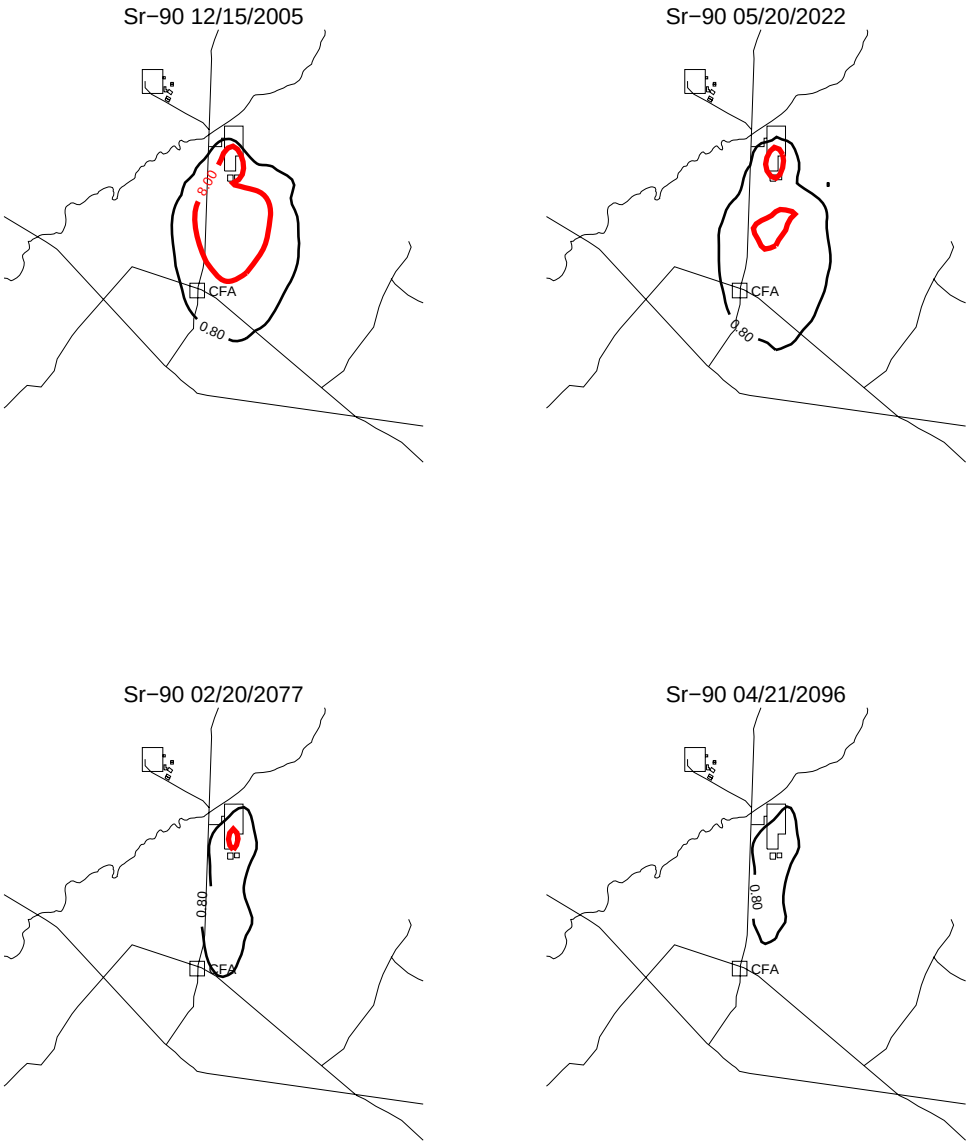

Figure J-11-57. Sr-90 aquifer concentration contours removing the production wells in 2096 (pCi/L) (MCL = thick red line, 10*MCL = thin red line, MCL/10 = black line).

Figure J-11-58. Sr-90 aquifer concentration contours removing the production wells in 2096 (pCi/L) (continued) (MCL = thick red line, 10*MCL = thin red line, MCL/10 = black line).

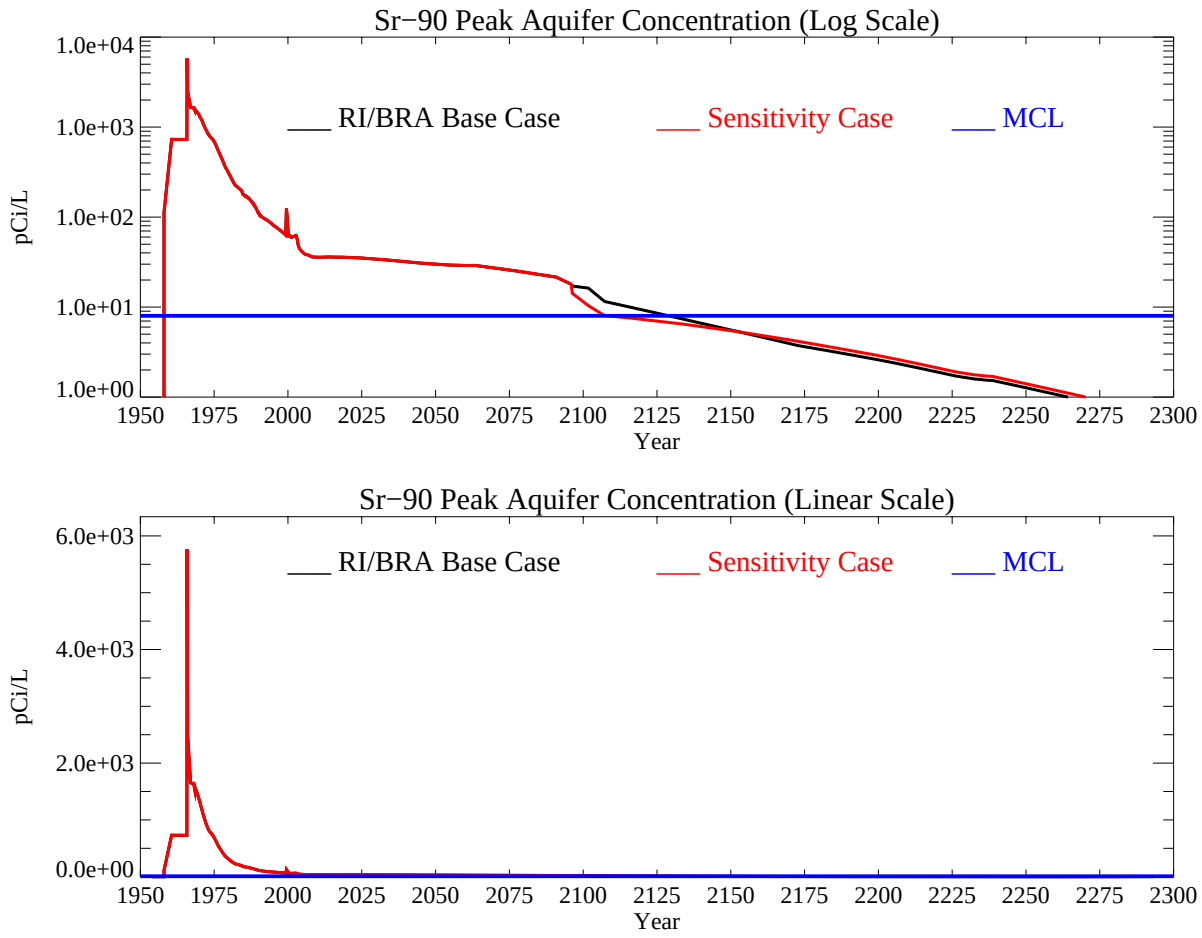

Figure J-11-59. Sr-90 peak aquifer concentrations removing the production wells in 2096 (pCi/L) with the MCL shown in blue, the RI/BRA model in black and this sensitivity run in red.

J-11.6 Larger Interbed Dispersivity

Dispersion is used to account for solute transport that occurs in addition to pure advection. In theory, it is the result of different flow velocities affecting the transport of solute particles moving through porous media. Assuming Fickian dispersion, this process will spread the solute in all directions. The amount of dispersion that occurs is a function of the heterogeneity of the media, the advective velocity, media porosity, water saturation, and concentration gradient. As a single measure, dispersivity tends to be a scale dependent phenomena with the magnitude on the order of 10% of the domain of interest in saturated groundwater systems, with decreasing dispersivity as the transport distance increases (Gelhar, 1986). In numerical models, advection and dispersion are accounted for through the implementation of the advective-dispersion transport equations. In addition, dispersion is introduced through spatial and temporal discretization. This later dispersion is model dependant, or dependant on the specific implementation incorporated in a given numerical code. As a result, a specific value for dispersivity has little actual meaning, but when incorporated into the simulation process, becomes a model fitting parameter. Fitting this parameter is done by first selecting a numerical model, gridding the system in time and in space, and by matching predicted concentration histories to measured field data for the transport of conservative (non-reacting) species. In other words, it becomes a calibration target.

The degree to which the final total model matches observed transport of Tc-99, H-3, and I-129 is a reflection of the complete calibration. In all of these cases, the observed perched water data was incomplete. Data was not collected early enough in time to capture the initial arrival of contaminants, the rise to peak concentrations, or the tailing off of the concentration history. A best-fit model was calibrated to those contaminants based on the available data. As a result, there is uncertainty in the derived model dispersivity.

The base grid vadose zone model used a 1 m longitudinal and 0.1 m transverse dispersivity. Larger dispersivity values can significantly affect peak aquifer concentrations for strongly sorbing and short lived contaminants such as Sr-90, where the bulk of the contaminant decays in the vadose zone because of sorption. The dispersive component increases the net transport, but reduces the aqueous phase concentration, and results in more of the contaminant being adsorbed on porous media. Although the dispersivity used in the RI/BRA model was derived for conservative tracers, looking at the sensitivity for Sr-90 is important. A larger dispersivity might allow lateral transport toward the MW-33-1 and MW-55-06 wells that are consistently being under predicted while dropping concentrations in wells that are consistently overpredicted nearer the tank farm. Transport sensitivity for Sr-90 to dispersivity in the vadose zone is evaluated here by increasing the longitudinal dispersivity to 15 m and increasing the transverse dispersivity to 1.5 m, values that are roughly 10% of the horizontal and vertical model dimensions.

J-11.6.1 Vadose Zone Sr-90 Simulation Results

Figures J-11-60 through J-11-63 illustrate the distribution of the Sr-90 in the vadose zone through the year 2293. The effect of increased dispersivity is very apparent in the contour plots presented for the vertical plain in years later than 2000. Increasing the dispersivity spreads the higher concentrations laterally above the 140 ft interbed. It affects sources in northern and southern INTEC, and allows the Sr-90 from both sources to merge in central INTEC.

Figure J-11-64 illustrates Sr-90 arrival in key perched water wells, and the comparison to field data is summarized for all of the perched water wells in Figure J-11-65. The subplots presented in Figure J-11-64 show that the model is better predicting concentrations in wells 33-1, MW-10-2, MW-18-1, MW-20-2, PW-2, PW-4, and USGS-50. Well 33-1 is just south of the tank farm, and the remainder of the better matches occur near the former percolation ponds. In the higher concentration wells near the tank farm, although increasing the dispersivity allows more lateral migration (needed to push the Sr-90 to the south and east), it also results in more adsorption and overall lower concentrations. The resulting effect is underpredicting concentrations in

those key wells. The plots of RMS suggest that the overall mean RMS in this sensitivity case is better (lower mean RMS) than in some of the other parameter sets appearing in the overall sensitivity study. If the average RMS value were biased toward the wells in which the highest concentrations occur (field data), the average RMS would actually be much higher and would indicate a poorer overall match in the 110 ft and 140 ft interbeds.

Peak vadose zone concentrations through time are given in Figure J-11-66 for this simulation by the red line. The dispersivity tends to damp the peak concentration response, but in general, the predicted peak concentration is not significantly different from the RI/BRA base case concentrations (black) throughout most of the time period.

The rate at which Sr-90 enters the aquifer is given by the red line in Figure J-11-67, and can be compared directly to the RI/BRA base case (black). It is interesting to note that increasing the dispersivity has resulted in significantly lower fluxes into the aquifer during the 2000-2200 time period.

Figure J-11-60. Sr-90 vadose zone concentration with increased dispersivity (horizontal contours) (pCi/L) (MCL=thick red line, 10*MCL = thin red line, MCL/10 = dotted line).

Figure J-11-61. Sr-90 vadose zone concentration with increased dispersivity (horizontal contours) (pCi/L) (MCL=thick red line, 10*MCL = thin red line, MCL/10 = dotted line).

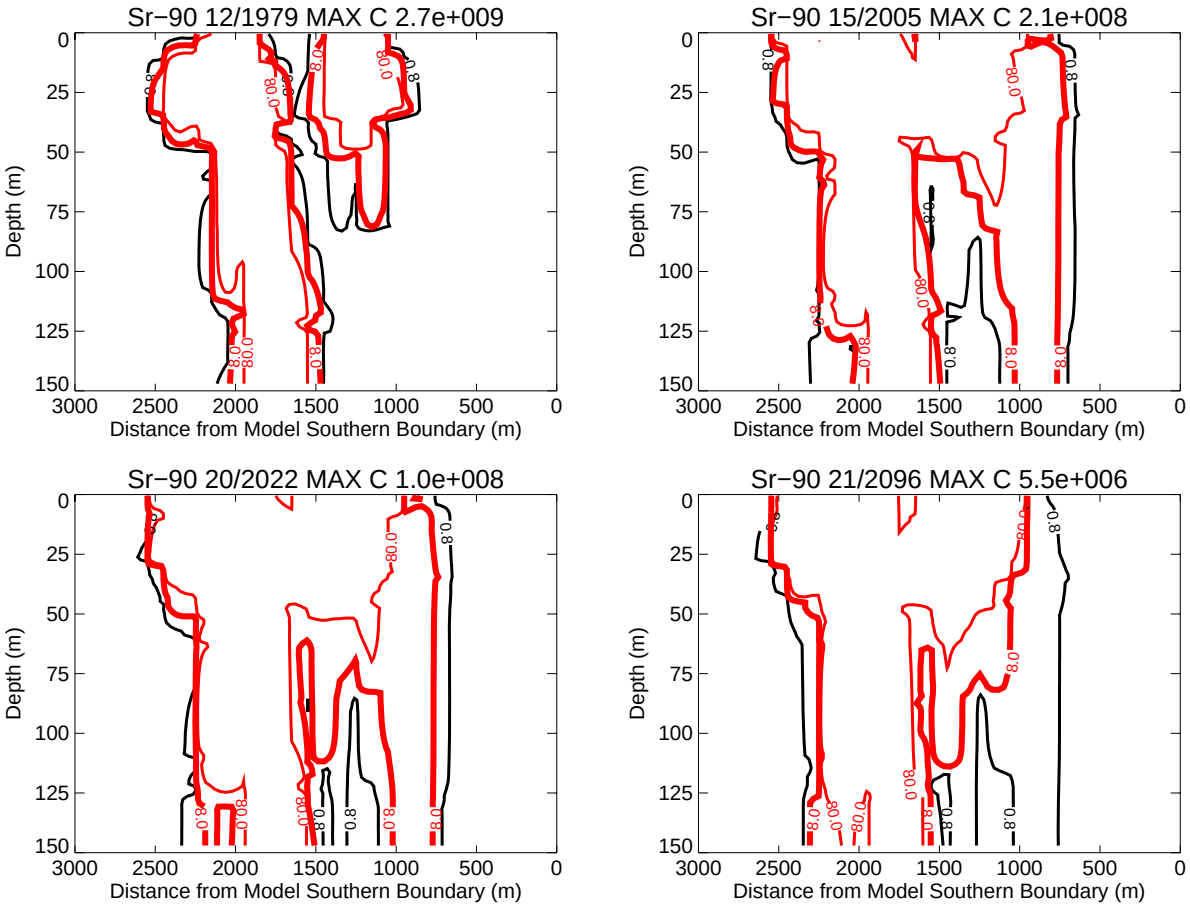

Figure J-11-62. Sr-90 vadose zone concentrations with increased dispersivity (vertical contours) (pCi/L) (MCL=thick red line, 10*MCL = thin red line, MCL/10 = dotted line).

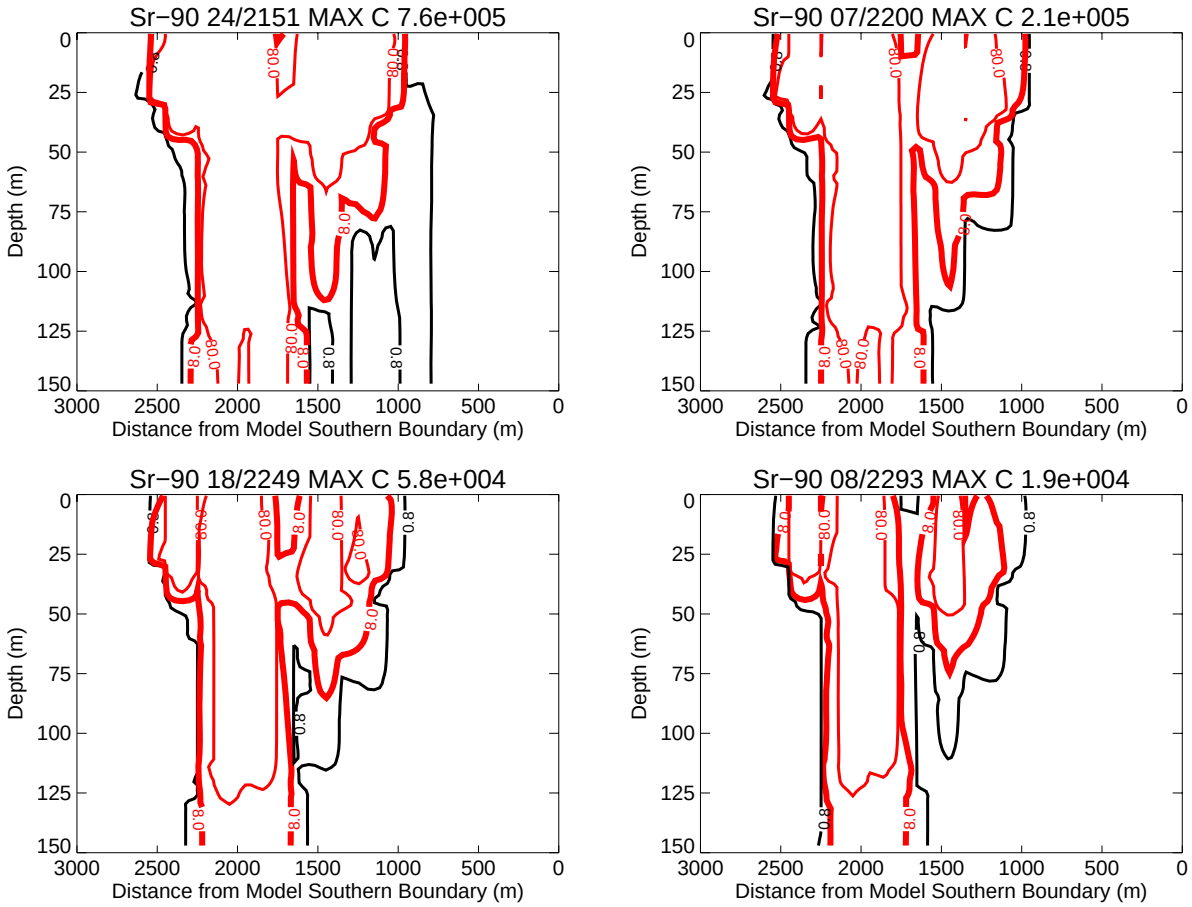

Figure J-11-63. Sr-90 vadose zone concentrations with increased dispersivity (vertical contours) (pCi/L) (continued) (MCL=thick red line, 10*MCL = thin red line, MCL/10 = dotted line).

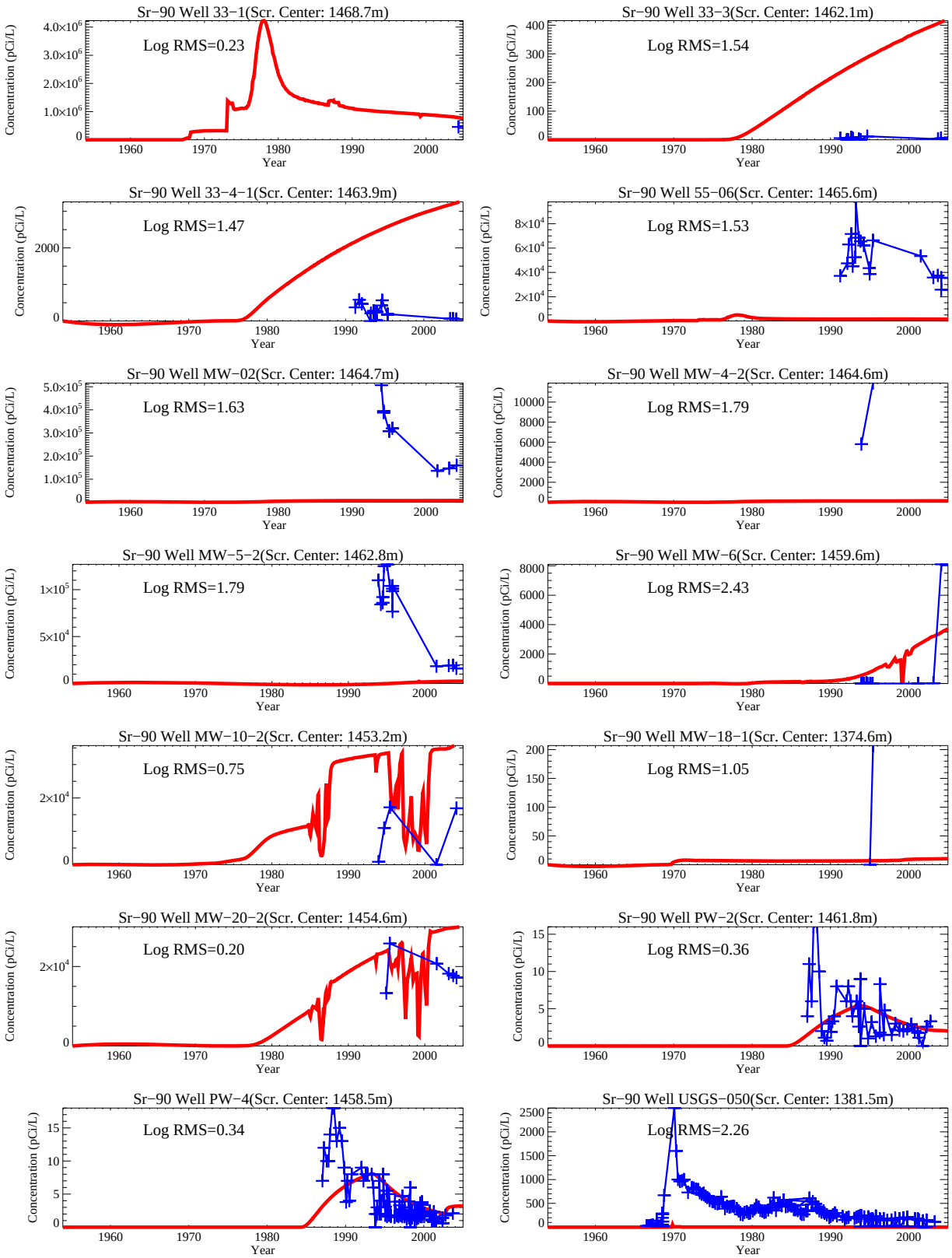

Figure J-11-64. Sr-90 concentration in perched water wells with increased dispersivity (pCi/L) (Measured values=blue crosses, Red=model at screen center).

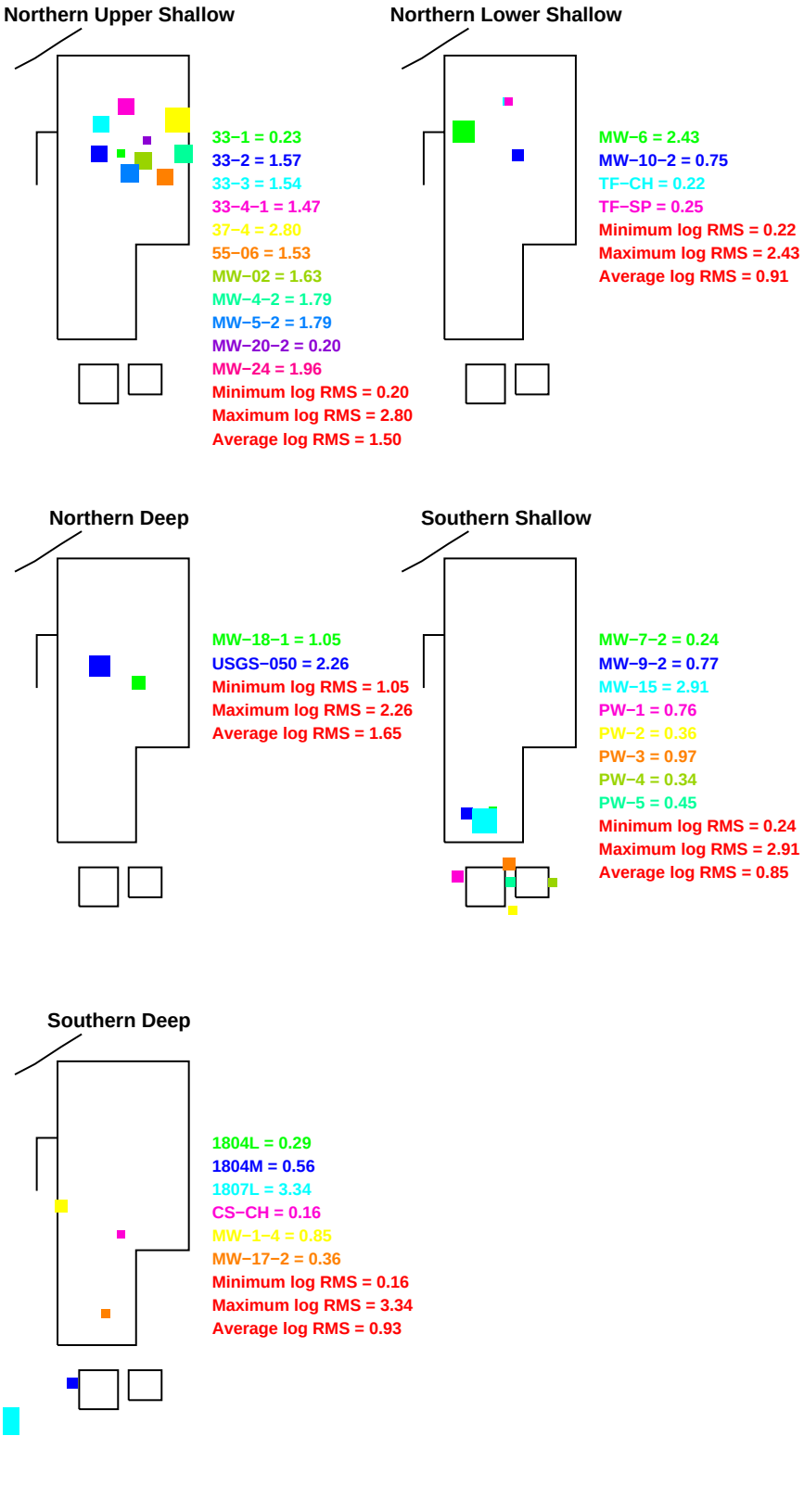

Figure J-11-65. Log 10 Root mean square error (RMS) by depth and northing with increased dispersivity.

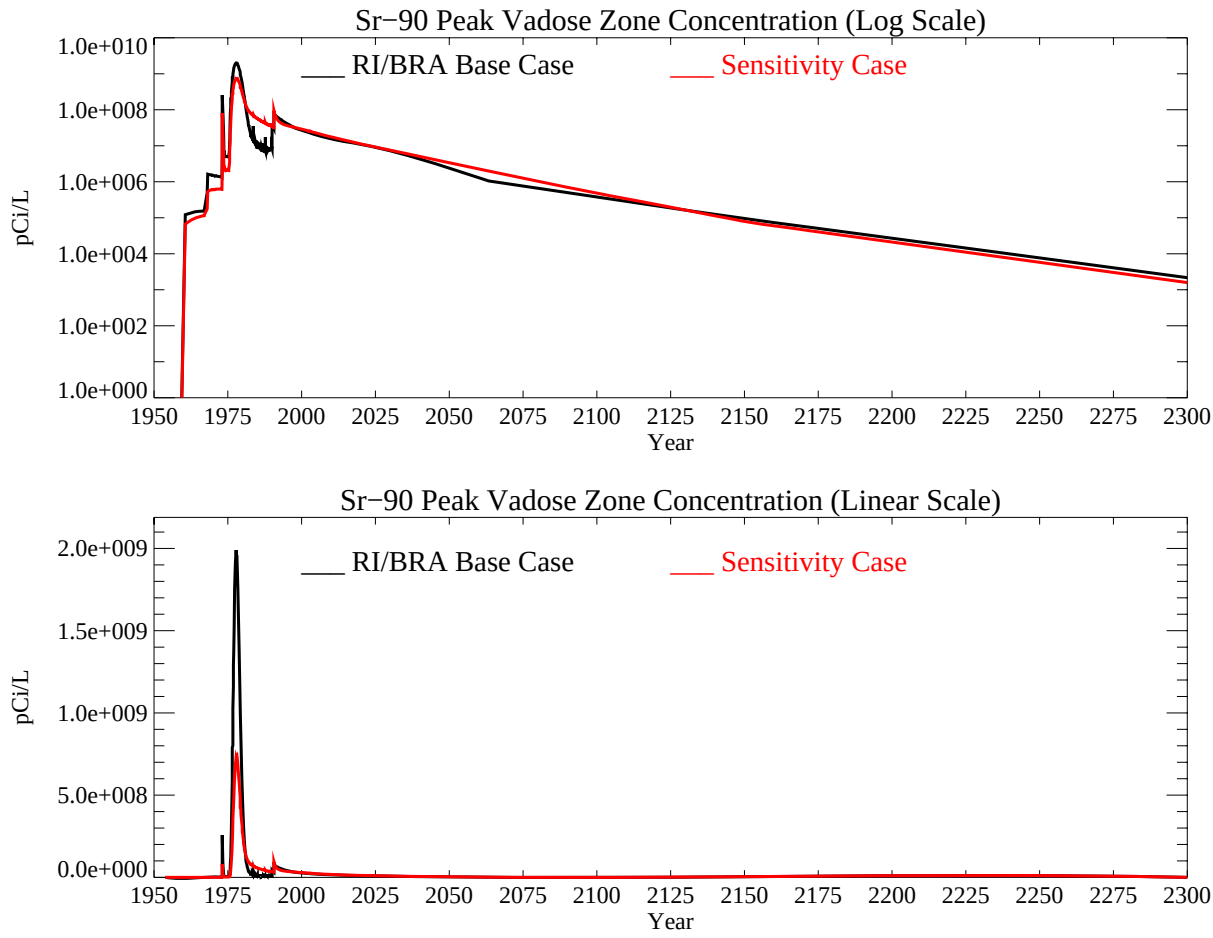

Figure J-11-66. Sr-90 peak vadose zone concentrations with increased dispersivity (pCi/L) The RI/BRA model is shown in black, and this sensitivity run in red.

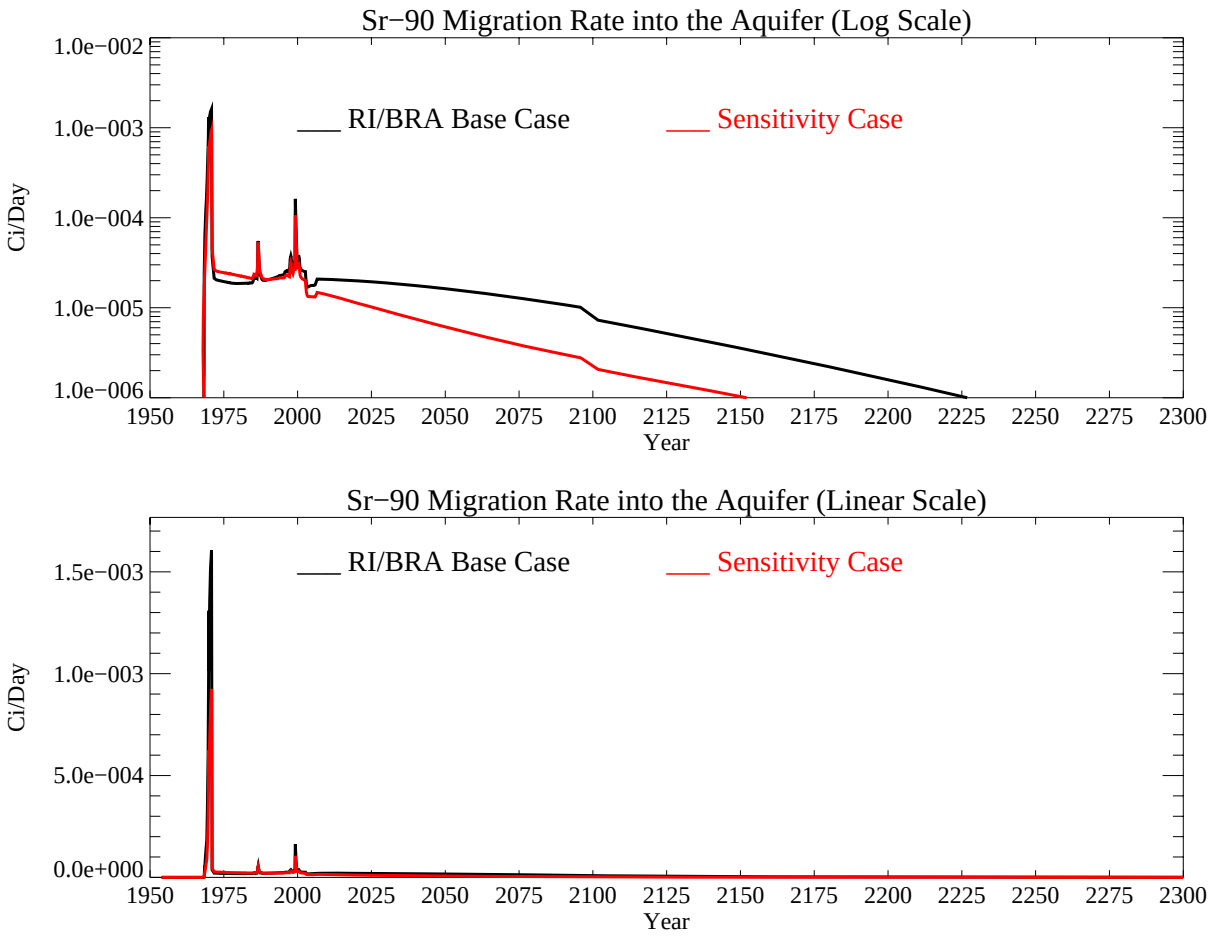

Figure J-11-67. Sr-90 activity flux into the aquifer with increased dispersivity (Ci/day). The RI/BRA model is shown in black, and this sensitivity run in red.

J-11.6.2 Aquifer Sr-90 Simulation Results

The distribution Sr-90 in the aquifer is given in Figures J-11-68 and J-11-69 contoured on the course and fine model grids, respectively. The area impacted by Sr-90 above the MCL is very similar to that predicted in the RI/BRA base case through year 2022. This area represents the long-term Sr-90 injection into the SRPA through the CPP-03 injection well. By year 2049, fluxes from the vadose zone arrive, and the decrease in flux rate is shown by the much smaller area enclosed by the 8 pCi/L contour line. As shown in Figure J-11-69, concentrations above the MCL are predicted to be between the former percolation ponds and the tank farm by year 2049.

The resultant peak aquifer concentrations are given in Figure J-11-70. With this increased dispersivity, the simulated Sr-90 concentrations are predicted to remain above the MCL from 1960 through year 2074. In year 2095, the predicted peak Sr-90 concentration is 4. pCi/L, about 21% of that predicted for the base case (18.6 pCi/L). During that period, the majority of the aquifer impact originates from direct injection rather than dispersive transport of Sr-90 from the tank farm.

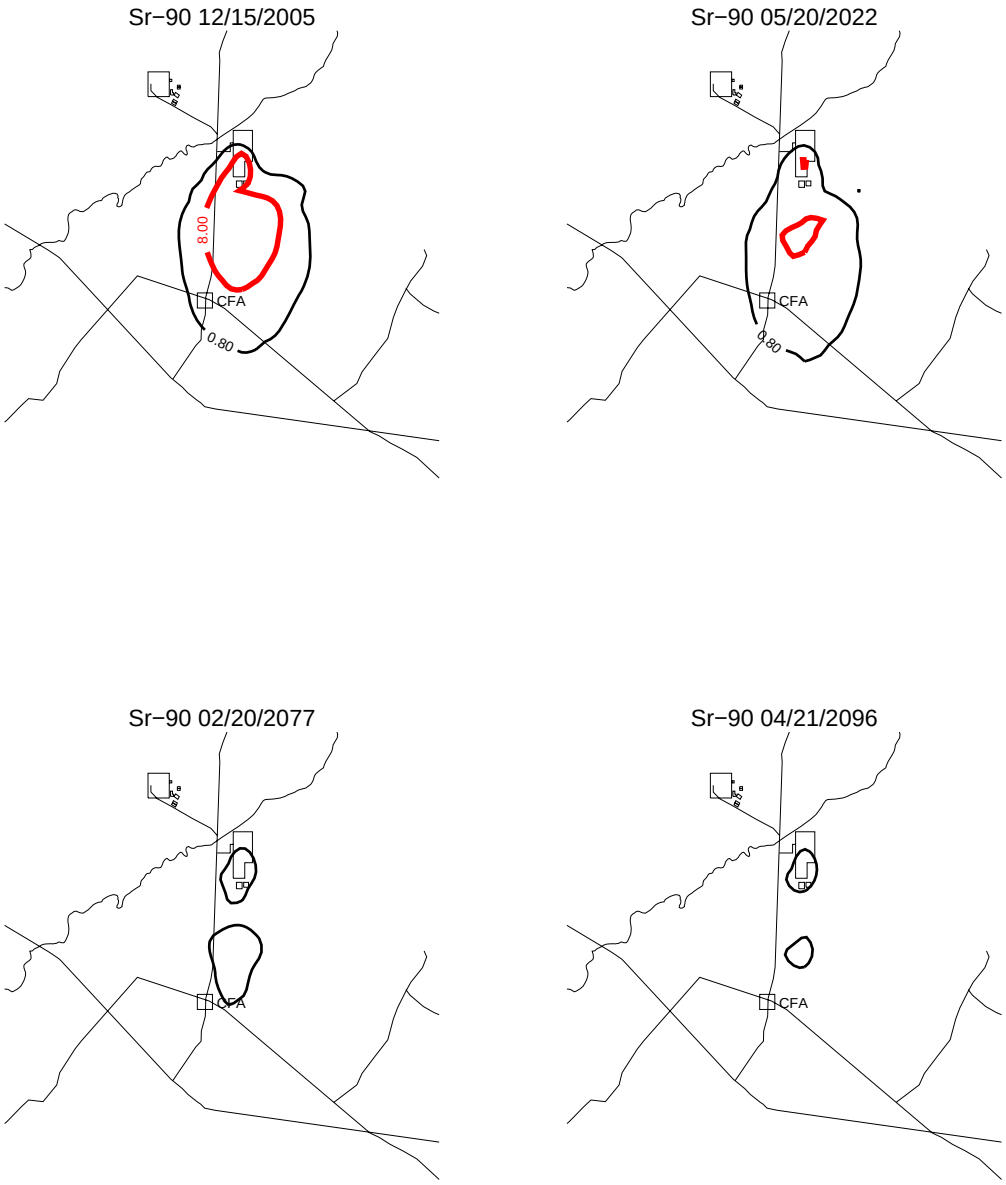

Figure J-11-68. Sr-90 aquifer concentration contours with increased dispersivity (pCi/L) (MCL=thick red line, 10*MCL = thin red line, MCL/10 = dotted line).

Figure J-11-69. Sr-90 aquifer concentration contours with increased dispersivity (pCi/L) (continued) (MCL=thick red line, 10*MCL = thin red line, MCL/10 = dotted line).

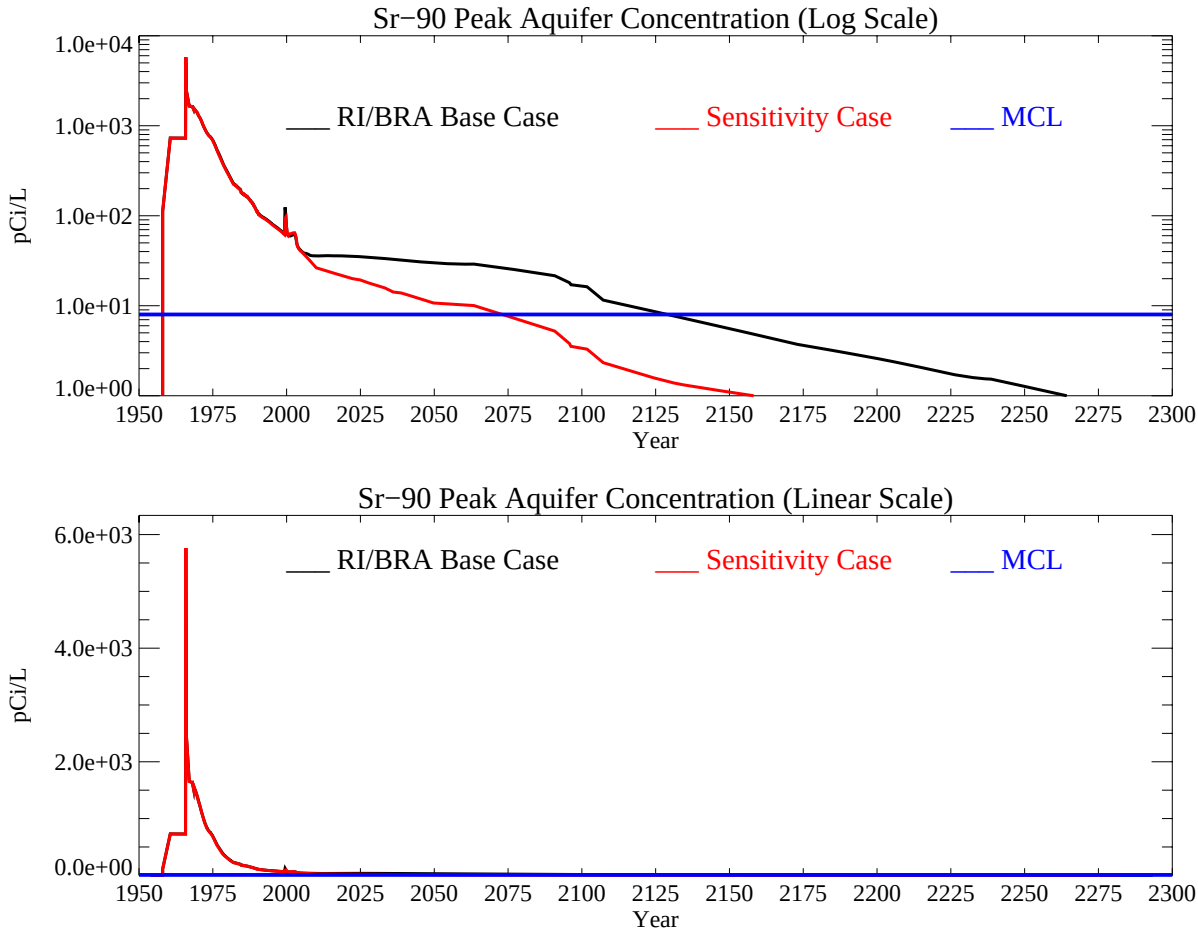

Figure J-11-70. Sr-90 peak aquifer concentrations with increased dispersivity (pCi/L) The MCL is shown in blue, the RI/BRA model in black, and this sensitivity run in red.

J-11.7 Summary of Sensitivity to Hydrologic Parameters

Under the hydrologic conditions examined in this sensitivity analysis, the geochemical processes observed in the one-dimensional model were preserved. We saw that in all cases, a fraction of the strontium moves relatively rapidly through the alluvium either complexed with nitrate ion, or because of inhibition of adsorption as a result of competition with elevated sodium and calcium concentrations in solution. The relative abundance of sodium and calcium are influenced by the saturation initially in the pore space of the alluvium and by the recharge rates through the alluvium. Once the sodium-bearing waste peak has passed through the alluvium, the remaining strontium on the ion exchange sites is released much more slowly. Within the parameters spanned here, the sodium-bearing waste pulse leaves the alluvium between 5 and 10 years after release (Table J-11-1).

In the RI/BRA base case, assuming an infiltration rate of 18 cm/yr, 12,336 Ci of Sr-90 were released within the first 10 years. In the case where the infiltration rate was increased to 39 cm/yr the HCO_3 became more abundant. This buffers the pH, reducing the amount of Sr-90 contained in the initial fast release from the alluvium. Increasing the infiltration rate dilutes the raffinate, resulting in less competition and complexing. Decreasing the infiltration rate increases the aqueous phase Sr^+ ion, which increases the amount of Sr-90 in that initial release, but it takes a little longer. Over the range of infiltration and wetting conditions representative of the tank farm liner and alluvium properties, there was considerable sensitivity in the amount of Sr-90 predicted to leave the alluvium within the first 10 years. At a low infiltration rate of 3 cm/yr, the Sr-90 leaving the alluvium at 10 years was predicted to be 7,243 Ci, while at 18 cm/yr and 39 cm/yr, the first released activity was 12,272 Ci and 5,536 Ci, respectively. This 6,736 Ci range produced a remarkably small difference in predicted 2095 peak aquifer concentrations. The relative insensitivity of aquifer concentrations to a seemingly large change in activity leaving the alluvium is due to the coupled hydrogeochemical processes, and is dominated by the fact that the Sr-90 arriving in the aquifer is transported via dispersion as opposed to pure advection.

This system is very sensitive to large changes in infiltration rate that result when it is assumed most of the anthropogenic water is released in northern INTEC. If the infiltration rate is on the order of 116 cm/yr in the regions outside of the tank farm, the six fold increase in infiltration rate increases peak aquifer concentrations by a factor of 18.4 Relatively large increases in infiltration rates produce higher saturations in the upper shallow and upper deep interbeds underlying northern INTEC. This increased the lateral spreading of contaminants, and also increases the vertical velocities. The 116 cm/yr corresponded to 52 million gallons/yr added to an infiltration rate from precipitation of 18 cm/yr. For comparison, the Big Lost River contributes on the order of 1.9 m/yr per meter of river length and its influence is apparent in all of the time-history plots of peak aquifer concentration. Although Sr-90 concentrations at INTEC are sensitive to high flux rates, removing a distributed water source had very little effect on predicted concentrations. When the anthropogenic water was assumed to be distributed throughout INTEC, stopping the water losses in year 2035 decreased concentrations in year 2095 by only 35%. The relatively small gain resulting in this case is attributable to the large difference between anthropogenic water losses and infiltration from precipitation. If it is assumed that the anthropogenic water is distributed throughout INTEC, as opposed to being focused in northern INTEC, precipitation is the dominant source of infiltration.

Predicted Sr-90 concentrations are sensitive to the assumed land-use scenario. If the production wells (CPP-1 and CPP-2) are removed from the influence of INTEC natural attenuation in central INTEC increases. At the same time concentrations are predicted to increase in northern INTEC. Increases occur in northern INTEC because when the production wells are in use the two production wells increase dispersion. There is some evidence that the two production wells also remove contaminants from the aquifer as a result of pumping. Contaminant sampling supports the latter observation (ICP 2004), and the relatively flat head gradient in central INTEC supports the former observation. Although predicted concentrations are sensitive to the presence of the production wells, they are not sensitive to their time of removal. The insensitivity is caused by continued arrival of Sr-90 from the vadose zone being larger than the natural attenuation processes in the aquifer.

Table J-11-1. Hydrologic parametric sensitivity summary. All Sr-90 activities are undecayed.

	Infiltration Rate (cm/yr)			Anthropogenic Water					Dispersivity
	I=39	**I=18**	**I=3**	**Focused in Northern INTEC**	**Losses Stopped in 2035**	**Pumping Stopped in 2012**	**Pumping Stopped in 2035**	**Pumping Stopped in 2096**	**10% of domain**
Alluvium Statistics									
Years after CPP-31	**Activity Leaving Alluvium (Ci)**								
5 yrs	1575	5187	1342	5187	5187	5187	5187	5187	5187
10 yrs	5536	12272	7243	12272	12272	12272	12272	12272	12272
15 yrs	5558	12310	7845	12310	12310	12310	12310	12310	12310
20 yrs	5580	12336	8037	12336	12336	12336	12336	12336	12336
Activity Remaining in Alluvium (Ci)	10320	3564	7863	3564	3564	3564	3564	3564	3564
Effective K_d (mL/g) at 20 years	13	2	6.4	2	2	2	2	2	2
Vadose Zone Statistics									
Peak Concentration (pCi/L)	3.0E9	2.0E9	1.9E9	4.0E8	2.0E9	2.0E9	2.0E9	2.0E9	7.3E8
Year Peaked	1979	1979	1978	1978	1978	1978	1978	1978	1978
Aquifer Statistics									
Peak Concentration (pCi/L) in 2095	27.3	18.6	8.9	343.0	12.0	11.9	11.9	18.6	4.0
Year C is below 8 pCi/L	2148	2129	2099	2214	2121	2108	2107	2108	2074

shaded cells = RI/BRA base case

J-12 VADOSE ZONE AND AQUIFER CALIBRATION

This section presents the aquifer and vadose zone calibration results. As observed in the RI/BRA simulations, the impact of varying the geochemical and hydrologic parameters on aquifer calibration is minimal. This insensitivity is due to the fact that Sr-90 in the SRPA prior to year 1990 is largely a result of the injection well (CPP-03), and its failure. The relatively small amount of Sr-90 arriving in the aquifer prior to 2005 (where we have field data) from land surface sources does not influence aquifer calibration. On the other hand, calibration to perched water is sensitive to the hydrogeochemical parameterization in both the alluvium and interbeds. The calibration to observed Sr-90 in aquifer wells is presented first, followed by the detailed discussion of vadose zone perched water calibration.

J-12.1 Aquifer Calibration Results

The primary source of Sr-90 was associated with the tank farm releases, with 18,100 Ci released in the tank farm, and 24.3 Ci discharged in the CPP-03 injection well. Field observations of Sr-90 in the aquifer are a direct result of the CPP-03 injection. Because of the retardation of Sr-90 in the vadose zone, most of the Sr-90 released in the tank farm will never reach the aquifer. The amount that has been predicted to reach the aquifer from surface sources is on the order of 1% of the amount injected in CPP-3. The disposal history for Sr-90 in the CPP-3 injection well is fairly complete as illustrated in Figure J-12-1. The raw data (Figure J-12-1 top) for releases were smoothed (Figure J-12-1 bottom) using an averaging process to facilitate incorporation into the numerical model.

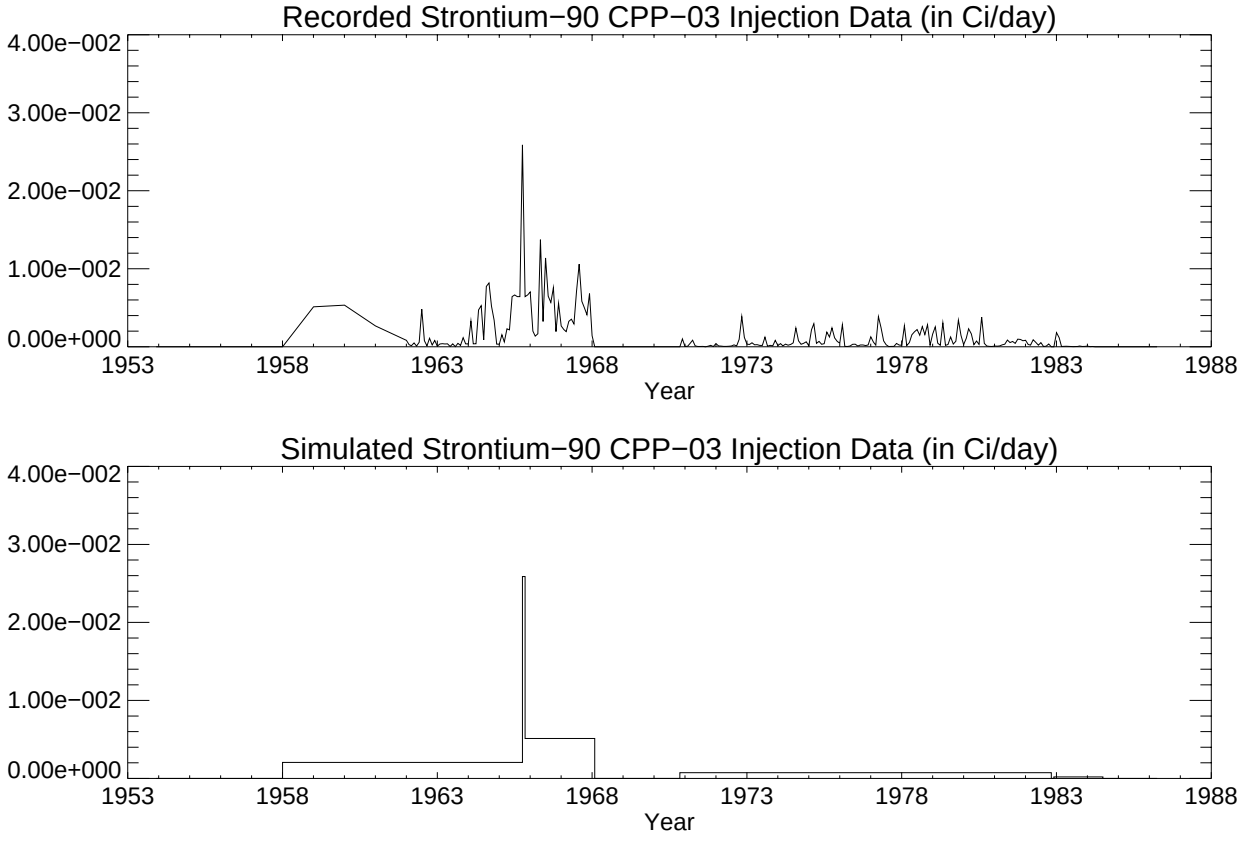

Figure J-12-1. Reported (top) and simulated (bottom) strontium-90 disposal in CPP-03 (Ci/day).

Matching the Sr-90 concentration history in the aquifer required adjusting the sorption coefficients in the aquifer materials. The best match between the arrival of discernible peaks and their concentrations were obtained by using a retardation factor of 4 for the basalt, corresponding to a K_d of 0.035 mL/g, and an H-I interbed K_d of 22 mL/g (from Appendix D).

Within the aquifer, Sr-90 has been monitored more frequently than contaminants with the exception of tritium. This data indicates that Sr-90 had traveled south as far as USGS-112 in the late 1980s. Predicted aquifer concentrations matching the southern extent are shown in Figure J-12-2. The model results shown in Figure J-12-2, are a simplification of the 3-dimensional concentrations predicted for the aquifer. To represent higher dimensional results in plan view, we have chosen the highest 15 m average concentration at any planar coordinate. This depth interval does not, in general, correspond to any particular well screen location, but does represent the highest pumpable concentration.

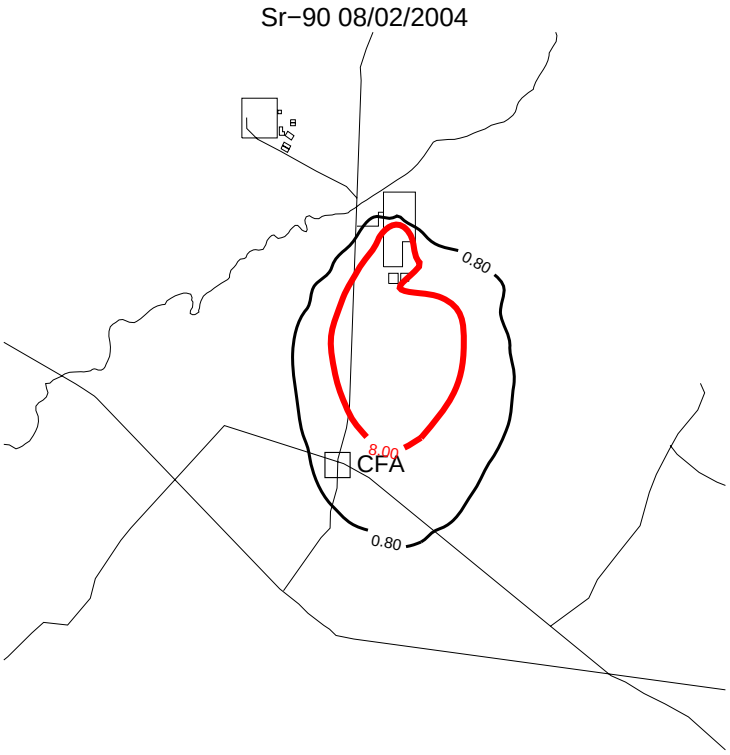

(a)

Figure J-12-2. Maximum simulated Sr-90 concentrations (pCi/L) on the base grid averaged over a 15m well screen in 2004 for the RI./BRA base case.

A 15 m well screen was chosen to represent peak concentrations throughout this analysis to account for real pumping effects. Concentrations representing the average are fairly insensitive to the assumed screened length prior to the arrival of Sr-90 in significant quantities from the vadose zone. This is largely due to Sr-90 currently in the aquifer being injected through a very large screened interval. The large screened interval distributes Sr-90 relatively uniformly over the vertical as shown in Figure J-12-3 for the ICPP-179x series wells located between the INTEC and the CFA. As shown by the 2003 data (asterisks) the vertically distributed range is small, and as shown by the RI/BRA model results (solid line), the predicted concentrations are also fairly uniform over the vertical.

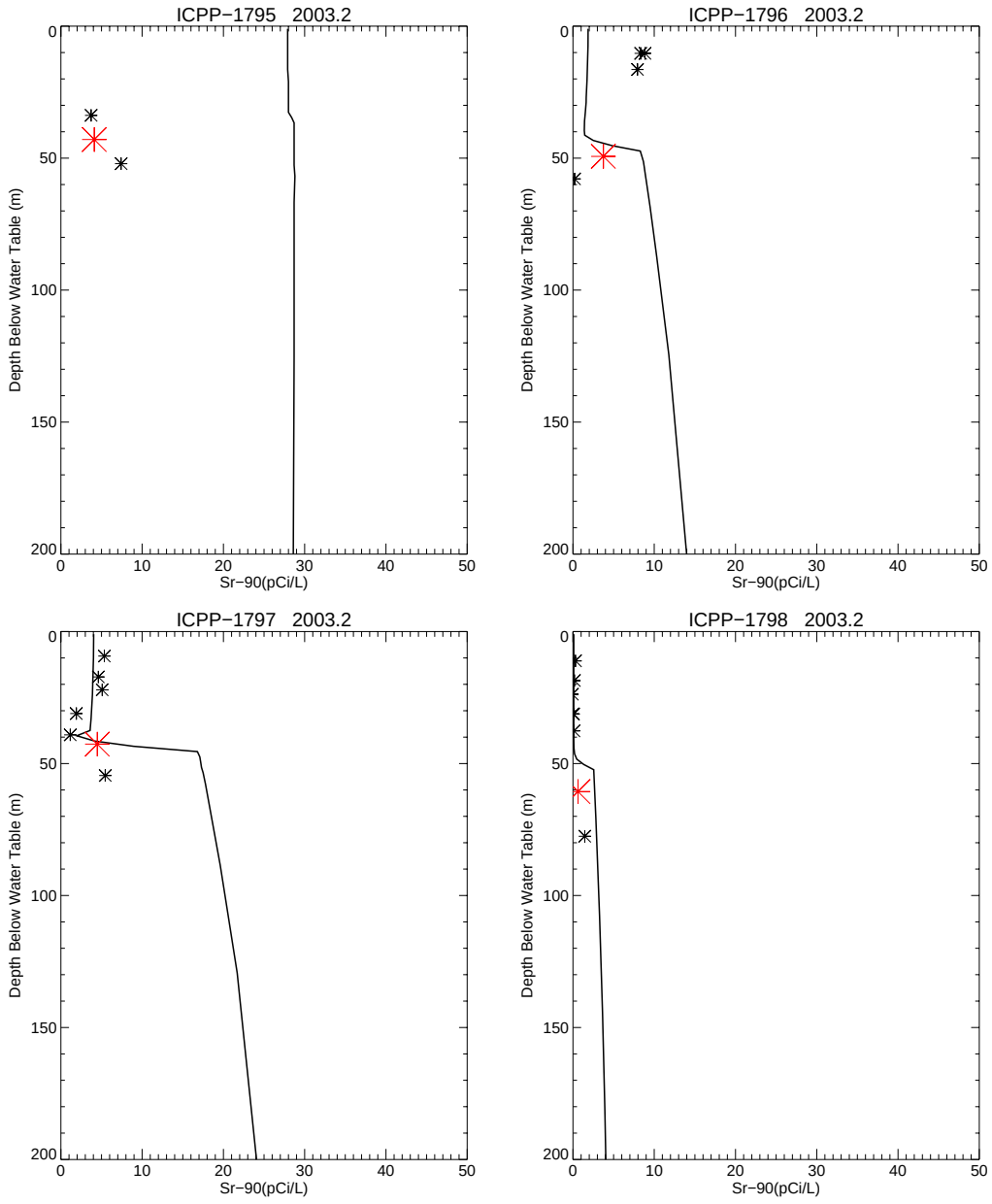

Figure J-12-3. Simulated and observed Sr-90 concentrations vs. depth in 2003 (simulated data using 15 m average=solid line, small asterisk=data taken in basalt, large red asterisk=data taken in the HI interbed, pCi/L).

Concentration histories for aquifer wells are given in Figures J-12-4 through J-12-8. A well -by-well comparison shows that although sampling was extensive, there are a large number of wells in which data collection did not begin until the mid 1980's. The presentation of these wells is sorted by distance from the CPP-03 with wells nearer CPP-03 presented first and wells closer to CFA presented last. The simulated concentrations plotted on these figures corresponds to the RI/BRA model.

In general, the timing and magnitude of predicted Sr-90 concentrations match the further wells quite well. On the other hand, the predicted arrival of peak concentrations in wells closer to INTEC occurs earlier than observed in the data, and predicted concentrations are too high. This disparity suggests that either there are two regions of velocity or there are two distinct regions of adsorption occurring in the aquifer. It is likely that a combination of both occurs, and that the combination is a function of the chemistry of the fluids injected with the Sr-90. The aquifer model assumes a uniform K_d throughout the aquifer domain, and does not account for potential changes in water chemistry as the injectate migrates down gradient from the injection well. It is possible that, like in the vadose zone, there are gradations in retardation in the aquifer as the sodium bearing injectate is diluted.

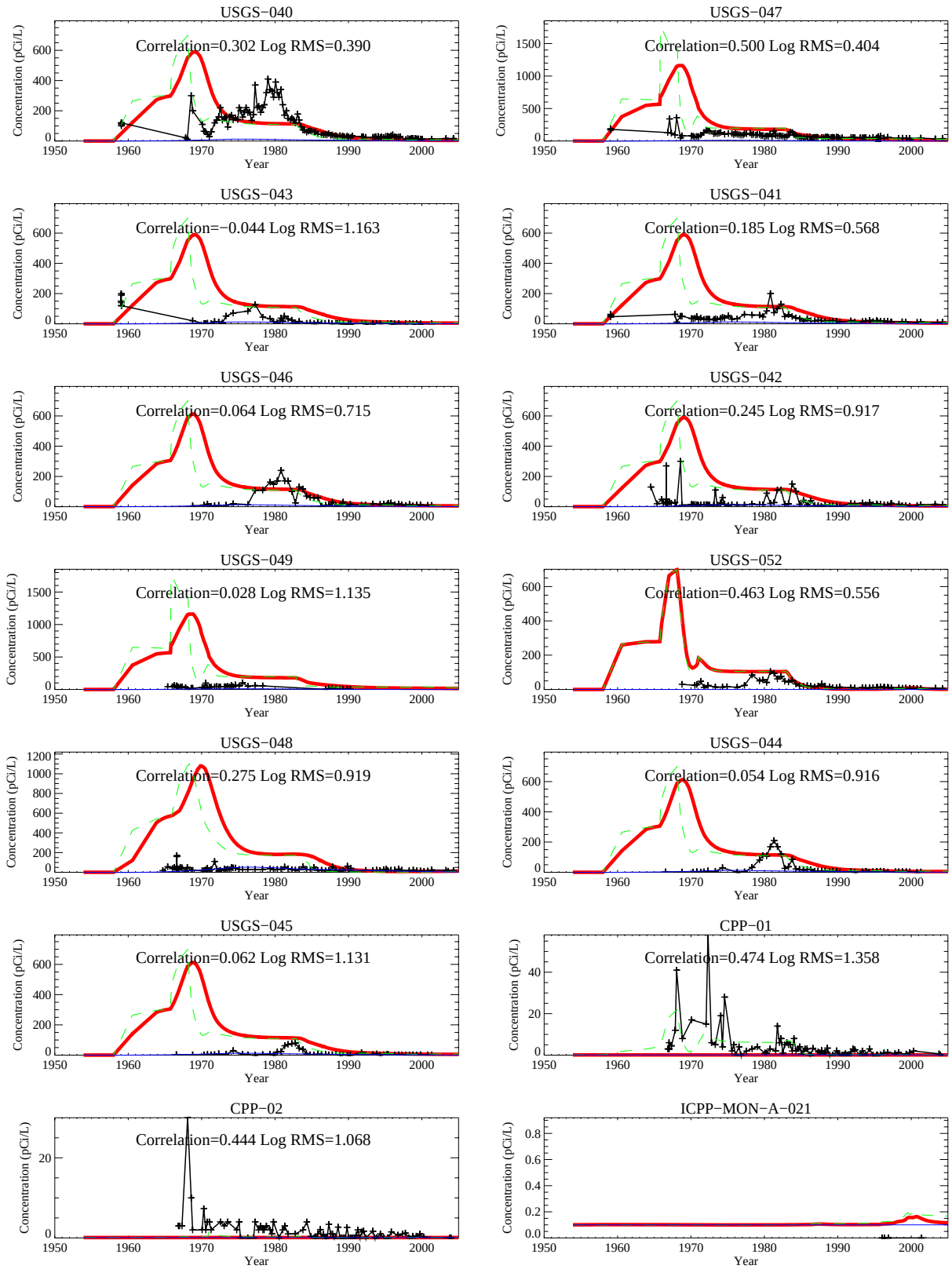

Figure J-12-4. Simulated and observed Sr-90 concentration histories (pCi/L) (measured=black crosses, thick red=model at screen center, dashed green=model top, blue=model bottom).

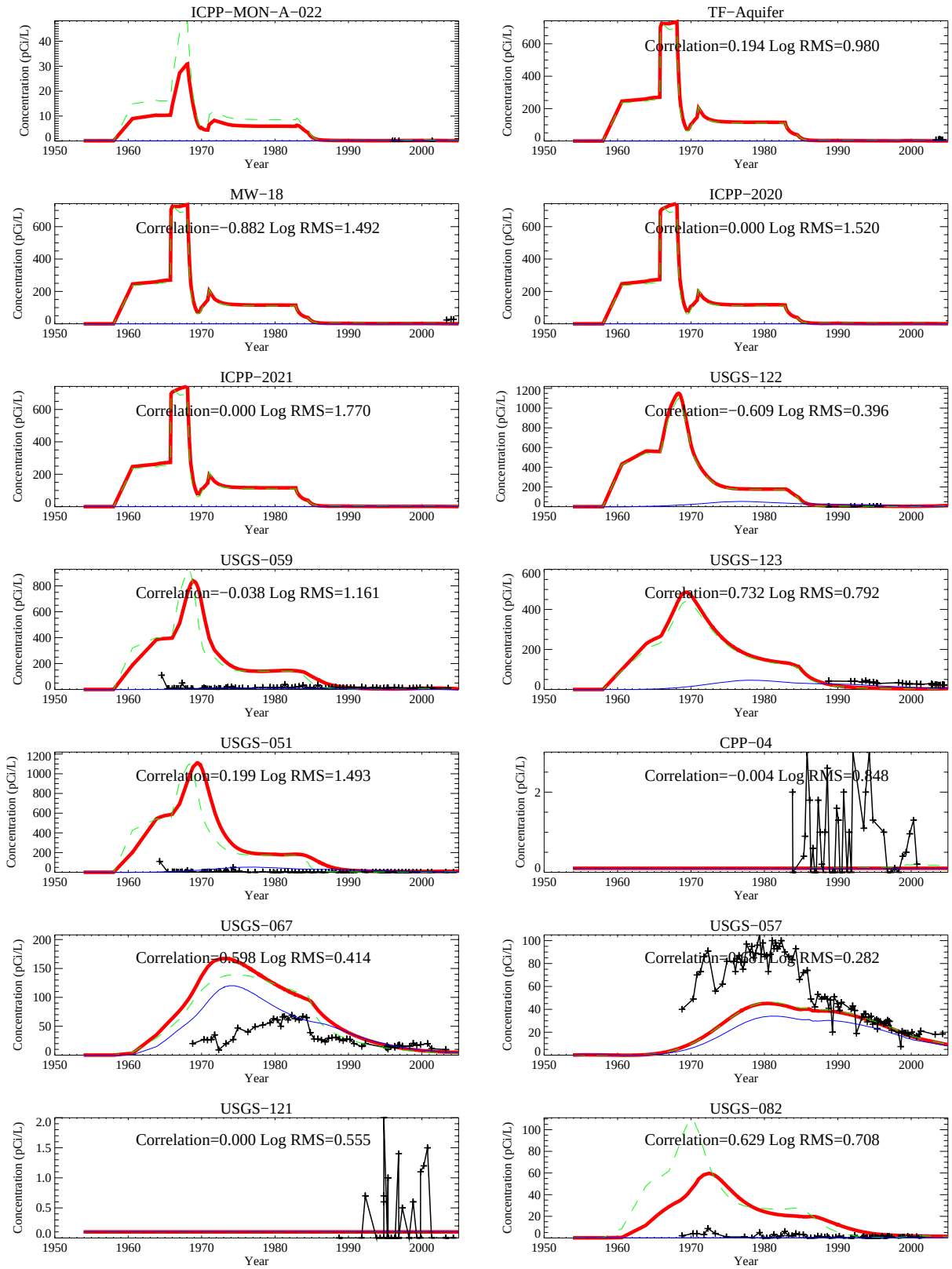

Figure J-12-5. Simulated and observed Sr-90 concentration histories (pCi/L) (measured=black crosses, thick red=model at screen center, dashed green=model top, blue=model bottom).

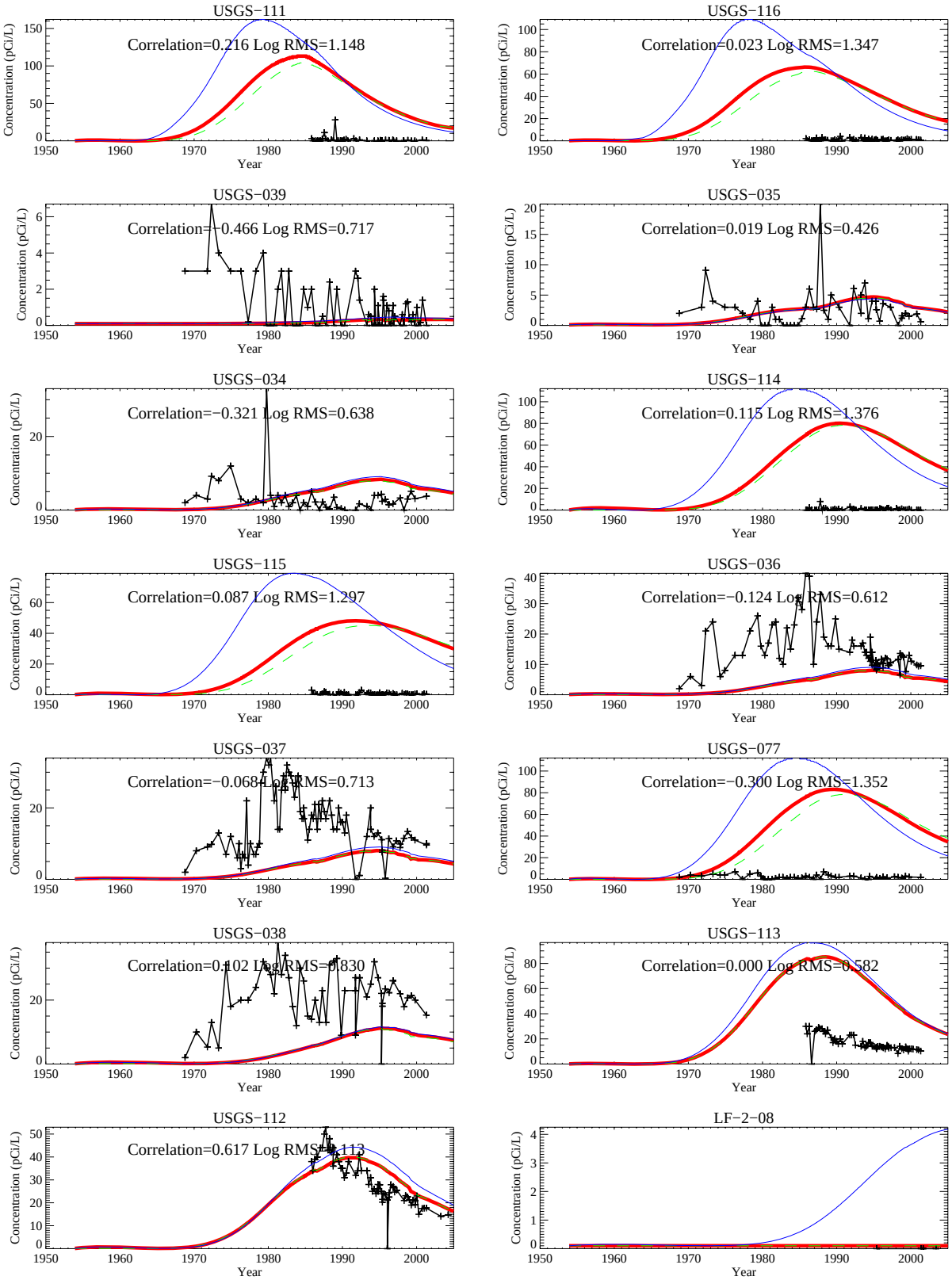

Figure J-12-6. Simulated and observed Sr-90 concentration histories (pCi/L) (measured=black crosses, thick red=model at screen center, dashed green=model top, blue=model bottom).

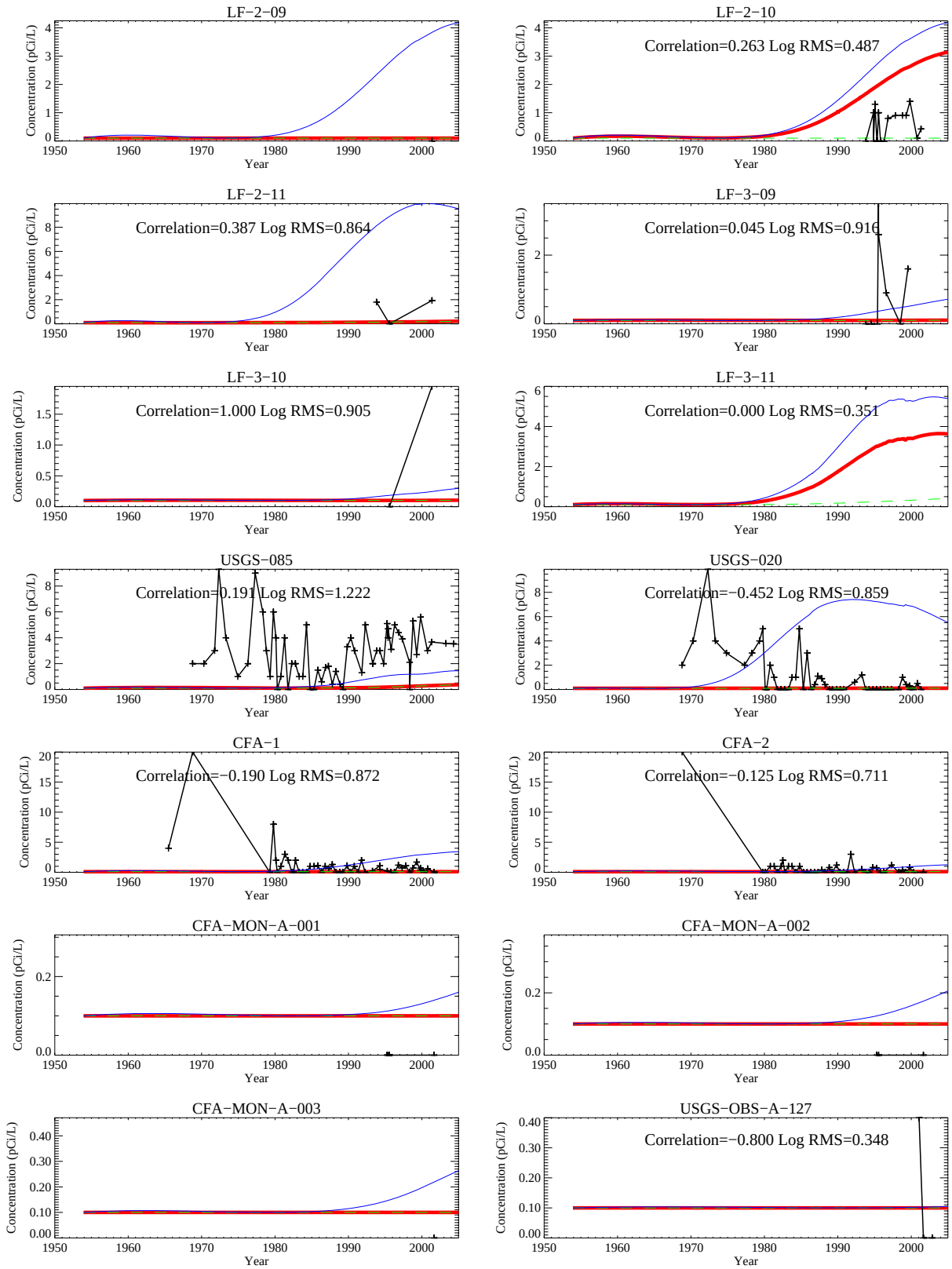

Figure J-12-7. Simulated and observed Sr-90 concentration histories (pCi/L) (measured=black crosses, thick red=model at screen center, dashed green=model top, blue=model bottom).

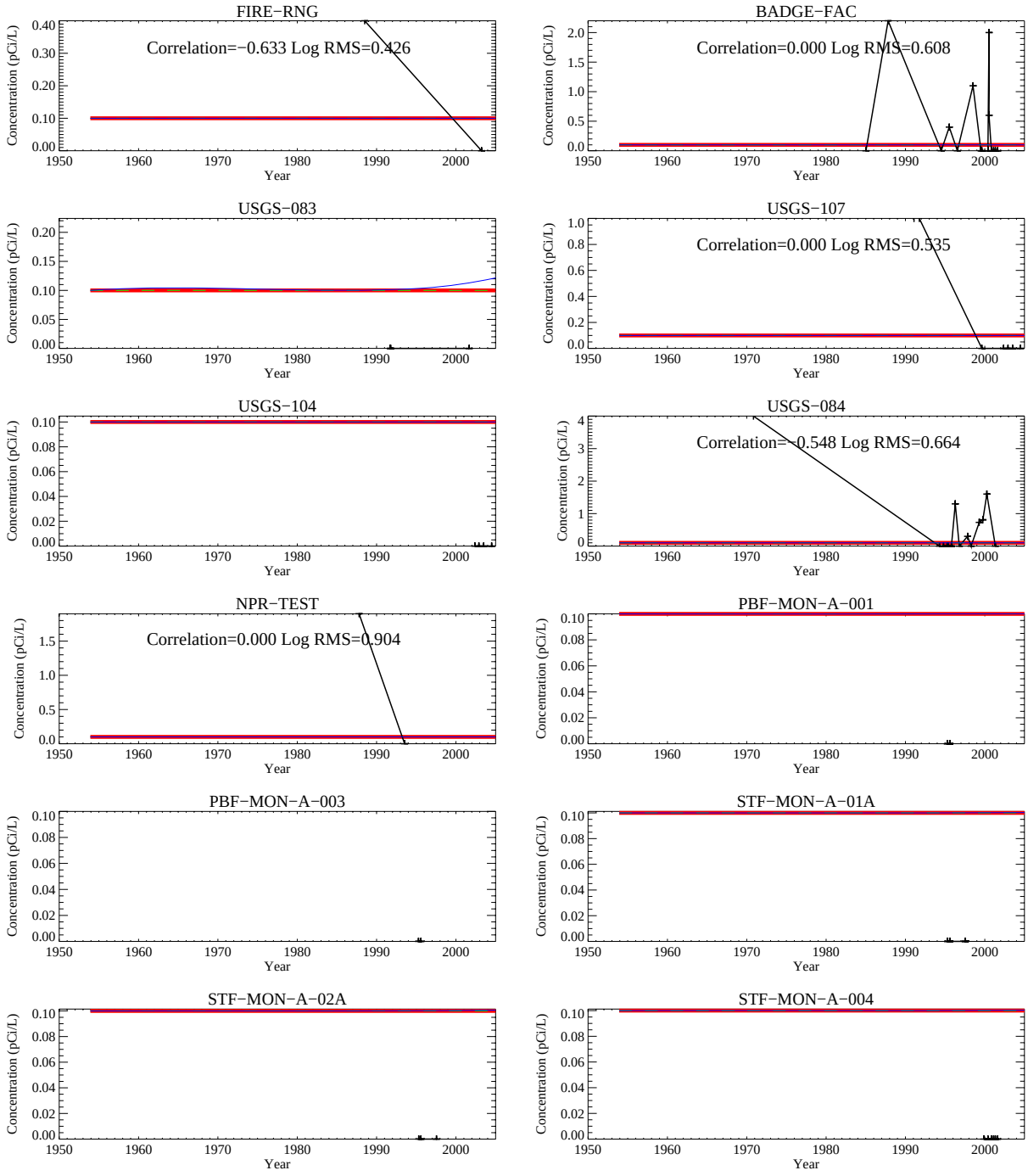

Figure J-12-8. Simulated and observed Sr-90 concentration histories (pCi/L) (measured=black crosses, thick red=model at screen center, dashed green=model top, blue=model bottom).

J-12.2 Vadose Zone Calibration Results For The RI/BRA MODEL

There are five primary regions of perched water that are considered in vadose zone calibration. These are the 1) northern upper shallow, 2) northern lower shallow, 3) northern deep, 4) southern shallow, and 5) southern deep perched waters. Each of these is influenced differently by the sources of Sr-90 contributing to their contamination, and by the hydrogeochemical parameters used in the model. The effect of model parameterization is discussed for each zone below.

J-12.2.1 Northern Upper Shallow Perched Water Sr-90

Data for the upper shallow perched water wells is presented in Figure J-12-9. In general, the data were collected well after Sr-90 initially arrived in this water body, and in many wells, the data only captures a small segment of the contaminated period. In only one well is a relatively complete concentration history available. This better data set was obtained for the CPP-55-06 well, where concentrations were fairly high.The key points to note in the available data include:

- High concentrations (above 10,000 pCi/L) have been observed in CPP-33-1, MW-5-2, MW-2, and MW-4-2. These wells are close to the tank farm with the exception of MW-5-2 which is further west and south. The highest concentration (458,000 pCi/L) was observed in 2004 in CPP-33-1, but only one data point is available in that well. Concentrations in MW-5-2 were near 100,000 pCi/L during the 1993-1995 time period, but have been below 20,000 pCi/L since 2001. Concentrations in Well MW-2 have followed a similar pattern to those in Well MW-5-2 and were measured at 514,000 pCi/L in 1993 and at 160,000 pCi/L in 2004. Sr-90 in Well MW-4-2 is also high and was measured at 5,800 and 11,900 pCi/L in 1993 and 1995, respectively.
- The other northern upper shallow perched water Sr-90 concentrations have been near or below 10 pCi/L except one measurement at well MW-6 in 2004 at 8,100 pCi/L. The previous observations dating back to 1993 were near 10 pCi/L.

The Sr-90 concentrations in the upper shallow perched water may be declining and peak concentrations in many of these wells may have occurred prior to 1995. Sr-90 concentrations in this region are declining more rapidly than would be predicted by radioactive decay alone, suggesting an active advective or dispersive flow component. Based on one measurement, concentrations in CPP-33-1 might be an exception.

The RI/BRA model predicted (red line) and observed (blue asterisk and line) Sr-90 concentrations for the northern upper shallow perched water wells are illustrated in Figure J-12-9. In general, the model agrees with the observed patterns of Sr-90 concentrations, but it tends to over predict the values observed in wells north and west of the tank farm, but under predicts the values south and east of the tank farm. It predicts that the highest simulated concentrations occur beneath the tank farm and immediately south and east of the tank farm. Overpredicting concentrations suggests that the model is overestimating north and west lateral water movement within and above the first interbed and underestimating lateral movement to the south and east.

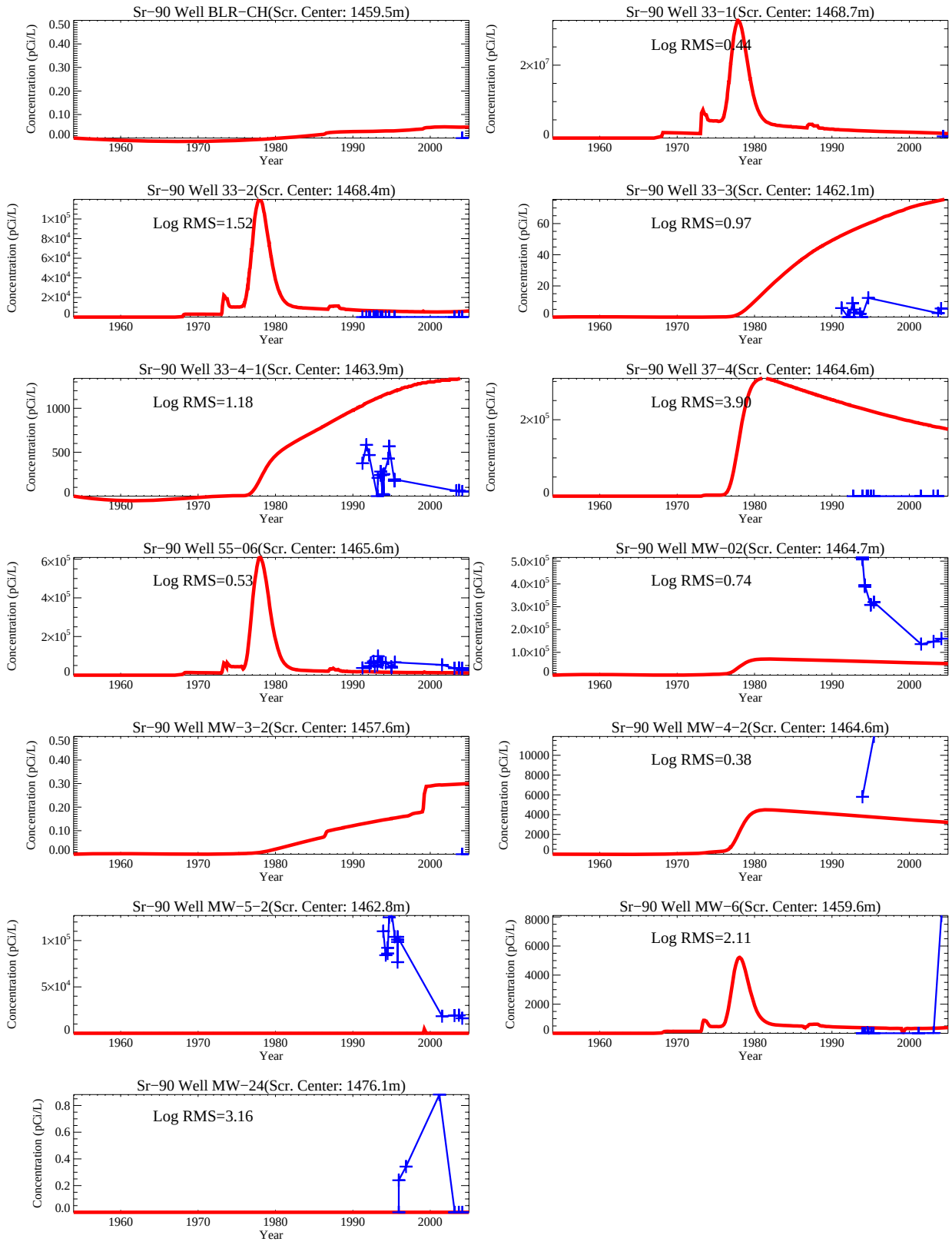

Figure J-12-9. Comparison of model predictions to field data for Sr-90 in the northern upper shallow perched water (red = predicted, blue = field data).

J-12.2.2 Northern Lower Shallow Perched Water Sr-90

In Figure J-12-10, data for wells in the northern lower shallow perched water are shown in blue. These figures show that wells within this region have not provided sufficient concentration-time data to assess whether the peak concentrations have been reached. Declining Sr-90 concentrations observed in the northern upper shallow perched water would suggest that the northern lower shallow perched water concentrations should be increasing -- reflecting the arrival of Sr-90 from the upper region. Available data in this lower region is sparse, and overall interpretation is uncertain. The key observations include:

- Declining concentrations have been observed in MW-20-2. The highest concentration (25,800 pCi/L) in this region was found in this well in 1995 has fallen to 21,224 pCi/L as of 2004.
- The concentration history in MW-10-2 is highly variable. Measured concentrations have ranged from 17,200 pCi/L in 1995, zero in 2001, and were back to 16,900 in 2004.
- Observed concentrations in the TF-SP and BLR-SP were near zero, but few measurements are available.

The spatial distribution of Sr-90 in the northern lower shallow perched water Figure J-12-10 is similar to that in the northern upper shallow perched water, and this distribution is reflected in the model predictions (red line). The highest simulated concentrations were predicted to be beneath the tank farm and immediately south and east of the tank farm. Like the upper region, simulated concentrations in this lower region were mostly higher than the observed concentrations. The large abrupt changes in concentrations predicted to occur in this region are due to the quarterly step change in the simulated Big Lost River recharge. The model predicts the 140-ft interbed is affected by the river to a greater extent than is the 110-ft interbed (see Appendix A, Section 6.2.2)

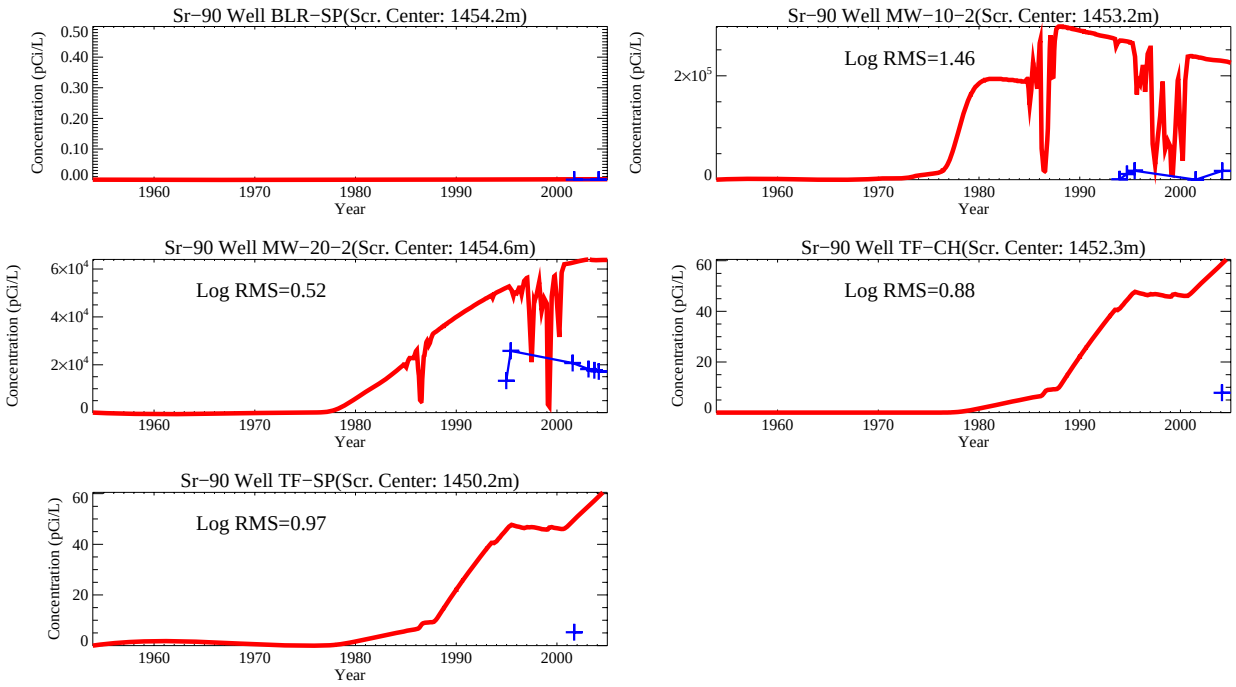

Figure J-12-10. Comparison of model predictions to field data for Sr-90 in the northern lower shallow perched water (red = predicted, blue = field data).

J-12.2.3 Northern Deep Perched Water Sr-90

Data for the wells completed in the northern deep perched water are shown in blue in Figure J-12-11. The Sr-90 retardation in the interbeds and the depth of the northern deep perched water make the tank farm an unlikely source of the Sr-90 in this region. The Sr-90 found in the northern deep perched water was most likely a result of the CPP-03 injection well failure. The highest observed Sr-90 concentrations found in this region coincide with the CPP-3 injection well repair date and the peak concentrations were close to the service waste water concentrations.

The highest observed Sr-90 concentrations (2,500 pCi/L) in this region were found in Well USGS-50 in 1970. The worst match in this water body occurred at well USGS-050, where concentrations are overpredicted by a factor of 400 ($380=10^{2.58}$). As discussed in Appendix A, Section ,6.3.2.1 the casing in this well has historically allowed downward migration of contaminants from higher elevations. The highest concentrations in the vadose zone pore water occur in the shallow interbeds with lowest concentrations appearing deeper. By allowing rapid migration through this well, the pore water near USGS-050 has much higher concentrations than observed in other deep wells. This leakage has not been accounted for in any of the vadose zone simulations presented here. In most of the key perched water wells, the difference between predicted and observed concentrations differs by less than a factor of 5 (log RMS< 0.76), which is very good given the overall complexity of the vadose zone at INL

The peak observed Sr-90 concentration in Well MW-18-1 was 207 pCi/L in 1995, and is most likely a reflection of the CPP-3 injection well because of the similarity to observed USGS-50 concentrations. Unlike predictions for the USGS-50 well, the simulated concentrations in Well MW-18-1 are persisting and begin to increase during the 1980s. This difference occurs because the model predicts the CPP-3 injection well water moving eastward towards Well MW-18 to a greater extent than northward towards Well USGS-50. The field data is inconclusive.

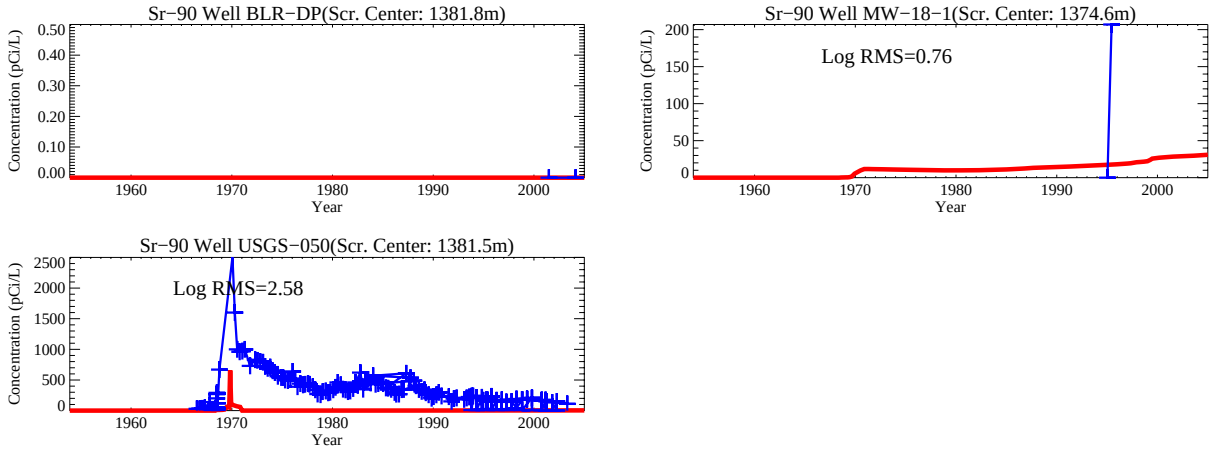

Figure J-12-11. Comparison of model predictions to field data for Sr-90 in the northern deep perched water (red = predicted, blue = field data).

J-12.2.4 Southern Shallow Perched Water Sr-90

Simulated (red) and observed (blue) Sr-90 concentration histories in the southern shallow perched water are illustrated in Figure J-12-12. This water body is associated with the 110-ft and 140-ft interbeds. Primary sources of Sr-90 in this region are the CPP-02 abandoned french drain and the former percolation ponds. The CPP-02 abandoned french drain operated from 1954 through 1966, received 4.78E7 gallons of water and 33.8 Ci of Sr-90. The percolation ponds operated from 1984-2002 and received service waste until the LET&D facility became operational in 1993. High concentrations in this region have been observed in MW-15 with much lower concentrations observed in other wells.

The highest Sr-90 concentrations were observed in Well MW-15 (22,100 pCi/L) in 1995, and high concentrations have been observed since its installation in 1994. This well is located near the southeast corner of CPP-603, and near site CPP-02. Concentrations at this location are too high to have originated in either the former percolation ponds, or the OU 3-13 Group-3 soil sites. For many years it has been known that elevated Sr-90 activities are present in the alluvium and shallow perched water near the CPP-603 spent fuel storage basins. Sections 2.2.6.1.1 and 2.3.2.2 of the OU 3-13 Work Plan (INEL, 1995) include detailed discussions of historical radionuclide concentrations in this area, and based on the low chloride concentrations, contaminated perched water in MW-15 is not believed to be derived from the former percolation ponds. Rather, the presence of Sr-90 and other fission products in the shallow perched water at this location is attributed primarily to historical releases of contaminated water from the spent fuel storage pools, including CPP-02 (Robertson et al. 1974).

Most of the observed data in the southern shallow perched water begins in the mid 1980s when the PW series wells were installed. A well defined concentration history is observable in this well series with first arrival coinciding with the percolation pond start up. The percolation ponds were excavated to basalt leaving sediments in topographical lows during their construction. The model placed the percolation pond water in the alluvium grid block immediately above the basalt, requiring injectate to migrate through the half-grid block of alluvium prior to entering the underlying basalt. The RI/BRA model used an alluvium K_d of 2 mL/g and an interbed K_d of 22 mL/g, which allows close approximation to wells PW-4, PW-5, and PW-2. The relatively low K_d allows migration from CPP-02 to arrive early in well PW-1, but by year 1990 concentrations are very close to measured values as shown by the RMS of 0.42 in that well. If anything, the simulated concentrations near the percolation pond is slightly delayed and of lower amplitude than observed in the data. The sodium concentration in the percolation pond water resulting from the INTEC water softening may have lowered the effective alluvium and interbed K_ds near the former percolation ponds below these assumed values. Concentrations of both Sr-90 and H-3 observed in Well PW-6 indicate percolation pond water reached this well. However, the model did not predict substantial amounts of percolation pond water arriving at this location.

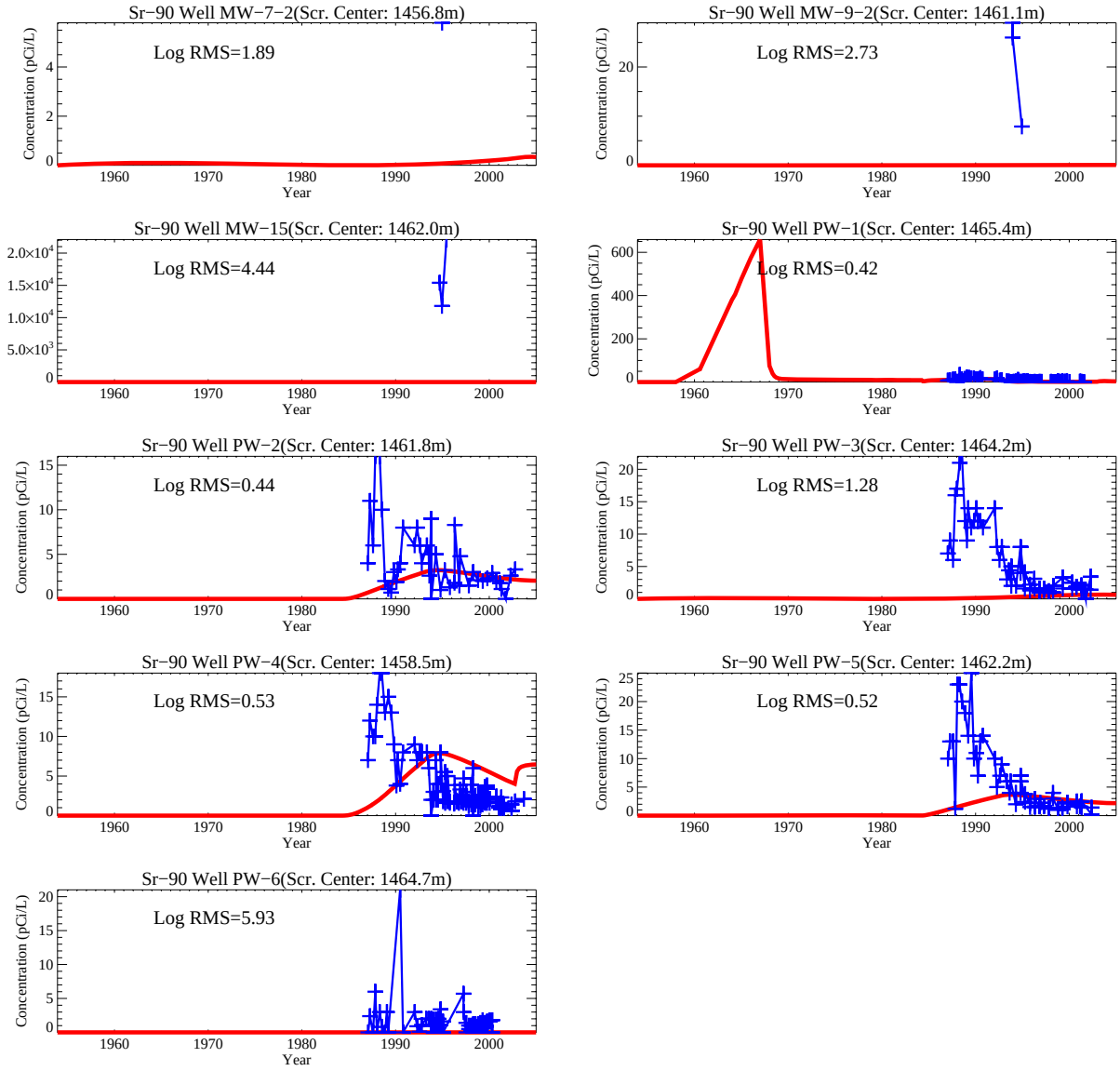

Figure J-12-12. Comparison of model predictions to field data for Sr-90 in the southern shallow perched water (red = predicted, blue = field data).

J-12.2.5 Southern Deep Perched Water Sr-90

The simulated and observed Sr-90 concentrations in the southern deep perched water wells is illustrated in Figure J-12-13 by the red and blue lines, respectively. The southern deep perched water is associated with the 380-ft interbed, but perched water has been encountered higher than 380-ft. As with the southern shallow perched water, the Sr-90s contamination sources are the CPP-02 abandoned french drain, the OU 3-13 group 3 soil sites and the service waste discharged into the former percolation ponds. Wells MW-1-4 and CS-CH lie near the northern most extent of the southern well grouping area and they most likely see contamination resulting from the CPP-3 injection well, OU 3-13 Group 5 soil sources, and possibly the tank farm releases.

The highest observed Sr-90 concentration in the southern deep perched water was found in Well 1804M at 16.9 pCi/L in 2002. Observed concentrations were 5.2 pCi/L in MW-1-4 at 5.2 pCi/L in 1994, 2.2 pCi/L in MW-17-2, and 1.1 pCi/L in well 1807L in 2002. Predicted concentrations using the RI/BRA model are quite close to these values in all but 1807L and MW-1-4 as indicated by the log RMS.

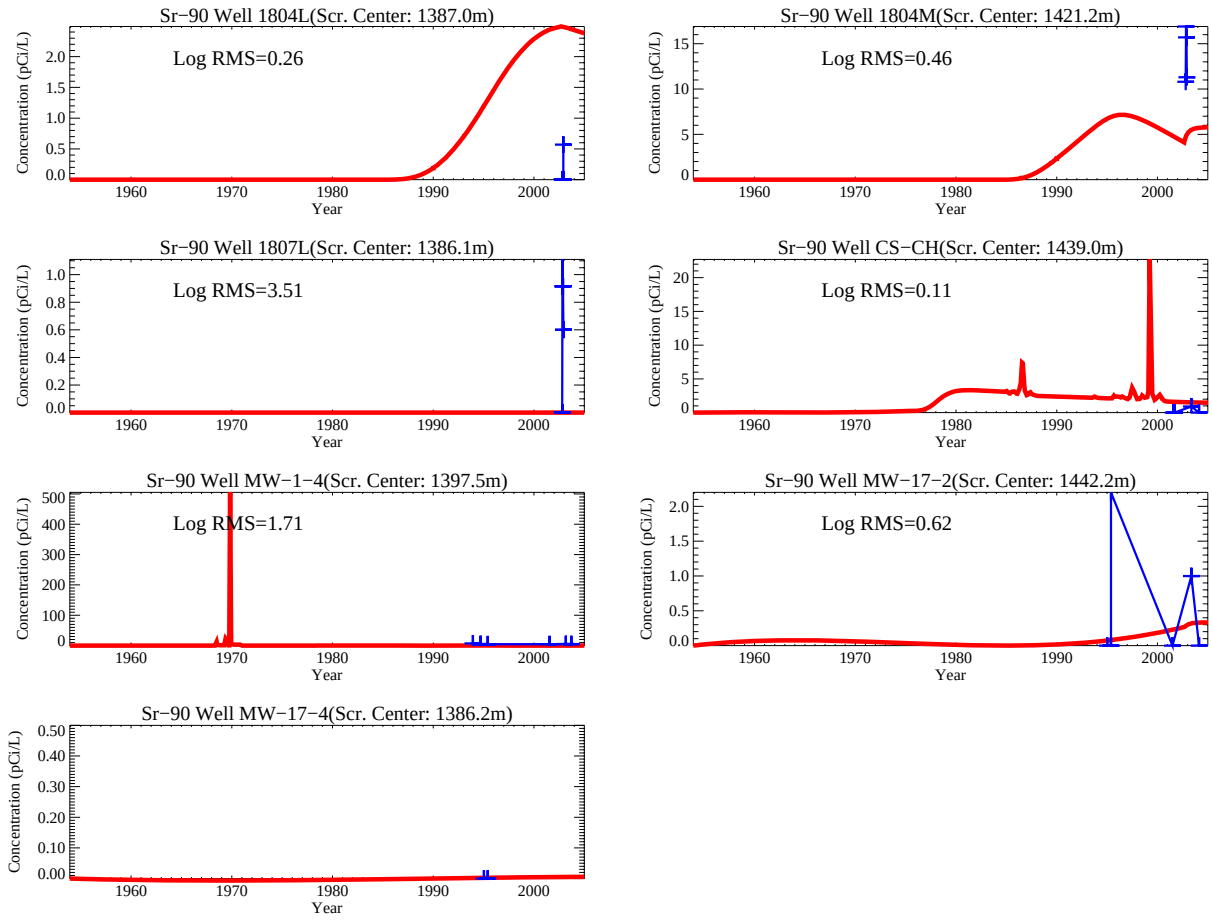

Figure J-12-13. Comparison of model predictions to field data for Sr-90 in the southern deep perched water (red = predicted, blue = field data).

J-12.3 Sensitivity of Perched Water Calibration to Hydrogeochemical Parameters

The log10 root mean square error for each of the sensitivity runs is summarized in Tables J-12-1 through J-12-10. The results are presented separately for each perched water zone, starting with the northern upper shallow perched water. In the discussion of each perched water body, there are two tables. In the first table, the minimum, average, and maximum log10 RMS is given with an indicator denoting the best match to field data and the figure in the body of the report in which the comparison to field data can be found. The second table contains the log10 RMS for each well used to derive the statistics in the first table. It is included to explain why the best match to field data does not always correspond to the smallest average log10 RMS error. The differences are largely related to the absolute maximum of observed field data. Even though the average error for a given simulation might be smaller, the average can be biased by wells in which the concentration is low. Prediction of long-term risk is driven by the highest concentrations, and the noted best match to field data takes this difference into account qualitatively.

J-12.3.1 Summary of Northern Upper Shallow Perched Water Calibration

The average log10 RMS (Table J-12-1) in the northern upper shallow perched water ranges from 1.04 to 1.50. In general, the lower mismatch errors were associated with the sensitivity run in which a CEC of 7 meq/100 g and interbed K_d of 50 mL/g were used. This parameter set probably overestimates the CEC, which is more likely in the 2-3 meq/100 g range. Decreasing the CEC increases the average log10 RMS because it results in overpredicting concentrations in wells far from CPP-31. Using only the highest concentration wells (MW 33-1, MW 33-2, 55-06, and MW-02), the lowest log10 RMS is obtained with more anthropogenic water in northern INTEC (Table J-12-2). As explained in Section J-11.3, the better match in this case occurs because more water allows flow above the 110-ft interbed.

Table J-12-1. Northern upper shallow perched water calibration summary.

Simulation	Minimum Log10 RMS	Average Log10 RMS	Maximum Log10 RMS	Figure #
RI/BRA Model: Alluvial CEC=2 meq/100 g, Interbed K_d=50 mL/g	0.38	1.33	3.90	J-8-14
Geochemical Parameter Sensitivity				
Alluvial CEC of 3 meq/100 g, Interbed K_d=50 mL/g	0.40	1.34	3.84	J-10-6
Alluvial CEC of 7 meq/100 g, Interbed K_d=50 mL/g	0.24	1.04	3.62	J-10-21
Alluvial CEC of 2 meq/100 g, Interbed K_d=22 mL/g	0.16	1.49	4.21	J-10-32
Alluvial CEC of 2 meq/100 g, Interbed K_d=78 mL/g	0.15	1.26	3.72	J-10-43
Hydrologic Parameter Sensitivity				
Lower 3 cm/yr Infiltration through the tank farm Liner	0.25	1.18	3.92	J-11-6
Higher 39 cm/yr Infiltration through the tank farm Liner	0.34	1.33	3.89	J-11-18
Anthropogenic Water Losses Focused in Northern INTEC	0.16	1.34	4.11	J-11-29
Anthropogenic Water Losses Stopped in 2035	0.38	1.33	3.90	J-11-40
Larger Interbed Dispersivity	0.20	1.50	2.80	J-11-64

.

Table J-12-2. Northern upper shallow perched water calibration by well and simulation

Simulation	Well Name										
	33-1	**33-2**	**33-3**	**33-4-1**	**37-4**	**55-06**	**MW-02**	**MW-4-2**	**MW-20-2**	**MW-24**	**MW-5-2**
RI/BRA Model: Alluvial CEC=2 meq/100 g, Interbed K_d=50 mL/g	0.4443	1.5244	0.9693	1.1809	3.8983	0.5346	0.7437	0.3771	0.5174	3.1556	0.0000
Geochemical Parameter Sensitivity											
Alluvial CEC = 3 meq/100 g	0.4013	1.4879	0.9165	1.1522	3.8428	0.4870	0.7896	0.4199	0.4663	3.4291	0.0000
Alluvial CEC = 7 meq/100 g	0.3752	1.4267	0.7197	0.9922	3.6192	0.4246	0.9608	0.5874	0.2417	0.0000	0.0000
Interbed K_d = 22 mL/g	0.4534	1.5582	1.5450	1.7933	4.2119	0.4299	0.4088	0.1619	1.1847	3.1550	0.0000
Interbed K_d =78 mL/g	0.4399	1.5149	0.6604	0.9078	3.7230	0.5410	0.9318	0.5574	0.1454	3.1583	0.0000
Hydrologic Parameter Sensitivity											
Tank Farm Liner Infiltration = 3 cm/yr	0.2760	1.4479	0.9620	1.1556	3.9179	0.7272	0.7695	0.4003	0.4349	2.6527	0.2501
Tank farm Liner Infiltration = 39 cm/yr	0.5458	1.7050	0.9641	1.1583	3.8928	0.3427	0.7093	0.3464	0.4895	3.1626	0.0000
Anthropogenic Water Losses Focused in Northern INTEC	0.1583	1.9068	1.5909	1.4150	4.1078	0.3177	0.2758	0.5902	0.8403	3.1026	0.3852
Anthropogenic Water Losses Stopped in 2035	0.4443	1.5244	0.9693	1.1809	3.8983	0.5346	0.7437	0.3771	0.5174	3.1556	0.0000
Larger Interbed Dispersivity	0.2332	1.5700	1.5447	1.4694	2.7967	1.5297	1.6295	1.7945	0.2017	1.9554	1.7920

J-12.3.2 Summary of Northern Lower Shallow Perched Water Calibration

The average log10 RMS in the northern lower shallow perched water (Table J-12-3) ranges from 0.91 to 2.02, for all simulations presented in this document. One of the better matches in this region was obtained with a larger dispersivity. As discussed in Section J-11.6, this is an artifact of weighting wells with lower concentrations equal to those with higher concentrations (Table J-12-4). As with the northern upper shallow perched water calibration, the second best match occurs with a slightly higher interbed K_d. In contrast with the northern upper shallow perched water calibration, increasing the anthropogenic water produced one of the worst matches. It is likely that there is more anthropogenic water being lost to infiltration than currently accounted for in the RI/BRA model. However, it is also likely that the interbed K_d is higher (closer to the 78 mL/g), and that not as much water as simulated in Section J-11.3 is lost to infiltration.

Table J-12-3. Northern lower shallow perched water calibration summary.

Simulation	Minimum Log10 RMS	Average Log10 RMS	Maximum Log10 RMS	Figure #
RI/BRA Model: Alluvial CEC=2 meq/100 g, Interbed K_d=50 mL/g	0.88	1.35	2.11	J-8-14
Geochemical Parameter Sensitivity				
Alluvial CEC of 3 meq/100 g, Interbed K_d=50 mL/g	0.83	1.31	2.08	J-10-6
Alluvial CEC of 7 meq/100 g, Interbed K_d=50 mL/g	0.64	1.16	2.00	J-10-21
Alluvial CEC of 2 meq/100 g, Interbed K_d=22 mL/g	1.55	1.79	2.23	J-10-32
Alluvial CEC of 2 meq/100 g, Interbed K_d=78 mL/g	0.51	1.12	2.06	J-10-43
Hydrologic Parameter Sensitivity				
Lower 3 cm/yr Infiltration through the tank farm Liner	0.86	1.36	2.17	J-11-6
Higher 39 cm/yr Infiltration through the tank farm Liner	0.90	1.40	2.22	J-11-18
Anthropogenic Water Losses Focused in Northern INTEC	1.48	2.02	3.33	J-11-29
Anthropogenic Water Losses Stopped in 2035	0.88	1.35	2.11	J-11-40
Larger Interbed Dispersivity	0.22	0.91	2.43	J-11-64

.

Table J-12-4. Northern lower shallow perched water calibration by well and simulation.

Simulation	Well Name			
	MW-6	MW-10-2	TF-CH	TF-SP
RI/BRA Model: Alluvial CEC=2 meq/100 g, Interbed K_d=50 mL/g	2.1067	1.4593	0.8763	0.9742
Geochemical Parameter Sensitivity				
Alluvial CEC = 3 meq/100 g	2.0776	1.4189	0.8256	0.9233
Alluvial CEC = 7 meq/100 g	1.9992	1.2741	0.6378	0.7302
Interbed K_d = 22 mL/g	2.2269	1.7527	1.5481	1.6271
Interbed K_d =78 mL/g	2.0646	1.3010	0.5079	0.6094
Hydrologic Parameter Sensitivity				
Tank farm Liner Infiltration = 3 cm/yr	2.1740	1.4367	0.8571	0.9574
Tank farm Liner Infiltration = 39 cm/yr	2.2190	1.4891	0.9021	0.9963
Anthropogenic Water Losses Focused in Northern INTEC	3.3289	1.4838	1.5915	1.6588
Anthropogenic Water Losses Stopped in 2035	2.1067	1.4593	0.8763	0.9742
Larger Interbed Dispersivity	2.4268	0.7489	0.2169	0.2455

J-12.3.3 Summary of Northern Deep Perched Water Calibration

The average log10 RMS in the northern deep perched water ranges from 1.1 to 1.96 (Table J-12-5 and J-12-6), for all simulations presented in this document. In general, the lowest mismatch errors were associated with the sensitivity run in which CEC=2 meq/100 g was used. In this specific case, the northern deep well that is really significant is USGS-050. In all cases, the peak concentration was under predicted in this well. As discussed above, this well was used as a temporary replacement injection well while CPP-03 was

repaired. Peak Sr-90 concentrations during the early 1970s were definitely introduced during the CPP-3 injection well failure, and the simulated and observed timing agrees. The measured concentrations in USGS-50 decline slowly after the 1970 repair period, where as the model predicts that concentrations would rapidly decrease after the repair. The continued high concentrations of Sr-90 in USGS-050 is attributed to leakage around the well casing that allows shallow high concentration perched water to directly enter the deep perched water zone.

Simulated concentrations in Well MW-18-1 are persisting and began to increase during the 1980s. This is because the model predicts that CPP-3 injection well water would move eastward towards Well MW-18 to a greater extent than northward towards Well USGS-50. The field data for well MW-18 is inconclusive.

Table J-12-5. Northern deep perched water calibration summary.

Simulation	Minimum Log10 RMS	Average Log10 RMS	Maximum Log10 RMS	Figure #
RI/BRA Model: Alluvial CEC=2 meq/100 g, Interbed K_d=50 mL/g	0.76	1.67	2.58	J-8-14
Geochemical Parameter Sensitivity				
Alluvial CEC of 3 meq/100 g, Interbed K_d=50 mL/g	0.78	1.70	2.63	J-10-6
Alluvial CEC of 7 meq/100 g, Interbed K_d=50 mL/g	0.85	1.87	2.88	J-10-21
Alluvial CEC of 2 meq/100 g, Interbed K_d=22 mL/g	0.09	1.10	2.11	J-10-32
Alluvial CEC of 2 meq/100 g, Interbed K_d=78 mL/g	1.09	1.96	2.84	J-10-43
Hydrologic Parameter Sensitivity				
Lower 3 cm/yr Infiltration through the tank farm Liner	0.77	1.67	2.57	J-11-6
Higher 39 cm/yr Infiltration through the tank farm Liner	0.75	1.66	2.57	J-11-18
Anthropogenic Water Losses Focused in Northern INTEC	0.07	1.13	2.20	J-11-29
Anthropogenic Water Losses Stopped in 2035	0.76	1.67	2.58	J-11-40
Larger Interbed Dispersivity	1.05	1.65	2.26	J-11-64

.

Table J-12-6. Northern deep perched water calibration by well and simulation.

Simulation	Well Name	
	MW-18-1	USGS-050
RI/BRA Model: Alluvial CEC=2 meq/100 g, Interbed K_d=50 mL/g	0.7558	2.5765
Geochemical Parameter Sensitivity		

Table J-12-6. Northern deep perched water calibration by well and simulation.

Simulation	Well Name	
	MW-18-1	USGS-050
Alluvial CEC = 3 meq/100 g	0.7774	2.6286
Alluvial CEC = 7 meq/100 g	0.8547	2.8755
Interbed K_d = 22 mL/g	0.0936	2.1101
Interbed K_d =78 mL/g	1.0893	2.8352
Hydrologic Parameter Sensitivity		
Tank farm Liner Infiltration = 3 cm/yr	0.7715	2.5691
Tank farm Liner Infiltration = 39 cm/yr	0.7489	2.5717
Anthropogenic Water Losses Focused in Northern INTEC	0.0678	2.1978
Anthropogenic Water Losses Stopped in 2035	0.7558	2.5765
Larger Interbed Dispersivity	1.0464	2.2624

J-12.3.4 Summary of Southern Shallow Perched Water Calibration

The average log10 RMS in the southern shallow perched water ranges from 0.85 to 3.04 (Table J-12-7) for all simulations presented in this document. Not considering the magnitude of observed concentrations, the lowest average RMS was obtained using a larger interbed dispersivity. Near the former percolation ponds, the better match was obtained with a lower alluvium K_d of 2 mL/g, allowing more rapid transport from the former percolation ponds. This suggests that the geochemical parameters of the alluvium are probably spatially variable, and are influenced by historical water chemistry. The highest concentrations in the southern shallow perched water correspond to wells MW-15, and PW-1. Table J-12-8 suggests that the best match occurs with an interbed Kd of 22 mL/g, but the log10 RMS for that case is quite similar to the log10 RMS for the RI/BRA base case.

Table J-12-7. Southern shallow perched water calibration summary.

Simulation	Minimum Log10 RMS	Average Log10 RMS	Maximum Log10 RMS	Figure #
RI/BRA Model: Alluvial CEC=2 meq/100 g, Interbed K_d=50 mL/g	0.41	2.02	5.93	J-8-14
Geochemical Parameter Sensitivity				
Alluvial CEC of 3 meq/100 g, Interbed K_d=50 mL/g	0.48	1.69	4.94	J-10-6
Alluvial CEC of 7 meq/100 g, Interbed K_d=50 mL/g	0.46	3.04	7.61	J-10-21
Alluvial CEC of 2 meq/100 g, Interbed K_d=22 mL/g	0.38	1.40	5.12	J-10-32
Alluvial CEC of 2 meq/100 g, Interbed K_d=78 mL/g	0.44	1.91	5.18	J-10-43
Hydrologic Parameter Sensitivity				
Lower 3 cm/yr Infiltration through the tank farm Liner	0.40	1.86	5.45	J-11-6
Higher 39 cm/yr Infiltration through the tank farm Liner	0.41	2.02	5.93	J-11-18
Anthropogenic Water Losses Focused in Northern INTEC	0.42	2.09	6.03	J-11-29
Anthropogenic Water Losses Stopped in 2035	0.41	2.02	5.93	J-11-40
Larger Interbed Dispersivity	0.24	0.85	2.91	J-11-64

.

Table J-12-8. Southern shallow perched water calibration by well and simulation

Simulation	Well Name								
	MW-7-2	**MW-9-2**	**MW-15**	**PW-1**	**PW-2**	**PW-3**	**PW-4**	**PW-5**	**PW-6**
RI/BRA Model: Alluvial CEC=2 meq/100 g, Interbed K_d=50 mL/g	1.8906	2.7342	4.4428	0.4150	0.4419	1.2760	0.5257	0.5196	5.9285
Geochemical Parameter Sensitivity									
Alluvial CEC = 3 meq/100 g	2.3033	3.1876	4.9380	0.4772	0.5084	1.4541	0.5338	0.5467	1.2352
Alluvial CEC = 7 meq/100 g	3.5212	4.2381	7.6058	0.4585	0.9570	1.8999	0.5700	0.6443	7.4526
Interbed K_d = 22 mL/g	0.4311	1.3931	3.1297	0.4759	0.3815	0.7761	0.4194	0.4794	5.1165
Interbed K_d =78 mL/g	2.6291	3.4487	5.1785	0.4400	0.5376	1.5885	0.5367	0.5845	2.2346
Hydrologic Parameter Sensitivity									
Tank farm Liner Infiltration = 3 cm/yr	1.6451	2.4631	4.1690	0.4501	0.4047	1.1371	0.5194	0.5006	5.4470
Tank farm Liner Infiltration = 39 cm/yr	1.8912	2.7342	4.4434	0.4150	0.4420	1.2759	0.5257	0.5197	5.9284
Anthropogenic Water Losses Focused in Northern INTEC	1.9949	3.0018	4.5691	0.4210	0.4419	1.3012	0.5258	0.5200	6.0283
Anthropogenic Water Losses Stopped in 2035	1.8906	2.7342	4.4428	0.4150	0.4419	1.2760	0.5257	0.5196	5.9285
Larger Interbed Dispersivity	0.2439	0.7717	2.9065	0.7551	0.3572	0.9692	0.3389	0.4520	0.0000

J-12.3.5 Summary of Southern Deep Perched Water Calibration

The average log10 RMS in the northern shallow perched water ranges from 0.93 to 1.28 (Table J-12-9) for all simulations presented in this document. Weighting high and low concentration wells equally, the best match was obtained with the larger dispersivity. However, looking at all of the comparisons there is very little overall variability, with the exception of well 1807L (Table J-12-10). That well is furthest from the percolation ponds. Although the higher dispersivity results in the lowest log10 RMS in this region, it resulted in large underpredictions of concentrations in the northern upper shallow perched water. With this under consideration, the best match in the southern deep perched water occurs with an interbed K_d of 22 mL/g. This is indicative of the ionic strength of the percolation pond water decreasing the interbed K_d in the perched water bodies above this one.

Table J-12-9. Southern deep perched water calibration summary.

Simulation	Minimum Log10 RMS	Average Log10 RMS	Maximum Log10 RMS	Figure #
RI/BRA Model: Alluvial CEC=2 meq/100 g, Interbed K_d=50 mL/g	0.11	1.11	3.51	J-8-14
Geochemical Parameter Sensitivity				
Alluvial CEC of 3 meq/100 g, Interbed K_d=50 mL/g	0.05	1.15	3.53	J-10-6
Alluvial CEC of 7 meq/100 g, Interbed K_d=50 mL/g	0.01	1.28	3.62	J-10-21
Alluvial CEC of 2 meq/100 g, Interbed K_d=22 mL/g	0.05	1.00	3.03	J-10-32
Alluvial CEC of 2 meq/100 g, Interbed K_d=78 mL/g	0.04	1.24	3.90	J-10-43
Hydrologic Parameter Sensitivity				
Lower 3 cm/yr Infiltration through the tank farm Liner	0.26	1.12	3.50	J-11-6
Higher 39 cm/yr Infiltration through the tank farm Liner	0.12	1.11	3.51	J-11-18
Anthropogenic Water Losses Focused in Northern INTEC	0.26	1.05	3.52	J-11-29
Anthropogenic Water Losses Stopped in 2035	0.11	1.11	3.51	J-11-40
Larger Interbed Dispersivity	0.16	0.93	3.34	J-11-64

.

Table J-12-10. Southern deep perched water calibration by well and simulation

Simulation	Well Name					
	1804L	1804M	1807L	CS-CH	MW-1-4	MW-17-2
RI/BRA Model: Alluvial CEC=2 meq/100 g, Interbed K_d=50 mL/g	0.2608	0.4560	3.5149	0.1096	1.7136	0.6233
Geochemical Parameter Sensitivity						
Alluvial CEC = 3 meq/100 g	0.2549	0.4475	3.5336	0.0457	1.7624	0.8383
Alluvial CEC = 7 meq/100 g	0.2261	0.4244	3.6154	0.0118	1.9362	1.4486
Interbed K_d = 22 mL/g	0.3510	0.8915	3.0309	0.0511	1.3292	0.3738
Interbed K_d =78 mL/g	0.1229	0.4457	3.8953	0.0430	1.9146	1.0235
Hydrologic Parameter Sensitivity						
Tank farm Liner Infiltration = 3 cm/yr	0.2656	0.4610	3.5015	0.2629	1.7273	0.5009
Tank farm Liner Infiltration = 39 cm/yr	0.2608	0.4560	3.5149	0.1186	1.6786	0.6237
Anthropogenic Water Losses Focused in Northern INTEC	0.2601	0.4569	3.5164	0.8597	0.5064	0.6773
Anthropogenic Water Losses Stopped in 2035	0.2608	0.4560	3.5149	0.1096	1.7136	0.6233
Larger Interbed Dispersivity	0.2946	0.5556	3.3359	0.1572	0.8509	0.3568

J-13 DATA SUMMARY

Sodium-bearing waste released to the tank farm alluvium in 1972 was very acidic, contained high concentrations of sodium, aluminum, and nitrate, and contained 15,000 Ci of Sr-90. Because of the highly dynamic geochemical evolution of pore water chemistry as the released sodium-bearing waste migrated through the tank farm alluvium, a competitive cation exchange model was evaluated as a method to provide better estimates of Sr-90 migration. Existing data were used in this competitive cation exchange model of Sr-90 transport in the tank farm alluvium. Where data did not exist, various methods were used to estimate the likely range of values the missing data would fall within.

J-13.1 Review of Geochemical Data

J-13.1.1 Mineral Data

Large amounts of data exist on mineralogy and grain-size distribution of INTEC alluvium. Sufficient data exist to conclude that calcite will be present at about 5 volume% in the alluvium to neutralize the acid. The simulations show that there is a large excess of calcium over the amount needed to buffer the sodium-bearing waste, and so the simulations will not be sensitive to significant changes in this number.

There are quite a few analyses of cation exchange capacity that are representative of alluvium at INTEC. Samples analyzed for CEC by the USGS in 1956, and by DOE in 1965 are either representative of *in situ* alluvium or are supported by sufficient data to permit adjustment of the CEC values to be representative of alluvium. The range of CEC values from these two data sets is relatively small, 2 to 4.5 meq/100 g. Using the PHREEQC geochemical code, an inverse calculation was performed on measured alluvium Sr K_d values to estimate alluvium CEC. The range of estimated alluvium CEC values was from 1.5 to 14 meq/100 g, with all but a few values below 4 meq/100 g. This agreement indicates a very narrow range of plausible alluvium CEC.

Direct measurements of Sr K_d values have been made on sedimentary interbed samples collected at 110 ft, 140 ft, and 380 ft below land surface at INTEC. These K_d values range from 140 to 240 mL/g with a single outlier at 60 mL/g. Comparing the major cation chemistry of the water used in the laboratory experiments to that of the perched water at INTEC shows that the laboratory experiments were conducted using water much lower in divalent cations than the perched water. Because the divalent cations compete most strongly with strontium for cation exchange sites, these measured K_d values were deemed to be too high. PHREEQC was used to calculate revised K_d values by using actual perched water chemical analyses. These revised K_d values ranged from 20 to 100 mL/g with a midpoint near 50 mL/g. This range of K_d values is based on a range of CECs estimated from the Liszewski data between13 and 24 meq/100 g. Measured CEC values from the SDA interbeds range from 5 to 45 meq/100 g with an average of 21 meq/100 g, supporting these estimated CEC values.

J-13.1.2 Selectivity Data

Good agreement on the order of selectivity preference for cations for a wide range of materials presented by a number of authors indicates that selectivity coefficients should vary over a fairly narrow range and be primarily controlled by the identity of the cation, not by the sedimentary materials. No site-specific selectivity coefficients have been measured on INL or INTEC materials. Laboratory data collected by Hawkins and Short in 1965 provide data from a series of sorption experiments that was used to evaluate the ion exchange model for INTEC sediments. Sorption of Sr to INTEC alluvium is well explained by ion exchange on planar surfaces of clay minerals using selectivity coefficients from the literature. Based on the concurrence in the literature on the order of selectivity preference of cations for ion exchange, and the ability of the selectivity coefficients adopted from the literature to match the laboratory experiments of Hawkins and Short, we conclude that the selectivity coefficients from the literature are applicable to the INTEC alluvium.

J-14 OVERVIEW AND SUMMARY

Future contaminant concentrations in the SRPA at INTEC were predicted using a single base case. The RI/BRA base case used the most defensible geochemical and hydrologic parameters to estimate exposure concentrations for a future groundwater receptor. These model simulations were based upon an interbed K_d of 50 mL/g and an alluvium CEC of 2 meq/100 g, which resulted in 12,336 Ci of Sr-90 leaving the alluvium during the first 20 year following the CPP-31 release. The RI/BRA base case provides the standard against which to compare the effects of various geochemical and hydrologic parameters during the sensitivity analysis. The RI/BRA base case is also used for future risk predictions.

The RI/BRA base case relies on several parameters to predict future groundwater concentrations. Most notably, the following parameters have the biggest impact on model predictions:

- An effective infiltration rate of 18 cm/yr from precipitation derived from field observations was used. This accounts for 85% of the total annual precipitation (21 cm/yr) that occurs at INTEC. No sensitivity analysis was performed to evaluate the range of observed infiltration rates at INTEC. For example, a previously used value of 10 cm/yr was not evaluated.
- A cation exchange capacity of 2 meq/100 g was used that results in 12,336 Ci of Sr-90 having left the alluvium during the 20 years following the CPP-31 release. This accounts for approximately 75% of the total Sr-90 in the tank farm being released to the underlying perched water, which cannot be accounted for using current monitoring data. Using the results from the sensitivity analysis, SRPA concentrations are linearly proportional to the contaminant mass leaving the alluvium, and therefore, reducing the mass by 1/2 will result in reducing the predicted SRPA concentrations by 1/2.
- An effective alluvium Kd of 2 mL/g was calculated based on the predicted ratio of aqueous phase to solid phase Sr-90. This low Kd is sufficiently large that after 20 years, the Sr-90 remaining in the alluvium does not contribute significantly to aquifer contamination. However, the Kd of 2 mL/g is approximately one order of magnitude lower than measured values outside of the influence of CPP-31.
- Interbed adsorption is the single most sensitive parameter, and is dependant on water chemistry and inherent spatial variability associated with mineralogic heterogeneity. The RI/BRA model was based on a singe midrange value that allows prediction of the mean behavior. The range of potential SRPA concentrations was evaluated using bounding values of the adsorption coefficient resulting in predicted concentrations that either about equal to the MCL by 2095, or are significantly higher than the RI/BRA model predictions.
- In all parameterizations, the model consistently over-predicts the Sr-90 concentrations in the SRPA wells located near INTEC, generally by a factor of between 3 and 6, but in some cases by as much as an order of magnitude. This over-prediction of current Sr-90 concentrations in the aquifer will impact predictions of future concentrations, but more importantly, will affect the time the aquifer is predicted to be above MCLs.

Model results are summarized in Table J-14-1. The RI/BRA base case has predicted that the peak Sr-90 concentrations in the SRPA at 2095 will be 18.6 pCi/L and be less than the MCL by 2129. Predicted SRPA concentrations are predicted to range from 4 to 343 pCi/L with the majority of concentrations in the 10-21 pCi/L range. To understand this range, it is important to understand the geochemical and hydrologic influences upon the model.

J-14.1 Geochemical Influences

Geochemical variables evaluated in this study included parameters of the alluvium and interbeds (CEC, Sr-90 selectivity, and K_d), and the geochemistry of the pore water (Na concentrations). These parameters determine 1) how much Sr-90 leaves the alluvium in the initial rapid release from CPP-31, 2) the mobility of the Sr-90 remaining in the alluvium, 3) and the mobility of Sr-90 in the interbeds of the vadose zone. Figure J-14-1 shows that the activity leaving the alluvium is a nearly exponential function of the cation exchange capacity of alluvium. The range of CEC evaluated spans 2-15 meq/100 g, with the most plausible values ranging between 2-7 meq/100 g. throughout the entire range, the activity leaving the alluvium is fairly sensitive, and differs by roughly 10,000 Ci. However, within this CEC and release range, the resultant peak aquifer concentration only ranges between 10 and 19 pCi/L.

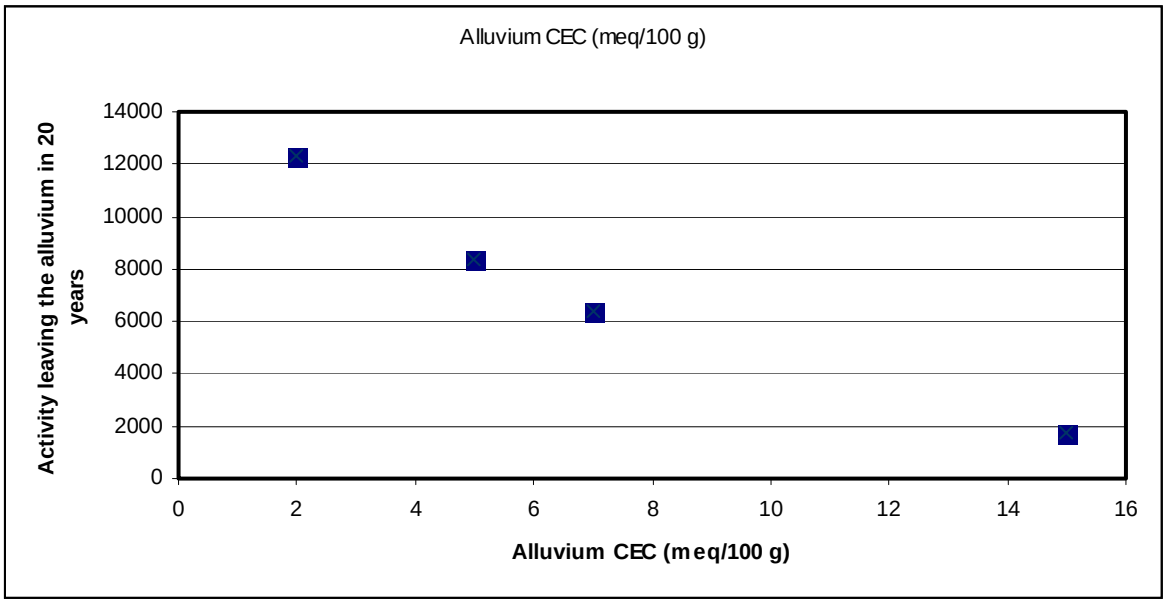

Figure J-14-1. Activity leaving the alluvium as a function of CEC.

As the released activity is removed from the alluvium through the cation exchange process, the remaining Sr-90 is held in place through a pseudo-steady state adsorption. Although more Sr-90 is predicted to remain in the alluvium at higher CEC, it is essentially immobile with a K_d approaching 50 mL/g as shown in Figure J-14-2. The most probable range of parameters places the K_d of residual alluvium Sr-90 in the 2-17 mL/g range, which is high enough to hold this remaining Sr-90 in the alluvium for an extended period of time. Table J-14-1 shows that the amount predicted to leave the alluvium at lower sodium concentrations falls within the range spanned by the plausible CEC range as does its effective K_d. This is also true for the range of Sr-90 selectivity coefficients simulated using the geochemical model. As a result, all of the sensitivity simulations evaluating alluvium geochemical characteristics fall within a fairly narrow range as shown in Figure J-14-3.

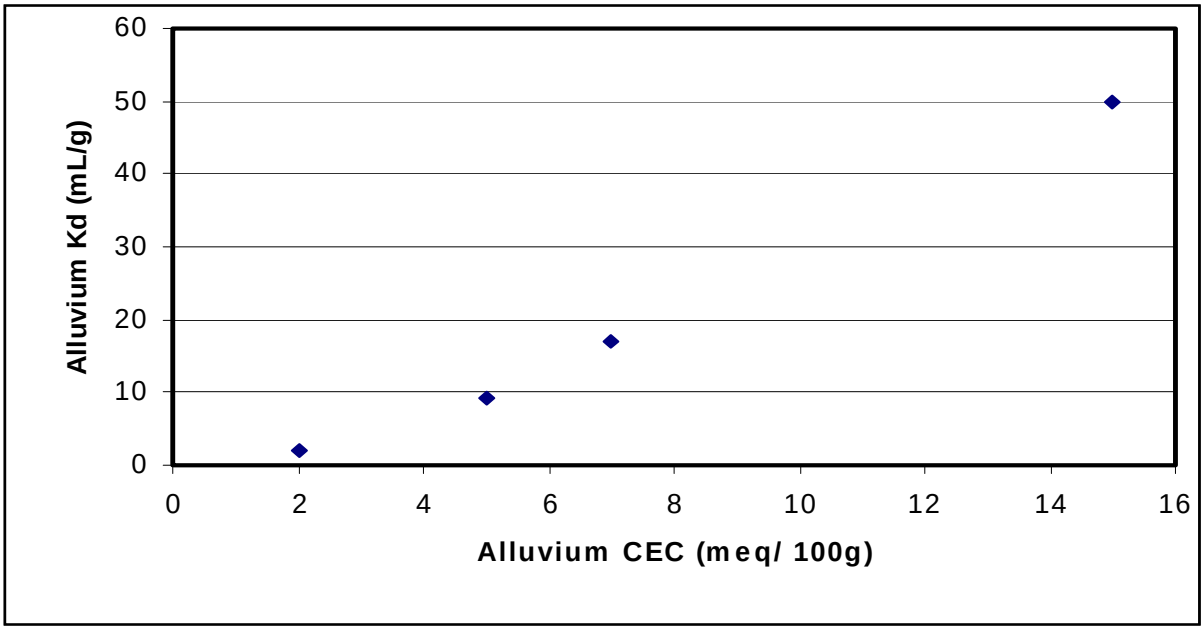

Figure J-14-2. Mobility of activity remaining in the alluvium as a function of CEC.

One of the outliers in the geochemical sensitivity study occurs in the simulation in which the interbed K_d was decreased to 22 mL/g (Figure J-14-3). This decrease affects not only the CPP-31 release, but also affects every other land-surface source of Sr-90. Sr-90 originating either from the OU 3-13 soil contamination, the failed injection well, or any of the OU 3-14 sources must pass through the interbeds in the vadose zone underlying INTEC. Because all of the sources are effected by adsorption in the interbeds, the K_d used to simulate transport through them is extremely important.Lowering the adsorption capacity affects peak aquifer concentrations by partitioning more of the Sr-90 into the aqueous phase off of the soils; by decreasing the travel time through the vadose zone and allowing less radioactive decay to occur; and by increasing the concentration gradients and resultant dispersive transport. In summary, the effects of interbed K_d are:

- The effective travel velocity is linearly proportional to the K_d: triple the K_d, triple the travel time.
- The half-life of Sr-90 is roughly 28 years. If the travel time is tripled, and given that the predicted time affected by peak aquifer concentrations is on the order of 200 years from now, the resultant residence time in the vadose zone is something like 600 years, or 20 half-lives.
- Aqueous concentrations are linearly proportional to the K_d, triple the K_d, cut the aqueous concentrations by one third.

Based on available data, a range of interbed K_ds is expected to span from 20-80 mL/g. At the low end (22 mL/g), the resultant concentration was predicted to be 110.8 pCi/L with concentrations remaining above the MCL through year 2263. At the high end, the resultant concentration would be 8.1 pCi/L with concentrations falling below the MCL by year 2096. Geochemical parameters used in the RI/BRA model were alluvium CEC=2 meq/100 g and interbed K_d=50 mL/g. Given these values, the peak concentration in the aquifer is predicted to be 18.5 pCi/L, and it falls below the MCL by 2129.

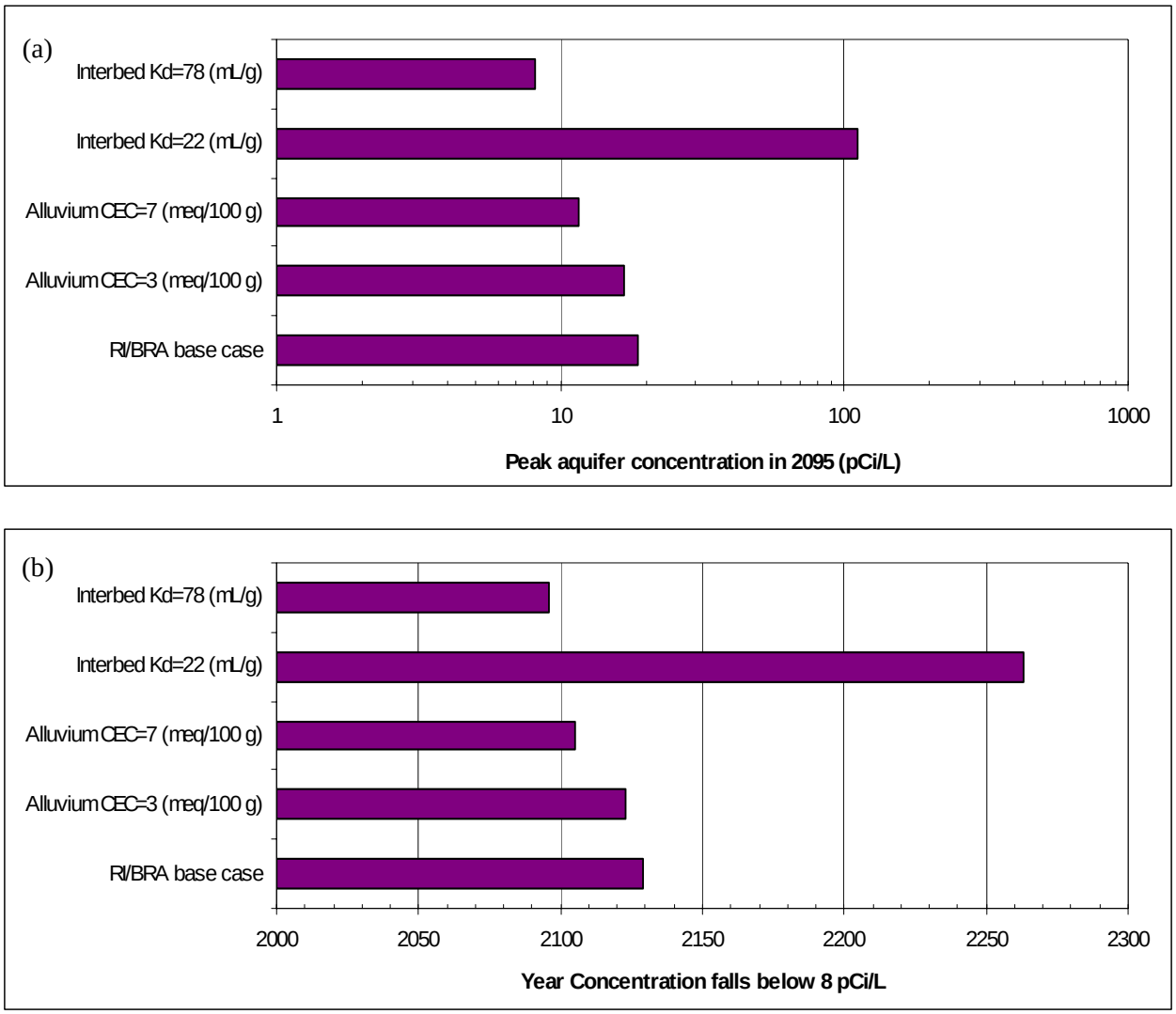

Figure J-14-3. Summary of geochemical sensitivity for the RI/BRA base case.

J-14.2 Hydrologic Influences

Hydrologic parameters studied here included infiltration rates through the tank farm, hydraulic characteristics of the interbeds, spatial distribution of unaccounted for anthropogenic water, and the land use scenario as impacted by the production wells. Figure J-14-4-A summarizes the predicted peak concentration and the year it falls below the MCL is summarized in Figure J-14-4-B. The highest peak value occurred when current estimates of the imbalance between pumped water and water discharges to the percolation ponds were focused near facilities in northern INTEC. The lowest value occurred when the dispersivity of the interbeds was increased in an effort to better match concentrations in CPP-55-06. Although increasing the dispersivity moved the Sr-90 out laterally, the predicted perimeter concentrations were much lower as a result of adsorption. As a result, the model underpredicted concentrations in wells with highest observed Sr-90 values. These two parameters also have the largest impact on the year during which the MCL is predicted to be exceeded. Of the two performance measures, the second is more sensitive overall. It is important because the time during which the MCL is exceeded dictates the duration of the remedial action. Sensitivity in this performance measure implies that cost estimates will also be subject to large uncertainty.

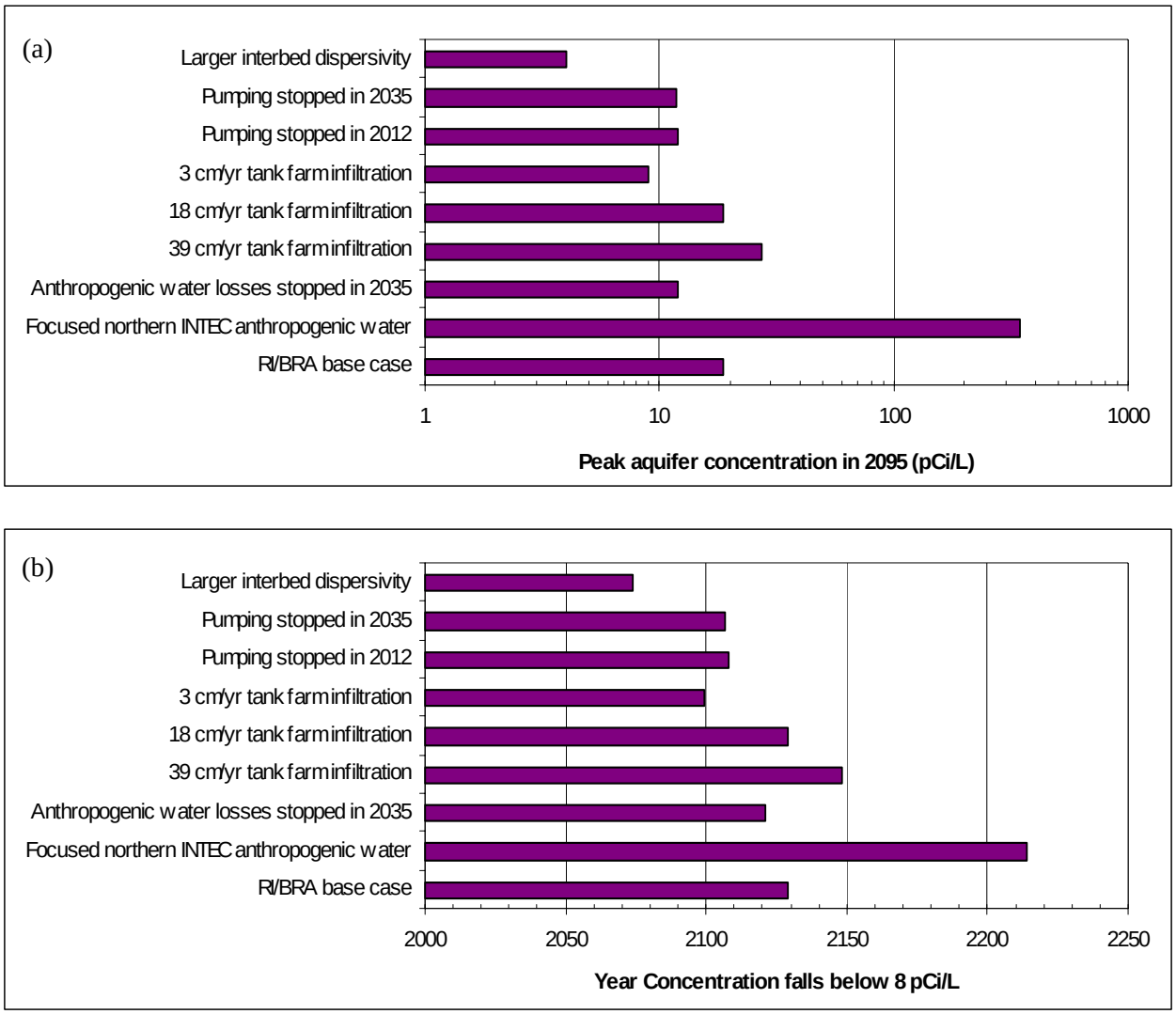

Figure J-14-4. Summary of hydrologic sensitivity for the RI/BRA base case.

Table J-14-1. Summary performance measures for all sensitivity simulations.

Simulation	Activity leaving alluvium within 20 years (Ci)	Activity remaining in alluvium at 20 years (Ci)	Effective K_d at 20 years (mL/g)	Peak Aquifer Concentration in 2095 (pCi/L)	Year C falls below 8 pCi/L
RI/BRA base case (CEC=2(meq/100 g)	**12336**	**3564**	**2**	**18.6**	**2129**
Geochemical Parameter Sensitivity Simulations					
Alluvium Properties					
CEC=3 (meq/100 g)	10864	5036	3.75	16.7	2123
CEC=5 (meq/100 g)	8380	7520	9.2		
CEC=7 (meq/100 g)	6403	9497	17	11.5	2105
$K_{Na/Sr}$=0.25	3378	12522	39		
$K_{Na/Sr}$=0.45	9480	6420	13		
Na^+ = 0.22 (mmol/L)	6517	9383			
Interbed adsorption coefficient					
K_d=22 (mL/g)	12336	3564	2	110.8	2263
K_d=78 (mL/g)	12336	3564	2	8.1	2096
Hydrologic Parameter Sensitivity Simulations					
Infiltration rate through tank farm liner (cm/yr)					
I=39	5580	10320	13	27.3	2148
I=18	12336	3564	2	18.6	2129
I=3	8037	7863	6.4	8.9	2099
Anthropogenic water					
Focused in Northern INTEC	12336	3564	2	343.0	2214
Losses Stopped in 2035	12336	3564	2	12.0	2121
Pumping Stopped in 2012	12336	3564	2	11.9	2108
Pumping Stopped in 2035	12336	3564	2	11.9	2107
Pumping Stopped in 2096	12336	3564	2	18.6	2108
Larger interbed dispersivity	12336	3564	2	4.0	2074

J-14.3 Summary

Important performance measures for evaluating the end state of Sr-90 are peak concentrations in 2095 and the time required for peak concentrations to be reduced below the MCL of 8 pCi/L. In all of the plausible parameters evaluated, we can conclude that:

- aquifer concentrations will exceed the MCL in 2095 in all but one of the RI/BRA results
- concentrations will exceed the MCL through year 2095, but will be below the MCL by 2263
- the predicted time frame that concentrations will exceed the MCL is very sensitive to interbed parameters
- the extent to which the MCL is exceeded is very sensitive to water chemistry and infiltration from anthropogenic water sources
- it is highly unlikely that the source of future aquifer contamination is from the Sr-90 that remains today in the alluvium
- it is believed that the existing contamination in the perched water and sorbed to the interbed that poses the greatest future risk.

J-15 REFERENCES

Appelo, C. A. J., 1994, "Cation and Proton Exchange, pH Variations, and Carbonate Reactions in a Freshening Aquifer," *Water Resources Research*, Vol. 30 (10), 2793-2805.

Appelo, C. A. J. and D. Postma, 1996, Geochemistry, Groundwater, and Pollution, A. A. Balkema, Rotterdam, Netherlands.

Barraclough, J. T., J. B. Robertson and V. J. Janzer, 1976, Hydrology of the Solid Waste Burial Ground, as Related to the Potential Migration of Radionuclides, Idaho National Engineering Laboratory, Open-File Report 76-471, IDO-22056, U. S. Geological Survey, Idaho Falls, Idaho, 1976, p.

Bartholomay, R. C., L. L. Knobel and L. C. Davis, 1989, *Mineralogy and Grain Size of Surficial Sediment from the Big List River Drainage and Vicinity, with Chemical and Physical Characteristics of Geologic Materials from Selected Sites at the Idaho National Engineering Laboratory, Idaho*, Open-File Report 89-384, DOE/ID-22081, U. S. Geological Survey, Idaho Falls, Idaho, July 1989, 74 p.

Bartholomay, R. C., 1990, *Mineralogical Correlation of Surficial Sediment from Area Drainages with Selected Sedimentary Interbeds at the Idaho National Engineering Laboratory, Idaho*, Water Resources Investigations Report 90-4147; DOE/ID-22092, U.S. Geological Survey, Idaho Falls, Idaho, 18p.

Bunde, R. L., J. Rosentreter, J. and M. J. Liszewski, 1998, "Rate of Strontium Sorption and the Effects of Variable Aqueous Concentrations of Sodium and Potassium on Strontium Distribution Coefficients of a Surficial Sediment at the Idaho National Engineering Laboratory," *Environmental Geology*, Vol. 34 (2/3), 135-142.

Bunde, R. L., J. Rosentreter, J., M. J. Liszewski, C. H. Hemming and J. Welhan, 1997, "Effects of Calcium and Magnesium on Strontium Distribution Coefficients," *Environmental Geology*, Vol. 32 (3), 219-229.

Del Debbio, J. A. and T. R. Thomas, 1989, *Transport Properties of Radionuclides and Hazardous Chemical Species in Soils at the Idaho Chemical Processing Plant*, WINCO-1068, Idaho National Engineering Laboratory, Westinghouse Idaho Nuclear Company, Idaho Falls, ID, October 1989, p.

DOE-ID, 2005, "Operable Unit 3-14 Tank Farm Soil and Groundwater Remedial Investigation /Baseline Risk Assessment (Draft)", DOE/NE-ID-11227, Rev. 0, U.S. Department of Energy Idaho Operations Office, May, 2005.

Hawkins, D. B. and D. C. Foster, 1963, *A Comparison of Two Methods of Sampling Gravel for the Evaluation of a Ground-Disposal Site for Radioactive Liquid Waste*, ID-12027, U. S. Atomic Energy Commission, Idaho Falls, ID, March 1963, 14 p.

Hawkins, D. B. and H. L. Short, 1965, *Equations for the Sorption of Cesium and Strontium on Soil and Clinoptilolite*, IDO-12046, U. S. Atomic Energy Commission, Idaho Falls, ID, November 1965, 33 p.

Hull, L. C., C. Grossman, R. A. Fjeld, J. T. Coates and A. W. Elzerman, 2004, "Hybrid Empirical - Theoretical Approach to Modeling Uranium Adsorption," *Applied Geochemistry*, Vol. 19 (5), 721-736.

ICP, 2004, *Evaluation of Tc-99 in Groundwater at INTEC: Summary of Phase 1 Results*, ICP/EXT-04-00244, Rev. 0, Idaho National Engineering and Enivronmental Laboratory, Idaho Completion Project, September 2004.

Leecaster, M. K. and L. C. Hull, 2003, *Spatial Distribution of Neptunium and Uranium Partition Coefficients (K_d) for Interbed Sediments at a Radioactive Waste Subsurface Disposal Area*, ICP/EXT-03-00088, Idaho Completion Project, Bechtel BWXT Idaho, Idaho Falls, ID, December 2003, 53 p.

Liszewski, M., J., J. J. Rosentreter, K. E. Miller and R. C. Bartholomay, 1998, *Strontium Distribution Coefficients of Surficial and Sedimentary Interbed Samples from the Idaho National Engineering and Environmental Laboratory, Idaho*, Water-Resources Investigation Report 98-4073, U. S. Geological Survey, Idaho Falls, ID, April 1998, 55 p.

Liszewski, M. J., J. Rosentreter, J. and K. E. Miller, 1997, *Strontium Distribution Coefficients of Surficial Sediment Samples from the Idaho National Engineering and Environmental Laboratory*, Water-Resources Investigations Report, 97-4044, U. S. Geological Survey, Idaho Falls, ID, 55 p.

Liszewski, M., J., J. J. Rosentreter, K. E. Miller and R. C. Bartholomay, 1998, Strontium Distribution Coefficients of Surficial and Sedimentary Interbed Samples from the Idaho National Engineering and Environmental Laboratory, Idaho, Water-Resources Investigation Report 98-4073, U. S. Geological Survey, Idaho Falls, ID, April 1998, 55 p.

McBride, M. B., 1994, Environmental Chemistry of Soils, Oxford University Press, New York.

Nace, R. L., M. Deutsch and P. T. Voegeli, 1956, *Geograph, Geology, and Water Resources of the National Reactor Testing Station, Idaho, Part 2: Geography and Geology*, IDO-22033-USGS, U. S. Geological Survey, Boise, ID, p.

Pace, M. N., J. J. Rosentreter and R. C. Bartholomay, 1999, Strontium Distribution Coefficients of Basalt and Sediment Infill Samples from the Idaho National Engineering and Environmental Laboratory, Idaho, Water Resources Investigations Report 99-4145, U. S. Geological Survey, Idaho Falls, ID, 56 p.

Reardon, E. J., 1981, "K_ds - Can They Be Used to Describe Reversible Ion Sorption Reactions in Contaminant Migration?" *Ground Water*, Vol. 19 (3), 279-286.

Rightmire, C. T., 1984, Description and Hydrogeologic Implications of Cored Sedimentary Material from the 1975 Drilling Program at the Radioactive Waste Management Complex, Idaho, Water-Resources Investigations Report 84-4071, DOE/ID-22067, U. S. Geological Survey, Idaho Falls, Idaho, June 1984, 33 p.

Roddy, M., 2005, *Geochemical Study for Perched Water Source Identification at INTEC*, EDF-5758, Rev 0, Idaho Cleanup Project, CH2M-WG Idaho LLC, Idaho Falls, ID, May 2005, 70 p.

Rosentreter, J., J., R. Nieves, J. Kalivas, J. P. Rousseau and R. C. Bartholomay, 1999, *The Use of Chemical and Physical Properties for Characterization of Strontium Distribution Coefficients at the Idaho National Engineering and Environmental Laboratory*, Water-Resources Investigations Report, 99-4123, U. S. Geological Survey, Idaho Falls, ID, 25 p.

Sparks, D. L., 2003, Environmental Soil Chemistry, Academic Press, Boston.

Steefel, C. I., S. Carroll, P. Zhao and S. Roberts, 2003, "Cesium Migration in Hanford Sediment: A Multisite Cation Exchange Model Based on Laboratory Transport Experiments," *Journal of Contaminant Hydrology*, Vol. 67 (1-4), 219-246.

Xu, T., E. Sonnenthal, N. Spycher and K. Pruess, 2004, *TOUGHREACT User's Guide: A Simulation Program for Non-Isothermal Multiphase Reactive Geochemical Transport in Variably Saturated Geologic Media*, LBNL-55460, Lawrence Berkeley National Laboratory, Berkeley, CA, May 2004, 192 p.

Zachara, J. M., S. C. Smith, C. X. Liu, J. P. McKinley, R. J. Serne and P. L. Gassman, 2002, "Sorption of Cs+ to Micaceous Subsurface Sediments from the Hanford Site, USA," *Geochemical Et Cosmochimica Acta*, Vol. 66 (2), 193-211.